2005
Annual Progress Report

AUTOMOTIVE LIGHTWEIGHTING MATERIALS

Less dependence on foreign oil, and eventual transition to an emissions-free, petroleum-free vehicle

FREEDOMCAR AND VEHICLE TECHNOLOGIES PROGRAM

U.S. Department of Energy
Energy Efficiency and Renewable Energy
Bringing you a prosperous future where energy is clean, abundant, reliable, and affordable

FreedomCAR & Fuel Partnership

21st CENTURY TRUCK PARTNERSHIP

Acknowledgement

We would like to express our sincere appreciation to QSS Group, Inc., Oak Ridge National Laboratory, and Argonne National Laboratory for their technical and artistic contributions in preparing and publishing this report.

In addition, we would like to thank all the participants for their contributions to the programs and all the authors who prepared the project abstracts that comprise this report.

U.S. Department of Energy
Office of FreedomCAR and Vehicle Technologies
1000 Independence Avenue S.W.
Washington, DC 20585-0121

FY 2005

Progress Report for Automotive Lightweighting Materials

Energy Efficiency and Renewable Energy
FreedomCAR and Vehicle Technologies

Edward J. Wall
Program Manager, FreedomCAR and Vehicle Technologies

Rogelio Sullivan
Materials Technologies Team Leader

Joseph Carpenter
Technology Area Development Manager

August 2006

CONTENTS

I. INTRODUCTION 1

II. AUTOMOTIVE METALS 7

A. Warm Forming of Aluminum II 7
B. Active Flexible Binder Control System for Robust Stamping 14
C. Die Face Engineering Project for Advanced Sheet Metal Forming 24
D. Electromagnetic Forming of Aluminum Sheet 31
E. Aluminum Automotive Closure Panel Corrosion Test Program 38
F. Improved Automotive Suspension Components Cast with B206 Alloy 51
G. Structural Cast Magnesium Development 57
H. Magnesium Powertrain Cast Components 68
I. Ultra-Large Castings of Aluminum and Magnesium 76
J. Cost Assessment of Emerging Magnesium Sheet Production Methods 85
K. Low-Cost Titanium Powder for Feedstock 95
L. Low-Cost Powder Metallurgy Technology for Particle-Reinforced Titanium Automotive Components: Manufacturing Process Feasibility Study 100
M. Powder Metal Performance Modeling of Automotive Components 104
N. High-Strength Steel Joining Technologies Project 120
O. Hydroform Materials and Lubricants Project 125
P. Sheet Steel Fatigue Characteristics Project 129
Q. Tribology 134
R. High-Strength Steel Stamping Project 136
S. Strain-Rate Characterization 141
T. Modeling of High Strain-Rate Deformation of Steel Structures 147
U. Lightweight Front End Structures 152
V. Future Generation Passenger Compartment 169
W. Evaluations of the Effects of Manufacturing Processes and In-Service Temperature Variations on the Properties of TRIP Steels 179

III. LOW-COST CARBON FIBER 187

A. Low-Cost Carbon Fiber from Renewable Resources 187
B. Advanced Stabilization of PAN Fiber Precursors 197
C. Advanced Oxidation of PAN Fiber Precursor 200
D. Low-Cost Carbon-Fiber Manufacturing Using Microwave Energy 204
E. Carbon-Fiber Systems Integration 208

IV. POLYMER COMPOSITES R&D 211

A. Development of Manufacturing Methods for Fiber Preforms 211
B. Development of Next-Generation Programmable Preforming Process 219
C. High-Volume Processing of Composites 229
D. Automotive Composites Consortium Focal Project 3 Composite-Intensive Body Structure 235

CONTENTS (CONT.)

E. Low-Cost Test Methods for Advanced Automotive Composite Materials: Creep Compression Fixture ... 243
F. Interphase Analysis and Control in Fiber-Reinforced Thermoplastic Composites ... 248
G. Performance Evaluation and Durability Prediction of Dissimilar Material Hybrid Joints ... 256
H. Durability of Carbon-Fiber Composites ... 260
I. Composite Crash Energy Management ... 268
J. Crash Analysis of Adhesively-Bonded Structures (CAABS) ... 281
K. Engineering Property Prediction Tools for Tailored Polymer Composite Structures ... 287
L. Simulation of Injection Molding of Thermoplastics Reinforced with Short and Long Fibers ... 299
M. A Hierarchical, Structure-Oriented and Stochastic Approach to Model Liquid Molding Processes Modeling and Simulation of Compression Resin Transfer Molding ... 303
N. Modeling and Simulation of Compression Resin Transfer Molding ... 310
O. Incorporating Higher-Order Tensors in the Computation of Polymer Composite Mechanical Properties ... 314

V. JOINING ... 321

A. Die-Cast Net-Shaped Hole Process Development for Application of Thread-Forming Fasteners ... 321
B. Forming Limits of Weld Metal in Aluminum Alloys and Advanced High-Strength Steels ... 330
C. Friction-Stir Spot-Welding of High-Strength Steels ... 336
D. Long-Life Electrodes for Resistance Spot-Welding of Aluminum Sheet Alloys and Coated High-Strength Steel Sheet ... 340

VI. NON-DESTRUCTIVE EVALUATION ... 349

A. NDE Tools for the Evaluation of Laser-Welded Metals ... 349
B. NDE Inspection of Resistance Spot-Welds in Automotive Structures Using an Ultrasonic Phased Array ... 350

VII. RECYCLING ... 361

A. Recycling Assessments and Planning ... 361
B. Baseline Assessment of Recycling Systems and Technology ... 366
C. Development of Technology for Removal of PCBs and Other Substances of Concern (SOCs) from Shredder Residue ... 374
D. Compatibilization/Compounding Evaluation of Recovered Polymers ... 383
E. Post-Shred Materials Recovery Technology Development ... 389

CONTENTS (CONT.)

VIII. Materials Crosscutting R&D 397

A. Technical Cost Modeling..... 397
B. Intermediate-Rate Crush Response of Crash Energy Management Structures 401
C. Structural Reliability of Lightweight Glazing Alternatives..... 406

1. INTRODUCTION

Automotive Lightweighting Materials R&D

As a major component of the U.S. Department of Energy's (DOE's) Office of FreedomCAR and Vehicle Technologies Program (FCVT), Automotive Lightweighting Materials (ALM) focuses on the development and validation of advanced materials and manufacturing technologies to significantly reduce automotive vehicle body and chassis weight without compromising other attributes such as safety, performance, recyclability, and cost.

The specific goals of ALM are to develop material and manufacturing technologies by 2010 that, if implemented in high volume, could cost-effectively reduce the weight of light-duty body and chassis systems by 50% with safety, performance, and recyclability comparable to 2002 vehicles.

ALM is pursuing five areas of research: cost reduction, manufacturability, design data and test methodologies, joining, and recycling and repair. The current Long-Range Plan for activities in these areas during the next 5 years is found at www.eere.energy.gov. Because the single greatest barrier to use of lightweight materials is cost, priority is given to activities aimed at reducing costs through development of new materials, forming technologies, and manufacturing processes. Priority lightweighting materials include advanced high-strength steels (AHSSs), aluminum, magnesium, titanium, and composites including metal-matrix materials and glass- and carbon-fiber-reinforced thermosets and thermoplastics. The inclusion of AHSSs is an example explaining the term "lightweighting" as opposed to "lightweight" in order not to imply focus on just lower density materials.

Collaboration and Cooperation

ALM collaborates and cooperates extensively to identify and select its research and development (R&D) activities and to leverage those activities with others. The primary interfaces have been and still are with entities of the "Big Three" domestic automotive manufacturers (DaimlerChrysler, Ford and General Motors), namely the FreedomCAR Materials Technical Team, the Automotive Composites Consortium (ACC), and the United States Automotive Materials Partnership (USAMP). These collaborations provide the means to determine critical needs, to identify technical barriers, and to select and prioritize projects. Other prominent U.S. partners include such organizations as the Auto/Steel Partnership of the American Iron and Steel Institute, the American Plastics Council, the Vehicle Recycling Partnership, and the American Foundry Society. ALM also coordinates its R&D activities with entities of other U.S. and Canadian federal agencies. Interactions with DOE's Office of Industrial Technologies Program (ITP), FCVT's High-Strength Weight Reduction (HSWR) Materials effort, and the Department of Natural Resources of Canada (NRCan) are especially important by virtue of overlaps of interests in lightweighting. Contacts with similar efforts in other countries besides Canada are being pursued. As mentioned below, projects at seven universities were initiated in FY 2005 under joint funding with the U.S. National Science Foundation (NSF), and another project at a university, jointly funded with DOE's Office of Science, continued.

Project Selection and Stages

In cooperation with USAMP and the FreedomCAR Materials Technical Team, a procedure has been established to help facilitate the development of projects in order to help move high-risk leveraged R&D to targeted research projects that eventually migrate to the original equipment manufacturers (OEMs) or suppliers as application engineering projects. R&D projects are assigned to one of three phases as depicted in the figure and defined below: concept feasibility, technical feasibility, and demonstrated feasibility. Projects are guided to meet the requirements of each phase before they move on to the next phase. Not all projects

must go through these phases under ALM funding; some may enter the technical or demonstrated feasibility stages from efforts funded elsewhere.

Concept Feasibility: Concept feasibility projects should contain a specific idea to address a need or to create something new. Projects are usually exploratory and small in monetary requirements and time, typically less than $200,000 total over 1–2 years. Projects should provide a yes/no answer to the value of the idea. All projects are required to have a detailed research plan, budget, and timing. They can be ended before proceeding to technical feasibility if there is a lack of technical progress or if the preliminary business case turns out to be unfavorable.

Technical Feasibility: Technical feasibility projects should continue R&D for ideas with proven merit or potential. These projects should identify the key barriers to implementing the technology and focus on overcoming them. Technical feasibility projects should have well-defined, industrial OEM and/or supplier participation and pull. They are usually larger and longer term than the concept feasibility projects with typical investment in the $1M to $2M range and length of 2–3 years or more. Technical feasibility projects can be ended before proceeding to demonstrated feasibility if there is a failure to overcome the key barriers to implementation or if the cost or business case does not develop as favorably as initially assessed.

Demonstrated Feasibility: Technology projects that need larger scale validation may become demonstrated feasibility projects. Not all technical feasibility projects will need a demonstration or validation program. These projects are few in number, much larger in scale, and may involve component or system fabrication and tests. Support and leverage from the industrial OEMs and/or suppliers is a key requirement.



Stage progression for projects

Once selected, R&D projects are pursued through a variety of mechanisms, including cooperative research and development agreements (CRADAs), cooperative agreements, university grants, R&D subcontracts, and directed research. This flexibility allows the program to select the most appropriate partners to perform critical tasks. The ALM efforts are conducted in partnership with automobile manufacturers, materials suppliers, national laboratories, universities, and other nonprofit technology organizations. These interactions provide a direct route for implementing newly developed materials and technologies. Laboratories include Argonne National Laboratory (ANL), Lawrence Berkeley National Laboratory (LBNL), Lawrence Livermore National Laboratory (LLNL), Oak Ridge National Laboratory (ORNL), Pacific Northwest National Laboratory (PNNL), and Sandia National Laboratories (SNL). ANL oversees recycling efforts and ORNL provides overall technical support and coordination, including for the DOE cooperative agreement with USAMP. The National Engineering Technology Laboratory (NETL) provides external projects management including the cooperative agreement with USAMP.

Research areas and responsible organizations

Coordinated area	Organization
Production and fabrication of aluminum	HSWR, ITP, Natural Resources of Canada (NRCan)
Production and fabrication of magnesium	International Magnesium Association, NRCan, HSWR
Recycling, reuse, repair of automotive parts and materials	Vehicle Recycling Partnership, American Plastics Council
Fabrication of steel and cast iron	American Iron and Steel Institute, the Auto/Steel Partnership, HSWR
Fundamental materials research	DOE Office of Science, National Science Foundation (NSF)
High-volume composite processing	Department of Commerce—National Institute of Standards and Technology's Advanced Technology Program
Crashworthiness	Department of Transportation
Production and fabrication of composites	American Plastics Council

FY 2005 Accomplishments

The Structural Cast Magnesium Development (SCMD) project work advanced far enough that General Motors decided to introduce the project's focal component, a front engine cradle, shown below, in its 2006 Chevrolet Corvette. The magnesium version is 34% lighter than the 2005 production aluminum engine cradle it replaces. See report 2.G.

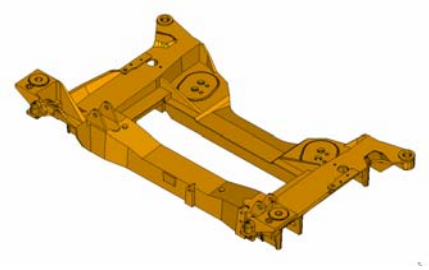


Image of Magnesium Front Engine Cradle

The Aluminum Consultants Group, in conjunction with PNNL, prepared a technical cost model that indicated that magnesium sheet produced by twin-belt casting and twin-roll casting probably can be economically viable for automotive applications. See report 2.J.

Bolstered by the successes in the SCMD and the Mg Powertrain Cast Components projects and the positive indications of the cost model above, the USAMP completed a strategic vision study outlining recommendations for North American automotive magnesium through the year 2020. The study will be published in 2006.

The Durability of Carbon-Fiber Composites project at ORNL concluded. A final report will be published in 2006. This culminates a ten-year campaign to develop and document initial, experimentally-based, durability-driven design criteria and damage-tolerance assessment procedures for representative fiber-reinforced polymer-matrix composite automotive structures in long-term (15 year) service. Earlier work on glass-fiber-reinforced epoxy-matrix composites provided enough assurance that commercial products developed. The later work of the campaign provided similar initial assurance for carbon-fiber-reinforced epoxy- and thermoplastic-matrix composites, and it is expected that, in time, commercial products in those materials will eventually emanate as well from further work by industry. See report 4.H.

The Active Flexible Binder Control System for Robust Stamping project built an advanced binder load control system and used it to successfully stamp liftgate panels from BH210 and DP500 steels, and A6111-T4 aluminum using the same set of tools (Fig. 1). The tryout time using the system was considerably less than those using conventional methods of reworking the die (welding, grinding, polishing and testing). Splits and wrinkles in stamped panels could literally be healed in minutes rather than in days by adjusting the tonnages

of the appropriate cylinders. Prior efforts to make the liftgate from A6111-T4 using conventional methods were unsuccessful. Fig. 2 shows the dramatic benefits of using closed loop control in eliminating wrinkles in a large steel pan. See report 2.B.

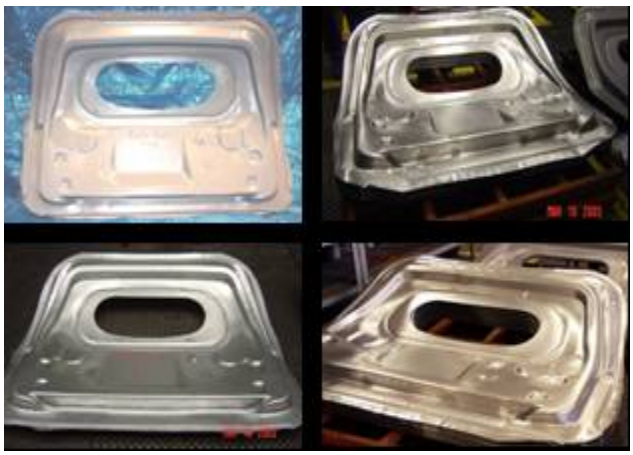


Fig. 1 Liftgate panels made from two steels (BH210, DP500) and two aluminum (A6111-T4) batches (lower photo)



Fig. 2 Steel Pan drawn without (upper photo) and with (lower photo) closed loop control

A recent cost study performed by Camanoe Associates, in conjunction with PNNL, concluded that the use of a low-cost titanium ore as the feedstock source in a continuous reduction process could drive down the cost of titanium sponge and powder substantially to the point that it could be considered for application in standard automotive components. The continuous process used in conjunction with a low-cost feedstock can produce powder at $2.00/lb compared to the nearly $90/lb for conventional atomized powder. PNNL is currently leading a program to develop this low-cost titanium processing stream. Working with E.I. DuPont de Nemours and International Titanium Powder (ITP), PNNL has employed low-cost, ilmenite-derived titanium tetrachloride (of the type used for titanium dioxide paint pigment) as the precursor in ITP's Armstrong titanium synthesis process. The resulting titanium powders, while containing additional impurities (primarily tin and silicon), still appear capable of meeting strength and ductility requirements for a wide range of automotive applications. See report 2.K.

A new multi-participant thrust on computational modeling for predicting the processing-dependent structures and properties of fiber-reinforced polymer-matrix composites (FRPMCs) was initiated late in this fiscal year. The ALM is supporting applied work at PNNL on the modeling and experimental verification work at ORNL; PNNL is working closely with a software vendor to implement the modeling into commercial code usable by industry. The ALM and the National Science Foundation are jointly supporting work at seven universities that will serve, in time, to improve the fundamental bases of the modeling. The entire thrust is being guided by a steering committee of researchers from the automotive and plastics industries. See reports 4.K to 4.O.

One concern about the use of FRPMCs has been whether they could be disposed of properly at the end of the vehicle's useful life. ANL supplied Changing World Technologies (CWT) of West Hempstead, New York with 3,000 lbs of auto shredder residue (ASR) or "fluff" which is mainly composed of the plastics left after the metals have been separated from the shredded vehicle body. CWT added a depolymerization step before their existing thermal pyrolysis step already operating commercially for poultry waste. The fuel produced seems comparable to fuel oil used in ships or industrial plants and, at current prices of such fuel; the

technology appears attractive enough for CWT to begin seeking funding for a full-scale plant to convert the ASR. See Report 7.E.

Future Direction

In FY 2002 and FY 2003, the FreedomCAR and Fuels Initiative formed from the 1994–2001 Partnership for a New Generation of Vehicles (PNGV). Thinking and planning on what replaces the ALM efforts that began in the PNGV in roughly 1999–2002 has continued since. The ALM and the FreedomCAR Materials Technical Team conducted a series of strategic reviews of various materials and manufacturing topics in FY 2004. Based on those reviews, carbon-fiber-reinforced polymer-matrix composites and magnesium will be emphasized in the next few years as they have the greatest weight-reduction potential, but there will be some efforts on AHSSs, titanium, and metal–matrix composites because these will contribute in niche roles to the overall FreedomCAR weight-reduction and cost neutrality goals. Material-crosscutting work in general manufacturing will continue to increase in joining, nondestructive evaluation (NDE), and recycling. Planning for the future NDE efforts will be concluded in 2006. Though technical feasibility (see figure above) projects will dominate as before, concept-feasibility and demonstrated-feasibility projects will also be pursued as will some university base-technology projects as mentioned above.

2. AUTOMOTIVE METALS

A. Warm Forming of Aluminum II

Principal Investigator: Ken Oikarinen
DaimlerChrysler Corporation
1030 Doris Road
Auburn Hills, MI 48326-2613
(248) 754-9763, Fax: (248) 754-9750, e-mail: kco3@daimlerchrysler.com

Principal Investigator: Peter Friedman
Ford Motor Company
Ford Research Laboratory
PO Box 2053, MD 3135/SRL
2101 Village Road
Dearborn, MI 48121-2053
(313) 248-3362, Fax: (313) 390-0514, e-mail: pfriedma@ford.com

Principal Investigator: Paul Krajewski
General Motors Corporation
GM R&D and Planning
Mail Code 480-106-212
30500 Mound Road
Warren, MI 48090-9055
(586) 986-8696, Fax: (586) 986-9204, e-mail: paul.e.krajewski@gm.com

Project Administrator: Constance J.S. Philips
National Center for Manufacturing Sciences
3025 Boardwalk
Ann Arbor, MI 48108-3266
(734) 995-7051; Fax: (734) 995-1150; e-mail: conniep@ncms.org

Technology Area Development Manager: Joseph A. Carpenter
(202) 586-1022; fax: (202) 586-1600; e-mail: joseph.carpenter@ee.doe.gov
Field Technical Manager: Philip S. Sklad
(865) 574-5069; fax: (865) 576-4963; e-mail: skladps@ornl.gov

---

Contractor: U.S. Automotive Materials Partnership
Contract No.: FC26-02OR22910

Objective

This project previously demonstrated the potential of warm-forming (WF) technology to significantly improve the formability of aluminum. The Phase I demonstration was done in "prototype" mode and demonstrated the expanded depth of draw that is possible with WF. The objective of Phase II is to:

- Develop and demonstrate a production process for the WF of aluminum for automotive body structures and measure the economic feasibility of the WF process for a production environment.

Approach

- Develop individual elements of the WF process in a laboratory environment including alloy characterization, lubricant development, forming simulation and process thermal modeling.
- Develop full-size demonstration of WF process and run tests in a production-like environment. Process will include blank preheating, lubricant application, WF press and die with modified thermal profile controls, and lubricant removal.
- Create a technical cost model that can generate cost comparisons between a warm-formed aluminum door inner and a same or similar door inner manufactured using conventional forming processes in steel and aluminum.

Significant improvements in the formability of aluminum are expected to be achieved through development of enabling WF process advancements including:

- Establishing the degree of improvement in formability of production-grade, commercial aluminum alloys.
- Developing a cleanable lubricant suitable for use in a WF process.
- Optimizing the temperature distribution of the die for improved thermal control and formability.
- Evaluating rapid preheating systems for blanks.
- Applying CAE simulation tools (finite element analysis) to modify the die to attain a production-quality part.
- Optimizing a process and layout design.
- Applying the results of the cost model to optimize process design.

To demonstrate the manufacturing and economic feasibility for a new production process such as the WF process, the definition of the process flow is paramount, as well as the development and application of a technical cost model that allows comparison of a product made in the WF process with a comparable component fabricated from aluminum or steel using current stamping technology.

Accomplishments

Achievements toward these goals through FY 2005 included the following:

- Completed aluminum alloy characterization and laboratory-based WF process studies, including aluminum-alloy sheet fabricated from custom-ormulated 5000 series alloys and commercial alloys 5182-O, 5182-H18, 5754-O and 5754-H18.
- Determined constitutive equation for AA5182 for formability simulation.
- Determined scheme for most uniform heating of die by adding new or relocating heaters, changing setpoints, wattage, and insulation/isolation.
- Completed die refurbishment based on forming simulation and prepared it for use in production demonstration.
- Identified a suitable lubricant through extensive laboratory-based studies. Lubricant application trials conducted and lubricant applied for WF trials.
- Developed a method for blank heating which would enable cycle times of 6-10 jobs/minute. However, the budget, established in 2001, did not allow for full-scale preheater and material handling automation design/build. It was decided that the demonstration would use an available OEM oven to preheat the blanks for the demonstration trials and the blanks would be moved manually, thereby allowing the project to remain within budget.

Future Direction

- Set up and conduct production demonstration – November 2005
- Evaluate the post-formed mechanical properties of the warm-formed parts – January 2006
- Employ the technical cost model to compare costs of WF and alternative processes.
- Create Mg sheet program – Sept 2006.

Introduction

The need to improve fuel economy has led automakers to explore lightweight materials such as aluminum for automobile body and closures. While attractive from a mass perspective, there are many challenges to the widespread use of aluminum including:

- Limited formability compared to steel
- Sliver management in trimming aluminum panels
- Appearance problems in most 5000-series aluminum panels

Phase II of the Warm Forming of Aluminum project was initiated after the initial technical feasibility of forming complex shapes at elevated temperatures was previously demonstrated in Phase I. It is a four-year development and demonstration program to establish the "production" feasibility of warm-forming aluminum-alloy blanks into automotive panels and to fully demonstrate a warm-forming process for cost-effectively manufacturing aluminum automotive panels that require a deep drawn shape. See Figure 1.

This project focuses on the following objectives:

- Developing and demonstrating a warm-forming process including the materials, equipment, and heating processes that can cost-effectively expand the forming limits of aluminum sheet.

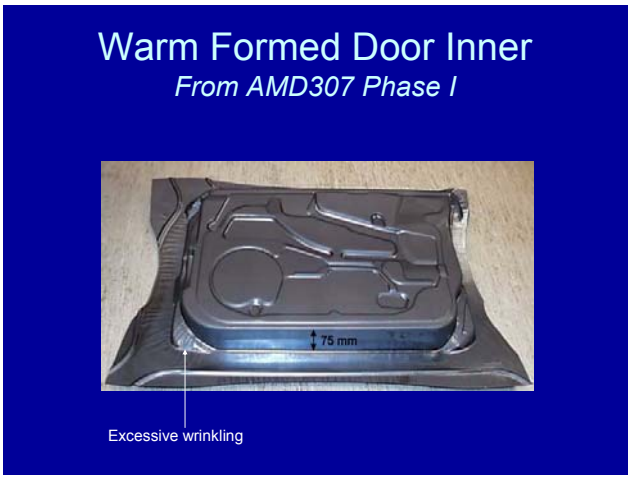


Figure 1. Warm-formed door inner from Phase I showing deep-drawn shape yielded by the Phase I die.

- Developing a technical cost model for the warm-forming process to evaluate the economic feasibility of the warm-forming process specific to component design.

The key enabling process improvements to make warm forming a production-capable process are the following:

- A high-temperature lubricant with good lubricity at warming-orming conditions, that is easy to clean prior to automotive painting.
- Temperature distribution management on the die surface during the forming operation.
- Identifying an effective preheating method for blanks.
- Identifying an optimum alloy for warm forming and characterizing its mechanical behavior at elevated temperatures.

Phase II Detail

Technical Cost Model: Technical cost model is complete. Camanoe Associates developed a detailed cost model based on a process sequence defined by the project team. Through use of the cost model, it was identified that aluminum-alloy cost accounted for over 70% of the cost of the end product and hence project research was refocused on commercially available alloys rather than "new" alloys with exotic alloying additives. Preliminary technical cost feasibility is positive and will be verified following the demonstration trials. Additionally, the model will be adjusted based on knowledge gained from the demonstration run. The cost model will allow warm forming of aluminum to be compared to conventional steel stamping and multi-piece assembly as a function of volume.

Alloy Selection: The University of Michigan completed analyses of the warm formability of commercial aluminum alloys and identified parameters affecting the sheet fabrication process for warm-forming-capable aluminum sheet.

Lubricant Selection: The performance of selected lubricants under various temperature, travel time, and load pressures was evaluated at the University of Michigan in collaboration with GM and Fuchs' Lubricants. Additionally, friction tests were conducted at Ford using pre-lubricated coupons to

establish optimum lube type and thickness to temperature relationships.

Die Thermal Analyses: University of Michigan's S. Wu Manufacturing Center performed initial Finite Element Analyses of temperature profiles on the warm-forming tooling for Neon Door Inners built in Phase I. Die geometry and heater location data were obtained from CAD models created in Phase I provided by Sekely Industries. See Figure 2.

In 2005, further thermal analyses were completed at GM using proprietary thermal analysis software. These analyses contributed to the final thermal distribution scheme for achieving the most uniform heating of the die by adding new or relocating existing heaters, changing setpoints, wattage, and insulation/isolation. Setpoints on the die and ring were determined for various thermal conditions ranging from 150°C to 350°C.

Blank Heating: Evaluations of infra-red heating and conduction heating methodologies for heating laboratory-scale blanks were investigated at The University of Michigan and Ford Motor Company, respectively. The results assisted the team in identifying the preferred heating methodology for blank pre-heating for a WF production process.

Alloy Fabrication: Pechiney Rolled Products-Alcan supplied the special formulation 5000 series and commercial AA5182 aluminum sheet for these formability studies. Magnesium Elektron (formerly Spectrulite) supplied commercial-grade magnesium sheet for the WF feasibility trials.



Figure 2. Picture of the warm-forming die constructed for the feasibility demonstration performed in Phase I.

Full-scale Process Demonstration: With the individual component processes validated at laboratory level for technical and economic process feasibility, the full-scale warm-forming demonstration using modified door inner stamping dies from Phase I will be conducted starting in November 2005. The process demonstration will be conducted in the local Detroit area allowing direct participation of the OEM team.

Post process inspection and material analyses: Coupons from warm-formed parts will be cut out and the materials properties will be evaluated by the OEMs. The typical properties to be evaluated will include strength, distortion, corrosion, cleanability, etc.

Phase II 2005 Accomplishments

Forming Simulation

FEA simulation was applied to WF die to understand forming process and guide die modification process. A CAD model was created of WF die by scanning in hot and cold state (NVision 3D and 3D Scan). Simulations were performed with various binder configurations (gaps) and coefficients of friction to find upper and lower bounds on final thickness prediction.

Simulation results will be correlated with experiment during post-form analysis of warm-formed panels.

Alloy and Formability Analysis - Pechiney (Alcan)/GM

GM and their subcontractor, MSU, completed the development of a constitutive equation for AA5182 supplied by Pechiney-Alcan for formability simulations done at Ford. Subsequently, the constitutive equation was provided to the WF OEM team. See Figure 3.

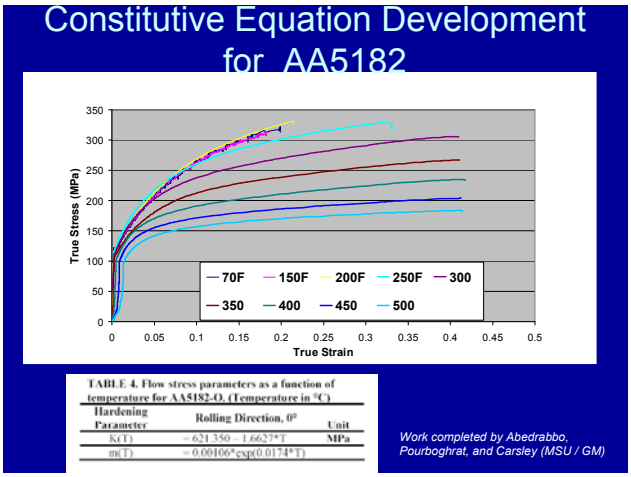


Figure 3. Constitutive equation for AA5182 for use in formability simulations.

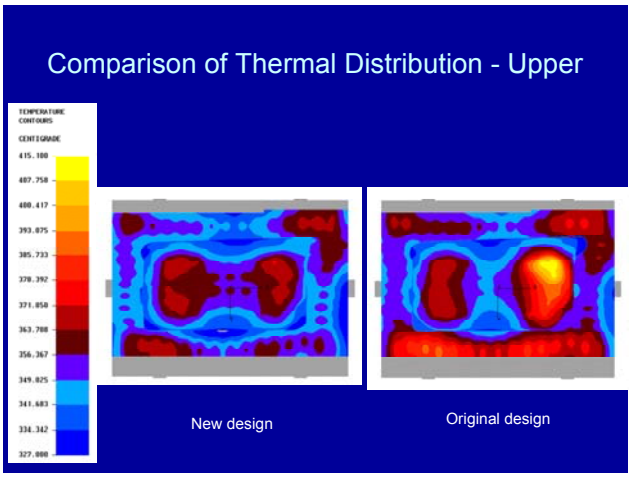


Figure 4. Thermal analyses before and after upper die design changes.

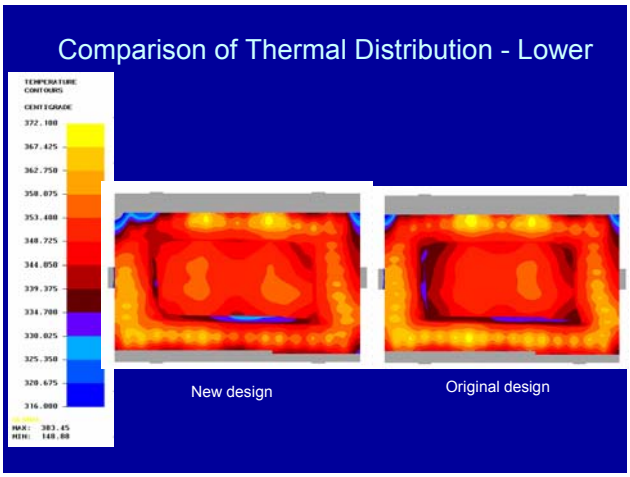


Figure 5. Thermal analyses before and after lower die design changes

Lubricant/Lubrication System

A production-viable, warm-forming lubricant and production-capable method of applying the lubricant was identified and implemented at a subcontractor to GM, Jay & Kay Manufacturing. Lubricant application trials were completed at Jay & Kay Manufacturing in August 2005. Additional laboratory friction screening was completed at Ford to test lubricity. Lubricant was applied for warm-forming trials scheduled for October-November 2005.

Thermal Analysis of Dies

A scheme for the most uniform heating of the die was determined involving the addition of new heaters, relocation, and removal of heaters, as well as changing setpoints, wattage, and installing new insulation for thermal isolation. Preliminary analysis was completed at GM using proprietary thermal analysis software in June 2005. See Figures 4 and 5. These thermal analyses resulted in being able to recommend new heaters and locations. Additionally, setpoints were determined for various thermal conditions for the die and ring ranging from 150°C to 350°C.

Modification of WF Die

The forming die and heating system was modified to improve part quality during 2005. The modifications included:

- Machining of cavity walls to remove tight spots.
- Machining rings to modify drawbeads.
- Modify heaters in punch based on results of thermal CAE studies.
- Addition of heaters in the corner of the punch and cavity.
- Refurbish heater controls.
- Add fasteners to hold down cavity, upper and lower rings.

Blank Heating System

In February 2005 it was determined that the project budget was insufficient to fund the design and building of a full-scale, blank-heating and material-handling automation system as evaluated in the laboratory trials performed at UM, GM and Ford. The laboratory evaluations of a conduction system would enable cycle times of 6-10 jobs/minute, and could be implemented by any of the OEMs for production applications. It was ultimately decided that the preheating and blank transfer system was not so unique so as to require the allocation of additional R&D budget in Phase II. Additionally, sufficient information exists from Phase II laboratory trials and supplier quotations to allow cost and cycle time data to be included in the technical process cost model. Therefore, it was decided that a GM oven (Figure 6.) would be used for blank preheating and blanks will be manually transferred between the oven and die during the demonstration trials.

Alloy Sheet Fabrication

Previously, the decision to use commercially-available material eliminated the need for further research to develop costly special alloys. In 2005, AA5182 was supplied by Pechiney – Alcan for the demonstration trials. Additionally, magnesium sheet for initial feasibility runs was purchased from Magnesium Elektron (MEL).



Figure 6. Picture of blank heating oven that will be used during warm-forming demonstration trials.

Process Demonstration

Substantial progress was made during 2005 to incorporate the various elements of WF process developed in this Phase II into a full-scale process demonstration. The demonstration was re-scoped and re-timed in February 2005 with the approval of the board of the USAMP's Automotive Metals Division (AMD). Significant steps made toward process scale-up included the selection of Troy Tooling Technologies as the source for die and controls rebuilding, press and hot-die fit-up, and demonstration trial implementation.

Demonstration trials are to include:

- Refurbished and thermally-optimized die
- Improved panel quality
- Hot machining
- New lubricant with production application
- Blank preheating with GM oven
- No extraction automation
- Include Mg blanks

Trials are set for November 2005.

Summary and Conclusions

Alloy Selection: 5182-O Al alloy has sufficient attributes for warm forming to support its use in the scale-up demonstration phase. Findings from the alloy characterization studies pertinent to the scale-up demonstration phase include the following:

- Full-hard 5182 aluminum has observable rolling-induced damage, which is absent in 5182-O.
- Full-hard 5182 alloy can be recrystallized by rapid heating; formability remains worse than 5182-O sheet.
- 5182-O alloy shows an improved cup height of 20 mm at 350°C as compared to room-temperature tests.
- 5182-O alloy has a biaxial forming limit of 40% x 40% (approximately) at 350°C.

In the demonstration phase, Mg sheet will be tested using the warm-forming demonstration process and tooling to empirically evaluate the result. Mg behavior and blank-forming results will help the

OEMs determine what developmental work may be required to warm form Mg.

Blank Preheating and Forming Studies: while lab trials demonstrated that an infra-red (IR) oven is capable of supplying ample heating for the warm-forming process, it did not appear to be the best solution for the production application due to the need for significant IR lamp overheating to achieve production-feasible heat-up times. Over-heating was believed to present the risk of melting the blank if the conveyer system were to stop for any period of time. The team fabricated and evaluated a laboratory-level conduction heater methodology. Conduction heating is believed to be a cost-effective and robust method of heating aluminum sheet. Laboratory tests indicated that forming temperatures can be reached within cycle time requirements of 6 to 10 jobs per minute.

In general, moly-disulfide lubrication produced equal or slightly inferior cup height in comparison to BN-coated samples, with values in the range of 18-21 mm. The Fuchs Lubricants 216 wax-based varieties with BN or moly-disulfide produced the best results. 216-BN was found to be the best lubricant exhibiting a cup height of 25 mm. Because it is a wax-based lubricant, a heavy, tenacious brown stain forms on the cup surface due to curing of the polymer base and bonding to aluminum. Future work may consider development of economical cleaning solutions for this lubricant.

For the 5182-O Al sheet alloys studied in the warm forming temperature range of 200-350°C and in the strain rate range of 0.015-1.33 s^{-1}, the following conclusions can be drawn:

- Uniaxial tensile elongation increases with increasing temperature and decreases with increasing strain rate. The maximum tensile elongation observed ranged between 60-100% at 350°C.
- Strain-rate sensitivity increases with increasing temperature, and the strain-hardening rate increases with increasing strain rate in keeping with dynamic recovery effects. Strain-rate hardening is deemed to play a dominant role in enhancing the elevated temperature plasticity in tensile deformation. Dynamic recovery effect increases with increasing stress level. And, at a specific stress level, the total amount of recovery effect increases with increasing temperature and/or decreasing strain rate.

Lubricant Studies: Fuchs lubricant 216 BN produced the best cup height of all formulations studied, exhibiting a cup height of ~25 mm, and appears to be a feasible lubricant for use in the scale-up demonstration. Cleaning options and methodologies will be defined during the demonstration trials.

Die and Blank Thermal Analyses: modeling performed by GM during 2005 completed the development of an FEA for determining optimal heater specifications for the tooling/process design. Future work on this task will verify FEA results against actual thermal data from the demonstration experiments. These data will then be incorporated into the FEA for determining optimal heater specifications for future OEM tooling/process design use.

Technical Cost Model: preliminary technical cost feasibility is positive and will be verified following the demonstration trials. Additionally, the model will be adjusted based on knowledge gained from the demonstration run. The cost model will allow warm forming of aluminum to be compared to conventional steel stamping and multi-piece assembly as a function of volume.

B. Active Flexible Binder Control System for Robust Stamping

Principal Investigator: Tom Balun
Forward Model Material Engineering Specialist
Stamping Business Unit - Die Engineering - Mfg Development Center,
Ford Motor Company
6000 Mercury Drive, Mail Drop 130 - FN1 Room AF008
Dearborn, MI 48126-2740
Cell: 313-805-4283; Fax: 313-59-44299; e-mail: tbalun@ford.com

Project Administrator: Mahmoud Y. Demeri
FormSys Inc.
40180 Woodside Drive South
Northville, MI 48167
Phone/fax: (734) 462-2742; e-mail: mdemeri@formsysinc.com

Technology Area Development Manager: Joseph A. Carpenter
(202) 586-1022; fax: (202) 586-1600; e-mail: joseph.carpenter@ee.doe.gov
Field Technical Manager: Philip S. Sklad
(865) 574-5069; fax: (865) 576-4963; e-mail: skladps@ornl.gov

---

Contractor: U.S. Automotive Materials Partnership
Contract No.: FC26-02OR22910

Objective

- Develop, build and demonstrate an optimized closed-loop flexible binder control system that can be installed in stamping presses to improve the quality of panels made from aluminum alloys and high-strength steels and to reduce the cost for developing and setting production tools.

Approach

- Conduct open-loop control demonstration of flexible binder technology.
- Develop methodology and guidelines for designing and building flexible binders.
- Develop computer simulation and process optimization capabilities for flexible binders.
- Develop a closed-loop flexible binder control system with appropriate sensors.
- Demonstrate closed-loop control of the flexible binder system on an industrial part.
- Evaluate the technical and economic feasibility of flexible binder technology.

Accomplishments

- The retrofitted Erie Press Binder Control Unit and GM liftgate tooling were tested in tryouts at TDM in Warren, MI using three different materials with varying thicknesses. Binder force trajectories generated by both trial-and-error and FEA were implemented and parts were successfully made. The tryout time using the system was considerably less than the estimated tryout time using conventional methods of working the die.
- A new 10-cylinder IFU binder control unit with pan tooling was tested successfully in a hydraulic press at the University of Stuttgart in Germany. Tests in a mechanical press, which are crucial to demonstrating the

applicability of binder control technology in mechanical systems, are scheduled at TDM in Warren, Michigan during November/December 2005.

- Three materials (A6111-T4, DP500 and BH210) were tested under biaxial deformation using the Viscous Pressure Bulge (VPB) test. This test yields more accurate information compared to the uniaxial tension test because stress conditions in stamping are often different from the ones present in the tensile test. Flow stresses from the test are used as input for FE simulation of the stamping process.
- Closed-loop control tests were run using the IFU unit equipped with wrinkle height sensors. The feedback controller was successful in maintaining the imposed wrinkle height limit by modulating the binder force on the six active cylinders. Test results show clearly that closed-loop control can produce a significant improvement in the quality of the drawn pan.
- FE simulation and optimization programs were applied to the GM liftgate and optimum blankholder forces (BHF) that are variable in space and constant in stroke have been obtained for A6111-T4. The optimization program, which was designed to run on Ohio State University's (OSU's) HP Unix, has been modified to run on GM's Sun Solaris operating system. The program was tested at GM as part of the verification and technology transfer plan.

Future Direction

- Conduct trials and demonstration on the GM liftgate using optimized BHF trajectories that varies in location and stroke.
- Conduct closed-loop trials and demonstration in a mechanical press using a new 10-cylinder binder load control unit equipped with feedback control system and wrinkle height sensors.
- Quantify technology benefits based on TDM's experiences with the flexible binder control system.
- Transfer developed technologies to OEMs and suppliers.
- Develop a commercialization plan including methods for efficient packaging and integration of hydraulic, electrical and control components.
- Identify commercial applications.
- Develop a business case for using this technology in the automotive industry.

Introduction

Traditional stamping uses rigid binders that do not address local forming conditions. Also, it cannot respond to process variations that may lead to stamping inconsistencies or even failure. Significant weight saving can be achieved by replacing parts made from mild steel with those made from lightweight and high specific-strength materials such as aluminum alloys and high-strength steel. But such materials are less formable and result in higher springback than mild steel. Forming such materials require innovative tooling and advanced controls.

Advanced binder load control systems can improve stamping quality, increase part consistency and reduce the time and cost for fine tuning of stamping tools. This new technology will have a significant impact on the US stamping industry.

One major task of this project was to retrofit the Erie Press Binder Control Unit to enable accurate binder load control in all 26 hydraulic force actuators. The unit has originally been fitted with a Xycom digital control system; however, poor performance and instability were observed during operation because the Proportional Integral Derivative controller could not handle the large flow-rate variation caused by the variable velocity profile of a mechanical press. Over the last three years, the project successfully developed and implemented an advanced control system for the unit based on mathematical modeling, computer simulation and experimental testing. The system hydraulics was repaired and the electrical system was rewired and retrofitted with a digital real-time control system and appropriate signal conditioning electronics. The unit was tested in a press at TDM using the GM liftgate tooling.

The Institute of Metal Forming at The University of Stuttgart (IFU) collaborated with two industrial suppliers in Germany, HYDAC and MOOG, to build a new binder load control unit equipped and instrumented with a large collection of advanced features: ten specially designed hydraulic cylinders, twelve proportional valves, two encoders for cushion position, one encoder for ram position, four punch force sensors, one wrinkle height sensor, one flow in sensor and one friction sensor. The unit has state-of-the-art cylinders, valves and controls. It also has three types of sensors for use in closed-loop control of the binder in a mechanical press environment. Testing of the unit in a hydraulic press in Germany has been completed. The IFU unit has been shipped to TDM in Warren, Michigan for installation in a mechanical press. Demonstration of the unit is scheduled for November/December 2005.

The Blankholder (BH) applies appropriate restraining force on the sheet metal blank to suppress wrinkles and eliminate splits during forming. Many studies have shown that variable blankholder force profiles increase the formability of stamped parts. In this project, Adaptive Simulation (AS) and Optimization (OPT) methods, coupled with FEM simulation, were developed and used to predict optimum constant and variable blankholder force (BHF) trajectories in single and multi-point cushion systems to reduce thinning and springback in the IFU part and the GM liftgate inner. FEM simulation and optimization programs were applied to the GM liftgate and optimum (BHF) trajectories that are variable in space and constant in time have been obtained. The optimization program, which was designed to run on OSU's HP Unix, has been modified to run on GM's Sun Solaris operating system. The program is being tested at GM as part of the technology transfer effort of the project. The simulation/optimization programs have also been converted to run on PAMSTAMP and LSDYNA software.

The following is a brief description of the work accomplished in the various tasks of the project.

Task 1: Conduct Open-Loop Control Demonstration of Flexible Binder Control Technology

1. The Erie Unit

Figure 1 shows the Erie Unit with the liftgate tooling installed in a mechanical press.

The tooling consists of an upper die, lower punch, inner blankholder, outer blankholder and guide for outer blankholder. The upper die, lower punch and the inner blankholder are made from Zn alloy (Kirksite material) commonly used in making prototype dies for stamping. The outer blankholder is made of cast iron using the segmented elastic blankholder concept developed by the University of Stuttgart (IFU). The inner and outer blankholders are attached to the 26-cylinder cushion system. Force applied by each cylinder can be independently adjusted and controlled during the stamping process. The required blankholder force is provided by the multipoint cushion system rather than the cushions in the press.

The die and punch geometry was initially designed by GM for use in a conventional rigid binder to stamp 1-mm-thick aluminum A6111-T4 liftgates using single-point cushions/nitrogen cylinders. However, the liftgate part could not be formed from A6111-T4 material with rigid blankholder despite several days of tryouts employing spotting the dies and adjusting the binder force in all the cushions.



Figure 1. TDM mechanical press with the 26-point cushion system (Erie Unit) and the GM liftgate tooling.

The die geometry was later modified by GM to form the part in production from 5xxx series aluminum alloy. Due to the complexity and difficulty in manufacturing the liftgate from A6111-T4 alloy, the die geometry was selected for the advanced binder control project to demonstrate the ability of multi-point cushion systems to solve difficult stamping problems. For this project, the conventional outer blankholder in the liftgate die was replaced by the segmented elastic blankholder developed by IFU. Also, the multipoint cushion system built by Erie Press was also used.

The retrofitted Erie unit with the liftgate tooling was installed in a TDM mechanical press and tested using both constant and time-varying blankholder force (BHF) trajectories. Liftgate panels were successfully made from BH210 steel, DP500 steel and A6111-T4 aluminum using the same set of tools.

The tryout time using the system was considerably less than the estimated tryout time using conventional methods of working the die. For example, the BH210 part was made in about 4 hours compared to about 5 days with die work, while the aluminum part was made in about 3 days. Splits could literally be healed in minutes by adjusting the tonnages of the appropriate cylinders. Prior efforts to make the part with aluminum A6111-T4 using conventional methods were unsuccessful.

Figure 2 shows liftgate inners made from BH210 (upper left) and DP500 steel (upper right). In both cases, the parts were formed without any splits on the first hit. However, there was some wrinkling which was corrected by trial-and-error adjustment of the cylinder tonnages.

In addition, binder force estimates from FEA were used for the tryout of aluminum. The FEA data for the 1.0 mm blank were provided by OSU while the FEA data for the 0.9 mm blank were provided by Alcoa. The 0.9 mm blank was 25 mm shorter in height. The OSU data were constant in stroke (time) but variable in space while the Alcoa data were variable in both space and time.

Figure 2 also shows the aluminum parts made using the OSU (lower left) and Alcoa (lower right) FEA

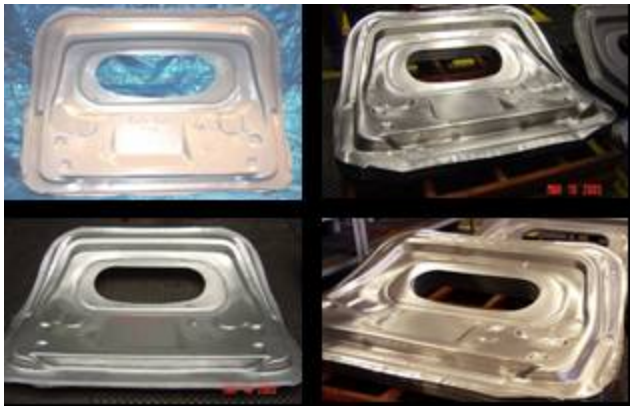


Figure 2. Liftgates made from BH210, DP500 and A6111-T4

simulation. The OSU simulation also predicted the observed side-wall wrinkling.

This task was completed with a successful demonstration of the unit to the project participants.

2. The IFU Unit

The IFU binder load control unit was built in Germany by a consortium which includes the University of Stuttgart, MOOG, HYDAC and the USCAR. The components of the unit were assembled and installed in a 20,000 kN hydraulic press at IFU in Stuttgart for validation and testing. Figure 3 shows the IFU unit in the hydraulic press. Figure 4 shows a more detailed picture of the flexible binder unit with the pan tooling.

The IFU unit has an easy to use Graphical User Interface (GUI), shown in Figure 5, to create, edit and upload a configuration file containing the force-

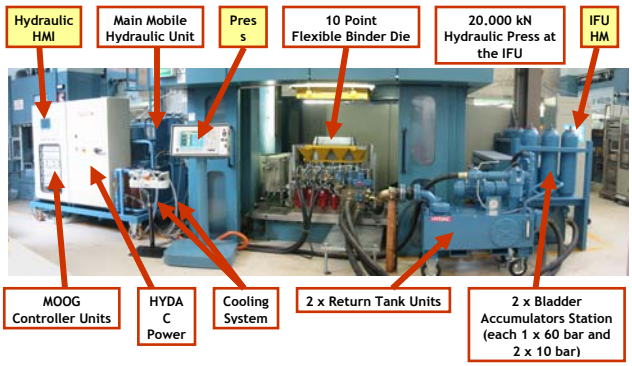


Figure 3. The IFU unit in a hydraulic press.



Figure 4. The flexible binder die in the press.

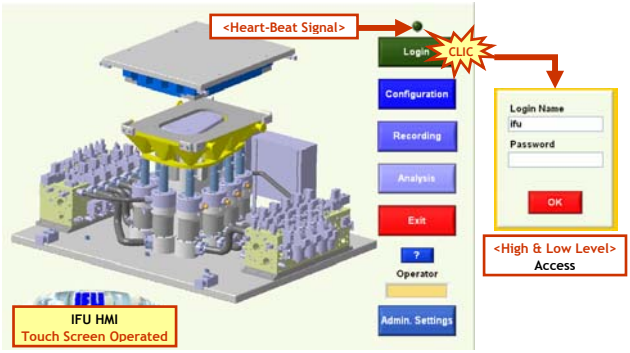


Figure 5. The IFU graphical user interface.

versus-stroke profile. The GUI was designed in LABVIEW to operate in combination with a touch screen. The unit operator needs only to login to access the configuration menu. The program has two operator levels. The high level gives the user access to the recorded data in order to perform data analysis.

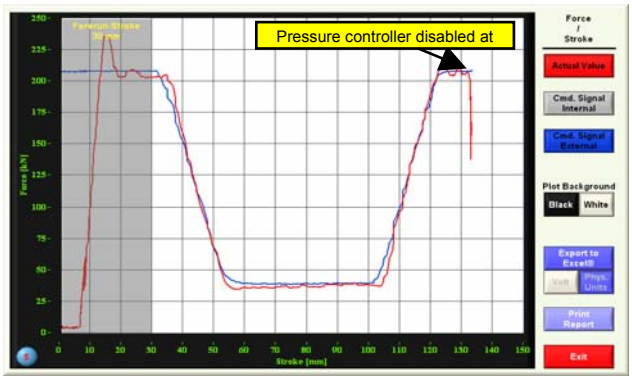
IFU Test Results

a. Control System Tests

IFU ran tests to verify that the pressure control system can track all command trajectories. Figure 6 shows an example of a flawless tracking force-versus-stroke trajectory in cylinder #5 at a slide velocity of 300 mm/s.

b. Closed-Loop Tests

IFU has performed tests on closed-loop control using wrinkle height sensors. The tests were run with and without closed-loop control to show that the closed-loop system can actually modulate the



Slide Velocity: 300mm/s
Pin Force: Variable and Constant
90%

Force over Stroke Pin

Figure 6. Force versus stroke trajectory.

binder force in-process to produce wrinkle free pans. The first set of tests was performed using IFU's hydraulic press in Stuttgart at a slide velocity of 20 mm/s without activation of the closed-loop control system. To produce wrinkles in a mild steel pan, a small binder force of 6 kN was applied to each of the six activated cylinders. This situation produced wrinkles so high (over 10 mm) that the drawing process had to be stopped at a depth of 100 mm for fear of damaging the die. In the second set of experiments, the 6 kN load was maintained on the six active cylinders, but this time the closed-loop control system was activated. A small constant wrinkle height value of 6 mm was set as a limiting wrinkle height that should not be exceeded. The controller was successful in maintaining the imposed limit by modulating the binder force on the six cylinders.

Figure 7 shows clearly that closed-loop control can produce a significant improvement in the quality of the drawn pan.

Status of the IFU Unit

The IFU Binder Control Unit has been shipped to the US for installation in a mechanical press at TDM in Warren, Michigan. Tryouts and demonstration of the unit are schedule for November/December 2005.

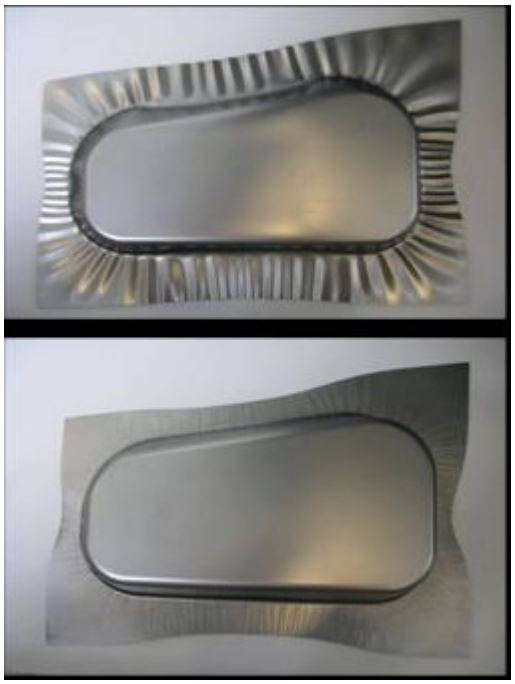


Figure 7. Pan drawn without (upper photo) and with (lower photo) closed-loop control.

Task 3: Develop Computer Simulation and Process Optimization Capabilities for Flexible Binders

a. Determination of Formability and Flow Stress Sheet Materials Using the Viscous Pressure Bulge Test

In stamping, the material properties of the sheet material (i.e., flow stress curve) greatly influence metal flow and product quality. This information is necessary as an input for Finite Element (FE) simulation of stamping processes. Usually the incoming material is tested using a uniaxial tensile test because this is a simple and inexpensive standardized test. Stress conditions in stamping are often different from the ones present in the tensile test. Therefore, it is useful to test the material under biaxial deformation conditions using the Viscous Pressure Bulge (VPB) test. Test equipment for VPB test is shown in Figure 8. A burst specimen for A6111-T4 is shown in Figure 9.

The maximum effective strain achievable in the VPB test without local necking is much larger (usually twice) than that in the tensile test. Flow stress estimated by VPB test would be used in the

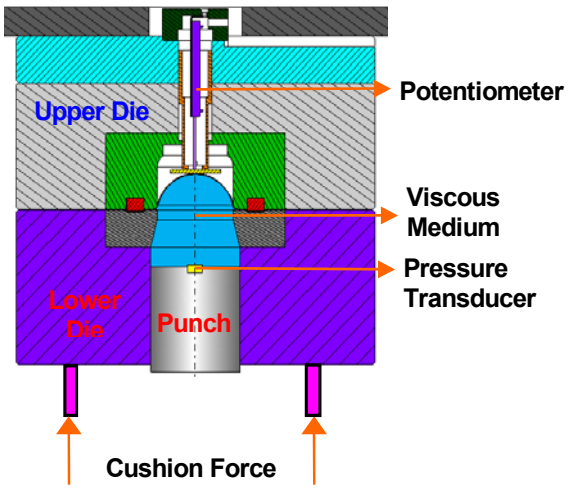


Figure 8. Test equipment for the Viscous Pressure Bulge (VPB) test.



Figure 9. A burst specimen of A6111-T4.

FE simulation to estimate the required blankholder force for forming the liftgate part.

To determine the flow stress of the sheet material, the instantaneous pressure, the dome height, the radius of curvature of the dome, and the thickness at the top of the dome are required. The instantaneous pressure and dome height are obtained from experiments while other parameters are obtained from a database. The database was generated through finite element simulation of the VPB test for different values of strain hardening index (n).

The flow stress and the formability of 1-mm (0.0394- in)-thick aluminum alloy A6111-T4, 0.8-mm (0.0315 in)-thick Dual Phase steel DP500 and 0.81-mm (0.0319 in)-thick Bake Hardened steel BH210 sheet material were determined using VPB

test. Figure 10 shows the flow curves of DP500, BH210 steel and A6111-T4. The figure shows that the flow stress for DP500 is higher followed by BH210 steel and A6111-T4 for any given strain value. This indicates higher strength exhibited by DP500 compared to BH210 steel and A6111-T4.

Figure 10 also shows that the maximum strains obtained from the bulge test for DP500, BH210 steel and A6111-T4 are 0.57, 0.60 and 0.41, respectively, indicating higher formability of BH210 steel followed by DP500 and A6111-T4.

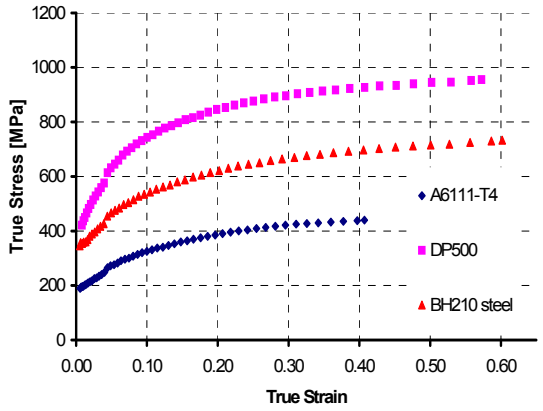


Figure 10. Flow curves for three materials determined by the VPB Test.

The dome height and pressure are measured during the experiment in real time. A press speed of 8 mm/sec was used for testing all the materials. However, the forming speed and strain rate do not affect the results significantly since the tests are conducted at room temperature. The dome height at bursting can accurately be obtained by monitoring the rapid drop in the pressure of the viscous medium. The measured dome height is an indication of the formability of the material. The consistency in the measured dome height and the burst pressure indicates that the quality of the incoming sheet material is also consistent. The average dome heights for the three materials are shown in Figure 11. As expected, the average dome height agrees with the known formability of the three materials.

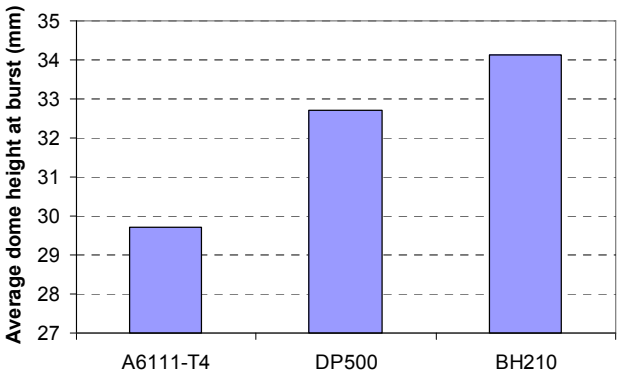


Figure 11. Average dome height for three materials measured by VPB Test.

b. Estimation of Blankholder Force Variable in Space and Constant in Time for theLiftgate Part

The FE simulation of the stamping process for the liftgate was conducted in three stages similar to the stamping operation in a single action tooling.

Stage I - Gravity simulation: The deformation of the sheet due to its own weight when placed on the blankholder.

Stage II – Holding simulation: Clamping of the sheet between the blankholder and upper die was conducted in two steps. In step I of the holding simulation, the sheet was clamped between the blankholder and the die by the movement of the upper die against the blankholder. In step II of the holding simulation, the sheet was clamped between the blankholder and the die with a gap of sheet thickness by applying force boundary conditions on the blankholder.

Stage III – forming simulation: In the forming simulation, the punch is moved against the die in the FE simulation to form the sheet to the desired shape.

The liftgate die consists of 26 independently controlled hydraulic cylinders. FE simulations coupled with optimization technique were used to estimate the optimal blankholder force in each cylinder to form the liftgate part. Due to symmetric boundary conditions, only 15 cylinder or cushion pins (pin 1 – 15) would be considered in the analysis.

Use of multipoint cushion system in stamping allows four possible modes of applying blankholding force during the forming process:

1. Constant in space and stroke: Constant blankholder force in all the pins that do not change during the punch stroke.
2. Constant in space and variable in stroke: Constant blankholder force in all the pins that change during the punch stroke.
3. Variable in space and constant in stroke: Different blankholder force in each pin that does not change during the punch stroke.
4. Variable in space and stroke: Different blankholder force in each pin that change during the punch stroke.

FE simulation coupled with optimization was used to predict the blankholder force varying in space and constant in stroke for liftgates made from 1-mm-thick aluminum alloy A6111-T4 sheets. Predicted optimized blankholder forces are given in Figure 12 and the corresponding pin locations are shown in Figure 13.

Currently, thinning and wrinkling are the only parameters used to monitor part quality.

Thinning Distribution Results

Figure 14 shows the thinning distribution predicted by FE simulation for the optimized blankholder force. Optimum blankholder force varying in space and constant in stroke resulted in maximum thinning of approximately 24%.

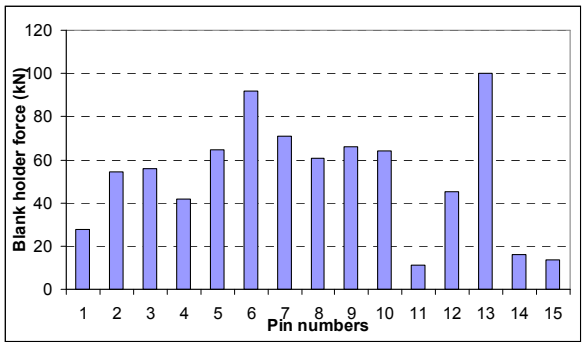


Figure 12. Predicted blankholder force variable in space and constant in stroke.

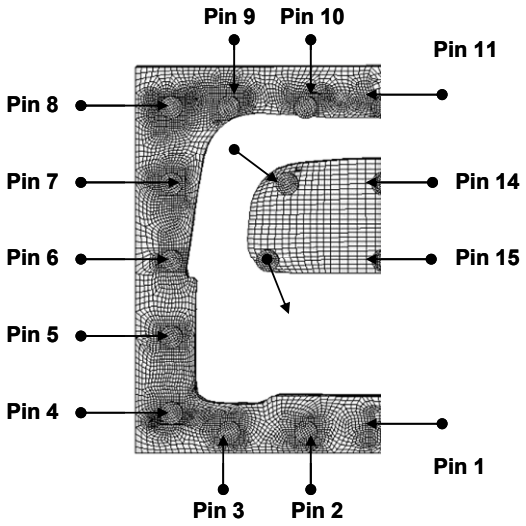


Figure 13. Pin locations in the liftgate simulation.

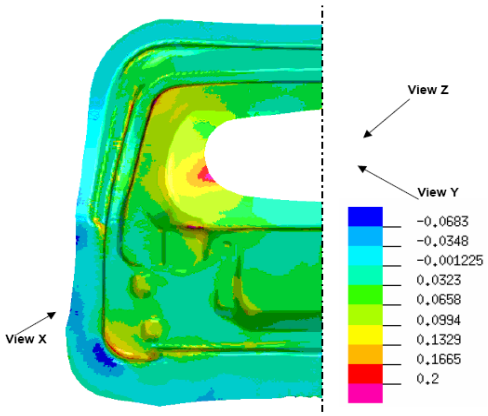


Figure 14. Thinning distribution predicted by FE simulation.

Wrinkling Results

Figure 15 shows possible location of wrinkling in the part for the predicted optimum blankholder force varying in space and constant in time. In the FE simulations, wrinkling was observed in the part at detail (A) in the Figure.

Further increase in the blank holder force did not result in elimination of wrinkles but increased thinning in the part. Even a large blankholder force of 125 kN in all the pins could not get rid of the wrinkles. This could be due to differences in the geometry between the FE model and the physical die at the wrinkle location.

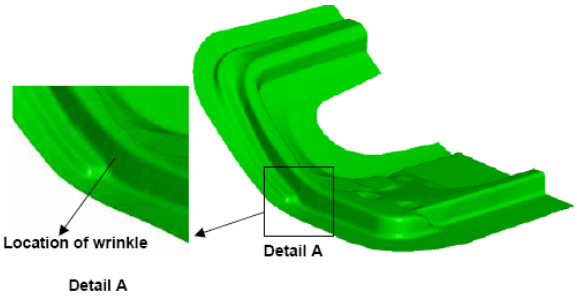


Figure 15. Locations of wrinkling in the part predicted by FE simulation.

Experimental Validation of BHF Profiles

Experiments/tryouts for forming the liftgate were conducted in a mechanical press at TDM using the multipoint cushion system and the flexible binder. Optimum blankholder force variable in space and constant during the stroke predicted by FE simulation coupled with optimization techniques was used in the tryout to form the part and validate the FE predictions.

Figure 16 shows the A6111-T4 blank geometry of thickness 1 mm used in the experiments/tryout. The edges of the blanks were deburred to avoid cracking during forming due to defects in blanking and piercing from the coil. The sheets were lubricated with dry thin-film lubricant precoated on the coil from the rolling mill.

Figure 17 shows that the liftgate was formed without splits. However minor wrinkles were observed in the flange geometry beyond the drawbeads on top and bottom and on one of the corners. Experiments carried out with very high blankholder force could not eliminate the wrinkles



Figure 16. Blank from A6111-T4 used in liftgate tests.



Figure 17. Successfully formed liftgate.

in the flange as observed in FE simulation. This further validates the FE model.

Major conclusions from the simulation study are:

- Predicted optimum blankholder force resulted in maximum thinning of 24 % in the part. Also, wrinkles were observed in the part.
- Wrinkling in the part predicted by FE simulation was found to be insensitive to the blankholder force. Even high blank-holder force of 125 kN did not result in elimination of the wrinkle.
- Tryouts on the liftgate verified FE simulation predictions. The panels were produced with minor wrinkles and no splitting.

Conclusions

The Erie Press Flexible Binder Unit was retrofitted with an advanced control system for hydraulic pressure control in all 26 cylinders. The unit was repaired hydraulically and retrofitted electrically to enable the control system to be effectively integrated. Binder force trajectories generated by both trial-and-error and FEA were implemented and liftgate panels were successfully made from BH 210 steel, DP 500 steel and AL 6111-T4 aluminum. The project was completed with a successful demonstration of the unit.

The new, 10-cylinder IFU binder control unit with pan tooling was tested successfully in a hydraulic press at the University of Stuttgart in Germany. Tests in a mechanical press, which are crucial to demonstrating the applicability of binder control technology in mechanical systems, will be conducted at TDM in Warren, Michigan.

Closed-loop tests show clearly that feedback control can produce a significant improvement in the quality of drawn pans.

FE simulation coupled with optimization technique was used to successfully predict the blankholder force varying in space and constant in stroke for the 1.0-mm-thick aluminum alloy A6111-T4 liftgate. The next step is to predict optimized blank-holder forces varying in both space and time.

Presentations and Publications

1. **Prediction of Blank Holder Force in Stamping Using Finite Element Analysis**
   Hariharasudhan Palaniswamy*, Arunkumar Thandapani*, Srikanth Kulukuru* and Taylan Altan*
   *ERC for Net Shape Manufacturing, The Ohio State University, 339 Baker Systems, 1971 Neil Ave, Columbus, OH, 43210, USA
   Presented and published at NUMIFORM Conference, Columbus, OH, May 2004

2. **Springback Control With Variable Binder Force – Experiments And FEA Simulation**
   Changqing Du*, Jin Wu*, Marcio Militisky¶, James Principe¶, Mark Garnett†, Li Zhang*
   *DaimlerChrysler, Advance Manufacturing Stamping Engineering
   ¶DaimlerChrysler, Body Material Engineering
   †DaimlerChrysler, Advance Manufacturing Engineering, Core Group
   Presentation and publication at the SAE Congress, Detroit, MI, March 2004

3. **Project Presentations**
   AMD Offsite Meeting, October 28, 2004.
   AMD Offsite Meeting, October 27, 2005.

C. Die Face Engineering Project for Advanced Sheet Metal Forming

Principal Investigator: Dr. Chung-Yeh Sa
General Motors Corporation
MC 480-111-S60
30200 Mound Road
Warren, MI 48090-9010
Phone: 586-947-0660, Fax: 586-986-8722, e-mail: chung-yeh.sa@gm.com

Principal Investigator: Laurent Chappuis
Ford Motor Company
VOGO - Advanced Stamping Engineering
17000 Oakwood Boulevard
Allen Park, MI 48101
Phone: 313-322-4470, Fax: 313-322-4359, e-mail: lchappui@ford.com

Principal Investigator: Li Zhang
DaimlerChrysler Corporation
CIMS 482-60-05
800 Chrysler Drive
Auburn Hills, MI 48326
Phone: 248-576-3117, Fax: 248-576-2230, e-mail: lz@daimlerchrysler.com

Project Administrator: Manish Mehta
TRC-National Center for Manufacturing Sciences
3025 Boardwalk
Ann Arbor, MI 48108-3266
Phone: 734-995-4938; Fax: 734-995-1150; e-mail: manishm@ncms.org

Technology Area Development Manager: Joseph A. Carpenter
(202) 586-1022; fax: (202) 586-1600; e-mail: joseph.carpenter@ee.doe.gov
Field Technical Manager: Philip S. Sklad
(865) 574-5069; fax: (865) 576-4963; e-mail: skladps@ornl.gov

---

Contractor: U.S. Automotive Materials Partnership
Contract No.: FC26-02OR22910

Objective

The ultimate project goal of the 3-year AMD 408 Die Face Engineering Project (DFEP) is to develop robust technology to improve die design and die processing so as to reduce manufacturing costs for all sheet metal parts using lightweight materials, by generating optimized sheet stamping dies from CAD surfaces (from FEM mesh) that compensate for springback while maintaining formability, eliminating the soft tool prototyping phase, and reducing die tryout phase.

The project deliverables include: (1) Integrated product-process finite element analysis capability that will more accurately predict springback for both closures (>90%) and structural parts (~80%); (2) Test results from simulations, panel trials and springback measurements that will be used to guide and validate the software development (done at private expense by vendors); and 3) Capability to automatically and consistently generate a machinable CAD surface of acceptable quality from FEM mesh.

Approach

The DFEP approach is to develop and validate improved simulation technology that provides more accurate and reliable springback predictions encountered in automotive sheet stamping operations.

The collaborating partners include Alcoa, DaimlerChrysler Corporation, Ford Motor Company/Volvo Cars Division, General Motors Corporation, ThyssenKrupp Budd Company, US Steel, Livermore Software Technology Corporation (LSTC), and Technologies Research Corporation of the National Center for Manufacturing Sciences (TRC-NCMS). The project tasks are being undertaken and reported in four main task areas:

A. Numerical Technology

B. Material Testing/Modeling

C. Field Validation

D. Surface Technology

- The DFEP approach has been to work with technology vendors and test laboratories to significantly improve the ability to: (a) analytically predict springback more accurately and validate for a broader range of closure and structural parts and (b) recommend optimized tool geometry (FEA mesh to CAD surface) so as to produce panels with the desired final shape after springback. The project will utilize results of the Springback Predictability NIST Project (1995-2000) incorporated in LS-DYNA, a commercial software from LSTC, and the USAMP Springback Compensation Project (SCP) AMD 311(2003).
- In Year 1, the DFEP team began to identify and classify part categories for which springback is still a challenge to predict (e.g., underbody parts), then conduct new simulations utilizing significant LS-DYNA improvements (developed at vendor expense and owned by vendor) and its linked modules to input original tool geometry, incorporate new material and process parameters, identify design variables, perform springback simulations, and output optimized tool geometry with material and process parameters.
- Springback predictions will be validated against dimensional measurement data obtained from tryout experiments with a "common" experimental die (incorporating challenging features for forming baseline panels of an underbody structural part in Year 1 and a trim die in Year 2) used to produce both aluminum and advanced high strength steel body panels with representative features.
- Finally, in Year 3, an integrated product design-analysis-formability capability will be demonstrated that combines improved springback simulation algorithms (material and surface contact) defined by the team and CAD-based die-face modification algorithms, which will be applied to the common die component. A new die surface will be generated for tryout and a second set of structural panels formed and measured to validate the prediction technology.
- A larger internal validation effort will be undertaken in Year 3 by the OEMs to industrialize "best practices" simulation standards and extend the integrated springback and CAD morphing technology to test additional challenging automotive parts.
- A technical cost model will be developed, comparing cost, quality and user-effort attributes of the improved simulation and tool development capability with the conventional (baseline) die build and tryout process.

Accomplishments

Reported under each Project Task Area:

Numerical Technology:

- DFEP Team conducted simulation experiments on an initial set of closure and structural parts to classify springback behavior, based on several end-user defined computational and prediction quality parameters. A consensus Springback Classification Table was developed.

- Developed smooth contact algorithms for improving geometric description of the products and springback predictive accuracy in FEM.
- Developed a new element with improved through-thickness stress variations that will help improve springback prediction.
- Conducted several detailed benchmark studies to understand the impact of various numerical technologies and define directions for further code improvements by the software vendor.

Material Testing/Modeling:

- Conducted literature review and performed baseline simulations of NUMISHEET benchmark parts and other simple geometries (e.g., Deep Draw Cup) to define critical material parameters, testing needs and modeling requirements for steel and aluminum sheet alloys. These models and measured parameters/coefficients will help drive the needed code improvements and accuracy in springback simulations. Material test data requirements include: tension and shear testing, stress-strain, tension-compression testing, and bending-unbending testing.
- Evaluated candidate test methods from team members and lab vendors, and contracted material testing to two selected laboratories to perform testing and validation of existing material models.
- Began implementing new material models into predictive code, such as non-linear isotropic and kinematic hardening models.

Field Validation:

- Designed and sourced pre-production stamping tooling for a "Common Die" structural automotive part geometry (previously defined in FY 2004) exhibiting challenging formability and springback behavior, for test and validation of incremental enhancements of new (privately developed) FEM software.
- Conducted baseline simulation experiments on the Common Die to predict formability and springback for high-strength steel sheets of DP 600, and DP 780 alloys, and aluminum 5754-O alloy.
- Completed all design modifications, draw die development, construction and tryout of the Common Die for the first phase of panel trials, which included 36 stamped panels of selected dual-phase steel and aluminum sheets.
- Conducted panel grid and strain measurement study on selected full- and half-size panels, using new global surface strain measurement technology.

Surface Technology:

- Developed and evaluated surface morphing criteria for facilitating efficient and accurate die development and modifications. This is an enabling technology for reduced lead times and labor in translating CAE designs/analyses to machinable CAD and NC programs.
- Evaluated current commercial CAD packages and established a baseline capability of CAD morphing performance, quality and computational goals for use in a FEM die design environment. Defined technology and performance gaps needed for improvement.
- Demonstrated and validated mesh-to-surface and surface-to-surface mapping algorithms with the same element topology.

Future Direction

- Expand the springback simulation and classification study to additional team-defined structural and closure components, and characterize springback behavior based on simulations and product measurements.
- Demonstrate feasibility of using enhanced springback prediction code with improved contact algorithms for various forming processes.

- Define technical and quality specification for achieving morphed CAD surfaces from FEM meshes of modified dies.
- Select CAD software vendors to partner with in demonstrating new mesh-to-CAD capability in die face engineering.

Introduction

Excellent progress was made in each of the Die Face Engineering Project (DFEP) focus areas described below in greater detail. The DFEP project has achieved two major technology improvements in simulation technology during the first year of the project, demonstrating results that are independent of input parameters. The first accomplishment is that the predicted springback results have been significantly improved using several new algorithms (vendor-owned) implemented in the project. Secondly, the predictive accuracy of the LS-DYNA FEM code has generally improved from 80% to over 90% in several product cases tested – code improvements to improve the consistency and reliability continue so that these predictive accuracies apply to a broader range of structural and closure panels and sheet materials. These advances have major implications to our goals to eliminate the soft tool trial, and reduction of lead time and cost for tryout of hard tools (up to 50%), and thus can help accelerate the application of advanced lightweight metals. Design refinements and baseline forming/springback simulations of a "Common Die" component were conducted early in Year 1. A capable die vendor was selected and contracted to source the insertable Common Die that has embedded difficult-to-predict springback features. The die tryouts on dual phase steel and aluminum panels were witnessed by DOE sponsors during the last quarter of Year 1.

Discussions were held with the Auto-Steel Partnership (A/SP) project team working on "High-Strength Steel Stamping and Springback Prediction Project" (see report 2.R). The A/SP project goal is to achieve springback control using process changes and modifications. The DFEP Team has formally involved A/SP project leadership, in order to exchange and leverage technical information.

Numerical Code Development:

- Springback Classification Study: The OEM members of the DFEP Team collaborated to conduct a study of springback behavior for a wide variety of production parts, based on measured springback data. These parts included rails, sills, pillars, etc.
- Surface Algorithms: The DFEP Team worked with FEM vendor LSTC to help develop and improve new surface algorithms for forming and springback predictions. The DFEP Team conducted validation studies on three production panels, one from each OEM. The feasibility demonstration of surface-based simulation capability for forming and springback prediction (a stretch target of the DFEP with high technical risk, and potential for high impact on project goals) were re-directed to a more efficient approach by using smooth contact algorithms.
- Smooth Contact Algorithms: Based on DFEP Team input, LSTC developed smooth contact algorithms aimed at improving the geometric description of the products and. therefore, springback predictive accuracy. The effect of the number of elements on the tooling radius was studied (# of elements ranged from 1 – 10). It was found that using the new mesh adaptivity feature, the number of elements in the corner of rigid tools now has a much smaller effect on the springback prediction results. Other studies have involved using three different contact scale factors (SLSFAC) combined with initial coarse mesh, initial coarse mesh with smooth contact, and initial fine mesh with smooth contact.
- Higher Order Element: LSTC also developed and implemented a higher-order element with improved through-thickness stress variations. The springback characteristics being studied include twisting, warping and out-of-plane bending, and are applicable to various forming processes (e.g., draw, trim and flanging).
- Benchmark Study: The DFEP Team and LSTC have jointly performed detailed simulation studies on benchmark components (e.g., Deep Draw Cup, NUMISHEET '93 U-channel – see Figure 1) to better understand the impact of various numerical technologies on computational efficiency and prediction

accuracy. Three different sheet materials and two different binder forces have been used. In Year 2, the Team will test these new features on real production panels.

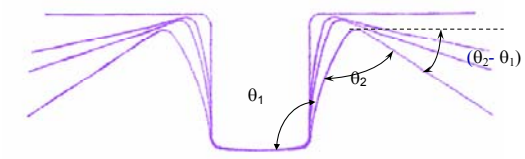


Figure 1. The NUMISHEET '93 U-channel Benchmark Showing Springback Predictions for Three Simulation Cases.

Material Testing/Modeling

- The motivation for undertaking this task was that currently available public domain material models do not seem to reflect the processing realities when sheet metal undergoes multiple bending-unbending cycles typical of a sheet forming operation. In order to assess the many theoretical models, a literature review of feasible material models was performed during the year, which helped in identifying candidate material models for further customization and characterization with input property and parameter measurements. This activity resulted in a gap analysis and model development roadmap to drive the property measurement tasks to validate existing models and subsequently implement into new FEM code. Candidate models included nonlinear isotropic and kinematic hardening. Highlights of the literature review were presented at the Team Offsite in December 2004, and disseminated to our NIST collaborators.
- Volvo's shear test method (Figure 2) was used to extend mechanical stress-strain behavior of the candidate DP 600 and aluminum 5742 alloys to levels beyond the conventional tensile test method. This method is particularly well suited for metals exhibiting small uniform elongations. Volvo is using the shear test to obtain the data at large strain levels, and apply the measurements for simulating the Common Die forming operations and springback.
- Additional test methods and capable vendors were identified for material testing and model fitting to develop a combined isotropic kinematic hardening model that (when implemented into numerical code) can improve springback predictions. These include the Fraunhofer tension-compression test method that can better characterize cyclic loading characteristics of material behavior that can be fit to the Chaboche material model. This method will impose material strain levels up to 15%.



Figure 2. Volvo's Large-Strain Shear Test Setup for Common Die Sheet Material.

Surface Development

- The primary goal of the Surface development task is to assist the CAE/Stamping Development engineer to quickly translate CAE die design (or modification information) directly into CAD data that can be used in machining dies.
- The Surface Team began in Year 1 by evaluating and developing an OEM-led, consensus set of morphing criteria for die development and modification. This first involved developing a collective understanding of how parametric design data is rendered into machinable CAD-quality surfaces. A CAD-NC tooling specialist from DaimlerChrysler facilitated this activity.

- The second major achievement was to conduct evaluations of current commercial CAD packages, and to establish baseline morphing capability. Three CAD vendors (whose products are compatible with a FEM design environment) were contracted to perform trial morphing on OEM-supplied component product data and target FEM meshes, ETA, D2M-Think3 and ICEM. Each OEM provided two CAD product data sets, a baseline FEM mesh and a modified (target) FEM mesh. Two example product geometries provided by the OEMs are shown in Figure 3. Evaluations performed by the CAD vendors included mesh-to-surface and surface-to-surface mapping algorithms with the same element topology. Final results remain to be evaluated, based on which a down-selection of vendors will be made to pursue new morphing technology developments in Year 2.

Field Validation

- A capable die vendor, Superior Cam, was selected by team consensus and contracted to source the insertable Common Die that has embedded difficult-to-predict springback features. The die enables the DFEP team to completely validate the springback predictability of certain key improvements in numerical codes and evaluate FEM technology implementations. The intent is to use this platform to build stamping dies "right the first time".
- Collaborative design refinements and baseline forming/springback simulations of a "Common Die" component were conducted early in Year 1 – the part geometry is shown in Figure 4. Existing (baseline commercial version) LS-DYNA code was used to generate baseline springback predictability at critical measurement locations.

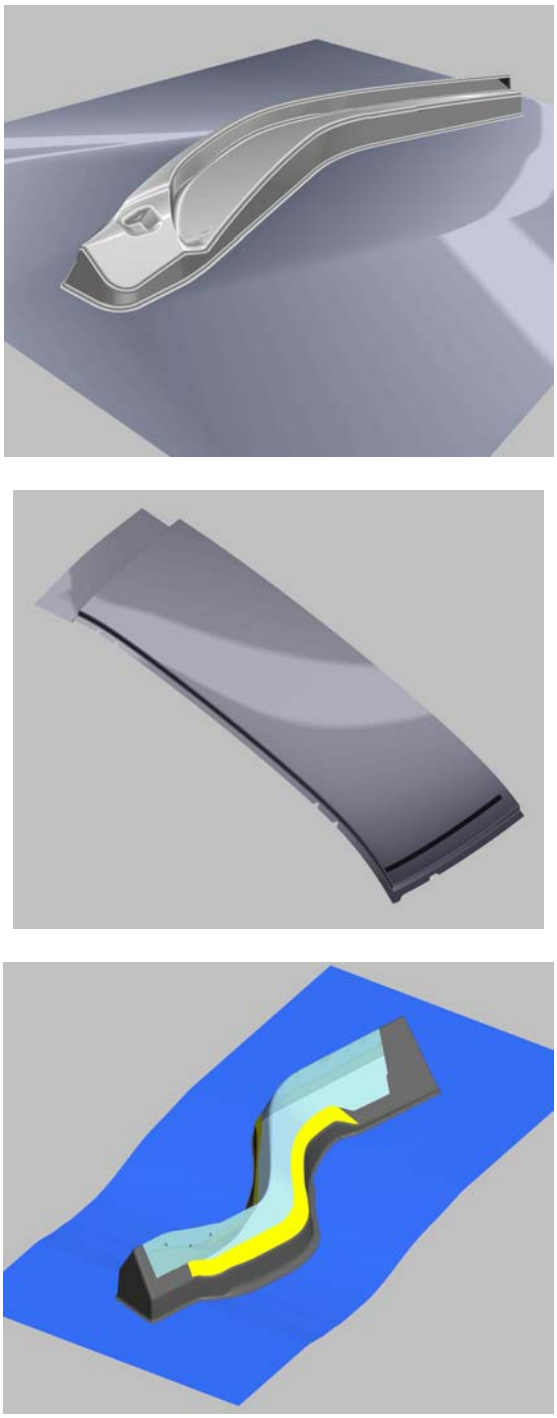


Figure 3. Example OEM Part Geometries Used in Conducting CAD Morphing Trials.



Figure 4. Illustration of Common Die Panel, Indicating Datum Points (Shown in Red).

- The preliminary forming (for die tuning) and die tryouts on dual phase steel and aluminum panels were held at American Tooling Corp. (ATC), and witnessed by DOE sponsors (Dr. Joe Carpenter and Rogelio Sullivan) during the last quarter of Year 1. The Team also attempted several forming trials on DP 780 sheet, which is a very challenging material to form due to its high stiffness; initial trials resulted in split panels. This effort is extra, and goes beyond the scope of the DFEP.
- During the last quarter, a total of 36 panels were formed at ATC for further study and specialized measurements, which included 9 gridded panels (for use with Auto-Grid technology for determining full-field-of-view surface strains), as shown in Figures 5 and 6. Sixteen aluminum 5754-O, 16 DP 600 steel and 4 DP 780 steel panels were stamped (16 full-sized and 20 half-sized panels). During the next quarter (FY 2006), the plan is to complete strain reading of all panels, scanning of all draw panels, and then to laser trim selected panels. All cases will have accompanying forming and simulation predictions, which will be compared with panel measurements, and then developed into validation metrics and guidance to the numerical code development task.



Figure 5. Tool-Shop Showing All DFEP Baseline Formed Panels Using the Common Die.



Figure 6. Close-up of a Half-Sized DP Steel Baseline Panel Formed on the Common Die.

Contributions of NIST

NIST Metallurgy Division (using internal laboratory funding) has also contributed by addressing certain fundamental science needs of the DFEP Material Testing/Modeling tasks that aim to improve the quality and precision of data. These contributions were in the following areas:

- Springback Deep-Draw Cup Test – to develop a standard test for evaluating the springback behavior of aluminum and steel alloy sheet.
- Surface Roughness/Friction – NIST began studies to a) accurately assess the relationships between surface roughening in the sheet and the friction that occurs during multi-axial deformation and b) improve the materials property data and constitutive equations to account for the variability exhibited in friction produced in the forming process.
- In-situ Multi-axial Stress Strain - Direct *in situ* measurement of multi-axial stress/strain of steel and Al sheet undergoing deformation using non-proportional loading paths.
- Small-Scale Tension/Compression Test - NIST is developing a test protocol to evaluate the work hardening behavior of a thin sheet during compression/tension cycles. Standardization through ASTM and ISO will be pursued.

D. Electromagnetic Forming of Aluminum Sheet

Principal Investigator: Richard W. Davies
Pacific Northwest National Laboratory
P.O. Box 999, Richland, WA 99352
(509) 375-6474, fax: (509) 375-4448, e-mail: rich.davies@pnl.gov

Principal Investigator: Frode Stavehaug
Pacific Northwest National Laboratory
P.O. Box 999, Richland, WA 99352
(509) 372-4766, fax: (509) 375-4448, e-mail: frode.stavehaug@pnl.gov

Technical Coordinator: Sergey Golovashchenko
Ford Motor Company
Ford Research Laboratory
2101 Village Road, MS3135, Dearborn, MI 48121-2053
(313) 337-3738, fax: (313) 390-0514, email: sgolovas@ford.com

Technology Area Development Manager: Joseph A. Carpenter
(202) 586-1022; fax: (202) 586-1600; e-mail: joseph.carpenter@ee.doe.gov
Field Technical Manager: Philip S. Sklad
(865) 574-5069; fax: (865) 576-4963; e-mail: skladps@ornl.gov

Participants:
Vladimir Dmitriev, EMF R&D, Ford Motor Company
Jeffrey Johnson, EMF System and Control, Pacific Northwest National Laboratory
Jeffrey Bailey, EMF Capacitor Bank Control, Pacific Northwest National Laboratory
Gary VanArsdale, EMF Coil Fabrication and Metal Forming, Pacific Northwest National Laboratory
Nick Bessonov, EMF Simulations, University of Michigan- Dearborn
Nick Klymyshyn, Computational Mechanics, Pacific Northwest National Laboratory

---

Contractor: Pacific Northwest National Laboratory
Contract No.: DE-AC06-76RL01830

Objective

- The purpose of this project is to develop electromagnetic forming (EMF) technology that will enable the economic manufacture of automotive parts made from aluminum sheet. EMF is a desirable process because the dynamic nature of the deformation results in benefits including increased forming limits and reduced springback. These benefits would result in increased use of aluminum and therefore more fuel-efficient vehicles due to mass reduction.

Approach

- Address analysis methods for forming system design.
- Address development of durable actuators (coils).
- Address industrial embodiment of the EMF process.

Accomplishments

- Completed a literature search for information on EMF, coil materials and coil design/durability.
- Completed design and assembly of a 150 kJ pulsed power unit at LANL.
- Ford Motor Company designed an integrated forming coil system for high-volume automotive stamping.
- LANL completed a literature review of patents, relevant coil materials, and the design of EMF coils.
- Installed the 150 kJ pulsed power supply at PNNL, demonstrated operation, and installed automated computer control system capable of automated cyclic testing and sheet metal forming.
- Completed fabrication of an experimental apparatus to evaluate coil durability.
- Established a CRADA to include Ford, PNNL, and Oxford Automotive.
- Performed cyclic testing of an EMF coil assembly for durability assessment and achieved more than 5,000 cycles.
- Developed conceptual layouts for industrial embodiment of EMF process.
- Demonstrated ability to improve formability of aluminum sheet by a factor of two-to-three times over conventional forming.
- Completed evaluation of EMF coil assembly cooling effectiveness.
- PNNL fabricated an enhanced coil assembly for improved coil cooling and durability.
- Established minimum cycle time limitations of the existing coil design assembly at PNNL.
- Developed EMF calibration process that reduces springback of parts.
- Design and experimental testing of flat coil with flat concentrator.
- Developed numerical simulation of the coil current density and pressure distribution on the blank during EMF restrike operation.

Future Direction

- Improve coil design to improve the thermal characteristics of the prototype coil assembly.
- Scale-up laboratory testing to include commercially-representative components.
- Further develop modeling capabilities that can assist in the design of EMF systems.
- Continue to investigate the industrial embodiment of EMF systems for automotive manufacturing.

Introduction

In the electromagnetic forming (EMF) process, a transient electrical pulse of high magnitude is sent through a specially designed forming coil by a low-inductance electric circuit. During the current pulse, the coil is surrounded by a strong transient magnetic field. The transient nature of the magnetic field induces current in a nearby conductive workpiece that flows opposite to the current in the coil. The coil and the workpiece act as parallel currents through two conductors to repel one another. The force of repulsion can be very high, equivalent to surface pressures on the order of tens of thousands of pounds per square inch. Thin sheets of material can be accelerated to high velocity in a fraction of a millisecond.

A recent interest in understanding the EMF of metals has been stimulated by the desire to use more aluminum in automobiles. The high workpiece velocities achievable using this forming method enhances the formability of materials such as aluminum. Also, the dynamics of contact with the forming die can help reduce or mitigate springback, an undesired effect that cannot be avoided in other forming techniques such as stamping. The commercial application of this process has existed since the 1960s. The large majority of applications have involved either the expansion or compression

of cylinders (tubes). The forming of sheet materials is considerably more complex and has received relatively little attention.

Project Deliverables

At the end of this project, methods and data to assist the economical design of EMF sheet forming systems will be documented. This will include materials information and design methods for durable coils, coil durability test data for selected materials and design concepts, dynamic and hybrid formability data, methods for modeling the forming process, and concepts for the industrial implementation of the technology in an automotive manufacturing environment.

Approach

This project addresses three main technical areas. The first technical area involves establishing analysis methods for designing forming systems. These methods will be based on developed knowledge of forming limits and relations between electrical system characteristics and deformation response for specific aluminum alloys of interest. The second area of technical challenge is in coil durability. Existing knowledge of electromagnetic forming and relevant knowledge from pulsed-power physics studies will be combined with thermo-mechanical analyses to develop durable coil designs that will be tested experimentally. Until a more thorough understanding is achieved of economic factors determining required durability, a nominal level of 100,000 cycle coil life will be the goal for this project. Finally, the third technical area involves the industrial embodiment of the EMF process. In this project, EMF is expected to be hybridized with conventional sheet metal stamping. Different approaches to hybridization will be analyzed for issues affecting the economic implementation in a modern stamping plant. Different system concepts will be developed and studied. Existing knowledge of the EMF process and technical achievements in this project will be combined to establish a methodology for designing hybrid forming systems that can be readily integrated into modern manufacturing facilities for the economic production of automotive sheet aluminum components. Some of the project focus areas and results are discussed in the following sections.

PNNL EMF System

The EMF system at PNNL has been operational since 2001. The system is typically operating at 6,500 V and current levels in excess of 225 kA have been demonstrated. Figure 1 shows a typical response of the EMF system during a 15 kJ discharge of the capacitor bank. The figure shows that the half-current (measuring half the total system current) of the system is approximately 86 kA, so that a total current of 172 kA passed through the load coil within 26 μs.

The system has also been cycled several thousands times at high current levels while supporting our coil durability experimental work. The custom designed control system was also successfully demonstrated in automated cyclic loading operating modes. During FY05, capacitor bank control system upgrades were complete that increased cycle-to-cycle reliability, and improved the efficiency of the data acquisition system used to sample the electrical response of the entire system as well as the changing response of the coil assembly.

Coil Design Concepts and Durability. During EMF, the high-intensity electromagnetic forces are applied to the turns of the coil. The coil, insulators and support structure must resist these forces, as well as related thermal cycles, without significant permanent deformation or material failure. In

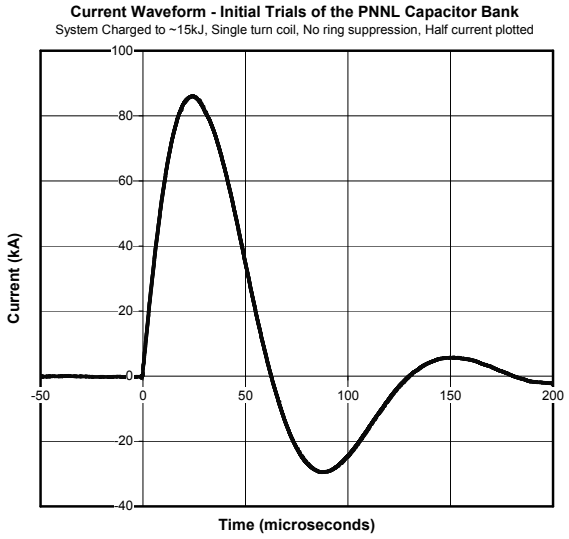


Figure 1. Typical EMF system waveform.

contrast to typical cylindrical coils, sheet forming will require coils with general three-dimensional shapes that are inherently less resistant to forces induced during forming. The key issues involve materials selection and design. Materials must be selected for both electrical conductivity and mechanical properties, and they must lend themselves to manufacturing. Materials may also need to be compatible with the presence of coolants and the forces generated during hybrid forming that combines conventional stamping and EMF. The design must integrate these elements while delivering the primary function of a spatial and temporal load distribution that achieves the desired deformations. Coil systems will have to be low-cost, modular, and have high durability (nominally 100,000 cycles) if they are to be relevant to automotive manufacturing.

During the first half of FY03, PNNL evaluated the performance of the original Ford and PNNL coil assembly designed and fabricated under this project. The experiments consisted of evaluating the forming effectiveness, measuring the coil's thermal characteristics, and starting durability tests under cyclic loading of the coil system. Figure 2 shows photographs of the forming die used, and the resulting formed aluminum sheet after testing. In this figure, the coil is directly below the aluminum sheet and the holes in the die are three inches in diameter. After a single EM pulse through the coil, the system forms three domes as shown in Figure 2 and Figure 3. These forming experiments were conducted to learn the necessary pulse magnitude in order to effectively form aluminum sheet. Subsequent to determining this critical EM pulse magnitude, PNNL initiated cyclic loading experiments on the coil system to determine the thermal and mechanical characteristics of the coil assembly to determine long-term durability. This original assembly has undergone cyclic testing at PNNL, and has achieved greater than 5000 cycles with no signs of coil degradation.

The PNNL coil durability experiments have focused on increasing the frequency of capacitor discharge to simulate high-repetition rate of automotive manufacturing. PNNL has increased the charge rate of the capacitor bank and refined the control system to achieve cyclic discharge rates to less than one per 10 seconds. This has allowed the project team to

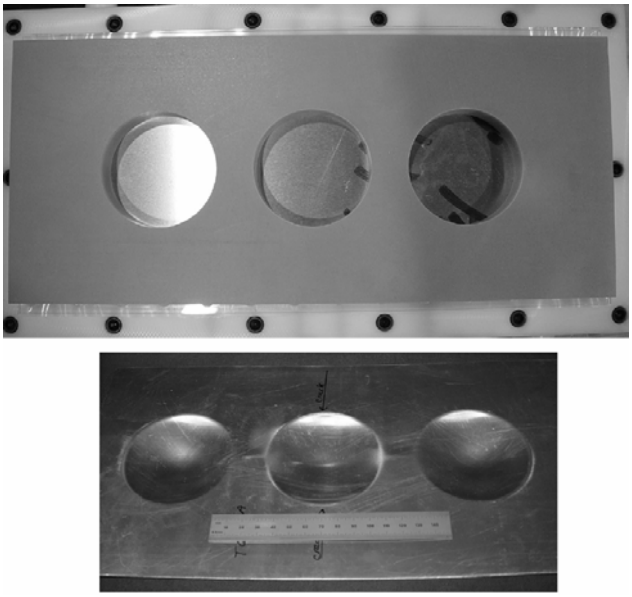


Figure 2. (top) Top view of the glass fiber reinforced plastic tooling on the coil assembly with aluminum sheet metal between the coil and the tool. (bottom) Photograph of the deformed sheet after one EM pulse through coil.

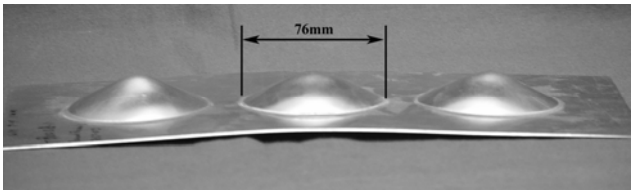


Figure 3. A formed aluminum sheet after a single EMF operation.

evaluate the structural performance of the coil and better understand the effect of coil operating temperature. One major focus at PNNL during the first half of FY04 was investigating the influence of coil assembly temperature and the ability to remove heat from the coil. Figure 4 shows the results of experiments at PNNL to evaluate the ability to remove heat from the coil using various proprietary techniques.

In the second half of FY04, PNNL redesigned the original coil assembly to increase the efficiency of cooling. The original design had limited cooling capacity and materials that had operating temperature ranges insufficient to support 10-second cycle times at high energy capacitor bank discharge. The redesigned coil incorporated a series of material substitutions and design refinements to increase the cooling efficiency, while attempting to retain the

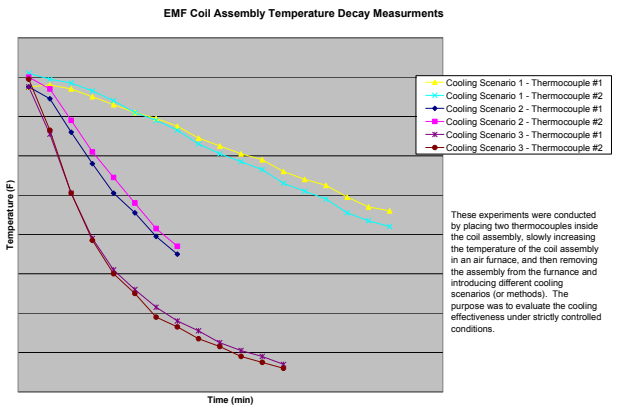


Figure 4. Plot showing the experimental results of heat removal from the coil assembly using three proprietary cooling scenarios. These experiments evaluated the rate of heat removal under controlled conditions to establish the effectiveness of each of the three cooling techniques.

successful mechanical support from the original design. This second-generation design was fabricated at PNNL. PNNL evaluated the cooling efficiency of this second-generation design under short cycle times at high energy capacitor bank discharge. During FY05, PNNL completed evaluations of this second generation coil assembly, and is making further design refinements to successfully maintain high repetition rates and suitable coil assembly temperatures.

Ford developed an EMF calibration process. The use of an EMF calibration process results in reduced springback of parts as shown in Figure 5.

Formability of Aluminum During EMF.
Ford Motor Company has conducted laboratory experiments to investigate the formability of aluminum alloy sheet during EMF. These laboratory experiments included free forming of domes and forming of sheet metal into V-shaped die cross-sections. Figure 6 shows a cross-section through a V-shaped forming die showing the coil, die, and the workpiece before and after deformation. This figure also shows the results of a typical strain grid analysis and the two-to-three times improvement in formability under these forming conditions. However, the experimental data have shown that the formability is sensitive to the shape of the die being used to evaluate the formability. Further investigation may be required in this area to better define the forming limits of the material under the



Figure 5. Improvement in springback by using EMF calibration process. (top) before, (bottom) after.

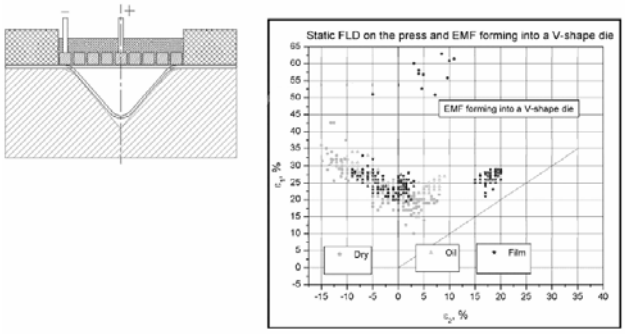


Figure 6. (left) A cross-section through a V-shaped die showing the coil, die, and workpiece before and after deformation. (right) Strain grid formability data showing the improvement in aluminum formability under these forming conditions.

varying biaxial and triaxial states of stress that develop during electromagnetic forming.

Numerical Simulation of EMF Process. The EMF process is challenging to simulate due to the need to simultaneously model electromagnetic, thermal, and elastic-plastic deformation of materials. Many of the commercial research codes have serious limitations and an inability to accurately predict the results of EMF processes. This project originally focused on integrating portions of existing commercial research codes to accurately predict the important characteristics of a three-dimensional electro-magnetic forming process. However, more recent work has focused on more accurate, custom process simulations.

The current work involves collaboration with Dr. Nick Bessonov in cooperation with University of Michigan – Dearborn. Figure 7 illustrates an example of a two-dimensional simulation of EM forming of aluminum sheet into a conical die with a fully-coupled electromagnetic-elastic plastic model. These models are currently being extended for use as a fully three-dimensional numerical simulation approach.

A numerical simulation of the current and the electromagnetic forces for the EMF restrike operation has been developed in support of the coil and concentrator work ongoing at Ford. The simulation accurately predicts the coil temperature rise, the current density in the coil cross-section, the electromagnetic pressure on the aluminum blank and the plastic strain distribution in the aluminum blank. Figure 8 shows a typical result of the numerical simulation for specific coil geometry.

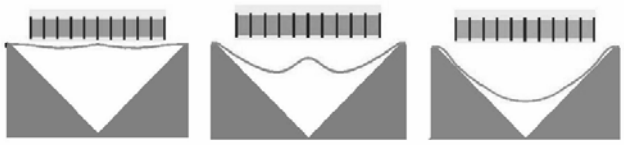


Figure 7. Example of a two-dimensional simulation of EM forming of aluminum sheet into a conical die with a fully-coupled electromagnetic-elastic plastic model. (Produced by Dr. Bessonov in cooperation with University of Michigan – Dearborn).

Industrial Embodiment. Oxford Automotive completed a study of the industrial embodiment of the EMF process, which is designed to analyze the potential methods to incorporate EMF into the highly-integrated manufacturing of automobiles. The study investigated integration into conventional sheet-metal stamping production facilities and the potential to create an entirely new and separate production line based on EMF technology for aluminum alloy sheet. Several variations of industrial deployment were identified and studied. One possible scenario is where the EMF system would be used as a separate forming station to perform a restrike function. This restrike operation would be employed to increase deformation in local regions requiring greater formability than conventional stamping will permit.

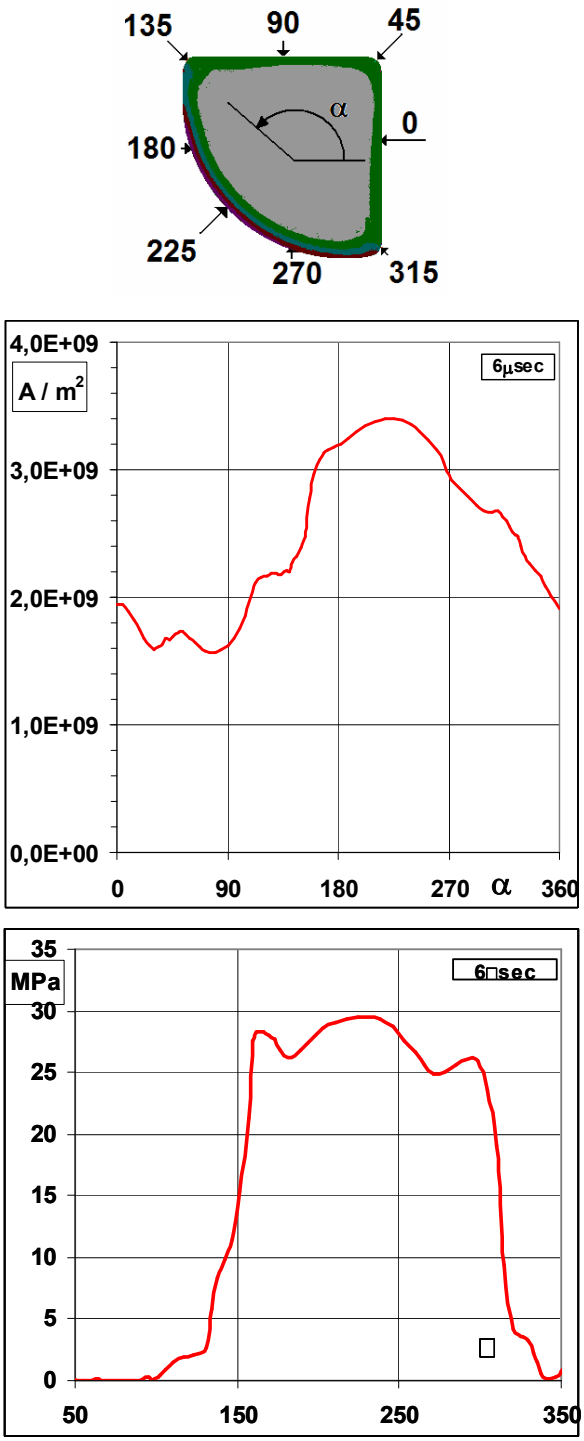


Figure 8. Numerical simulation of the (middle) coil current density and (bottom) pressure distribution on the blank during EMF restrike operation using the coil geometry (top).

Conclusions

Technical feasibility of EMF for aluminum sheet in an automotive application has been demonstrated, during both this project and prior USCAR projects. The durability of relevant coils systems and methods for the economical design, construction and implementation of forming systems are yet to be demonstrated. However, the current project has made significant progress in demonstrating coil durability at commercially relevant conditions. There is also a need for additional dynamic formability data of relevant aluminum alloys. This project targets these issues. Progress has been made in assessing the current state of knowledge for materials, coil design, formability, and system design. Also, a pulsed power system has been designed and fabricated to serve in experimental testing of coil systems. This project has also shown that EMF can be performed using aluminum sheet while achieving intermediate coil life (~5,000 cycles). As this project progresses, a balanced combination of analysis and experiment will be applied to demonstrate more durable coil systems that meet the performance requirements of automotive manufacturing. A numerical simulation tool has been developed that accurately predicts the coil temperature rise, the current density in the coil cross-section, the electromagnetic pressure on the aluminum blank and the plastic strain distribution in the aluminum blank. This tool contributes to developing modeling capabilities that can assist in the design of EMF systems.

E. Aluminum Automotive Closure Panel Corrosion Test Program

Project Co-Chair: Tracie Piscopink-Jafolla
General Motors Corporation
Mail Code 483-370-101
3300 General Motors Road
Milford, MI 48380-3726
(248) 676-7014; fax: (248) 685-5279; e-mail: tracie.l.jafolla@gm.com

Project Co-Chair: Francine Bovard
Alcoa Technical Center
100 Technical Drive
Alcoa Center, PA 15069
(724) 337-3249; fax: (724) 337-2044; e-mail: francine.bovard@alcoa.com

Technology Area Development Manager: Joseph A. Carpenter
(202) 586-1022; fax: (202) 586-1600; e-mail: joseph.carpenter@ee.doe.gov
Field Technical Manager: Philip S. Sklad
(865) 574-5069; fax: (865) 576-4963; e-mail: skladps@ornl.gov

---

Contractor: U.S. Automotive Materials Partnership
Contract No.: FC26-020R22910

Objective

- Develop a standardized cosmetic corrosion test for finished aluminum automotive body panels that provides a good correlation with in-service testing and field performance.

Approach

- Define test matrix.
- Specify and obtain materials.
- Specify phosphate and paint system.
- Pretreat and paint large reservoir of test specimens.
- Conduct laboratory testing, outdoor exposures, test-track exposures and in-service testing.
- Evaluate test data to determine which accelerated tests correlate with in-service testing.
- Conduct iterative laboratory testing to improve correlation between lab tests and on-vehicle exposures, and to determine reproducibility and repeatability of lab tests down-selected based upon initial data.

Accomplishments

- Initial laboratory tests, test-track exposures and outdoor exposures completed.
- On-vehicle tests have been exposed for two years out of five planned.
- Initial evaluation of test-track exposures laboratory test samples completed
- Corrosion product analyses conducted for some laboratory tests.
- Analysis of initial laboratory test data completed and second iteration of lab tests defined

Future Direction

- Complete second round of laboratory tests
- Continue long-term in-service testing.
- Conduct corrosion product analyses for in-service tests.

Introduction

The use of aluminum closure panels such as hoods, deck lids and lift-gates is increasing as the need to lower overall vehicle weight and thereby improve fuel economy increases. One of the key requirements for closure panel materials is a very high degree of corrosion resistance and excellent paint durability. Although aluminum closures have been used for many years, the general level of confidence and ability to predict corrosion lifetimes in service remains uncertain. Over the years, many laboratory corrosion test environments have been used to evaluate the performance of painted closure panels. Although the results of these tests can sometimes be useful for relative comparisons of alloy substrates and/or paint systems, the correlation of these lab test results with in-service performance has not been established in a systematic way. Extensive studies have been carried out in order to establish this correlation for finished cold-rolled and galvanized steel substrates [1] through cooperative efforts between the automotive companies and steel, pretreatment and paint suppliers. With the increased use of aluminum, it was recognized that a program was required to establish the correlation between lab test results and in-service performance for finished aluminum closure panels.

In response to this need, a group composed of representatives from the auto companies, the aluminum industry and associated suppliers was established in June of 2000 to formulate a program that would provide this correlation. The establishment of a standard test method for corrosion of aluminum closure panels through this effort will accelerate the adoption of lightweight aluminum materials to lower overall vehicle weight and reduce manufacturing costs by eliminating multiple test programs. A single corrosion test accepted throughout the industry could also be used to allow rapid selection and verification of alloy, pretreatment and paint performance. In this report, an outline of the test program, evaluation procedures and discussion of the preliminary results from initial laboratory tests, outdoor tests, test-track exposures and on-vehicle exposures are presented.

Experimental

Materials

In 2001, the first step in the development of a new cosmetic corrosion test occurred with the establishment of a reservoir of painted panels. These panels would then be used in the subsequent evaluation of all test methods. As listed in Table 1, the substrate materials, metal finish and paint processing variables were selected to give a range of cosmetic corrosion performance. Several aluminum alloys used in the Unites States and in Europe, both current and historical, were included. Electro-zinc-coated steel and uncoated cold-rolled steel were included as reference materials. Two aluminum alloys were processed to simulate metal finishing in an automotive assembly plant body shop.

Table 1. Materials

Code	Alloy	Metal finish	Paint System
A	AA6111-T4PD	No	Standard
B	AA6111-T4PD	No	Low F-
C	AA6111-T4PD	No	E-coat Only
D	AA6111-T4PD	Yes	Standard
E	AA6016	No	Standard
F	AA6022-T4E29	No	Standard
G	AA2036	Yes	Standard
H	EG 60 Steel	No	Standard
I	CRS	No	Standard

The materials were painted with a typical automotive paint system. This paint system included zinc phosphate pre-treatment, medium-build cathodic electrophoretic priming (e-coating), and spray painting with a primer surfacer and white basecoat - clear topcoat system for a total paint film thickness of approximately 100 μm. An additional set of 6111 panels was processed through the

phosphate pre-treatment with lower fluoride concentration (comparable to the fluoride level used for steel-only vehicles). Also, since qualification testing is often done on panels that are processed only through the electrophoretic primer (e-coat) step, another set of 6111 panels was processed only through the e-coat step, i.e., standard fluoride for Al but no basecoat or clear coat applied.

Panels were prepared for testing with two parallel scribes penetrating through the coatings to the substrate. The painted and scribed samples were then sent to laboratories for testing in a variety of environments, including laboratory, static outdoor exposure, proving-ground, and on-vehicle tests.

Evaluation Method

The evaluation of scribe corrosion has traditionally been performed visually with a simple ruler by measuring creepage distance. While this simple technique of measuring creepage distance has provided some quantitative measure of corrosion severity, the one-dimensional interpretation (length only) of this manual technique provides only a partial quantification of the two-dimensional creepage phenomena. In the case of filiform corrosion found in aluminum substrates where creepage does not propagate uniformly along the scribe line as in steel substrate but rather forms thread-like, circuitous filament lines, this one-dimensional manual technique of measuring straight-line distance may incorrectly quantify corrosion.

Optical macro-imaging is a proven instrumentation technology that, when applied to the evaluation of two-dimensional surface defects, provides more reliable and accurate measurements of geometrical shapes than are obtainable with traditional human visual evaluation methods or one-dimensional extrapolative analysis of two-dimensional shapes. For this study, an optical imaging system developed by Atlas Material Testing Technology LLC was employed to quantitatively interpret the degree of filiform corrosion. The imaging system employs controlled illumination conditions (geometry and intensity), high-resolution digital image capture and advanced algorithm-based image and data analysis methodologies. The use of optical imaging techniques eliminates the influences of human subjectivity by digitally capturing all sample images under the same enhanced illumination conditions and then subjecting them to a consistent image analysis administered by objective computer software [2-6].

For this study, four geometrical attributes were measured: area of corrosion, maximum creepage, minimum creepage, and average creepage. The area of corrosion was found to be the most representative and comprehensive measurement. Because the size of the panels and therefore the scribe lengths for the lab tests were different from the other tests, the corrosion area was normalized to the length of the scribe (i.e., area per length). The normalized corrosion areas for triplicate panels (2 scribes per panel) were then averaged and the results are reported as “normalized average area.”\

Laboratory Tests

Ten existing laboratory test methods were identified by the task group for the initial laboratory testing (Table 2). Triplicate sets of the materials in Table 1 were evaluated in each test. Each test was repeated at a second laboratory as a limited check on the lab-to-lab reproducibility of the initial results. The fully-prepared painted and scribed test panels were provided to the testing laboratories.

After comparing the initial round of test results to preliminary on-vehicle exposure results, three of these tests (APGE, ASTM G85-A2, and HCl Dip)

Table 2. Lab Tests

TEST METHOD	# OF LABS
Ford APGE (35/70 Cycles)	2
ASTM B117 (650/1000 hours)	2
ASTM D2803 (50/80/100% RH)	2
ASTM G85-A2 (3 weeks)	2
CCTIV (35/70 Cycles)	2
GM9540P-B (40/80 Cycles)	3
HCl Dip (8 weeks)	2
J2334 (40/60/80 Cycles)	2
KWT	1
VDA 621-415	2

were selected for further evaluation. Round-robin testing of these test methods is currently in progress. The duration of the tests is being varied in an attempt to further improve the correlation of these accelerated tests with the results from the on-vehicle exposures. Each test will be conducted at five laboratories to more thoroughly evaluate the repeatability and reproducibility of the test methods.

In-service (On-vehicle) Exposures

It is critical when developing a laboratory-based test that test-to-field correlation be performed. In an effort to capture real-world data in developing this test it is necessary to expose these panels to severely corrosive environments that represent "worst case" real-world service environments. Suitable environments exist in the northeastern United States, southeastern coastal areas of the United States, and southeastern Canada. The five sites selected for this study were: 1.) Detroit, Michigan; 2.) Orlando, Florida; 3.) St. John's, Newfoundland; 4.) Montreal, Quebec; and 5.) Ohio-New York Truck Route.

Two sets of 2" x 4" test panels are exposed on each vehicle (two vehicles per site). Each set of 24 (three each of eight material variables) are attached to a mounting panel (16" x 12") using double-backed tape prior to mounting on vehicle. At the Detroit, St. Johns, and Montreal sites, one set is mounted on the hood of each vehicle (horizontal orientation) and one set on the right front door of each vehicle (vertical orientation). At the Florida and Ohio-New York sites, the panels are mounted beneath the trailer frame behind the front wheels (vertical orientation only). Each panel contains 2 diagonal scribe lines which are 2" long and 1" apart. The panels will be exposed for a total of 5 years of in-service exposure. Intermediate evaluations will be conducted when possible.

OEM Test-Track Exposures

Proving-ground tests have historical background and are based on extensive test-to-field correlation studies on steel automotive body panels. The four proving grounds selected for this study were: 1.) GM – Milford, Michigan; 2.) Ford – Flagstaff, Arizona; 3.) DCX – Chelsea, Michigan; and 4.) ARL – Aberdeen, Maryland.

Each site exposed two sets of 24 test panels which are 2" x 4" with pre-cut edges. Each set of 24 (three each of eight material variables) will be attached to a mounting panel (16" x 12") using double-backed tape prior to mounting on vehicle. One set will then be on the hood of each vehicle (horizontal orientation) and one set on the right front door of each vehicle (vertical location). Each panel contains two diagonal scribe lines which are 2" long and 1" apart. The panels were exposed for durations that prior testing indicates should be representative of ~10 years of field exposure.

Outdoor Exposures

In addition to on-vehicle and OEM test-track exposures, static exposure for the products at the following test sites were elected for this study: 1.) ARL Exposure Site in Cape Canaveral, Florida and 2.) Alcoa Exposure Site in Pittsburgh, Pennsylvania.

Each test site exposed a set of 24 (three each of eight material variables) test panels which are 4" x 6" with pre-cut edges and a 5/16" diameter hole for mounting. Each panel contains two diagonal and parallel scribe lines which are 4" long and 1" apart. The panels will be exposure for two years of static outdoor exposure. The panels were manually sprayed with a 5% NaCl solution 2 times per week throughout the two-year exposure.

Corrosion Product Analysis

In order to state categorically that any lab test correlates well with in-service corrosion performance, it is essential that the chemical nature of the corrosion products formed on lab tested materials match those on identically prepared materials exposed to in-service environments. Apart from the extent of corrosion found on painted coupons, the chemical composition of the corrosion products from laboratory and in-service exposure should be the similar if a good correlation exists. To initiate this comparison, the corrosion products from samples of AA6111 that had been exposed to some of the laboratory tests were analyzed using a variety of electron-optical techniques. This work was carried out in cooperation with the Surface Science group at the University of Western Ontario. A more detailed description of this work was presented at

the SAE 2004 Congress [7], so only a very brief description of this work is provided below.

Electron-optical techniques were selected to do this analysis because the amount of corrosion product on aluminum closure panels is very small, making more traditional analytical procedures impractical. In addition, the use of these methods allows not only for a measurement of the chemical species present, but also for an analysis of the distribution of these species in and around the corroded area on the panel. Work to date has shown that some lab tests, such as the SAE J2334, result in corrosion product formation where high localized concentrations of certain elements such as chloride are found at the periphery of the corrosion site, whereas in other tests such as the CCT IV, the distribution of chemical species is much more homogeneous throughout the corrosion product. It is anticipated that initial comparisons of corrosion products in lab tests and in-service environments will be carried out in late 2005 and early 2006.

Results and Discussion

Panels from the test tracks, outdoor tests, preliminary on-vehicle exposures and initial lab tests have been analyzed. At this point only a very limited amount of service-relevant results from the on-vehicle exposures is available. From these preliminary on-vehicle results it is qualitatively apparent that the panels with metal finishing (D & G) have significantly more corrosion than the other substrates (Figure 1). The preliminary results for normalized average area from on-vehicle service relevant exposures are plotted in Figure 2. Based on these preliminary results, accelerated tests that also show a significant difference between the substrates with metal finishing (i.e., sanding) and those without metal finishing would appear to correlate better with the preliminary observations from on-vehicle testing. Many of the accelerated lab tests do not show a significant difference between the substrates with and without metal finishing. Of the laboratory test methods evaluated thus far in the program, the ASTM G85-A2 test and the HCl dip test appear to show a significant difference in corrosion performance between the substrates with metal finishing (i.e., sanding) and those without metal finishing as illustrated in Figures 3 and 4. Also, the APGE test showed this difference for one test lab, but not the second test lab as illustrated in Figure 5.

Likewise, test-track or proving-grounds tests that show a difference in performance related to metal finishing would qualitatively correlate better with the preliminary field test observations. One of the OEM test-track exposures appears to exhibit differences in the performance of substrates with and without metal finish that are consistent with the preliminary on-vehicle observations, but the other two OEM test tracks are not consistent with this difference as illustrated in Figure 6.

The actual appearance or morphology of the corrosion is also an important consideration. Ideally, the morphology of the corrosion generated by the accelerated laboratory test should mimic that observed in the on-vehicle exposures in Figure 1. Examples of the morphology observed from the three lab tests that quantitatively differentiated the corrosion performance based metal finish are shown in Figure 7. Of these, the APGE test appears to mimic the field tests better in that the corrosion is blister-like and localized. The HCl dip test and the ASTM G85-A2 test generated corrosion more uniformly along the entire scribe line.

Conclusions

Correlation of accelerated tests with on-vehicle exposures is critical for this test development effort. Three accelerated tests that have shown signs of possible correlation with on-vehicle tests (APGE, HCl Dip and ASTM G85-A2) have been selected for further evaluation. Additionally, it was shown that only one of the three OEM test tracks correlated reasonably well with preliminary on-vehicle exposure results. The reproducibility of the tests is also an important consideration, which will require additional testing to evaluate. A few additional accelerated laboratory tests will also be considered in an effort to find a lab test with improved correlation to in-service vehicle testing and the correct morphology.

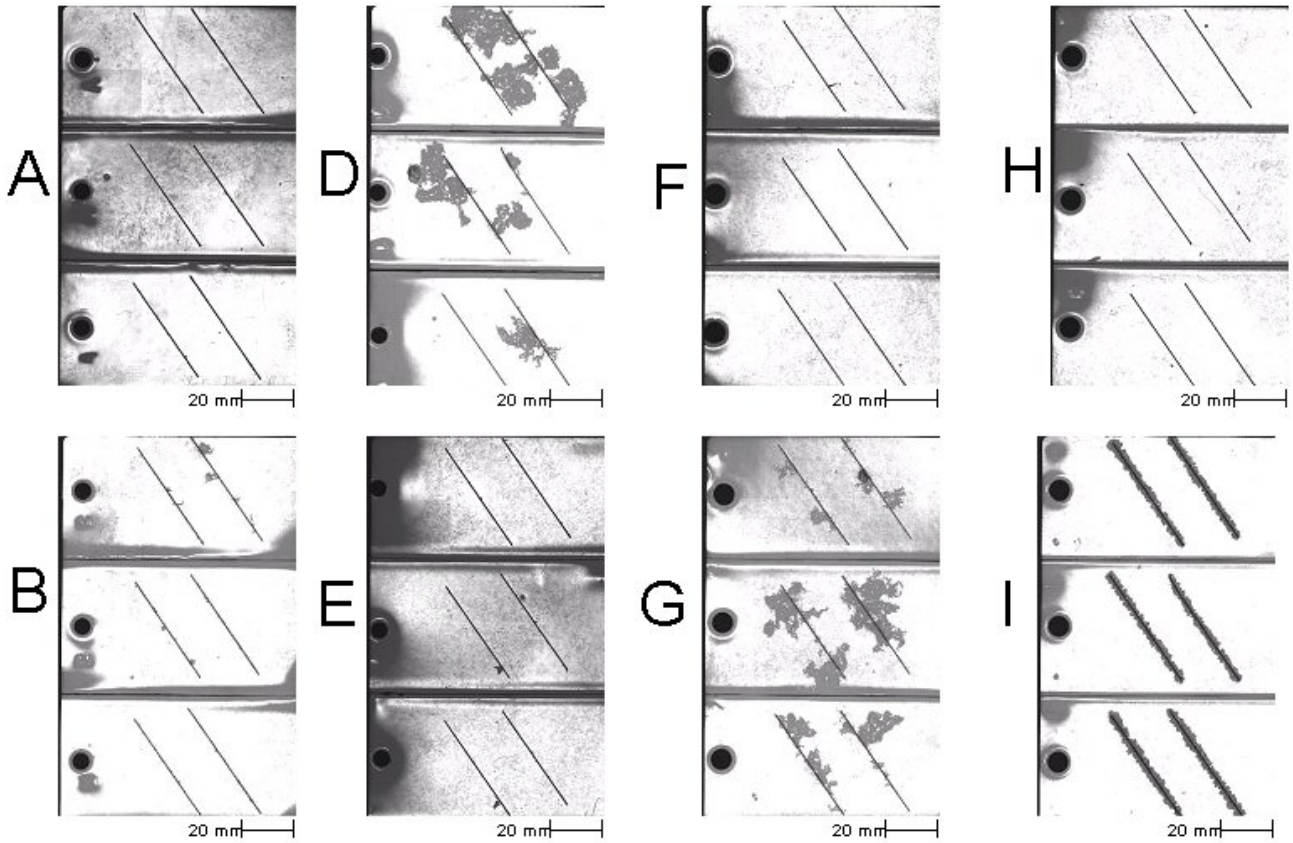


Figure 1. Representative images of panels from the Detroit On-Vehicle Test after 1.5 years in-service exposure.

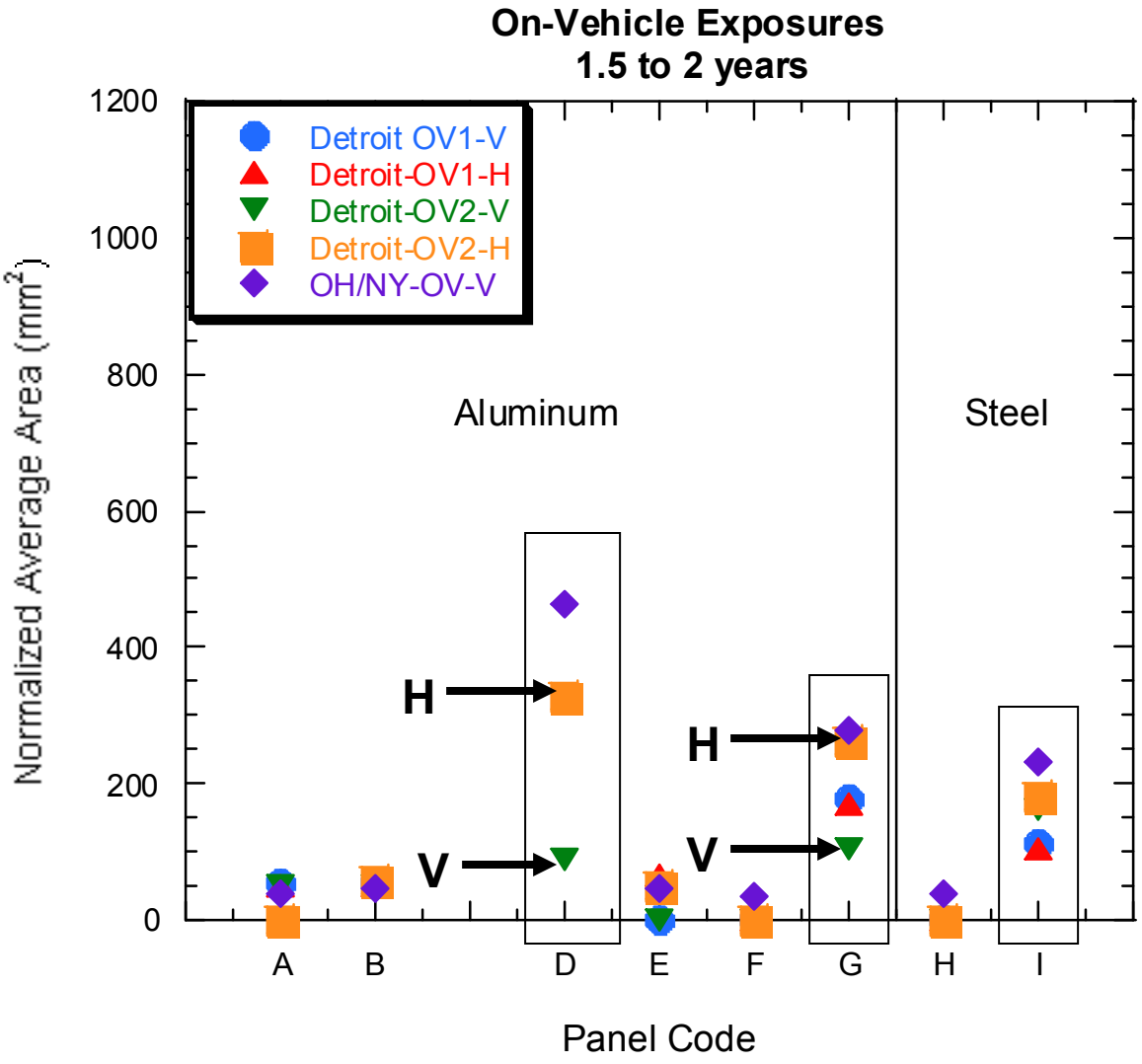


Figure 2. Normalized average area for preliminary on-vehicle service-relevant exposures.

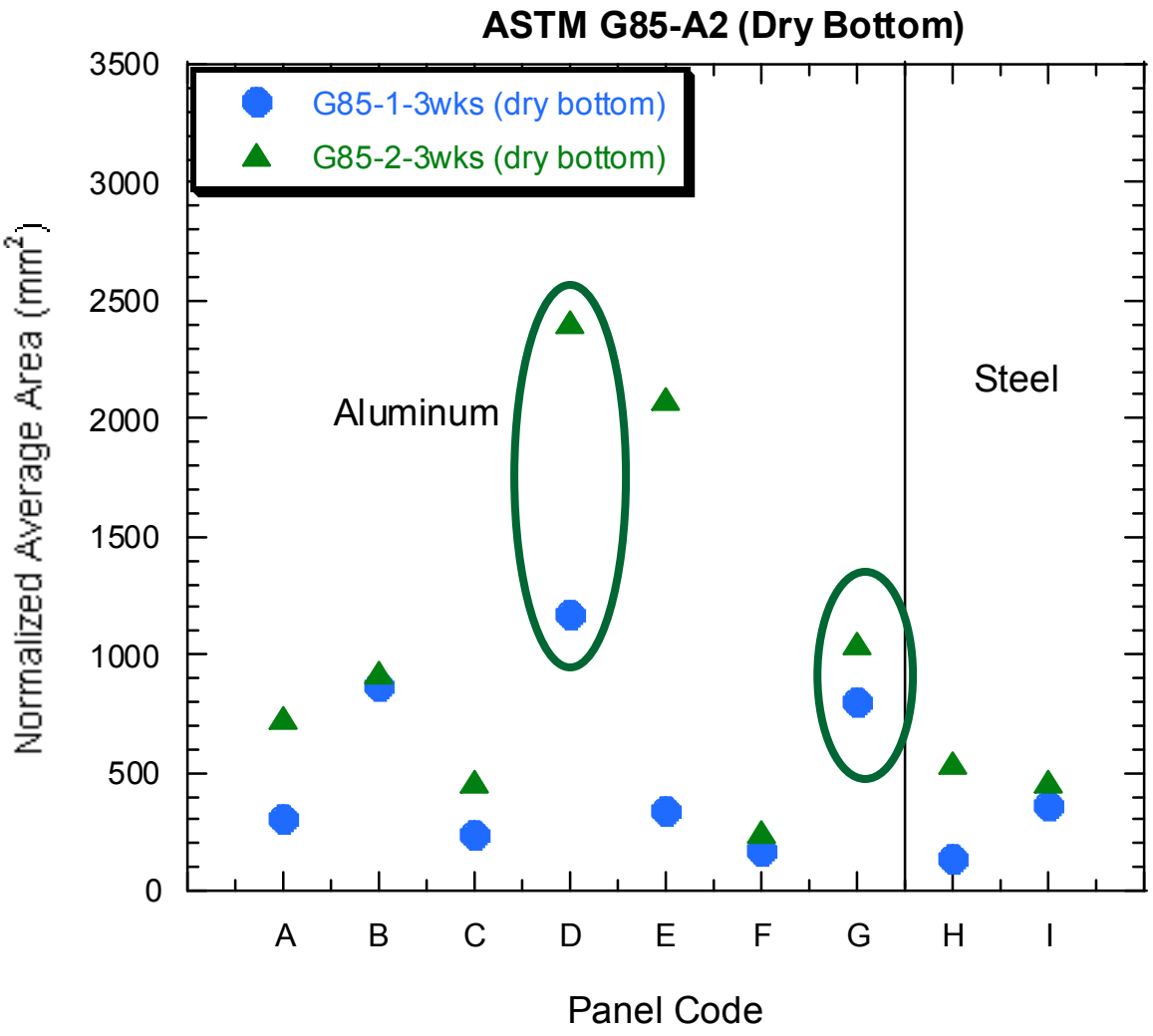


Figure 3. Normalized average area of corrosion for ASTM G85-A2.

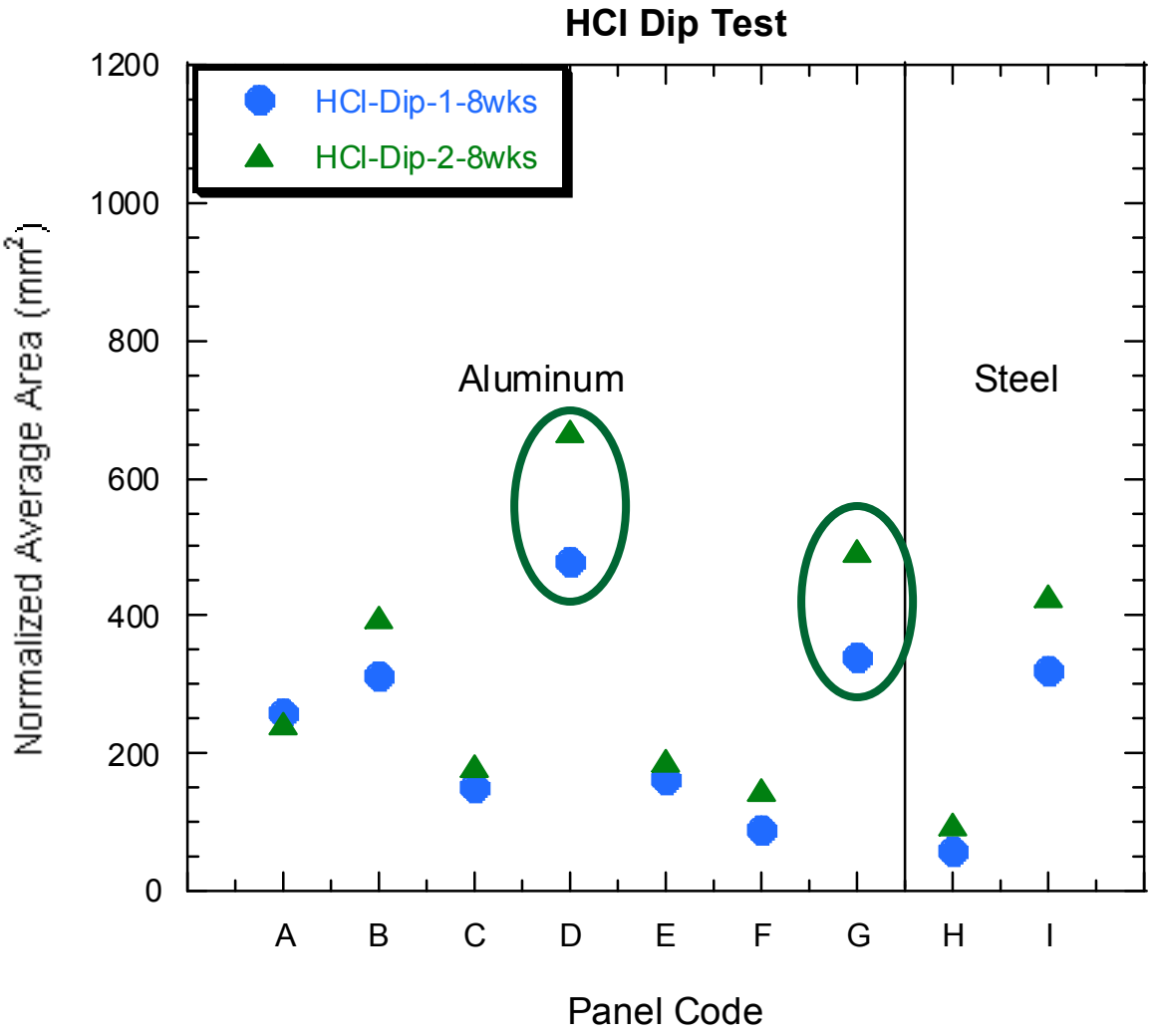


Figure 4. Normalized average area of corrosion for HCl Dip Test.

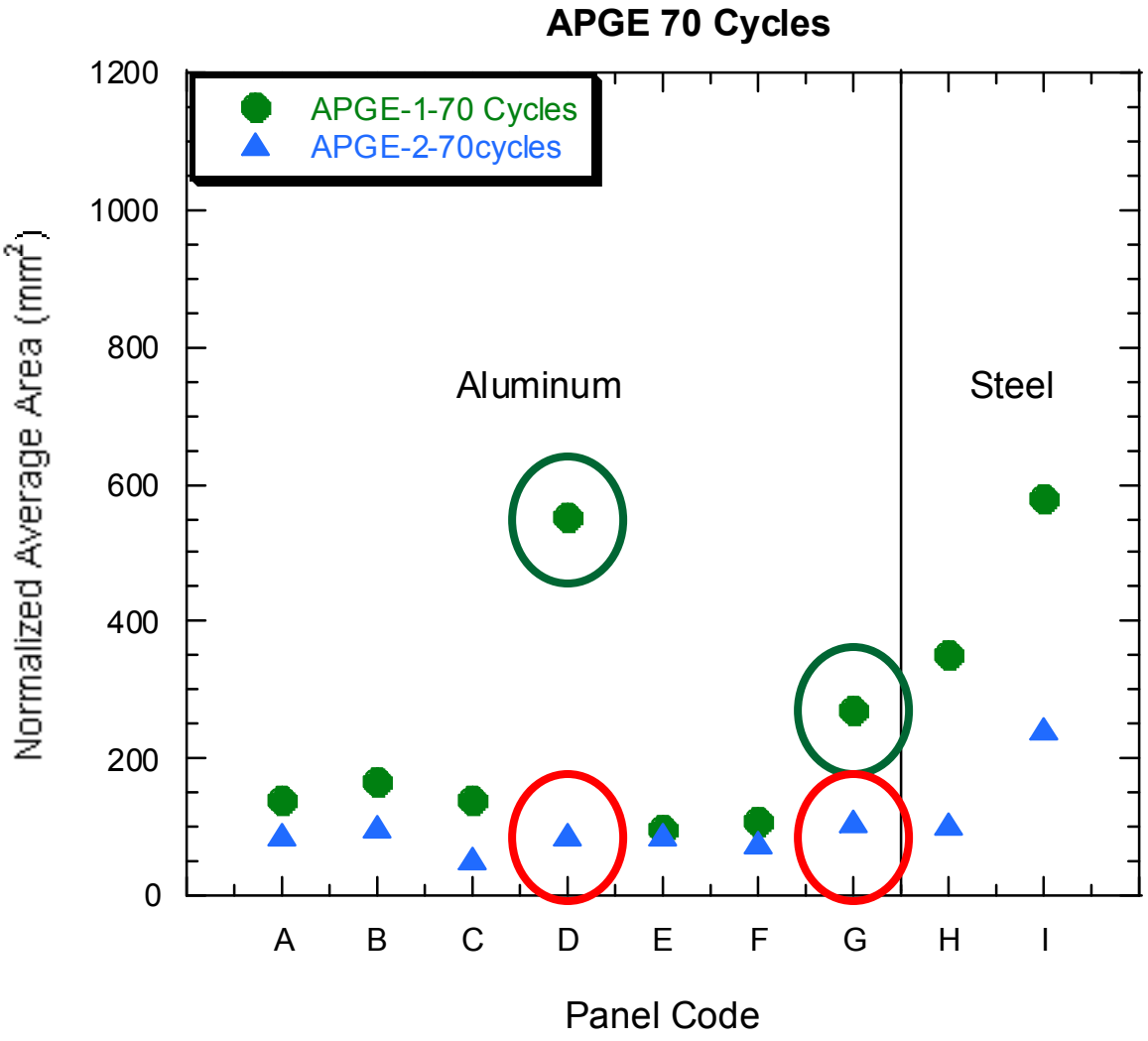


Figure 5. Normalized average area of corrosion for APGE.

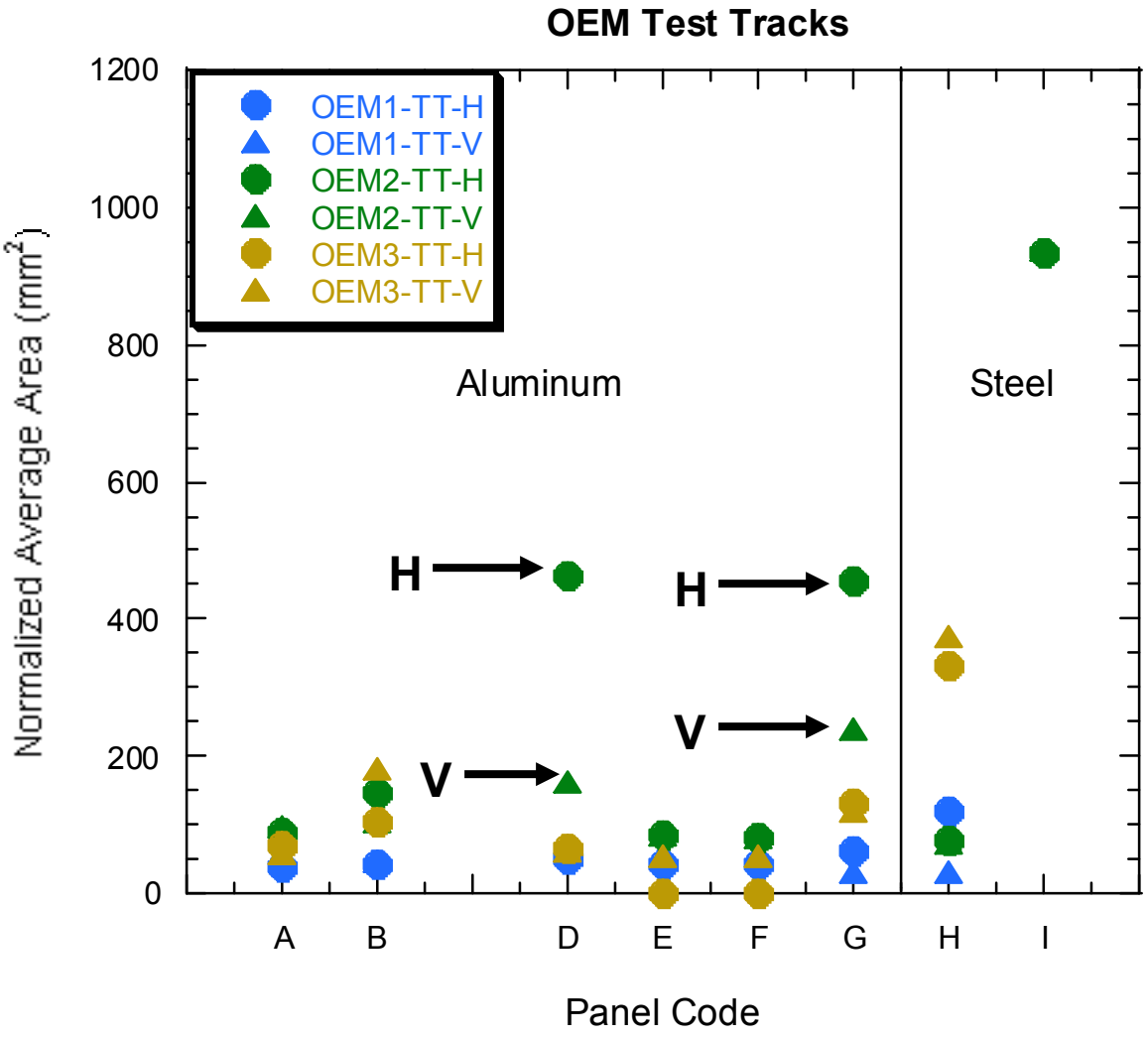


Figure 6. Normalized average area of corrosion for OEM test tracks

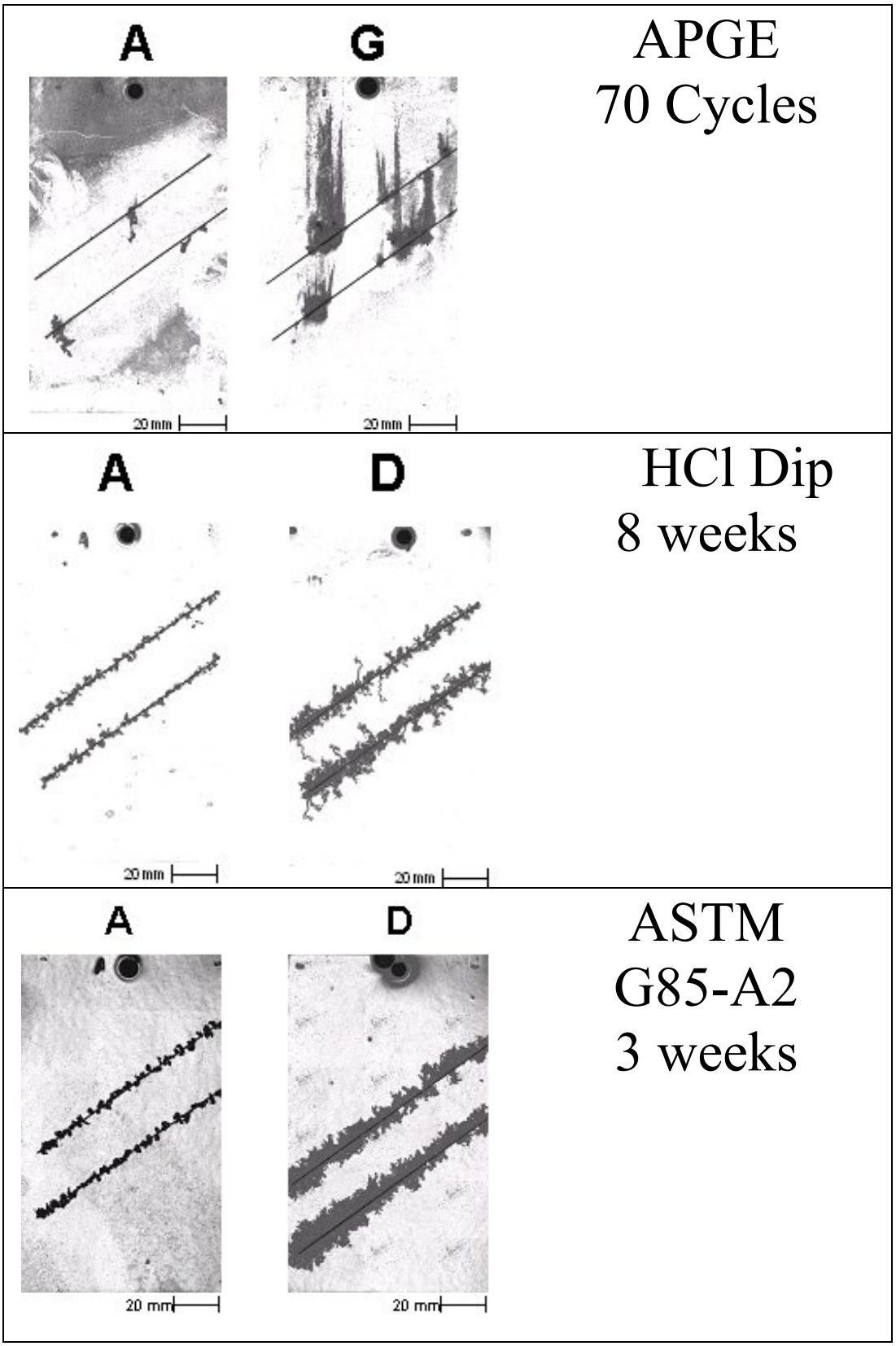


Figure 7. Representative images from APGE, HCL Dip and ASTM G85-A2.

References

1. SAE J2334, "Cosmetic Corrosion Lab Test", Society of Automotive Engineers, Warrendale, PA, June 1998.
2. Lee F, Ryntz, R, Britz, D., "Analysis of Scratch Resistance Using Optical Imaging and Automatic Classification", 4th International Coatings for Plastics Symposium, June 4-6 2001, Troy, MI
3. Lee, F., Pourdeyhimi B, and Adamsons, K, "Analysis of Coatings Appearance and Surface Defects Using Digital Image Capture/Processing/Analysis, The International Symposium on a Systems Approach to Service Life Prediction of Organic Coatings, Breckenridge, CO, Sep.14-19, 1997
4. Pourdeyhimi, B., and Lee, F. *European Coatings Journal*, 1995, 11, 804.
5. Wypych, G., Lee, F., Pourdeyhimi, B., Durability of Building and Construction Sealants, Ed. A. T. Wolf, RILEM, 2000.
6. Lee, F., Pourdeyhimi, B., and Martin, J., "Comparative Study of Standard Weathering Test Methods Using Image Analysis," *Durability 2000: Accelerated and Outdoor Weathering Testing, ASTM STP 1385*, J.D. Evans and W.D. Ketola, Eds., American Society for Testing and Materials, West Conshohocken, PA, 2000.
7. Corrosion Product Analysis of Aluminum Closure Panels, S. Ramamurthy et al., SAE paper 05B-417, 2005

Presentations/Publications/Patents

SAE 2002B-203
SAE 2003-01-1235
SAE 2005-01-0542

F. Improved Automotive Suspension Components Cast with B206 Alloy

Principal Investigator: Dr. Geoffrey K. Sigworth
GKS Engineering Services
1710 Douglas Avenue, Dunedin, FL 34698
Phone and Fax: (727) 733-2179
E-Mail: gsigworth@earthlink.net

Technology Area Development Manager: Joseph A. Carpenter
(202) 586-1022; fax: (202) 586-1600; e-mail: joseph.carpenter@ee.doe.gov
Field Technical Manager: Philip S. Sklad
(865) 574-5069; fax: (865) 576-4963; e-mail: skladps@ornl.gov

---

Contractor: U.S. Automotive Materials Partnership
Contract No.: FC26-02OR22910

Objective

To establish the commercial viability of B206 alloy for suspension components, by providing needed fundamental information on this alloy system and by overcoming technical issues that limit the lightweighting applications of this alloy. Once the important technical issues are solved, we should be able to provide mechanical properties equivalent to forged aluminum suspension components in net-shaped B206 alloy castings. This would allow us to lightweight automobiles and trucks in a cost-effective manner.

Approach

Four major technical focus points have been identified for this project. Accordingly, the work will be conducted in four separate phases:

1. Determine the effect of alloy composition on mechanical properties in the T4 and T7 heat-treated conditions and establish the feasibility of using less-expensive versions of the alloy.
2. Study heat treatment of B206 alloy and establish combinations of aging time and temperatures which produce desirable stress-corrosion immunity. This portion of work will also determine the feasibility of using improved T7 heat-treatment cycles to increase elongation in this temper.
3. Create cost models for automotive suspension components produced by different processes and different materials.
4. Produce control-arm castings using two different casting processes. Test components produced in the T4 and T7 tempers to provide required engineering information and establish the feasibility of using cast B206 alloy components to replaced forged aluminum parts.

Accomplishments

Kick-off meetings officially began this project early in October, 2004. Unfortunately, portions of the project were affected by delays in establishing contractual agreements and issuing of purchase orders. However, all purchase orders were in place in February, 2005.

The task 1 work is nearly complete. A study of tensile properties versus alloy composition was conducted by researchers at Alcan International. These results show that best results are obtained with two separate alloy compositions, depending on whether the T7 or the T4 temper is used. These two alloy compositions are:

1. T4 Temper
The alloy contains 4.7 to 4.9% Cu, 0.35 % Mg and 0.2 % Mn. by weight. The expected tensile properties are (yield strength (YS), ultimate tensile strength (UTS), elongation): 250-260 MPa, 430-450 MPa, and 18-22%, respectively.

2. T7 Temper
The alloy contains 4.0 to 4.2% Cu, 0.15% Mg and 0.2% Mn, and the expected tensile properties are (YS, UTS, elongation): 350-370 MPa, 430-450 MPa, and 7-10%, respectively.

The first alloy composition falls within the present composition limits specified for 206 alloy. The second is closer to 204 alloy.

In addition to the above results, a set of casting guidelines has been prepared for foundrymen who want to pour B206 alloy.

A second stage of task 1 casting trials was completed in September, 2005 by Nemak researchers at their Central Development and Technology Center near Monterrey, Mexico. Several different alloy compositions were prepared and 'wedge' castings were made. The 'wedge' castings were poured to establish the tensile properties of the alloy as the solidification rate varied from 30 seconds to 30 minutes. In addition, hot-crack test castings were poured to determine the effect of alloy composition on castability. The mechanical testing of the Nemak castings is still underway, and a technical report summarizing the results should be available in December, 2005. Once the report on the Nemak experiments is issued, this will complete phase 1 of the project.

Task 2 is being conducted at the University of Windsor under the direction of Prof. Jerry Sokolowski. Alcan International is also assisting this phase of the project by providing additional testing. A survey study of the aging of B206 alloy has been completed. Samples were aged at temperatures between 125 and 225°C for times ranging from two to forty-eight hours. The hardness and electrical conductivity were measured, and the samples were subjected to a corrosive medium to establish their vulnerability to intergranular attack. A report of these experiments was issued in October, 2005. Additional studies will establish the kinetics of the solution heat treatment process and attempt to develop an alternative T7 aging process to increase elongation in that temper.

Although preliminary discussions have taken place, no work on task 3 (the cost modeling) has been conducted.

The design work needed for task 4 has been completed at Hayes-Lemmerz, and they are ready to cut the tooling needed to produce molds for the control-arm casting. Casting trials will be conducted at their plant in Wabash, Indiana. Casting simulation and design studies are underway at Nemak. This work should be completed during the first quarter of 2006, and the tooling required to pour control-arm castings will be available two to three months later. Mercury Castings has recently come on board to this project as an additional industrial partner. They will produce test-bar castings in B206 alloy using a new semi-solid SOD (Slurry on Demand) process, which they are developing. Mercury will also produce castings from an extrusion alloy, 6061, and from two common casting alloys, 356 and 357. The mechanical properties of the SOD castings will be provided by Mercury Castings.

Future Direction

Now that the task 1 casting trials are complete, attention will be focused on the task 4 casting trials. Production of the first prototype suspension components should commence during the first half of CY 2006.

In the T7 temper, theoretical considerations suggest that it is possible to increase elongation significantly by changing the aging cycle used. This will be the primary objective of additional task 2 heat-treatment studies at the University of Windsor. We will also attempt to reduce the cost of heat-treatment by studying the kinetics of the solution heat-treatment process in B206 alloy. The cost of solution heat-treatment is on the order of 0.5

cents per pound for each hour of treatment. Reducing the solution time will also result in energy savings; about 0.03 kw-hr (330 Btu) per pound per hour.

Work on the cost models (task 3 of this project) will begin early in 2006.

Introduction

206 alloy is significantly stronger than 356 alloy and has mechanical properties approaching some grades of ductile iron. It also has excellent high-temperature tensile and low-cycle fatigue strength. Consequently, this material could be used in a number of applications to reduce vehicle weight. Cost savings may also result, because less material would be required to provide the strength needed for the application. In spite of its excellent properties, however, 206 alloy is seldom used because of its propensity for hot cracking. GKS Engineering has discovered a better method to grain refine this alloy, which reduces the tendency for hot cracking. This material has a number of potential applications, but its high strength and excellent ductility make it an ideal candidate for suspension components. Consequently, in the first stage of work (Project AMD 305 -- completed in May, 2002) control arms were produced via a tilt-pour/permanent-mold casting process to establish the viability of this material for these safety-critical components.

The work completed under AMD 305 showed that extremely high mechanical properties can be obtained. The tensile properties of permanent-mold B206 alloy control arms were nearly the same as (or slightly better than) those found with many forged aluminum components, and the low-cycle fatigue life of B206 alloy is ten times that of A356 alloy castings for an equivalent stress level. AMD 305 also showed that the permanent-mold casting process, although suitable, may not be the best manufacturing process for 206 alloy. Traditional sand casting and composite casting methods (such as Nemak´s semi-permanent-mold precision sand-casting process) are more forgiving of hot cracking. The additional work proposed in this project will examine the technical feasibility of producing B206 alloy suspension components in three other casting processes. Other important technical and commercial issues related to B206 will also be addressed. The object is to provide the technical and economic data needed to justify commercial use of this material in suspension components.

Justification

Automakers are under increased pressure to reduce CO_2 emissions and improve fuel economy through increased CAFE standards. Because of its higher strength, B206 alloy structures have the potential to reduce vehicle mass, which is directly linked to improved CAFE and vehicle performance. There is also a potential for cost savings, because less material would be required when compared to conventional aluminum castings.

Program and Deliverables

This project will take 30 months to complete and will proceed in four tasks. Below is a description of the deliverables for each of the four tasks of the project.

Phase 1

The main alloying elements in 206 alloy (Cu, Mg, Mn) will be varied in a series of statistically-designed experiments. Test bars will be cast at each composition and heat treated to the T4 and T7 tempers. Hot-crack test castings will be made to study the effect of alloy composition on castability, and ‘wedge’ castings will also be poured to determine the effect of solidification rate on tensile properties. These tests will determine the effect of alloy composition on mechanical properties and castibility, and will allow design and casting engineers to better tailor mechanical properties for any specific application. The minor impurity elements (Fe and Si) will also be varied to determine the effect of these elements on mechanical properties. It appears that the maximum limits for Fe and Si, presently listed in the AA specifications for the 206 alloys, are lower than necessary for most automotive applications. Increasing these limits by a modest amount would reduce the cost of the alloy. These tests will be conducted at the Research and Development Center of Alcan International and at Nemak.

Phase 2

Parts made in 206 alloy are immune to stress-corrosion in the T4 and T7 tempers; parts that have been aged, however, are susceptible. Published information on other Al-Cu-Mg alloys suggests that relatively short aging times may induce stress-corrosion, and that the susceptibility to stress-corrosion may occur before any change in hardness is found. For example, the temperatures and times used in powder coating may cause a problem. This part of the study will map out the dangerous areas which must be avoided. It will also examine alternative T7 treatments, to see if there is a way to improve material properties (especially elongation) in this temper. The use of alternative methods to test for stress-corrosion resistance will also be evaluated. The standard test is cumbersome, and takes 30 days to complete. A simpler, more rapid test is desirable. This phase of work will be carried out at the University of Windsor in Windsor, Ontario, and at Westmoreland Mechanical Testing Laboratories. Additional support will be provided by the laboratories of Alcan International.

Phase 3

A cost model will be constructed for suspension components manufactured using different processes and materials. A General Motors front-lower control arm forged in 6xxx alloy will serve as a mule for this economic study. The following component cases will be considered:

- forged 6xxx alloy
- sand-cast B206 alloy
- semi-permanent-mold cast B206 alloy
- permanent-mold cast A356 alloy

Creative Concepts will assist GKS Engineering in formulation of the cost models in this portion of the study. Sync Optima will also do finite element method (FEM) studies of the different cases, to determine changes required in the design (and weight) of the control arm as the material is changed from the base condition (forged 6xxx alloy).

Phase 4

In this final stage of work, control-arm 'Mule' castings will be manufactured by the composite precision sand-casting process at Nemak and at Hayes-Lemmerz International. Semi-solid cast parts will also be made at Mercury Castings.

In AMD 305, parts were made and heat treated to the T4 temper. In this new work, additional castings will be made and tested in both the T4 and T7 tempers. In this way, a complete set of mechanical property data will be obtained for the castings.

For this portion of the project, the compositions used to produce castings will be the optimum alloy compositions mapped out in phase 1 of the project.

Westmoreland Mechanical Testing and Research will do testing of castings made in this phase of work.

Measurable Success Indicators

The successful result desired from each of the four phases of work is outlined below:

Phase 1

Mechanical properties as a function of cast material composition will be provided, allowing automotive design engineers to optimize component properties at lowest possible cost. Information will be provided which may allow us to increase upper limits for dissolved Si and Fe and reduce costs in 206 alloy.

Phase 2

Optimum heat-treatment schedules, which avoid stress-corrosion problems, will be established and recommended. Simple and rapid tests for stress-corrosion susceptibility will also be evaluated.

Phase 3

Cost models will be provided for the production of suspension components using several manufacturing processes and different materials. This model will assist automotive design engineers to optimize component performance, and at the same time to help realize production cost savings.

Phase 4

Control-rm castings will be produced using two different casting processes, and a complete battery of material property tests of the components will provide the technical database needed to design,

manufacture and use suspension components cast in B206 alloy.

Technical Results

The results of the phase 1 casting trials have been used to map out the range of mechanical properties that can be obtained from B206 alloy castings. For permanent-mold test bars, which have a relatively rapid solidification rate (20-30 seconds), the tensile properties found in the T4 temper are shown in Figure 1. The irregular polygon in this figure indicates the variation of tensile properties (UTS or ultimate tensile strength and YS or yield strength (in MPa) and % elongation) that one may expect as the composition is varied between the upper and lower limits for this alloy in the Aluminum Association specifications. The amounts of Cu, Mg, Mn, Fe and Si in the alloy were all allowed to vary.

The corresponding range of mechanical properties available in the T7 temper are indicated below in Figure 2.

In addition to the above results, two of the Alcan alloy compositions were poured into an end-chill mold. Tensile samples were cut at three distances from the chill (ranging from ½ to two inches). The tensile properties obtained from these castings are

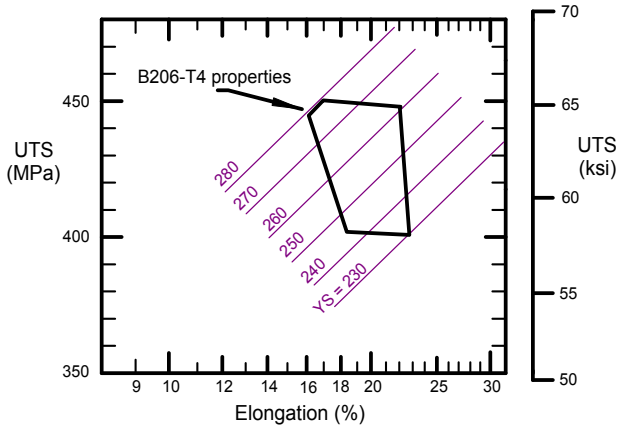


Figure 1. B206-T4 Tensile Properties

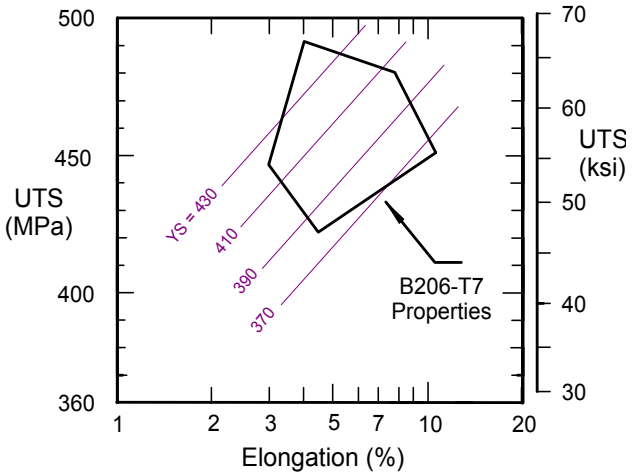


Figure 2. B206-T7 Tensile Properties

shown in Figure 3 together with data published for the more commonly used aluminum casting alloys.

The solidification time is indicated in this figure by numerical values for the secondary dendrite arm spacing (SDAS), or the cell size in the case of B206 alloy. (The data for A357 alloys are for heavily chilled sections of aerospace castings only.) It can be seen that B206 alloy exhibits mechanical properties superior to the conventional Al-Si-Mg and Al-Si-Cu casting alloys.

A number of B206 alloy samples were aged and tested for intergranular attack by corrosion. A test procedure outlined in Mil Spec MIL-H-6088 and ASTM specification G110 was used. This procedure correlated well with the results of a standard

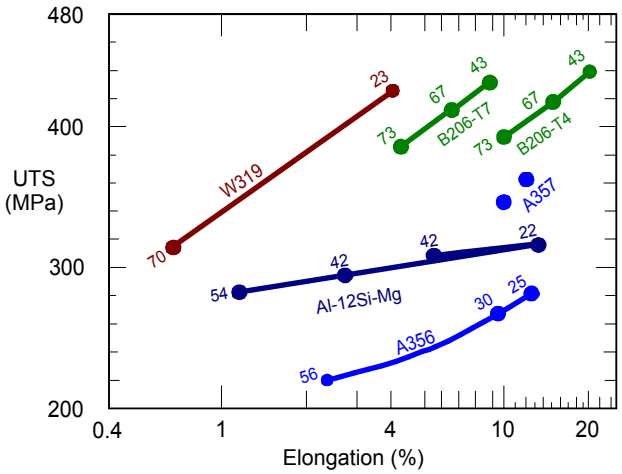


Figure 3. Range of Mechanical Properties in Five Aluminum Casting Alloys

alternate immersion test in 201 alloy,[1] and so it was adapted for use in phase 2 of this study. The average depth of the intergranular attack by corrosion (in microns) is plotted in Figure 4, as a function of aging time and aging temperature.

In this plot, the safe aging conditions are indicated by the hatched areas. (These areas indicate aged samples where the average intergranular corrosion depth was less than 20 microns deep.) The areas of worst corrosion attack are 'in between' the safe areas, at aging temperatures between 100 and 180º C. The next step in phase 2 of our program is to conduct alternate immersion stress-corrosion tests. Then, the results of the two corrosion tests will be correlated.

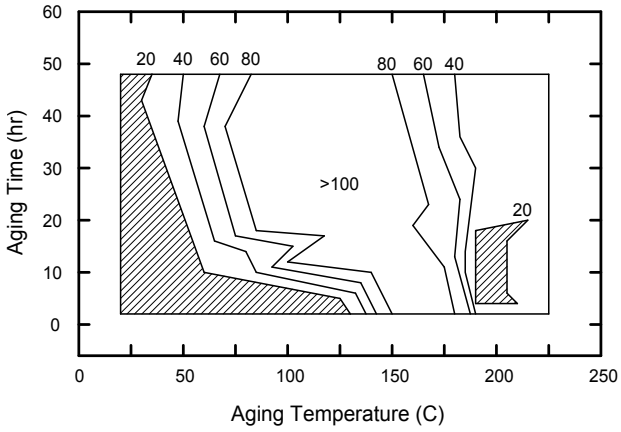


Figure 4. Average Depth of Corrosion

Presentations and Publications

No publications, presentations or patents have resulted from this project to date.

[1] M.S. Misra and K.J. Oswalt: "Corrosion Behavior of Al-Cu-Ag (201) Alloy," Metals Engineering Quarterly, Vol. 16, pp. 39-44 (1976).

G. Structural Cast Magnesium Development

Principal Investigator: Richard J. Osborne
General Motors Corporation
Mail Code 480-210-3B1
30001 Van Dyke Road
Warren, MI 48090-9020
(586) 575-7039; fax: (586) 575-8163; e-mail: richard.osborne@gm.com

Project Administrator: D.E. Penrod, P.E.
Manufacturing Services and Development, Inc.
4665 Arlington Drive
Cape Haze, Florida 33946
(941) 697-5764; fax: (941) 697-5764; e-mail: dep@gls3c.com

Technology Area Development Manager: Joseph A. Carpenter
(202) 586-1022; fax: (202) 586-1600; e-mail: joseph.carpenter@ee.doe.gov
Field Technical Manager: Philip S. Sklad
(865) 574-5069; fax: (865) 576-4963; e-mail: skladps@ornl.gov

---

Contractor: U.S. Automotive Materials Partnership
Contract No.: FC26-02OR22910

Objective

Overcome technical and manufacturing issues (high-integrity castings, corrosion & joining) that limit the light weighting application of structural cast magnesium automotive components. Then demonstrate the successful application of a magnesium engine cradle in a volume production type vehicle.

Approach

- Improve our scientific understanding of magnesium alloys.
- Develop a cost model that compares cast magnesium chassis component costs to other materials and processing techniques.
- Provide comprehensive database and design guidelines.
- Develop improved casting processes.
- Identify and/or develop methods to improve corrosion resistance.
- Improve joining technologies.
- Transfer knowledge and lessons learned to industry.
- Complete all of the scientific project tasks relevant to microstructure-property modeling, corrosion mitigation, joining behavior and nondestructive evaluation (NDE) methods.
- Convert an existing aluminum cradle to magnesium and have the parts ready for testing and approved for Corvette's Job #1 for 2006. Both industry and the scientific development part of this project worked simultaneously to solve all aspects of the project (see Figure 1) to meet the time schedule.

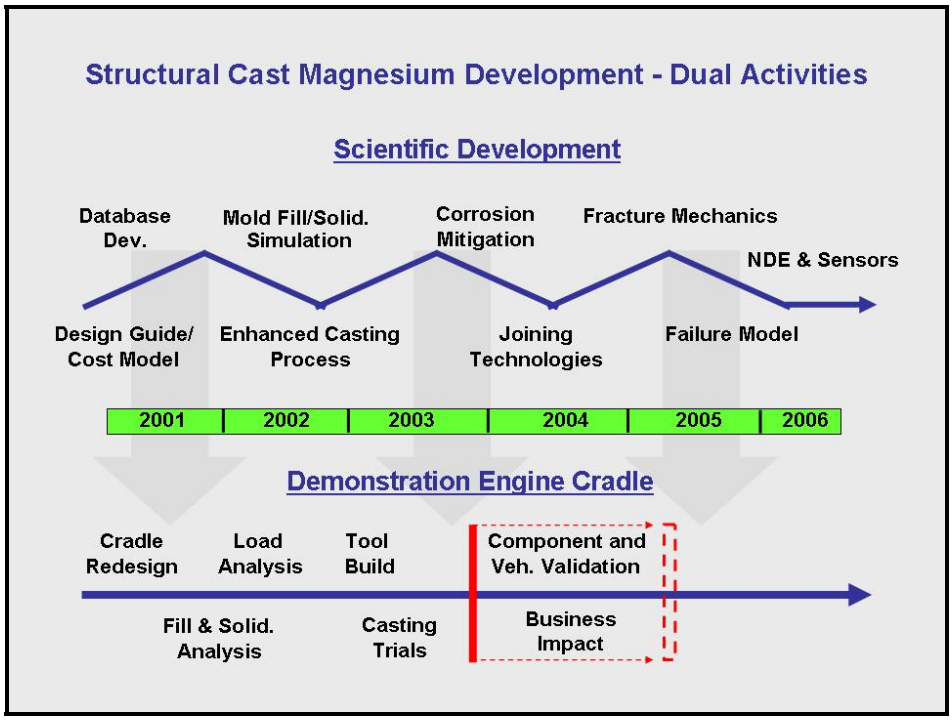


Figure 1. Dual-project path for science and magnesium demonstration casting validation activities.

Accomplishments

- Completed magnesium to aluminum cradle re-design and FEA analysis.
- Full vehicle and subsystem validation testing has been completed for 150 prototype cradle castings with no issues reported to date.
- The magnesium cradle (see Figure 2) achieved a 5.5 kg reduction in weight (35%) with respect to the current aluminum cradle now used in production applications.
- Completed mechanical property and microstructural characterization of numerous magnesium alloy production components.
- A new, high-temperature, creep-resistant alloy, AE44, was developed by participating team member Hydro Magnesium, which successfully completed at-bench and on-vehicle testing.
- CANMET's corrosion studies showed the need for dissimilar metal isolation requirements.
- Bolt Load Retention (BLR) CANMET analysis demonstrated that the cradle attachments would meet vehicle performance requirements.
- SCMD team developed and implemented successful galvanic corrosion mitigation strategy which proved successful in at-bench and on-vehicle validation testing. SCMD Database material testing was completed and provides CAE properties.
- Mississippi State University and Sandia National Lab completed material testing quantitative microstructure characteristics and they are beginning to exercise the Damage model.
- Lawrence Livermore National Lab completed fabrication of several ASTM E505 Radiographic Inspection Standards (RIS) which will improve casting evaluation sensitivity.
- Project demonstration cradle passed all validation requirements with no issues and is now in volume production on the 2006 Z06 Corvette.

- SCMD and MPCC (see report 2.H) project teams developed and published a Magnesium 2020 document which outlines a North American Strategic Vision (from 2005 through the year 2020) for Automotive Weight Reduction using magnesium components.
- SCMD database has been improved with a new navigation system and additional property inputs.
- SCMD Principal Investigators and core team members published and presented 46 papers in 2005.

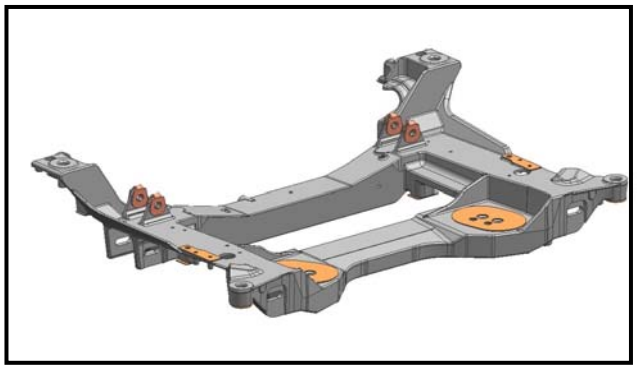


Figure 2. Machined Magnesium Cradle

Future Direction

- SCMD project has made significant scientific and application progress, but this project alone is insufficient for Mg to realize its full vehicle weight-saving potential without a dedicated, long-term vision to focus future research and development efforts. Therefore, the scope of the SCMD project was increased on 3/9/05 to develop an industry vision that will outline the potential to increase the use of magnesium (North American Automotive) from 10 #/typical vehicle in 2005 to 250 #/typical vehicle in 2020. The document was completed and reviewed by the SCMD participating companies, the AMD USAMP Board and a representative from the DOE on 10/11/05 and it will soon be distributed by a representative from USCAR.
- The SCMD Core Team continues to work and develop the Structural Cast Magnesium Development (SCMD) Project's Statement of Work (SOW) Tasks to complete both the scientific and manufacturing aspects of the project.
- The SCMD Core Team continues the investigation of the LPPM casting process to cast a duplicate magnesium cradle by this alternative casting process. Progress reports are reviewed at all SCMD meetings.

Introduction

The SCMD project has focused on resolving critical issues that limit the large-scale application of magnesium castings in automotive components. The project activities combine the science and manufacturing technology necessary to implement front and rear structural cradles. Such components offer all of the difficult manufacturing issues, including casting process (high-pressure die, semi-solid, low-pressure, squeeze, etc) and joining, along with harsh service environment challenges such as corrosion, fatigue, and stress relaxation associated with fasteners.

The project team includes personnel from:

- The "Big Three" automotive companies
- 34 companies from the casting supply base
- Academic personnel
- Independent testing and research labs
- American Foundry Society (AFS)
- Technical Associations
- Oak Ridge National Laboratory (ORNL)
- Sandia National Laboratory (SNL)
- Lawrence Livermore National Laboratory (LLNL)
- Natural Resources Canada (CANMET)

Industry Participants

An existing aluminum engine cradle (that is currently in production use) was redesigned for two different magnesium casting processes: High-Pressure Die-Casting (HPDC) and Low-Pressure Permanent Mold (LPPM). Utilization of computer simulations (prior to tooling design) indicated good correlation of casting fill operation (and their effects) to actual production experiences (see Figure 3).

Tooling and castings have been made for both processes. Several hundred HPDC production prototype castings were distributed to SCMD project participants and to GM Corvette Team for the vigorous testing procedures that were required for the HPDC cradle (See Figure 4). Based on the results of the ongoing tests, the Corvette Team decided to start a parallel production program for the implementation of using a magnesium cradle for the 2006 Z06 Corvette.

The Low Pressure Permanent Mold (LPPM) process (see Figure 4-A) has had another project extension to complete the results of this process investigation.

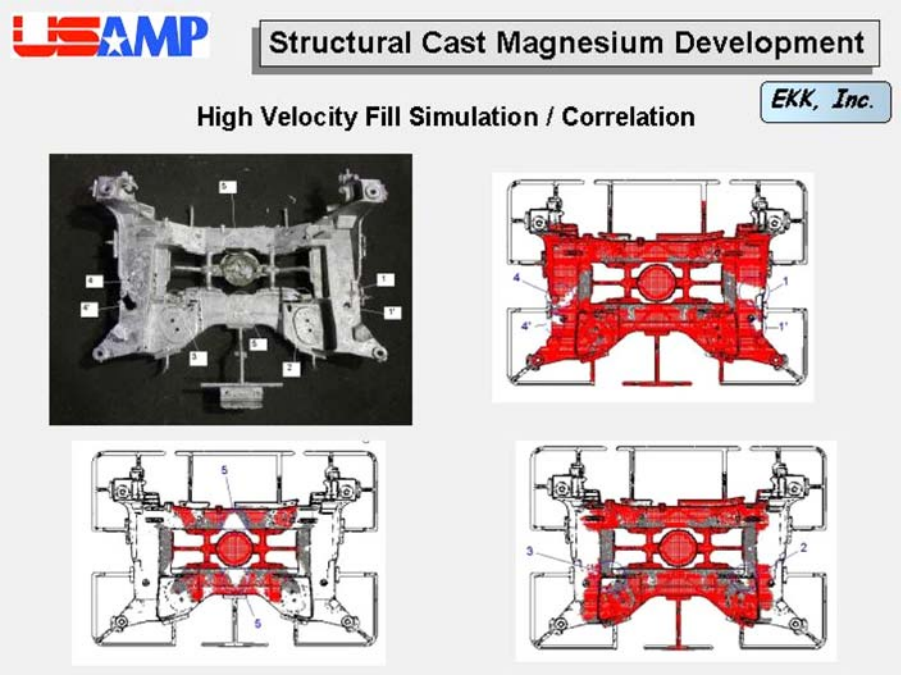


Figure 3. EKK, Inc. cavity fill simulations show excellent correlation with short fill HPDC castings.



Figure 4. Initial machined HPDC cradle castings



Figure 4-A. Initial LPPM magnesium cradle

Importance/Significance: Utilization of up-front computer modeling (used for both HPDC and LPPM processes) resulted in significant savings (time and costs) and eliminating casting defects in the initial castings. Based on the prototype castings produced by both processes, there is an estimated 35% weight savings in the magnesium cradle versus the current aluminum production part. The investigation of producing the same casting by the two different processes (HPDC and LPPM) has a great potential for the utilization of existing aluminum casting companies to expand their operations into magnesium, without huge capital and facility expenditures.

Project progress/status vs. targets

The most recent project targets were to complete the outstanding Statements of Work for the final project report to meet Job #1 2006 objective for Corvette (completed), and to complete the Magnesium 2020 document (completed).

Remaining Technical Challenges and Plans

The SCMD project will complete the outstanding Statements of Work for the final project report. In addition, the project team was recently assigned an additional task of completing the LPPM casting process that was heretofore stopped due to insufficient funds. This task will be completed before the final report is published in June of 2006.

Milestones

Cooperative Agreement

Magnesium front cradles (HPDC process) have passed all at-bench and on-vehicle testing; actual testing results have coincided with predicted computer modeling techniques; all tasks were completed on time to meet Corvette's evaluation of installing a similar Mg cradle for Job #1-2006 production vehicle.

A new, high-temperature, creep-resistant alloy, AE44, was developed by a participating project team member who successfully completed bench and vehicle testing.

Detailed quantitative microstructural characterization continues for other production components cast with AZ91D, AM 50, and AM 60 magnesium alloys. CANMET's corrosion studies showed (see Figure 6) the need for dissimilar metal isolation. CANMET's Bolt Load Retention (BLR) analysis (see Figure 6) demonstrated that the Mg cradle attachments would meet vehicle performance requirements.

Cooperative Research and Development Agreement (CRADA)

ORNL—ORNL continues the investigation of modeling software from four of the supply teams. The results of the investigation will be applied to the ORNL models using current commercial software; ORNL continues investigating the effects of using die lube for HPDC and LPPM operations (see Figure 5).

Importance/Significance: These investigations (real-time and software-proven) have already indicated that gas can be generated from the lube when molten metal (higher temperature) is introduced into the mold cavity. The gas then disperses throughout the casting, causing various types of porosity defects.

SNL/MSU—SNL is coordinating and collecting project data from all the SCMD project testing sites and then using the data to expand the mathematical "failure model" (see Figure 7).

Importance/Significance: Designers can use the multiscale fatigue model to develop castings, with the accurate knowledge of providing known failure points**.**

LLNL—LLNL has completed the fabrication of several ASTM E505 Reference Quality Indicators that will improve casting evaluation sensitivity (see Figure 8); performing radiographic analysis of production parts and test samples to determine discontinuity types and grades at predicted high-stress locations; investigating the possibility of using fiber-optic, in-mold; thermal monitoring system for HPDC continues in a high-volume production facility; working with suppliers to provide a system to detect impurities in the metal that is charged into the furnace.

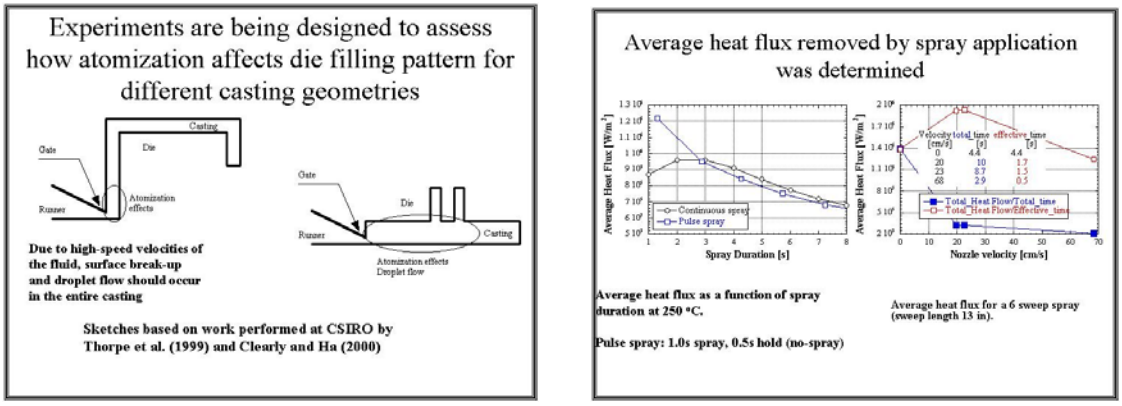


Figure 5. ORNL Die-Lube Investigation Work

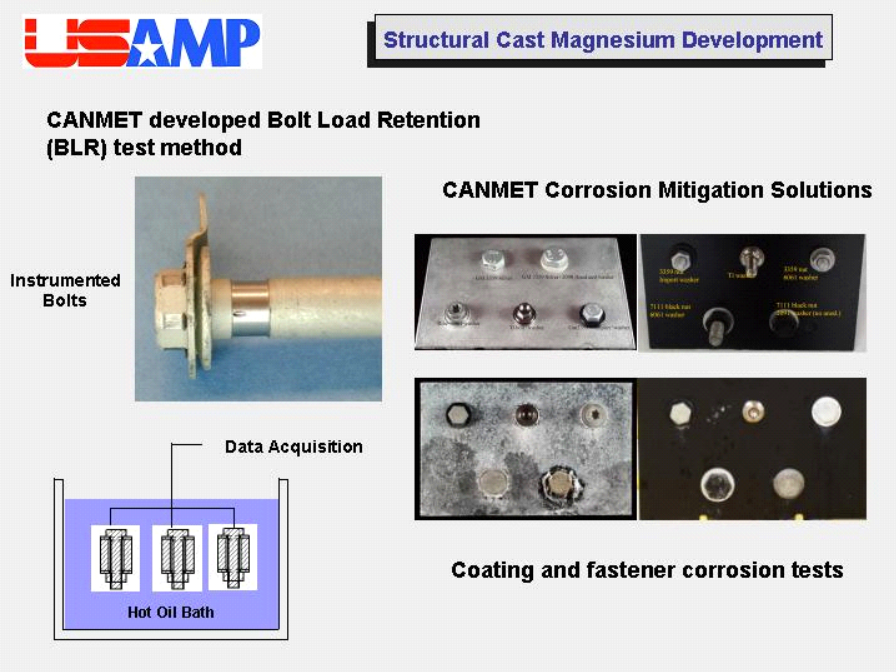


Figure 6. CANMET bolt load retention testing and corrosion studies developed knowledge required for product implementation.

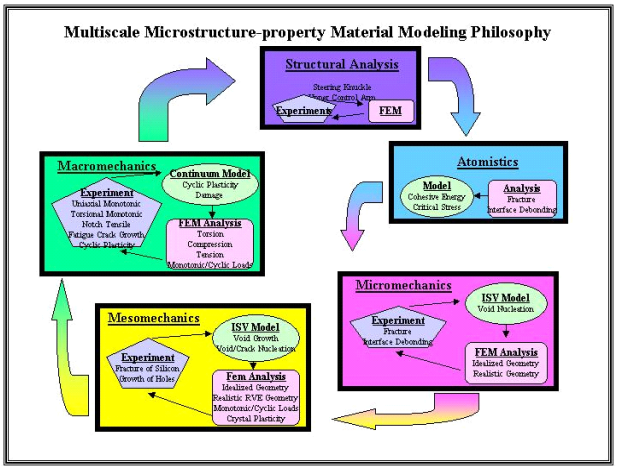


Figure 7. SNL damage model for simulating component material properties.

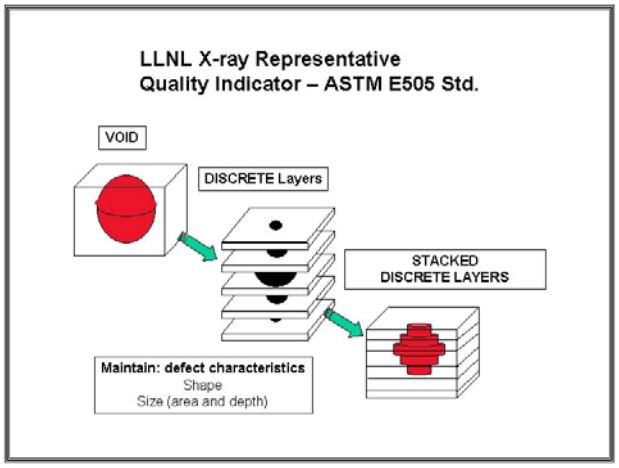


Figure 8. LLNL development activities.

Importance/Significance: All of the above procedures and investigations will provide more consistent and measurable standards that are required for improved quality control and to improve the safety-critical components that are cast in magnesium.

Academia participants: Academia participation in the SCMD project is involved with: the investigation of and characterization of crack nucleation and growth; the investigation into the cause of casting defects and the ability to separate gas and shrinkage effects that are generated (in the casting) by the various processes. (See Figure 9).

Importance/Significance: The importance of understanding the crack nucleation and the results of gas generated in magnesium castings will help to provide tools to manufacturing (or change process parameters) to eliminate casting defects. Both of these investigations by academia are working with the information supplied by ORNL and sample parts provided by the manufacturing team. The understanding of the gas effects in castings, generated by die lube could be a major breakthrough in understanding defects in magnesium castings.

Project Benefit

Expected DOE and U.S. industry benefits derived from successful completion of this project will include vehicle mass savings for ground and air transportation, leading to reduction in fuel consumption, emissions, and less dependence on foreign oil.

The North American auto industry currently uses approximately 70,000 MT/year of magnesium, which is equivalent to some 3.5 kg per vehicle. The ability to significantly increase magnesium usage will help the auto industry meet future Federal CAFE targets and reduce exposure to CAFE penalties. Cast magnesium structures have the potential to reduce 100 Kg of vehicle mass, which could reduce emissions by 5% and reduce fuel consumption by approximately 1.0 mpg (ignoring secondary mass savings).

Light metal alloys have greater recycling value with reduced energy consumption versus plastics (including melting, machining, handling, and transportation energy requirements).

The Big Three's competitive global postures will increase as a result of designing and manufacturing vehicles that offer greater consumer value. This can improve the U.S. trade balance with countries that market higher-fuel-efficiency vehicles than those produced in North America.

Health and environmental issues for workers are reduced during light-metal casting operations when compared to ferrous foundries and polymer molding operations.

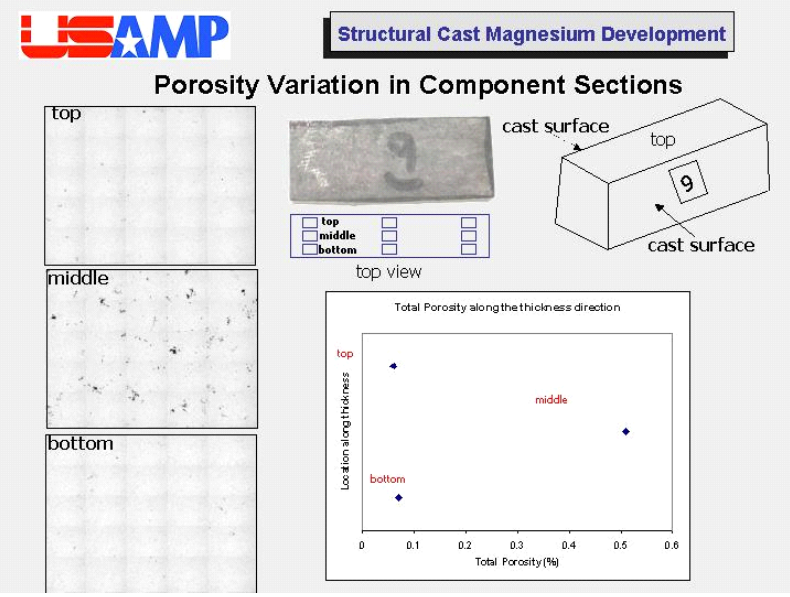


Figure 9. Georgia Institute of Technology characterization of AE44 alloy HPDC cradle section.

National laboratories are provided with valuable manufacturing development and product application experience.

Another benefit is the dual-purpose role of providing the national laboratories (and academia) an opportunity to develop math-based simulation models and NDE technologies that benefit both the auto industry and Federal ongoing technology programs.

The successful casting of a magnesium cradle (by low-pressure die-casting) will indicate to the existing aluminum casting industry that the transfer of casting technology (aluminum to magnesium casting) can be achieved at a low facility cost.

Conclusion

USAMP prototype and GM production cradles have passed all validation criteria except for galvanic corrosion. Process and production simulation, galvanic corrosion, joining and enhanced casting process development continue to be top cost issues for structural castings.

The SCMD project has been extended through 12/06 to complete additional testing and investigation of the LPPM process, and to develop a plan for the increase use of automotive magnesium through the year 2020.

Most important, the project success to date has proven that the technical and manufacturing issues (high integrity castings, corrosion & joining) that has heretofore limited the light weighting application of structural cast magnesium automotive cradles has been successfully solved.

In conclusion, the SCMD project has proven the successful casting (and recent production use) of a magnesium engine cradle is a major accomplishment for the North American magnesium casting industry.

Presentations

Numerous SCMD Core team presentations to attendees at 2005 SAE World Congress.

SCMD Core team presentations to attendees at 2020 Magnesium Document Review Meeting 10/11/05 at USCAR Office.

S. G. Lee, A. M. Gokhale, and G. R. Patel, “Macro-Segregation in High-Pressure Die-Cast AM60B Alloy” Magnesium Technology 2005 Symposium, TMS Annual Meeting, San Francisco, CA, February 14-17, 2005.

S. G. Lee, G. R. Patel, A. M. Gokhale, and Mike Evans, "Effects of Liquid Metal Gate Velocity on the Porosity in High-Pressure Die-Cast AM50 Alloy", *Magnesium Technology 2005 Symposium,* TMS Annual Meeting, San Francisco, CA, February 14-17, 2005.

A. Sreeranganathan, Soon Gi Lee, and A. M. Gokhale: "Quantitative Characterization of AM50 and AS21X Magnesium Alloys to Correlate the Variability in the Fracture Properties to Microstructure", *Automotive Alloys 2005 Symposium,* TMS Annual Meeting, San Francisco, CA, February 14-17, 2005.

Soon Gi Lee, Arun Sreeranganathan, and A.M. Gokhale: "Simulation of Mechanical Behavior of Die-Cast Magnesium Alloy Based on Three-Dimensional Porosity and Finite Elements Method," *Symposium on Computational Aspects of Mechanical Properties of Materials: Meso-Scale and Continuum Modeling,* TMS Annual Meeting, San Francisco, CA, February 14-17, 2005.

Soon Gi Lee and A.M. Gokhale: "On the Formation of Gas (Air) Induced Shrinkage Porosity in Pressure Die-Cast AM60 Mg-Alloy," Symposium on Defect Formation, Detection, and Elimination During Casting, Welding, and Solidification: Processing, Microstructure, and Properties, *Materials Science and Technology 2005* (MS&T 2005), Pittsburgh, PA, September 26, 2005.

Soon Gi Lee, G. R. Patel, and A.M. Gokhale: "Variability in Tensile Ductility of High-Pressure Die-Cast AE44 Mg-Alloy," Symposium on Defect Formation, Detection, and Elimination During Casting, Welding, and Solidification: Processing, Microstructure, and Properties, *Materials Science and Technology 2005* (MS&T 2005), Pittsburgh, PA, September 26, 2005.

S. Robison, D. Weiss, G. Gegel, G. Woycik, M. Mariatt, B. Cox, "Designing an Engine Cradle for Magnesium Semi-Permanent Mold Casting", *AFS CastExpo 2005.*

S. Robison, D. Weiss, G. Gegel., G. Woycik, M. Mariatt, B. Cox, "Designing an Engine Cradle for Magnesium Semi-Permanent Mold Casting", *International Conference on High Integrity Light Metal Castings;* Indianapolis, IN, October 31, 2005.

Publications

McLaughlin, M., Kim, C.W., Backer, G., Prindiville, J., Gokhale, A.M., and Lee, S.G. "An Application of Trapped-Air Analysis to Large, Complex High-Pressure Magnesium Casting", accepted in Die Casting Engineer, September 2004

A.M. Gokhale and G. R. Patel: "Origins of Variability in the Fracture Related Mechanical Properties of a Tilt-Pour-Permanent-Mold Cast Al-Alloy," Scripta Materialia, Vol. 52, no. 3, PP 237-241, 2004.

A.M. Gokhale and G. R. Patel: "Quantitative Fractographic Analysis of Variability in Tensile Ductility of a Squeeze Cast Al-Si-Mg-Base Alloy," Materials Characterization, Vol. 54, no. 1, PP 13-20, 2005.

A.M. Gokhale and G. R. Patel: "Analysis of Variability in Tensile Ductility of a Semi-Solid Metal Cast A356 Al-Alloy," Materials Science and Engineering, Vol. 392, PP 184-190, 2005.

S. G. Lee, A. M. Gokhale, and G. R. Patel: "Inverse Surface Macrosegregation in High-Pressure Die-Cast AM60 Magnesium Alloy and its Effects on Fatigue Behavior," Scripta Materialia, Vol. 52, PP 1069-1074, 2005.

S. G. Lee, G. R. Patel, and A.M. Gokhale, "The Effect of Inverse Macro-Segregation on Fatigue Behavior of Die-Cast AM60B Magnesium Alloy," Materials Science Forum, Vol. 488/489, PP. 713-717, 2005.

S. G. Lee, A. M. Gokhale, and G. R. Patel, "Macro-Segregation in High-Pressure Die-Cast AM60B Alloy" Proceedings of Magnesium Technology 2005 Symposium, TMS, Warrendale, 2005, PP 376-380.

S. G. Lee, G. R. Patel, A. M. Gokhale, and Mike Evans, "Effects of Liquid Metal Gate Velocity on the Porosity in High-Pressure Die-Cast AM 50 Alloy", Proceedings of Magnesium Technology 2005 Symposium, TMS, Warrendale, 2005, PP 377-380.

S.G. Lee, G.R. Patel, A.M. Gokhale, A. Streeranganathan, M.F. Horstemeyer, "Variability in the Tensile Ductility of High Pressure Die Cast AM50 Mg Alloy," *Scripta Materials*, Vol. 53,pp 851-856, 2005.

S. G. Lee, A.M. Gokhale, and G.R. Patel: "Characterization of the Effects of Process Parameters on Macrosegregation in a High-Pressure Die-Cast Magnesium Alloy", Materials Characterization, Vol. 55, No. 3, PP 219-224, 2005.

S. G. Lee, A. Sreeranganathan, G.R. Patel and A.M. Gokhale, "Quantitative Characterization of AM50 Magnesium Alloy to Correlate the Variability in the Mechanical Properties to Microstructure," TMS Letters, Issue 2, PP 47-48, 2005 (on-line).

S. G. Lee and A. M. Gokhale: "Phenomena of Formation of Gas Induced Shrinkage Porosity in High-Pressure Die-Cast Magnesium Alloys," Proceedings of Magnesium Technology 2006 Symposium, in press.

S. G. Lee, A. M. Gokhale, G. R. Patel, and M. Evans: "Effect of Process Parameters on Porosity Distributions in High-Pressure Die-Cast AM50 Mg-Alloy," Materials Science and Engineering, Submitted (in review)

S. G. Lee, A.M. Gokhale, and A. Sreeranganathan: "Visualization and Representation of Three-Dimensional Porosity in a High-Pressure Die-Cast Mg-Alloy," Materials Science and Engineering, Submitted.

S. G. Lee, G.R. Patel, A.M. Gokhale, A. Sreeanganathan, and M. F. Horstemeyer: "Quantitative Fractographic Analysis of Variability in the Tensile Ductility of High-Pressure Die-Cast AE44 Mg-Alloy," Materials Science and Engineering, Submitted.

S. G. Lee, A. M. Gokhale, and Jackie L. Milhans, "Reconstruction, Visualization, and Characterization of Three-Dimensional Microstructure of High-Pressure Die-Cast AE44 Magnesium Alloy," Transactions of American Foundry Society, Submitted.

K. Gall, G. Biallas, H. J. Maier, M. F. Horstemeyer, and D. L. McDowell, "Environmentally Influenced Microstructurally Small Fatigue Crack Growth in Cast Magnesium," Materials Science and Engineering A, 2004.

S. Xu, V.Y. Gertsman, J. Li, J.P. Thomson and M. Sahoo, "Role of Mechanical Twinning in Tensile-compressive Yield Asymmetry of Die Cast Mg Alloys", *Canadian Metallurgical Quarterly*, Vol. 44, No. 2, 2005, pp. 155-165.

S. Xu, G. Williams, R. Bouchard, J.P. Thomson and M. Sahoo, "Bolt-load Retention Testing of Magnesium Alloys for Automotive Engine Cradle Applications", *Proc. 2nd International Conference of Light Metals Technology (LMT 2005),* H. Kaufmann, Ed., St. Wolfgang, Austria, June 8-10, 2005, LKR, Austria, pp. 283-288.

V.Y. Gertsman, J. Li, S. Xu, J.P. Thomson and M. Sahoo, "Microstructure and Second Phase Particles in Low and High Pressure Die Cast Magnesium Alloy AM50", *Metall. Mater. Trans. A*, Vol. 36A, 2005, pp. 1989-97.

Fan, J., Gao, Z., and Zeng, X., "Cyclic Plasticity across Micro/Meso/Macroscopic Scales," *Proceedings of the Royal Society London,* 460, 2004, 1477-1503.

Chen, B., Peng, X., Fan, J. and Chen, S., "A Constitutive Model for Casting Magnesium Alloy ZL 105 Based on the Analysis of Spherical Void Evolution, "Int. *J. of Plasticity* (in press).

Chen, B, Gao, Z, Peng, X, Fan, J, and Cai, C. Micro-macro combined study for a porous constitutive model based on the analysis of a cylindrical void, *Key Engineering Materials*, 227, 101-112.

Jinghong Fan, Wenyue Zheng, Xiangguo Zeng, Yansong He and C. Derushie, Corrosion Fatigue of AM50 and AE44 Alloys at Various Temperature and R-Ratio, SAE Paper 2006.
S.G. Lee, G.R. Patel, A.M. Gokhale, A. Streeranganathan, M.F. Horstemeyer, "Variability in the Tensile Ductility of High

Pressure Die Cast AM50 Mg Alloy," *Scripta Materials*, Vol. 53,pp 851-856, 2005.

Hammi, Y., Horstemeyer, M.F., and Bammann, D.J., "An Anisotropic Damage Model for Ductile Metals", *International Journal of Damage Mechanics*, Vol. 12, no. 3, pp 245-262, 2003.

Aragones, J., Goundan, K., Kolp, S., Osborne, R., Ouimet, L., Pinch, W., "Development of the 2006 Corvette Z06 Structural Cast Magnesium Crossmember" *Society of Automotive Engineering,* 2005 #05M-36.

N. Li, R. Osborne, D. Penrod, "The USCAR Structural Cast Magnesium Development Project," *Magnesium Technology*, TMS, San Francisco, CA 2005.

N. Li, R. Osborne., B. Cox, D. Penrod, "Magnesium Engine Cradle-The USCAR Structural Cast Magnesium Development Project," *SAE Paper* 2005-01-0337.

Conrad, C., McLaughlin, M., and Kim, C.W., "Computer Simulation of High Pressure Die Casting of Magnesium Engine Cradle," *2005 SAE World Congress*, April 2005, 2005-01-1815.

Kim, C.W., and Kubo, K., "Recent Advancements on Porosity Simulation in High Pressure Die Casting", *CastExpo '2005*, April 2005, 05-059.

Kim, C.W., Siersma, K., and Kubo, K., "A Porosity Simulation for High Pressure Die Casting", *2006 TMS Conference* (submitted 2005 for publication in 2006).

Sabau, A.S., Predicting Interdendritic Cavity Defects during Casting Solidification, *JOM*, 2004, Vol. 56, pp. 54-56.

Sabau, A.S. and Wu, Z., Evaluation of a Heat Flux Sensor for Spray Cooling for the Die Casting Processes, Submitted for publication to the *Journal of Materials Processing Technology*, November 2005.

Sabau, A.S. and Wu, Z., Measurement of Heat Flux During Lubricant Application for the Die Casting Process, *North American Die Casting Association (NADCA)-CastExpo 2005*, St. Louis, Missouri, USA, April 2005.

Sabau, A.S., Measurement of Heat Flux at Metal-Mold Interface during Casting Solidification, Accepted for publication in the *International Journal of Cast Metals Research*, Sept. 2005.

Wenyue Zheng, R. Osborne, C. Derushie, J. Lo, "Corrosion Protection of Structural Magnesium Alloys: Recent Development, "Submitted and presented at *SAE 2005 World Congress."*

H. Magnesium Powertrain Cast Components

Project Manager: Bob R. Powell
GM Research & Development Center
MC 480-106-212
30500 Mound Road
Warren, MI 48090-9055
(586) 986-1293; fax: (586) 986-9204; e-mail: bob.r.powell@gm.com

Project Administrator: Peter P. Ried
Ried and Associates, LLC
6381 Village Green Circle, Suite 10
Portage, MI 49024-2680
(269) 327-3097; fax: (269) 321-0904; e-mail: pried_imagineer@netzero.net

Technology Area Development Manager: Joseph A. Carpenter
(202) 586-1022; fax: (202) 586-1600; e-mail: joseph.carpenter@ee.doe.gov
Field Technical Manager: Philip S. Sklad
(865) 574-5069; fax: (865) 576-4963; e-mail: skladps@ornl.gov

---

Contractor: U.S. Automotive Materials Partnership
Contract No.: FC26-02OR22910

Objective

- Demonstrate and enhance the feasibility and benefits of using magnesium alloys in place of aluminum in structural powertrain components, thereby achieving at least 15% mass reduction of the cast components.

Approach

- Identify, benchmark, and develop a design database of the potentially cost-effective, high-temperature magnesium alloys and, using this cast-specimen database, select the alloys that are most suitable for the magnesium components. (Task 1)
- Design, using finite-element analysis (FEA), an ultra-low-mass engine containing potentially four magnesium components (cylinder block, bedplate, structural oil pan, and front engine cover) using the most suitable low-cost, recyclable, creep- and corrosion-resistant magnesium alloys. (Task 2)
- Create a cost model to evaluate alloy, manufacturing, and technology costs to predict the cost-effective performance of the engine. (Task 2)
- During the execution of Tasks 1 and 2, identify and prioritize the critical gaps in the fundamental science of magnesium alloys and their processing that are barriers either to the progress of the project or to the use of magnesium in future powertrain applications. Seed-fund the most critical research, and promote additional identified needs to support further development of the magnesium scientific infrastructure in North America, thereby enabling more advanced powertrain applications of magnesium. This will be one aspect of the technology transfer deliverables of the Magnesium Powertrain Cast Components (MPCC) Project. (Task 3)
- Note that before addressing Tasks 4–6 and funding Task 3 research, an in-depth review of the engine design, including performance and durability predictions, alloy requirements and measured alloy properties, cost model, and predicted mass reduction will be conducted. Passing this gate review is necessary for entry into the second-half of the project, which has the goal of demonstrating/validating the engine design with respect to castability, manufacturability, performance, durability, and cost.

- Refine the engine component designs as necessary (updating to match the properties of the alloy selected for each component), design and build tools and patterns, and cast the engine components. (Task 4)
- Excise specimens from the cast components and develop a full mechanical and corrosion design database for the alloys. Create an original equipment manufacturer (OEM)—common material specification for magnesium powertrain alloys. (Task 5)
- Assemble complete powertrains, dynamometer-test the components, and conduct end-of-test teardowns. Refine the cost model to support determining the cost-effective performance of the engine. (Task 6)

Accomplishments

- In the years 2001-2004 Tasks 1 and 2 were completed. A successful gate review for entering Phase II was accomplished, involving (1) the selection of alloys for each magnesium engine component and revision of the component designs based on the properties of the selected alloys, (2) the issuance of contracts to project teams for tooling and casting each component, and (3) the selection of five basic research projects in support of the objectives of Task 3. The 2005 accomplishments follow.
- Completed the cylinder-block design using properties of the Australian Magnesium Technologies alloy SC-1 and issued a contact for low-pressure sand casting the magnesium block to Fonderie Messier (a division of Honsel, Inc.), in Arudy, France. This was a critical accomplishment following a 2004 fire at the Eck Industries foundry and the decision by Denison Industries that casting the cylinder block would be too great a challenge for their capability.
- Tooling design and build were completed by Becker CAD CAM CAST for the cylinder block and eight prototype castings were made during the reporting period at Fonderie Messier using gating developed with EKK and MAGMAsoft simulation software.
- Filing of a patent application for the structural details of the magnesium cylinder block was approved by the USAMP leadership and in process.
- The structural oil pan tooling design and build were completed by HE Vannatter using properties of Dead Sea MRI 153M alloy. Casting trials were performed by Spartan Light Metal Products using gating designs based on casting simulation by Technalysis. The combination of limited available gating area and the solidification behavior of the alloy have made this a difficult component to cast. Ongoing changes have improved the castings, but at reduced mass savings.
- The front engine cover tooling design and build were completed by EXCO and Extech using properties of the Dead Sea MRI 230D alloy. The components were cast by Intermet and, as in the case of the oil pan, required fine tuning of the gating system and casting conditions to produce sound castings.
- The rear seal carrier tooling design and build were completed by PCMI using properties of Dead Sea MRI 153M alloy. The component is being produced via thixomolding by Thixomat.
- Completed the first phase of adhesion tests for a wear-resistant coating to be used in the engine cylinder bores. Several surface preparations and two coating deposition methods were evaluated with excellent adhesion to magnesium being demonstrated.
- Made further improvements to the architecture for the magnesium alloy property database, including adding thermophysical and fatigue properties. Began working with the Structural Cast Magnesium Development project (see report 2.G) team for distribution of the combined databases.
- Launched five basic research projects in support of the Task 3 objectives: (1) Computational Thermodynamics and Phase Equilibria to Penn State University; (2) Hot Tearing Susceptibility to CANMET; (3) Creep Mechanisms to the University of Michigan; (4) Corrosion and Corrosion Mechanisms to the Universities of Michigan at Dearborn and Ann Arbor; and (5) Recycling of Creep-Resistant Alloys to Case Western Reserve University and CANMET.

Future Direction

- Complete casting, machining, and sub-assembly of magnesium components, with documented machining observations for each of the magnesium components to comprehend any potential differences between the chosen magnesium alloys and aluminum.
- Excise specimens from cast magnesium engine components and test to create an excised-specimen property database of the three selected magnesium alloys, which will complement the cast-specimen database completed during Phase I.
- Complete assembly and dynamometer testing, teardown, and analysis of the magnesium-intensive engines.
- Input data from all stages of the manufacture of the die-cast oil pan and front engine cover and the sand-cast cylinder block into the cost model to determine the cost-effective performance of the magnesium-intensive engine.
- Continue monitoring and reviewing the five basic research projects to their respective completion dates.
- Deliver final reports for the project by June 30, 2006.

Introduction

Since launch in 2001, the Magnesium Powertrain Cast Components (MPCC) project team has been working toward the ultimate goals of determining and then demonstrating the readiness of magnesium (Mg) alloys to be used to reduce the mass of automotive powertrains. The project team exceeded their 15% mass reduction target for the Mg-intensive engine, selected alloys for each Mg component, and completed the engine component design revisions using the respective properties for each selected Mg alloy. In FY 2005 the following milestones were accomplished: (1) tooling for each of the four Mg engine components was designed and built, (2) initial casting trials were completed and good progress was made to achieving sound parts for both engine testing and the excised specimen database, and (3) all five research projects in the critical areas, as identified by the project team, were launched. In addition, good progress was made developing the bore treatment for the cylinder block and for selection of the coolant to be used during the engine dynamometer testing.

The Magnesium Engine Components

The magnesium-intensive V-6 engine design was based on the aluminum 2.5/3.0L Ford Duratec engine. The final design (using the selected alloy properties for each component) resulted in overall mass reduction that significantly exceeded the original 15% target set by the MPCC project team. The major MPCC project activity in FY 2005 was to design and build tooling for casting each of the four magnesium components. This was accomplished and casting trials of all of the components were begun, with varying degrees of success. Nevertheless, it is expected that all of the parts will be cast and machined within the timing required to begin engine testing.

Cylinder Block: The Australian Magnesium Technologies alloy SC-1, a sand-casting alloy, was selected for this component. Prior experience (MPCC Project Phase I) with this alloy indicated that it would be necessary to use low-pressure casting, rather than gravity casting to produce sound parts. When it became apparent that neither Eck nor Denison Industries had the capability to do this, the project team contracted Fonderie Messier (a division of Honsel) to cast the cylinder blocks. The gating design was developed using casting simulations by MAGMAsoft and EKK. The tooling was designed and built by Becker CAD CAM CAST. The use of thermocouple-instrumented molds to validate the gating design and the solidification behavior of the castings also contributed to the rapid progress that Fonderie Messier is making.

Fonderie Messier cast the block pan rail up in a completely closed system to enable mold purging. Chills and crank-bore inserts were incorporated into the mold and the inserts were successfully cast-in-place. Excellent insert/Mg interface integrity was observed and this integrity was maintained even after heat treating. Some porosity has occurred in the thick regions of the casting but this is being addressed by use of chills and additional risers.

Figure 1 shows the as-cast block from which the risers and gating having been removed.

Structural Oil Pan: The Mg alloy chosen for this component was Dead Sea MRI 153M. The major changes to the final design of this component were made to address "noise, vibration, and harshness" (NVH) issues, particularly with respect to the sump area of the oil pan; see Figure 2. It is required that the Mg-intensive engine equal the performance of the Al engine. Accordingly, the NVH concerns were addressed by adding ribs to increase stiffness. In other areas of the casting, material was removed to minimize mass, generally reducing the wall thickness from 3.5 to 2.5 mm.

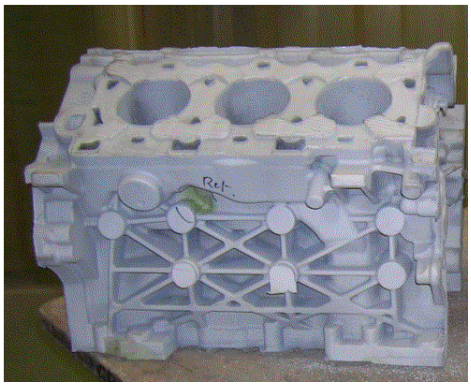


Figure 1. The Mg cylinder block, as cast at Fonderie Messier.

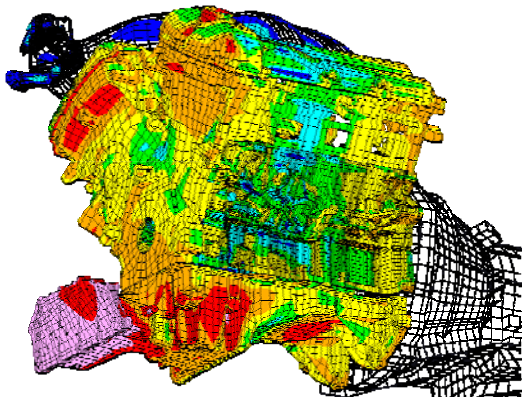


Figure 2. NVH analysis of the Duratec engine. Note the acoustic intensity of the oil pan sump.

The tooling for this high-pressure die casting was designed and built by HE Vannatter and the gating was designed by Spartan LMP using the simulations done by Technalysis. Unfortunately, the oil pan has been very difficult to cast for the following reasons: the complex geometry of this component, in particular, the sump and the slides needed; the arrangement and size of the ribs; and the solidification behavior of the alloy. As a result, the die has been evolving over the course of several casting trials. These changes include increasing the wall thickness in critical areas and changing the number of ribs, their locations, and sizes. Castings are being made, but these will require repair for hot cracking, so further die changes are being considered.

The cover for the sump will be a friction-stir-welded (FSW) plate. The use of FSW enables further mass reduction and part simplification by eliminating the attaching bolts. FSW will be done by Hitachi-North America.

Front Engine Cover: The major redesign focus of this component, like that of the oil pan, was NVH performance. Interestingly, the NVH model predicted that wall thinning will not adversely affect NVH performance if additional ribs are used in critical areas.

The alloy chosen for this part is Dead Sea MRI 230D even though the creep resistance of this alloy is greater than needed for the application. The MPCC team did this because they wanted to evaluate a very-high-creep-resistant alloy in anticipation of a high-pressure die-cast (HPDC) cylinder block. In this sense, the front engine cover is serving as a surrogate for the HPDC cylinder block. The tooling for the front engine cover was designed and built by EXCO and Extech. The casting was done by Intermet. The cast parts showed some hot cracking. As was done with the oil pan, preventing hot cracking required increasing the gate area, fine tuning of the shot profile, and reducing the dwell time. Also, radii were softened and texturing was used to facilitate metal flow. The castings are currently being leak tested and sorted for delivery to the machining site. The front engine cover is shown in Figure 3.

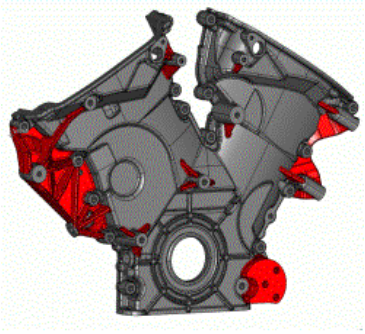


Figure 3. The Mg front engine cover.

Rear Oil Seal Carrier: The Mg version of the V-6 engine requires the use of a rear oil seal carrier, as shown in Figure 4. The Thixomat thixomolding process was used to achieve this near-net-shape part. The alloy chosen is Dead Sea MRI 153M, the same alloy as being used for the oil pan. As a result of the first casting trials, some changes to the die are being made and parts are expected to be ready when required.

Engine Bore Development

The Al Duratec engine uses iron liners in the cylinder bores. Iron bores were not considered for the MPCC Mg engine; instead, the project team chose to develop a spray-deposited, wear-resistant bore coating. This approach will save mass, enable better heat transfer, and improve block stiffness by allowing thicker bore walls. Thicker walls will reduce bore distortion and provide greater flexibility with respect to designing for creep management and head-gasket sealing. Two deposition processes and a range of surface preparations are being evaluated.



Figure 4. The Mg rear oil seal carrier.

The ASTM C-633 adhesion test has been used to screen the coatings using Mg blocks that were cast in Phase I of the project. The adhesion results have been excellent. A specification for maximum porosity on the bore surfaces to be coated has been incorporated into the requirements that Fonderie Messier has for the cast cylinder blocks. Additional development work will proceed as soon as the prototype blocks have been provided.

Engine Coolant

Four coolants were tested in Phase I for hot-surface corrosion (ASTM D4340) and galvanic corrosion (ASTM D1384) with each of the HPDC and sand-casting alloys. Since selecting SC-1 for the cylinder block, each of the coolant suppliers has been working to improve their coolants with respect to this alloy. Corrosion testing of the new coolants is being done to identify the coolant to be used in the engine dynamometer tests.

An additional coolant test was introduced during Phase II. This test, based on the ASTM D1384 test for galvanic corrosion, was developed by Victor Reinz to determine the durability of the Mg in the vicinity of the head gasket. In this region, an "electrolytic cell" has been created by the system, which comprises the stainless steel head gasket, the Mg cylinder block, the aluminum cylinder head, and the coolant. The sample configuration for this test is shown in Figure 5. The concern being addressed by this test is whether or not transition metals from the gasket will plate out on the Mg, where they will act as cathodic centers and lead to pitting corrosion.

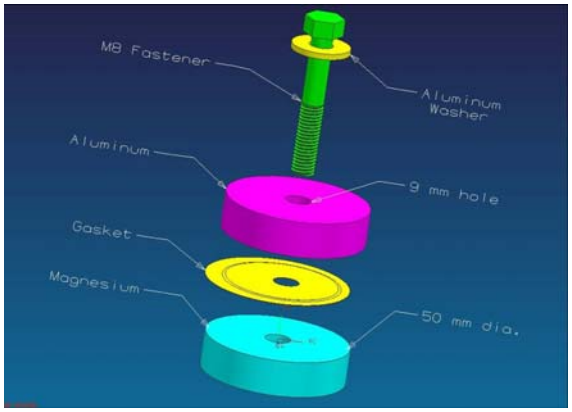


Figure 5. Head-gasket corrosion test assembly.

Test results show that pitting does occur with some metal-coolant combinations. Further testing will be done with the advanced coolants. In addition, coolant samples will be taken during the engine dynamometer tests to detect any corrosion and breakdown, if it occurs.

Engine Dynamometer Test Program

Engine testing is the ultimate measure of the technical readiness of Mg for powertrain applications. The test program was developed to validate the engine design model and its predictions about the durability and NVH performance of the engine. These tests will also help to verify that the selected alloys can be used in production engines. The test program and supporting statement of work were completed and a request for quotes yielded five quotes.

Seven tests comprise the program: (1) hot scuff, (2) cold scuff, (3) deep thermal shock, (4) high speed durability, (5) key life thermal, (6) long-term engine system, and (7) piston-skirt marking. Full engine disassembly and teardown analysis will be performed subsequent to all tests.

Critical Scientific Needs for Powertrain Magnesium Alloys

During Phase I of the project, numerous gaps in the technical understanding of Mg alloys and/or processing were identified and documented. These gaps were determined to be critical for future applications of Mg to automotive powertrains. It was an original objective of the MPCC project to identify such gaps and to either start new or expand existing research in North America that addressed these gaps. The procedure for accomplishing this has been described in the 2004 Progress Report. Five projects were launched in FY 2005.

Computational Thermodynamics and Alloy Development of Magnesium Alloys: Funding was awarded to Z.K. Liu at Penn State University to develop first-principle models for incorporation into computational thermodynamics databases. These models will be used to predict phase equilibria in critical alloy systems including magnesium-aluminum-calcium and magnesium-calcium-tin. Key aspects of this project are the sharing of data and experimental verification of the phase equilibria predictions. The collaborative group has been expanded to include researchers at the University of Michigan at Ann Arbor, the University of Wisconsin, and the Technical University of Clausthal. This interaction is already providing critical review of the Penn State University predictions and the sharing of data is benefiting research collectively and independently.

Hot Tearing Behavior of Magnesium Alloys

Funding for this project was awarded to D. Emadi at CANMET-NRC. His objective is two-fold: (1) to optimize an experimental system for quantifying the hot-tearing susceptibility of Mg alloys and (2) to determine the microstructural basis for hot tearing in these alloys. Hot tearing is related to the solidification behavior of the alloy and the tendency of a particular alloy to hot tear has a large impact on its castability and the economics of the casting process. Hot tearing has been an issue for each of the components that have been cast in the MPCC project, though in most cases it has been addressed successfully.

Creep, Bolt Load Retention, and Microstructural Analysis of High Temperature Magnesium Alloys: This project was awarded to W. Jones et al., at the University of Michigan at Ann Arbor. Creep is perhaps the single most important requirement for Mg alloys if they are to be used in powertrain applications. Creep is the slow plastic deformation of a material subjected to sustained load at high temperature. The research team will be developing mechanistic models for creep and seeking the microstructural basis for the observed creep rates.

Evaluation of Magnesium Corrosion by Various Methodologies and Surface Composition of Magnesium Alloys by Rutherford Backscattering: The first phase of this project was begun at the University of Michigan at Dearborn under the leadership of P.K. Mallick. In this phase, all of the high-temperature Mg alloys considered in the MPCC project were corrosion tested using several different methodologies. The differences observed among the methods were documented and extensive research has been conducted to explain those differences on the basis of the operating corrosion mechanisms. In the second phase of the work, Rutherford Backscattering (at the University of

Michigan at Ann Arbor) will be used to study the corrosion interface to further reveal the microstructural basis for Mg corrosion. The results of this work will contribute to the development of improved alloys and/or improved corrosion mitigation strategies.

Fluxless Recycling Methods and Process Control for Creep-Resistant Magnesium Alloys: Funding for this project was awarded to D. Schwam at Case Western Reserve University and E. Essadiqi at CANMET-NRC. Recycling of current automotive Mg alloys is generally well understood. However, the new alloys, those that have the necessary creep resistance for powertain applications, contain additional alloying elements such as calcium, strontium, tin, and rare earths. These elements are not amenable to current flux-based recycling methods because they react with the flux. The significance of this on the practice and economics of recycling has yet to be determined. The first phase of this project will be to conduct an in-depth survey of the industry and the scientific literature to determine the scientific and technical barriers to recycling and the progress made to date to address them. The second phase of the work will be research to further overcome the identified barriers.

Conclusions

The MPCC Project has made excellent progress since its inception in 2001. The science and engineering property database for the high-temperature, creep-resistant magnesium alloys which was developed after extensive casting and testing has been combined with the Structural Cast Magnesium Development and the Design for Product Optimization databases of ambient-temperature alloys and is being readied for joint distribution to the respective project teams. The MPCC properties enabled revised engine component designs and the design and build of the tooling to cast the components. Casting is ongoing and it is expected that testing of assembled engines will begin in mid-FY 2006. Documentation of the engine design and cost model to predict cost-effective performance of the Mg-intensive engine and the engine tests will be completed in 2006. The basic research projects begun in FY 2005 will continue beyond the engine test part of the MPCC project into 2007 and, along with successful engine testing, represent the legacy of the MPCC project.

Acknowledgements

The success of this project is due to the dedicated efforts of a large number of team members, in particular, the author's colleagues at Ford, DaimlerChrysler and General Motors. The many other companies and organizations making up the project team were listed in the FY 2003 Progress Report. However, the author would like to acknowledge the MPCC core team for their work: John Allison, Joy Hines, and Robert McCune from Ford; Randy Beals and Lawrence Kopka from DaimlerChrysler; Larry Ouimet, James Quinn, and Grant Tappen and William Miller from General Motors; and Peter Ried from Ried and Associates. The continuing support of our respective companies and the U.S. DOE is gratefully acknowledged.

Presentations/Publications/Patents

1. "Light-Weight Magnesium-Intensive Engine Developments," published in the 2004 FreedomCAR Highlights.
2. "Overcoming the Barriers to the Magnesium-Intensive Engine," B.R. Powell, presented at the joint meeting of the Ohio and Mid-Western Sections of the American Foundry Society and the American Society for Quality Control, Bowling Green, Ohio, February 2, 2005.
3. "The USAMP Magnesium Powertrain Cast Components Project," B.R. Powell, L.J. Ouimet, G.K. Tappen, J.E. Allison, J.A. Hines, R.C. McCune, R.S. Beals, L. Kopka, and P.P. Ried, presented at the 16th Annual Magnesium in Automotive Seminar of the International Magnesium Association, Livonia, Michigan, March 17, 2005.
4. "The USAMP Magnesium Powertrain Cast Components Project: Testing the Magnesium-Intensive Engine," B.R. Powell, L.J. Ouimet, G.K. Tappen, J.E. Allison, J.A. Hines, R.C. McCune, R.S. Beals, L. Kopka, and P. P. Ried, presented at the Magnesium Technologies session of the 2005 Society of Automotive Engineers World Congress, Detroit, Michigan, April 11, 2005.
5. "The USAMP Magnesium Powertrain Cast Components Project: Testing the Magnesium-Intensive Engine," B.R. Powell, L.J. Ouimet,

G.K. Tappen, J.E. Allison, J.A. Hines, R.C. McCune, R.S. Beals, L. Kopka, and P. P. Ried, presented at the Achieving Lightweight Vehicles session of the 2005 Society of Automotive Engineers World Congress, Detroit, Michigan, April 14, 2005.

6. "The USAMP Magnesium Powertrain Cast Components Project: Testing the Magnesium-Intensive Engine," B.R. Powell, L.J. Ouimet, G.K. Tappen, J.E. Allison, J.A. Hines, R.C. McCune, R.S. Beals, L. Kopka, and P. P. Ried, presented by R.S. Beals at the 62nd International Magnesium Association International Congress in Berlin, Germany, May 24, 2005.
7. Magnesium Powertrain Cast Components Project," B. R. Powell, presented at the AMD Board Casting Off-Site, USCAR, Southfield, Michigan, September 29, 2005.
8. A patent application is in preparation.

I. Ultra-Large Castings of Aluminum and Magnesium

Principal Investigator: Michael H. Maj
Ford Motor Company
Research and Advanced Engineering
2101 Village Road
Dearborn, MI 48121
(313) 337-6700; fax: (313) 390-0514; e-mail: mmaj@ford.com

Project Administrator: Thomas N. Meyer, Ph.D.
TNM Contract Engineering and Consulting Services
3987 Murry Highlands Circle
Murrysville, PA 15668
(724) 325-2049; e-mail: TNMENG@aol.com

Technology Area Development Manager: Joseph A. Carpenter
(202) 586-1022; fax: (202) 586-1600; e-mail: joseph.carpenter@ee.doe.gov
Field Technical Manager: Philip S. Sklad
(865) 574-5069; fax: (865) 576-4963; e-mail: skladps@ornl.gov

---

Contractor: U.S. Automotive Materials Partnership
Contract No.: FC26-02OR22910

Objective

Assess the manufacturing feasibility, economics and mass-reduction potential of thin-wall structural castings of aluminum and magnesium applied to automotive weight reduction.

Project Approach

The Ultra-Large Casting (ULC) project builds on the findings of a U.S. Department of Energy-funded contract to the American Foundry Society (Project ORNL-12401) which benchmarked various casting processes to assess their suitability for manufacturing large light-metal castings. Based on this background work and continuing research, the ULC project approach is listed below.

- Further describe and substantiate the rationale for using light-metal castings in place of conventional stamped and welded steel automotive body structures to reduce vehicle weight.
- The project will be executed in two concurrent phases. *Phase I* is focused on process selection and capability analysis. Pha*se II* is focused on designing, analyzing, producing and testing a "real-world" vehicle application that meets the ULC Team's ultra-large-casting criteria.
- The main objective for *Phase I* is to utilize the selected processes to improve the quality of cast components vs. conventional casting processes by achieving a more homogeneous distribution of properties while demonstrating consistent and predictable mechanical properties having improved strength and ductility.
- The major tasks for *Phase I* consist of part design, flow and solidification modeling, tool design/analysis/fabrication, correlation with casting trials, material characterization, process capability studies and an economic analysis.
- The main objective for *Phase II* is a “Real-World” application of an Ultra-Large Casting that will demonstrate a mass reduction of 40% - 60% at a competitive cost compared to conventional steel

construction. Additionally, it is desired to demonstrate parts consolidation, reduced investment cost in tooling and dies and improved energy absorption.

- The major tasks supporting Phase II are FEAs for static, durability, noise-vibration-harshness (NVH) and crash analyses; system-level and full-vehicle prototype fabrication; durability testing; dynamic crash testing; and an economic analysis.

Accomplishments

Since October 1, 2004 the following has been accomplished:

- Selected THT Sub-Liquidus Casting (SLC) and Thixomolding for process capability evaluation. While SLC focus will be on aluminum, it is also possible to cast magnesium. Thixomolding is limited to magnesium.
- Industry participants selected. COSMA, a division of MAGNA International, through MAGNA's PROMATEK Research Center, will demonstrate the THT SLC process on their 1000-ton THT casting machine. G-MAG, another division of MAGNA, will demonstrate Thixomolding while applying hot-runner technology on a 1000-ton Husky Thixomolding machine. Husky Injection Molding Systems, Ltd. will support G-MAG with access to their 1000-ton machine and necessary hot-runner technology.
- Ford conducted a preliminary cost study that indicates the economics of ultra-large cast structural parts are competitive with conventional stamped steel automotive structures.
- A "test part" has been designed that embodies the geometric elements and manufacturing challenges that will be encountered in a much larger component**.** This part will be used to evaluate the capabilities of the SLC process. A "real world" part targeted for implementation on a Ford vehicle program will be used to evaluate the capabilities of the Thixomolding process.
- Detailed statements of work have been developed with major purchase orders issued to both Promatek and G-MAG to cover test-part design, flow and solidification modeling, tool design and tool construction.
- Flow and solidification modeling of the test part is in progress under a subcontract to Promatek. Modeling has been subcontracted to EKK and Hitachi by G-Mag.
- Design geometry/solid modeling for the "real-world" part is nearing completion. Preliminary FEA studies for static crash, dynamic crash, and durability analyses have been completed by Ford.
- A newly developed manufacturing process, Ablation Casting, appears to be adaptable and scalable to potentially produce high-quality ULCs. A purchase order to Eck Industries has been issued to produce a “test part” geometry very similar to that pursued by MAGNA/Promatek. These parts are scheduled for production near the end of 2005 and will be evaluated by the ULC Team.

Future Direction

The ULC Team will continue toward its ultimate goal of demonstrating how light-metal cast body structural parts can provide a 40% to 60% weight reduction at a competitive cost compared to today's conventional stamped steel approaches. The weight reduction is certainly achievable. The key is to have a robust process to produce such parts. The immediate focus of the ULC team is to assess the capabilities of SLC and Thixomolding, which are semi-solid die-casting processes. It may, however, become necessary to change direction and explore other manufacturing processes if insurmountable difficulties arise that inhibit attaining desired casting mechanical property levels or inhibit process scalability. Therefore, if other suitable processes are identified and appear to have potential, the ULC team will consult the AMD Board of Directors to request modifications to the project scope, timing and funding.

The Rationale for Ultra-Large Castings

The majority of mass-market automobile and light truck body structures are constructed of sheet metal stampings fastened together with resistance spot welding. This method of construction tends to increase the weight of the body because it introduces structural redundancies. For example: an outer panel requires an inner panel for stiffness, which in turn might require local reinforcements. The casting process enables all of these structural elements and features to be integrated into a single piece, and thus has the potential to significantly reduce weight. This logic is illustrated with the example in Figure 1 which shows how a multi-piece stamped steel liftgate inner structure could be integrated into a single casting. There are numerous examples in the industry literature to be cited, however, the basic justification for ultra-large castings (ULCs) is the ability to *reduce cost* by integrating components and *reduce weight* by taking advantage of the casting process to eliminate structural redundancies and additionally using lower density material such as magnesium or aluminum. A comprehensive, definitive case study comparing a true structural casting to conventional multi-piece stamped and welded construction has yet to be completed. Such a case study is essential for substantiating the rationale for ULCs and will be undertaken by the ULC Team.

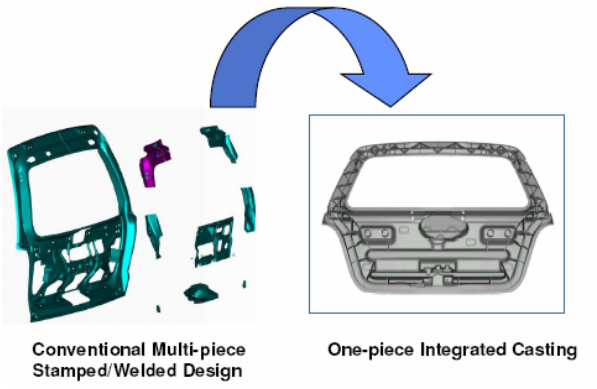


Figure 1. Single casting integrated from a multi-piece stamped steel liftgate inner structure.

Existing Applications of Large Light-Metal Castings

There are many examples in the industry of what are considered ultra-large castings such as die-cast magnesium instrument panel structures, seat structures, closure inner structures, etc. However, it is more appropriate to describe these applications as quasi-structural because they are not totally integrated into the body structure. These quasi-structural components demonstrate the light-weighting potential of large castings replacing conventional stamped steel structures.

A notable example of an ultra-large structural casting is the current Ford F-150 radiator support structure shown in Figure 2. It is a one-piece, thin-walled magnesium casting that replaces seven major stamped steel parts for a 25-pound weight saving. It is integrated into the body structure where it contributes to torsional stiffness and plays a role in crash.



Figure 2. An example of an ultra-large structural casting.

If applications of ultra-large structural castings like the F-150 radiator support and other large quasi-structural parts already exist, why is there a need for an Ultra Large Casting project? Because these particular components are manufactured using the conventional High-Pressure Die Casting (HPDC) process, which has some inherent limitations in achieving consistent mechanical properties.

Current Manufacturing Processes

The F-150 radiator support and most large quasi-structural automotive magnesium castings are manufactured with the HPDC process. While they perform adequately in many applications, HPDCs may not be suitable for other primary structures like pillars, rails or bodysides that have to manage large amounts of crash energy. HPDCs of magnesium lack the level of ductility and other desirable mechanical properties for these structural applications. Therefore, further uses of magnesium HPDCs beyond today's applications are limited by the process capabilities and by the mechanical properties achievable with conventional die-casting. Although premium vacuum HPDC's of aluminum are utilized for large structural components, costs are not competitive with conventional steel assemblies. Modest properties are achieved with solution heat treatment and this requires a costly dimensional management process. Current premium aluminum structural HPDC parts are relatively expensive.

Utilizing a relatively simple process such as HPDC to make structural parts is highly desirable by the industry. Unfortunately, the presence of porosity in magnesium HPDCs has a detrimental effect on mechanical properties. A plethora of countermeasures have been developed to combat porosity (and other shortcomings) of the HPDC process by introducing into the process vacuum, non-turbulent filling of the shot sleeve and "squeezing" during solidification. There are also expensive specialty heat-treatable alloys that are used along with one or more of the countermeasures to lower porosity levels. In spite of these enhancements and spin-off HPDC-based processes, HPDCs continue to be plagued by porosity and non-uniform mechanical properties. This inhibits the wide use of HPDCs as primary structural parts. Besides porosity and non-uniform mechanical properties, adapting HPDC to ultra-large castings presents other challenges, such as low yield. In some cases, over 50% of the shot weight consists of biscuits, runners and overflows. This has an effect on economics, especially for magnesium die castings since magnesium is not able to be recycled in-process. As casting size increases, runner systems become larger and more complex, increasing tooling cost and necessitating the use of larger tonnage die-casting machines. This significantly increases the cost of capital equipment.

Alternatives to HPDC.

An attempt to demonstrate production feasibility of ultra-large, thin-wall structural castings to achieve weight reduction at competitive costs resulted in a major effort by Alcoa and DOE[1] in the late 1990's. A novel, low-pressure, multiport, hot-chamber injection process was pursued but technical difficulties arose relative to the metal-injector system. Alcoa regarded the ULC market to be futuristic and elected not to direct additional funds and resources to address the technical issues. At the 1999 end of this three-year effort by Alcoa and DOE, a number of minivan inner panels were cast for evaluation; a panel is shown below in Figure 3. This is a single casting that replaces an assembly of 11 stampings. However, DOE, working with the AFS, continued to pursue ULCs. As a result, two documents [2,3] demonstrating the potential value of ULCs were produced. These studies showed that ultra-large components could be produced at costs competitive with steel structures for vehicles in the range of 70,000 units per year. At the higher volumes, traditional steel stampings become more cost attractive. The primary difference for the volume transition is the lower tooling costs associated with castings versus tooling required for stampings and subsequent assembly.

In addition to an economic impact of ULCs, a complete life-cycle energy analysis indicated that such structures of aluminum will ultimately provide an overall reduction in energy required for transportation. A similar analysis for magnesium is likely to yield the same conclusion.



Figure 3. A single casting that replaces an assembly of 11 stampings.

The efforts by AFS and DOE identified candidate processes suitable for ULC's and these included:

a) multiport hot-chamber injection at pressures compatible with typical permanent-mold systems;
b) Single gas plenum driving metal to fill a ULC permanent mold;
c) the Brocast process (France) utilizing gas-driven metal for filling, pressures up to 15 bars, vacuum levels to 50 mbars producing both magnesium and aluminum alloy castings;
d) the THT Inc., sub-liquidus casting process, "SLC," to produce aluminum castings via a semi-solid process;
e) the Thixomolding process to form magnesium solids into quality cast components in a semi-solid process without having to handle molten magnesium.

Fundamental technical challenges need to be resolved in a) and b) above. Both economic and technical issues are present in the Brocast process (i.e., item c) above. Casting hardware and technology is rapidly emerging for the last two processes, d) and e), and these were selected for demonstration of ULC technology. THT's SLC process is a system that is compatible with the use of multiple injectors. In addition, the process has been shown to produce castings in a T5 temper having properties approaching those requiring a full solution heat treatment (e.g., T6). It has long been concluded that thin-wall aluminum ULCs must be used in an "as-cast" condition or a T5 condition. The high costs due to dimensional management (i.e., straightening) associated with solution heat-treatment process must be avoided. Finally, small magnesium automotive structural parts are now manufactured utilizing the Thixomolding process. Recently, hot-runner technology has been developed and demonstrated by Husky. The combination of larger available machines (e.g., 1000 ton and greater) coupled with hot-runner technology makes the Thixomolding process a very attractive candidate for producing ULCs.

The ULC Project picks up where the AFS/DOE benchmarking left off by seeking to evaluate the potential of SLC and Thixomolding processes to produce ULCs. Both of these processes involve semi-solid metal (SSM) casting. SSM has been practiced across the U.S. for approximately 35 years. Several advantages of the SSM process include:

- product complexity, close dimensional tolerances, near net shape, thin walls and excellent surface finish compared to conventional die castings;
- exceptional soundness -- in most cases SSM castings contain less than 0.1% porosity, better than any other mass production casting process;
- ability to utilize a variety of alloys;
- low process temperature resulting in short cycle times and low stress on tooling;
- ability to undergo a T-5 heat treatment without losing ductility. This allows the castings to achieve required mechanical properties without the dangers of blistering, distortion or quench stresses associated with the full T-6 heat treatment required of other structural casting processes.

The SLC Process

The SLC process[4] is the latest approach to SSM casting, developed by THT Presses, Inc., Dayton, Ohio. The SLC process uses normal foundry ingot, primary or secondary, and requires no processing equipment extraneous to the casting machine or processing time outside of the normal die-casting cycle. SLC is suitable for casting both aluminum and magnesium.

The SLC machines (See Figure 4) have a vertical shot and a horizontal die-parting configuration. While the machine is somewhat smaller, it offers an equivalent shot capability of a larger, more conventional machine. Also, because of their unique shot sleeve and piston design (See Figure 5), the machines are capable of larger shots than machines of higher tonnage.

The SLC process employs a large-diameter, short-stroke approach. This feature allows for larger shots and enables tight control of the metal temperature

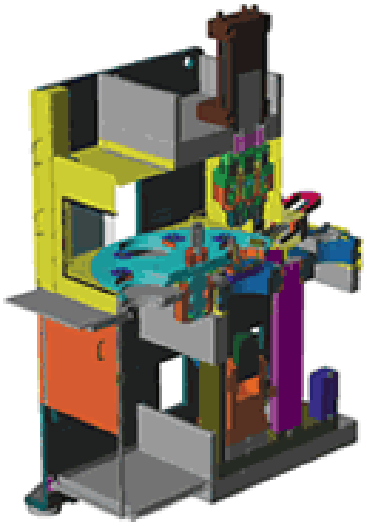


Figure 4. THT SLC casting machine.

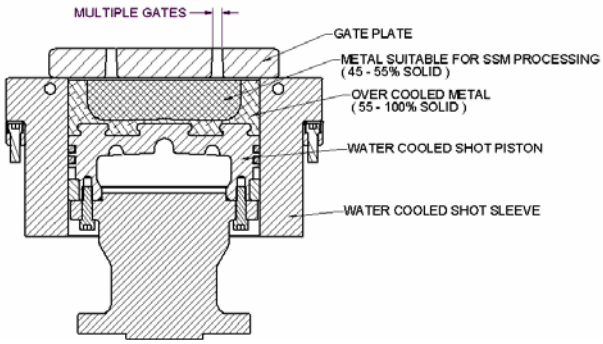


Figure 5. SLC shot sleeve.

required for SSM slurry processing. This reduces plunger speed necessity, drastically reducing impact pressures at the conclusion of each shot. This also provides the opportunity for multiple-cavity gating.

The indexing table feature enables pouring molten metal into a shot tube at one station, making appropriate temperature adjustments and achieving required slurry ripening, then making the actual shot in the next shot tube and removing the biscuit in the last station. Unlike other SSM slurry approaches, the SLC process requires virtually no slug pre-preparation equipment or processing time outside of the casting machine.

The SLC slot sleeve design (depicted in Figure 5) naturally provides both the time necessary in the semi-solid temperature regime to gain the globular structure desired and a major portion of the poured shot suitable to enter the die cavity (more than 60%). This all can occur within the normal machine cycle.

Suitable SSM structures can be achieved in the SLC process. When starting with normally grain-refined melt, the process provides globule sizes in the range of 75 microns. Mechanical properties achieved in castings from slurries are comparable to, and sometimes higher than, those realized from magnetohydrodynamics-stirred, billet-based SSM castings.

The Thixomolding Process

Another SSM casting variation is the Thixomolding process, which offers higher ductility magnesium castings with high strength and low wall thickness. Thixomolding combines conventional die-casting and plastic injection molding into a one-step process for the net-shape molding of magnesium alloys (See Figure 6).

The process requires no investment in molten-metal process and handling equipment and eliminates the safety hazards of handling molten magnesium. The injection system, which is similar to plastic injection molding machines, consists of a high-temperature screw and barrel coupled to a high-speed shot system that drives the reciprocating screw.

In the process (Figure 6), magnesium alloy feedstock is thermally processed by the rotating screw. The temperature is then raised to a semi-solid region and, after determining the desired temperature and shot size, is injected into a preheated metal mold. The screw is driven forward, filling the die cavity.

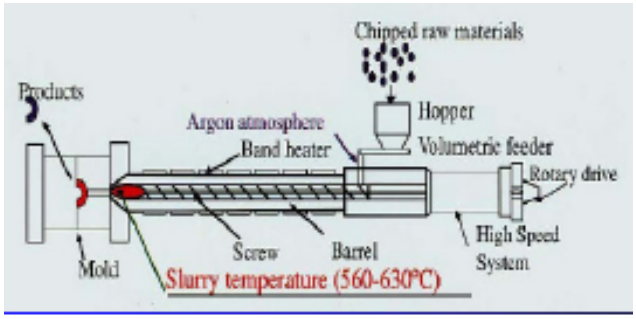


Figure 6. Thixomolding schematic.

The small amount of turbulence allows thixomolded components to have low levels of porosity and gives designers dimensional stability with precision and repeatability. Also, since the process does not require any external foundry or material handling, it is considered environmentally friendly.

Process Evaluation

The key component of Phase I is development of a test part that presents the fundamental challenges of an ultra-large, thin-wall casting and requires inexpensive tooling but produces **key process understanding.** After a number of meetings and discussions, the "test part" shown in Figure 7 resulted. This part includes options to gate at 1, 2, 3 or 4 locations. It enables flow lengths as great as 48" before forming knit lines. This gating provides significant flexibility in the testing. In addition, typical features characteristic of a structural component are included (e.g., ribs, steps, round bosses, "D' bosses, "C" channels, and "X" bracing). The target for nominal thickness is 2 mm but it is realized that this may need to be increased to as much as 3 mm for production of quality castings.

Simpler casting fluidity trials utilizing a constant thickness (2 to 3 mm) with uniform width (25 mm) will be the first action step in Phase I. The flow path will follow the same outline as the test part. Following the fluidity trials, materials characterization will be conducted prior to casting the test parts. The fluidity trial will provide the first comparison between computer process simulation and the actual results. Based upon these results, the



Figure 7. Test part geometry.

part nominal thickness will be selected and the test-part design finalized. The materials characterization will involve casting of components to assess mechanical and corrosion properties. Properties will include:

a) tensile
b) compression
c) Poisson's ratio
d) Modulus
e) Low-cycle fatigue
f) Microstructural examination
g) Toughness (K_{IC} and da/dN)

A much smaller number of these tests will be utilized to adjust the process in an attempt to optimize process conditions. For example, the conditions for part removal and quench will be evaluated with respect to mechanical properties.

During the materials characterization, a ring geometry will be produced that clearly produces a knit line. A test will be conducted to evaluate the quality of the knit line. In cases of failure, the fracture region will be evaluated relative to oxide content and general cause of knit-line failure.

Finally, approximately 20 to 25 castings will be selected at random during the production of over 200 cast test parts. Approximately eight locations will be selected for tensile, yield, and elongation evaluation in addition to conducting some microstructural analyses in at least two key areas of the casting. The Phase I effort evaluating only the SLC process will be conducted on the 1000-ton THT machine that was installed in late 2004 and now fully operational at the Promatek Research Center (Brampton, Ontario).

At this point, the test-part geometry will only be used to evaluate the SLC process using aluminum alloy. The same test part geometry could also be used to evaluate magnesium cast with the SLC process.

Evaluation of the Thixomolding process, which is much more mature than SLC, will focus directly on the "real world" vehicle cast part (Figure 8).

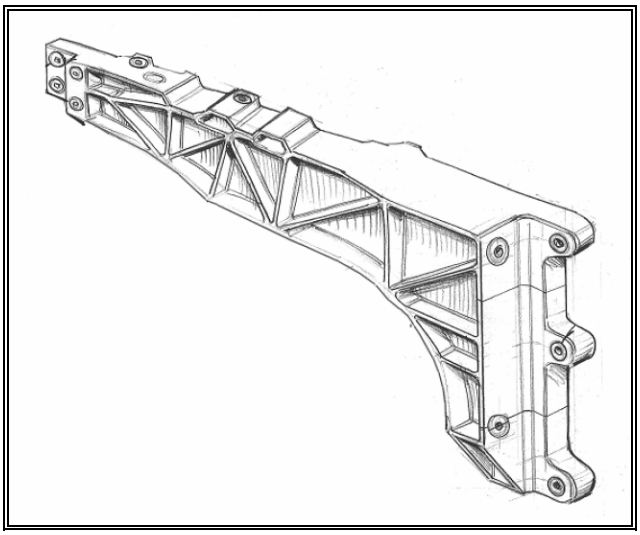


Figure 8. "Real World" application (shotgun).

Materials characterization will likely be based upon excised specimens from the cast vehicle parts.

"Real-World" Vehicle Application

It is important to demonstrate that the process knowledge gained can be applied to real-world vehicle light-weighting. The demonstration chosen by the ULC team is to replace the conventional multi-piece steel structure that forms the inner front fender—known in the industry as a "shotgun"-- with a single casting (See Figure 8).

While this particular component would not necessarily be considered "ultra-large", it embodies the geometric elements and manufacturing challenges that might be encountered in a much larger component, such as an entire body side. The shotgun application is of further interest to researchers because it is integrated (See Figure 9) into the body structure where it contributes to stiffness (which has durability and NVH implications) and plays a role in conducting and absorbing crash energy (See Figure 10).

Furthermore, the shotguns will attach to a radiator support that *is* an ultra-large casting in its own right. The end result of this study will be a front-end structure for large body-on-frame pickup or SUV constructed entirely of castings, demonstrating a weight savings of 50% to 60 % compared to conventional steel architectures.

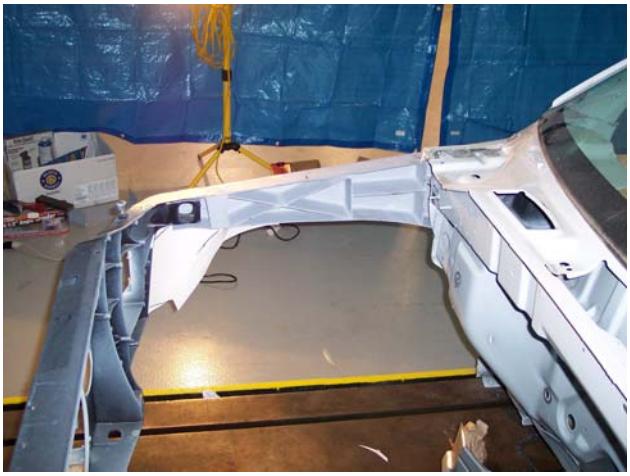


Figure 9. Cast shotgun is integrated with the body structure.



Figure 10. Shotgun must manage crash energy.

Conclusions

The ULC Project has made good progress since its October 2004 kickoff. Building on the foundation laid in the Joint AFS/DOE benchmarking study, the ULC Team has identified two emerging casting processes, Sub-Liquidus Casting and Thixomolding with Multiple Hot Runners. The Thixomolding process has the potential to produce low-cost large magnesium castings with mechanical properties much better than those achievable with High Pressure Die Casting (the industry's preferred process). The SLC similarly offers the potential to produce aluminum ULC parts having properties and production costs not achievable by premium vacuum die-casting processes. In addition to the fundamental research required to evaluate these emerging casting processes, the Team has developed a real-world automotive application that is targeted for an OEM vehicle program. In fiscal year 2006, the team expects to continue to assess the capabilities of SLC

and Thixomolding by analyzing parts produced by both processes.

Presentations and Publications

No publications or presentations have been made at this time.

References

1. Final Report 2000 April 28 Subcontract No. 86X-SU545C, Development of a Casting Process for Ultra-Large Automotive Components
2. AFS Project ORNL-ULC, July 16, 2002
3. AFS Project ORNL-ULC-II, July 30, 2003
4. "Sub Liquidus Casting (SLC) Process: Concept and Product," J. Jorstad, M. Thieman, R. Kamm, M. Loughman and T. Woehlke, 2003 AFS Transactions, No. 03-162.

J. Cost Assessment of Emerging Magnesium Sheet Production Methods

Principal Investigator: Darrell R. Herling
Pacific Northwest National Laboratory
P.O. Box 999, MS: K2-03, Richland, WA 99352
Ph: (509) 375-6905, Fax: (509) 375-4448, E-Mail: darrell.herling@pnl.gov

Technology Area Development Manager: Joseph A. Carpenter
(202) 586-1022; fax: (202) 586-1600; e-mail: joseph.carpenter@ee.doe.gov
Field Technical Manager: Philip S. Sklad
(865) 574-5069; fax: (865) 576-4963; e-mail: skladps@ornl.gov

---

Contractor: Pacific Northwest National Laboratory
Contract No.: DE-AC06-76RL01830

Objective

Magnesium has the highest specific stiffness and second highest specific strength of all structural metals. Because of this, there is an increasing global interest in using magnesium for structural components. A number of research activities are under way to develop approaches for producing magnesium sheet at the volume and cost levels demanded by automotive applications. The economics associated with some of these emerging yet promising technologies are unclear. The United States Council for Automotive Research (USCAR), in an effort to better understand the cost factors and potential for low-cost production, commissioned a study to develop a technical cost model on magnesium sheet production. The Aluminum Consultants Group, in conjunction with Pacific Northwest National Laboratory, prepared a technical cost model for magnesium sheet production alternatives.

Approach

In developing the cost model, options for producing magnesium sheet were identified and processing details studied. The model focuses on the two most commercially prominent continuous-casting processes, twin-belt casting and twin-roll casting. The design and data used in the model are largely based on information and experience with aluminum continuous casting, with anticipated modifications required for magnesium sheet production. Supplemental information specific to magnesium continuous casting was obtained from the literature and solicited directly from organizations involved in each of the processes. The model focuses on three primary elements: metal cost; casting process cost; and sheet rolling cost.

Accomplishments

For the continuous-cast magnesium sheet model, two “base cases” were developed to provide a starting point for subsequent sensitivity analyses. These two base cases used the same inputs for the metal cost and rolling cost elements, with a difference in the casting costs. The projected production costs for twin- roll and twin-belt casting of 1.5-mm-thick magnesium sheet are $1.97 per pound and $2.43 per pound, respectively. This compares to an industry-quoted price (including profit and overhead costs) of $4.50 per pound for magnesium sheet currently produced by conventional ingot metallurgy methods.

Future Direction

Though production costs for continuous casting are estimated to be significantly less than for conventional methods, to meet targeted performance properties, much still needs to be learned about processes. An increased understanding is needed of how alloy composition and process conditions produce the resulting microstructures. Modeling of continuous-casting processes has been a focus of research and can be applied to

magnesium alloys along with critical experiments. In addition, future research must establish the envelope of continuous-casting capabilities for magnesium, addressing aspects such as strip width, as-cast strip thickness, and casting rate and their effects on important issues such as segregation, cast grain structure, and surface quality. Underlying all of these studies is a better understanding of the relationship of alloy microstructure and sheet formability as well as other mechanical properties such as corrosion resistance, all of which are necessary for automotive applications.

Introduction

The growth of interest in and use of magnesium in automotive applications has been primarily in the area of cast components, similar to aluminum in the past. Because magnesium has the highest specific stiffness and second highest specific strength of any metal, there is an increasing global interest in extending its potential weight-saving opportunities into auto body and structural components. This would necessitate the use of formable magnesium sheet. Currently, little infrastructure exists for the production of magnesium sheets because its application in highly specialized uses such as photoengraving sheet is limited. Because of this limited production capacity and the inherent difficulties in thermomechanical processing of magnesium due to its hexagonal close-packed crystal structure, magnesium sheet prices are presently well above the levels that would be considered acceptable for automotive applications.

Worldwide activities are underway to develop approaches for producing magnesium sheet at the volume and cost levels demanded by automotive application. These approaches include efforts to better understand and improve the conventional processing of magnesium sheet via ingot-casting, hot-rolling, and cold-rolling methods, as well as some alternatives such as nearer-net-shape continuous-casting type processes.

The Materials Technical Team of the United States Council for Automotive Research (USCAR) sought to better understand the cost drivers of magnesium sheet production and the potential impact that alternative processing approaches could have. The Aluminum Consultants Group, in conjunction with the Pacific Northwest National Laboratory, prepared a technical cost model for magnesium sheet production alternatives. The results of this effort are the substance of this report. Specifically, the three objectives of this study were to:

- Provide a framework for understanding the primary cost elements for the production of magnesium sheet by conventional as well as alternative processing methods.
- Evaluate the effects of a range of potential values for key variables to identify the key cost drivers.
- Suggest areas of focus for research and development (R&D) activities based on these results.

Magnesium Sheet Cost Model

To begin to understand the main cost drivers and potential benefits of alternative processing routes for production of magnesium sheet, a technical cost model was developed. The model focuses only on the two most commercially prominent continuous casting processes, twin-belt casting and twin-roll casting, and does not directly address the technical cost elements of conventional magnesium sheet processing methods.

The design and data used in the model are largely based on information and experience with aluminum continuous casting, with anticipated modifications required for magnesium sheet production. The model focuses on three primary elements, specifically:

- Metal cost
- Casting process cost
- Sheet rolling cost.

A few caveats about the modeling approach are needed. First, this model is intended for scoping analysis only and clearly is not intended to be a rigorous modeling of production cost. Second, the model does not include profit considerations.

Within the framework of the model, the selection of input values to produce useful outputs is the next critical step. For the Continuous Cast Magnesium Sheet Model, two “base cases” were developed to

provide a starting point for subsequent sensitivity analyses. These two base cases used the same inputs for the Metal Cost and Rolling Cost components with a difference in the Casting Cost section. Specifically, a base case was developed for each of the two continuous casting processes of interest, twin-roll casting and twin-belt casting. In this section, values used for the base cases and the rationale for their selection are provided. Also, the output for a total cost per pound for magnesium sheet using the base case assumptions is provided.

For the base case, a standard product and desired production volume were selected. The values used were 1.5-mm(0.40 in)-thick x 1-m(40 in)-wide sheet at a production volume of 10,000 tons per year (tpy). The sheet thickness and width are considered of interest for automotive body panels, while the production volume represents a roughly 10x increase over the current sheet production volume by conventional processing.

Metal Cost Inputs

The base metal price input for the base case, using AZ31 alloy, was set using the prices of the individual constituents (Mg, Al, and Zn) at the June 2005 American Metal Market free-market price in proportion to their concentration in the alloy. The resulting input price used was $1.47 per pound. The recycle component is calculated from the assumed rolling recovery; in the base case, it is 25%.

Melt loss is assumed to be on the higher end of that typical for aluminum, although no specific data were found for magnesium. A value of 5% melt loss is used in the base case.

Casting Cost Inputs

Some inputs were common for both the twin-roll and twin-belt casting cases. The as-cast strip width was selected to be 48 inches to result in a 40-inch-wide sheet, accounting for edge losses during rolling. Variable costs per hour were established at $200 for both processes.

Twin-Belt Casting

For twin-belt casting, base case values were used that reflected lower range values for aluminum processing, adjusted only for the density differences between magnesium and aluminum. Thus, a continuous-casting productivity value for the base case of 700 lb/hr-in was used, which is roughly 0.7 times the lower-range value for aluminum twin-belt casting. Using this productivity value and assuming 6,720 hours of production time per year, a casting capacity of roughly 112,000 tons was calculated, which is consistent with reported values for casting capacity in the literature (Hamer et al. 2002). Adjustments were made to the number of operating hours per year to produce the required casting output.

Based on information obtained from discussions with a supplier of twin-belt casting equipment[(a)], capital cost for a unit consisting of a caster and associated in-line rolling stands is approximately $80 million, resulting in a fixed cost per machine of 15% of that amount. Because the required casting output for this base case is roughly 10% of the machine capacity, the fixed cost per ton is significantly higher than if the machine were producing at full capacity.

Twin-Roll Casting

For twin-roll casting, a continuous-casting productivity of 45 lb/hr-in was used, again representing roughly 0.7 times the lower end of the aluminum range. Based on this productivity, one casting machine is not adequate to meet the casting output requirement, necessitating two machines in the base case.

Again, information from a supplier of twin-roll casters indicated that a casting unit costs $6 million[(b)], and the fixed cost per machine is calculated accordingly. Using the base case production target level, two casting machines are operated near capacity. Along with their lower overall capital cost, this results in a lower fixed cost per ton for the twin-roll casting base case than for the twin-belt casting case.

---

[a] Peter Regan, Hazelett, personal communication with Gerald Cole, Lightweight Strategies LLC, February 2005.

[b] Chris Romanowski, FATA Hunter, personal communication with Gerald Cole, Lightweight Strategies LLC, February 2005.

Rolling Cost Inputs

For both base cases, an as-cast thickness prior to downstream rolling of 0.12 inches was selected, consistent with capabilities described in the literature for aluminum (Hamer et al. 2002, von Gal 2000). In twin-belt casting, this is actually not the true as-cast thickness but rather the as-cast thickness further reduced by the in-line rolling capability that is part of a twin-belt casting unit. In twin-roll casting, this is the true as-cast thickness. A reduction-per-pass value of 30% is used, which is in the mid-range of reports for warm rolling of magnesium in the literature (Liang and Cowley 2004, Park et al. 2004). A rolling cost/pass of $0.05 per pound was used based on information from discussions with suppliers[c]. It is somewhat higher than the cost for aluminum, recognizing in particular the need for heating prior to each pass. No specific assumptions were made regarding rolling speeds due to a lack of available data. Finally, a rolling recovery of 75% was selected for this base case.

Conclusions from Cost Modeling

Using the input values described above, the model was run to calculate the estimated cost for magnesium sheet produced by the twin-belt casting and twin-roll casting methods. Summary spreadsheets for the twin-belt cast and twin-roll cast base cases are provided in Tables 1 and 2, respectively. The results are tabulated in Table 3, and the percent of total cost for each element is shown in Figure 1. Estimated production cost for twin-belt and twin-roll continuous casting is $2.43 and $1.97 per pound, respectively.

For comparison, a price quote for the same sheet size and production volume was obtained from SCI, a subsidiary of Magnesium Electron Ltd., the producer of conventionally-rolled AZ31 sheet. The price quoted was $4.50 per pound. It is important to note that this is a price quote, including factors related to profit and capital recovery, while the model predictions are cost estimates.

Sensitivity Analyses

While the estimated cost values derived from the base-case assumptions are interesting and potentially useful alone, another purpose of creating the spreadsheet cost model is to allow assessment of the effects of changes in the values of input variables on the estimated cost with a goal of identifying the variables that are most sensitive. This information in turn can be used to determine the areas where further R&D would provide the most cost leverage. Four variables were the focus of sensitivity analyses based on their expected impact; specifically, metal price, annual sheet production volume, caster productivity, and rolling parameters of reduction per pass and rolling recovery. For each case, values of the variable of interest were changed while other base-case assumptions were held constant. The results for each analysis will be reviewed in turn.

Metal Price

Metal price can vary depending on the source of the alloy and market conditions. Two additional metal price values were examined besides the base-case assumption of $1.47 per pound. A value of $0.84 per pound was used as a lower bound assumption based on information that this is a typical price for AZ31 in Europe (AMM 2005). A higher value of $1.60 per pound was also examined based on historical data (Kramer 2004). Running the model with these variations results in the total cost per pound listed in Table 4. Because metal price is such a significant fraction of the total sheet cost, it is not surprising that changing the input metal price has a large effect on the estimated final sheet cost.

Annual Production Volume

While the production volume level of 10,000 tpy used in the base case is a significant increase over the volume of magnesium sheet now produced by conventional processing, it is still modest by automotive volume standards. Three higher values of annual production volume were analyzed, and the results are shown in Table 5.

Increasing annual production volume had the largest effect on the sheet cost produced by the twin-belt casting process, primarily through better utilization

[c] Chris Romanowski, FATA Hunter, personal communication with Gerald Cole, Lightweight Strategies LLC, February 2005.

Table 1. Base Case Results for Twin-Belt Casting

Base Case Twin-Belt Casting					
Metal Cost Input		**Casting Cost Input**		**Rolling Cost Input**	
Base metal price/lb	$1.47	Strip width (in)	48	As-cast thickness (in)	0.12
Recycle component (%)	25	Cont. casting productivity (lb/hr-in)	700	Final Thickness (in)	0.06
Melt loss (%)	5	Casting capacity/machine (tpy)	112896		
		Number of machines	1	Reduction per pass (%)	30
		Total casting capacity (tpy)	112896	Number of rolling passes	3
		Fixed cost/machine (per yr)	$12M	Rolling cost/pass	$0.05
		Fixed costs (per ton)	$900		
		Variable costs (per hr)	$200	Rolling recovery (%)	75
		Uptime (%)	80		
		Shifts per week	20		
		Weeks of operation	6		
		Operating hours per year	794		
Cost/finished/lb	$1.62	Cost/finished/lb	$0.61	Cost/lb	0.20
Total cost/lb					**$2.43**
		Casting output/(tpy)	13334	Annual production vol (tpy)	10000
		Under/over capacity (tpy)	99562		

Table 2. Base Case Results for Twin-Roll Casting

Base Case Twin-Roll Casting					
Metal Cost Input					
Base metal price/lb	$1.47	Strip width (in)	48	As-cast thickness (in)	0.12
Recycle component (%)	25	Cont. casting productivity (lb/hr-in)	45	Final Thickness (in)	0.06
Melt loss (%)	5	Casting capacity/machine (tpy)	7258		
		Number of machines	2	Reduction per pass (%)	30
		Total casting capacity (tpy)	14515	Number of rolling passes	3
		Fixed cost/machine (per yr)	$12M	Rolling cost/pass	$0.05
		Fixed costs (per ton)	$900,000		
		Variable costs (per hr)	$135	Rolling recovery (%)	75
		Uptime (%)	80		
		Shifts per week	21		
		Weeks of operation	46		
		Operating hours per year	6173		
Cost/finished/lb	$1.62	Cost/finished/lb	$0.15	Cost/lb	0.20
Total cost/lb					**$1.97**
		Casting output/(tpy)	13333	Annual production vol (tpy)	10000
		Under/over capacity (tpy)	1182		

Table 3. Results for Base Cases

Process	Metal Cost/Finished lb	Casting Cost/Finished lb	Rolling Cost/Finished lb	Total Cost/lb
Twin-Belt	$1.62	$0.61	$0.20	**$2.43**
Twin-Roll	$1.62	$0.15	$0.20	**$1.97**

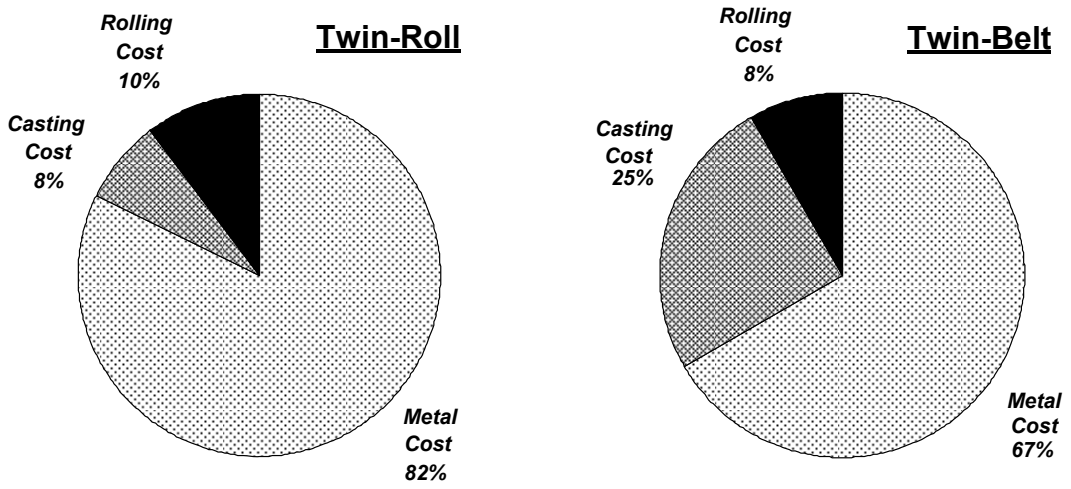


Figure 1. Percentage of total cost for each primary cost element

Table 4. Metal Prices

Metal Price/lb	Sheet Cost (twin-belt casting process)	Sheet Cost (twin-roll casting process)
$0.84	$1.73	$1.28
$1.47 (base case)	$2.43	$1.97
$1.60	$2.57	$2.11

Table 5. Annual Production Volume

Annual Sheet Production Volume (tons)	Sheet Cost (twin-belt casting process)	Sheet Cost (twin-roll casting process)
10,000 (base case)	$2.43	$1.97
20,000	$2.12	$1.94
30,000	$1.97	$1.92
60,000	$1.92	$1.92

of the higher production capacity of this process that is greatly underutilized in the base case. Only modest reductions in cost per pound for the sheet produced by the twin-roll casting process as a function of increased production volume are seen, provided by reduced variable costs per pound since capital utilization is already high.

Caster Productivity

In the base case, the assumption was made that the caster productivity would equal that of the lower end of the published range for aluminum on a density-compensated basis. However, there is no published information on continuous-casting productivity for magnesium sheet, and the possibility exists that caster productivity values could be higher or lower than that chosen for the base case. The effect of caster productivity was analyzed at two annual production volume levels for both of the continuous-casting processes.

For the twin-belt casting process, higher value of productivity equivalent to the high range of published values for aluminum on a density-compensated basis was used. On the lower side, an equal interval from the base case was studied on the assumption that magnesium continuous casting may have much lower productivity. The results are summarized in Table 6. The results in this table indicate that the overriding influence in the twin-belt casting process is not productivity but capital utilization, which is better at the higher production volume level.

For the twin-roll casting process, again a higher productivity value was used based on the published values for twin-roll casting of aluminum compensated for the difference in density for magnesium. Also a substantially lower productivity value was used to assess the effect of changes in the value of this variable. The outputs are shown in Table 7. For the twin-roll casting process-based product, sheet cost is reduced by increased productivity by less than 10% over the range of values examined with minor effects of production volume.

Rolling Process

Because the rolling process for magnesium sheet is reported to be more complicated and costly than aluminum, the sensitivity of sheet cost to variation in key rolling process variables was assessed. In this analysis, reduction per pass was varied from 20 to 50%, bracketing the 30% base-case value. Rolling recovery ranged from 50 to 90% to assess sensitivity. In this initial analysis, the low values of each variable were paired, as were the two high values. The results are shown in Table 8. Clearly there is a significant effect of rolling process parameters on final sheet cost over the range of values studied.

Direct Sheet Production

Recognizing the effect of rolling process costs and the potential sensitivity of cost to changes in the potentially realistic values for this process, another analysis was done using the extreme assumption that the continuous-casting processes could produce final thickness and width sheet without further rolling. We know that there are likely metallurgical aspects of the sheet structure that will require some finishing rolling process. Nevertheless, as a lower bound of sheet cost, a direct sheet processing route assuming 95% recovery of sheet from the metal input was determined. The results, calculated at two levels of production volume for each of the continuous-casting processes, are shown in Table 9. Elimination of the separate rolling process could have a significant positive effect on project sheet cost if technically feasible.

Summarizing the results of the cost modeling discussed above, the key conclusions are:

- Metal price is the key component for magnesium sheet price. It represents 66 to 82% of the total sheet cost in the base cases. Changes in metal price over a range of values representing differences in supply, source, and market conditions can result in as much as $0.83 per pound variability in the final sheet cost.
- For a continuous-casting process perspective, twin-belt casting was found to be very sensitive to assumed production volume in the range

Table 6. Caster Productivity--Twin-Belt

Caster productivity (lb/hr-in)	Sheet cost (10,000 tpy production volume)	Sheet cost (60,000 tpy production volume)
400	$2.43	$1.93
700 (base case)	$2.42	$1.92
1000	$2.42	$1.92

Table 7. Caster Productivity--Twin-Roll

Caster productivity (lb/hr-in)	Sheet cost (10,000 tpy production volume)	Sheet cost (60,000 tpy production volume)
20	$2.07	$2.01
45 (base case)	$1.97	$1.92
80	$1.93	$1.88

Table 8. Effect of Rolling Process

Reduction per Pass (%)	Rolling Recovery (%)	Sheet Cost (twin-belt casting process)	Sheet Cost (twin-roll casting process)
20	50	$3.07	$2.39
30 (base case)	75 (base case)	$2.43	$1.97
50	90	$2.19	$1.81

Table 9. Costs of Direct Sheet Production

Process	Sheet cost (10,000 tpy production volume)	Sheet cost (60,000 tpy production volume)
Twin-belt casting	$2.16	$1.66
Twin-roll casting	$1.70	$1.69

studied. Twin-roll casting was less sensitive. This is consistent with experience using these processes for aluminum, i.e., that twin-belt casting is best for serving large established markets with high volume requirements, while twin-roll casting is better suited to market development scenarios in which incremental buildup of volume is expected.

- Twin-roll casting is slightly more sensitive to changes in caster productivity than twin-belt casting, but final sheet cost is relatively insensitive to both. Effective use of the production capacity of the equipment has a stronger effect on sheet cost.
- Rolling process variables such as rolling reduction per pass and recovery have strong effects, with a variability of $0.58 to $0.88 in sheet cost over the range studied. Higher reductions per pass and rolling recovery, or even elimination of downstream rolling, would greatly reduce projected sheet cost.

Implications of Results on Magnesium R&D

A primary goal of the technical cost modeling exercise was to attempt to identify those factors that have the greatest influence on the projected cost of magnesium sheet as a potential driving force for technical development. This section discusses potential R&D directions.

Perhaps, as expected, the largest component of magnesium sheet cost in a scenario where alternate processing by continuous casting is used is the base metal price. While market factors will have the

primary effect on metal cost, its importance dictates that the lowest cost processes are those that maximize conversion of metal units into final sheet product. One recommendation in this regard is to produce the cast sheet as close to final sheet thickness as continuous casting technology and final product microstructure, property, and surface quality requirements allow. A second approach is to develop alloys and processing schemes that enable magnesium to be rolled with high reductions and minimal edge cracking. Of course, this latter suggestion, if developed, would benefit magnesium sheet produced by conventional processes as well. There are reports of research in this area by Deakin University in Australia, where they are exploring magnesium alloys with the potential for 90% cold reduction (Deakin 2005).

To meet the objectives of reducing the production cost of magnesium sheet while achieving the targeted performance properties, much needs to be learned about composition, structure, processing, and property relationships. With specific relevance to the continuous-casting process routes that have been the primary subject of this study, an increased understanding of how alloy and process conditions produce the resulting microstructures is needed. Modeling of continuous-casting processes has been a focus of research and can be applied to magnesium alloys, coupled with critical experiments. Beyond this fundamental understanding we must establish the envelope of continuous-casting capabilities for magnesium, addressing aspects such as strip width, as-cast strip thickness, and casting rate and their effects on important issues such as segregation, cast grain structure, and surface quality. Underlying all of these studies is a better understanding of the relationship of alloy microstructure and sheet formability as well as other mechanical properties such as corrosion resistance, all of which are necessary for automotive applications.

Magnesium sheet production R&D has been addressed on a worldwide basis over the past few years. Efforts on twin-roll casting are being carried out in Australia at CSIRO (Liang and Cowley 2004), in Korea (Park et al. 2004), and in Germany at Thyssen Krupp Stahl (AMM 2001). Generally, these efforts, based on reports in the literature as well as personal communication with representatives from the various organizations, are focused at the pilot-scale, producing strip widths in the 600- to 700-mm width range and exploring a range of conventional and less conventional alloys. Process development work is focused not only on the continuous-casting process itself but also downstream rolling.

No apparent work is being done on twin-belt casting of magnesium, although one producer has indicated that technical feasibility was established by Dow some fifty years ago[(d)]. This may be an area of interest due to the concatenation of the casting and hot-rolling steps in the process, which would seem especially well suited to magnesium sheet production. The large volume capability and resultant capital cost of twin-belt casters may be an impediment to actively pursuing this route until the magnesium sheet market becomes much larger.

A final area of potential R&D emphasis would be in development of the spray-rolling process for magnesium sheet. While clearly at a much more developmental stage compared with twin-belt and twin-roll casting, the unique features of this process may fit well with the requirements and limitations of continuously cast magnesium alloys.

Presentations/Publications/Patents

- W.H. Hunt Jr., "Technical Cost Model for Magnesium Sheet Production," presented to USCAR, Materials Technical Team, Southfield, MI, June 8, 2005.
- W.H. Hunt Jr. and D.R. Herling, "Cost Assessment of Emerging Magnesium Sheet Production Methods," PNNL-15368, Sept. 2005.

References

1. American Metal Market. July 5, 2001. "TKS Forms Company to Perform Magnesium Sheet Output R&D." http://www.findarticles.com/p/articles/mi_m3MKT/is_129_109/ai_76473393.
2. American Metal Market. June 2, 2005. "MB Europe free market price, magnesium." http://www.findarticles.com/p/articles/mi_m3MKT/is_30-3_112/ai_n6135784.

[d] Peter Regan, Hazelett, personal communication with Gerald Cole, Lightweight Strategies LLC, February 2005.

3. Deakin University. 2005. "Wrought Magnesium Research." Advanced Materials, Manufacturing, and Performance Group, School of Engineering, Deakin University. http://www.deakin.edu.au/engineering/research/ammp/?188.
4. Hamer S., B. Taraglio, and C. Romanowski. October 2002. "Continuous Casting and Rolling of Aluminum: Analysis of Capacities, Product Ranges, and Technologies." *Light Metal Age*, pp. 6-17.
5. Kramer, D.A. 2004. "Magnesium in the Third Quarter 2004." *Mineral Industry Surveys.* U.S. Geological Service, Washington, D.C. http://minerals.usgs.gov/minerals/pubs/commodity/magnesium/mgmis3q04.pdf
6. Liang, D. and C.B. Cowley. May 2004. "The Twin-Roll Strip Casting of Magnesium." *JOM*, pp. 26-28.
7. Park, S.S., J. Lee, H. Lee, K. Shin, and N. Kim. 2004. "Development of Wrought Mg Alloys via Strip Casting." *Magnesium Technology 2004.* The Minerals, Metals, & Materials Society, Littleton, Colorado, pp. 107-112.
8. von Gal, R. January 2000. "The Aluminum Sheet Mill for the New Millennium." *Aluminum*, Vol. 76, pp. 1010-1014.

K. Low-Cost Titanium Powder for Feedstock

Principal Investigator(s): Curt A. Lavender and K. Scott Weil
Pacific Northwest National Laboratory
P.O. Box 999/K2-44
Richland, WA 99352
(509) 372-6770; Fax: (509) 375-4448; e-mail: curt.lavender@pnl.gov
(509) 375-6796; Fax (509) 375-4448; e-mail: scott.weil@pnl.gov

Technology Area Development Manager: Joseph A. Carpenter
(202) 586-1022; fax: (202) 586-1600; e-mail: joseph.carpenter@ee.doe.gov
Field Technical Manager: Philip S. Sklad
(865) 574-5069; fax: (865) 576-4963; e-mail: skladps@ornl.gov

Participants:
Lance Jacobsen, International Titanium Powder, Inc., 20634 W. Gasken Drive, Lockport, IL 60441
Michael Hyzny, DuPont, (302) 999-5252 e-mail:michael.t.hyzny@USA.dupont.com
Tim Soran, ATI Allvac, (509)372-1711; e-mail:Tim.Soran@Allvac.com
Paul Jablonski, Albany Research Center, Albany, OR 97321
Mahi Sahoo, CANMET, Ottawa, Ontario Canada K1A 1M1

Contractor: Pacific Northwest National Laboratory
Contract No.: DE-AC06-76RLO1830

Objectives

- Investigate alternate powder and melt-processing methods for low-cost titanium materials.
- Evaluate processing methods to produce powder metallurgy (P/M) titanium products with International Titanium Powder, Inc. (ITP) powder.
- Evaluate the suitability of emerging titanium technologies for the production of low-cost titanium products for automotive applications.

Approach

- Perform characterization and analysis of the sintering behavior of the ITP powder. Provide feedback of results to ITP for use in process design.
- Develop low-cost feedstocks for P/M use in automotive applications from low-cost titanium chloride (TiCL4)
- Perform thin-section slab castings and roll to sheet to simulate and evaluate the use of continuous-casting methods to produce sheet materials.
- Survey the emerging technologies for the low-cost production of titanium powders and evaluate for use in automotive applications.

Accomplishments

- Developed press-and-sinter cycles that produced greater than 97% dense plates of cold-pressed (CP) titanium from the ITP powder. Tensile tests from the plates exhibited no measurable ductility.

- Plates pressed and sintered from CP titanium ITP powder hot rolled with a 2.5:1 reduction, exhibited limited ductility in tensile tests. Fracture surface evaluation showed that, although densities were high, large amounts of the powder had not sintered.
- Designed and fabricated in cooperation with Albany Research Center and CANMET, graphite molds for plate casting trials to determine the effect of solidification rate on the reduction of area required to produce wrought properties. Castings 1/8, ¼ and ½ inch in thickness were prepared.
- Evaluated step-plate castings for mechanical properties which indicated that castings made in permanent molds without hot isostatic pressing (HIP) can exhibit adequate mechanical properties.

Future Direction

- Perform dilatometry, thermogravimetric (TGA), microstructural analysis and x-ray diffraction (XRD) analysis to develop a sintering cycle that can eliminate Na impurities and improve sinterability at lower pressing pressures.
- Continue the development of sintering cycles for the ITP powder with an emphasis on understanding the sintering mechanisms of the powder to increase ductility.
- Evaluate alternate low-cost titanium feedstocks for powder or melt processing to wrought products.

Introduction

An automobile design trend that has received much attention has been the reduction of vehicle mass. Reducing mass can improve both performance and fuel economy. While design changes can play a large role in reducing mass, large reductions ultimately will require the substitution of higher specific strength/stiffness materials in place of carbon steel. Primary contenders in this race are high-strength steels, aluminum, and fiber-reinforced polymer composites. One material, not on this short list, but one that could provide further reductions, is titanium. Although titanium is light and strong, its role in the automobile has been almost nonexistent because of its exorbitant price. This high price is a direct result of the current production route, the Kroll process, which is time-consuming; energy-, capital-, and labor-intensive; and batch-based.

However, new technologies are emerging that may change the characteristics of the titanium market. In particular, these technologies may reduce the titanium price sufficiently to allow it to compete in high-volume markets, possibly even automotive. This project examines the powder metallurgy (P/M) behavior of titanium powder produced by a new process being developed by ITP.

Approach

The production of low-cost titanium for automotive applications will require cost reductions in both raw materials and secondary processing operations. The approach to this project will be to evaluate the suitability of emerging titanium beneficial technologies for the production of low-cost automotive components. The ITP powder process produces an alloy powder with morphology very similar to other emerging technologies, Fray-Farthing-Chen (FFC) Cambridge and MER anodic reduction. Because ITP can produce powders in sufficient quantity for evaluation, the ITP process will be used as the basis for the evaluation.

Results and Discussion

Previous reports [1, 2, 3] of ITP powder processing indicated that sodium compounds were assumed to be limiting the density and tensile ductility of the sintered pressing. Thermo-gravimetric (TGA) results of ITP powders indicated that sodium compounds were present and began to decompose at temperatures near 500°C. Using previously reported 1150°C sintering cycles [4] plates were pressed, consolidated and tested for mechanical properties using a standard ASTM E8 tensile sample tested at 12 mm/mm/minute strain rate. The tensile tests exhibited little or no ductility in the as-sintered condition. The failure strength of the as-sintered sample was 510 MPa and occurred slightly after yield of the sample. The measured strain in the as-sintered sample was less than was less than 0.07%. The samples that were as-sintered and rolled exhibited yield and ultimate strengths of 560 and 570 MPa, respectively with an elongation of 4%.

A sample 12-mm-diameter by 12-mm-long was vacuum hot-pressed at 750°C using the hot press at Wright Paterson Air Force Material Laboratory. From the vacuum hot-pressed bar, sub-scale tensile samples were machined and tested at a constant crosshead speed of 12 mm/mm/minute. The vacuum hot-pressed sample exhibited 100% density, yield and ultimate tensile strengths of 525 MPa and 570 MPa, respectively and an elongation of 17%. Tensile test results for the powder processed materials are given in Table 1.

Analysis of the fracture surface of the pressed, sintered and rolled tensile sample indicates that relatively complete consolidation of the powder has been achieved, as shown here by Figure 1.

The low-cost, ilmenite-based $TiCl_4$ and standard grade of $TiCl_4$ provided by DuPont had the compositions given in Table 2. The low-cost $TiCl_4$ exhibited elevated Sn and Si concentrations of 406 and 55 ppm, respectively, compared to standard $TiCl_4$ where Sn and Si are less than 50 and 10 ppm,

Table 1. Tensile properties measured from parts processed from ITP powder using various consolidation methods. Typical properties for ASTM CP TI Grade 3 have been included for comparison.

	Yield Strength	Ultimate Strength	Elongation
Processing Conditions	MPa	MPa	%
Pressed and Sintered	N/A	510	<0.07
Pressed, sintered and rolled	560	570	4
Vacuum Hot Pressed at 750°C	525	590	17
Grade 3 CP Ti, Typical	455	560	20

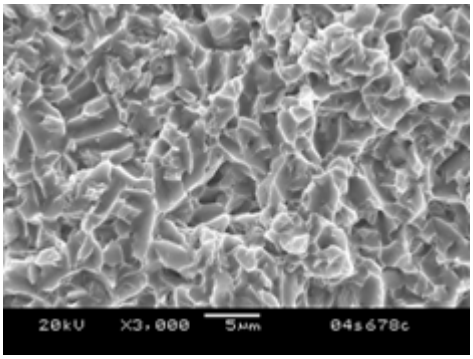


Figure 1. Fracture surface of sintered compacts of ITP powder indicating that relatively complete sintering of the compact has been achieved.

Table 2. Comparison of chemical composition of standard and low-cost, ilmenite based $TiCl_4$.

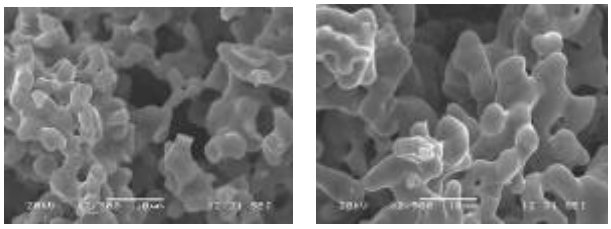
Element	Standard $TiCl_4$	Low-Cost, Ilmenite-Based $TiCl_4$
	ppm	ppm
Sn	50.00	408.3
Si	10.00	55.4
Mg	10	8.6
Ca	10	4.6
V	3.00	3.9
Cu	1	3.7
Sb	5.00	3.3
Zn	5	2.9
Fe	1.00	1.9
Al	2	1.5
Pb	5	1.5
As	2.00	1.4
Cd	N/A	1.4
Mn	1	1.4
Ni	25	1.4
Nb	N/A	1.4
Zr	10	1.4
Ba	1.4	1.4
Cr	1	0.7
Co	1.4	tr
Hg	<0.35	<0.35

respectively. The ilmenite-based $TiCL_4$ produced by DuPont had less than 2 ppm Fe as a result of a distillation process used to produce FeCl for sale to the chemical industry (resulting in reduced $TiCl_4$ cost).

The low-cost, ilmenite-based $TiCl_4$ feedstock received at ITP has been processed to powder using the "Engineering Loop." No processing problems were encountered with low-cost $TiCl_4$. Figure 2 is a micrograph of the ITP standard and low-cost $TiCL_4$ powder. No obvious difference in powder morphology was observed when comparing the standard and ilmenite based $TiCl_4$ ITP powders, shown in Figure 2.

The powders produced by ITP exhibited an open-pore structure shown in Figure 3 and, as a result, have a relatively low tapped density of approximately 7%. Although a tapped density of 7% is workable for many P/M applications, ideally the tapped density will be higher.

As a result, milling trials were initiated at PNNL to break down the powder and develop a higher tapped density. Ideally, the powder would fracture at the



(a) (b)

Figure 2. ITP powder produced with low-cost, ilmenite-based $TiCl_4$ (a) and standard $TiCl_4$ (b) indicating little change in powder morphology. Note the ligament type structure in the as-received powders.

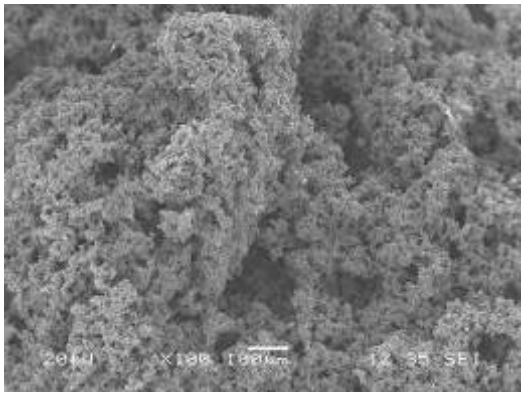


Figure 3. Typical as-received ITP powder that exhibits a tapped density of approximately 7% of theoretical.

ligaments shown by Figure 2 and produce a fine sub-micron powder size; however, the ITP powder is very ductile-cold-welded readily into agglomerates as shown by figure 4. The finest powder sizes achieved are represented by Figure 5 and resulted in tapped densities in excess of 35%.

All Ti6Al4V step-cast plates were completed and delivered to CANMET for evaluation. Figure 6 has been included to illustrate the typical step-cast plate developed by AlRC and PNNL and delivered to CANMET. Each step of the casting was evaluated for tensile properties using sub-size (4 mm) ASTM E8 tensile samples.

The ultimate strength for the plates increased from 928 to 984 MPa as the section thicknesses decreased from 25 to 3.2 mm. No discernable differences in yield strength and elongation were observed with section thickness. Table 3 has been included and summarizes the tensile results reported by CANMET[5].

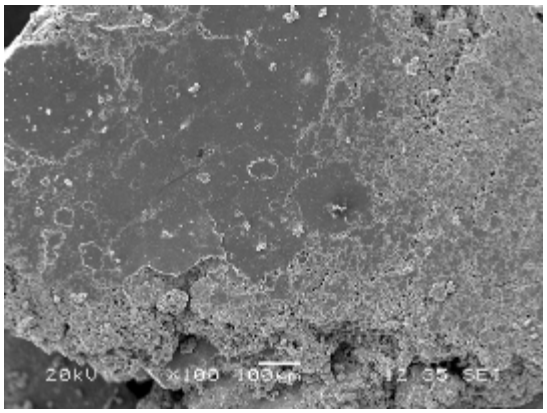
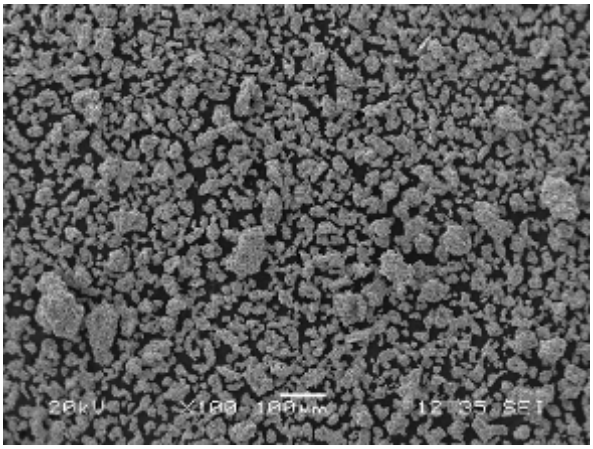
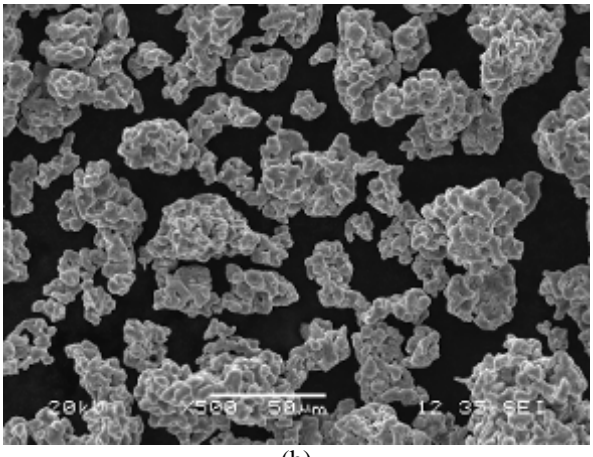


Figure 4. Cold-welded agglomerates due to over-milling of the very ductile ITP powder.



(a)



(b)

Figure 5. Milled ITP powder that exhibits tapped density in excess of 35% at 100x (a) and 500x (b).

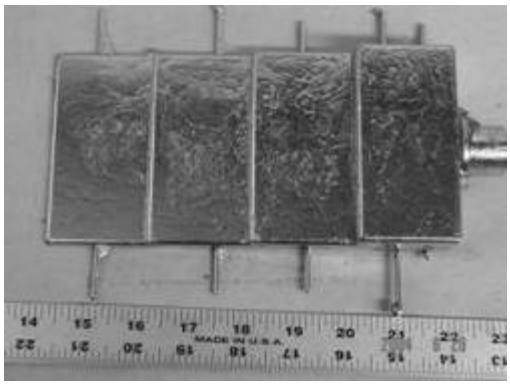


Figure 6. Step-plate castings developed for evaluation at CANMET.

Table 3. Tensile properties measured by CANMET from the step-plate castings produced by AlRC.

Section Thickness	0.2% Offset Yield Strength	Ultimate Strength	Elongation
Mm	MPa	MPa	%
25	823	928	7
13	836	951	7
6.3	817	958	9
3.2	824	984	6
Ti6A14V – Cast and HIPed	870	960	10

Ti6Al4V cast plates have been prepared at AlRC for additional characterization for tensile and fatigue strength developed by low levels of hot rolling. Characterization of the plates prior to hot rolling has been initiated. An example of the plates to be used for evaluation of solidification rate and property relationships has been included in Figure 7.



Figure 7. Monolithic cast plate to be used for hot rolling and Solidification-rate analysis.

Conclusions

- As indicated by the strength and ductility levels produced in the vacuum hot-pressed samples, the powder produced by ITP can develop near wrought-like properties in CP Ti.
- Sintering conditions for the ITP can be developed to produce ductility. Optimization of the sintering cycle must be performed to maximize ductility.
- The low-cost, ilmenite-based $TiCl_4$ -produced powder is visually very similar to the standard $TiCl_4$ powders.
- The impurities observed in the low-cost ilmenite-based $TiCl_4$ are Sn and Si after FeCl removal by distillation.
- The sintering mechanism of the ITP powder is different than atomized powder and conditions must be developed to maximize the volume of powder sintered.
- Thin-plate castings of Ti6Al4V can produce properties near that of cast and HIPed casting using a simulated permanent mold made from graphite.

References

1. S. Abkowitz, S. M. Abkowitz, H. Fisher and P. Schwartz, Final Report of Contract No. 409117AU7, *Low-Cost Titanium Evaluation*, Dynamet Technology, Inc., November 29, 2002.
2. S. Abkowitz, S. M. Abkowitz, H. Fisher and P. Schwartz, Final Report of Contract No. 7283, *Low-Cost Titanium Evaluation*, Dynamet Technology, Inc., July 29, 2003.
3. Gerdemann, S.J. and Alman, D.E., *Characterization of a Titanium Powder Produced through a Novel Continuous Process*, Advances in Powder Metallurgy and Particulate Materials 2000, MPFI, Princeton NJ.
4. FY 2004 Progress Report for Automotive Lightweighting Materials, Energy Efficiency and Renewable Energy, Office of Freedom CAR and Vehicle Technologies, Advanced Materials Technologies, http://eere.energy.gov.
5. Canadian Lightweight Materials Research Initiative (CLiMRI), POL Annual Report (PAR) 2004-2005.

L. Low-Cost Powder Metallurgy Technology for Particle-Reinforced Titanium Automotive Components: Manufacturing Process Feasibility Study

Russell A. Chernenkoff
Ford Motor Company
SRL MD3135
2101 Village Road, Dearborn, MI 48124
(313) 594-4626; e-mail: rchernen@ford.com

Dr. William F. Jandeska
General Motors Corporation, GM Powertrain
895 Joslyn Ave. Pontiac, MI 48340
(248) 857-2184; e-mail: william.jandeska@gm.com

Dr. Jean C. Lynn
DaimlerChrysler
800 Chrysler Dr. East, CIMS 482-00-15, Auburn Hills, MI 48326
248-512-4851; e-mail: jcl6@daimlerchrysler.com

Technology Area Development Manager: Joseph A. Carpenter
(202) 586-1022; fax: (202) 586-1600; e-mail: joseph.carpenter@ee.doe.gov
Field Technical Manager: Philip S. Sklad
(865) 574-5069; fax: (865) 576-4963; e-mail: skladps@ornl.gov

---

Contractor: U.S. Automotive Materials Partnership
Contract No.: FC26-02OR22910

Objective

- Demonstrate production-intent process scheme for fully-densified titanium-alloy, powder-metallurgy (PM) composite samples.
- Benchmark process capability using commercial-grade titanium powder feedstock and follow with one of the proposed low-cost titanium powder materials. Blend additives to achieve final titanium-alloy material with reinforcement.
- Perform microstructure characterization and interfacial studies.
- Confirm test specimens are crack-free by nondestructive evaluation method (Lawrence Livermore National Laboratory).
- Generate static mechanical properties and perform failure analysis.
- Perform a technical cost modeling study on the novel ADMA Products, Inc., process and establish sensitivity of each processing step for cost-effectiveness.

Approach

- Use titanium metal feedstock to produce blanks in simple shapes via the ADMA manufacturing process that will then be machined into coupons for mechanical property determination.
- Conduct microstructural and interfacial studies together with mechanical property testing.
- Perform a technical cost model on the ADMA manufacturing process.

Accomplishments

- Produced powder blends of Ti-6Al-4V material from Sodium Reduced Ti sponge fines with and without reinforcement (benchmark material).
- Received powder blend of Ti-6Al-4V material from International Titanium Powder (ITP) without reinforcement (low-cost alterative).
- Die-pressed powders in 0.500-in.-diameter carbide tooling to 0.500-in. thickness for metallographic examination.
- Compacted and processed powder blends into 3 inch x 5 inch blanks for tensile samples.
- Sintered in vacuum furnace, optimized heat treatment.
- Machined blanks into tensile samples.
- Completed metallographic examinations and tensile tests.
- Completed fracture analysis on composite material.

Introduction

The goal of this concept feasibility study is to develop a low-cost PM manufacturing process to obtain fully dense parts based on current commercial-grade materials and a novel processing technology. The study will use particle-reinforced titanium metal feedstock in conjunction with PM press-and-sinter technology to manufacture simple parts for testing. A technical cost model will be performed to document the cost of the manufacturing process. The decision gate criteria are (1) a cost-competitive manufacturing process and (2) acceptable microstructure and mechanical properties that have been identified for connecting rods targeted for high-performance reciprocating engine applications.

Materials

Sample blanks (plates) have been manufactured using a baseline aerospace-quality Ti material (RMI) and a low-cost alterative material from International Titanium Powder (ITP). Small samples of the materials were mounted and polished followed by etching for eight seconds using Kroll's reagent. Photomicrographs were taken using a digital camera connected to a Leco metallograph.

Ti-6Al-4V from Sodium Reduced Ti sponge fines (RMI "commercial" product): The density of un-reinforced samples after compaction and sintering was greater than 99% of theoretical full density. Metallographic analysis revealed homogeneous microstructure with a basket weave morphology (Figure 1). Level of detected porosity is less than

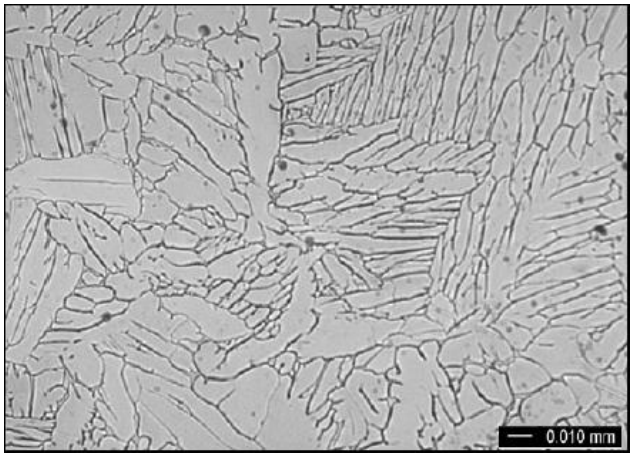


Figure 1. Ti-6Al-4V from Sodium Reduced Ti sponge fines (RMI "commercial" product).

1%. Samples reinforced with titanium carbide (TiC) had densities greater than 90% of theoretical full density. TiC was formed from elemental powder (Ti and graphite). Figures 2 and 3 show Ti-6Al-4V(RMI) with 10% and 20% TiC, respectively.

Ti-6Al-4V from International Titanium Powder: The ITP powder was compacted and sintered without TiC reinforcement. After an initial sintered density of 65% of theoretical full density, several compaction and sintering iterations were required to obtain a sintered density of 90+%. Figure 4 shows the microstructures of the compacted and sintered ITP material at 65%, 86%, and 90+% density.

Mechanical Properties

Tensile test results from Ti-6Al-4V Sodium Ti samples without TiC reinforcement and with10%

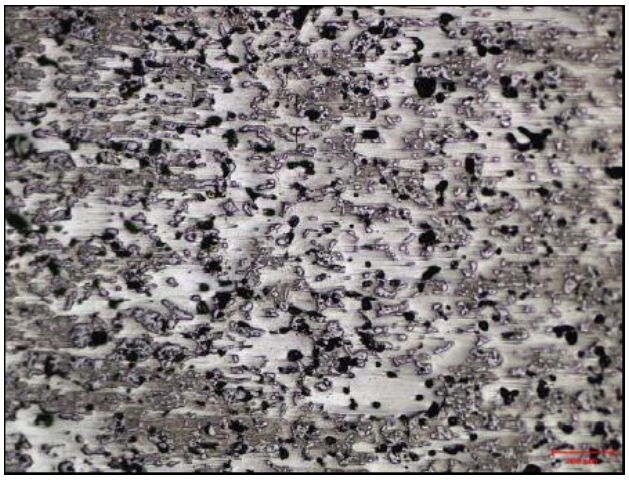


Figure 2. Ti-6AAl-4V + 10% TiC from Sodium Reduced Ti sponge fines (RMI "commercial" product).

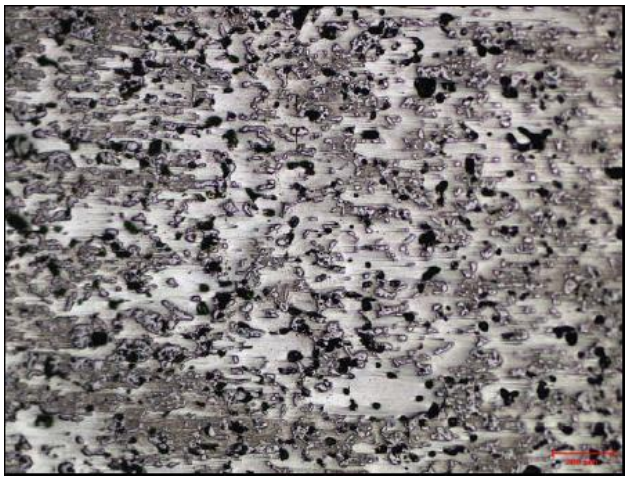


Figure 3. Ti-6AAl-4V + 20% TiC from Sodium Reduced Ti sponge fines (RMI "commercial" product).

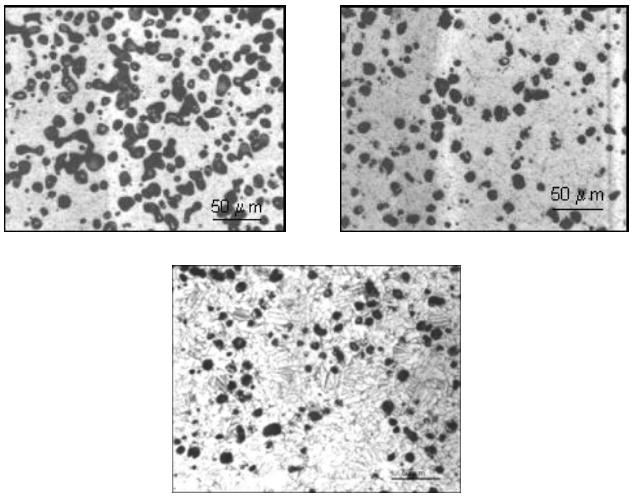


Figure 4. Ti-6AAl-4V ITP material at 1) 65%, 2) 86%, and 3) 90+% density.

and 20% TiC reinforcement and are shown in Table I. The Ultimate (UTS) and Yield (0.2%YS) strength are higher than that specified by ASTM (UTS -130 ksi and 0.2%YS – 120 ksi) for both the un-reinforced material and the material with 10% TiC reinforcement. Tensile testing on the ITP material is in progress.

On-Going / Future Work

- Complete cost model on ADMA manufacturing process.
- Assess cost model and mechanical properties against decision gate criteria.
- Complete USAMP final report.
- Begin process for phase II (manufacture component – connecting rod).

Table 1. Mechanical Properties of Ti-6Al-4V

Composition	Sample No.	Tensile Strength (ksi)	Yield Strength (ksi)	Elongation, %	Modulus of Elasticity, MSI
Ti-6Al-4V from sodium reduced Ti sponge fines (RMI "commercial" product)	1	143.2	123.1	12.2	16.9
	2	143.6	123.7	13.8	18.3
	3	142.6	122.8	11.4	16.7
	4	142.7	123.1	11.8	16.8
Ti 6Al-4V + 10% TiC	1	150.3	143.5	3.0	17.7
	2	151.4	137.9	3.0	17.7
	3	150.4	142.4	3.0	17.9
	4	150.1	143	2.0	18.1
	5	148.5	141.1	2.0	17.5
Ti 6Al-4V + 20% TiC	1	115	115	2.0	18.3
	2	119.2	119.2	1.0	19
	3	124.5	124.5	2.0	20.1
	4	122.3	122.3	2.0	19.5
	5	121.5	121.5	2.0	19.6
Ti-6Al-4V from ASTM Standard B348-03 Grade F-5		130	120	10.0	

M. Powder Metal Performance Modeling of Automotive Components

Project Manager: Mark Osborne
Group Leader - Materials Engineering
Casting Development and Validation Center GM Powertrain
1631 North Washington
Saginaw, MI 48601
(989) 757-0014; fax: (989) 757-0373; e-mail: mark.osborne@gm.com

Principal Investigator: Mark F. Horstemeyer (Paul Wang, Youseff Hammi)
CAVS Chair in Solid Mechanics & Professor, Mechanical Engineering
Mississippi State University
206 Carpenter Bldg., P.O. Box ME
Mississippi State, MS 39762
(662) 325-7308; fax: (662) 325-7223; e-mail: mfhorst@me.msstate.edu

Russell Chernenkoff, Technical Specialist
Ford Motor Company
2101 Village Road, Room 2022B, MD 3135
Dearborn, MI 48124
(313) 594-4626; fax: (313) 390-0514; e-mail: rchernen@ford.com

Jean Lynn, Senior Specialist
Daimler Chrysler
800 Chrysler Drive, CIMS 482-00-15
Auburn, MI 48326
(248) 512-4851; fax: (248) 576-7490; e-mail: JCL6@daimlerchrysler.com

Howard Sanderow, President (CPMT Rep)
Management & Engineering Technologies (MET)
161 Copperfield Drive
Dayton, OH 45415
(937) 832-1583, fax: (937) 832-0858; e-mail: metgroup@earthlink.net

Technology Area Development Manager: Joseph A. Carpenter
(202) 586-1022; fax: (202) 586-1600; e-mail: joseph.carpenter@ee.doe.gov
Field Technical Manager: Philip S. Sklad
(865) 574-5069; fax: (865) 576-4963; e-mail: skladps@ornl.gov

---

Contractor: U.S. Automotive Materials Partnership
Contract No.: FC-26-02OR22910

Objective

- Develop and evaluate math-based models for powder metallurgy component design and performance prediction. An existing U.S. Automotive Materials Partnership (USAMP) microstructure-property model for castings will be extended to powder metallurgy (P/M) for practical application in low strain-rate (design and durability) and high strain-rate (toughness-driven impact strength) environments. This model will be utilized to evaluate and optimize two component designs (a main bearing cap and a gear) as affected by material and manufacturing processes (compaction and sintering), and will accommodate each

companies' analytical codes (Abaqus, LS-Dyna, Ansys, etc.). The flexibility of this model will facilitate the evaluation of lightweight materials (such as aluminum and titanium) for future component applications.

Approach

- Determine current powder metallurgy standards publications, component design guidelines, manufacturing, and evaluation methodologies. Provide a selection of metal powders that can satisfy design performance requirements, component design guidelines, and manufacturing and testing specifications across industry participants (Task 1)
- Evaluate and develop numerical modeling techniques to predict mechanical properties throughout P/M component sections. The transition of current materials and designs to process structural automotive P/M components creates the need to predict the properties of the component in all sections of the design. In addition, there is the necessity to provide the least-cost, lowest-mass product designs and reduced development lead-time. Adapt and/or re-develop existing math-based models which are capable of accurately predicting P/M component structures and properties throughout the compaction and sintering processes (section size, density variation, dimensional tolerances, potential for cracking), alloys and process parameters (machine functions, tool and powder temperatures, strain rate, friction and pressure). Capture the history of a P/M part through its pressing, sintering, and life-cycle performance history using the developed multiscale methodology. (Task 2)
- Develop component and vehicle-level testing to validate durability, quality control and performance of P/M automotive parts. Quality control for P/M parts production involves several process factors such as powder properties, press settings, tooling design, and furnace condition. Determine these process factors in terms of their impact on process variations and quality improvement. Use optimization and statistical techniques to help determine the main factors affecting the final component. Perform validation experiments in which actual boundary conditions from real processes will be used to fracture the components. This will ensure us understanding the quality effects on the product along with the modeling effort. (Task 3)
- Manage and report program activities. The proper execution of this task will greatly enhance the value of the overall program. The type of reports and guidelines, which will be generated form this program will be in accordance with DOE and USCAR requirements. (Task 4)
- Perform Technology/Commercial transfer throughout the automotive value chain. Unlike aluminum, plastics and steel, there are no major R&D/technical institutions fostering the necessary infrastructure to support the large-scale application of automotive P/M components. It is for this reason, that if the auto industry wishes to take advantage of P/M's potential weight and cost reduction opportunities, it will have to nurture it through programs sponsored and directed by USCAR. The project team will request the professional support of societies to publish notices of meetings, and project information as released by the project team. (Task 5)

Accomplishments

- Identified the metal and alloy powders that are able to meet manufacturing and component durability requirements.
- Identified and standardized the performance test methods.
- Identified the testing instrumentation to characterize the metal powder properties.
- Identified all the P/M techniques to process auto parts (production, mixing/blending, cold and warm compaction, sintering, heat treatment, optional finishing operations, etc.).
- Identified the existing numerical techniques for simulating P/M forming processes.
- Identified the important parameters that influence the compaction processes.
- Identified and evaluated the existing powder material models that will simulate P/M compaction processes.

- Developed a constitutive law based on the Modified Drucker-Prager cap model mixed with the microstructure-based plasticity model to predict the material state during compaction. The model is composed of several material parameters that are density-dependent.
- Developed an algorithm to implement the compaction constitutive model into the finite element code ABAQUS/Explicit using the user material subroutine VUMAT.
- Defined a powder metallurgy test matrix, which will be used to create a microstructure-property database for validation of model constants and accurate prediction of powder mechanical behavior.
- Performed Finite Element Analysis on 3D cylinder, gear and main bearing cap with virtual material parameters, geometries and tool motions to illustrate the capability of the model for simulating powder compaction of automotive components.

Future Direction

- Perform microstructural evaluations and mechanical property tests on P/M cylinder geometry to determine microstructure-property relations during compaction, sintering, and in-service duty life. With the above software developed, the model will be correlated to these microstructure-property relations.
- Determine the interparticle friction coefficient, using a simple Coulomb law of friction by measuring the tangential forces at the contact surface and determine the influencing parameters contributing to the friction effects.
- Perform atomistic simulations for different diameter particles (3.52 nm, 7.04 nm, and 14.08 nm) with a BCC particle arrangement with periodic boundary conditions to examine the effect of particle size on the density distribution of the sample after compression.
- Develop algorithm and implement the developed compaction model into the finite element code ABAQUS/Standard to predict the springback of a compacted part during ejection.
- Modify the existing sintering model from Pennsylvania State University to insert internal state variables and link it to the compaction model. Develop algorithm and implement the sintering model in ABAQUS/Standard
- Predict the material state during the powder compaction and sintering processes with the developed math-based models for a main bearing cap and gear.
- Validate process model (including tool geometry, friction, tool and metal temperatures, die rate and pressure) and property models on P/M bearing cap and gear with experiments.
- Document the progress by writing final reports for the second year project by October 31, 2006.

Introduction

In October 2004, the Computational Manufacturing and Design Department at the Center for Advanced Vehicular Systems (CAVS) started the Powder Metallurgy Performance project with the guidance from the Big Three automakers (General Motors, Ford and DaimlerChrysler), and the Center for Powder Metallurgy Technology of North America (CPMT). The project employs the accomplishment of a previous USAMP Lightweight Metals Group project where a microstructure-based plasticity material model has been able to capture the plasticity and damage effects for A356 aluminum and AM60 magnesium, and where it was shown that the model can be used to optimize a control arm made of this latter material [Horstemeyer et al., 2002]. Using the same methodology, the objectives and benefits of this current project are (1) cost reduction (eliminating tooling iterations and prototype components), (2) shortening the lead-time from the concept to implementation for new components, (3) optimization of current components for increasing performance and reducing weight, (4) the availability of modeling tools to evaluate material substitution in components, and (5) the improvement of our scientific understanding of powder metallurgy.

During the first project year, significant progress was made in the area of simulation where all the

numerical techniques needed to perform multiscale and multistage modeling were identified. Also, the microstructure-based plasticity material model was integrated with the Modified Drucker-Prager Cap Model to capture the plasticity of the powder during compaction. In the area of experimentation, a test matrix was established to build a complete microstructure property database for compaction, sintering, performance and fatigue. The project team is currently looking for industrial partners to provide iron and aluminum powders and specimens to CAVS, and also to perform experiments using equipment that is not available at CAVS site.

P/M Manufacturing Process

Powder metallurgy, or P/M, is a process for forming metal parts by compacting and heating metal powders to just below their melting points. Although the process has existed for more than 100 years, over the past quarter century it has just become widely recognized as a robust process for producing high-quality parts for a variety of important applications. This success is due to the advantages the process offers over other metal forming technologies such as forging and metal casting, advantages in material utilization, shape complexity, near-net shape dimensional control, among others [German, 1994]. In reality, P/M comprises several different technologies for fabricating semi-dense and fully dense components. In this project, we will study the conventional P/M process, referred to as press- and-sinter, which is used to make the two automotive parts, gear and bearing cap.

In this conventional process, P/M parts are formed by a sequence of processes. The first few steps are the selection of suitable powder forms, the production of powders, and the weighing and mixing of them. The blended powders are then pressed or compacted into a desired shape in a tool set, consisting of punches, a die and core rods. The green compacts are then sintered. To improve the properties of the sintered products, finishing operations may be carried out.

Mixing/Blending

The blending of metal powder, which is done under controlled conditions (i.e., air, inert atmosphere, or liquid) to avoid contamination and deterioration, fulfills several purposes:

- Produces a uniform distribution of particle sizes and shapes.
- Allows different metals to be mixed to obtain specific physical properties.
- Improves metal powder interaction and prolongs the life of dies used when metal powder is blended with lubricant.

Compaction

Powder compaction is the most critical stage in the P/M manufacturing process. During this operation, the blended powder undergoes significant dimensional changes as the powder height is reduced. The powder is compacted to form the shape of the desired part. The density after compaction (also called green density) depends on the compaction pressure, dimensions of the compacted part, tooling motions and powder yield strength.

Sintering

Sintering follows the process of compacting and shaping the powdered material. After compaction, the strength of the material is low. Sintering, then, increases both the physical and mechanical properties of the material. Sintering is the process of heating the material to a temperature below the melting temperature but high enough to allow bonding or diffusion among the individual particles. Continuous sintering furnaces are used for most production. These furnaces have three chambers:

- A chamber to volatilize the lubricants in the green compact in order to improve bond strength and prevent cracking. It is called the burn-off chamber. It slowly raises the temperature of the compound in a controlled manner.
- A high-temperature chamber for sintering. It is the site of actual solid-state diffusion and bonding between the powder particles. The time during the second stage of sintering must be sufficient to produce the desired density and final properties.
- A cooling chamber.

The furnace thermal profile should be properly controlled to obtain successful sintering and optimum properties. During the sintering process a wide variety of physical, chemical, and metallurgical phenomena occurs within the mass of metal powder

particles. These phenomena are influenced by the sintering conditions, such as time, temperature, and atmosphere, and the chemical composition of the powder mass.

Finishing Operations

Finishing operations are usually performed after sintering. For better dimensional accuracy, different machining operations such as coining and turning are performed. Heat treating (quench and temper, steam treat) the sintered part will improve its strength, hardness, and wear resistance. Finishing operations are also performed to improve the surface characteristics of the part.

Numerical Methods for P/M Modeling

To perform the modeling of automotive P/M parts, the P/M manufacturing process can be divided into a number of distinct stages: powder transfer, powder compaction, ejection, sintering and heat treatment. Different numerical techniques and constitutive laws can be used for modeling these stages of the P/M process. Linking the different models is a requirement to synthesize the whole P/M process and to make the procedure history-dependent (Figure 1). Using multiscale methods and techniques for bridging scales from atomistic to continuum can be very helpful in understanding the fundamental relationship between microstructure and important macroscopic materials properties [Horstemeyer and Wang, 2003]. In this project, the numerical techniques considered are Molecular Dynamics, the Finite Element Method and eventually the Discrete Element Method.

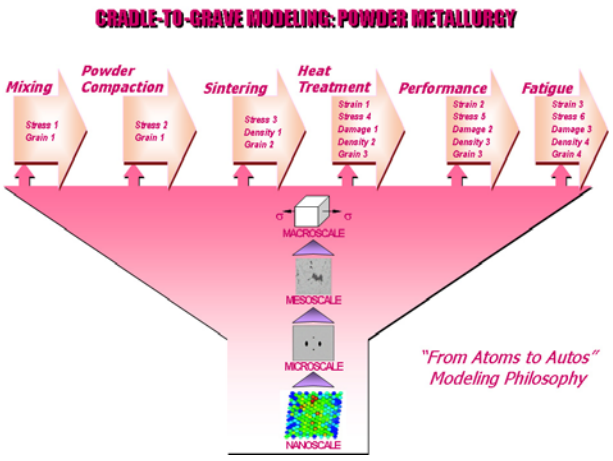


Figure 1. Cradle-to-Grave modeling of P/M process.

Molecular Dynamics

The molecular dynamics method was first introduced by Alder and Wainwright in the late 1950's [Alder and Wainwright, 1957 and 1959] to study the interactions of hard spheres. At the nanoscale level, Molecular Dynamics techniques address the response of individual atoms under mutual interactions. Due to the limitations imposed by computer speed and memory, the total number of atoms is of the order of a couple of millions and the total real time of simulation is of the order of picoseconds. Molecular Dynamics simulations are considered here as 'numerical experiments' to quantify the appropriate cause-effect relations between the microstructure and the mechanical properties for P/M compaction, sintering, and sizing processes at the macroscopic level. By varying packing arrangement (Figure 2), nanoparticle size and compacting temperature, we can understand the deformation and diffusion mechanisms which occurred in an assembly of the particles, such as dislocation slip, diffusion through dislocations, grain boundary sliding, interparticle friction and void/crack nucleation during the P/M consolidation process.

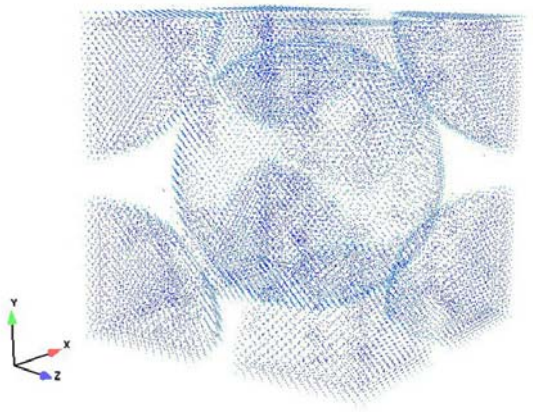


Figure 2. Molecular Dynamics – Nanoscale simulations of powder compaction with BCC packing configuration

The macroscale internal state variable constitutive theory can then be correlated and validated with these atomistic simulations of nanocrystalline powder to quantify the level of influence by these material parameters: inter-particle friction, length scale effects and particle size effects. These results associated with the experimental database constitute part of the effort to build comprehensive microstructure-property relationships of the P/M process.

Discrete element analysis

Discrete element methods (DEM), also known as distinct element methods, were first developed for granular materials by Cundall and Strack [1979]. It has been mainly applied to soil mechanics and many other researchers have used it for a variety of granular dynamics simulations. It consists of numerical simulations of interacting individual particles that provide significant information on particle motion, and contact forces. To formulate motion equations, the particles are treated as individual entities with Newtonian motion in a gravitational field. This method has been advanced by many researchers and it has been used extensively to study the flow and deformation mechanisms of granular materials.

The purpose of using DEM simulations in this project is to study and improve the flowability of metal powder during mixing, die filling and powder transfer. The DEM model can analyze the sensitivity of the interparticle and particle/die friction coefficients, the geometry of the particles, and the particle size distribution. Therefore, the determination of an apparent density distribution right before the onset of pressing by using DEM simulations should only increase the accuracy of the powder compaction modeling (Figure 3).

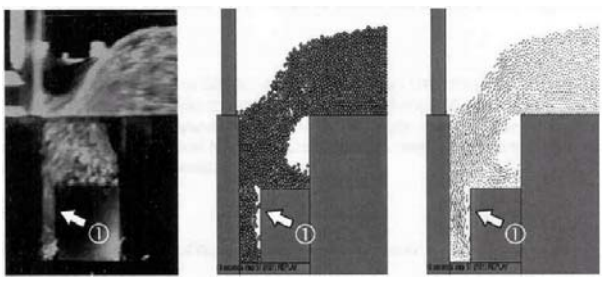


Figure 3. DEM simulation of die filling [Gillia et al., 2002].

Finite Element Method

In recent years, finite element (FE) analysis has received wide attention for its applicability to powder metallurgy (P/M) industry. With a significant level of reliability and proven quality control, these techniques provide a valuable tool in predicting density and stress distributions in the pressed compact prior to the actual tooling design and manufacturing process.

In this project, the finite element method (FEM) is the primary numerical tool for simulating die compaction and sintering, and for design and performance optimization of the P/M automotive parts. By implementing user-defined routines (UMAT and VUMAT) for both compaction and sintering processes into the general purpose finite element program ABAQUS [2003], quantitative predictions of density distributions and shape distortions can be obtained as well as the stresses in the tool components. Further, by employing optimization techniques to the simulation of powder processing steps, the final properties and design of P/M parts can be tailored by specific levels as desired.

Test Matrix and Characterization Method

For constitutive laws to be successful, computer simulation should be accompanied by a complete experimental database. The accuracy of numerical prediction depends on appropriate experimental data to calibrate and validate the powder material model.

In the first phase, a test matrix (Table 1) has been established to perform microstructural and mechanical property tests on P/M specimens so as to determine microstructure-property relations during compaction, sintering, and in-service life performance. As the compaction model is developed and implemented into the finite element code, the next task is to perform closed-die, isostatic and triaxial compaction tests to correlate the model with the microstructure-property relations. Many researchers have observed that the metal powder material model can be improved by updating the elastic and plastic properties (elastic moduli, cap eccentricity, material cohesion, internal friction, green strength) with the relative density $\tilde{\rho}$.

Table 1. Test Matrix for Compaction, Sintering, Performance and Fatigue

	Experiments	Model Calibration
COMPACTION	Determination of Tap Density	Initial Density before compaction
	Closed-die Compaction	Compressibility Curves Cap Hardening parameters for Pressure-Density curve
	Isostatic Compaction	Compressibility curves Cap Hardening
	Triaxial Compaction Isostatic Compaction	Yield Surfaces (density dependent) Cap Eccentricity parameters
	Elastic Properties of compacted powder at different density level	Density-Dependent Elastic parameters Young's Modulus E(r) Bulk modulus K(r)
	Measurement of Internal and die-wall friction	Friction parameter β as function of density
SINTERING	Sintering	Heat Transfer Mass and Dimensional changes Densification Phases
PERFORMANCE	Monotonic Tension Monotonic Compression Monotonic Torsion	Mechanical Properties at different densities of post-sintered P/M parts
FATIGUE	Uniaxial Fatigue Mean Stress Bauschinger Effect	Fatigue Life at different densities of post-sintered P/M parts

For example, the elastic Young's modulus E and the bulk elastic modulus can be deduced from the tests as a function of the density, and the Poisson's ratio can be derived from these two moduli [Pavier and Doremus, 1999]. Figure 4 shows variations of these two moduli with respect to the density (g/cm^3) for an iron-based powder. The Young's modulus for wrought iron is of the same order of magnitude (210 GPa) as the bulk modulus (175 GPa). Therefore, under high compressive stresses the powder has an elastic-plastic behavior similar to its constituent material. Also, the failure line, which is assumed to be linear in the model, can be determined by measuring the green strength in at least two test configurations with different stress triaxiality, such as the compression test, the Brazilian disc test, and the four-point bending test [Coube and Riedel, 2000]. Isostatic compaction is needed to determine the compressibility curves (density versus hydrostatic compacting pressure). More expensive triaxial tests are necessary to determine the shape of the cap. It is expected that exact knowledge of the cap curvature may have a minor influence on the final density distribution in most practical cases. In special cases, however, when a considerably profiled upper punch intrudes into the powder, the shape of the cap can influence the predicted density distribution significantly, so that more reliable values of the eccentricity parameter are needed. In addition, friction measurements should be performed, especially if simulations of slender parts are intended, Fig. 5.

Recently, Coube and Riedel [2000] allowed the material parameters, internal friction μ and material cohesion d, to be internal state variables and they are functions of both volumetric and equivalent plastic strain rates, Figure 6. The evolution equations of these variables exhibit a more pronounced softening on the failure line. Note that the objective of this formulation is to describe the cracking as a process of strain localization.

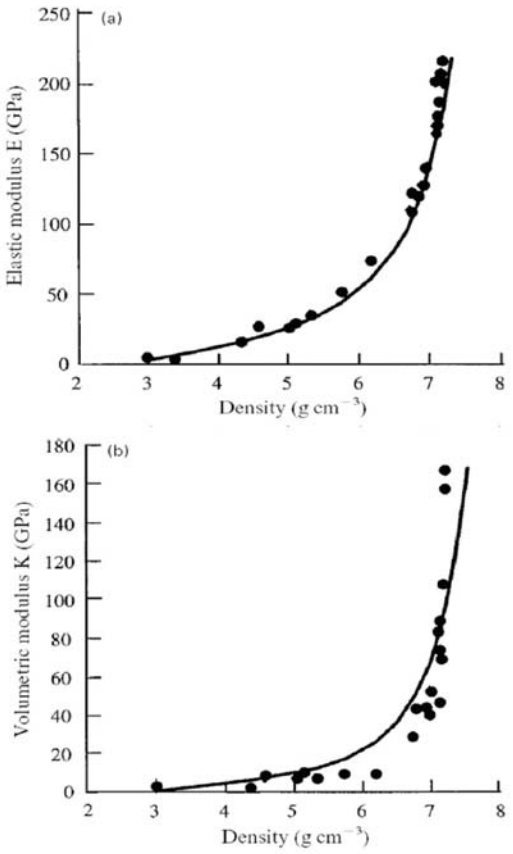


Figure 4. Evolution of given elastic moduli as function of density [Pavier and Doremus, 1999].

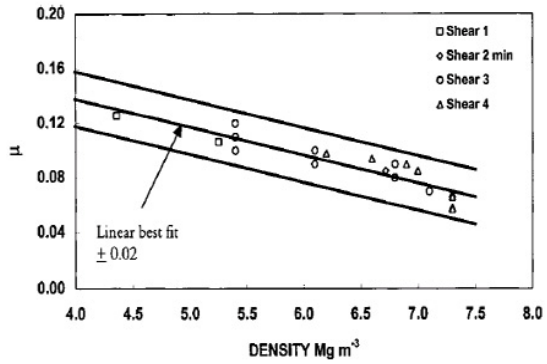


Figure 5. Measurement of internal friction [PM Modnet Methods & Measurements Group, 2000]

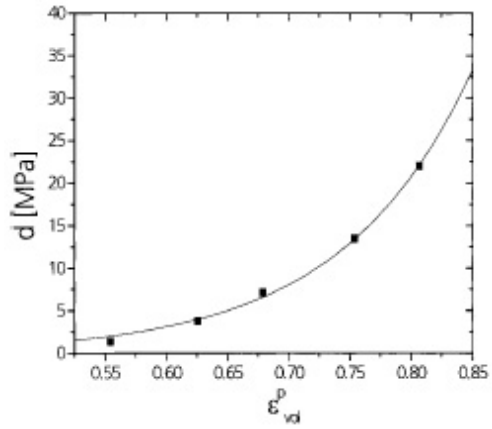


Figure 6. Cohesion strength d versus plastic volumetric strain [Coube and Riedel, 2000]

Modeling of Powder Compaction

The powder compaction is the most critical stage in the Powder Metallurgy (P/M) manufacturing process. Final part density, homogeneity, and strength are highly affected by this crucial operation. According to Khoei and Lewis [1998], a successful model for powder compaction process should reflect the frictional and compressible-densification yielding characteristics of the powder. A powder compaction model also needs the ability to describe the evolution of the porosity or density and the plasticity of the ductile metal particles subject to complex-shape geometries under multiaxial stress states. The density distribution is dependent on the combination of many factors such as geometrical shape, mechanical properties of the powder, and powder-tool frictional behavior.

In order to formulate a physically-based constitutive model, we need to distinguish the importance of three different scales during the deformation processes:

- the deformation of the powder aggregate idealized as a continuum – the classic macroscopic level,
- the deformation of the individual particles – the particle or microscopic level,
- the nanoscale dislocation mechanisms and the interparticle reactions.

Therefore, to have an accurate description of the different scales for metal powder analysis, the material model needs to reflect the following properties as defined by Trasorras et al. [1994], to accurately describe the following:

- Elastic deformation of the powder aggregate
- Plastic deformation of the powder aggregate
- Geometric hardening of the powder aggregate as a result of densification and a very large reduction in volume
- Plastic deformation of the particle according to the behavior described by classical plasticity with isotropic hardening as the powder aggregate is compacted
- Strain hardening of the particle.

In this project, the proposed compaction model consists of mechanical constitutive equations of the plastic deformation of the powder aggregate and the deformation-induced hardening of the particles. The structure of the constitutive equations of a porous material reflects volumetric inelastic deformation and marked pressure dependences. The macroscopic continuum framework assumes the porous medium as a macroscopically equivalent, isotropic, homogenous continuum with the relative density (or void volume fraction/damage) as a scalar internal variable. The anisotropic effects due to orientation and shape of the grains or voids are assumed to be small and are neglected at this moment.

Many mathematical models have been proposed for simulating the behavior of metal powders during rigid die compaction. For the case of macromechanical modeling of the metal powder compaction, the Cap model is one of the most popular constitutive models. The Cap model was originally developed to address the effects of stress state on geological types of materials such as sand, rock, and concrete. It was then adapted for ceramic and hard metal powders and most recently, for ductile metal powders [Gurson and Posteraro, 1994]. Such a model may be directly used for ceramic powders and the like. However, most metal powder compaction operations deal with ductile powders, and the Cap model suffers from a limited ability to incorporate the material property changes in ductile metal particles that accompany densification and deformation of the powder mass. Therefore, to allow hardening of the failure shear envelope, the model should then correlate the hardening of the overall aggregate with the plastic hardening of the particles and the relative density of the compact.

During the powder compaction process, large material rotations and deformation occur. To describe the deformation of ductile metal particles, an internal state variable (ISV) plasticity model is used [Bammann, 1990; Bammann et al., 1993]. The evolution equations for these state variables are motivated from dislocation mechanics and their use enables the prediction of strain-rate history and temperature history effects. The assumption of linear elasticity can be written

$$\underline{\sigma} = \underline{\underline{C}}(\rho) : \underline{\varepsilon}^{e} \tag{1}$$

where $\underline{\underline{C}}(\rho)$ is the elastic stiffness function of the relative density ρ, $\underline{\varepsilon}^{e}$ the elastic deformation, and $\underline{\sigma}$ is the Cauchy.

To characterize the behavior of the powder aggregate, we use a Modified Drucker-Prager/Cap material model. This double surface plasticity model consists of an elastic region in stress space, bounded by a friction-failure line F_s in the low-pressure region, and an elliptic yield cap F_c in the high-pressure region. The mechanical behavior of powders in compression can arise from adhesion and frictional sliding at particle interfaces, fracture of particles, and plastic deformation of particles. Because the metal powder is considered as a ductile material, the yield cap is also influenced by plasticity.

To reduce the conditional branching in the algorithm and to avoid numerical instabilities, a smooth function is introduced to replace the corner intersection between the two surfaces associated with the cap model, i.e., the failure envelope and isotropic-hardening cap surfaces of the Drucker-Prager/Cap model originally proposed by DiMaggio and Sandler [1971]. The modified Drucker-Prager failure surface of the smooth cap model is defined as:

$$F_s = \left|\underline{\sigma} - \underline{\alpha}\right| - F_e(p) = 0 \tag{2}$$

with

$$F_e(p) = d + p\tan\beta - F_p(p) \qquad (3)$$

where β is the material's angle of friction and d is its cohesion strength; $\underline{\alpha}$ is the kinematic hardening tensor; p is the first invariant of the stress tensor $\underline{\sigma}$. The deviatoric stress tensor, $\underline{s}$, is defined as

$$\underline{s} = \underline{\sigma} + p\underline{I} \qquad (4)$$

The hydrostatic stress, p, is written as:

$$p = -\frac{1}{3} I_1 \quad \text{with} \quad I_1 = \text{trace}(\underline{\sigma}) \qquad (5)$$

Following standard conventions in soil mechanics, compression and compaction are assumed to be positive. The key modification to connect the failure yield surface smoothly with the cap yield surface is to include another function F_p in the failure yield surface F_s. The pressure dependent function F_p is here defined by:

$$F_p(p) = H(p - p_c)\left[\frac{p - p_c}{p_a - p_c}\right]^{p_a - p_c} \tan\beta \qquad (6)$$

where p_a is the hardening parameter, $H(\cdot)$ is the Heaviside function:

$$H(p - p_c) = \begin{cases} 1 & \text{if } p \geq p_c \\ 0 & \text{if } p < p_c \end{cases} \qquad (7)$$

The variable p_c is defined by:

$$p_c = p_a - p_d \qquad (8)$$

where p_d is a material parameter.

The cap yield surface has an elliptical shape with constant eccentricity in the meridional $|s\text{-}\alpha|$–p plane (Figure 7). The cap surface hardens or softens as a function of the volumetric plastic strain: volumetric plastic compaction (when yielding on the cap) causes hardening, while volumetric plastic dilation (when yielding on the shear failure surface) causes softening. The cap yield surface is written as

$$F_c = \sqrt{|s - \alpha|^2 - \frac{1}{R^2}[p - p_a]^2} - F_e(p_a) = 0 \qquad (9)$$

with $$F_e(p_a) = d + (p_a - 1)\tan\beta \qquad (10)$$

where R is a material parameter called the cap eccentricity that controls the shape of the cap. The cap hardening variable p_a is an evolution parameter that represents the volumetric plastic strain-driven hardening/softening.

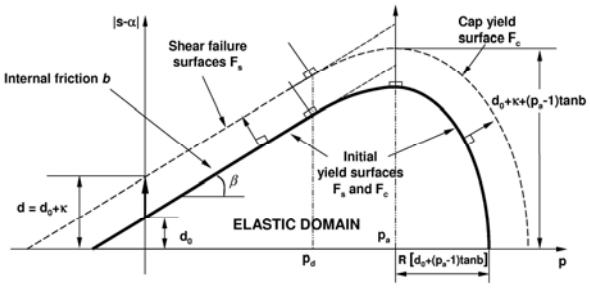


Figure 7. Modified Drucker-Prager/Cap Model: yield surfaces in the |s-α|–p plane

The evolution parameter p_a is a hardening parameter that controls the motion of the cap surface, and p_b defines the geometry of the cap surface. The ellipticity of the cap surface is determined by the material parameter R that relates the hardening parameter p_a to p_b through the relation

$$p_b = p_a + RF_e^*(p_a) \qquad (11)$$

with

$$F_e^*(p_a) = d_0 + (p_a - 1)\tan\beta \qquad (12)$$

where d_0 is the initial material cohesion. Because the ellipticity of the cap surface may also be influenced by the incompressible plasticity, the cap hardening evolution does not take into account the increase in the material cohesion d due to the isotropic plasticity of the particle.

Sandler and Rubin [1979] proposed a relationship to define the evolution of the cap's motion, which is defined by the isotropic cap hardening rule

$$\bar{\varepsilon}_{vol}^{p} = W\left(1 - \exp\left[-c_1 p_b^{c_2}\right]\right) \qquad (13)$$

In which W is the maximum plastic volumetric strain (at hydrostatic compression *'lockup'*), c_1 and c_2 are material shape factor parameter, and $\bar{\varepsilon}_{vol;}^{p}$ is the effective volumetric plastic strain defined by integrating

$$\dot{\bar{\varepsilon}}_{V}^{p} = \begin{cases} \dot{\varepsilon}_{vol}^{p} & \text{if } p_a > 0 \text{ and } I_1 > 0 \\ 0 & \text{otherwise} \end{cases} \qquad (14)$$

where ε_{vol}^{p} is the plastic volumetric strain. The density can also be defined by an associative or a non-associative flow rule with pressure dependent deviatoric [Marin and McDowell, 1996].

The form of the elastic domain is defined in terms of the failure shear and cap yield surfaces as

$$F_s(|s|, p) < 0 \quad \text{and} \quad F_c(|s|, p) < 0 \qquad (15)$$

For multisurface plasticity, an appropriate statement of the flow rule relies on Koiter's generalization, which, using the flow potentials F_s and F_c, takes the form

$$\underline{\dot{\varepsilon}}^{p} = \dot{\gamma}_s \frac{\partial F_s}{\partial \underline{\sigma}} + \dot{\gamma}_c \frac{\partial F_c}{\partial \underline{\sigma}} \qquad (16)$$

where $\dot{\gamma}_S$ and $\dot{\gamma}_c$ are the plastic consistency parameters. Plastic loading or elastic loading/unloading is formulated in Kuhn-Tucker form by means of the relation

$$\dot{\gamma}_s, \dot{\gamma}_c \geq 0, \; F_s, F_c \leq 0 \text{ and } \dot{\gamma}_s F_s + \dot{\gamma}_c F_c = 0 \qquad (17)$$

The plastic hardening of the particles allows the hardening of the failure shear envelope and the cap surface. The cohesion of the powder aggregate d will then increase as follows

$$d = d_0 + \kappa + V(\theta)\sinh^{-1}\left[\frac{\dot{\bar{\varepsilon}}^{p}}{f(\theta)}\right] \qquad (18)$$

The cap hardening evolution is based on the material cohesion d_0 and is then not affected by the dilatancy of the cap surface due to particle hardening of particles. The material cohesion d_0 is given by

$$d_0 = d_1 \exp\left[d_2 \bar{\varepsilon}_{vol}^{p}\right] \qquad (19)$$

In Figure 8, we observe the evolution of the cap yield surface during densification where only the plasticity of the powder aggregate is considered (no deformation of individual particles) and the cap eccentricity R is function of the density as follows

$$R = \frac{R_1 - R_2}{1 + \left(\rho / \rho_c\right)^{k}} + R_2 \qquad (20)$$

where d_1, d_2, R_1, R_2, ρ_c and k are material parameters.

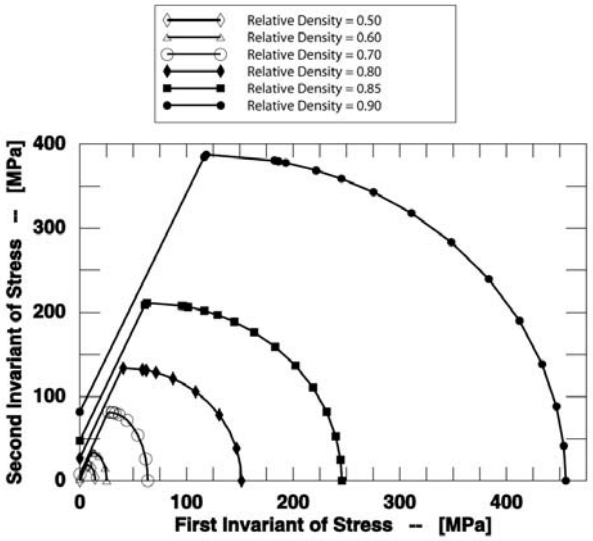


Figure 8. Evolution of the cap yield surface during densification.

Fundamental: Nanoscale Friction Analysis

The Molecular Dynamics research is focused on modeling the interparticle behavior between two nanoparticles during compression for friction analysis. Each particle is conveniently represented by a sphere. Nickel is chosen as the powder material since nickel particles are spherical and its Embedded Atom Method (EAM) potential is already defined. The purpose of this nanoscale analysis is to study the interparticle friction for different lattice orientation and particle packing configuration, and to understand its influence on macroscopic material properties.

Atomistic simulations using EAM potential were performed for various model setups, as shown in Figure 9. The model setups consisted of two contacting particles of various sizes, crystal orientations, and misorientation angles to analyze the effect of these parameters on nanoparticle behavior. Boundaries were defined as free surfaces in the *x*- and *z*-directions, and by applying a compressive load along the *y*-direction by defining an applied velocity. The imposed velocity resulted in very high strain rates, on the order of $10^8\ s^{-1}$.

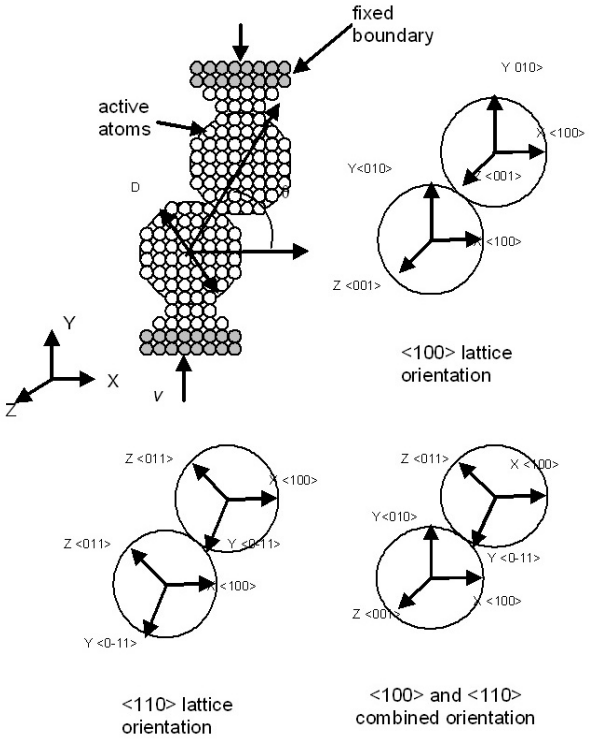


Figure 9. Model configuration with θ=30°, 60°, 90°, D = 3.52 nm, 10 nm, 20 nm, applied velocity v = 0.022 *Å/ps*, and various crystal orientations.

Before the velocity is applied, a Nose-Hoover thermostat was used to enforce a constant temperature of 300 K, and to equilibrate the system accommodating any surface relaxation the system may have. At the completion of the equilibrium phase, a linear *y* velocity profile $v_y = \dot{\varepsilon} y$ is applied to all atoms. This is done in order to avoid an initial shock wave, which otherwise would result from the instantaneous application of the boundary conditions on the $\pm y$ surfaces. Figure 10 shows the model configuration for the various particle sizes investigated in the analysis. These results were after 10 psec of temperature equilibrium, but prior to the applied velocity.

Figure 11 shows stress-strain results from the molecular dynamics simulation for two 3.52 nm particles at 30 degree misorientation angle. Each dot in the figure represents an individual nickel atom with a centrosymmetry value, a measure of an atom's disturbance for its crystalline lattice position, greater than 2.0. Several locations of micro-yield, where the stress-strain behavior deviates from elastic linearity, were identified on the curves.

The first location of micro-yield was when the initial dislocations were emitted from the grain boundaries. The steep drops in the stress-strain response were due to the formation of shear bands. Size effects on the axial stress strain results show that as particle size increases, the yield strength decreases, which is consistent with experimental results. Misorientation angle effects on the axial stress-strain response result in the highest yield stress for the 90 degree case and smallest yield stress for the 30 degree case. Lattice orientation effects on the axial stress-strain response show the most severe shear band formation occurred on the <110> crystal orientation.

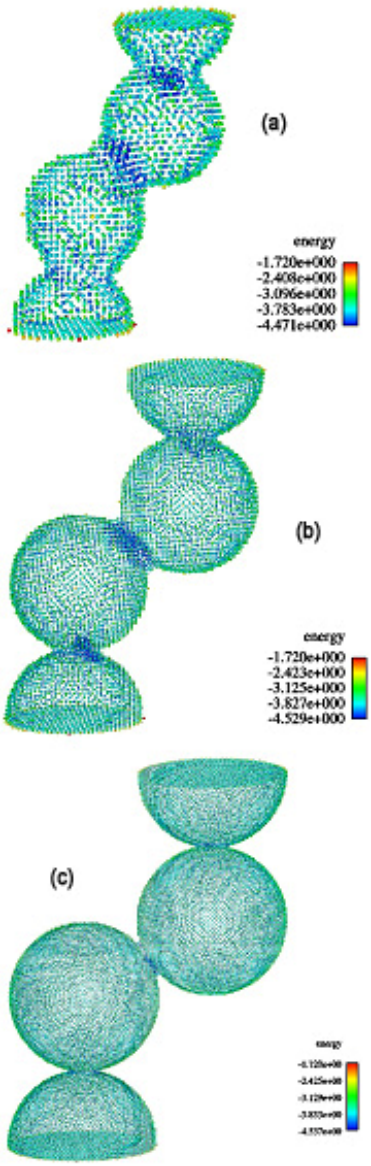


Figure 10. Atomistic model for (a) 3.52 nm (2123 atoms per particle), (b) 7.04 nm (16757 atoms per particle), and (c) 14.08 nm diameter particles (134000 atoms per particle), after 10 ps of temperature equilibrium and no applied velocity.

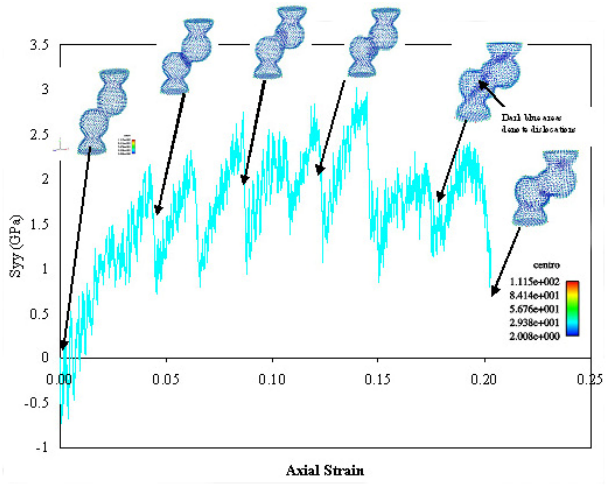


Figure 11. Compressive stress vs. Axial strain results for 3.52 nm particles with <100> crystal orientation at 30 degree misorientation angle during compression with 5E8/s applied strain rate.

Application: FE Analysis of Compaction

In order to illustrate the applicability of the developed compaction model, the powder behavior during the compaction of a set of complex forming processes are analyzed numerically in ABAQUS/ Explicit. Two different geometries have been selected; a 3D cylinder and a gear. Simulations of the 3D cylinder will be used in the second phase for correlation and validation of model constants, and the gear and bearing cap are the two chosen automotive components for durability, quality control, performance and design optimization.

The two geometries were simulated by using displacement control when increasing the punch movement. The parameters were chosen arbitrarily and do not really represent any existing metal powders. Numerical results presented in this section do not reflect any experimental data or results in the literature. The goal is to illustrate how the model can capture the density distributions during compaction. In both analyses, the dies were represented by rigid bodies and a friction coefficient of value 0.1 was applied at the interface powder/die. The upper and lower punches were moving at the same speed and in opposite directions. The theoretical density is 7.8 g/cc and the initial density is equal to 4.13 g/cc, which represents 53% of the theoretical density.

The 3D cylinder was set with initial height of 100 mm before compaction, the diameter was

12.5 mm. Figure 12 shows the relative density distribution after compaction, which corresponds to a height of 60 mm. It is noteworthy that the neutral zone is located at the center of the cylinder and on the lateral surface, and the highest relative density (93%) is at the end surfaces on the corner next to the die wall. The density gradient along the cylinder axis is due to the die wall friction. Figure 13 shows the compressibility curve of a given point.

The inner, root and outer diameters of the gear were respectively 8 mm, 20 mm and 27 mm, the thicknesses before and after compaction were 8 mm and 4.8 mm (Figure 14). Note that the behavior of density gradient along the gear axis and next to the die wall or core rod is the same as that in the

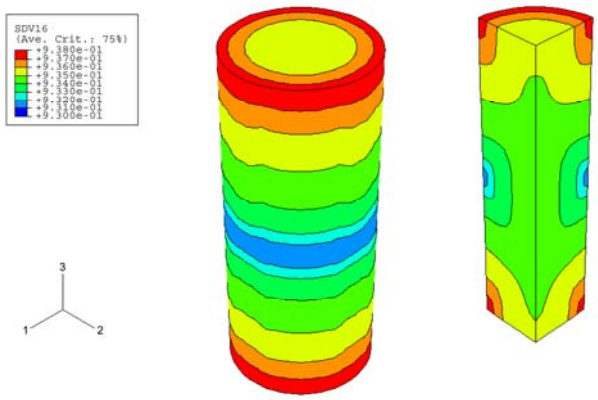


Figure 12. Relative density distribution in a 3D cylinder.

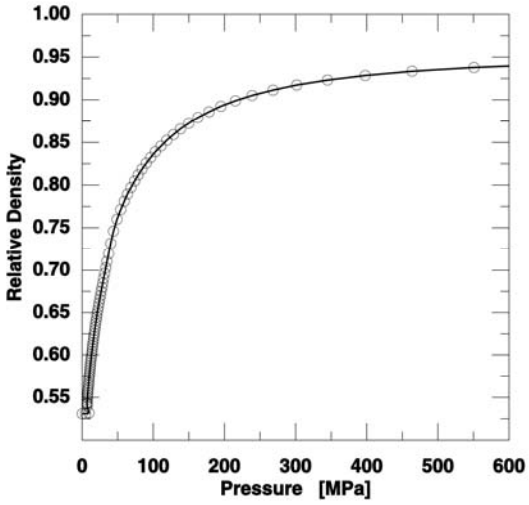


Figure 13. Compressibility curve.

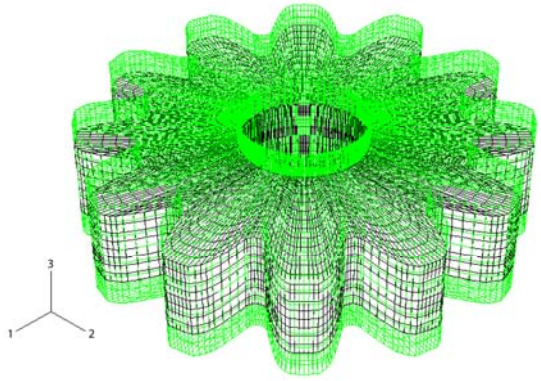


Figure 14. Undeformed and deformed meshes of a gear.

cylinder case before due to the die wall friction. The highest density (7.3 g/cc) is at the gear tooth arcs, next to the die wall and the punches, and at the inner diameter, next to the core rod. The density distribution between the inner and root diameters is mostly homogeneous due to the relative small thickness of the gear.

In the next year effort, we will focus on the comparison between numerical simulations and experimental validations of gears and bearing caps.

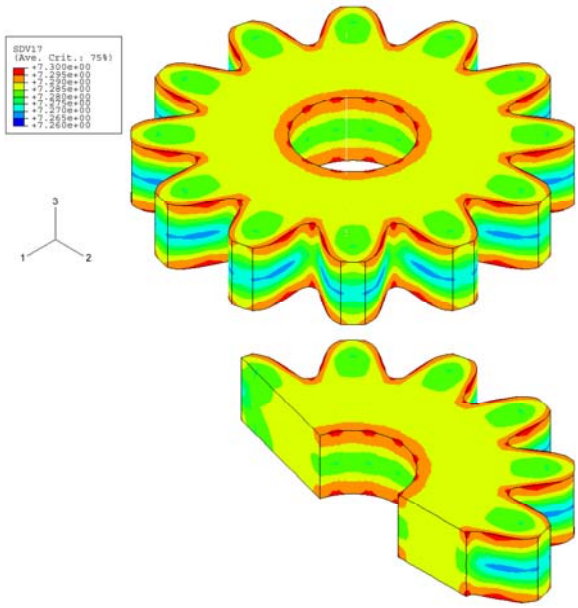


Figure 15. Density distribution in a gear (g/cc).

Conclusions

The Powder Metallurgy Performance Modeling of Automotive Components Project has made significant progress especially in the area of modeling where a constitutive law to predict material state during powder compaction was developed and implemented into a finite element code. This constitutive model is based on the Modified Drucker-Prager cap model and mixed with the microstructure-based plasticity. It also includes different density-dependent material parameters. Other project accomplishments include identification and standardization of performance test methods; identification of testing instrumentation to characterize the metal powder properties; establishment of a test matrix to build a complete microstructure property database for compaction, sintering, performance and fatigue. In fiscal year 2006, the project team expects to conduct experiments on powder compaction defined in the test matrix, complete sintering modeling and link that model to the compaction model, perform atomistic simulation to determine the interparticle friction coefficient, and finally write a documentation report of the second phase of the project in October 2006.

Acknowledgements

The authors would like to acknowledge funding from the Center for Advanced Vehicular Systems at Mississippi State University and from USAMP Lightweight Materials Group. We also acknowledge valuable guidance received from Howard I. Sanderow (MET and Center for Powder Metallurgy Technology – CPMT), Russell A. Chernenkoff (Ford Motor Company), William F. Jandeska (Center for Powder Metallurgy Technology – CPMT), Jean C. Lynn and Scott Burrell (DaimlerChrysler).

Presentations/Publications/Patents

1. "Design of Powder Metallurgy Components Considering History and Multiscale Effects," H.I. Sanderow, P. Wang, Y. Hammi, T.Y. Stone and M.F. Horstermeyer, presented at the 2005 MPIF Fall Management Conference and 61st Annual Meeting, October 11, 2005, Key Biscayne, Florida.
2. "Constitutive Modeling for Powder Compaction and Densification," Y. Hammi, T.Y. Stone and M.F. Horstermeyer, presented at the PM^{2}TEC 2005 International Conference on Powder Metallurgy & Particulate Materials, June 21, 2005, Montreal, Canada.
3. "Constitutive Modeling of Metal Powder Behavior during Compaction," Y. Hammi, T.Y. Stone and M.F. Horstermeyer, presented at the SAE 2005 World Congress, April 12, 2005, Detroit, Michigan.

References

1. Abaqus, User's Manual, Version 5.8, Hibbit, Karson & Sorensen, Inc., 2003.
2. Alder, B. J. and Wainwright, T. E. J. Chem. Phys. 27, 1957, pp. 1208.
3. Alder, B. J. and Wainwright, T. E. J. Chem. Phys. 31, 1959, pp. 459.
4. Bammann, D.J. "Modeling Temperature and Strain Rate Dependent Large Deformations of Metals," Appl. Mech. Rev.,Vol. 1, 1990, pp. 312–318.
5. Bammann, D.J., Chiesa, M.L., Horstemeyer, M.F. and Weingarten, L.I. "Failure in Ductile Materials Using Finite Element Methods," In: Jones, N., Wierzbicki, T. (Eds), Structural Crashworthiness & Failure, Elsevier, Amsterdam, 1993, pp. 1–54.
6. Coube, O. and Riedel, H. "Numerical Simulation of Metal Powder Die Compaction with Special Consideration of Cracking", Powder Metallurgy, Vol. 43, No. 2, 2000, pp. 123–131.
7. Cundall, P.A. and Strack, O.D.L. "Discrete Numerical Model for Granular Assemblies", Geotechnique, Vol. 29, No. 1, 1979, pp. 47–65.
8. DiMaggio, F.L. and Sandler, I.S. "Material Models for Granular", Journal of Engineering Mechanics", ASCE, Vol. 97, EM3, 1971, pp. 935–950.
9. German, R.M. *Powder Metallurgy Science*, Metal Powder Industries Federation, Princeton, NJ, 1994.
10. Gillia, O.T., Dihoru, L., and Cocks, A.C.F., Modeling Die Filling, In: A. Lawley, J.E. Smugeresky, L. Smith, (Eds.), Process Modelling in Powder Metallurgy & Particulate Materials, MPIF, Princeton, NJ, 2002, pp. 161-165.

11. Gurson, A.L. and Posteraro, R.A. "Yield functions for metal powders for use in the numerical simulation of powder compaction", TMS Annual Meeting, 1994, pp. 3.
12. Horstemeyer, M.F., Lathrop, J., Gokhale, A.M. and Dighe, M. "Modeling Stress State Dependent Damage Evolution in a Cast Al-Si-Mg Aluminum Alloy", Theor. Appl. Fract. Mech., Vol. 33, 2002, pp. 31–47.
13. Horstemeyer, M.F., Osborne, R., and Penrod, D., "Microstructure-Property Analysis and Optimization of a Control Arm", American Foundry Society, AFS Transactions, 02-036, 2002, pp. 297–314.
14. Horstemeyer, M.F. and Wang, P. "Cradle-to-Grave Simulation-Based Design Incorporating Multiscale Microstructure-Property Modeling: Reinvigorating Design with Science", Journal of Computer-Aided Materials Design, Vol. 10, No. 1, 2003, pp. 13–34.
15. Johnson, G.C. and Bammann, D. J. "Discussion of Stress Rates in Finite Deformation Problems", International Journal of Solids and Structures, Vol. 20, No. 8, 2004, pp. 725–737.
16. Khoei, A.R. and Lewis, R.W. 1998, "Finite Element Simulation for Dynamic Large Elastoplastic Deformation in Metal Powder Forming", Finite Elements in Analysis and Design, Vol. 30, No. 4, pp. 335–352.
17. Marin, E.B. and McDowell, D.L. "Associative Versus Non-Associative Porous Viscoplasticity Based on Internal State Variable Concepts", International Journal of Plasticity, Vol. 12, No. 5, 1996, pp. 629–669.
18. Pavier, E. and Doremus, P. "Triaxial Characterisation of Iron Powder Behaviour", Powder Metallurgy, Vol. 42, No. 4, 1999, pp. 345–352.
19. PM Modnet Methods and Measurement Group. "Measurement of Friction for Powder Compaction Modeling – Comparison with Laboratories", Powder Metallurgy, Vol. 43, No. 4, 2000, pp. 364-374.
20. Trasorras, J.R.L., Armstrong, S., and McCabe, T.J.. "Modeling the compaction of steel powder parts," Advances in Powder Metallurgy and Particulate Materials, v 7, 1994, p 33.
21. Sandler, I.S. and Rubin D. "An Algorithm and a Modular Subroutine for the Cap Model", Int. J. Numeri. Analy. Meth. Geomech., Vol. 3, 1979, pp. 173–186.

N. High-Strength Steel Joining Technologies Project

Project Manager: Michael S. Bzdok
Auto/Steel Partnership
2000 Town Center, Suite 320
Southfield, MI 48075-1123
(248) 945-4778; fax: (248) 356-8511; e-mail: mbzdok@a-sp.org

Co-chair: James W. Dolfi
Dolfi AWS LLC
16883 Shrewsbury
Livonia, MI 48154
(734) 427-8117; fax: (734) 427-1827; e-mail: dolfi@www.net.com

Co-chair: John C. Bohr
General Motors Corporation – Controls, Robotics, and Welding
30300 Mound Road – Mail Code 480-109-164
Warren, MI 48090-9015
(810) 602-8276; fax: (586) 947-1039; e-mail: johnc.bohr@gm.com

Technology Area Development Manager: Joseph A. Carpenter
(202) 586-1022; fax: (202) 586-1600; e-mail: joseph.carpenter@ee.doe.gov
Field Technical Manager: Philip S. Sklad
(865) 574-5069; fax: (865) 576-4963; e-mail: skladps@ornl.gov

---

Contractor: U.S. Automotive Materials Partnership
Contract No.: FC26-02OR22910

Objective

The objective of the High-Strength Steel Joining Technologies project team is to provide welding and joining expertise to the Auto/Steel Partnership (A/SP) lightweighting projects to facilitate the increased use of advanced high-strength steels (AHSS). Additional project objectives include augmenting the technical knowledge pertaining to welding of AHSS through applied research and development of industry standards for quality acceptance and weldability testing of AHSS.

Approach

- Determine welding parameters to produce quality welds, then statically and dynamically test welds produced at these parameters to quantify individual weld structural performance (See Figure 1). Tensile shear strength, impact energy and fatigue life are typically evaluated.
- Develop procedures for testing of AHSS and evaluating weld performance, where there is a lack of applicable standards.

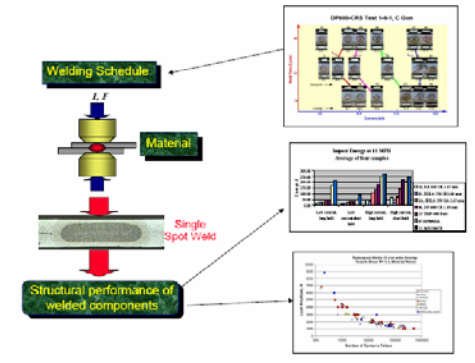


Figure 1. Resistance Spot Welding Process Approach Example

- Focus on materials classified as Group 3 and 4 (See Figure 2), as well as specific materials recommended by the A/SP Lightweight Structures Group.

Group	Min Tensile Strength	Typical Products
1	< 350 MPa	MILD 140/270 BH 180/300 BH 210/320 BH 240/340
2	350 - 500 MPa	BH 260/370 HSLA 280/350 HSLA 350/450 DP 300/500
3	> 500 - 800 MPa	DP 350/600 TRIP 350/600 DP 500/800 TRIP 500/800 CP 700/800
4	> 800 MPa	DP 700/1000 Mart 950/1200 Mart 1150/1400 Mart 1250/1520

Figure 2. IISI Steel Classifications for Welding

- Secure material in sufficient quantities from membership companies to fabricate samples and complete structural performance testing according to a predetermined project plan or matrix.
- Investigate the use of process finite element modeling to predict weld quality characteristics and optimize weld process parameters (See Figure 3). Simulate, using finite element modeling, where applicable, future projects for weld process optimization and weldability assessments. Validate simulation results with experimental data.

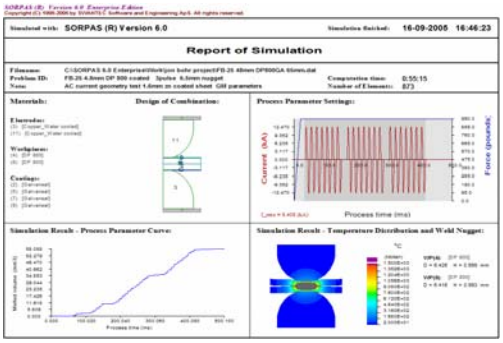


Figure 3. Process Simulation Report for RSW of DP780 Utilizing B-Nose Electrode and 3-Pulse Weld Schedule

Accomplishments

- Developed weld parameters for specified material grade and thickness combinations for the A/SP Lightweight Front End Structures Group (LWFES, report 2.U), provided technical direction, and applied welding practices to fabricate a prototype AHSS vehicle front structure.
- Provided equipment evaluation and set-up support at the prototype build shop and provided the post-crash weld performance report for inclusion in the final LWFES prototype build report (See Figure 4).



Front view showing bumper reinforcement and rail collapse. All welds were acceptable.



Left-hand side view showing integrity of spot welds on the AHSS rail assembly between bumper and dash.

Figure 4. Lightweight Front End Structures – Crash Test Photos

- Reviewed the draft report and completed additional work to support the referenced American Iron and Steel Institute (AISI)/Edison Welding Institute (EWI) project that addresses the effect of tempering welds made with dual-phase (DP), Martensitic, and transformation-induced plasticity (TRIP) steels.
- Provided technical direction and coordination for material selection to conclude the Steel Institute AISI/EWI project, Technology Roadmap Program #0114, DE-FCO7-97ID13554, which addresses the effect of tempering welds made with DP, Martensitic, and TRIP steels.
- Developed the test-plan matrix for evaluation of weld processes including metal inert gas (MIG), laser-assisted MIG, and plasma-assisted MIG. Obtained and provided the necessary materials and completed testing and review of the welds, resolved process issues, and approved process samples (See Figures 5 and 6).
- Completed projection weld fastener resistance weld process and simulation study. Worked with the University of Waterloo to model the projection welding of a hex-flanged weld nut using SORPAS with a cylindrical block model. Weld test results have correlated with the model. A final project report is under review.
- Produced and tested samples for low-temperature impact-strength study. Test data are undergoing review and analysis.
- Provided direction and post-test samples of tensile shear and impact tests for committee review, provided data to support development of AHSS resistance-weld quality standard, submitted data and participated in SAE/AWS D8 standard development of AHSS weld quality documents, and provided technical support for development of AHSS fracture classification matrix for standardization. (See Figure 7).

Future Direction

Future team activities include supporting welding development for the recently formed A/SP AHSS Application Guidelines Project Team and developing welding parameter and joint performance data for specific applications on AHSS automotive body prototypes.

- Assess capability to perform drawn-arc stud welding on AHSS.
- Develop a Design of Experiment (DoE) methodology for material characterization and for assessing manufacturing feasibility of spot-welding AHSS.
- Develop software application to support common deployment and analysis of the AHSS DoE test method.
- Develop weld process modeling and joint prediction models to reduce weld testing.
- Assess paint bake and sub-zero thermal cycle effects on welds.
- Support collaborative agreement with LeTourneau University for testing and post-mortem analysis of fracture surfaces of welds from other A/SP resistance-welding efforts.

SWSG First AHSS Sample for Approval, a Robotically Welded Section of 3.40 mm DP600 Bare to 3.40 mm DP600 Bare

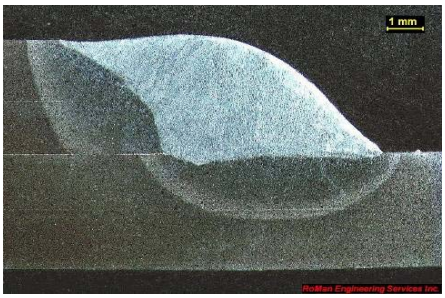


Figure 5. Approval sample cross-section 3.40 mm DP600 Bare to 3.40 mm DP600 Bare

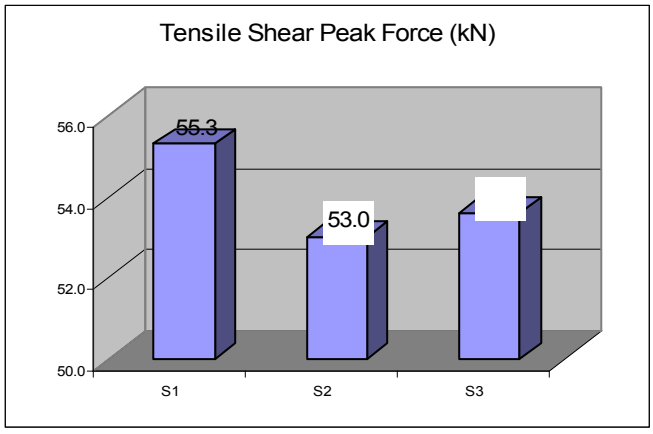


Figure 6. Structural Weld Sub-Group Stack up 1 3.40 mm DP600 Bare to 3.40 mm DP600 Bare Robotically Produced MIG Weld

PROPOSED STANDARD FRACTURE CLASSIFICATION Submitted to AWS D8 Automotive Standards Committee

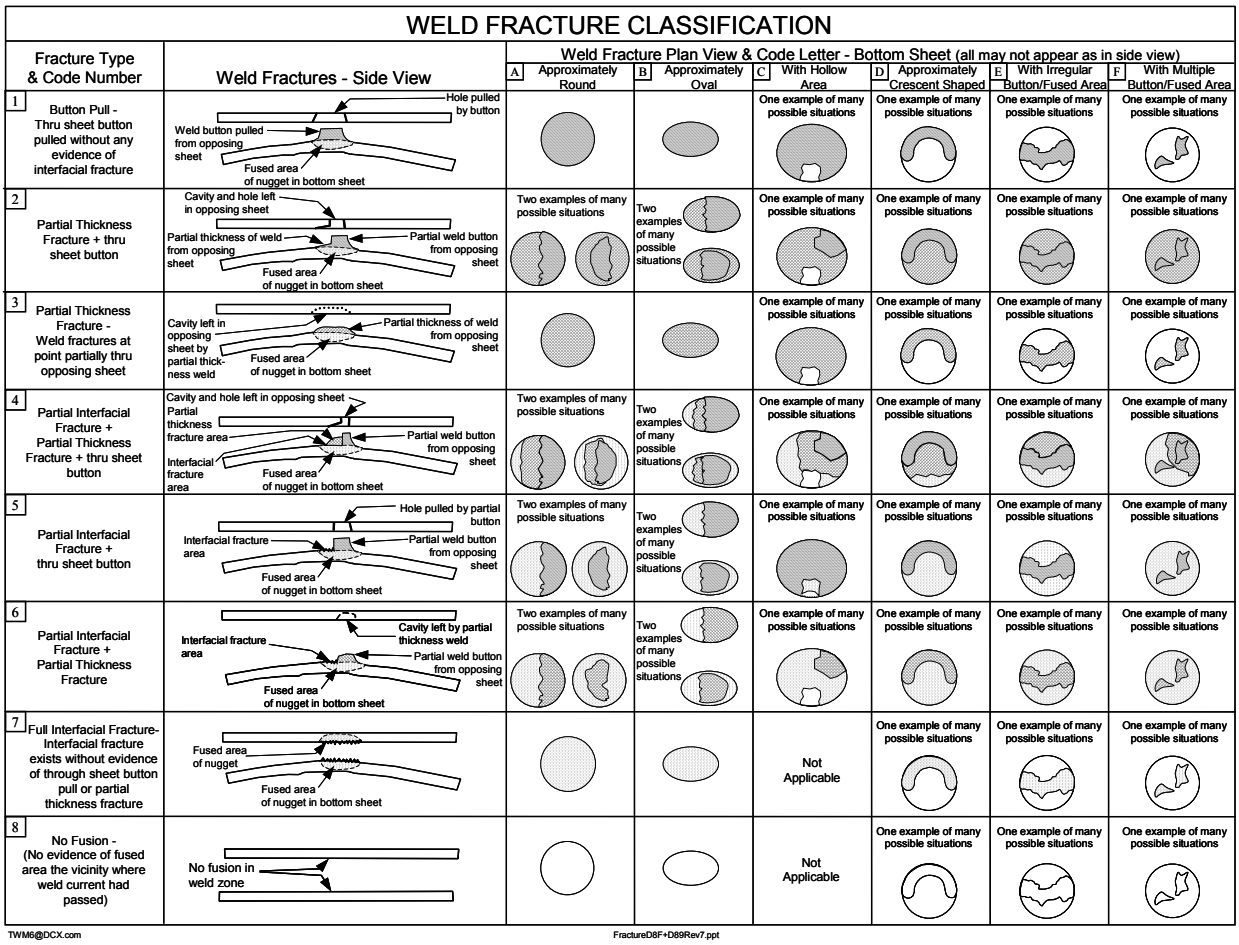


Figure 7. Proposed fracture classification matrix.

O. Hydroform Materials and Lubricants Project

Project Manager: Gene Cowie
Auto/Steel Partnership
2000 Town Center, Suite 320
Southfield, Michigan 48075-1123
(248) 945-4779; fax: (248) 356-8511; e-mail: gcowie@a-sp.org

Chairperson: Ronald Soldaat
Dofasco, Inc.
1330 Burlington Street East
P.O. Box 2460
Hamilton, Ontario, Canada L8N 3J5
(905) 548-7200; fax: (905)5480-4250; e-mail: Ronald_Soldaat@dofasco.ca

Technology Area Development Manager: Joseph A. Carpenter
(202) 586-1022; fax: (202) 586-1600; e-mail: joseph.carpenter@ee.doe.gov
Field Technical Manager: Philip S. Sklad
(865) 574-5069; fax: (865) 576-4963; e-mail: skladps@ornl.gov

---

Contractor: U.S. Automotive Materials Partnership
Contract No.: FC26-02OR22910

Objective

- Develop mechanical test procedures and forming-limit diagrams for tubes.
- Improve the accuracy and confidence in finite element modeling of tubular hydroforming.
- Investigate the fabricating and performance characteristics of tailor-welded tubes.
- Develop an understanding of steel and lubricant requirements for hydroforming using a combination of experiments and finite element modeling.
- *Support the work of other Auto/Steel Partnership (A/SP) project teams when they investigate hydroformed structural components.*
- Validate the performance benefits of hydroforming in automotive structures.

Approach

The approach taken on this project is to gain a basic understanding of the hydroforming process and potential issues. The investigation encompasses various grades and gauges of steel tubing, including tailor-welded tubes, in free-expansion and corner-fill processes using several types of lubricants. The work has been divided into six phases.

1. Phase 1 – Free-expansion and corner-fill characteristics
2. Phase 2 - Effects of end feeding and pre-bending on hydroforming limits
3. Phase 3 - Investigate some of the pre-bending parameters for the hydroforming process
4. Phase 4 - Investigate some of the bending parameters for advanced high-strength steel tubing
5. Phase 5 - The experimental forming limits of steel tubes
6. Phase 6 - Empirical prediction of tube forming limit diagrams and analysis of hydroforming data

Delays in obtaining sheet stock and tubes caused Phases 3 and 4 to follow 5 and 6.

Accomplishments

During the report period (October 1, 2004 – September 30, 2005) the following were accomplished.

- Completed tube-bending tests comprehending two materials (IF and DP600), two bending speeds and two lubricants.
- Conducted inside and outside corner-fill tests on pre-bent DP 600 tubes.
- Conducted inside and outside corner-fill tests on pre-bent IF tubes.

Future Direction

During fiscal year 2006, the Hydroforming Materials and Lubricant plans to accomplish the following:

- Support the work performed by Lightweight Front End Structures (ASP080, see report 2.U) on a hydroformed front frame rail.
- Fabricate tailor-welded tubes for evaluation.
- Conduct free-expansion and straight-tube corner-fill tests on tailor-welded tubes.
- Begin to validate the performance benefits of tube hydroforming in automotive vehicle structures using tubes that simulate real-world applications.

Introduction

Hydroformed steel tubes have been used in the automotive industry to form components that meet structural objectives, particularly strength and rigidity, at optimal mass. One of the most significant advantages of tubes is that they are monolithic closed sections and, as such, exhibit many times more stiffness in torsion than conventional open sections, such as “C” and “hat” shapes. Their use is limited largely by a lack of knowledge about the capabilities and parameters of hydroforming processes and the effects of the processes on the tubes.

This project was undertaken to investigate and quantify the capabilities and parameters of various hydroforming processes so that automotive designers and engineers can utilize the tube configurations that are available and predict the performance of components made by hydroforming. Hydroforming tubes made from high-strength and advanced high-strength steels and fabricating and hydroforming tailor-welded tubes are of particular interest because of the potential reduction of mass associated with materials of higher strength and optimal thickness.

Discussion

Hydroforming is a process in which a tube is placed into a die, which is shaped to develop the desired configuration of the tube. Water is introduced into the tube under very high pressures, causing the tube to expand into the die. The tube ends can be held stationary or moved inward during the process to end-feed material into the die cavity.

The process has two distinct stages, shown in Figure 1. The first stage is free expansion (Figure 1a). It continues until the tube contacts the die wall (Figure 1b). In the second stage, corner filling, the tube is in contact with the surface of the die, which constrains subsequent deformation (Figure 1c). During this stage, the tube expands into the corners of the cavity, accomplishing corner fill. A tube that has been hydroformed is shown with the die in Figure 2. Note that the test was continued until the tube failed.

During corner fill, the tube slides against the die; therefore, friction between the tube and die affects the process, and the lubricant used in the process becomes a significant parameter.

During both stages, the tube undergoes plastic strain. The amount of plastic strain that can occur before the material fractures is predicted in stamping processes that utilize flat sheet steel by using a forming-limit diagram (FLD). The FLD is determined by the properties of the material. The hydroforming process is preceded by tube forming

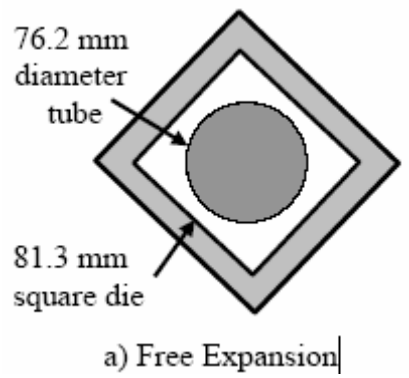


Figure 1a

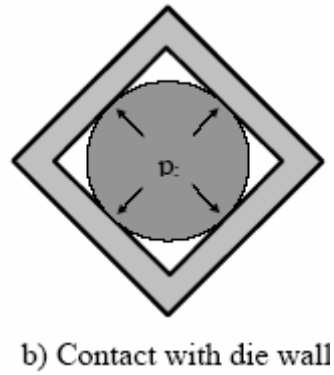


Figure 1b

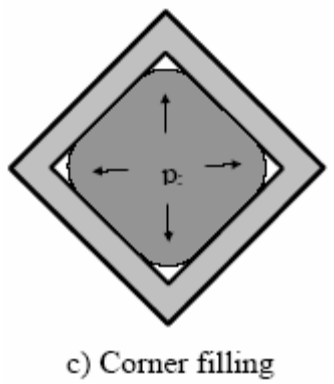


Figure 1c

Figure 1. The Hydroforming Process

and sometimes pre-bending of the tube, both of which induce strains in the material and alter its properties. Before an FLD can be developed for the hydroforming process, the strain history, that is, the strain induced in the material prior to hydroforming, must be known.

An FLD is required for any successful computer simulation of hydroforming. Therefore, in addition to experiments with tube expansion to determine the



Figure 2. A hydroformed tube and die

effects of axial compression and tension in combination with internal pressurization, the effects of pre-bending and pre-forming on subsequent formability was addressed. Collected data were used to develop forming-limit diagrams for tubular hydroforming of straight tubes. These data will be used to develop guidelines for optimizing bending operations.

Presently, the formability limits for pre-bent steel in tubular hydroforming are poorly understood. Accuracy needs to be addressed and improved to allow optimum application of tubular hydroforming in the lightweighting of vehicles.

Tube bending-phases 3 and 4, which were delayed while obtaining the selected sheet steel and converting to tube, began in November, 2004. The bending tests comprehend three variables: material, lubricant and bending speed. The materials are interstitial free (IF) and dual-phase (DP600); a water-based and a mineral oil-based lubricant were selected. Bending speeds were selected. The results will be evaluated to determine the effects of these variables on tube surface quality and hydroforming formability.

The Hydroforming Materials and Lubricants Project Team have begun to evaluate the potential of tailor-welded tubes for the hydroforming process. This phase of testing will be conducted on 76.2-mm (3")-OD tubes made from two material grades and two thicknesses. The test will consist of five iterations as follows:

1. Baseline: 1.5 mm DP600 single material tube (20.00 inches long)
2. 1.5 mm DP600 butt-welded to 1.5 mm DP600
3. 1.2 mm DP600 butt-welded to 1.5 mm DP600
4. 1.5 mm HSLA350 butt-welded to 1.5 mm DP600
5. 1.5 mm HSLA350 butt-welded to 1.2 mm DP600

The tubes will be analyzed and then utilized for hydroforming tests.

Requests for quotation have been sent to two tube fabricators and one has been selected. A request for Purchase Order has been issued and is currently being processed.

Future Work

During the 2006 fiscal year, the Hydroforming Materials and Lubricants Team plan the following work:

1. Procure the five sets of tubes for the tailor-welded tube evaluation.
2. Analyze the tubes.
3. Perform hydroforming tests.
4. Continue to support the work of ASP080 Lightweight Front End Structures.
5. Validate the performance benefits of tube hydroforming in automotive vehicle structures.

Conclusions

Analysis of tests run during this reporting period indicates that:

- Bending speed had no measurable effect on the inside bend geometry and strain patterns for both the DP600 and IF tubes. The speeds evaluated were 22.5°/ sec and 30°/sec (4 sec. and 3 sec. to bend 90°) for DP600 tubes and 22.5° /sec. and 36°/sec. (4 sec. and 2.5 sec. to bend 90°) for IF tubes.
- Lubricant choice had a measurable effect on both bending and corner-fill hydroforming.

P. Sheet Steel Fatigue Characteristics Project

Project Manager: Gene Cowie
Auto/Steel Partnership
2000 Town Center, Suite 320
Southfield, Michigan 48075-1123
(248) 945-4779; fax: (248) 356-8511; e-mail: gcowie@a-sp.org

Chairman: John Bonnen, Ph.D.
Ford Motor Company
Ford Research Laboratory
20000 Rotunda Drive
Dearborn, Michigan 48121-2053
(313) 322-9127; fax: (313) 390-0514; e-mail: jbonnen@ford.com

Technology Area Development Manager: Joseph A. Carpenter
(202) 586-1022; fax: (202) 586-1600; e-mail: joseph.carpenter@ee.doe.gov
Field Technical Manager: Philip S. Sklad
(865) 574-5069; fax: (865) 576-4963; e-mail: skladps@ornl.gov

---

Contractor: U.S. Automotive Materials Partnership
Contract No.: FC26-02OR2290

Objective

- Compile the test data generated in the previous phases of the program into a user-friendly database that can be used in all phases of design and structural analysis of sheet steel vehicle bodies.
- Investigate the fatigue life of joints formed by spot welding, adhesive bonding and weld bonding (a combination of welding and adhesive bonding).
- Explore the fatigue response of advanced high strength steels (AHSS) after being subjected to metal inert gas (MIG) and laser-welded joining and compare this behavior with that of standard automotive steels.
- Help Joining Technologies team (See report 2.N) identify optimum welding parameters for laser- and MIG-welded joints, and develop a fatigue test program.

Approach

- Investigate the fatigue characteristics of resistance spot welding, a fusion process in which the metal pieces to be joined are melted and re-solidified via a brief high-voltage electrical pulse, forming an alloy with a distinctly different microstructure than that of the metals that are joined. In addition, the weld nugget, or button, may contain discontinuities, which can become sites at which fatigue cracks form. The amount and type of discontinuities, and thus the fatigue properties, are affected to a considerable extent by the welding process. The microstructures of the joined metals are also changed in the area adjacent to the weld, which is known as the heat-affected zone (HAZ).
- Investigate the fatigue characteristics of adhesive bonding, which substitutes an entirely different material in place of the weld to act as the load-bearing connection. The adhesive must adhere to the metals being joined and resist fatigue failure at the adhesive/metal interface and within itself.
- Investigate the fatigue characteristics of weld bonding.

- Investigate the previously unknown, or at best little known, factors that are expected either to improve or impact durability, and facilitate modeling and simulation.
- Reduce the spot-welded, adhesive-bonded and weld-bonded test data to a form that is useful to design engineers who perform vehicle structural analysis.
- Develop a test program to investigate the fatigue characteristics of MIG welding, a fusion process akin to spot welding that introduces a third "filler" metal, forms alloy microstructures different from the metals being joined, but also results in continuous joints.
- Identify the parameters of MIG-welded joints including metal grades, metal thicknesses, coatings and joint configurations that impact fatigue.

Accomplishments

- Defined the parameters of the sheet steel fatigue database and engaged a contractor to perform the work. The database has been constructed and has undergone several evaluations by team members. Work is expected to be complete by the end of 2005.
- Selected 27 combinations of steel grades and coatings for discontinuous-joint fatigue testing. Of the combinations, 22 were spot welded, and all are completed. Two of the combinations were weld bonded, and both have been completed. Three of the combinations were adhesive bonded, and have been completed.
- Re-inserted several tests that had previously been dropped, and have begun tests on spot-welded DQSK and Boron steels.
- Performed data reduction on spot-weld tests and issued a report.
- Contacted several consultants, invited them to present proposals for fatigue testing MIG welds, and selected one to develop a test program. The project team has approved the program and materials have been procured.
- Began a program to test MIG and laser welds in support of the Joining Technologies Project ASP070. Two test laboratories have been selected, and a contractor has been selected to perform the welding.

Future Direction

During the next fiscal year, the project team will do additional testing of spot-welded samples of mild steel and ultra high-strength boron steel. Upon completion, the information will be made available on the A/SP website and in published form through SAE. The project team will also begin its own program of fatigue testing MIG welds.

Introduction

Future and near-future vehicle designs are faced with several stringent requirements that impose conflicting demands on the vehicle designers. Safety must be improved while weight and cost are contained. Advanced high-strength steels, judiciously selected and applied, are currently the best candidates offering low-cost (compared with aluminum, magnesium and plastics), reliable materials for meeting these mandates. As structural components are optimized and thinner-gauge, higher-strength materials are assessed, fatigue life of the component and the areas where loads are transferred become increasingly important considerations. To assess the performance of a component in the design phase, the fatigue characteristics of the base material and the joints, where loads are transferred, must be known. This project has essentially completed testing various grades of steel that have been spot-welded, adhesively-bonded and weld-bonded, and is currently initiating tests on DQ and boron steel. Testing of MIG- and laser-welded joints is under way.

Discussion

Spot-Weld, Adhesive-Bonding and Weld-Bond Testing

The effort to evaluate the fatigue characteristics of spot-welds began in the 2002 fiscal year with presentations by key researchers on the current state of the work at DaimlerChrysler Corporation, Ford Motor Company, and General Motors Corporation. Based on these presentations, the Sheet Steel Fatigue Project Team (See report 2.P) has produced results beneficial to all three companies. Early in the planning, the Auto/Steel Partnership (A/SP) Joining Technologies Team was consulted, and that team prepared the samples to be tested. This interaction ensured that the samples were joined using procedures that were properly controlled and in adherence to the best current practices in sheet metal joining.

The following test parameters were agreed upon and carried out:

Two modes of testing: tensile shear (Figure 1) and coach peel (Figure 2).

Since weld fatigue performance is independent of metal thickness for mild steels, high-strength low-alloy (HSLA) grades and advanced high-strength steels (AHSS), tests on these grades utilized only one metal thickness (1.6 mm).

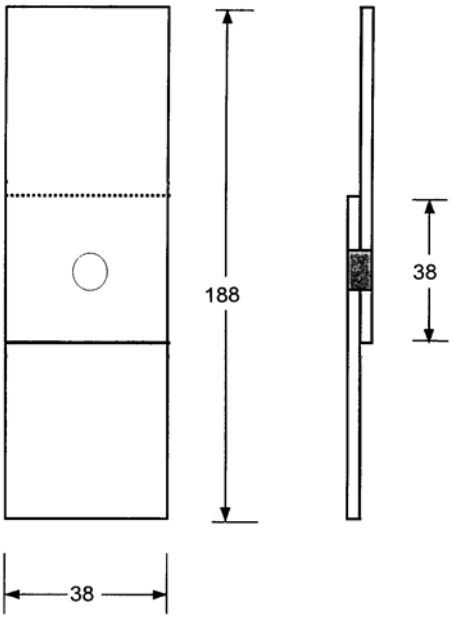


Figure 1. Spot-Welded Lap Shear Test Specimen

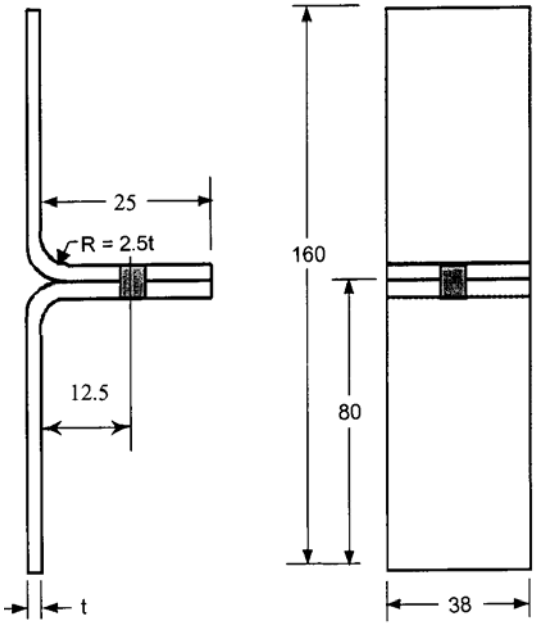


Figure 2. Coach Peel Test Specimen

Because no such data were available for AHSS, several grades in this class were tested at two thicknesses (1.6 mm and 0.7 mm).

Testing was done at two R ratios: 0.1 and 0.3. The stress ratio R is defined as the ratio of the minimum stress to the maximum stress in the test cycle. Maximum and minimum values are algebraic, with tension designated as positive and compression negative.

Eleven steel grades were tested. Most of the testing was performed on spot-welded joints. Several tests were also performed on adhesive-bonded and weld-bonded joints.

Two sources, of the nine invited to submit testing proposals, were selected to perform the work: The University of Missouri in Columbia, Missouri, and Westmoreland Mechanical Testing and Research, Inc. in Youngstown, Pennsylvania.

As the testing progressed and results were analyzed, the following tests were added for comparison purposes:

1. Testing at specified R ratios means that the maximum and minimum loads are constant throughout a given test. However, as the maximum load is increased to generate fatigue curve data, the minimum loads also increase. This process is valuable for establishing base-line data. However, in the real world, loads can be expected to vary. For this reason, two sets of automotive spectrum load tests, set to different predetermined load scalings, were run.
2. Two studies were performed on samples with a different welding schedule that produced a smaller weld button.
3. At the request of the Joining Technologies Team, three tests were run using wide samples (125 mm vs. the standard 38 mm). The wider samples minimize rotation of the weld under load.

Metal Inert Gas (MIG)-Welded Joints

MIG welding is the second most common welding process used on vehicle structures, and applications are expected to increase. MIG welds are used not only on body members and sub-frames, but also in frames for larger passenger vehicles, light trucks and sport-utility vehicles (SUV). Therefore, the test samples will be made from two thickness ranges: 1.6 mm for body applications and 3.4 mm for frame applications (boron steel will be tested at 1.8 mm thickness). These are target thicknesses based on material availability, and variations will be made where necessary on approval of the team.

Frame members do not generally require as much formability as body members, and they offer excellent opportunities for mass reduction through downgaging. Therefore, tests on frame joints will ultimately employ higher strength materials than those specific to body members.

The Team agreed to four modes of testing: butt weld (Figure 3), single-lap shear (Figure 4), double-lap shear (Figure 5), and perch mount (Figure 6).

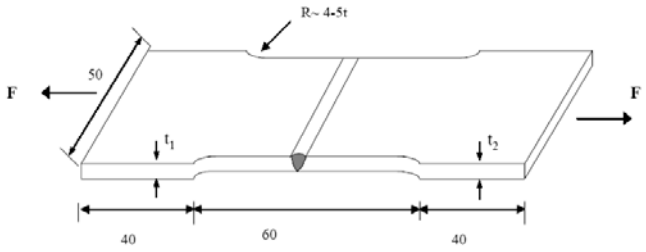


Figure 3. MIG-Butt-Welded Specimen

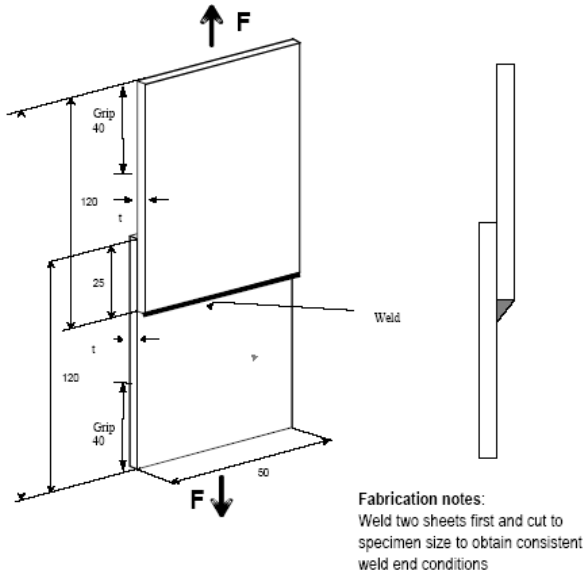


Figure 4. MIG Welded Single-Lap Shear Specimen

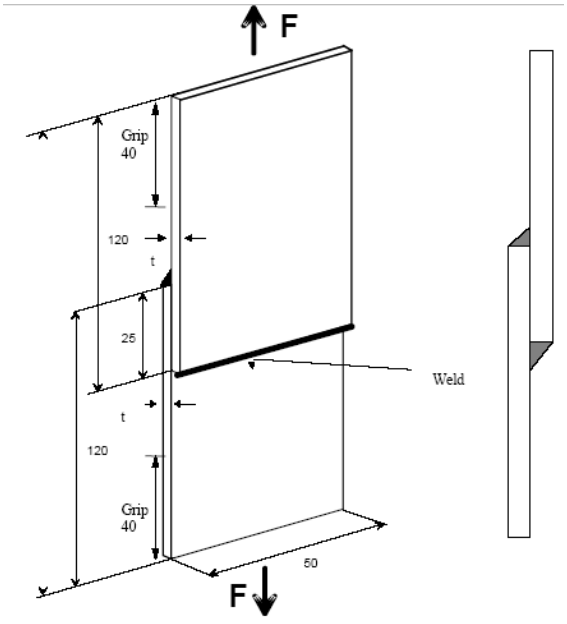


Figure 5. MIG Welded Double-Lap Shear Specimen

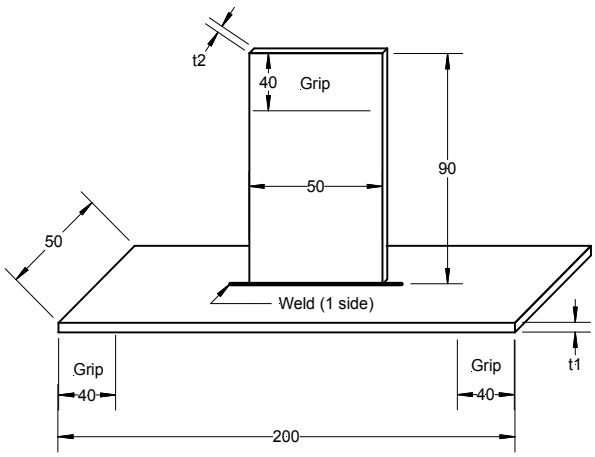


Figure 6. MIG-Welded Perch Mount Specimen

Conclusions

Analysis of test results indicates that the fatigue performance of a spot weld is independent of the materials being welded. This finding supports the initial understanding that the melting and resolidifying processes associated with spot welding form new alloys and make the properties and coating of the material(s) being joined, and the welding parameters, insignificant contributors to fatigue performance.

Q. Tribology

Project Manager: Pat V. Villano
Auto/Steel Partnership
2000 Town Center Drive, Suite 320
Southfield, Michigan 48075-1123
(248) 945-4780; fax: (248) 356-8511; e-mail: pvillano@a-sp.org

Project Chairman: Alan Pearson
General Motors Corporation
Metal Fabricating Division
2000 Centerpointe Parkway
Mail Code 483-520-042
Pontiac, Michigan 48341
(248) 753-2056; fax: (248) 753-2344; e-mail: alan.pearson@gm.com

Technology Area Development Manager: Joseph A. Carpenter
(202) 586-1022; fax: (202) 586-1600; e-mail: joseph.carpenter@ee.doe.gov
Field Technical Manager: Philip S. Sklad
(865) 574-5069; fax: (865) 576-4963; e-mail: skladps@ornl.gov

---

Contractor: U.S. Automotive Materials Partnership
Contract No.: FC26-02OR22910

Objectives

- Conduct stamping simulation tests to study the effects of tribological conditions on the stamping performance of advanced high-strength steels (AHSSs). Stamping performance in this project is defined as minimizing die wear and identifying the optimum die materials and lubricants for AHSSs.
- Include these ultimate benefits:
  - Improve test procedure to simulate die wear.
  - Define a model for prediction of die wear.
  - Optimize lubricant/die combinations for AHSSs.
  - Maintain common lubricants among automotive companies and steel suppliers.

Approach

- Examine wear rates of different die materials, die surface treatments and lubricants with AHSSs.
- Comparison of wear rates with different lubricants and die materials.
- Evaluation of methods of improving die life.
- Optimized lubricants/die combinations for AHSSs.
- Project consisting of L16 (DOE) two material grades, two thickness, two sheet coatings, two bead radii, two lubricants and two bead coatings.

Accomplishments

- Completed Phase 1 report "Enhanced Stamping Performance of High Strength Steels with Tribology."
- Completed Phase 2 report "Effect of Stroke Length and Penetration on Die Wear."
- Obtained steel coils of galvannealed AKDQ, HSLA340, and DP600 supplied by partner companies. The materials are used in the wear tests for Phase 3.
- Collected data for the eight test conditions.
- Completed Phase 3 report "Enhanced Stamping Performance of High Strength Steels with Tribology – Report on Phase 3 Testing."

Future Direction

- Develop wear-rate model to predict die life.
- Gather wear test data to substantiate model.
- Correlate model with production data as AHSSs come into production.

Progress Report

October 1, 2004 to September 30, 2005:

A project was initiated to improve the understanding of the effects of lubricants on die wear and part dimensional variation (springback due to interfacial friction) associated with stamping of high-strength steels. Die material will also be studied. Advanced high-strength steels (AHSSs) may require different lubricant and/or die material to minimize die wear, achieve consistent friction, and reduce part variation.

This Phase will examine wear rates of different die materials; die surface treatments and lubricants with AHSSs. The TribSys wear test apparatus was used to evaluate wear tests under various conditions. The test simulates the forming of 48,000 parts. Changes in process conditions and physical wear of the die will be evaluated. The project also builds on and extends knowledge it gained in the previous studies. It established a baseline of die wear from three (3) sheet materials (AKDQ, HSLA, and DP600) and two (2) lubricants (prelube and mill oil) with one die material (flame-hardened G3500). This study will compare the baseline results to D2 die material with and without chromium nitride (CrN) coating. The performance of dry film lubricants will also be compared to mill oil on galvannealed and hot-dipped galvanized AHSS.

TribSys Inc. will conduct experiments to evaluate die wear on drawbeads under the following conditions.

1. A 2" wide steel strip will be pulled through a set of three (3) beads. The center bead will be used to evaluate die wear.
2. Coils will be coated with mill oil and dry film lubricant prior to testing.
3. For each test condition, 48,000 pulls of 2" length will be performed using the TribSys Wear Test Apparatus.
4. Results will be analyzed using statistical analysis and analytical methods (scanning electron microscope/surface roughness). Analysis of wear will be presented in a report.

The timing of the project fell behind due to delays in obtaining master steel coils of various grades and gauges from the steel suppliers. But, at this time the entire required master coils of the various steel grades and gauges have been received at the steel processor. The coils were processed into 2" widths, 50% bare and 50% with dry film lube coating to satisfy the test requirements. All of the coils were then shipped to TribSys Inc. for completion of the die wear tests. The testing shall begin in October 2005.

R. High-Strength Steel Stamping Project

Project Manager: Michael S. Bzdok
Auto/Steel Partnership
2000 Town Center, Suite 320
Southfield, Michigan 48075-1123
(248) 945-4778; fax: (248) 356-8511; e-mail: mbzdokl@a-sp.org

Co-chair: James Fekete
General Motors Corporation
Body Manufacturing Engineering
2000 Centerpointe Parkway
Pontiac, Michigan 48341
(248) 753-5324; fax: (248) 753-4810; e-mail: jim.fekete@gm.com

Co-chair: Changqing Du
DaimlerChrysler Corporation
800 Chrysler Drive
Auburn Hills, Michigan 48326
(248) 576-5197; fax: (248) 576-0230; e-mail: CD4@DCX.com

Technology Area Development Manager: Joseph A. Carpenter
(202) 586-1022; fax: (202) 586-1600; e-mail: joseph.carpenter@ee.doe.gov
Field Technical Manager: Philip S. Sklad
(865) 574-5069; fax: (865) 576-4963; e-mail: skladps@ornl.gov

---

Contractor: U.S. Automotive Materials Partnership
Contract No.: FC26-02OR22910

Objectives

- Determine how to accurately predict and control the amount of springback and other deviations from the desired stamping geometry for parts made from high-strength steel (HSS) and advanced high-strength steel (AHSS) prior to construction of the production tooling.
- Develop part design and manufacturing process guidelines that can be recommended to automotive design and manufacturing engineers for the purpose of reducing springback and other part distortions.

Approach

The approach of the HSS Stamping Project is twofold:

1. AHSS stamping springback predictability through finite element analysis (FEA).
2. AHSS stamping springback control by developing knowledge of part design geometries that affect flange springback and die processes that control springback.

Several different types of dies have been constructed or are on loan to the Auto/Steel Partnership (A/SP) for the stamping process development.

Accomplishments

- Identified additional processes to control springback, sidewall curl and panel twist.
- Modified tooling for stretch-forming processes of AHSS auto body structural components to neutralize the residual stresses that cause springback and sidewall curl. Predictable results have been shown for HSLA 350 and DP600 MPa. The tooling was additionally modified for DP780 MPa and DP980 MPa. Panel measurements and data analysis are being completed.
- Modified panel geometry to show that this will also control springback. Effective use of stiffening beads and other part shape modifications are being recommended to product designers for control of twist, undercrown and springback.
- Built a new Multi-Process Master Shoe Die and Sub-Die inserts that are capable of a variety of part shapes and processes. The master shoe has a high-pressure hydraulic cushion that can be programmed for various process control features. Sub-die inserts for two Underbody Longitudinal Rails and a Cowl Cross Bar were also built. A Body Center Pillar sub-die is in the tryout stage for completion by November 2005.

Future Direction

- Die trials with the new Multi-Process Die and programmable hydraulic cushion are continuing. This die is designed as a master die set and pressure system that will accept sub-die inserts to produce a variety of structural parts, such as underbody rails, cross bars and side-structure pillars. Stamping processes for draw or form die actions can be developed with this tool.

Introduction

Owing to the mechanical properties of advanced high-strength steel (AHSS), the springback after forming and the geometric dimensional control of the stamped parts have been critical issues in stamping tool construction and in stamping production. Because the actual dimensions of AHSS stampings off the tooling are unpredictable with current tools and technology, the average die face re-machining may be four to six times normal and result in two to three months of lost tryout time.

Computer simulation technology has been widely applied in the stamping industry and has been recognized as a virtual stamping tool to identify formability issues and evaluate solutions before the actual stamping dies are made. Although computer simulation provides accurate prediction for splits and buckles, experience has shown that computer simulation data have not been reliable in predicting the amounts and modes of the springback, twist or sidewall curl. These distortions must be controlled if the AHSS is to be used successfully for lightweight body structures. Innovative stamping processes that neutralize residual stresses resulting from the metal deformation may control springback and other distortions in high-strength steel stampings. These processes will involve some type of stretch forming in order to give the stamping "shape set". The work of this project group is to determine the most effective means of researching and applying these "shape set" processes. Computer simulation is also being analyzed to improve the data input for accurate formability prediction.

Progress Toward Meeting Deliverables

Fender Rail Die

To assess the accuracy of the current forming/springback control theories, a full-scale fender rail-stamping die was used (Figure 1). A lockstep was added to the die to provide sidewall stretch. Several different AHSS materials, including Dual Phase 600, 780 and 980 Mpa were used to stamp fender rails and the finished panels were measured by laser scan. Springback control experiments were conducted using tooling designed to replicate actual production stamping die processes. These experiments confirmed the importance of stretching the sidewalls during the stamping process in order to reduce residual stress, flange springback and part-to-part variation. However, DP600 MPa and lower-strength materials were the only materials that could be stretched with

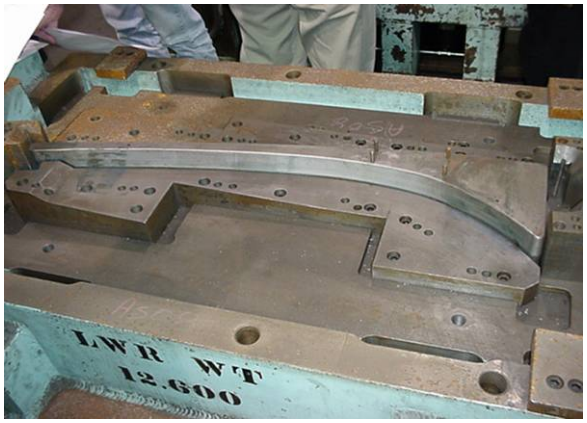


Figure 1. Fender Rail Die – Lower Half

a two-break lockstep. Higher-strength materials (DP780 MPa and DP 980 MPa) required a four-break lock step for effective stretch results (Figure 2).

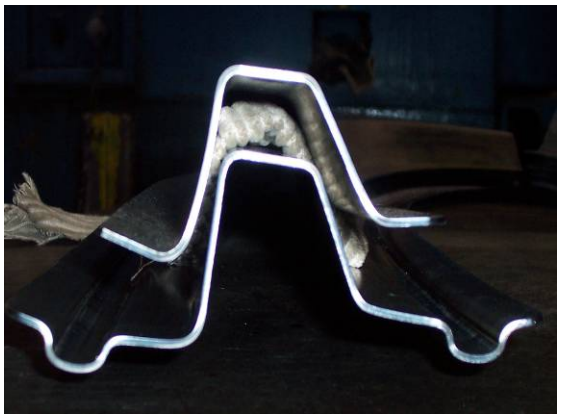


Figure 2. Effect of stretch with four-break lock step. Note that top section was not stretched.

Multi-Process Master Shoe Die

Currently, the Project Group is focused on experimenting with a multi-process research die with sub-die inserts (Figure 3) to produce various automotive structural components by a variety of processes. This die has the necessary higher holding pressures and controlled processes required for working the higher-strength materials. A programmable hydraulic-pressure cushion is the main component of this system that provides the means of stretch forming the metal and controlling springback. Four sub-die inserts are planned for this tool by the end of 2005.

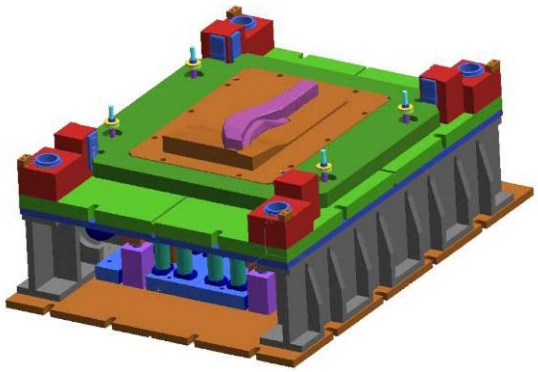


Figure 3. Lower Half of Multi-Process Die

Sub-die inserts in the multi-process master shoe die enable stamping of underbody, cross-car and side structural components with a variety of stamping processes.

Rear Longitudinal Rail Sub-Dies

Tryouts of the three different stamping processes and with 1.6 mm and 2.2 mm DP600 MPa steel and 1.6 mm DP780 MPa and DP980 MPa steels have shown that the higher-strength materials tend to split when drawn and are more readily formed than drawn. Reductions in tooling temperatures, tool wear and lubrication requirements were noted when using the forming process. Material utilization was also much more efficient when using the forming process (Figure 4). Future efforts will feature continued work with the higher-strength grades to



Figure 4. Rail Stampings. Three Processes.

improve the springback control with "shape set" features, such as lock steps, added to the forming process.

Cowl Cross Member Sub-Die

A Cowl Cross Member sub-die is part of the program. This stamping tryout also shows that the higher-strength steels are more easily formed than drawn for some panel configurations (Figure 5). Additional stampings will be produced with DP600, 780 and 980 MPa materials using various blank configurations. These stampings have been laser scanned and the dimensional data has been recorded and is being analyzed to determine the effectiveness of each process.



Figure 5. Cowl Cross-Bar. Two Processes.

Future Work

Body Side Center Pillar Sub-Die

Another sub-die for a Body Center Pillar will be completed by November 2005 (Figure 6).

This part is crucial to the body side structure for meeting side impact requirements. It is also typically difficult to stamp in medium-strength grades due to springback, twist and undercrown. The higher-strength grades will increase the manufacturing difficulties.

By recording the results of innovative forming processes, case studies for specific structural parts will be presented, along with product design and stamping process guidelines for industry reference,



Figure 6. Body Side Center Pillar

when making product applications of the AHSS materials.

In addition, stamping press tonnages are being recorded, along with impact loads, press signature analysis and die cushion pressure requirements for the stamping industry's information. This will aid in better understanding the machine and equipment requirements for manufacturing components from this material.

Further stamping tryouts of DP600, DP780, and DP980 MPa will be conducted on typical automotive underbody, cross–car and side structural members with new tooling and multiple processes. These materials, in lighter gauges than currently employed, will assist the weight reduction and structural performance goals of the Future Generation Passenger Compartment (see report 2.V) and other lightweighting project groups in the A/SP.

Conclusions

The dual-phase steels of 600 MPa to 980 MPa can be formed more readily than drawn. Product should be designed to allow a form-die process for structural parts in the higher-strength grades.

Draw-die processes and stretch-form processes will be required for large outer "skin" panels of 500 MPa and lower. Product design modifications may be required to use these materials instead of lower-strength grades.

When AHSS is formed, a "shape set" stretch should be added at the bottom of the press stroke for springback compensation.

Stretch flanges are very susceptible to edge cracking and flange-edge stretch must be minimized by product design. Trim-edge quality will be critical.

Presentations and Publications

Advanced High-Strength Steels Materials, Product Design and Stamping Processes *Presented at the March 9, 2005 seminar "Great Designs in Steel"* in Livonia, MI

S. Strain Rate Characterization

Project Manager: Pat V. Villano
Auto/Steel Partnership
2000 Town Center Drive, Suite 320
Southfield, Michigan 48075-1123
(248) 945-4780; fax (248) 356-8511; e-mail: pvillano@a-sp.org

Chairman: David J. Meuleman
General Motors Corporation-Metal Fabricating Division
2000 Centerpoint Parkway
Pontiac, Michigan 48341
MC 483-520-266
(248-753-5334; fax: 248-753-4810; e-mail: david.meuleman@gm.com

Lead Scientist: Srdan Simunovic
Oak Ridge National Laboratory
P.O. Box 2008, MS6164
Oak Ridge, TN 37831-6359
(865) 241-3863; fax: (865) 574-7463; e-mail: simunovics@ornl.gov

Technology Area Development Manager: Joseph A. Carpenter
(202) 586-1022; fax: (202) 586-1600; e-mail: joseph.carpenter@ee.doe.gov
Field Technical Manager: Philip S. Sklad
(865) 574-5069; fax: (865) 576-4963; e-mail: skladps@ornl.gov

---

Contractor: U.S. Automotive Materials Partnership
Contract No.: FC26-02OR22910

Objectives

- Develop new experimental setups for characterization of crashworthiness and strain-rate sensitivity of both high-strength steels (HSSs) and structural designs.
- Replicate impact conditions that occur in automotive impact by simpler and more manageable experiments in order to generate meaningful data for computer modeling.

Accomplishments

- Developed experimental setup procedures for new crashworthiness characterization test based on parallel-plates buckling, a procedure developed at the University of Dayton Research Institute (UDRI).
- Developed and conducted constant-velocity crash experiments on circular tubes made of mild steel, dual-phase and transformation-induced plasticity steels.
- Developed graphics-oriented tools for data analysis from parallel-plate and tube crush experiments.

Future Direction

- Develop experiments for characterizing strain and strain-rate history in tubular components in octagonal, spot-welded double-hat tube crush tests.
- Provide high-quality data for material and finite-element modeling (FEM) development.

Introduction

Crashworthiness characterization of HSS requires testing of materials and structures under increased strain rates, large plastic strains, and large displacements that are characteristic of actual impact events. Aside from providing a physically quantitative measure of crashworthiness, the experiments also provide benchmarks for verification of FEM models that are used for automotive design and analysis. Typical crashworthiness experiments involve crushing of tubular objects, such as circular or rectangular tubes. Due to a combination of relatively high velocities and force levels required for progressive crushing, the experiments are usually conducted in inertia-based equipment, such as drop towers or impact sleds. For example, in a drop tower the drop height and the drop mass can be adjusted to generate desired crush force and length. However, there are practical limits on the mass and the velocity that can be used in a drop tower. The kinetic energy of the impact must be such that it can be expended in the deformation of the specimen and the safety restraints in order not to damage the testing equipment. Vibrations of the falling mass are practically impossible to eliminate, and the lateral forces are not easily measured nor controlled. The velocity of impact cannot be kept constant and gradually reduces from the onset of impact.

The objective of this project is to develop and conduct coupon- and component-level experiments for the characterization of crash-worthiness of HSS. The project will also provide high-quality data for development of material and structural FEM models, and, therefore, enable more accurate modeling and design of lightweight crashworthy vehicles.

Design of Experiments

Tube Crush Experiments

To improve experimental investigations of the material and structural behavior for automotive impact, the Oak Ridge National Laboratory (ORNL) and the Automotive Composites Consortium (ACC) of USCAR have developed a new integrated virtual and physical test system for hydraulic, high-force, high-velocity crashworthiness experiments of automotive materials and structures. The unique system, a test machine for automotive crashworthiness (TMAC), permits controlled, progressive crush experiments at programmable velocity profiles and high force levels. More details about the TMAC system can be found on http://www.ntrc.org.

The tube crush experiments were conducted at the National Transportation Research Center user facility in Oak Ridge, Tennessee. The TMAC system is shown in Figure 1.

The ability to control displacement (velocity) and the large lateral stiffness of the machine allows for strain history measurements that are not practical in drop-tower equipment. TMAC's high load capacity allows for constant-velocity history during the test. This can be seen from the displacement history in Figure 2. The figure shows the progression of the displacement of the loading plate during the 4 m/s crush test. The slope of the displacement denotes velocity, which was constant for the duration of the first 18 milliseconds corresponding to the investigated tube crush length.



Figure 1. Test machine for automotive crashworthiness.

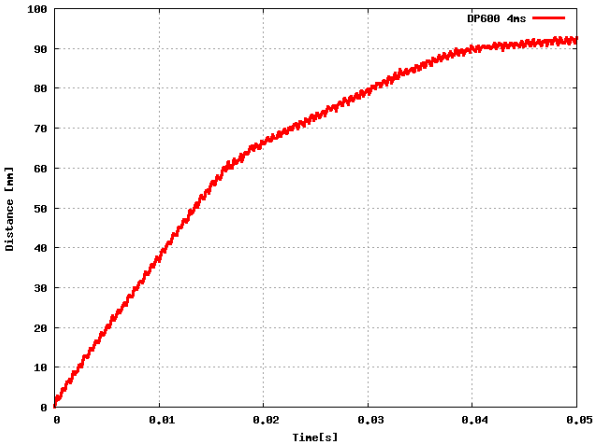


Figure 2. Displacement history for the 4 m/s tube crush

The Auto/Steel Partnership (A/SP) supplied experimental tube specimens. A relatively large diameter provides better bonding with the strain gages and relatively tight manufacturing tolerances alleviate uncertainties due to imperfection sensitivity of the circular tubes. Geometry of the tube specimens is defined by tube length, 178 mm (7 in), diameter, 50 mm (2 in), and wall thickness, 1.6 mm (0.063 in). The first set of materials tested in FY 2005 included mild steel (DQSK), High Strength Low Alloy (HSLA) 350 MPa and Dual Phase (DP) 600 MPa steels. The test velocities were 0.06 m/s, 0.6 m/s and 4 m/s.

The goal of the project is to measure and investigate the strain and strain-rate regimes that material experiences during the crush in order to improve predictive capabilities of the numerical models. The principal tools for strain-rate history measurement are electric resistance strain gages. The material experiences large strains during progressive crush and, therefore, high elongation gages have to be used. The gage placement, bonding and data acquisition were determined in the previous studies. The tube force was measured by a set of load cells and a load washer. The data from load sensors, displacement trace, and high-speed camera are synchronized, and together provide comprehensive information about the progressive crush and crashworthiness.

Deformation modes of circular tubes are very imperfection-sensitive since the characteristic energy dissipation of different modes is very similar. Such uncertainty can also be exploited as different modes of deformation can be triggered with appropriate modifications of tube geometries and boundary conditions. We have considered several test configurations for inducing various symmetric and asymmetric deformation modes. Axially-symmetric crush in mild steel (DQSK) and High Strength Low Alloy (HSLA) tubes was triggered using the developed pre-crush adapter. The loading adapter generates symmetric deformation as shown in Figure 3.

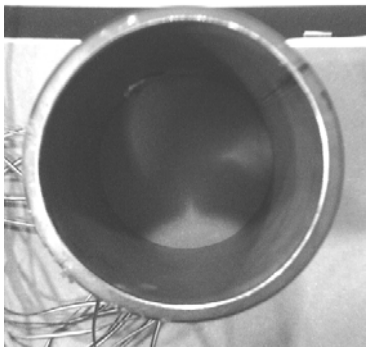


Figure 3. Pre-crush for mild steel tube

The pre-crushed specimens are then crushed with different test velocities. Axially-symmetric crush of a mild steel tube is shown in Figure 4.

Specimens tested with different velocities for the same crush length are shown in Figure 5.

The force-time histories for two different specimens crushed with 4 m/s are shown in Figure 6.

The effect of crush speed on the overall force levels can be analyzed by comparing force-distance signals for tests. Figure 7 compares the force levels for tests run at 2 velocities, 0.6 m/s and 4 m/s, respectively.

Asymmetric tube crush is more prevalent in automotive crush, as the structural component geometries have more complex shapes and loading conditions. Asymmetric crush modes in circular tube specimens were triggered by tube height modifications. This mode is also more likely in the high-strength steel structures.

The crush speed sensitivity of HSLA and DP steels is shown in Figures 8 and 9. The tubes were crushed in unsymmetric modes.

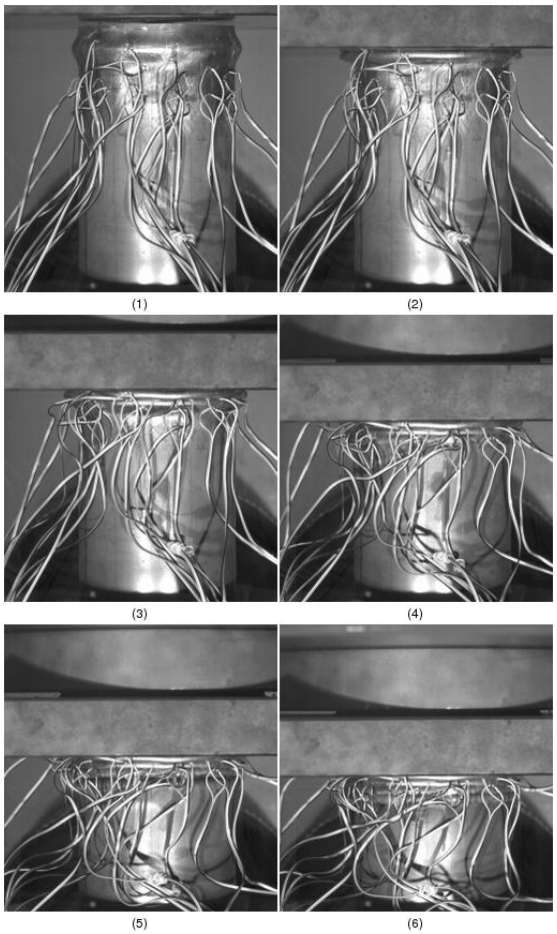


Figure 4. Progressive crush of a mild steel tube under constant velocity of 2 m/s. (Numbers below the photographs denote the relative time sequence)

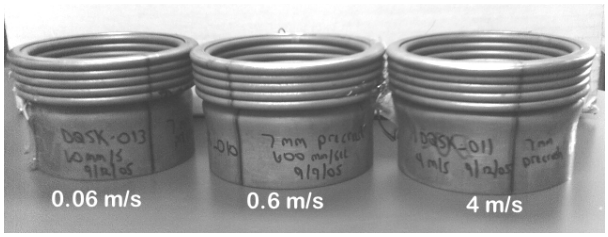


Figure 5. Specimens crushed under different velocities (Numbers in photograph denote crush speeds)

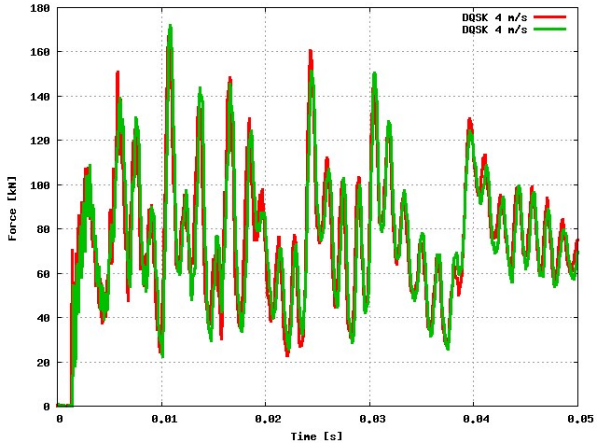


Figure 6. Crush force history of mild steel tubes for the symmetric crush at 4 m/s. (The overlap of the force traces indicates the repeatability of the test).

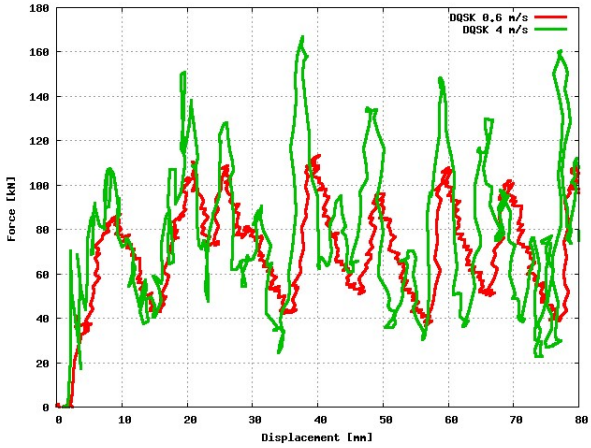


Figure 7. Force-crush distance data for crash tests at two velocities

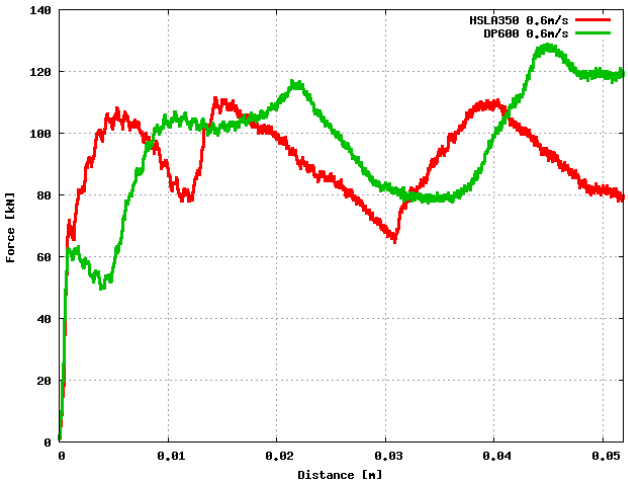


Figure 8. Crush test with 0.6 m/s

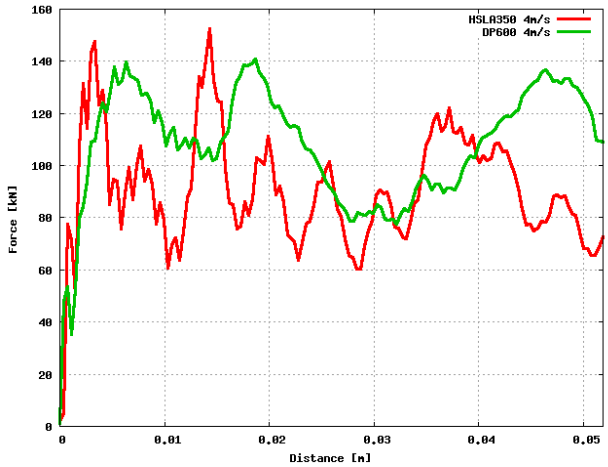


Figure 9. Crush test with 4 m/s

Figure 8 compares impact forces for HSLA 350 and DP 600 materials under crush speed of 0.6 m/s, whereas Figure 9 shows force traces less than 4 m/s crush. The results show different trends of the two materials and indicate higher crush speed sensitivity of DP 600 materials than can be deduced from the coupon-level uniaxial-loading data available in the literature. This, in turn, indicates that constitutive model modifications are necessary in order to account for this behavior as lower strain-rate sensitivity of DP 600 material in uniaxial configurations would result in corresponding force-level sensitivity in crush tests.

Each specimen is instrumented with multiple strain gages that record strain histories in axial and hoop directions of the tube. A typical recording of the axial strain gages during 4 m/s crush test is shown in Figure 10. Label numbers indicate gage identifiers that in turn are ordered away from the crushed end.

The strain histories of the gages positioned at the same location but for the different crush velocities can be compared in order to investigate loading conditions for different velocities. Figure 11 shows strain histories as functions of crush length for crash tests at 0.6 m/s and 4 m/s, respectively.

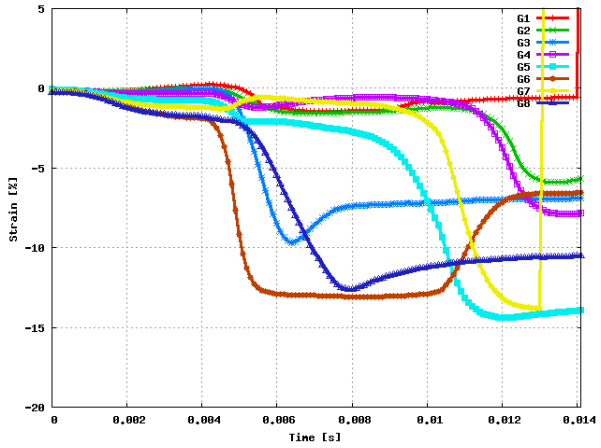


Figure 10. Strain history of axial strain gages for DP tube during 4 m/s crush

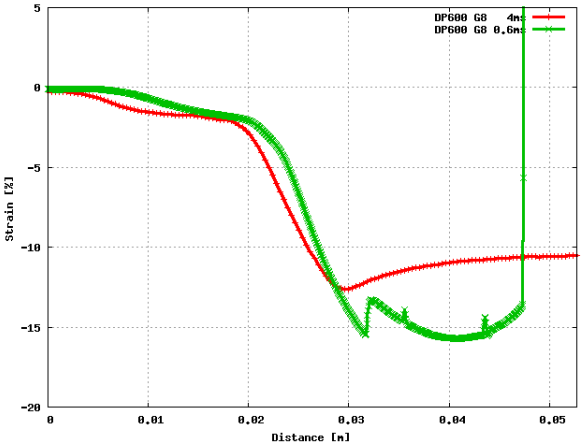


Figure 11. Axial strain gage data for crush tests at two different velocities.

The figure above indicates that the strain rate experienced by the material is proportional to the crush speed. The overall magnitude of the strain rate is recorded, as well. Such information is used to determine the range of testing conditions at the coupon level that are needed for material characterization.

A new analysis environment for tube crush data has been developed using DIADEM software from National Instruments. Computer programs were developed to synchronize multiple data channels to allow for simultaneous analysis of crush sequence, deformation, forces and velocities. The results are then viewed by a DIADEM viewer and distributed to the project participants. The results are shown in Figure 12.

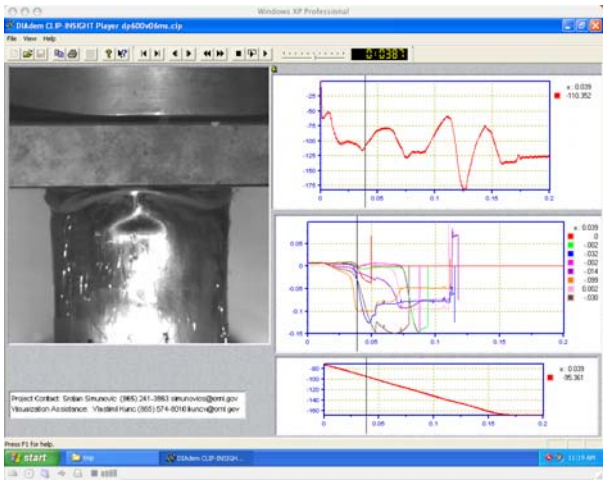


Figure 12. Tube crush data presentation

Such a coupled form of information has not yet been available in the automotive impact analysis and together with the unique experimental facility, provides new information for material analysis and benchmark for material and FEM model evaluation and development.

Conclusions

New experimental setups have been developed for characterization of crashworthiness of HSS. The experiments are based on hydraulic-based testing systems. The systems provide unique tightly controlled testing environments for structural and material characterization. The experimental data are used for validation and evaluation of modeling approaches, and for development of modeling guidelines for HSS materials and structures under impact loads. The high-quality data is combined into a comprehensive viewing format.

Acknowledgments

Support from the Auto/Steel Partnership Strain Rate Characterization Team is acknowledged.

Future Work

The future work on the project will focus on two remaining topics:

1. Circular tube crush experiments in TMAC test machine for various steel sheet materials.
2. Crushing of octagonal tubes in TMAC test machine. The geometry is characteristic to the front-end designs of new prototype vehicles.
3. Development of new coupon and structure-level crash characterization experiments.

T. Modeling of High Strain-Rate Deformation of Steel Structures

Co-Principal Investigator: Srdjan Simunovic
Oak Ridge National Laboratory, P.O. Box 2008 MS6164, Oak Ridge TN 37831-6164
(865) 241-3863, fax: (865) 241-0381; e-mail: simunovics@ornl.gov

Co-Principal Investigator: J. Michael Starbuck
Oak Ridge National Laborator, P.O. Box 2008 MS6053, Oak Ridge TN 37831-6053
(865) 576-3633, fax: (865) 574-8257;e-mail: starbuckjm@ornl.gov

Technology Area Development Manager: Joseph A. Carpenter
(202) 586-1022; fax: (202) 586-1600; e-mail: joseph.carpenter@ee.doe.gov
Field Technical Manager: Philip S. Sklad
(865) 574-5069; fax: (865) 576-4963; e-mail: skladps@ornl.gov

---

Contractor: Oak Ridge National Laboratory
Contract No.: DE-AC05-00OR22725

Objectives

- The objective of the project is to develop numerical modeling guidelines in order to realistically assess the influence that the properties of strain-rate dependent materials exert in crashworthiness computations. The dynamic loading problems are modeled using diverse combinations of modeling approaches (sub-models) that are essential in describing strain-rate sensitivity in computational simulations. Sub-models examined include finite element method (FEM) formulations, constitutive materials models, material properties under different strain rates and loading conditions, contact conditions, etc, as well as material property changes caused by component processing.

Accomplishments

- Investigated effects of stress transients for high-strength steel (HSS) and their effects on peak impact force
- Developed experimental setup for new crashworthiness characterization test based on parallel-plates buckling
- Developed program for analysis of history of strain-rate calculations
- Analyzed history of strain rates in unsymmetric crushing
- Determined modeling effects on strain-rate history in unsymmetric crushing
- Developed new constitutive models for HSS to account for strain-rate history and transients
- Investigated forming and welding effect on steel tube crashworthiness
- Developed model for tube roll-forming and validated it against manufacturing process
- Developed experimental guidelines based on the two parallel-plates and tube crush tests

Future Direction

- Develop new constitutive models for modeling of damage and tearing of HSS during impact
- Conduct and analyze octagonal tube crush experiments replicating HSS front rail
- Determine optimal FEM formulations for modeling of crushing of tubes with corners

---

Introduction

The objective of the project is to develop numerical modeling guidelines for strain-rate dependent materials in crashworthiness computations. The scope of the project is to study specific structural problems in automotive impact, develop new experimental and analytical techniques for characterization of strain-rate sensitivity of HSS and modeling of complex strain and strain-rate histories. The dynamic loading problems are modeled using diverse combinations of modeling approaches (sub-models) that are essential in describing strain-rate sensitivity in computational simulations. Sub-models to be examined include finite element formulations, constitutive materials models, contact conditions, etc. The trends, influences, and direct effects of employed modeling techniques will be identified and documented. The relative significance of employed sub-models is established, particularly in relation to the strain-rate effects resulting from the material constitutive models.

The research project is conducted as a team effort between the ORNL and the Auto/Steel Partnership (A/SP) Strain Rate Characterization Group (see report 2.S).

Simulation of Double-Plate Experiment

A new experimental setup has been developed for investigation of progressive crush in high-strength steel. The objective of the experiment is to replicate components of loading conditions that occur during progressive crush of tubular structures in a simple structure to minimize the complexity of the problem [1]. The simplicity of the specimen allows for semi-analytical extraction of data and simple correlation with the FEM experiments. The experiment has been used for investigation of inertia and strain-rate effects in Type II structures by Tam and Calladine [2]. Since then, numerous interpretations of the test have been conducted using analytical or computational models. Our version of experiment is conducted for three different crushing velocities in order to assess the effect of crushing speed and to correlate the computational models with experiments.

The effects of material model types, model parameters, FE shell element formulations and spatial discretizations have been included in the study.

A typical test configuration is shown in Figure 1. The specimen is made of two pre-bent parallel plates and is impacted from the bottom and crushed with constant velocity.

Figure 1 shows the edge view of the specimen. The forming process has been simulated using the quasi-static material properties. A result of a typical forming simulation for DQSK steel is shown in Figure 2. The edge of the simulated formed plate is superimposed over the image from the experiment and shown in red and marked as “Simulation”. In order to match the formed shape of the specimen, it was necessary to use element discretization that was very close to the plate thickness. This result also illustrates a necessity of a fine discretization for modeling of progressive crush using the current FEM shell element technologies. It also indicates the need for development of new FEM shell formulations that would allow for localized behavior in larger shell elements. The current discretization that is proportional to shell thickness is close to the limit of shell element applicability since the shell element formulation is developed on the basis of assuming that the element thickness is negligible to the shell curvature.

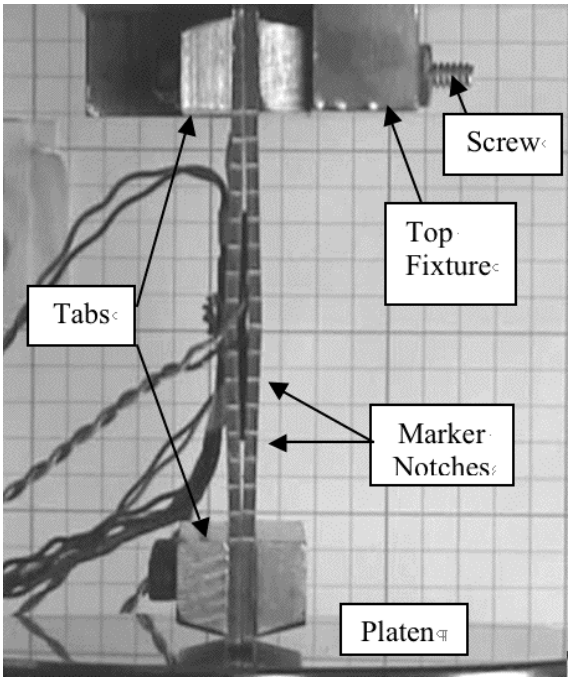


Figure 1. Double-Plate impact configuration

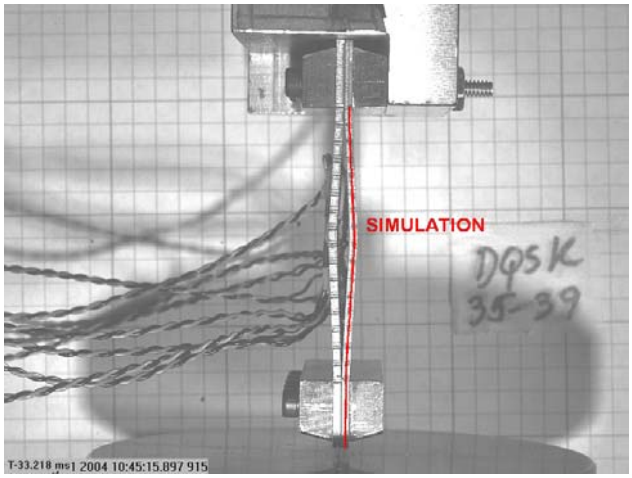


Figure 2. Simulation of the forming process

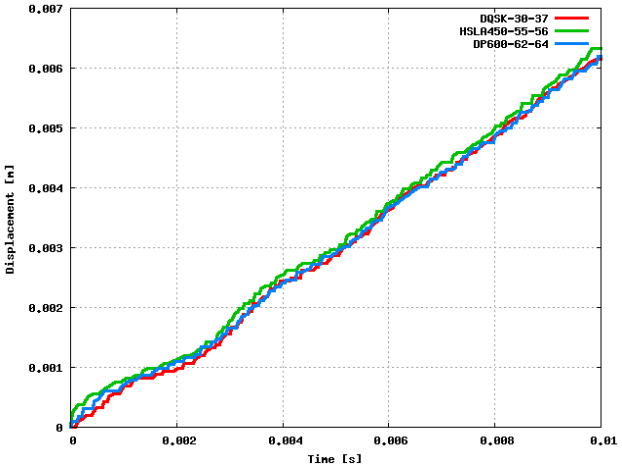


Figure 3. Loading displacement for impact test

The formed plates are assembled into a test specimen as shown in Figure 1. The residual strains from forming simulations are used in the impact simulations of the experiment. The simulated forming strains were also compared with the strain calculated from the analysis of the curvature distribution in the experiment and were found to be in a close agreement.

The impact simulation phase was conducted using the same discretization as was used in the forming phase. The material properties now include strain-rate effects. The loading was imposed using the displacement history of the loading plate as obtained from the experiment. A typical history of the displacements for the intermediate velocity test of 0.6 m/s is shown in Figure 3.

Images of the simulations superimposed over the experimental results from the high-speed camera test are shown in Figure 4. The images are ordered in time sequence. The material tested was mild steel (DQSK).

Simulation results exhibit more flexibility compared to the experiments in all materials tested. During early phase of impact after contact between the loading plate and the specimen, models buckle faster than experiments.

Experiments later catch up with the simulations and the two are overlapped during the majority of the test duration. Several reasons for the discrepancy are possible, and are currently being investigated. The transient stress enhancement during the sudden strain rate increase [3, 4] has been considered, as well as effects of element discretization and specimen flexibility. The increase in buckling load can be achieved by changing the material model to account for stress transients and by using a larger element size. The combination of the two effects is used as a guideline for the modeling of progressive crush in larger structures. A relative simplicity of the test also allows for semi-analytical interpretation for certain portions of the test. The semi-analytical approach is combined with the FEM simulations to determine the best combination of modeling parameters. These parameters are correlated with local measures of strain and strain-rate effect and provide verified modeling combination that otherwise could not be provided in an automotive component or tube crush tests.

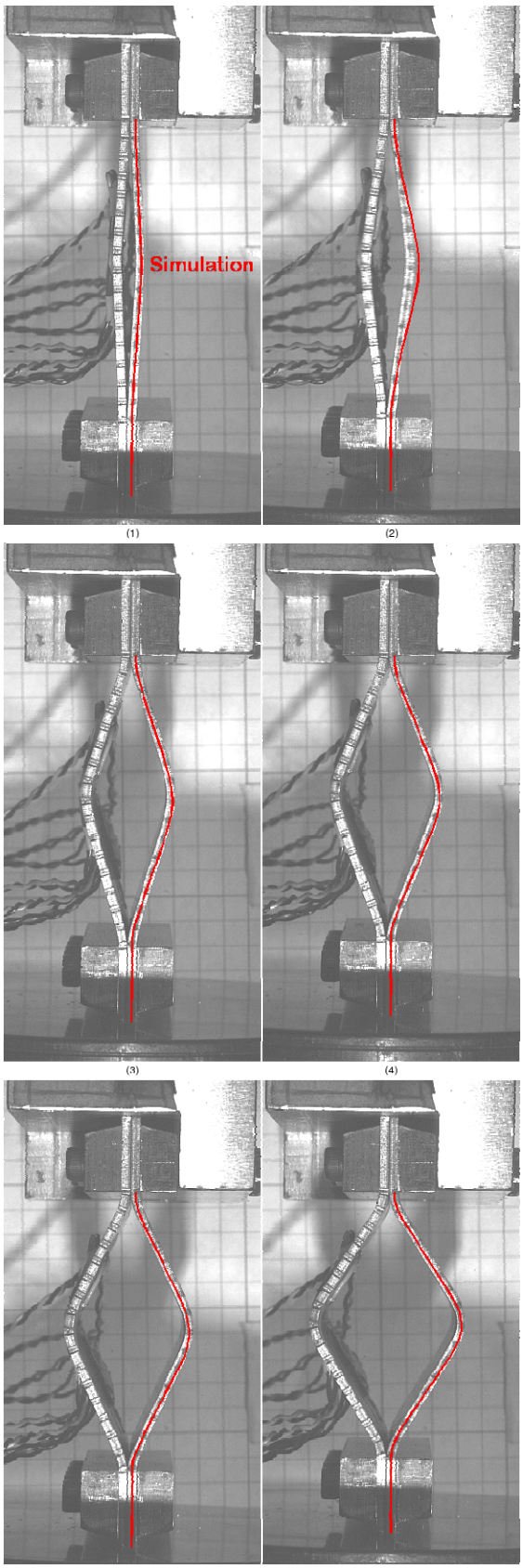


Figure 4. DQSK plate crush test. Crush velocity 0.6 m/s

Simulation of Tube Crush Tests

Structural component experiments have been developed using the new, velocity-controlled, high-speed hydraulic Test Machine for Automotive Crashworthiness (TMAC) at ORNL. Components are crushed in different modes to investigate crush efficiency, characterize material response and validate models. Different modes of progressive crushing lead to different amounts of energy dissipation in impact. The models are compared to crush tests of different steel grades under various impact velocities. Figure 5 shows typical crushed tubular specimens and the respective crush velocities.

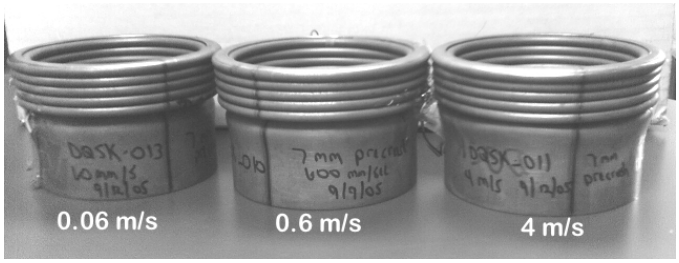


Figure 5. Crushed tube specimens

The comparison between the measured and simulated impact force is shown in Figure 6. The material model used in the simulation uses the latest information from the A/SP experiments and shows the very good agreement with the test. The difference between the measured and simulated force peaks indicates, as in the duble-plate test, that modifications in the material may be needed to account for sudden strain-rate increase.

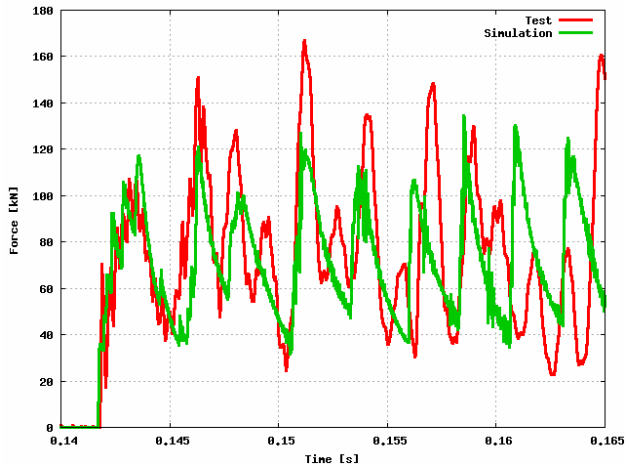


Figure 6. Comparison of test and simulation for tube crush at 4 m/s

Conclusions

The current project concentrates on investigation of different FEM modeling approaches for modeling of impact in HSS structures. The research is performed in collaboration with an experimental program on characterization of HSS under impact. The modeling is also used for development of new high strain-rate material and structural characterization tests. The results of the project are used for development of more accurate modeling approaches for automotive design. The research results are also applicable in high strain-rate forming operations.

Future Work

The future work on the project will focus on four topics:

1. Support of the strain-rate experiments on coupon and component level.
2. Development and validation of material models and modeling techniques.
3. Modeling of HSS octagonal tubes.
4. Development of models and experiments for damage and fracture of HSS in crash

The remaining most important aspect to address from the modeling of HSS crashworthiness are the methods to model the crush of tubes with rectangular (polygonal) cross section, modeling of damage that the HSS experiences during the deformation, and incorporation of processing into the models.

Acknowledgments

The research was performed at the Oak Ridge National Laboratory (ORNL), which is managed by UT-Battelle, LLC for the U.S. Department of Energy under contract DE-AC05-00OR22725. The tubes for the TMAC experiments were donated by the US Steel Corporation. The support of Auto/Steel Partnership Strain Rate Characterization Team is acknowledged.

Contact

For additional information on details on the research project please contact Srdjan Simunovic, simunovics@ornl.gov. Dr. Simunovic is a senior research staff member in the Computational Materials Science Group (http://www-cms.ornl.gov) at the Oak Ridge National Laboratory.

References

1. M. Avalle and G. Belingardi, “Experimental evaluation of the strain field history during plastic progressive folding of aluminum circular tubes,” *International Journal of Mechanical Sciences*, 39(5), 575–583 (1997).
2. L.L. Tam and C.R. Calladine, “Inertia and strain-rate effects in a simple plate-structure under impact loading,” *International Journal of Impact Engineering*, 11(3), 349–377 (1991).
3. Campbell JD. Dynamic Plasticity of Metals. New York: Springer, 1972.
4. Simunovic S., Nukala, K.V.V., Modeling of Strain Rate History Effects in BCC Metals, 3rd MIT Conference on Computational and Solid Mechanics, Bathe K. J. Ed., Elsevier, 2005.

U. Lightweight Front End Structures

Project Manager: Pat J. Villano
Auto/Steel Partnership
2000 Town Center Drive, Suite 320
Southfield, Michigan 48075-1123
(248) 945-4780; fax (248) 356-8511; e-mail: pvillano@a-sp.org

Co-Chairman: John Catterall
General Motors Corporation
Body Systems Center
Engineering West
Mail Code 480-111-W23
30200 Mound Road
Warren, Michigan 48090
(586) 986-3541: fax (586) 986-4184; e-mail: john.1.catterall@gm.com

Co-Chairman: Jody R. Shaw
Marketing Manager, Automotive
United States Steel Corporation
5850 New King Court
Troy, Michigan 48098-2608
(248) 267-2608: fax (248) 267-2581; e-mail: jrshaw@uss.com

Technical Area Development Manager: Joseph A. Carpenter
(202) 586-1022; fax: (202) 586-6109; e-mail: Joseph.Carpenter@ee.doe.gov
Field Technical Manager: Philip S. Sklad
(865) 574-5069; fax: (865) 576-4963; e-mail: skladps@ornl.gov

---

Contractor: U .S. Automotive Materials Partnership
Contract No.: DE-FC05-02OR22910

Objective

- The objective of the Auto/Steel Partnership (A/SP) Lightweight Front End Structure (LWFES) project is to benchmark, develop and document solutions that balance the interaction of material, manufacturing and performance in the lightweighting of steel automotive structures. The initial phase of this study focused on automotive front-end system solutions that address high-volume manufacturing and assembly. Furthermore, example solutions were manufactured and physical testing was performed to evaluate the advanced high-strength steel (AHSS) designs.
- The AHSS solutions will provide choices and consequences that address real-world challenges faced in the vehicle development process. A comprehensive knowledge-base design tool was developed to capitalize on a set of robust AHSS automotive design guidelines relating choices to consequences.

Approach

- An existing Front Rail System from a donor vehicle was retrofitted with AHSS Dual Phase (DP) 800 steel to save 22% of the mass. In addition, a front bumper made from DP 980 steel replaced the existing bumper design.
- The AHSS rail system and bumper were manufactured and tested to compare performance with the conventional design it replaced.

- Analytical and physical testing was carried out on both the original and the redesigned rail system.
- Comparisons will now be drawn and recommended practices documented.

Accomplishments: Additional Phase 2 Deliverables

- Selected a stamped rail concept.
- Obtained final optimized stamped rail and bumper designs.
- Completed formability simulation of the stamped design.
- Generated Computer Aided Design (CAD) data for manufacturing of the new stamped rail and bumper designs.
- Developed prototype tools for manufacturing rail and bumper stampings.
- Manufactured prototype dies for the rails, rail extensions and bumper.
- Developed new welding schedules for AHSS joining.
- Developed static and dynamic stiffness Design of Experiment (DoE) Finite Element (FE) Models.
- Developed static stiffness DoE response surface.
- Developed dynamic stiffness DoE response surface.
- Stamped and assembled rails, rail components and bumpers.
- Prepared the donor vehicle to accommodate the new rails and bumper.
- Installed the new AHSS rails and bumper into the vehicle.
- Conducted a successful (certified) Insurance Institute for Highway Safety (IIHS) 35-mile-per-hour crash test of the retrofitted vehicle and recorded the results.
- Correlated the vehicle crash test data with the analytical results.
- Updated Proteus, a knowledge-base tool, with the findings of this project.
- Published a final report detailing all of the findings of this project, including lessons learned.
- Tech transfer of project results (Deep Dive Presentation) conducted at DaimlerChrysler.
- Project results "display" was completed and used in road show presentations.

Future Direction

- The original Phase 1 and Phase 2 have been completed**.**

Manufacturing Feasibility

The primary intent of the Lightweight Front End Structures (LWFES) project was to demonstrate the mass savings potential of advanced high-strength steels (AHSSs) combined with efficient design in an existing production vehicle package space while addressing manufacturing feasibility. To ensure manufacturing feasibility, several A/SP enabler teams were utilized to review the design recognizing that the members of these teams represent the manufacturing interests of their companies and ensured that the project developed a solution that addressed manufacturing feasibility. The enabler teams were consulted to assist in developing designs, and designs were modified to accommodate enabler teams' design review comments.

The LWFES team would like to recognize the efforts of the A/SP High-Strength Steel Stamping team (see report 2.R), Hydroformed Materials and Lubricants team (see report 2.O), Strain-Rate Characterization team (see report 2.S) and the High-Strength Steel Joining Technologies team (see report 2.N) for their overview and support of the project.

The project team went to every effort, within the confines of the program, to demonstrate manufacturing feasibility. The project does not address manufacturing capability required to

understand the influence of the many variables of a high-volume manufacturing environment. The extent to which manufacturing feasibility is addressed is documented in the following sections.

The manufacturing feasibility report is composed of the input from many of the participants of the program. Detailed chapters are provided for each of the key manufacturing areas. The following is a summary of the manufacturing feasibility section of the report.

Materials

The redesigned rail bumper system relies on DP 780 and DP 980 steels, grades that are commercially available from North American sheet steel producers. The existing rail design utilizes steel in strength ranges from BH 210 to HSLA 340 compared to the new optimized design, which utilizes DP 780 and DP 980. The mass-saving potential of different steel grades in a crash event can best be compared by the relative area under the true-stress true-strain curve between 0 and 10%, as shown in Figure 1.

It is the high ductility of these grades that enable the stamping of the components and application to the rail/bumper system. In comparison, a HSLA 800 grade has a total elongation of 3% to 4% compared to 16% to 19% for DP780. Prior to applying the AHSS grades to automotive applications, such limitation in ductility has prevented the stamping of steels at these strength levels into rail and bumper components.

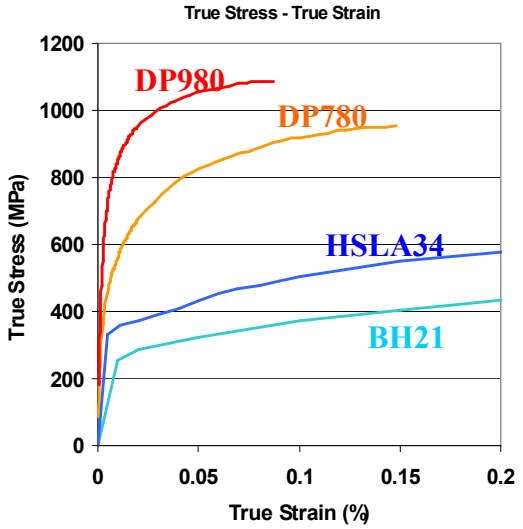


Figure 1. True Stress-True Strain Curves

Laser-Welded Blanks

Six of the 12 stampings comprising the redesigned rail bumper system are produced using laser-welded blanks (LWBs) (Figure 2) of DP 780 and are a key design feature required for structural efficiency and affordability.



Figure 2. Rail inner and rail outer laser-welded blanks

The LWBs are primarily responsible for the part consolidation achieved in the redesign, reducing the part count from 27 in the original design to 13 on the redesigned system. The blanks were manufactured under production conditions, with no special edge preparations in the blanking operations and the equipment run at production speed.

Laser-weld seam quality was evaluated for geometrical imperfections and tested with an Olsen tester. The testing indicated the blanks met all quality requirements. The weld seam produced by the laser-welding process was usually convex, displayed a narrow weld seam and a very small heat-affected zone (HAZ). Examples of microstructures for DP 780 Hot Dip Galvanized (HDG) steel after laser welding are shown in Figure 3. Micro-hardness values indicate that the welds are typical of a good quality laser-welding process and demonstrate high feasibility for industrial applications of DP 780 LWBs.

The most severe testing placed on the laser-welded blanks was during the actual stamping operations and in the crash event where the laser welds performed as expected and without incident.

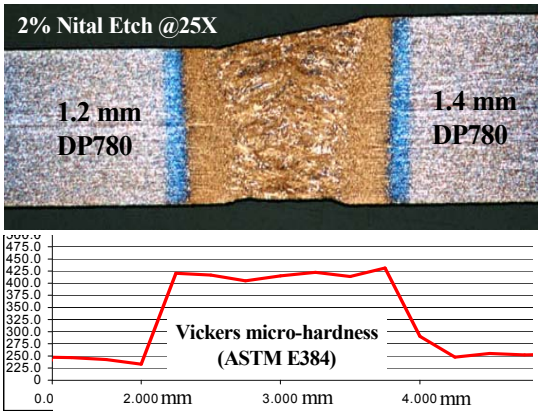


Figure 3. Laser weld's HAZ and micro-hardness.

Stamping

Steel stamping dies were built to produce the prototype components, with the exception of the rail extension, which used a soft tool for the draw operation. The process is designed to produce components representative of a production operation. The process is also intended to investigate and address manufacturing feasibility within the confines of the project. The detailed report describes each component as in the following example of the rail extension, which was the most difficult stamping.

A prototyping process was developed to produce the part, in this case, a five-stage operation.

Finite element analysis (FEA) simulation was used to address the feasibility of forming the component. In this case, failure was predicted but it was felt a solution could be developed during die development.

Blank optimization was utilized to allow the steel to draw into the die and address potential splitting and wrinkling concerns.

A single-piece draw die was used to form the part. As predicted by the forming simulation, the parts did demonstrate forming problems. Several design changes were required to address splitting issues, including opening the sidewalls and changing the binder pad surface to improve material flow.

A re-strike tool was required to finish-form the sidewall and correct the sidewall springback.

Finally, a checking fixture was used to confirm conformance to design and understand and address springback issues. A graphic representation of the above is shown in Figure 4.

It was anticipated that trimming was to be accomplished by laser or saw operations in prototyping. However, the parts configuration accommodates a typical trim-die operation.

A recommended production process is accomplished for each component. This is a conservative approach and the intent would be to look for design concessions and process improvements to reduce the number of operations.

Tooling reports

Tooling reports were performed on each of the stampings to understand final part severity and the need for additional work on each part. The tooling report for the rail extensions is shown in Figure 5. The analysis shows that several locations on the parts are not safe and additional die modifications or part concessions are required for a production-ready stamping.

The forming strain evaluations shown in Figure 6 indicate that, in addition to the rail extension, the rail extension reinforcement and the bumper stampings do not meet a safe criterion. The dies have been assigned to the A/SP High-Strength Steel Stamping team for additional development and the improved understanding required for production of these steel grades.

Spot Welding

The A/SP High-Strength Steel Joining team developed weld schedules for the stack-ups required by the design as shown in Figure 7. All resistance welds were produced using standard, portable gun-tyle welders typical of a body shop that uses manual welding.

Where single-side access was the only access to weld joints, material was drilled out on the top sheet to provide effective MIG puddle welds. This technique was used where the donor body was attached to the rail assembly. This was a restriction of the prototype vehicle build and not indicative of

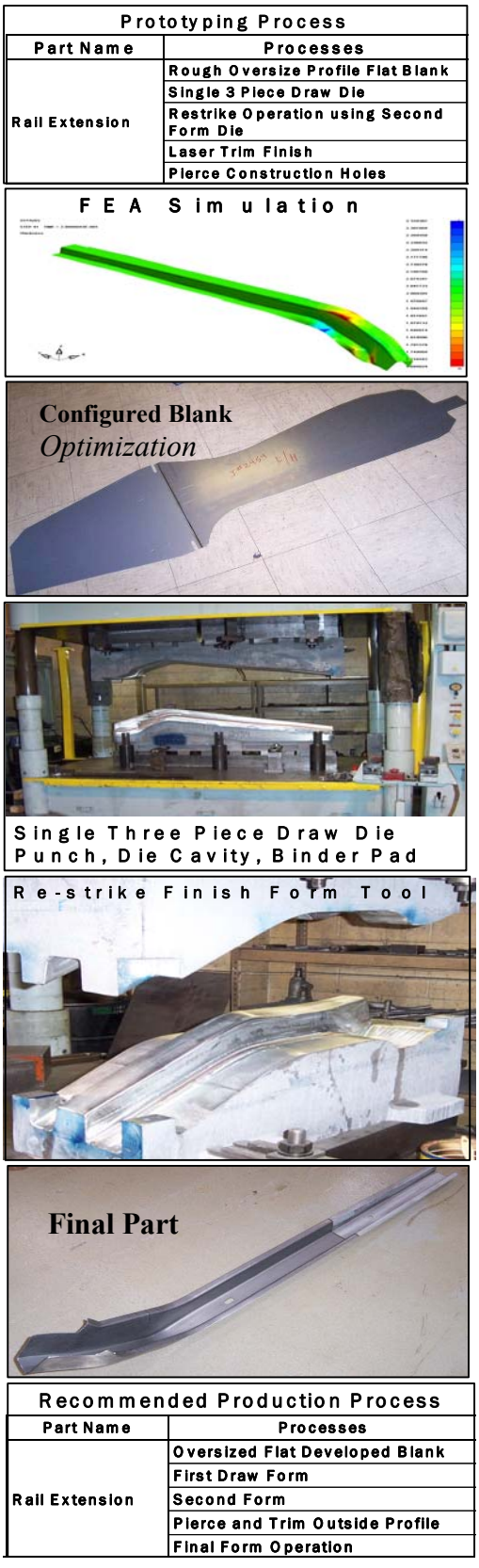


Figure 4. Stamping process flow diagram

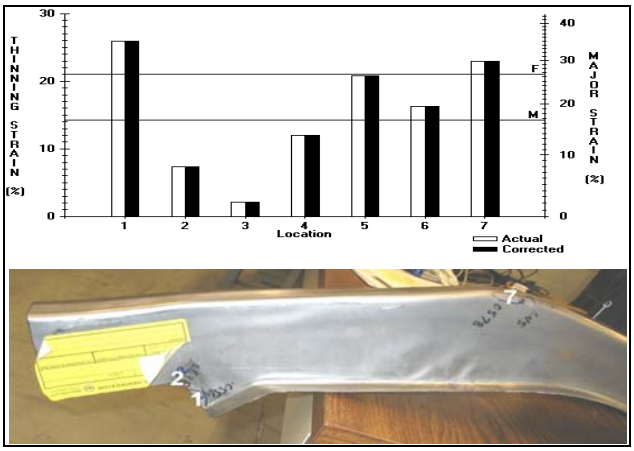


Figure 5. Rail extension tooling report

Table 1 - Stamping Material Properties and Component Forming Evaluations

Part	Grade & Gauge & Coating	YS (MPa)	TS (MPa)	%El	n-value (terminal)	Part Forming Status	
						Status	Safety Margin
Rail Inner (3 pc. LWB)	DP780 1.0mm GA	489	875	16.6	0.116	Safe	18.50%
	DP780 1.2mm GA	508	896	16.4	0.113	Safe	10.80%
	DP780 1.4mm GA	429	837	19.2	0.118	Safe	12.90%
Rail Outer (3 pc. LWB)	DP780 1.0mm GA	489	875	16.6	0.116	Safe	18.50%
	DP780 1.2mm GA	508	896	16.4	0.113	Safe	13.30%
	DP780 1.4mm GA	429	837	19.2	0.118	Safe	13.50%
Rail Inner Reinf.	DP780 2.0mm GA	495	892	13.6	0.111	Safe	16.70%
Rail Extension (2 pc. LWB)	DP780 1.2mm GA	508	896	16.4	0.113	Safe	11.90%
	DP780 2.0mm CR	517	806	23.0	0.111	Critical	-8.30%
Rail Ext. Reinf.	DP780 1.4mm GA	429	837	19.2	0.118	Marginal	6.10%
Bumper Inner	DP980 1.0mm CR	814	983	14.0	0.084	Marginal	1.20%
Bumper Outer	DP980 1.0mm CR	814	983	14.0	0.084	Critical	-3.80%

Figure 6. Tooling Report Summary Table

what would be accomplished in a production assembly.

A post-crash inspection of the welds was undertaken to assess performance of the welds in the crash event. Observation of all visually-accessible rail welds indicated that no welds separated without pulling buttons from adjacent material. The welds performed as expected in the crash event.

The study suggests that conventional equipment and processing would be able to deliver acceptable welds for these material combinations.

Assembly

The assembly was a "one-off" build and is the least representative aspect of a production process, and little was gained toward the demonstration of manufacturing feasibility. An assembly fixture, shown in Figure 8, was used for the assembly of the rail and then for attachment to and alignment on the donor vehicle.

Weld Schedules Specified For Materials In LWFES Rail Assembly.

Stack up ID	Material Location	AISI	Metal grade, gage	Weld cycles	I min-Imax (kA)	Nom Current kA (1)
114	TOP	-	DP980-1.03 mm			
	BOTTOM	-	DP890 1.03 mm	22	8.8-11.6	10.5
115	TOP	-	GA DP800 1.0 mm	22	8.8-12.4	11(2)
	BOTTOM	-	GA DP800 1.0 mm			
116	TOP		GA DP800 1.20 mm	22	9.0-10.8	10
	BOTTOM	208	GA DP800 1.20 mm			
117	TOP	209	GA DP800 1.40 mm	22	9.0-10.4	10.5(2)
	BOTTOM	209	GA DP800 1.40 mm			
118	TOP	210	HDG DP800 2.0 mm	22	10.0-11.5	10.8
	BOTTOM	209	GA DP800 1.40 mm			
119	TOP	208	GA DP800 1.20 mm	22	10.0-12.0	11.0(2)
	BOTTOM	210	HDG DP800 2.00 mm			
120	TOP	209	GA DP800 1.40 mm	22	10.0-11.5	10.8
	BOTTOM	210	HDG DP800 2.00 mm			
121	TOP	209	GA DP800 1.40 mm	22	9.8-11.0	10.8(2)
	MID	210	HDG DP800 2.00 mm			
	BOTTOM	209	GA DP800 1.40 mm			

Nominal force 1500 lbs, nominal hold 30 cycles, tips 45-degree truncated with 7.0 mm face.
GA = Galvanneal
HDG = hop dip galvanized

NOTES:
(1) Nominal current produced better than 97% good welds without weld tip stabilization.
(2) Required tip stabilization to obtain buttons on tip (point) evaluation test.

Figure 7. Weld schedules for specified materials



Figure 8. Modified rail assembly on check fixture

It was noted that the parts fit together without the need for excessive clamping, indicating that the parts were near desired shape.

The project does not comprehend all of the manufacturing variables prevalent in a high-volume manufacturing environment. However, this project does address several aspects of meeting those goals and can be used in the accumulation of knowledge needed to develop robust manufacturing practices suitable for AHSS.

Testing

The AHSS rail and bumper designs were validated by conducting a New Car Assessment Program (NCAP) 35-miles-per-hour rigid-barrier impact test at the Transportation Research Center in East Liberty, Ohio. The bumper and the front section of the rails crushed completely and there was no significant deformation of the A-Pillar, B-Pillar, roof rails and rail extension rear. The B-pillar acceleration peak of the new AHSS design was lower than that of the baseline design; however, the time-to-stop of the new AHSS design was longer than that of the baseline design.

There are two observations to be noted relating to the condition of the test vehicle:

- it had been driven prior to this test, and
- the engine and engine mounts from a previously crashed vehicle were used.

Overall, the new AHSS design had an NCAP performance similar to that of the baseline design.

Photos 1 through 7 provide visual and graphic representation of pre- and post-test conditions.



Photo 1. NCAP Test – Left-Hand (LH) Side Views



Photo 2. NCAP Test - Front Views

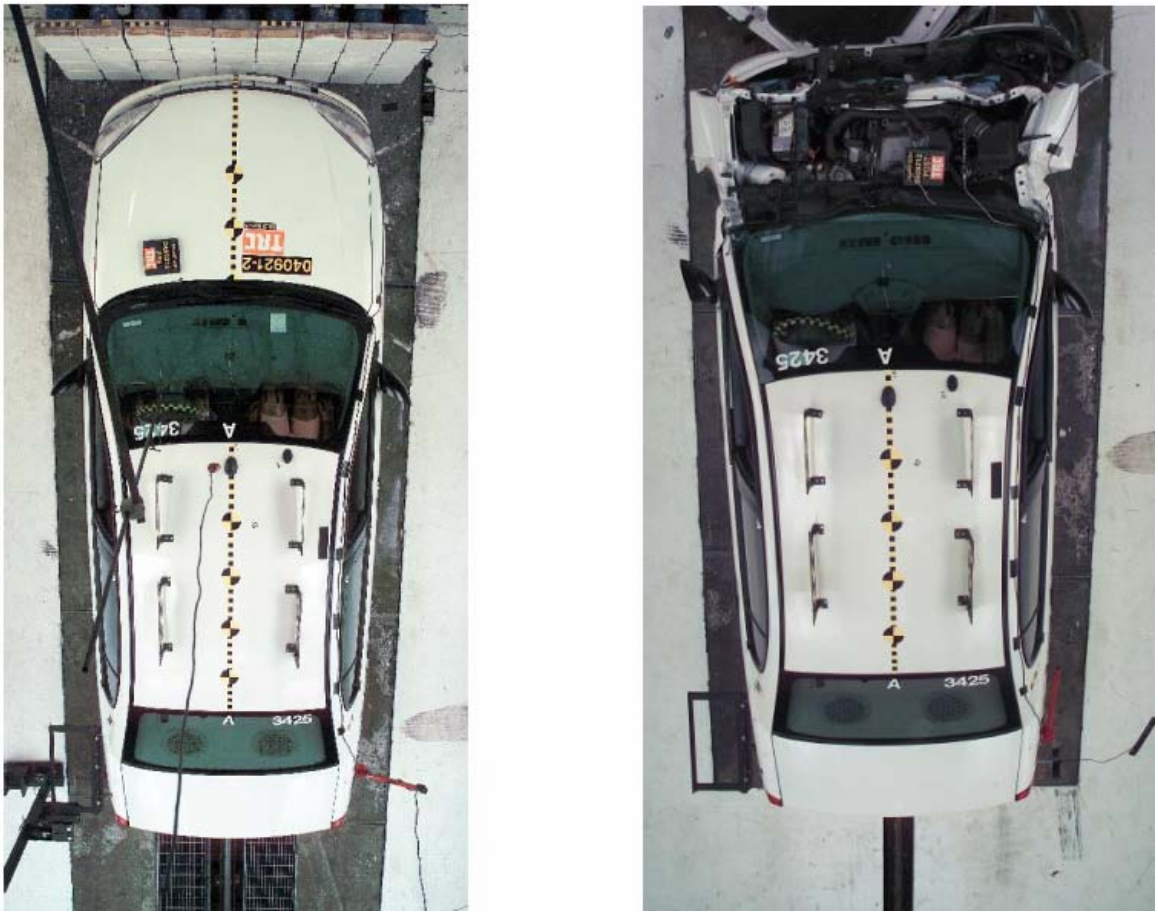


Photo 3. NCAP Test - Top Views



Photo 4. NCAP Test - Underbody Views



Photo 5. NCAP Test – Front End/Bumper View



Photo 6. NCAP Test - Bumper Close-up Views

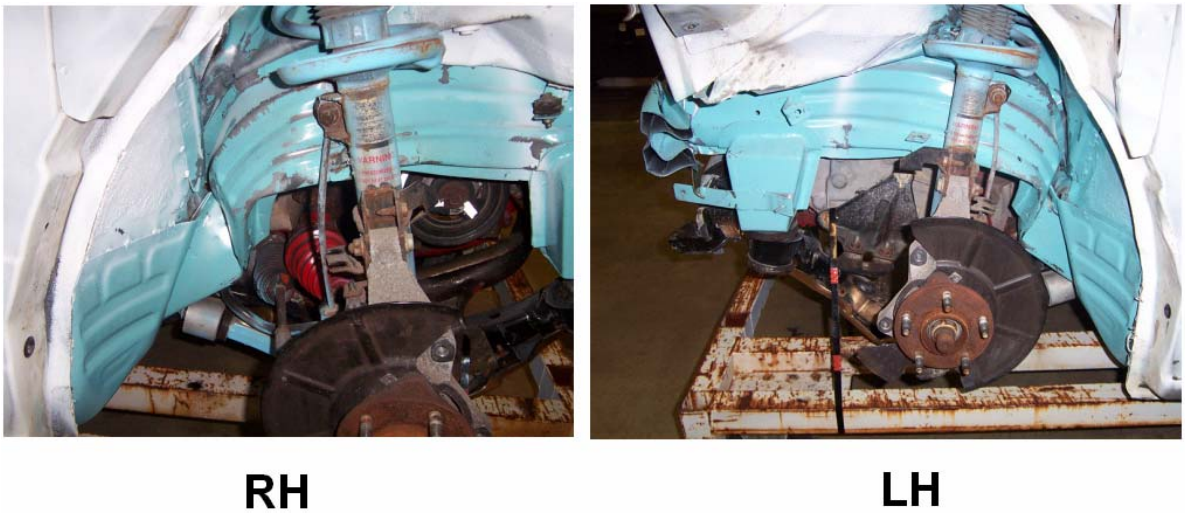


Photo 7. NCAP Test - Front Rail Views

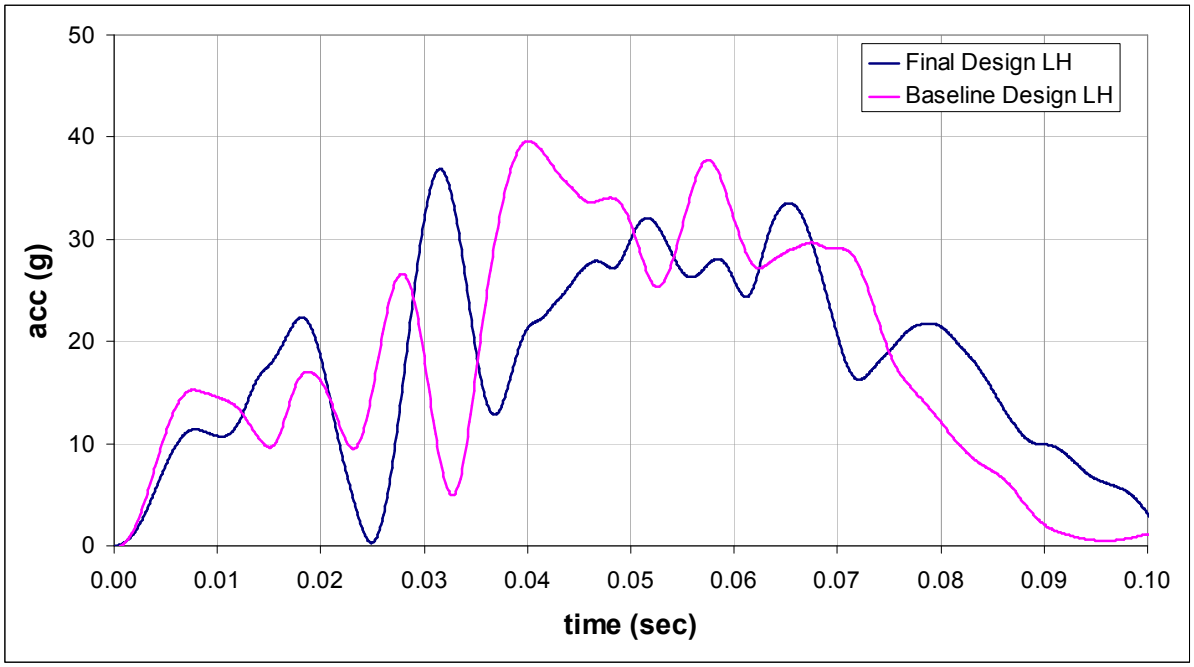


Figure 9. NCAP Test – Left-Hand B-Pillar Acceleration Pulse Comparison

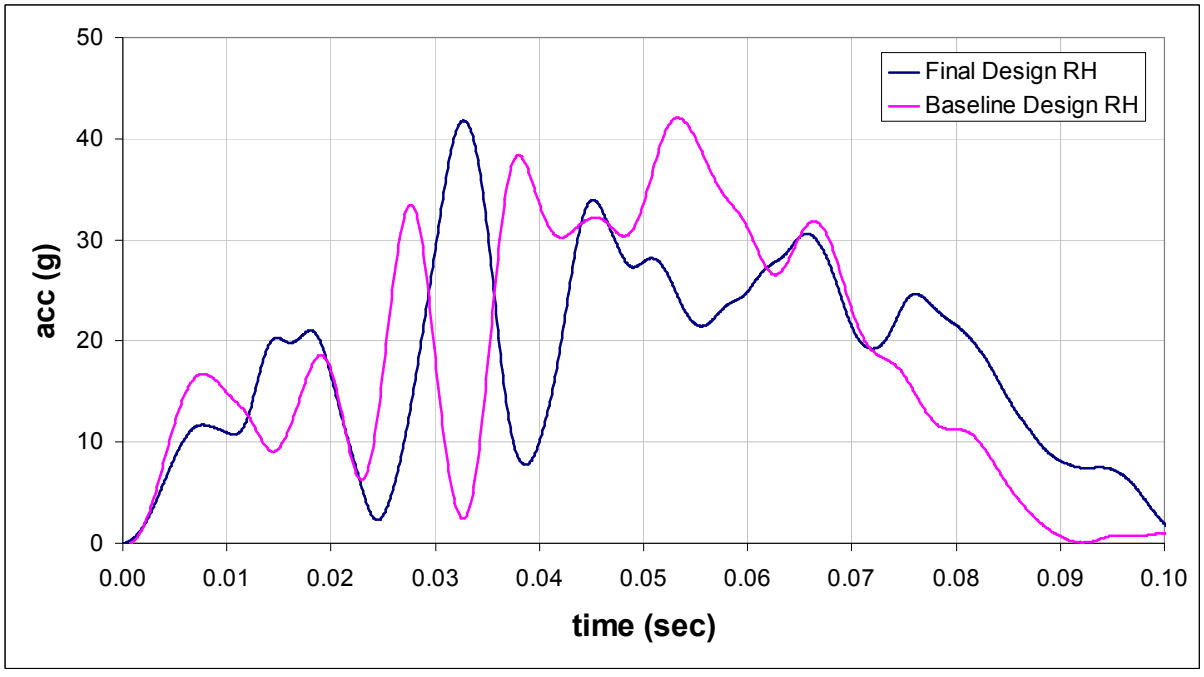


Figure 10. NCAP Test – Right Hand B-Pillar Acceleration Pulse Comparison

Post-Crash Report of Weld Performance

The crash test was performed with all front structure components in place, including engine, suspension and heating and air-conditioning equipment. The original-design structural components are painted white. All structural adhesive and sealers were applied per the production requirements of the original design. The AHSS components that were redesigned to replace the original steel rails are painted blue. The apron assembly, or shock tower, was not part of the redesigned LWFES rail project.

The body structure was mounted on a 45-degree viewing rack to allow easy access to areas of interest. Due to the mounting, the most easily photographed rail components were on the right-hand (RH) side of the body.

Where single-side access was the only access to weld joints, material was drilled out on the top sheet to provide effective metal inert gas (MIG) puddle welds. This technique was used where the donor body was attached to the rail assembly. One joint on the rail assembly restricted access of the weld gun and plug welds were used in place of resistance spot-welds (RSW) for some welds in this joint. The bumper reinforcement attachment bracket was also arc-welded to the end of the rail assembly. All resistance welds were produced using standard portable gun-style welders typical of a body shop that employs manual welding. All arc-welding was performed using standard body-shop MIG welding equipment and E70 filler wire. Observation of the post-rash weld conditions suggests that conventional equipment and processing should be able to deliver acceptable welds for these material combinations.

Observation of all visually-accessible rail welds did not indicate that any welds separated without pulling buttons from adjacent material. Photos 8 through 17 show principal views of the rails and associated assemblies. The performance of the welded rail assembly is largely unremarkable as welds performed as intended.

Weld pitch was approximately 37 mm for the heavier stock. The closest pitch for RSW was approximately 25 mm.

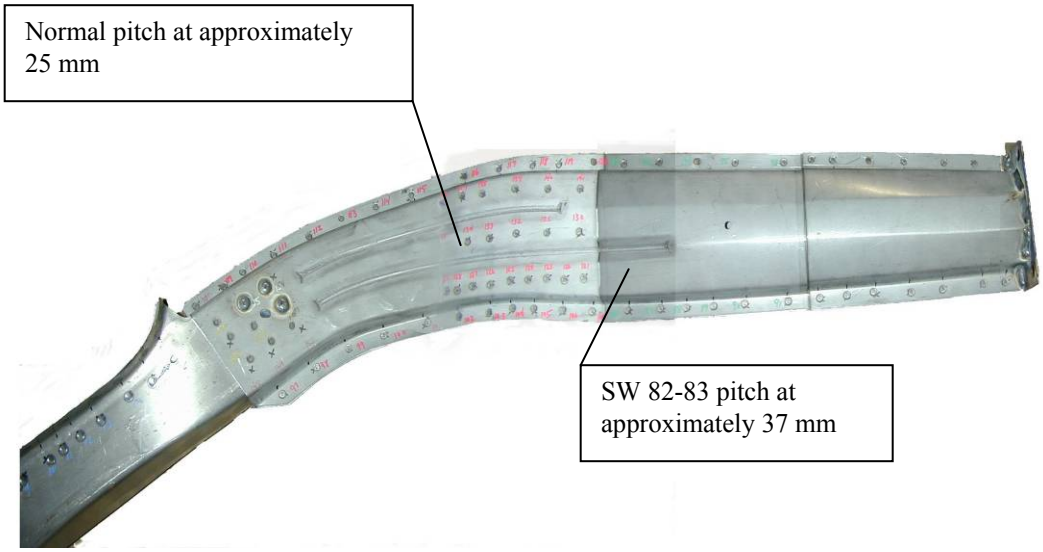


Photo 8. A portion of the right-hand rail assembly showing spot pattern layout prior to crash testing. This view does not include the rail length extending under the floor pan of the body.



Photo 9. Pitch for spot welds from bumper attachment to end of tailor-welded blank.



Photo 10. Standard MIG puddle welds were used where RSW guns would not fit into the box section.

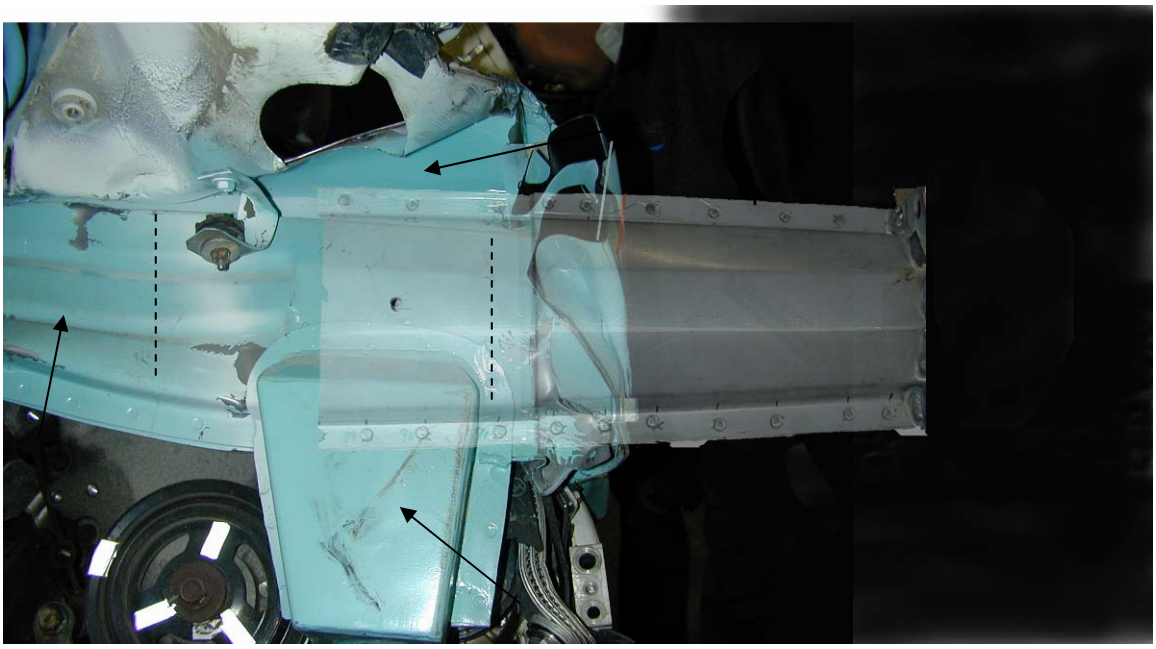


Photo 11. View showing right-hand rail assembly with phantom view of original rail superimposed. Dashed lines are approximate location of the laser-welded blank joints.

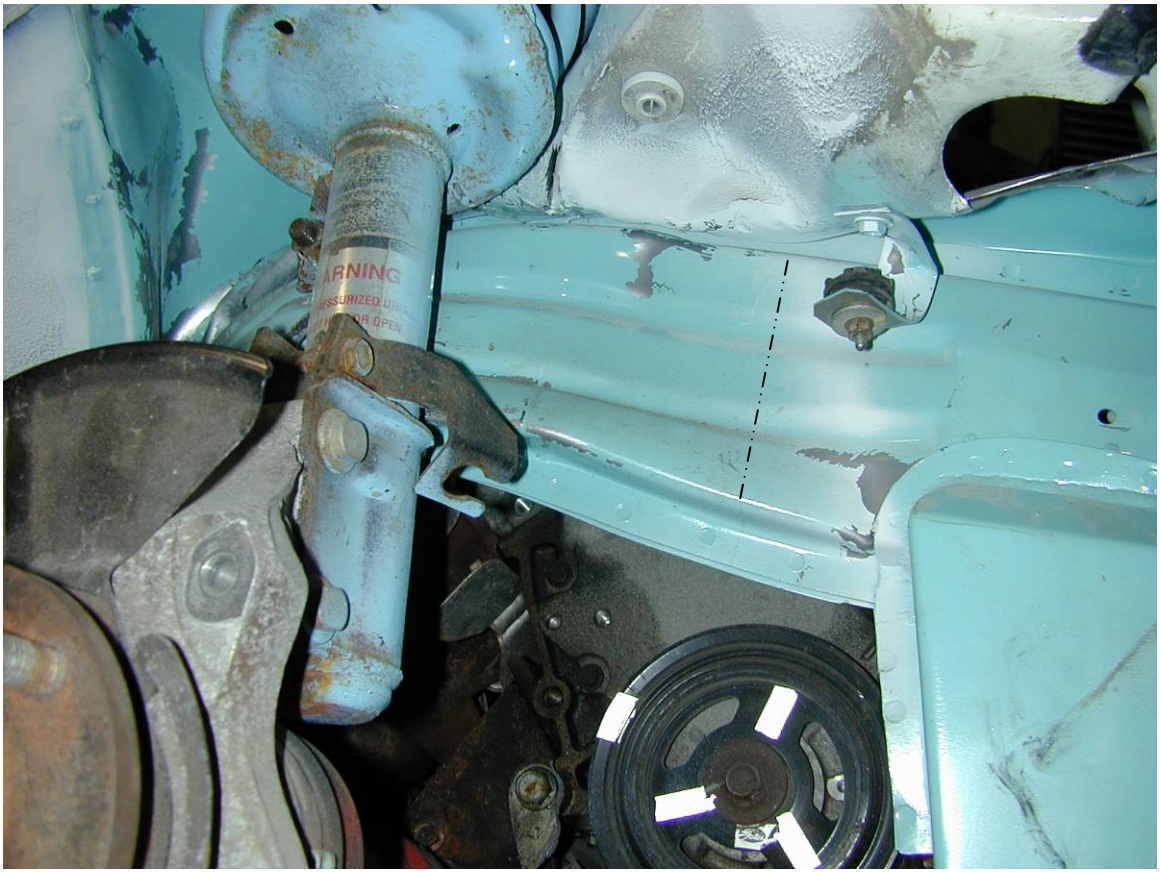


Photo 12. Right-hand rail aft of laser-welded blank joints.

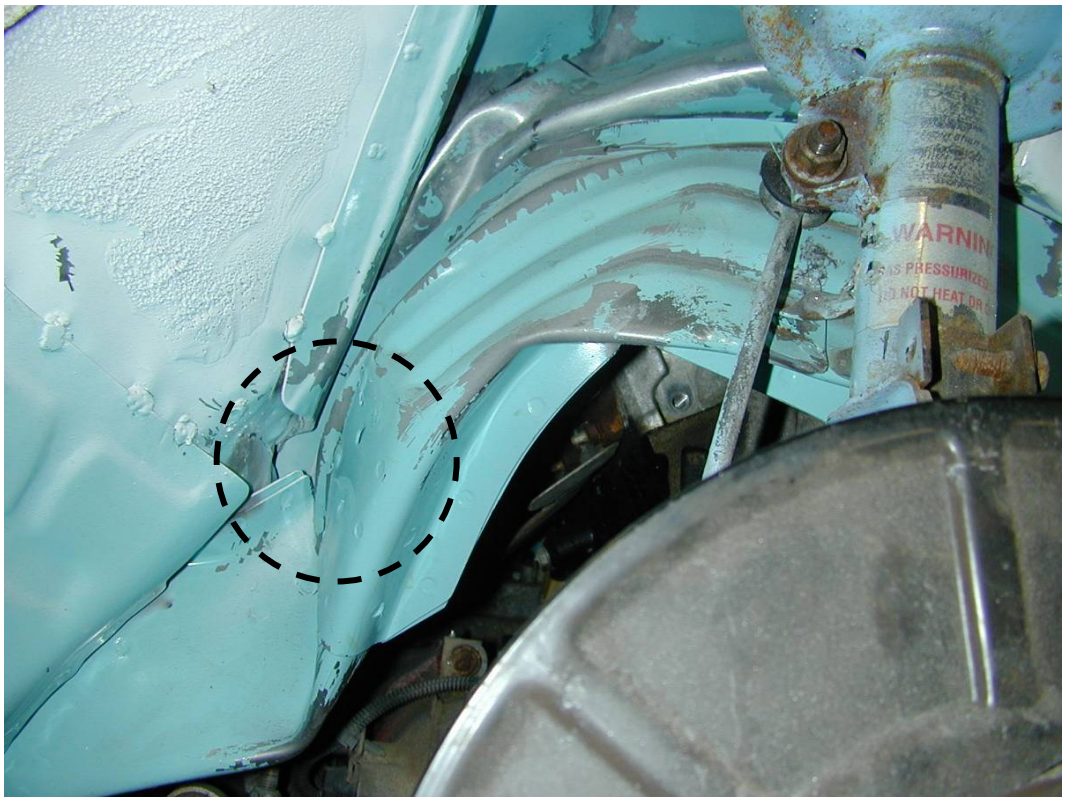


Photo 13. Slip joint with resistance spot and MIG puddle welds highlighted.



Photo 14. Left-hand rail-to-bumper reinforcement collapse. Weld buttons were pulled from the AHSS materials when separation was observed.

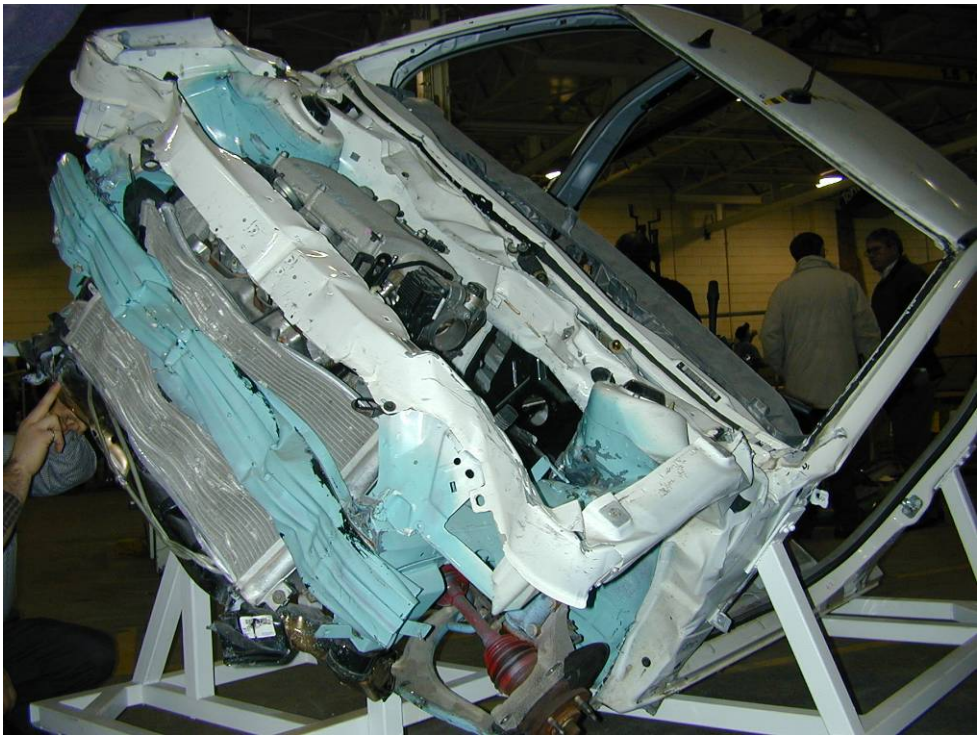


Photo 15. Front view showing bumper reinforcement and rail collapse. All welds were acceptable.



Photo 16. Left-hand side view of test vehicle.

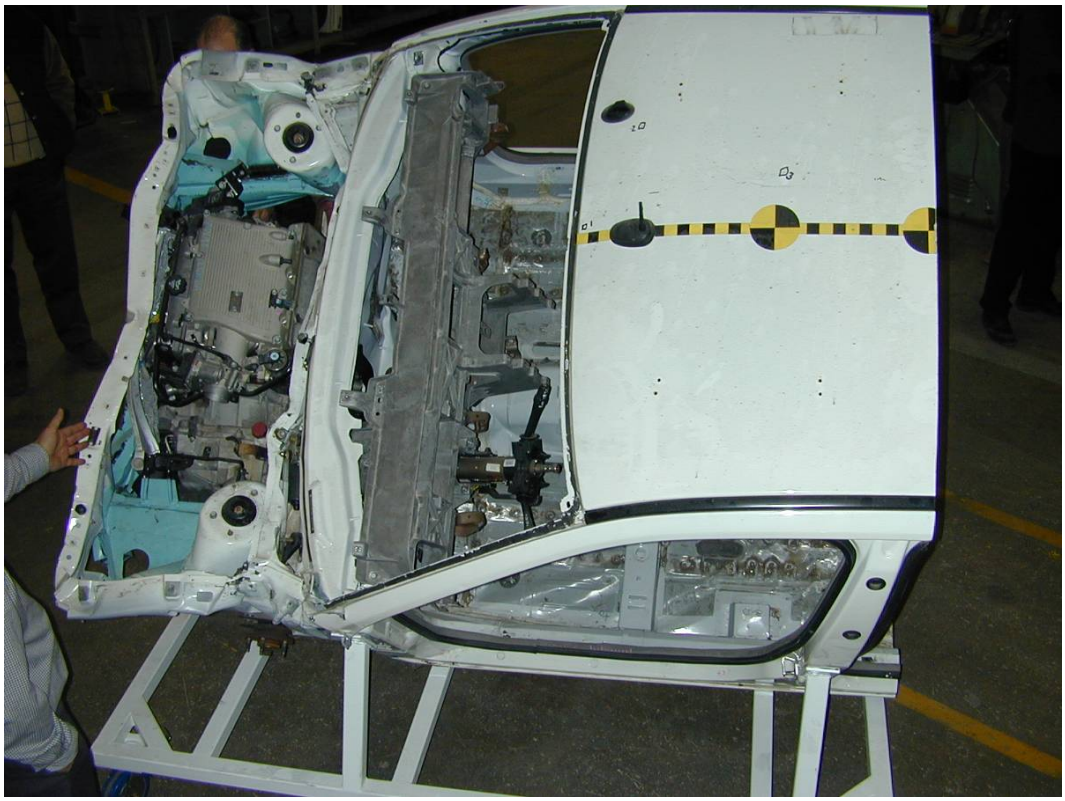


Photo 17. Body top view. Note powertrain components contacting radiator support and dash panel.

Conclusion

The front rails and bumper were designed and fabricated using AHSS DP 800 and DP 980. The AHSS design achieved a mass reduction of 8.77 kg (22.36%) compared to the baseline design. The performance of the AHSS design was similar to that of the baseline design. Conducting an NCAP 35-mph rigid-barrier impact test on the donor vehicle fitted with the AHSS rails and bumper, validated the AHSS design.

It can be concluded that the use of AHSS in conjunction with effective part design can result in significant mass reductions without compromising crash performance. Priority should be given to design stability and load path as opposed to maximizing sections. Parts can be manufactured using DP 800 and DP 980 steels, provided proper attention is given to manufacturing constraints early in the design process.

Technology Transfer

Final results from Phase 1 and Phase 2 were rolled out at "Great Designs in Steel" seminar held in March 2005, including the completion of the display and backdrop with the crash vehicle front end and project results.

Subsequently, a deep-dive presentation was given to DaimlerChrysler (DCX) engineers by the project team and a workshop conducted. A front end for a future DCX vehicle was selected to allow a comparison by the A/SP project team representatives against the project results.

Future deep-dive type presentations are scheduled with General Motors and Ford Motor Company as a means to allow their product engineers to compare future vehicles with these results in a similar manner.

The engineering final report with project results is being finalized and will be made available on the Auto/Steel Partnership website, as well as media and public opportunities.

V. Future Generation Passenger Compartment

Project Manager: Pat J. Villano
Auto/Steel Partnership (A/SP)
2000 Town Center Drive, Suite 320
Southfield, Michigan 48075-1123
(248) 945-4780; fax (248) 356-8511; e-mail: pvillano@a-sp.org

Co-Chairman: John Catterall
General Motors Corporation
Body Systems Center
Engineering West
MailCode 480-111-W23
30200 Mound Road
Warren, Michigan 48090
(586) 986-3541: fax (586) 986-4184; e-mail: john.1.catterall@gm.com

Co-Chairman: Jody R. Shaw
Manager, Automotive Marketing
United States Steel Corporation
5850 New King Court
Troy, Michigan 48098-2608
(248) 267-2608: fax (248) 267-2581; e-mail: jrshaw@uss.com

Technology Area Development Manager: Joseph A. Carpenter
(202) 586-1022; fax: (202) 586-1600; e-mail: joseph.carpenter@ee.doe.gov
Field Technical Manager: Philip S. Sklad
(865) 574-5069; fax: (865) 576-4963; e-mail: skladps@ornl.gov

---

Contractor: U.S. Automotive Materials Partnership
Contract No.: FC26-02OR22910

Objective:

The objective of the Future Generation Passenger Compartment (FGPC) project is to incorporate current propulsion systems and fuel-cell technologies into concept architectures. The project is separated into five (5) phases: Phase 1 - Concept Development; Phase 2a - Validation on a donated vehicle; Phase 2b – Development of Advanced Steels; Phase 3 – Roll-out learnings into advanced vehicle development; and Phase 4 - Production design. Phases 3 and 4 are Original Equipment Manufacturer (OEM) internal.

Approach:

The FGPC project team will benchmark, develop and document integrated solutions that will balance the interaction of materials, manufacturing, performance and cost. The study will focus on solutions that will address high-volume manufacturing and assembly applied to fuel-cell technology vehicles. The project supports the goals of FreedomCar as follows:

- High-strength steels are a mass-efficient solution in crash-dominated vehicle structures (e.g., body, closures, chassis, etc.) at a significant cost advantage versus other materials.
- A passenger compartment is thus an enabler to facilitate the application of other lighter weight materials to achieve half the vehicle mass while maintaining affordability.
- Steel has the proven and existing infrastructure for high-volume production and 100% recycling.

- This and other projects also allow the industry to migrate to lightweight structures that will accommodate fuel-cell powertrains.
- Immediate project initiation is required to establish the foundation required to develop a FreedomCAR solution.

Accomplishment:

A benchmarking study and fuel-cell development calibration baseline have been completed.

Future Direction:

- Validation of the Phase 1 results into a donated vehicle.
- Develop additional advanced high-strength steels.
- Roll-out learnings into advanced vehicle development.
- Incorporate into future production vehicles.

Project Progress: October 1, 2004 to September 30, 2005.

The project was initiated on January 1, 2005.

The Future Generation Passenger Compartment (FGPC) project is divided into nine (9) sections. Each of these sections will have a presentation and report.

1.0 Benchmarking
2.0 Calibration Baseline
3.0 IIHS/ Roof Crush DoE Study
4.0 Concept Design Study
5.0 Design Concept Analysis Check
6.0 Final DoE Mass Optimization
7.0 Final Design Check
8.0 CAD Data for the final Design
9.0 Final Report

The following definitions are used throughout this report:

ULSAB-AVC: Ultra Light Structure Automobile Body-Advanced Vehicle Concept
FGPC: Future Generation Passenger Compartment
FGPC-D: Diesel Vehicle
FGPC-F: Fuel-Cell Vehicle

1.0 Benchmark Study completed:

The goal of the Benchmarking Study was to gather information that would identify the latest technology trends used by worldwide OEMs for crashworthiness in general and specifically the Insurance Institute for Highway Safety (IIHS) side-impact and rollover tests. The FGPC project team members will use this knowledge to enhance the OEM designs for better performance.

The strength or weakness of a particular design investigated during benchmarking is a relative statement and could only be graded if the design targets and their performance constraints were known. Therefore, we have to believe each design has its own philosophy.

Design philosophy is defined as a target that designers would like to achieve for overall vehicle behavior and vehicle component behavior in different proving-ground tests and attributes, such as front crash, side impact and rear crash.

The design philosophy or vehicle definition is based on target performance, development cost, vehicle rank, manufacturing, material, styling, etc. Definitions should be known so one can identify whether or not a particular design is within that design envelope. Since the design philosophy and constraints of the benchmarked vehicles are not known, the team would not categorize a design as good or bad. Such a categorization is also not within the scope of this project.

The key question in the crash and safety environment of the auto industry is how it should meet Federal Motor Vehicle Safety Standards (FMVSS), New Car Assessment Program (NCAP), IIHS, Japanese and other regulations within one vehicle system package with no major architectural

changes in the packaging and tooling to control cost and weight.

At the same time, there exists a challenge to meet all safety issues, reduce the vehicle mass, and make the vehicle fuel efficient for current and future types of drivetrains, including future vehicles with a Hydrogen Fuel-Cell drivetrain.

Most automakers and their key suppliers predict that hydrogen fuel-cell technology would be able to demonstrate commercial feasibility and production validation by 2010, with vehicles ready for public sale by 2015.

OEMs worldwide are developing crash load paths using all available tools to meet FMVSS, ECE, IIHS and NCAP front, side and rear crash requirements. Although crash load paths are similar on all vehicles, each manufacturer has its own strategies for managing the crash energy and load paths.

- For front impact, the trend is to more evenly distribute loads to improve passenger protection, and to be more crash-compatible with vehicles of differing ride heights using energy management and load path mechanisms.

- For side impact, controlling the B-pillar intrusion and deformation mode by balancing the lower and upper regions of the body structure is critical. Reinforced B-pillar, rocker, and roof structures are generally needed to meet performance targets.

- For rear crash, similar strategies as used in front impact are under development, using energy-management and load-path mechanisms within one system to meet all rear crash scenarios.

All benchmarked vehicles in this study have used all of the above techniques to meet the targets. However, some, more than others, used layers of reinforcements with steel material to resist the loads. It is predicted that future technological advancements may provide an alternative approach to meeting crash and safety goals.

Overall, it has been observed that a few vehicles have incorporated a considerable amount of reinforcement within the body side in the rocker, A-pillar, B-pillar and roof rail sections. It is possible that the original architecture was not designed for some events and designs had to be reconfigured by adding reinforcements to meet specific targets.

Other design features that were found to be common in this benchmarking effort include the use of bulkheads, used for the prevention of local buckling, and a wider B-pillar section, which provides better resistance in side impact and rollover and better load transformation for vehicle dynamics and also helps to stiffen the body in torsion. This could reduce the number of reinforcements that are used inside of the B-pillar, or weight reduction using geometry. Styling could be an issue in this type of design.

A deep rocker section with multiple-layer reinforcements is used because it will not allow the section to collapse in FMVSS 214 and ECE side impact where the barrier hits the rocker section. The rocker is used for the load path for front crash as well.

To meet the requirements of rollover, IIHS front and side impacts, we observed a deep section in the roof rail between the A and C pillars. This contrasts the strategy used by many vehicles that use a smaller section with multiple reinforcements.

If all these ideas are used properly based on design philosophy, it is considered a smart design, one that if it is used outside of its envelope, it would be considered over-designed.

In the design of vehicle components, beading will be used to improve local and overall stiffness and crash modes of body panels.

In summary, the strategy to meet FGPC Project Team objectives will be:

1. The use of geometry to design the load path to meet crashworthiness performance, while absorbing energy using total-system topology optimization.

2. Investigate the usage of advanced high-strength steel (AHSS) materials and manufacturing

techniques (e.g., tailor-welded blank) that can reduce weight and increase performance.

2.0 Fuel Cell Development Calibration Baseline Report was also completed:

The purpose of this report is to document the design and packaging effort that provided a baseline configuration for the subsequent CAE assessment of vehicle performance for different crashworthiness scenarios.

A/SP provided the initial vehicle model, which was developed for the ULSAB-AVC program. The model was validated and used as the baseline configuration. Two variations were developed:

- Fuel-cell power (FGPC-F)
- Conventional rear-wheel drive with diesel engine (FGPC-D)

Objective:
To provide evaluation of the FGPC design for fuel-cell and traditional engine configurations for five different performance attributes:

- FMVSS 208 Front Crash (US-NCAP)
- IIHS Front Crash
- IIHS Side Impact
- FMVSS 301 Rear Crash
- FMVSS 216 Roof Crush

The objective is 1) to compare the FGPC vehicle performance with ULSAB-AVC in all above mentioned attributes and 2) to compare the performance of the fuel-cell and traditional engine configurations for each crash attribute and then use the worst case to evaluate the performance of the vehicle with the new underbody design.

A new underbody was designed based on the ULSAB-AVC vehicle platform for FGPC. The new underbody was modified and packaged to allow the vehicle structure to be capable of having two different types of drive train: traditional rear-drive diesel engine and fuel-cell power. Engineering Technology Associates (ETA), Engineering Design, Inc. (EDAG), and A/SP team members developed fuel-cell packaging requirements based on information gathered in the benchmarking phase and from the OEMs (GM, Ford and DCX). These requirements include the mass of fuel-cell components, and volume of fuel-cell tanks and modules. The packaging and design of the new underbody was targeted in a way that the volumes of the fuel-cell storage tanks are maximized and shapes of the fuel-cell tanks are acceptable to be manufactured today or by 2010. The final design of the fuel-cell modules includes two oblong-shaped tanks under the rear seat and a conical-shaped fuel cell tank under the modified center tunnel.

The FGPC program vehicle targets were developed based on ULSAB–AVC performance targets:

1. Front Crash – Meet U.S.-NCAP and IIHS 40% Offset Deformable Barrier (OBD) Impact structure performance
2. Rear Crash – Meet FMVSS 301
3. Side Impact – Meet IIHS Dynamic Side Impact
4. Roof Crush – Meet FMVSS216

The scope of the design and packaging effort includes the following tasks:

- Review available space for packaging
- Determine and subsequently maximize volume of fuel-cell storage tanks
- Develop alternative body design options
- Review sections of fuel-cell storage
- Evaluate possible alternative shapes for fuel storage if applicable
- Study possible concessions in packaging
- Incorporate suspension data (if available)
- Establish material thickness of fuel storage containers

The first portion of the design study was to determine the overall volume of the space that was available for fuel-cell storage using the existing ALSAB/AVC-PNGV vehicle structure.

The packaging of the components for the fuel cell option was determined using dimensions obtained from the A/SP team. These components (fuel-cell stack, batteries and electronic box) were positioned in strategic areas and reviewed by the committee members to best determine a viable location. The repositioning of the components in the front engine compartment was the starting point for all

components and acceptability would be determined using the analytical front-end crash results.

Multiple fuel-cell shapes and sizes were packaged to determine the actual fuel storage area that would be available with the existing structure and possible alternative revisions that could be made were determined. A revision to the tunnel area in size and shape was one option along with other revisions to the existing structure. Some considerations include:

- The width of the tunnel remained the same and the joint connections to the rail members did not change. The height of the tunnel was raised, holding the front portion at its present height but raising the rear connection to the rear floor pan and kick-up panel as high as possible; this would impact the middle rear seat passenger (Figure 1).
- Alternative shapes other than cylindrical were considered (oblong, conical and irregular). These would be held as possible options and would be packaged with the various revisions to the current structure (Figures 2-4).

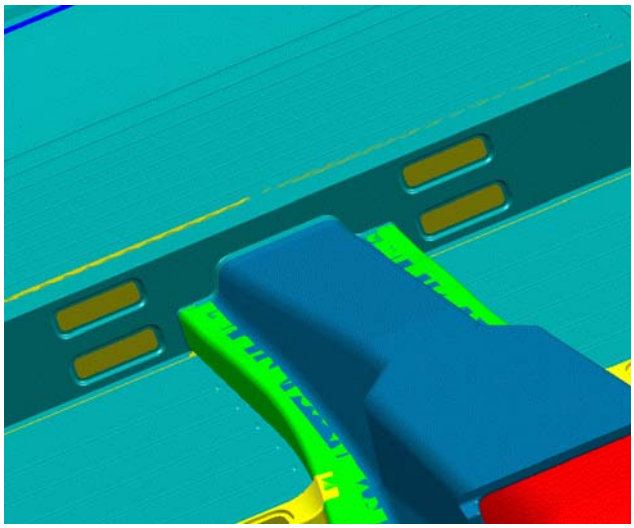


Figure 1. Revised Transmission Tunnel.

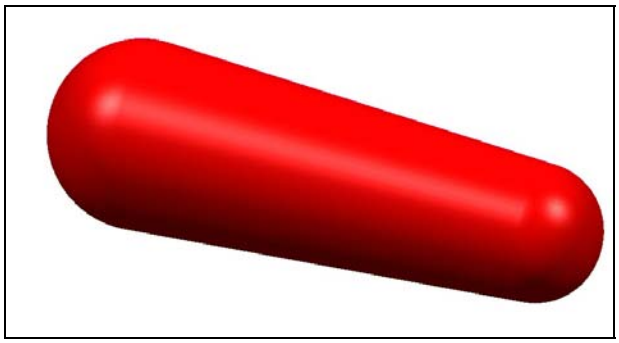


Figure 2. Cone shape for tunnel fuel storage 79,390,000 cmm at a weight of 20.65 kg.

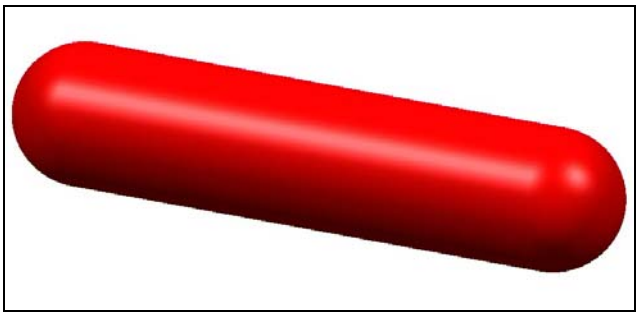


Figure 3. Cylindrical shape for the tunnel fuel storage 50,710,000 cmm at a weight of 13.18 kg.

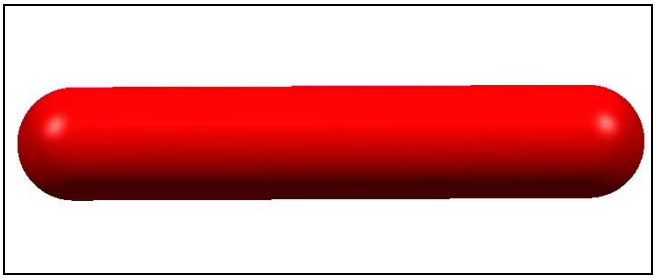


Figure 4. Fuel storage tank under rear seat.

The cylindrical shape for under the rear seat and the trunk was 23,920,000 cmm at a weight of 6.22 kg. Six tanks would be utilized for this space, 3 cylinders under the seat area and 3 cylinders under the trunk. The total weight would be 37.32 kg at a total volume of 143,520,000 cmm.

After initial review of the various fuel-cell storage alternatives with the team, one fuel-cell tank would be considered in the tunnel and cylindrical tanks or oblong tanks would be considered under the rear seat and trunk. After reviewing all the design options, it was decided that an irregular fuel-cell shape would be used for the tunnel space to maximize the volume (94,450,000 cmm at 24.56 kg)

(Figure 5). An oblong shape would be used under the rear seat and the depression for the cushion on the floor in that area would be eliminated in order to maintain maximum height for the fuel-cell tank (95,950,000 cmm at 24.96 kg) (Figure 6). Another oblong fuel-cell tank of duplicate shape and size would be positioned under the trunk floor. Figures 7-9 show the fuel tanks' positions in the vehicle. Brackets were developed to support the fuel-cell storage tanks. No revision was made to the trunk floor for packaging the storage tank.

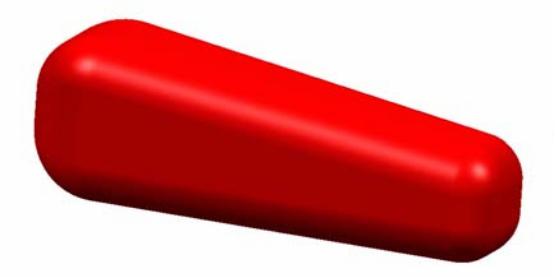


Figure 5. Final Front Fuel Tank Shape.



Figure 6. Final Rear Fuel Tank Shape.

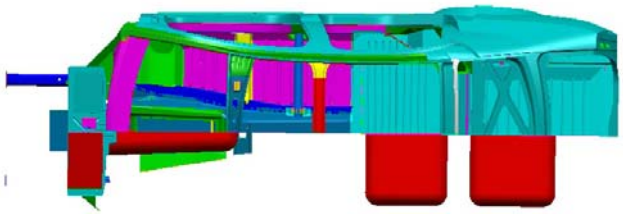


Figure 7. Centerline split view showing body structure and fuel tank - top view.

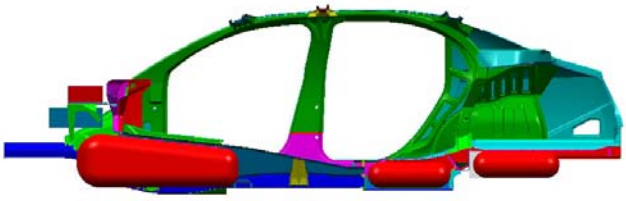


Figure 8. Centerline split view showing body structure and fuel tank - side view.

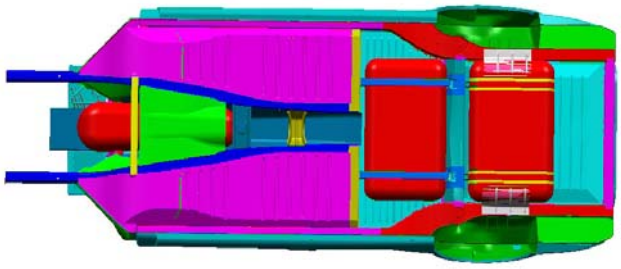


Figure 9. Underbody showing fuel-cell tank locations and tunnel fuel shield.

- A possible revision to the rail member was evaluated by straightening its shape from the front seat to the rear running parallel to the centerline of the vehicle. This could possibly obtain additional width at the tunnel between the rails and create more space for fuel-cell storage. If feasible, this would change the width of the tunnel and could possibly affect the rear seat passenger's foot clearance (Figure 10).
- The fuel-cell storage in the rear compartment area (trunk) could only be utilized in the forward area because of the intrusion zone identified from the rear-impact analytical run. This would be taken into consideration when attempting to package the fuel-cell storage in this location.

The existing ground clearance was a determining factor for the size and location of many of the fuel cells, and was therefore used as a guideline for the packaging of the fuel cells.

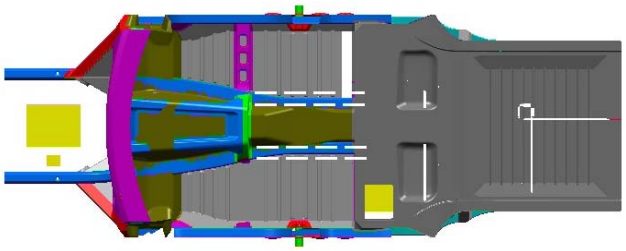


Figure 10. Revisions for passenger's foot clearance.

To accept the height change and shape through the tunnel area, crossmembers were redesigned and the kick-up area from the front to rear floor was revised (Figure 11).

The crash results showed buckling in the floor pan at the tunnel in the kick-up area. This was possibly due to the kick-up area on the floor and the kick-up reinforcement being revised from the original design. It was agreed to revise this area and to obtain a cross-car vertical wall connection on the floor pan, tunnel, and the reinforcement. The kick-up reinforcement would then revert to a single-piece part. The tunnel would also be revised to accommodate this change.

The straightening of the rail members was eliminated from the options due to intrusion into the foot space of the rear-seat passenger.

Fuel-cell components were packaged under the hood and a front package tray was designed to support these components.

The tubular support extending laterally that was utilized as an attachment point for the rearward portion of the front seat was revised due to the height of the tunnel being raised. The original design crossed over the top of the tunnel but had to be cut off at the tunnel because of the height change (Figure 11). A connecting bracket was placed at either side of the tunnel to accommodate the attachment of this tube. A bracket was designed in the tunnel at this location in an attempt to continue the flow of a cross-car support from a side impact.

The team wanted the configuration of the top of the tunnel to the rear floor to have the same plane transition, meaning the top of the tunnel would be at the same height as the rear floor at the rear seat area. The step-down area on the revised tunnel was changed per the request from the previous meeting. This made the rear kick-up reinforcement two parts compared to one in the original, because of the height of the tunnel. The joint connections to the tunnel were revised to accommodate the change. The front tunnel reinforcement was also revised to agree with the tunnel revision, and it kept its basic shape with minor alterations.

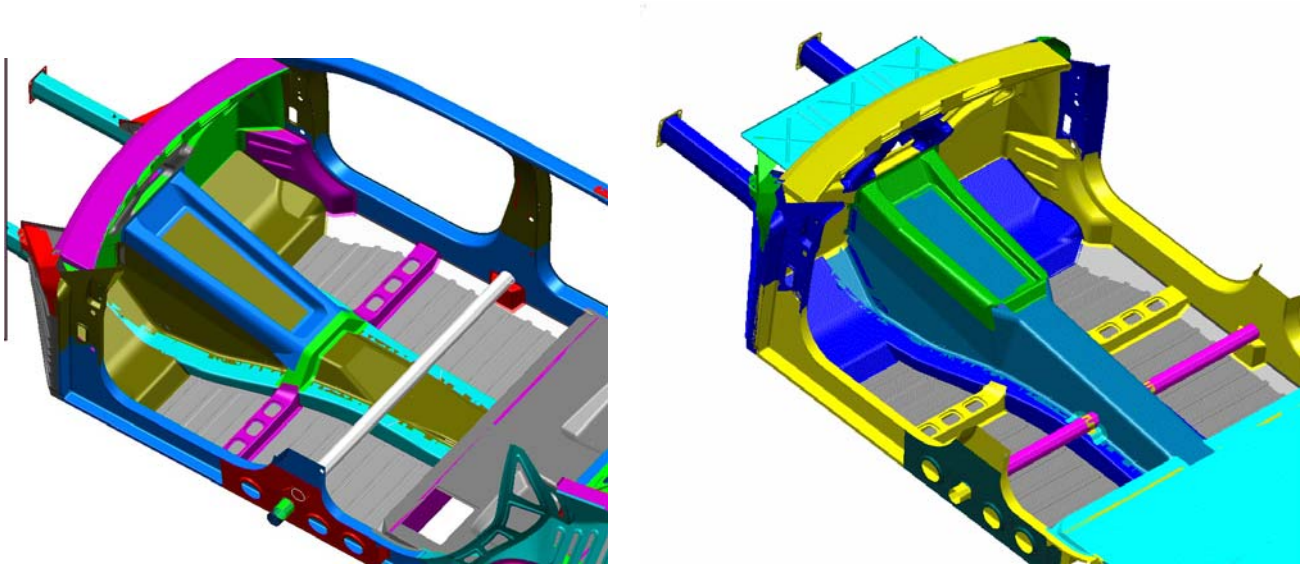


Figure 11. Modifications required to increase tunnel height.

A shield was designed for the tunnel fuel cell trying to incorporate two functions:

- Utilize as a support for the fuel-cell tank
- Utilize as a protective barrier

Brackets for the front shield were designed to assist in supporting the shield, and the shield was revised to better accommodate the routing of the fuel-cell lines (Figure 9).

To strengthen the upper load path for side impact, a roof bow was designed at the B pillar similar to the roof bow used on the C-Class vehicle. Subsequent analysis results showed the roof bow needed revision, so three separate roof bows were designed:

- Move roof bow rearward to be more in-line with the B-pillar from the side view (Figure 12).
- A wider roof bow was positioned strategically at the B-pillar (Figure 13).
- A double roof bow in the area of concern at the B-pillar along the side roof rail (Figure 14).

The front-end crash results showed intrusion of the motor into the shield and tank. The shortening of the tunnel fuel-cell tank will be investigated based on additional information for tank hook-up. The fuel-cell motor dimensions were revised slightly to address the front-end crash intrusion. The original volume was maintained but the front of the box was set further rearward.

2.3 Conclusions

2.3.1 Front Impact

NCAP – Uses Baseline Model

Simulation results for front-impact analysis indicate that the performance of FGPC-D case is similar to the ULSAB-AVC model, whereas the FGPC-F performance degraded compared to ULSAB-AVC. The front fuel-cell tank contacted the electric motor/gear box causing a higher deceleration pulse, which resulted in lower dynamic crush resistance.

IIHS-ODB – Uses Baseline Model

Simulation results for offset-impact analysis indicate that the performance of FGPC-F vehicle degraded from the ULSAB-AVC model as the fuel-cell footwell intrusion is much greater than the FGPC-D model. The reason is because the subframe impacts the fuel-cell tank causing an increase in bending of the longitudinal rails.

In summary, the evaluation of the vehicle performance of both drivetrains for NCAP and IIHS case showed that Fuel-Cell Engine configuration is the worst case compared with the traditional engine configuration. Also, the vehicle will not meet NCAP flat rigid-barrier and IIHS front-crash structural performance requirements with the fuel-cell powertrain. In the fuel-cell configuration, the conical front fuel storage tank will be impacted by the motor/transmission. The IIHS vehicle performance measure was moved from good status to acceptable level; also the fuel-cell tank was impacted by front structure components.

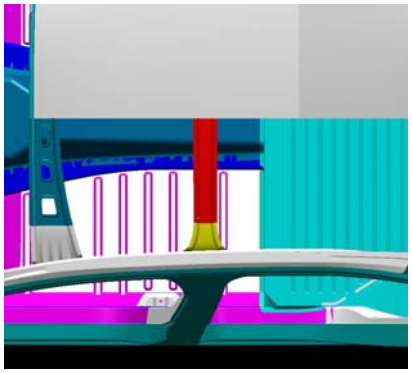


Figure 12. Roof Bow at B-Pillar.

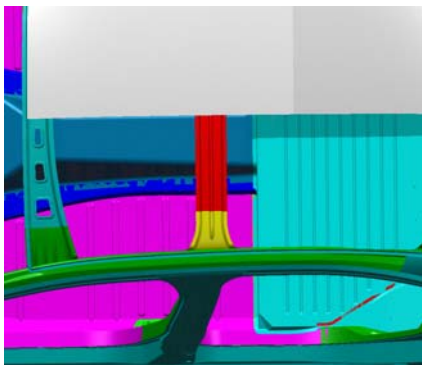


Figure 13. Wider Roof Bow.

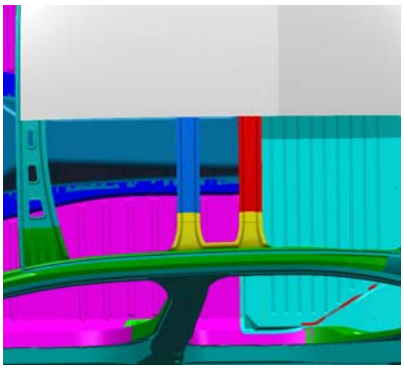


Figure 14. Double Roof Bow

2.3.2 Side Impact – Uses Baseline and Modified Models

In IIHS side impact regulation, the vertical range considered for the structural rating extends from the base of the B-pillar interior up to a point that is 540 mm above the H-point measurement taken with the seat in full-rear and full-down position are summarized in Table 1 below.

Evaluation of the vehicle side-impact performance for each drivetrain configurations showed that both the traditional-engine and fuel-cell configurations showed weakness. ETA added a roof bow at the B-pillar to the side-rail intersection in order to improve the performance of both vehicle configurations that have different mass distributions. The results showed that vehicle performance is below "good" status (125 mm intrusion, see IIHS side impact requirements) for both conditions. However, the results showed that vehicle structural performance with the conventional engine is better than fuel-cell powertrain case. The conventional engine configuration is therefore identified as the baseline for the IIHS side-impact optimization study, which is Task 3 of this project.

2.3.3 Rear Crash – Uses Baseline Model

The worst-case evaluation of the rear-crash vehicle performance showed that the fuel-cell configuration performs the worst in comparison with the traditional-engine design. Analysis results showed that the modified ULSAB-AVC vehicle would meet rear crash FMVSS 301 requirements for both drivetrain cases. The oblong fuel cell and traditional-engine fuel tank would survive and there would not be any fuel leakage.

Simulation results for rear-impact analysis indicate that both the diesel and fuel-cell configurations of the FGPC can withstand the 35-mph rear-impact test without fuel- tank damage.

The fuel pipe of the diesel model has some plastic (permanent) deformation, but the value is small, only 3 % plastic strain. The diesel fuel tank is well secured.

2.3.4 Roof Crush – Uses Modified Model

The vehicle would meet roof crush targets for both drivetrains. The worst case would be the heavier vehicle, which would be the fuel-cell vehicle, because the force requirement is based on vehicle mass.

Table 1. Side-Impact Results Summary: Distance between B-Pillar and Centerline of Seat (Reference Figure 15).

	Baseline Model	Modified Model (Added tunnel and modified rear floor crossmembers, added roof bow)	Remarks
Fuel Cell	85 mm	100 mm	29.4 %*
Diesel	70 mm	105 mm	50.0 %*

*Improvements based on iteration #1

Good	**>**	**125 mm**
Acceptable	**>**	**50 mm**
Marginal	**>**	**0 mm**
Poor	**<**	**0 mm**

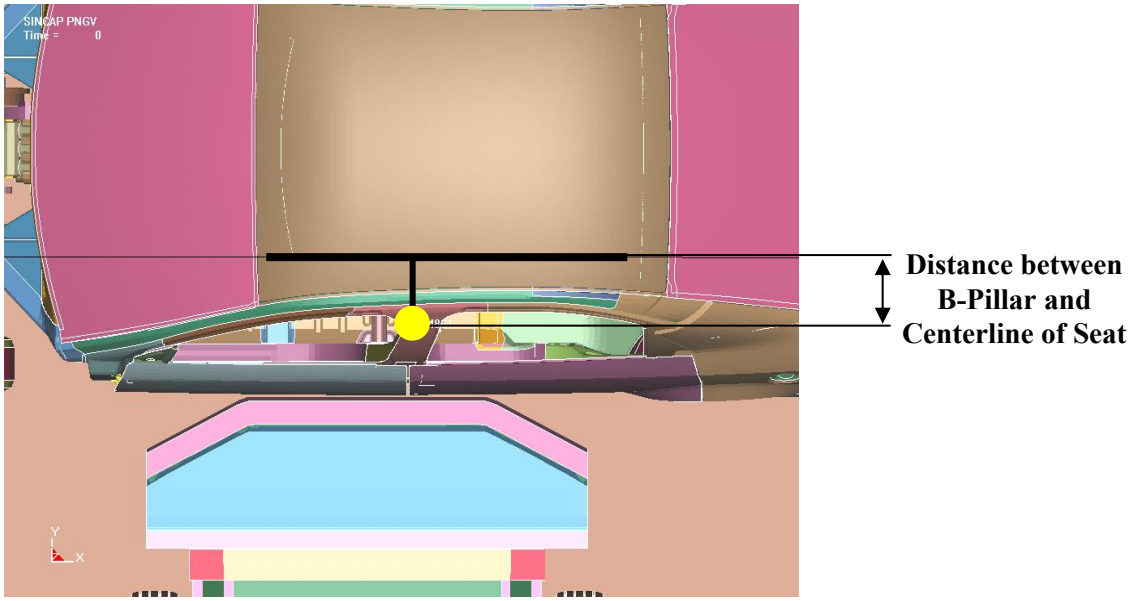


Figure 15. Side-Impact Measurement Definition.

W. Evaluations of the Effects of Manufacturing Processes and In-Service Temperature Variations on the Properties of TRIP Steels

Principal Investigator: Moe Khaleel
Pacific Northwest National Laboratory
(509) 375-2438; fax: (509) 375-6605; e-mail: moe.khaleel@pnl.gov

Technology Area Development Manager: Joseph A. Carpenter
(202) 586-1022; fax: (202) 586-1600; e-mail: joseph.carpenter@ee.doe.gov

Field Technical Manager: Philip S. Sklad
(865) 574-5069; fax: (865) 576-4963; e-mail: skladps@ornl.gov

---

Contractor: Pacific Northwest National Laboratory
Contract No.: DE-AC06-76RL01830

Objective

- Develop an understanding of the effects of typical automotive manufacturing processes, such as welding and forming, on the retained properties of advanced Transformation Induced Plasticity (TRIP) steels.
- Evaluate the effects of in-service temperature variations on the properties and energy absorption characteristics of TRIP steels.
- Compare the sensitivity of mechanical properties of a range of TRIP steel grades produced by various domestic and international steelmakers.

Approach

- Develop mechanical property versus in-service temperature relationships for the available grades of TRIP steels to determine their suitable vehicle applications and allowable thermal processing histories for manufacturing. A temperature range of -40°C to 93°C is considered.
- Determine the effects of welding and forming processes on the retained mechanical properties of different grades of TRIP steels. Tensile samples are prepared from formed and/or welded parts. The samples are tested at three different temperature levels to determine the effects of primary forming on the subsequent performance and properties of TRIP steel.

Recent Accomplishments

- Demonstrated stable transformation of austenite to martensite under a temperatures range of -40°C to 93°C for TRIP steel materials.
- Completed base metal characterization (mechanical properties and chemical composition) for all four TRIP steel populations.
- Performed experiments to quantify the effect of primary forming processes on the retained austenite volume fraction.
- Completed a preliminary study to determine the required weld sizes in resistance spot welds of TRIP 800 steels.
- Held a mid-year technical review meeting with project participants from Ford, GM and DCX.
- Presented project results at the annual project review of steel projects funded by DOE. The meeting was sponsored by DOE and the Auto Steel Partnership.

Future Direction

- Complete the quantification of retained austenite volume fraction by performing microstructure characterization on deformed TRIP steels.
- Follow Phase II proposed approach to model the kinetic transformation of retained austenite to martensite under different thermal-mechanical loading paths and to develop a micromechanical model to aid in the performance prediction of TRIP steels. Validate the models by performing welding and forming experiments.

Introduction

This project is a collaborative effort between DOE, Pacific Northwest National Laboratory (PNNL), and the USAMP of the U.S. Council for Automotive Research (USCAR). The work started in July 2004.

Because of the excellent strength and formability of "Transformation Induced Plasticity" (TRIP) steels, they offer the potential for reduced vehicle weight and improved vehicle crash performance. The enhanced ductility of TRIP steels is the result of a phase transformation, therefore, thermal cycling, forming, and welding could be expected to impact the final microstructure, and thus final material properties. Although the combination of strength and energy absorbing capabilities of TRIP steels make them attractive, their sensitivity to thermal processing and in-service temperature variations has not been sufficiently established. In order to introduce TRIP steels into critical areas of the body structure (such as crash energy management areas), the automotive OEM's must know what the retained properties of the material are after exposure to a range of manufacturing and in-service conditions.

This project examines key aspects of the manufacturing process that TRIP steels would be exposed to, and systematically evaluate how the forming and thermal histories affect final strength and ductility of the material. The project evaluates in-service temperature variations, such as under hood and hot/cold cyclic conditions, to determine whether these conditions influence final strength, ductility and energy absorption characteristics of several available TRIP steel grades. As part of the manufacturing thermal environment evaluations, stamping process thermal histories are included in the studies. As part of the in-service conditions, different loading rates are also included.

At the completion of the study, a thermal history/material property relationship is established over a full range of expected thermal histories and selected loading rates. Establishing these relationships will allow OEM designers to select TRIP steels for proper vehicle applications, and to specify manufacturing process conditions that yield reliable final material property levels.

Base Metal Mechanical Property Characterization under Different Temperatures

Since TRIP steels are relatively new for the automotive OEMs, there are many uncertainties on the feasibility of this class of steel in the domestic automotive industry and whether the desired phase transformation and enhanced ductility will occur under different manufacturing and operating temperatures.

Another issue with this class of steel is the supplier dependency. These steels are so called "performance-based steels", which means that each supplier could basically 'cook' their recipes differently to achieve the same strength and ductility requirements with different steel chemistry and thermal-mechanical processing. This puts a lot of strain on OEM manufacturing engineers. Because of the lack of fundamental understanding of these steels, each material batch would need extensive characterization and forming and welding trials. This would significantly prolong the material insertion process. Also, as shown previously by the U.S. Council for Automotive Research (USCAR) Joining Team, there is a lack of weld acceptance criterion on spot welds. Welding engineers have to go to great length and use some very exotic welding schedules to achieve the current weld acceptance criterion without knowing the actual benefit on weld performance.

In order to answer these feasibility questions, four TRIP steel materials from different suppliers were obtained and tested at -40°C, room temperature and

93°C. The four suppliers are from North America, Europe and Asia. Material B is a TRIP700 grade, and the remaining three are TRIP800. The chemistry compositions for the four steels are shown in Table 1. Materials A and C have very similar composition and are both CMnSi TRIP steels. Materials B and D are both CMnAl TRIP steels.

Table 1. Steel chemistry comparison (weight percent).

	C	*Mn*	*Si*	*P*	*Al*	*S*
Material A	0.191	1.83	1.17	0.009	0.032	0.003
Material C	0.18	1.75	1.62	0.014	0.03	0.002
Material D	0.20	2.21	0.07	0.013	1.41	0.002
Material B	0.22	1.64	0.046	0.012	1.51	0.001

Figure 1 shows the room temperature stress versus strain behaviors for three TRIP800 as-received base materials. Even though they are all TRIP800, the mechanical properties of these steels can vary quite significantly. Materials A and D have very similar and consistent behaviors, with total elongation around 27%. Material C has the similar initial yield level as materials A and D, however, it does not have the typical 'elongation at yield', the so-called EAY point. In addition, its transformation rate and therefore initial work hardening is higher, and it has relatively low ultimate elongation.

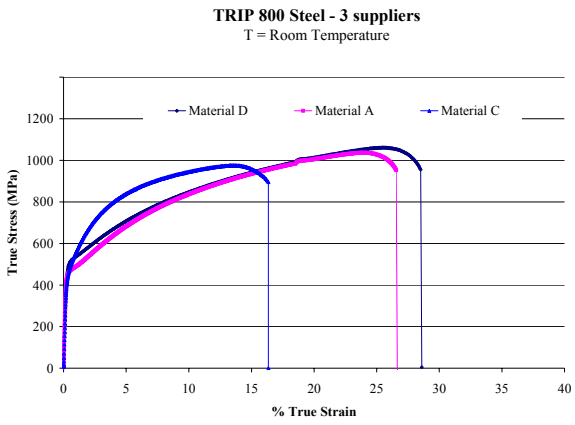


Figure 1. Base material room temperature stress versus strain curves.

Figures 2 and 3 show the stress versus strain curves for three TRIP800 materials tested at 93°C and -40°C, respectively. Slightly higher elongations were observed for all the three materials at 93°C with small degrees of strength reductions compared to their room temperature behaviors. At -40°C, materials A and D have much higher initial work hardening rate and lower total elongation compared to their room temperature behavior. Material C's stress versus strain behavior is less sensitive to test temperature which suggests that it has lower level of initial retained austenite in its microstructure.

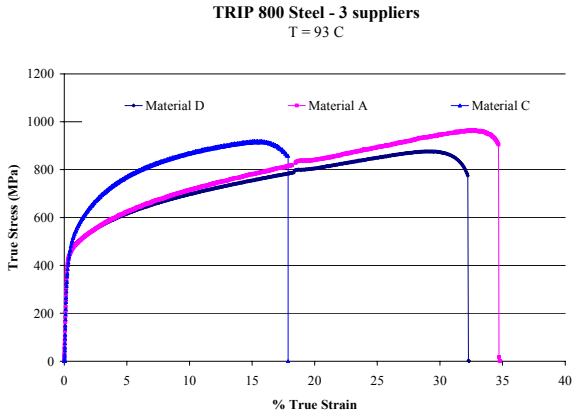


Figure 2. Base material stress versus strain curves under 93°C.

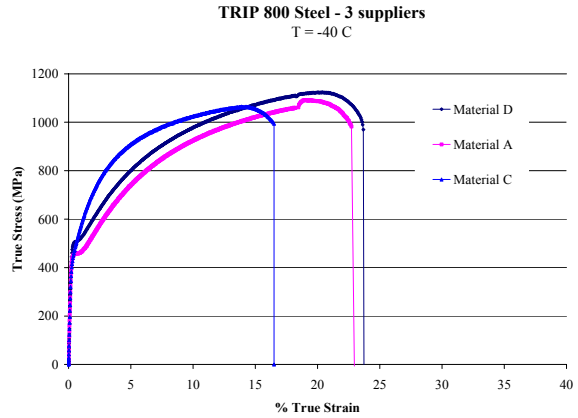


Figure 3. Base material stress versus strain curves under -40°C.

Figures 4 and 5compare the different stress versus strain behaviors for materials A and D at different test temperatures and the transformation kinetics of retained austenite (RA) as measured by electron back-scattered diffraction (EBSD). The as-received austenite volume fraction is about 8% for material A and 17% for material D.

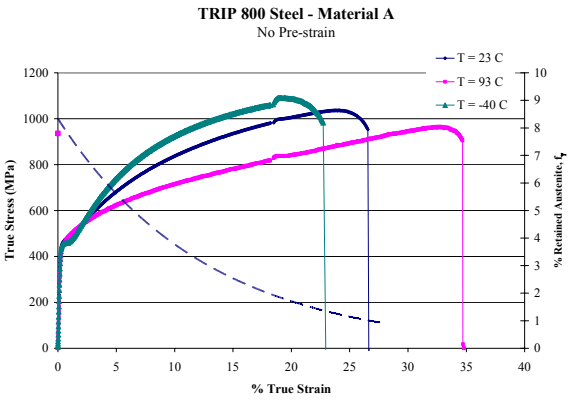


Figure 4. Stress vs. strain curves for material A under different test temperature and RA volume fraction evolution during deformation.

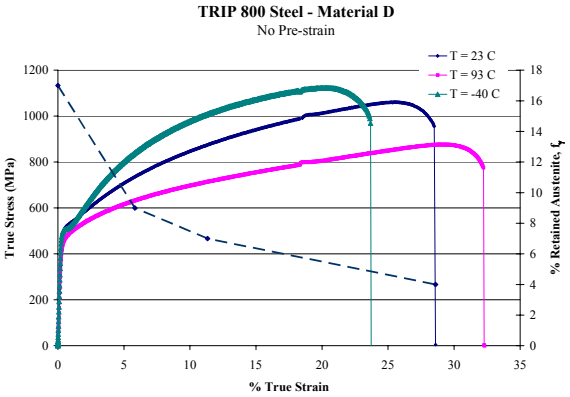


Figure 5. Stress vs. strain curves for material D under different test temperature and RA volume fraction evolution during deformation.

Figure 6 shows the typical EBSD measurement for material A at fracture. Its retained austenite volume fraction is only about 1%. The detailed transformation kinetics under different deformation temperature are still under investigation. The second phase of this project will focus on modeling of the transformation kinetics and provide automotive engineers with appropriate constitutive laws describing various grades of TRIP steels based on different chemistry compositions and associated thermal-mechanical processes.

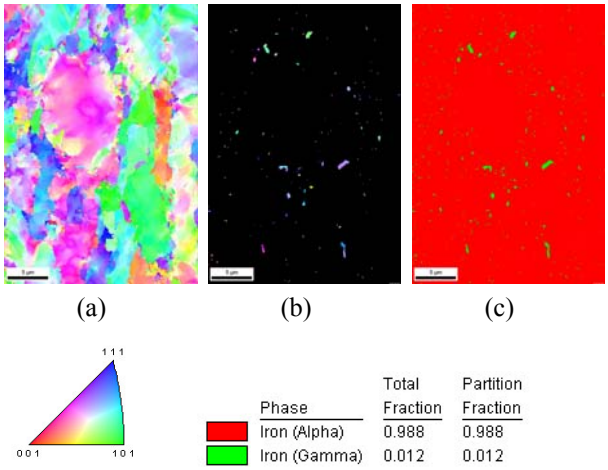


Figure 6. Typical EBSD measurements for Material A at fracture. (a) The total data orientation map; (b) the retained austenite orientation map; and (c) the retained austenite phase map.

Effects of Primary Forming and Different Loading Paths on Stress-Strain Behaviors

In this section, the effects of pre-straining or primary forming on subsequent stress versus strain characteristics are studied. Three pre-strain levels were considered: 5%, 10% and 15%. Pre-straining was carried out by stretching a large sheet of sheet material under plane-strain condition. Sub-sized ASTM E8 specimens were then prepared from the pre-stretched sheet and subjected to subsequent tensile testing at different temperatures (Figure 7).

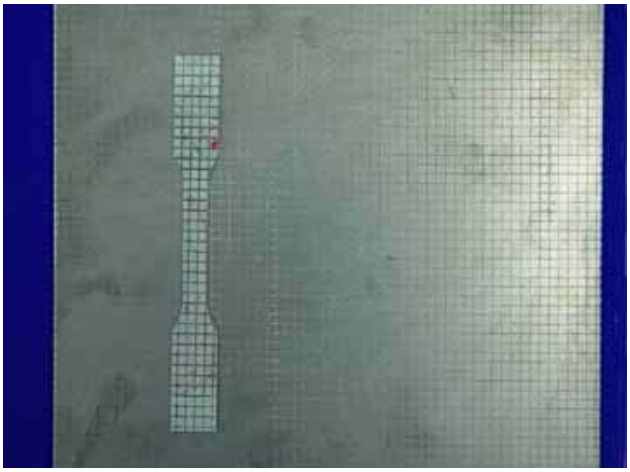


Figure 7. Pre-straining of tensile samples.

It should be noted that since the pre-straining is performed under plane-strain condition, more austenite should have transformed into martensite compared to the uniaxial samples at the equivalent strain levels. Pre-straining allows retained austenite to partially transform into martensite. Depending on the pre-strain levels and temperatures at which pre-straining is performed, materials of completely different microstructure and therefore different stress/strain characteristics will be generated. For example, Figure 8 illustrates the effects of room temperature pre-straining on material A. The pre-strained samples all have lower strengths in comparison to the strength of the non-pre-strained samples at the equivalent strain level. This indicates possible softening/aging response with tendency for strain localization. The final elongation values plus the corresponding levels of pre-strain are slightly higher than that of the non-pre-strained samples at room temperature testing. This is consistently observed for all the four materials studied.

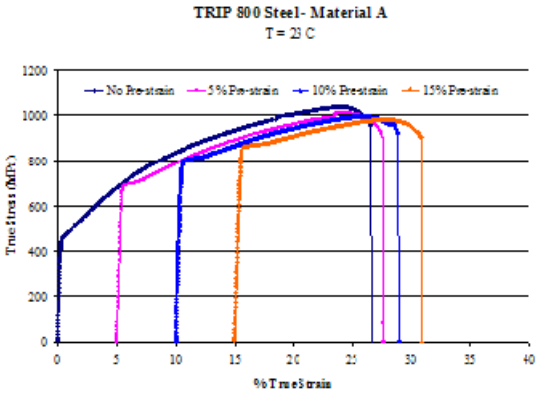


Figure 8. Effects of pre-straining on stress versus strain characteristics for Material A.

Figures 9 and 10 show the effects of room temperature pre-straining on the subsequent tensile behaviors at 93°C for material D and -40°C for material B. Consistent behaviors are observed for all other materials.

At 93°C, samples with room-temperature pre-strains have considerably higher initial yield levels than samples without pre-strains. This is because faster transformation occurs at room temperature than at 93°C (see Figures 4 and 5). Hence, the volume fraction of martensite in the pre-strained samples at any strain level is higher than those without pre-strains. More martensite in the pre-strained samples also renders the samples to have less total ductility at 93°C.

Completely different pre-straining effects are observed for samples tested at -40°C (see Figure 10 for material B). Since the samples are pre-strained at room temperature, less austenitic transformation occurs for the pre-strained samples than those tested at -40°C at the same strain levels. Therefore, the pre-strained samples have lower initial yield strength, more prominent Luders Band, and inhomogeneous shear deformation. The total ductility levels of the pre-strained samples are higher than those without pre-strain.

The effect of automotive paint bake was also examined for material B (see Figure 11). Minimal influence is observed on the samples' ultimate

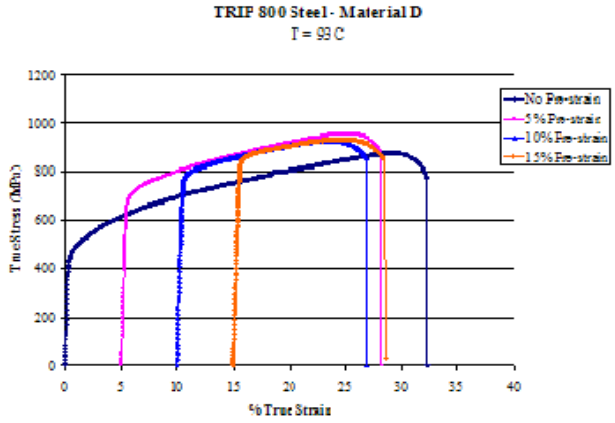


Figure 9. Effect of room temperature pre-straining on tensile properties under 93°C for Material D.

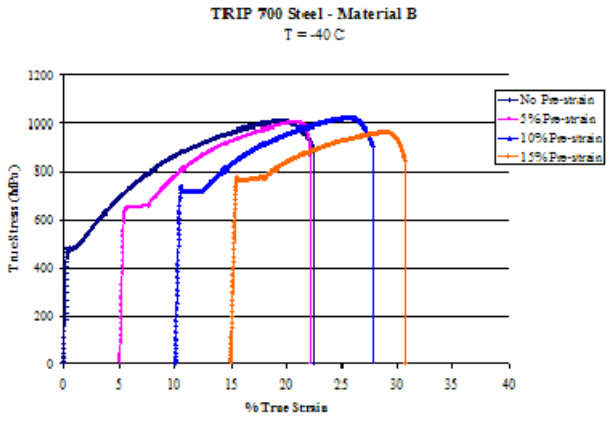


Figure 10. Effect of room temperature pre-straining on tensile properties under -40°C for material B.

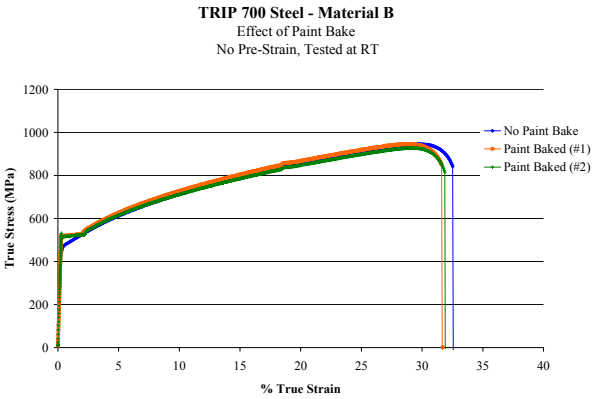


Figure 11. Effect of paint bake on base material properties.

tensile strength (UTS) and elongation. There is only a slight positive bake hardening effect on initial yield level for material B.

Resistance Spot Welds (RSW) of TRIP800- Effect of Fusion Zone Size

The effects of fusion zone size on failure modes, static strength and energy absorption of resistance spot welds of TRIP800 are also studied. The main failure modes for spot welds are nugget pullout and interfacial fracture. Partial interfacial fracture is also observed. Static weld strength tests using cross tension samples were performed on three joint populations with controlled fusion zone sizes. The resulted peak load and energy absorption levels associated with each failure mode were studied for all the weld populations using statistical data analysis tools.

Figures 12 and 13 show the effects of fusion zone size and weld failure mode on the peak load and total energy absorption of the RSW samples. The large slopes in Figures 12 and 13 for the TRIP800 small population indicate large scatters in peak load and energy absorption for the welds that failed by interfacial fracture. On the other hand, the much tighter slopes for the pullout welds in TRIP800 nominal and large populations indicate that welds failing by nugget pullout have well-controlled peak loads and energy absorption distributions with less performance variations. It is also interesting to note that even though the smallest weld in the TRIP800 large population failed by interfacial fracture mode, its peak load and energy absorption levels are comparable with the welds that failed by nugget pullout. In addition, the two interfacial fracture welds in the TRIP800 nominal population also indicate a large scatter in peak load and energy absorption. Note that the peak load and energy absorption levels for the TRIP800 nominal and large populations are about the same. This can be attributed to the significant weld indentation and expulsions for the TRIP800 large population.

The results in this study show that spot welds with fusion zone size of $4\sqrt{t}$ (t being the sheet thickness in mm) can not produce nugget pullout mode for the TRIP800 material examined. The critical fusion zone size for nugget pullout should be derived for individual materials based on different base metal properties as well as different heat affected zone (HAZ) and weld properties resulted from different welding parameters.

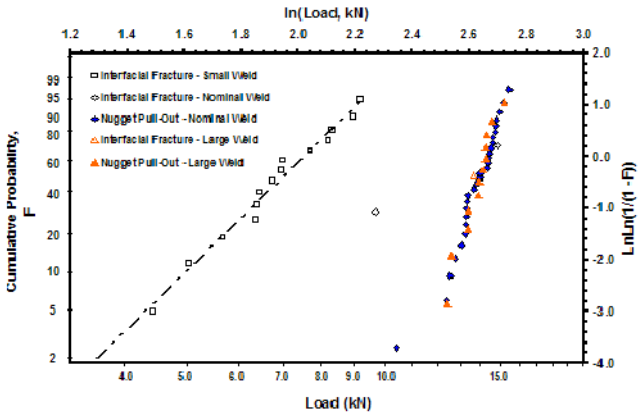


Figure 12. Peak load distributions for three weld populations in TRIP800.

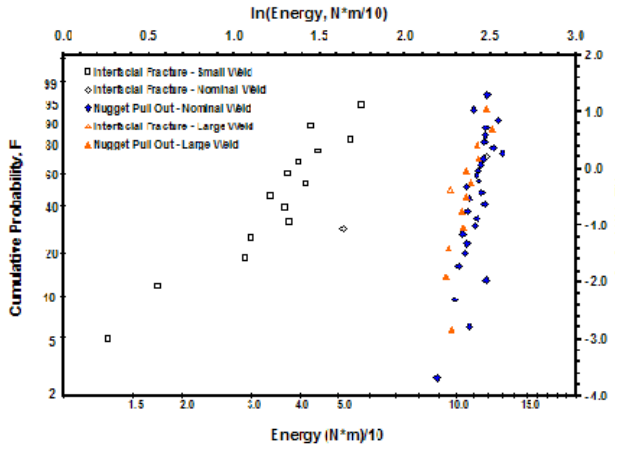


Figure 13. Distributions of energy absorption level for three weld populations in TRIP800.

Conclusions

- TRIP steels are performance-based steels; therefore, different suppliers have different chemistries and surface coatings on the same steel grade resulting in different base material properties.
- Four TRIP steels (TRIP 700 and three TRIP 800) manufactured by various domestic and international suppliers were evaluated.
- For the four TRIP steels tested, retained austenite transformation is stable under temperature range tested: -40°C to 93°C.
- Different pre-straining levels (i.e., primary forming processes) and test temperatures influence the yield strength and total elongation.
- Automotive paint bake has very little effect on the stress versus strain behaviors of TRIP steels.
- The critical fusion zone size for nugget pullout for TRIP800 should be derived for individual materials based on different base metal properties as well as different heat affected zone (HAZ) and weld properties resulted from different welding parameters.

Presentations

- Sun X, EV Stephens, and MA Khaleel. 2005. *"Effects of Manufacturing Processes and In-Service Temperature Variations on the Properties of TRIP steels - Concept Feasibility Study."* Presented by Moe Khaleel, Xin Sun and Elizabeth Stephens (Invited Speaker) at A/SP annual program review with DOE, Southfield, MI on September 21, 2005. PNNL-SA-46610.
- Sun X, EV Stephens, and MA Khaleel. 2005. *"Effects of Manufacturing Processes and In-Service Temperature Variations on the Properties of TRIP steels - Concept Feasibility Study."* Presented by Xin Sun and Elizabeth Stephens at Semi-Annual Program Review, Southfield, MI on March 10, 2005. PNNL-SA-44524.

3. LOW-COST CARBON FIBER

A. Low-Cost Carbon Fibers from Renewable Resources

Project Contact: F. S. Baker, W. L. Griffith, A. L. Compere
Oak Ridge National Laboratory
Post Office Box 2008
Oak Ridge, TN 37831-6087
(865) 241-1127: fax: (865) 576-8424; e-mail: bakerfs@ornl.gov

Technology Area Development Manager: Joseph A. Carpenter
(202) 586-1022; fax: (202) 586-1600; e-mail: joseph.carpenter@ee.doe.gov
Field Technical Manager: Philip S. Sklad
(865) 574-5069; fax: (865) 576-4963; e-mail: skladps@ornl.gov

---

Contractor: Oak Ridge National Laboratory
Contract No.: DE-AC05-00OR22725

Objective

- Carbon-fiber resin composites could greatly decrease the weight of passenger vehicles resulting in substantial increases in fuel efficiency. However, carbon fiber is currently too expensive for large-scale use in production vehicles. This project will demonstrate methods for the use of new precursor materials, largely based on renewable resources, which decrease cost and increase availability of carbon fiber that meets the performance and price requirements of the automotive market. The project goal is to identify at least one precursor formulation, comprising both renewable and recycled materials, which could be used to produce industrial-grade carbon fiber at a cost in the range of $3-5 per pound. In addition to precursor, cost savings will also be achieved through improved processing methods and more efficient energy utilization.

Approach

- Provide the data needed to scale up process steps to industrial levels and to consistently achieve desired fiber properties on an industrial scale.
- Develop the technical knowledge base required to support production of lignin-based, carbon-fiber precursor feedstock on an industrial scale, comprising:
  - Lignin isolation to obtain the best molecular weight, low-volatile, and low-salt content material.
  - Spinning technology, including production die structure, plasticizers, and nucleating agents.
  - Oiling and sizing technology.
  - Selection of appropriate polyesters.
  - Plasma treatment and sizing technology to make the fiber compatible with selected resin systems.
  - Properties and economics of carbon-fiber and composite systems.
- Scale and transfer the technology for the production of carbon-fiber precursors from lignin-blend feedstock:
  - Evaluate melt-extrusion properties of lignin-based feedstock at increasing scale using near-industrial equipment that can be readily obtained by fiber manufacturers.
  - Evaluate production of carbon fiber using research and pilot-scale production lines.
  - Evaluate mechanical and composite compatibility properties of graphitized lignin-based fibers.
  - Collaborate with partners to evaluate, define and develop process metrics, economics and standards.
- Transfer technology and intellectual property for the production of lignin-based carbon fibers to industry.

Accomplishments

- Proof-of-concept demonstration of the melt extrusion of 28-filament tow of lignin-based fibers was made. This validated selected compositions, processing methods, and testing technologies. It also provided a basis for understanding the process improvements required for large-scale manufacture of lignin-based, carbon-fiber precursor.
- Significant amounts of 28-filament tow were successfully spun at the University of Tennessee at Knoxville (UTK) using a two-step process. No sticking problems were apparent and fiber diameter was reduced from ~ 45 microns to ~15 microns with an apparent improvement in mechanical properties.
- Preliminary data indicate that carbon-fiber yields of 50% are feasible, consistent with lignin carbon content.
- Preliminary evaluation of a plasma surface treatment (plus silanation) of lignin-based, carbon fibers indicated a significant improvement in fiber-resin bonding compared to conventional carbon fibers.
- Small epoxy-resin composites made using carbon fibers produced from 28-filament lignin-based fiber tow, exhibited target composite mechanical properties.
- Identified sources of volatiles within lignin and developed purification methods which selectively remove residual carbohydrates, one source of volatiles, in a single process step.
- Developed potential process-control technologies for the production of low salt content (low-ash) lignin.
- Developed preliminary specification for lignin precursor and demonstrated bench-scale methods to produce lignin meeting the specification.

Future Direction

- Methods for production of industrial-quality carbon fibers from lignin feedstocks will be developed. Work will include:
  - Optimization of lignin isolation conditions to achieve the target specifications with respect to contaminant content (salts, carbohydrates and particulates) and provide the best molecular weight.
  - Identification of conditioning and spinning processes which remove volatiles both prior to and during precursor fiber production.
  - Selection of plasticizers and nucleating agents for melt-spinning of lignin-based precursor materials.
  - Design of spinning dies to provide the best internal structure of the fiber.
  - Development of techniques for spooling and oiling lignin-based precursor fibers at each step.
  - Identification of methods for surface treating and sizing the surface of carbon fibers to improve compatibility with proposed resin systems. This is particularly critical for chopped- fiber composites.
- Collaborate with industrial, government and academic partners to:
  - Address raw fiber production issues (lignin, preconsumer recycled polyesters, plasticizers, spinning and winding technologies, process scale-up).
  - Demonstrate carbon-fiber production from lignin-based, multifilament tow using a pilot-scale industrial process line.
- Transfer the low-cost carbon-fiber production technology to industry.

Introduction

The use of carbon-fiber resin composites would greatly reduce the weight of passenger vehicles, resulting in substantial increases in fuel efficiency. However, carbon fiber is presently too expensive and too limited in production capacity to support large-scale use in production vehicles. To address these impediments to the commercial use of carbon-fiber in the automotive industry, this project is directed to the development of methods for the production of carbon-fiber feedstock from high-volume, low-cost materials based on renewable resources and recycled materials. The goal is the development of technologies which will reduce precursor and processing costs, and which could be implemented to produce low-cost carbon fiber on a scale sufficient to support its large-scale use in passenger vehicles. Use of renewable and recycled materials also decreases sensitivity of carbon-fiber

cost to changes in petroleum production and energy costs.

Proof-of-concept production of single fibers from a variety of natural, renewable and recycled materials available in high volume was demonstrated. Single-fiber, melt-spun from blends of Kraft hardwood lignin (an inexpensive, high-volume, wood-pulping byproduct) and small amounts of routinely recycled polyolefins and polyesters, could be processed using conventional stabilization (oxidizing atmosphere), carbonization, and graphitization (inert atmosphere) furnace technologies to yield carbon fibers. Carbon-fiber mechanical properties improved when the fibers were stretched during thermal treatment. Graphite content, as measured by x-ray diffraction, increased with increasing temperature of treatment. Carbon-fiber yield from the lignin-based feedstocks was ~ 50%. Physically, the fibers were dense, smooth-surfaced, and uniformly round.

Larger quantities of a lignin-polyester (recycled) feedstock were melt-spun as a multifilament tow (4-28 fibers) using a 27-mm-diameter twin-screw Leistritz extruder at the University of Tennessee at Knoxville (UTK) to meet a September, 2003 composite preparation and testing milestone. This Leistritz machine is the smallest member of a line of commercial melt extruders, and can be used to obtain data to design larger-scale, melt-spinning equipment. Meeting the milestone showed that: 1) lignin-polyester blend can be melt-extruded as a small tow using near-commercial-scale melt-spinning equipment; 2) resin-fiber composites made using the graphitized lignin-polyester-based carbon fibers exhibited normal fracture patterns; and 3) although very smooth surfaced, lignin-polyester-based carbon fibers can be plasma treated and silanated to provide good fiber/resin adhesion.

Analysis of the samples obtained indicated that bubbles and inclusions were the major flaws in the lignin-polyester-based carbon fibers. Flaws are known to decrease the strength of carbon fibers and are typically the initiation point for fiber breakage. Inclusions were typically natural particulates associated with wood and the pulping process, namely, sand, cellulose, and water. Bubbles were caused by water trapped in carbohydrates co-precipitated with lignin during conventional processing of lignin for commercial products. Methods were developed to mitigate these problems. Additionally, methods for controlling salt content in the fibers and for pre-filtering black liquor prior to lignin isolation were developed.

Project Deliverables

Goal: By the end of this multi-year program, production of one or more environmentally-friendly, economically-feasible, carbon-fiber precursors will be demonstrated and transfer of production technologies and related intellectual property to industry initiated.

In FY 2004, major milestones, including the initial tests of the effect of lignin molecular weight on fiber properties were completed on time.

FY 2005, milestones included development of a lignin feedstock specification that will facilitate industrial production of carbon fibers meeting program goals (5/2005) and establishment of basic rheology for extruding and winding lignin-fiber bundles with improved handling characteristics (9/2005).

FY 2006 milestones comprise production of significantly larger quantities of lignin-based carbon fiber, with near-target mechanical properties, needed to demonstrate use in automotive composites. Also, demonstration by a pulping company of the ability to produce, in a cost-effective manner, purified lignin material meeting the specifications for ash, particulate, and volatile contents.

Planned Approach

Production of industrial-grade carbon fibers from a radically new type of feedstock requires the simultaneous development of methods for feedstock recovery, characterization, preparation, blending, spinning, handling, and spooling in addition to the thermal processing, stretching/orientation, oiling, and sizing technologies required for conventional fibers. These are combined with evaluations of fiber quality and suitability for use in composites.

First priority was placed on developing cost-effective, environmentally-friendly, precursor-fiber preparation and thermal processing conditions. Carbonization of lignins, which typically do not contain aromatic nitrogen, does not result in the

cyanide emissions typical in the processing of acrylic fibers. Lignins can also be melt-spun or dry-spun, which eliminates the petrochemical solvents used in producing raw acrylic fiber.

Use of modern thermal processing techniques, such as hot-stretching and controlled-atmosphere treatment, will be evaluated to improve the properties and yield of carbon fiber from the lignin feedstock.

Industrial partners have worked with project staff on the selection of polymers to blend with lignin, strategies for production of cleaner (purer) lignin, and spinning of fiber. In the later stages of the project, quantities of lignin-based, carbon-fiber tow sufficient for composite fabrication will be produced using a pilot-scale fiber production line.

Transfer of project technology, including intellectual property, is planned.

Lignin Feedstock Quality

Lignins are inexpensive, high-volume forest- and biomass- industry byproducts. A number of different commercial processes produce lignin streams from which carbon fibers could be manufactured, including: 1) alkaline pulping processes (Kraft and soda); 2) ethanol production from wood and other biomass; and 3) organosolv pulping. The ORNL research work has been focused on alkaline pulping liquors because these represent about 80% of the total domestic pulping industry. In both processes, liquid streams containing lignin are concentrated and burned to provide both process energy and pulping chemicals recycle.

Historically, only two Kraft mills worldwide have isolated dry lignin for commercial sale as chemicals, but all Kraft pulp mills could, in principle, isolate lignin as a potential precursor material for carbon-fiber production. This is accomplished by acidification of black liquor to form a loose gel which is recovered as a precipitate, washed, dried, and marketed for use in many high volume applications, including dyestuff dispersants, asphalt emulsifiers, concrete additives, lead-acid battery plate extenders, soil micronutrients, and metallurgical mold releases. These applications are, however, relatively insensitive to the presence of contaminants such as particulates, cellulose fibers, water, volatiles, and inorganic pulping chemicals entrained during lignin precipitation.

Production of a cost-effective, industrially-feasible, lignin-based, carbon-fiber feedstock will require the development of methods to effectively remove salts, particulates, and volatiles from the crude lignin isolated from conventional pulping operations. The methods developed at ORNL, which typically involve purification of the liquid streams from which lignin is recovered, are discussed below. Using these methods, it was possible to produce very high-quality lignins from alkaline pulping liquors.

It is also possible to extract low-salt-content, low-volatile-content lignins using novel pulping technologies that are emerging on a commercial scale. Novel biomass-derived lignins produced by project partners were evaluated for potential use as carbon-fiber precursor materials.

Evaluation of Purified Lignins from Conventional Alkaline Pulping

Alkaline pulping technologies, which include Kraft pulping ($NaOH + Na_2S$) and soda pulping (NaOH), dominate domestic production of pulp for use in paper products. In alkaline pulping, wood chips are contacted with the alkaline solution and cooked at high temperature and pressure. At the end of the cooking cycle, a lignin-rich stream, “black liquor,” is separated from the wood pulp. Black liquor is concentrated by evaporation and burned to recover the pulping chemicals (>99% recovery) and to provide energy for the pulping and paper production operations (some mills include power co-generation, providing a net energy gain).

Because the process uses wood chips, alkaline pulping is a year-round industry, with the potential of providing a large volume of lignin for use as carbon-fiber feedstock. To put this into perspective, approximately 10% of the lignin passing through alkaline pulping operations, could, if used for carbon-fiber production, supply enough carbon fiber to replace approximately half of the ferrous metals used in passenger transport vehicles.

It is important to keep in mind, however, that pulp and paper mills operate under demanding economic and environmental standards. For example, mills must meet Environmental Protection Agency Cluster Rule emission and effluent standards. To apply the technology developed in this project to the production of enough purified lignin to support widespread automotive use of carbon fiber, the lignin isolation/purification process technology must be tailored to mill needs.

Commercial lignin products isolated from black liquor typically contain a variety of solid materials (sand, diatoms, cellulose fibers) and chemicals (salts, carbohydrates, wood extractives). In order for this lignin to be used as a feedstock for production of carbon fibers, which are typically <10 micron in diameter, solids >1 micron in diameter must be removed. This can be accomplished by micron-scale filtration of the black liquor prior to lignin isolation. Additionally, carbohydrates, which sorb water, can be precipitated and removed by filtration prior to precipitation of the lignin itself. Using commercial filter media, selectively precipitated and coagulated carbohydrates can be removed from alkaline pulping liquors in a single step.

Thermogravimetric analysis (TGA) curves for desalted, carbohydrate-stripped Kraft and low-sulfur soda hardwood lignins are shown in Figure 1, revealing that these lignins exhibited low volatiles content (<5% weight loss at 250°C). Furthermore, as shown by the solution nuclear magnetic resonance (nmr) spectroscopy data in Figure 2, the carbohydrate-stripped Kraft and soda hardwood lignins contained only very small amounts of residual carbohydrate material.

Biomass Lignins from Ethanol Production

One of the emerging leading processes for production of ethanol from biomass involves: 1) pretreating the biomass by alkaline or organosolv pulping; 2) hydrolyzing the cellulose fibers to sugars; and 3) fermenting the sugars to ethanol. The mills are being deployed to meet Kyoto-treaty requirements for production of fuels and chemicals

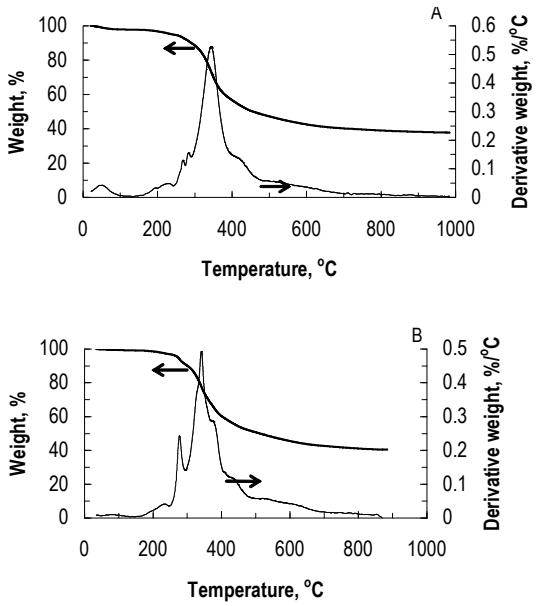


Figure 1. Thermogravimetric analyses of desalted, carbohydrate-stripped, soda-anthraquinone (A) and Kraft (B) hardwood lignins.

from biomass. Operators of these mills are interested in developing markets for the significant quantities of lignin byproduct which they currently produce. Although this process is not being tested in domestic bioethanol plants, increasingly high petroleum prices could make these biomass ethanol processes attractive in the U.S. Woody biomass wastes have good year-round availability. A fraction of the ethanol produced from the cellulose pulp is used in the pulping process, and the overall process energy is supplied by burning part of the lignin precipitated during ethanol recovery and recycle.

Granit, a project partner, started pulping-based ethanol production mills this year, and is already able to supply about 10,000 tons/year of lignin, i.e., enough precursor material to support the equivalent of 20% of the worldwide production capacity of carbon fiber. Similarly, Lignol Innovations has started construction of an ethanol-organosolv pulping test facility in which conversion of wood residues, such as sawdust and insect-damaged trees, to alcohol is being evaluated. Deployment of this biomass technology is accelerating because the ethanol fuel produced from the process plays a key part in Kyoto-treaty compliance strategies for many countries. In the U.S., it would provide an attractive opportunity for reuse of smaller or older non-profitable pulp mills.

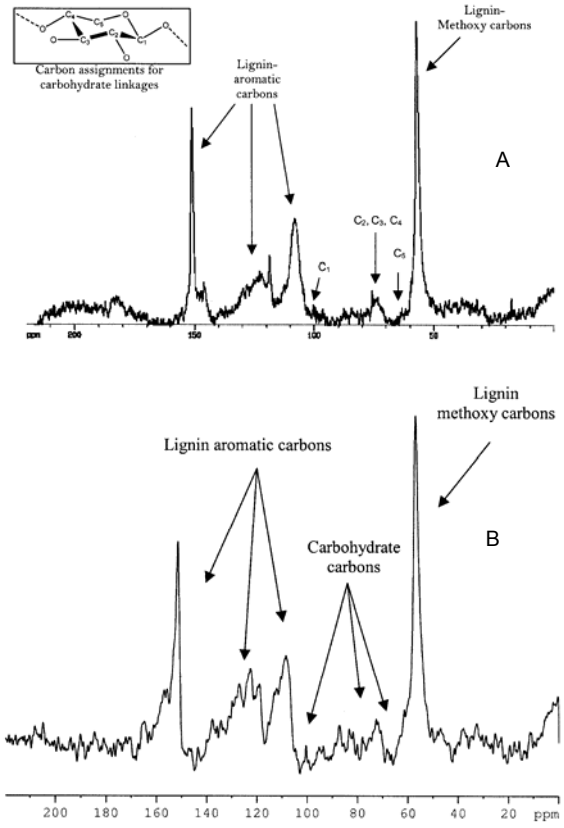


Figure 2. Nuclear magnetic resonance spectra of desalted, carbohydrate- stripped, Kraft (A) and soda-anthraquinone (B) lignins.

Because the lignins in biomass feedstocks, such as grass or flax, are different in composition and chain length from those typical of wood-derived lignins, their basic properties have been evaluated in this project.

In Figure 3, TGA curves are shown for three lignins derived from biomass ethanol production: Sarkanda grass ("Ecobind 100SA140"); flax ("Ecobind100FA"); and a Lignol Innovations experimental lignin produced from softwood sawdust. From the TGA curves and data in Table I, it is apparent that the Lignol softwood lignin showed potential as carbon-fiber feedstock, at least on the basis of its low volatile content (3%) and low ash content (0.2%), which almost met the target specification (0.1%). The grass and flax lignins exhibited higher volatile contents of 8 and 10%, respectively, about twice the target specification of <5%. Both also exhibited lower residual carbon contents (< 30% at 1000°C) compared to

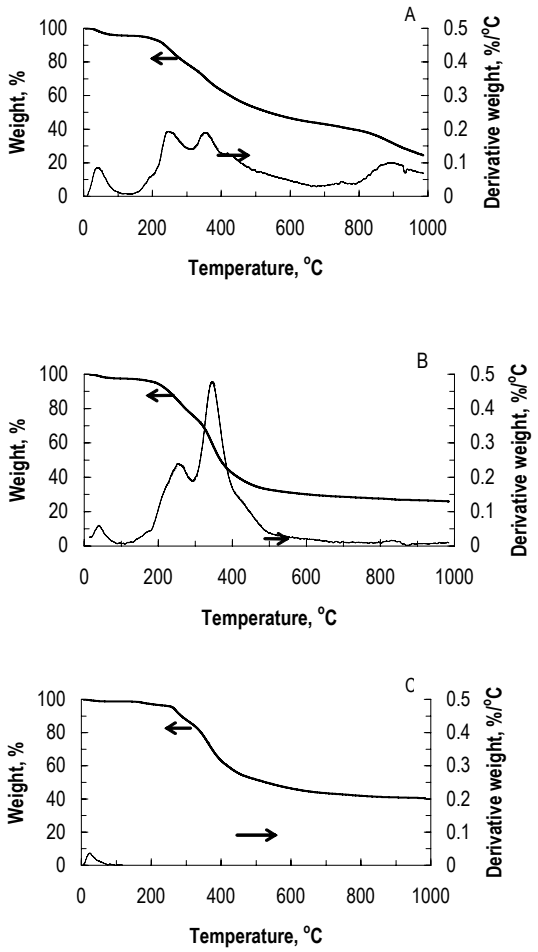


Figure 3. Thermogravimetric analyses for Sarkanda grass (A), flax (B), and Lignol Innovations (C) lignins (derived from biomass ethanol production).

Table 1. Ash and volatiles in biomass lignins

Lignin	Ash, %	Volatiles, %
Lignol Innovations	0.2	3
Flax	0.6	10
Sarkanda grass	3	8

commercial Kraft hardwood lignin (40%). In keeping with commercial, alkaline-pulped, softwood-lignin products, the Lignol softwood lignin exhibited a carbon content of ~40%. Furthermore, as shown by the nmr spectroscopy data in Figure 4, the Lignol experimental softwood lignin contained very low levels of residual carbohydrate.

A major difficulty associated with biomass lignins would be variability in lignin properties due to changes in either the type or condition of biomass feedstock to the pulp mill. Additionally, some

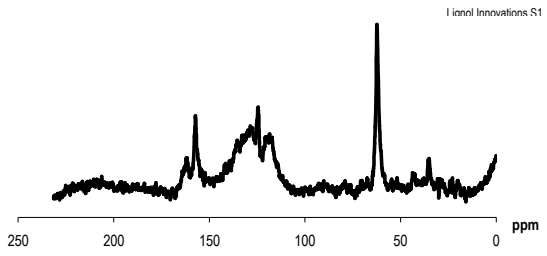


Figure 4. Nuclear magnetic resonance spectra of Lignol Innovations ethanol organosolv lignin.

biomass feedstocks, such as rice straw, contain significant concentrations of insoluble inorganic materials, such as silicates.

The ash content of the Sarkanda grass lignin was 3%, comparable to that of commercial Kraft hardwood-lignin products. Almost all of this ash material could be removed as base-insoluble, filterable particulates. The flax lignin exhibited a lower ash content of 0.6% and, as already noted, the Lignol experimental softwood lignin exhibited a notably low ash content of 0.2%, which would facilitate its purification for use as a carbon-fiber feedstock. Microscopic examination revealed that the particulates in all three of the biomass-ethanol lignins predominantly comprised cellulosic residues from the pulped biomass.

Biomass-lignin production technology is, for the most part, being developed outside of the US as part of the effort to meet Kyoto-treaty compliance goals. However, the low cost and potentially high volume of ethanol production from pulped wood wastes and annual biomass could drive the use of these two technologies into the U.S. market. Additionally, both the Granit and Lignol processes could be adopted by Mexican or Canadian companies with near-border plants. Furthermore, the technologies could be retrofitted into older or smaller pulp mills, which would significantly increase the availability of domestic commodity lignin.

Solvent Extraction Lignins

Although fractions of commercial lignins are soluble in some solvents, carbohydrates and salts are relatively insoluble in both alcohols and ketones. Therefore, MeadWestvaco, a project partner, felt that it should be possible to produce low-salt, low-carbohydrate lignins by solvent extraction of commercial dry lignin. Several such lignin samples were produced for evaluation.

The ash and volatiles contents of these materials are shown in Table 2. As shown by the TGA data in Figure 5, there was considerable variation in the thermogravimetric behavior of the different solvent-extracted lignins evaluated. Although most of the samples showed relatively high volatile contents at temperatures well below probable melt-spinning temperatures, the LPX-83777-OID sample exhibited low volatile content (4% at 250ºC) and a high carbon content (40% residue at 1000ºC). Nuclear magnetic resonance spectra of the samples also showed considerable variation in carbohydrate content, with the LPX-8377-OIA sample exhibiting particularly low carbohydrate content.

Ash and particulate levels in the solvent-extracted samples were also variable. As expected for this lignin source, most of the samples had ash levels around or below 1%. However, the LPX-377-61-M sample exhibited a high ash content of 2.6%, but nevertheless still comparable to that of commercial lignin products.

With optimization, solvent-extracted lignins could potentially be useful carbon-fiber feedstocks or feedstock constituents.

Table 2. Solvent extracted lignin ash and volatiles content

Lignin	Ash, %	Volatiles, %
LPX-8377-OID	0.3	11.2
LPX-8377-61-M	2.6	14.5
LPX-8377-OIA	0.2	8.5
LPX-8393-48	0.6	9.2
LPX-8393-49	0.2	8.6
LPX-8393-50	0.1	2.5
LPX-8393-49	0.1	4.6

Lignin Specification

Industrial partners requested that ORNL develop an initial specification for lignin to be used as a precursor material for the production of carbon fibers. The preliminary specifications established are based on data for commercial pitch-based carbon fiber and on the requirements for the twin-screw extrusion of textile fibers, such as polyesters, at 250°C. The lignin specifications comprise:
< 1000 ppm ash, < 500 ppm non-melting

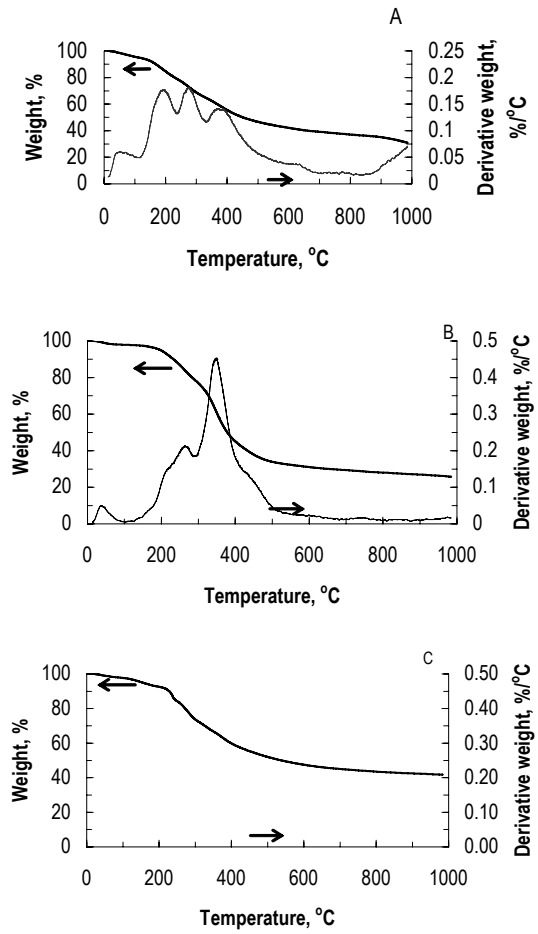


Figure 5. Thermogravimetric analyses of solvent extraction lignins LPX-8377-61-M (A), LPX-8393-48 (B), and LPX-8377-OID (C).

particulates (e.g., cellulosic fibers), <5% volatiles by 250°C, and the removal of all particulates >1 micron in size.

The volatiles and non-melting particulate-content requirements were developed to match the standard requirements for high-temperature textile melt-spinning. The specifications for ash and particulates contents were set on the basis of early pitch fiber data, with the objective of minimizing inclusions and defects which weaken carbon fibers. These specifications have been met with lignins purified at ORNL using a bench-scale process.

With increasing experience and better understanding of the factors that influence lignin melt-spinning, the specifications will be extended to include relevant physical and chemical properties of lignins deemed suitable for carbon fiber feedstocks.

Future Directions

Production of lignin-based multifilament tow (28 filaments) and successful use of this material in small resin-fiber composites was demonstrated in FY 2003. The project was re-proposed and extended to permit evaluation of methods for producing high-quality, lignin-based feedstocks for low-cost production of automotive carbon-fiber resin composites.

Having established proof-of-concept, the project staff is systematically addressing the technical issues required to produce industrial-grade, lignin-based carbon fiber at prices and properties meeting automotive need. Because domestic lignins evaluated by this process are derived from alkaline (Kraft and soda) pulping, a major concern has been the need to develop an understanding of the levels and types of contaminants in the lignins which are detrimental to multifilament spinning. This work has been paired with efforts to develop cost-effective, scaleable process technology for selective removal of carbohydrates, non-melting particulates, and ash from lignin.

Using project-developed technologies, it has been possible to consistently produce bench-scale quantities of purified lignin material which meets the preliminary specifications. The specifications will be upgraded and broadened as requirements for a satisfactory precursor material are better defined, e.g., to include physical and chemical properties relevant to blending and melt-spinning.

The techniques for precipitation and purification of lignin are expected to evolve and improve. The goal is an industrially-practicable method which permits one-step removal of better than 90% of the hemicellulose carbohydrate in black liquor prior to lignin precipitation. The carbohydrate material isolated by this means could potentially be reused in paper manufacture if only small amounts of flocculants are used and if the carbohydrate structure is preserved. Incorporating the recovered carbohydrate material (hemicellulose) into paper would enhance the mechanical properties of the paper, as well as offset lignin cost. Alternatively, the hemicellulose carbohydrate could be returned to the black-liquor recovery boiler for energy and chemical recycle.

Efforts in FY 2006 will be focused on the development and demonstration of a commercially viable process for the production of lignin-based precursor material meeting the specifications established for carbon-fiber production. Working in partnership with Pacific Northwest National Laboratory (PNNL) and MeadWestvaco (MWV), a combinatorial chemistry approach will be used to screen a large permutation of process conditions to establish the most cost-effective means of producing purified, melt-spinnable lignin on a commercial scale. Economic analyses will be an integral part of the effort to ensure that the lignin could be produced at a cost consistent with the target for finished carbon fiber. In addition to establishing commercially-viable lignin processing technology, the deliverable from the proposed PNNL/ORNL/ MWV program of work is several hundred pounds of on-spec lignin precursor material that can be used to produce carbon-fiber tow for composite testing (in mid-FY 2007).

Studies on biomass-derived lignins will continue, but with reduced emphasis. Biomass utilization is an emerging business, and it is still too early to gauge its potential for commercial success. Nevertheless, if the Granit and Lignol processes for ethanol production from biomass materials are commercially successful, worldwide production of dried biomass lignin could increase by more than 50,000 tons per year, each year. On the downside, shipping costs could be too high for its cost-effective use as a carbon-fiber precursor material. In this context, the major question is whether and to what extent pulp-based biomass ethanol production will become commercially feasible in the U.S., as well as near-border areas of Mexico and Canada.

Die designs for spinning of lignin-based fibers will be further evaluated. Initial test data indicated that the high-shear dies similar to those used for spinning pitch-based feedstocks create a more uniform internal structure in the raw fiber. Spinning parameters, including rheology of the blend, will be optimized for multifilament production.

Production techniques that provide high-quality, handleable, spoolable, raw lignin-based fiber are required, and will be evaluated. The techniques include selection and evaluation of plasticizers and nucleating agents, raw fiber coatings and oils, and spooling.

Following carbonization/graphitization of the lignin-based fiber, the carbon fiber must be surface treated and sized to increase its compatibility with a given resin system. Fiber-resin compatibility is particularly critical in automotive applications, because the current program plan calls for use of chopped, rather than woven or wound fiber.

As the project work progresses and challenges are resolved, project partners expect to become increasingly involved in scaling up the processes with respect to lignin production and purification, and to melt-spinning and thermal processing of the fibers.

Partnerships

A number of partners have been instrumental in helping to develop the lignin-based, carbon-fiber technology. During the early part of the project, North Carolina State University spun a variety of lignin-polymer blends into single fibers, which were used for the initial feasibility evaluations. Similarly, the University of Tennessee (Knoxville) produced significant quantities of multifilament tow for project use.

The participation of several wood-pulping and biomass companies has greatly improved project access to a variety of different lignin materials. Since its inception, the project has benefited from the participation of MeadWestvaco Corporation, which provided hundreds of pounds of softwood and hardwood lignin products for project use, including a wide variety of research lignins. MeadWestvaco is currently the only producer of lignin products derived from alkaline pulping (specifically the Kraft process).

Later, in FY 2004, the project attracted interest and participation from three other pulp and paper companies: Weyerhaeuser, Granit, S.A.; and Lignol Innovations. The participation of these companies has broadened the variety of lignins available to the project, including biomass-derived lignins which exhibit lower volatile contents.

Conclusions

The project was re-proposed in FY 2003 and, in FY 2004, re-tasked to focus on larger-scale production of carbon-fiber feedstock. Relationships with MeadWestvaco Corporation, Eastman Chemical Company, and Granit, S.A., were formalized. A third paper company, Weyerhaeuser, informally furnished samples of black liquors from which lignins were isolated for melt-spinning evaluation.

Initial evaluations of the melt-spinning of small lignin fiber tow demonstrated the feasibility of producing precursor fibers by melt-spinning and that carbon fibers could be produced from the lignin fiber, successfully surface treated, and used to prepare small resin composites. However, it was clear from an examination of the carbon fibers that the contaminants inherently present in commercial Kraft lignin products had to be reduced. This was necessary to both improve melt- spinnability of the lignin precursor fiber and to decrease the subsequent contaminant levels (particulates and volatile materials) in the carbon fibers themselves, which caused small defects that adversely impacted mechanical properties.

During this period, purification technologies were demonstrated on a lab-scale. Carbohydrate, in the form of cellulosic polysaccharides coprecipitated with lignin, was found to contribute significantly to evolution of gas during lignin fiber spinning and also to production of char if held for long periods above 200°C. Carbohydrate-stripped lignins showed significantly reduced volatile evolution between 150 and 250°C.

Initial technical evaluations indicate that the carbohydrates recovered prior to lignin separation and purification could be simply incorporated into cellulose pulp with significant increases in tensile and burst indices of the paper (+15%). Recovery of this carbohydrate, primarily hemicellulose, could provide a significant revenue stream to offset the cost of lignin production.

Additionally, preliminary specifications were established for lignin precursor suitable for melt-spinning into fiber. The specifications, which define acceptable levels of ash, particulates, and volatiles, were based on a combination of the specific requirements for spinning lignin fiber tow and the specifications used for commercial production of pitch-based carbon fibers. Small amounts of lignin purified on a bench scale consistently met the specifications.

Overall, using a combination of desalting and carbohydrate-stripping techniques, it has been possible to significantly improve, by >75%, the strength and stiffness of lignin-based carbon fibers produced as single filaments. A 7 kg batch of purified Kraft hardwood lignin material was produced to support further efforts to demonstrate multifilament spinning and rewinding.

Presentations/Publications/Patents

W. L. Griffith; A. L. Compere; and C. F. Leitten, Jr., 2004. “Lignin-Based Carbon Fiber for Transportation Applications”. In *Proceedings of the 36th International SAMPE Technical Conference*, San Diego, CA, 15-18 November, 2004. Covina, CA: Society for the Advancement of Material and Process Engineering. (CD, no paper or page number.)

A. L. Compere; W. L. Griffith; C. F. Leitten, Jr.; and J. M. Pickel. 2005. “Evaluation of lignin from alkaline-pulped hardwood black liquor”. ORNL/TM-2005/88.

Invention Disclosure: “Method for Improving Separation of Carbohydrates from Wood Pulping and Wood or Biomass Hydrolysis Liquors”; William L. Griffith, Alicia Compere, and Carl F. Leitten, Jr. Submitted on July 19, 2005; elected for patent application on August 16, 2005. Lab Docket No. 1300001598. DOE No. S-105, 200.

B. Advanced Stabilization of PAN Fiber Precursor

Principal Investigator: Felix L. Paulauskas
Oak Ridge National Laboratory
PO Box 2008, Oak Ridge, TN 37831-6053
(865) 576-3785; fax: (865) 574-8257; e-mail: paulauskasfl@ornl.gov

Project Manager, Composites: C. David Warren
Oak Ridge National Laboratory
P.O. Box 2008, Oak Ridge, TN 37831-6065
(865) 574-9693; fax: (865) 576-4963; e-mail: warrencd@ornl.gov

Technology Area Development Manager: Joseph A. Carpenter
(202) 586-1022; fax: (202) 586-1600; e-mail: joseph.carpenter@ee.doe.gov
Field Technical Manager: Philip S. Sklad
(865) 574-5069; fax: (865) 576-4963; e-mail: skladps@ornl.gov

Principal Participants:
Christopher J. Janke, Oak Ridge National Laboratory
Daniel Sherman, Atmospheric Glow Technologies
Professor Amod Ogale, Clemson University
Dr. Marshall Cleland, Ion Beam Applications

Contractor: Oak Ridge National Laboratory
Contract No.: DE-AC05-00OR22725

Objectives

- Develop an improved technique for stabilizing carbon-fiber precursor with increased line speed and reduced carbon-fiber cost.
- Verify that finished fiber properties satisfy automotive and heavy-vehicle manufacturers' requirements.
- Conduct a preliminary evaluation of the cost impact of the new stabilization technique.
- Integrate the stabilization module into an advanced technology pilot-line.

Approach

- Investigate thermochemical, ultraviolet, and electron-beam processing stabilization routes.
- Select one of the aforementioned stabilization routes for detailed equipment and process development.
- Develop fiber-handling protocols for continuous processing.
- Conduct parametric studies to correlate processing parameters and fiber properties.
- Characterize fibers to confirm that they satisfy program requirements.

Accomplishments

- Developed project plan including prospective stabilization routes and appropriate partnerships.
- Initiated subcontract negotiations with Clemson University for ultraviolet processing and Atmospheric Glow Technologies for thermochemical processing routes.

B. Advanced Stabilization of PAN Fiber Precursor

Principal Investigator: Felix L. Paulauskas
Oak Ridge National Laboratory
PO Box 2008, Oak Ridge, TN 37831-6053
(865) 576-3785; fax: (865) 574-8257; e-mail: paulauskasfl@ornl.gov

Project Manager, Composites: C. David Warren
Oak Ridge National Laboratory
P.O. Box 2008, Oak Ridge, TN 37831-6065
(865) 574-9693; fax: (865) 576-4963; e-mail: warrencd@ornl.gov

Technology Area Development Manager: Joseph A. Carpenter
(202) 586-1022; fax: (202) 586-1600; e-mail: joseph.carpenter@ee.doe.gov
Field Technical Manager: Philip S. Sklad
(865) 574-5069; fax: (865) 576-4963; e-mail: skladps@ornl.gov

Principal Participants:
Christopher J. Janke, Oak Ridge National Laboratory
Daniel Sherman, Atmospheric Glow Technologies
Professor Amod Ogale, Clemson University
Dr. Marshall Cleland, Ion Beam Applications

Contractor: Oak Ridge National Laboratory
Contract No.: DE-AC05-00OR22725

Objectives

- Develop an improved technique for stabilizing carbon-fiber precursor with increased line speed and reduced carbon-fiber cost.
- Verify that finished fiber properties satisfy automotive and heavy-vehicle manufacturers' requirements.
- Conduct a preliminary evaluation of the cost impact of the new stabilization technique.
- Integrate the stabilization module into an advanced technology pilot-line.

Approach

- Investigate thermochemical, ultraviolet, and electron-beam processing stabilization routes.
- Select one of the aforementioned stabilization routes for detailed equipment and process development.
- Develop fiber-handling protocols for continuous processing.
- Conduct parametric studies to correlate processing parameters and fiber properties.
- Characterize fibers to confirm that they satisfy program requirements.

Accomplishments

- Developed project plan including prospective stabilization routes and appropriate partnerships.
- Initiated subcontract negotiations with Clemson University for ultraviolet processing and Atmospheric Glow Technologies for thermochemical processing routes.

- Met with Ion Beam Applications and commenced planning for electron-beam processing experiments.

Future Direction

- Develop an inexpensive stabilization technique that complements advanced oxidation and carbonization/graphitization processes.
- Conduct parametric studies and fiber characterization to better understand process effects and the processing window and to quantify fiber properties.
- Install advanced stabilization module in advanced-technology pilot-line.

Introduction

The purpose of this project is to investigate and develop a technique to rapidly and inexpensively stabilize a polyacrylonitrile (PAN) precursor. New processing techniques are being developed for the purpose of reducing the cost of carbon-fiber conversion. Previous and ongoing research at ORNL has demonstrated that plasma processing shows great promise for inexpensively and rapidly oxidizing, carbonizing, and graphitizing polymer precursors to convert them to carbon fibers. However, to date, all plasma processing protocols tried by ORNL have damaged virgin precursor, i.e., the precursor needs to be lightly stabilized, or cross-linked, before it is exposed to plasma. A rapid, inexpensive, and robust stabilization technique is needed to complement the aforementioned advanced process modules, and enable the development of an integrated, advanced-technology conversion line that converts polymer precursor fibers into carbon fibers at significantly lower cost than conventional conversion technology.

This project, therefore, intends to develop an advanced stabilization module that integrates with other advanced fiber processing modules to produce inexpensive carbon fiber with properties suitable for use by the automotive industry. Critical technical criteria include (1) ≥ 25 Msi tensile modulus and ≥ 1.0% ultimate strain in the finished fiber; (2) uniform properties over the length of the fiber tow; (3) repeatable and controllable processing; (4) and significant unit cost reduction compared with conventional processing.

Project Deliverable

At the end of this project, we will have demonstrated satisfactory PAN-precursor-fiber stabilization in a multiple-tow stabilization module operating at line speed exceeding that typical of conventional carbon-fiber conversion lines. The project deliverable is an equipment and processing specification from which advanced stabilization equipment can be purchased and operated in a subscale, advanced-technology, pilot conversion line.

Technical Approach

The researchers are investigating three prospective PAN-precursor-fiber stabilization routes: electron-beam processing, thermochemical processing, and ultraviolet processing. All three routes are based on discoveries previously made in other carbon-fiber projects, and each appears to offer certain advantages. After initial feasibility studies, the researchers will select the most promising route for detailed process development, with the principal criterion for selection being finished fiber cost. The preferred route will then undergo detailed parametric studies to develop the processing recipe, and will be scaled up in both speed and tow count to the point where equipment can be designed and purchased for operation in a subscale, pilot conversion line.

Progress

The project was initiated late in FY05, with sufficient time remaining for planning only. ORNL has engaged partners to provide equipment and assist with or lead the study of each processing route. The researchers have met with Ion Beam Applications, which will provide irradiation services at its Long Island facility, and experiment planning is underway for first electron-beam processing experiments in November 2005. Contract negotiations are ongoing with Atmospheric Glow Technologies, Inc. and Clemson University, the respective providers of thermochemical and ultraviolet processing equipment and services. First experiments for each of these routes are likely to also occur in the November

2005 time frame, assuming there are no unusual delays in contract execution.

Future Direction

FY 2006 will be devoted to parallel studies of the proposed stabilization routes, with down-selection to a single route in early FY 2007.

Education

Educational institutions participating in this project include Clemson University and UT. A Clemson post-doctoral researcher will conduct ultraviolet processing studies under the direction of Professor Amod Ogale. Two University of Tennessee (UT) materials science graduate students will provide characterization support to the project under the guidance of Professor Roberto Benson.

Partners

In addition to the aforementioned partners, ORNL gratefully acknowledges contributions to this project by TohoTenax America and Hexcel. Both have generously provided raw materials and offered technical consultation. Additionally, technical and programmatic consultation has been provided by the Automotive Composites Consortium.

Conclusions

Three prospective, nonthermal processing routes are proposed to lightly stabilize polymer precursors in an advanced carbon-fiber conversion line. Contract negotiations and experiment planning are underway with first experiments scheduled in November 2005.

C. Advanced Oxidation of PAN Fiber Precursor

Principal Investigator: Felix L. Paulauskas
Oak Ridge National Laboratory
P.O. Box 2008, Oak Ridge, TN 37831-8048
(865) 576-3785; fax: (865) 574-8257; e-mail: paulauskasfl@ornl.gov

Project Manager, Composites: C. David Warren
Oak Ridge National Laboratory
P.O. Box 2008, Oak Ridge, TN 37831-6065
(865) 574-9693; fax: (865) 576-4963; e-mail: warrencd@ornl.gov

Technology Area Development Manager: Joseph A. Carpenter
(202) 586-1022; fax: (202) 586-1600; e-mail: joseph.carpenter@ee.doe.gov
Field Technical Manager: Philip S. Sklad
(865) 574-5069; fax: (865) 576-4963; e-mail: skladps@ornl.gov

Participants:
Terry L. White and Kenneth D. Yarborough, Oak Ridge National Laboratory
Professor Joseph Spruiell, University of Tennessee
Daniel Sherman, Atmospheric Glow Technologies

Contractor: Oak Ridge National Laboratory
Contract No.: DE-AC05-00OR22725

Objectives

- Develop an improved technique for oxidizing carbon-fiber precursor with increased line speed, reduced carbon-fiber cost, and reduced equipment footprint.
- Verify that finished fiber properties satisfy automotive and heavy-vehicle manufacturers' requirements.
- Conduct a preliminary evaluation of the cost impact of the new oxidation technique.
- Integrate the oxidation module into an advanced-technology pilot-line.

Approach

- Develop a plasma process for oxidation in an atmospheric-pressure plasma reactor.
- Develop fiber-handling protocols for continuous processing.
- Conduct parametric studies to correlate processing parameters and fiber properties.
- Characterize fibers to confirm that they satisfy program requirements.

Accomplishments

- Demonstrated complete oxidation of "pre-stabilized" 3k PAN-precursor tow in atmospheric-pressure plasma using a continuous process at 0.05 m/min line speed.
- Fully oxidized "pre-stabilized" fiber in atmospheric-pressure plasma at less than half the residence time of conventional oxidation.
- Submitted a provisional patent application for the plasma oxidation process.

Future Direction

- Continue refining the reactor design and processing protocols to achieve high speed, multiple large tow, continuous, plasma oxidation process.
- Develop "pre-stabilization" technique.
- Conduct parametric studies and fiber characterization to better understand process effects and the processing window and to quantify fiber properties.
- Conduct rate-effect studies and update cost analysis.

Introduction

The purpose of this project is to investigate and develop a plasma processing technique to rapidly and inexpensively oxidize a polyacrylonitrile (PAN) precursor. Oxidative stabilization is a slow thermal process that typically consumes 70% or more of the processing time in a conventional carbon-fiber conversion line. A rapid oxidation process could dramatically increase the conversion line throughput and appreciably lower the fiber cost. A related project has already demonstrated the potential for greatly increasing line speed in the carbonization and graphitization stages, but the oxidation time must be greatly reduced to fully exploit faster carbonization and graphitization. This project intends to develop a plasma oxidation module that integrates with other advanced fiber-processing modules to produce inexpensive carbon fiber with properties suitable for use by the automotive industry. Critical technical criteria include (1) ≥ 25 Msi tensile modulus and ≥ 1.0% ultimate strain in the finished fiber; (2) uniform properties over the length of the fiber tow; (3) repeatable and controllable processing; (4) and significant unit cost reduction compared with conventional processing.

Project Deliverable

At the end of this project, we will have demonstrated satisfactory fiber oxidation in a multiple-tow, plasma oxidation module operating at line speed exceeding that typical of conventional carbon-fiber conversion lines.

Technical Approach

We are investigating PAN-precursor-fiber oxidation using nonequilibrium, nonthermal plasma at atmospheric pressure. Plasma processing is believed to enhance oxygen diffusion and chemistry in the PAN oxidation process. Atmospheric-pressure plasma provides better control over the thermal environment and reaction rates than does evacuated plasma, in addition to eliminating the sealing problems accompanying evacuated plasma processing. Various fiber characterization tools and instruments are used to conduct parametric studies and physical, mechanical, and morphological evaluations of the fibers to optimize the process. An evacuated plasma reactor is useful for bench-scale studies, because it allows a greater degree of manipulation and control over reactive species and related parameters. Early in the project, processing tests were conducted in an evacuated plasma reactor, and that same reactor is now used for conducting the bench-scale parametric studies.

Atmospheric-Pressure Plasma Processing Results

Exposure in plasma at or near atmospheric pressure provides superior thermal control because the gas flow should convectively heat or cool the fibers. This is deemed particularly important to avoid fiber melting from the exothermic reactions associated with the PAN cross-linking that occurs during stabilization. However, the mean-free-path of the chemically reactive species is shorter by orders of magnitude than it is in an evacuated environment, and this makes it very difficult to find a combination of process parameters that will oxidize the fibers with acceptable residence time.

Conventional PAN oxidation is typically accomplished in three or four thermal stages (stages can be physically separate furnaces or zones in a single physical furnace) in air, at temperatures increasing from about 200 to 250°C. In FY 2004, the researchers demonstrated the ability to reproduce the oxidation advancement in each of the conventional furnaces two, three, and four. The virgin PAN is chemically fragile; hence, we have not yet

discovered a satisfactory nonthermal processing protocol that reproduces the oxidation advancement in the first conventional furnace. The researchers previously reported that they had been able to reproduce, with plasma oxidation, the process for each of the individual conventional furnaces 2, 3, and 4 (schematically shown in Fig 1).

During the first half of FY2005, the researchers refined the operating parameters to enable full oxidation of "pre-stabilized" precursor in a single step. i.e., the oxidation advancement achieved in a single, plasma, batch reactor was equivalent to that achieved in sequential processing through conventional furnaces 2, 3, and 4. This is shown schematically by the longest solid arrow in Figure 1. After batch oxidation was satisfactorily demonstrated, the researchers turned their attention to continuous processing. In the second half of FY2005, a continuous reactor was designed and built. The continuous- reactor design includes many innovations not present in earlier designs, but pictures and design details are not included herein due to the sensitive nature of that information. At the end of FY2005, the researchers demonstrated complete oxidation, starting with a "pre-stabilized" precursor, at a continuous processing line speed of 0.05 m/min.

Another very important achievement during this period was a significant reduction in oxidation residence time. The aforementioned single-stage, batch and continuous, plasma oxidation processes were achieved in less than half of the residence time required for conventional processing through furnaces 2, 3, and 4.

The researchers continued identifying the parameters that most affect the oxidation rate and optimizing those parameters within the reactor. For patent protection and export control reasons, the detailed results are not published, but they are periodically disclosed to the relevant program managers in oral briefings.

Pre-Stabilization

As previously mentioned, the precursor must be lightly stabilized before it can withstand the plasma environment. Late in FY2005, a new project was initiated to focus on developing an advanced "pre-stabilization" technique (See report 3.B, "Advanced Stabilization of Pan Fiber Precursors"). The pre-stabilization module and the plasma oxidation module will eventually be incorporated into an advanced-technology pilot-line.

Future Direction

In FY 2006, the project focus will be on carbonizing plasma-oxidized fiber to validate its mechanical properties; parametric studies to improve the process; and commence scaling studies to increase line speed, tow size, and tow count.

Patents and Publications

A provisional patent application was filed describing the plasma oxidation method.

Education

The materials characterization has been conducted in partnership with the University of Tennessee's (UT's) materials science department. Two UT graduate students were engaged to provide characterization support to the project.

Partners

ORNL gratefully acknowledges contributions to this project by Fortafil and Hexcel. Both have generously provided raw materials and offered technical consultation. Additionally, technical and programmatic consultation has been provided by the Automotive Composites Consortium and by Delphi Corporation.

Conclusions

During FY 2005, the researchers have fully oxidized "pre-stabilized" PAN in a single-step, batch process and in a continuous process, in less than half of the residence time required for analogous conventional thermal processing. The next steps are to validate mechanical properties and commence scaling studies.

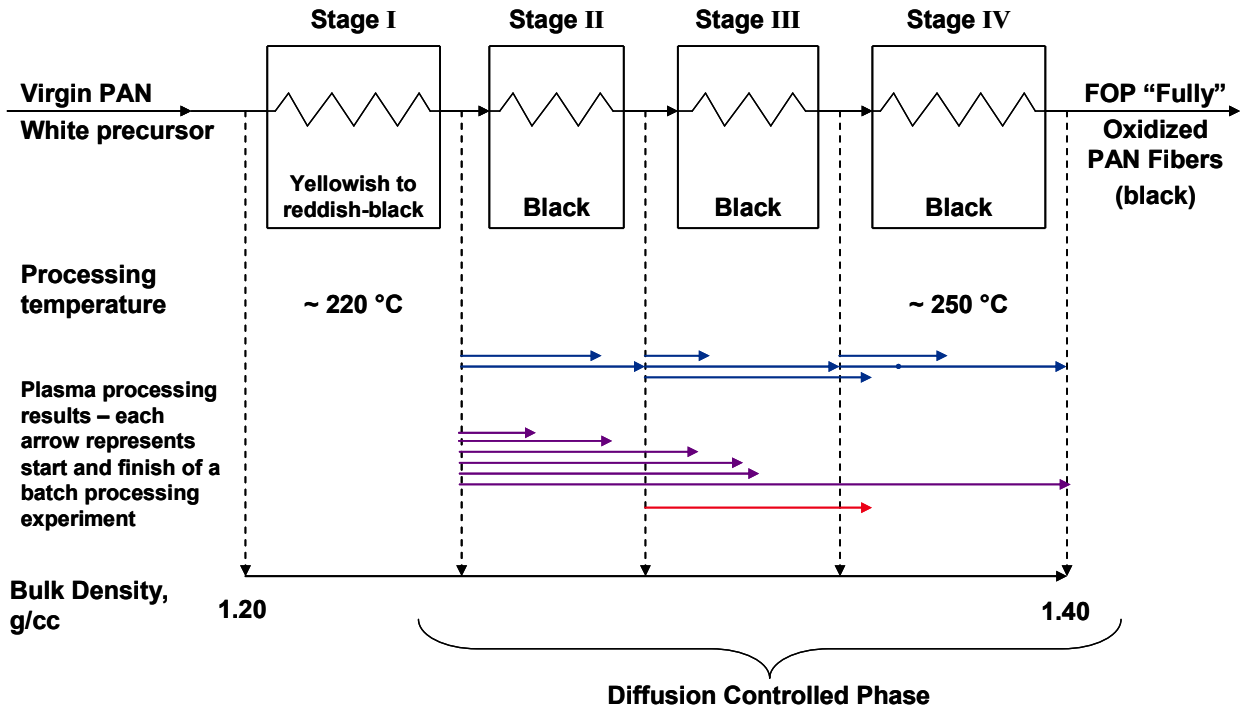


Figure 1. Oxidation advancement–arrows show degree of advancement achieved in various batch plasma processing experiments. Different arrow patterns represent different schemes.

D. Low-Cost Carbon Fiber Manufacturing Using Microwave Energy

Principal Investigator: Felix L. Paulauskas
Oak Ridge National Laboratory
P.O. Box 2008, Oak Ridge, TN 37831-8048
(865) 576-3785; fax: (865) 574-8257; e-mail: paulauskasfl@ornl.gov

Project Manager, Composites: C. David Warren
Oak Ridge National Laboratory
P.O. Box 2008, Oak Ridge, TN 37831-6065
(865) 574-9693; fax: (865) 576-4963; e-mail: warrencd@ornl.gov

Technology Area Development Manager: Joseph A. Carpenter
(202) 586-1022; fax: (202) 586-1600; e-mail: joseph.carpenter@ee.doe.gov
Field Technical Manager: Philip S. Sklad
(865) 574-5069; fax: (865) 576-4963; e-mail: skladps@ornl.gov

Participants:
Terry L. White, Oak Ridge National Laboratory
Kenneth D. Yarborough, Oak Ridge National Laboratory
Professor Roberto Benson, University of Tennessee

Contractor: Oak Ridge National Laboratory
Contract No.: DE-AC05-00OR22725

Objective

- Investigate and develop a microwave-assisted technical alternative to carbonize and graphitize polyacrylonitrile (PAN)-based precursor.
- Prove that carbon fiber with properties suitable for use by the automotive industry can be produced inexpensively using microwave-assisted plasma (MAP) processing.
- Demonstrate that MAP processing can produce acceptably uniform properties over the length of the fiber tow.
- Show that for specified microwave input parameters, fibers with specific properties may be controllably and predictably manufactured using microwave furnaces.
- Demonstrate the economic feasibility for producing approximately 30-Msi-modulus fibers at a significant cost reduction relative to those produced conventionally.

Approach

- Demonstrate the ability to deliver high fiber-mass throughput by increasing line speed and tow count.
- Conduct parametric studies on the continuous carbon-fiber processing pilot unit to continually improve the system design, process parameters, and fiber properties.
- Characterize MAP-processed carbon fibers to confirm that they satisfy program requirements.
- Continually evaluate, develop, and characterize “spin-off” technology, hardware, and ideas that improve upstream or downstream processing, or facilitate more efficient utilization of fiber.

Accomplishments

- Completed relocation of the carbon-fiber conversion laboratory to ORNL main campus.
- Achieved what we believe to be record spatial resolution in measuring spatial distribution of surface functional groups.
- Correlated surface topography and spatial distribution of surface chemistry.

Future Direction

- Re-assemble and commission the MAP carbonization module at ORNL main campus location.
- Increase multiple-tow line speed.
- Continue parametric studies and fiber characterization to better understand process effects and processing window and to quantify fiber properties.
- Integrate into advanced technology, subscale carbon-fiber pilot conversion line (future project).
- Develop partnership(s) to commercialize the technology.

Introduction

The purpose of this project is to investigate and develop a microwave-assisted technical alternative to carbonize and partially graphitize the polyacrylonitrile (PAN) precursor. The project is to prove that carbon fiber with properties suitable for use by the automotive industry can be produced inexpensively using microwave-assisted plasma (MAP) processing. It is to be demonstrated that MAP processing can produce acceptably uniform properties over the length of the fiber tow. The project is also to show that for specified microwave input parameters, fibers with specific properties may be controllably and predictably manufactured using microwave furnaces. Lastly, but most importantly, this project is to demonstrate the economic feasibility for producing approximately 30-Msi-modulus fibers at a significant cost reduction below those produced conventionally.

Project Deliverables

At the end of this project, a continuous, multiple-tow, scalable, high-production-line-speed MAP carbon-fiber prototype unit will have been developed, constructed, and tested. A final report will be issued with the test results of the carbon fibers processed with this unit. Appropriate industry briefings will be conducted to facilitate commercialization of this economically-enabling technology.

Facility Relocation

In FY 2005 the carbon fiber conversion laboratory and associated equipment were moved from the Y-12 site to the ORNL main campus. Most of the equipment has now been re-assembled at the new facility. Completion of reassembly, installation, and checkout is scheduled in early FY 2006.

Characterization

Carbon-fiber surface chemistry greatly affects bonding to the resin, and hence the composite material properties. MAP carbonization has been shown to produce different, and apparently superior, surface chemistry than conventional carbonization. While spatially-averaged surface chemistry is useful information, it is extremely desirable to understand the spatial variation of surface chemistry and how it correlates with surface topography.

PAN-based carbon fibers are typically covered by ridges that run approximately parallel to the fiber axis and are somewhat regularly spaced. Typical ridge height and width both tend to be on the order of 100 nm, so any technique for correlating surface topography and surface chemistry must include the ability to locate surface functional groups with about 10 nm spatial resolution. Furthermore, depth-of-field needs to be in the nanometer range so as to focus on the top atomic layers.

Auger Electron Spectroscopy (AES) satisfies spatial and depth-of-field resolution requirements. By using chemical derivitization techniques, AES can identify

elemental composition and indirectly determine the chemical states present on the sample surface. ORNL's High Temperature Materials Laboratory employed this technique to produce the images shown in Figure 1. AES and secondary images were both obtained in the same instrument (PHI 680, Physical Electronics, Cahnhassen, MN). In the AES images, high carboxyl concentration is indicated by dark (blue for readers who are viewing color images) areas. The images clearly show the high carboxyl concentrations imparted by plasma treatment, as well as the correlation between microstructural features and the distribution of acid groups. The researchers are unaware of previous measurements of surface chemical spatial distribution at this resolution. It is observed that most carboxyl groups were distributed along the bottoms or sides of valley regions. Functional groups are believed to attach to the edges of graphene planes, so it appears that, compared to ridges, there are more graphite edge sites located along the valley. This is surprising, as the conventional view has been that functional groups attach to the ridge tops. The orientation of graphene planes with regard to the fiber surface in both ridges and valleys, and the graphitic organization in both areas, i.e., any distortion present, need to be further investigated.

Patents and Publications

An invention disclosure was submitted to ORNL's patent office on the design details of the MAP system. The patent will be filed in early FY 2006.

Education

The materials characterization, notably utilizing Auger microanalysis and x-ray photoelectron spectroscopy (XPS), has been conducted in partnership with the University of Tennessee's Materials Science Department. A doctoral candidate provided characterization support to the project. This work forms the basis of her doctoral thesis.

Conclusions

Relocation of the carbon-fiber conversion lab commenced during the first half of FY 2005.

The researchers developed a method to accurately determine the spatial distribution of surface functional groups and their correlation with topographical surface features. A noteworthy achievement was that, to our knowledge, the spatial resolution of these measurements was the best ever achieved in measuring functional group locations.

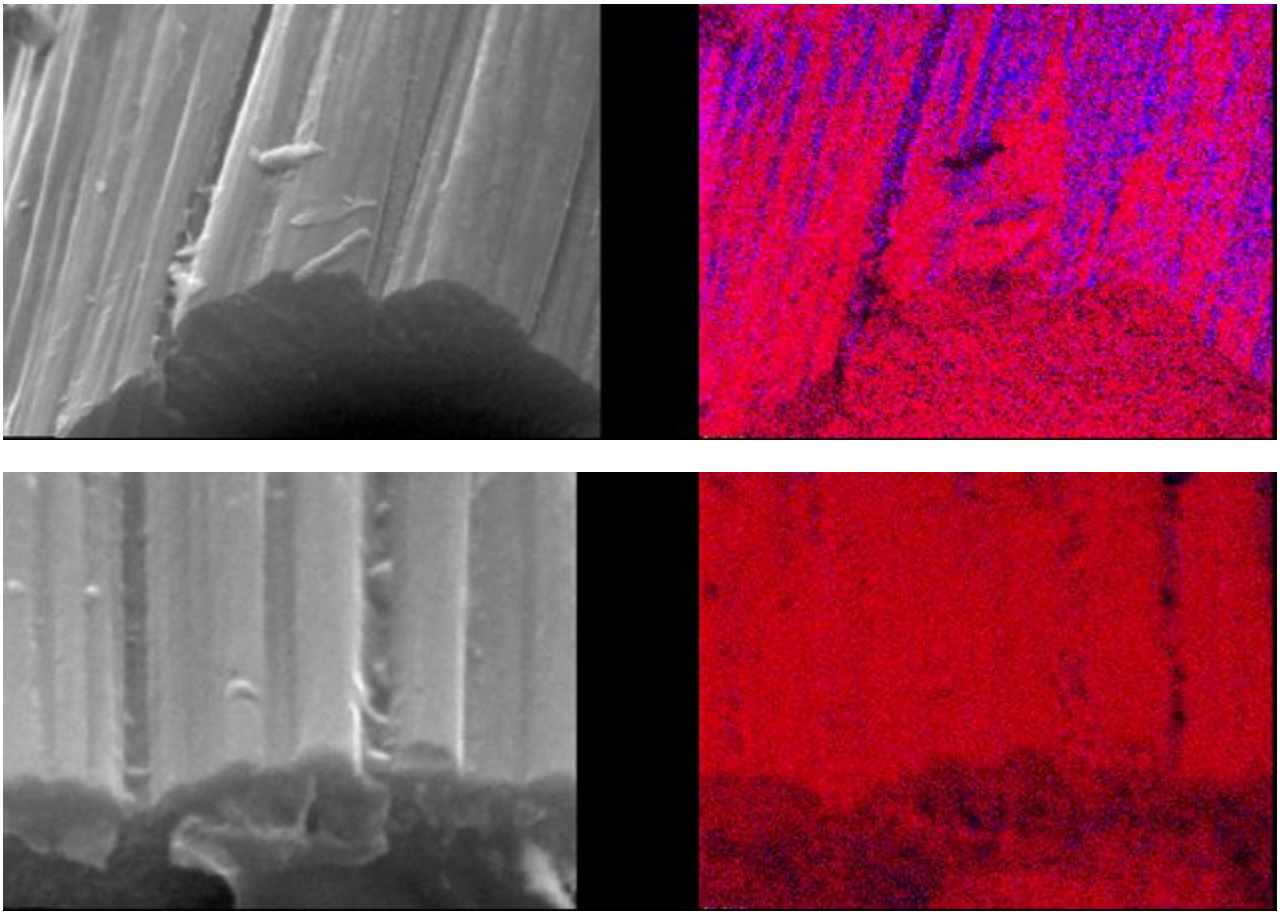


Figure 1. Images of carbon fiber. Top: untreated, unsized commercial fiber. Bottom: Plasma-treated fiber. Left: scanning electron micrograph. Right: Auger electron spectrograph, in which dark (blue, for readers viewing color images) areas indicate high carboxyl concentrations.

E. Carbon Fiber Systems Integration

Principal Investigator: Felix L. Paulauskas
Oak Ridge National Laboratory
P.O. Box 2008, Oak Ridge, TN 37831-8048
(865) 576-3785; fax: (865) 574-8257; e-mail: paulauskasfl@ornl.gov

Project Manager, Composites: C. David Warren
Oak Ridge National Laboratory
P.O. Box 2008, Oak Ridge, TN 37831-6065
(865) 574-9693; fax: (865) 576-4963; e-mail: warrencd@ornl.gov

Technology Area Development Manager: Joseph A. Carpenter
(202) 586-1022; fax: (202) 586-1600; e-mail: joseph.carpenter@ee.doe.gov
Field Technical Manager: Philip S. Sklad
(865) 574-5069; fax: (865) 576-4963; e-mail: skladps@ornl.gov

---

Contractor: Oak Ridge National Laboratory
Contract No.: DE-AC05-00OR22725

Objectives

- Develop a subscale, modular test facility for carbon-fiber conversion technology.
- Provide capability to test conversion subsystems or modules.
- Provide a capability for converting a range of polymer precursors into finished carbon fibers
- Provide the capability to produce small quantities of finished carbon fiber.

Approach

- Procure and install a conventional carbon-fiber pilot line.
- Construct advanced technology carbon-fiber pilot line using equipment and process specifications developed in other carbon-fiber conversion projects.
- Highly instrument the pilot line for process characterization.
- Locate the advanced technology and conventional lines adjacent to each other, and equip them with versatile fiber transport equipment.

Accomplishments

- Acquired and installed a used conventional pilot line.
- Commenced installation of MAP-carbonization, advanced-technology module.

Future Direction

- Complete conventional pilot line acceptance testing.
- Complete installation and commissioning of MAP carbonization module.
- Procure, install, and commission other advanced-technology modules when the processes and equipment designs are sufficiently mature.
- Perform precursor studies and parametric process studies.

- Investigate and demonstrate stable operating envelope, as well as system reliability, availability, and maintainability.
- Develop partnership(s) to commercialize the technology.

Introduction

The purpose of this project is to develop a user facility for testing and demonstrating new carbon-fiber conversion technology. The facility will be designed specifically for processing tows of commercial-grade (large tow) fiber, but will be sufficiently versatile that it can also process some aerospace-grade fibers. It will be designed to process a variety of polymer precursors; it may be adaptable to pitch precursors, but that is not a project requirement. As a user facility, it will be made available for use by government laboratories, universities, and industry partners.

The heart of the facility will be two adjacent, subscale, carbon-fiber conversion lines. One line will be based on conventional pre-treatment, conversion, and post-treatment processes and the other will embody advanced technology processes. The facility will be highly instrumented for characterizing fiber properties and process parameters. It will also be highly modular, and will be equipped with versatile tow transport equipment, so that tows can be routed through any combination of conventional and advanced technology conversion, pre-treatment, or post-treatment modules. The pilot line will be capable of running a single tow or any number of tows up to its maximum capacity, which will be at least five 50k tows. The pilot line may eventually be mated with upstream or downstream processes. The facility is shown schematically in Figure 1.

Project Deliverables

At the end of this project, a modular, flexible, and highly instrumented user facility for testing carbon-fiber conversion technology will be operational. The user facility will embody all pre-treatment, conversion, and post-treatment processes in parallel pilot lines for both conventional and advanced technologies, with the ability to route one to at least five large tows through any combination of the available processing modules.

Current Status

During FY2005, ORNL acquired a used conventional pilot line from Toho Carbon Fibers Inc. in Rockwood, TN and installed it in the 7625 building at ORNL. This pilot line has the capability to convert eight large tows at line speed of 0.2 m/min. The speed limit is the oxidation units; if oxidation is bypassed, the maximum line speed is 0.5 m/min. Acceptance testing will be conducted in early FY 2006.

Also in FY 2005, the MAP carbonization equipment was moved from the Y-12 site to its new home in ORNL building 7625 and installation was completed except for some minor piping connections. MAP carbonization installation will be completed and testing commence in early FY 2006.

Conclusions

The development of a DOE “carbon-fiber systems integration” facility for testing and demonstrating new carbon fiber manufacturing technology has commenced. A conventional carbon-fiber pilot line has been acquired and installed. The MAP-carbonization, advanced-technology module is being installed in the same laboratory. The end goal is to operate adjacent complete, subscale conventional- and advanced-technology pilot lines that will allow testing of either new precursors or new conversion technology.

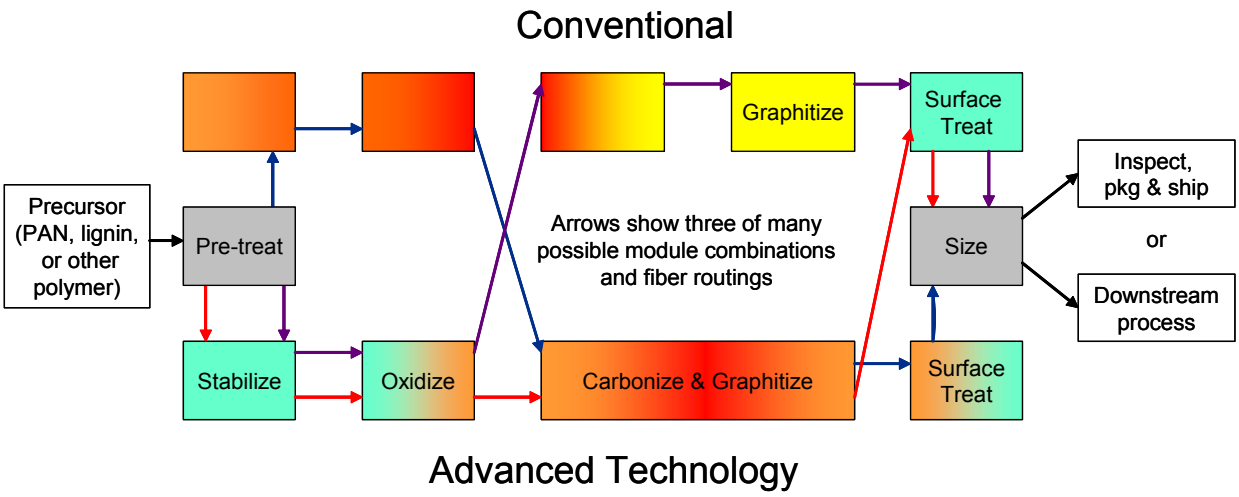


Figure 1. Schematic of carbon-fiber pilot lines

4. POLYMER COMPOSITES R&D

A. Development of Manufacturing Methods for Fiber Preforms

Principal Investigator: Jeff Dahl
Ford Motor Company, Research and Innovation Center
P.O. Box 2053, MD 3135 RIC, Dearborn, MI 48121-2053
(313) 845-1039; fax: (313) 390-0514; e-mail: jdahl@ford.com

Project Manager: C. David Warren
Oak Ridge National Laboratory
P.O. Box 2009, Oak Ridge, TN 37831-8050
(865) 574-5069; fax: (865) 574-0740; e-mail: warrencd@ornl.gov

Technology Area Development Manager: Joseph A. Carpenter
(202) 586-1022; fax: (202) 586-1600; e-mail: joseph.carpenter@ee.doe.gov
Field Technical Manager: Philip S. Sklad
(865) 574-5069; fax: (865) 576-4963; e-mail: skladps@ornl.gov

---

Contractor: U.S. Automotive Materials Partnership
Contract No.: FC26-02OR22910

Objective

- Develop and demonstrate new fiber preforming processes to decrease cost, increase manufacturing rates and improve reproducibility of large preforms for composite molding.
- Provide process development support to the Automotive Composites Consortium's (ACC) Focal Project-3.

Approach

- Identify carbon-fiber properties required to permit rapid processing and achieve desired performance levels.
- Investigate materials, process equipment, and tooling technology to further reduce the cost and enhance the quality of chopped-fiber performs.
- Characterize chopped-fiber preforms utilizing experimental carbon-fiber rovings to determine important characteristics (permeability, light transmission, areal density distribution, etc.).
- Explore the extension of automated preforming technology to make preforms with a thermoplastic matrix.

Accomplishments

- Toho Tenax carbon-fiber roving development program progressed with successful direct splitting of carbon-fiber rovings.
- Preforming process development conducted on the Focal Project 3 B-pillar test section.
- Initiated preliminary thermoplastic P4 (TP-P4) processing studies

Future Direction

- Experimental preforming and molding evaluation of mechanically-split, low-filament-count Toho Tenax carbon-fiber rovings.
- Further characterization and investigation of low-cost, carbon-fiber rovings with reduced individual bundle size.
- Investigate the use of thermoplastic-matrix materials in the P4 process and develop the TP-P4 process concept.

Introduction

This project has focused on the development of the P4 process, a fully-automated robotic preforming process. A prototype, two-station manufacturing cell was designed, fabricated and installed at the National Composite Center (NCC) in Kettering, Ohio. This equipment is currently being utilized to support preforming and material development efforts within the Automotive Composites Consortium (ACC).

In order to obtain higher mass savings with composites relative to steel (50-70%), carbon fiber must be utilized as the reinforcing fiber. The extension of this preforming technology to manufacture carbon-fiber preforms is now in progress to support the development of ultra-light weight vehicle structures. A major focus of this program is the development of a carbon-fiber material suitable for chopped-fiber processes. Current production carbon-fiber materials are not amenable. Advances in carbon-fiber roving and preforming technology will be demonstrated in the structural automotive parts designed and prototyped as part of the ACC's Focal Project 3 (see report 4.D).

Preliminary investigation to determine the feasibility of using a modified P4 process (i.e., TP-P4) to generate thermoplastic/glass fiber preforms and blanks for compression molding was initiated.

Carbon-Fiber Roving Development

To date, chopped carbon-fiber preforming research and development has been limited due to material format issues. In order to address fundamental material format issues with off-the-shelf carbon fibers, development programs have been initiated with two carbon-fiber manufacturers (Hexcel and Toho) to expedite material research. The focus of these programs is to investigate the technology required to achieve a reduction in bundle size, to determine the effects of bundle size in the preforming/molding processes and to ascertain the effect on composite material performance.

Hexcel Carbon Fibers

A carbon-fiber roving development program to investigate the effect of individual bundle size on preforming, molding and composite material performance using Hexcel carbon fibers is nearly completed. The development effort focused on assessing the effect of individual bundle size on P4 preforming, structural reaction injection molding (SRIM), and the resultant composite material performance. It was theorized that a reduction in bundle size would improve material distribution in the preforming process and, therefore, positively impact the mechanical performance of molded structures. Based upon the data gathered to date, composite material mechanical performance was positively impacted by a reduction in bundle size.

Evaluation of the carbon-fiber rovings is nearly complete with preform permeability evaluation remaining. Remaining preform fabrication includes permeability samples, both in-plane and through the thickness. Upon completion of preform permeability test equipment at ORNL, in-plane and through-thickness permeability measurements will be conducted using preforms fabricated with each of the seven carbon-fiber rovings previously manufactured.

Toho Tenax Carbon Fibers

A research program to develop carbon-fiber rovings more amenable to the P4 preforming process was originally developed and initiated with Fortafil Fibers. Toho Carbon Fibers acquired Fortafil on September 1, 2004; therefore, the program is now officially with Toho Carbon Fibers. This program focuses on developing cost-effective methods to reduce the individual carbon-fiber bundle sizes within a roving by using relatively low-cost, 80k carbon fiber as the input material. A carbon-fiber

roving specification was developed jointly between the ACC and Fortafil as the target material for this program. The overall program is comprised of five phases.

Toho Tenax CF Phase 1: The first phase of the work was to investigate whether or not splitting the precursor could give a final carbonized tow with fiber bundles of the desired dimensions.

The major effort at Toho was focused on evaluating precursor samples produced by spinning small-filament-count strands through spinnerets selectively blanked to give the desired number of filaments. In total, four samples were evaluated at Toho. The first three contained 42 strands of 2,000 filaments each; the last sample contained only 28 strands but was spun with greater separation between the spinneret hole sections. All samples were spun as 1.5 denier/filament (dpf) and grouped into bundles containing 167k total filaments. The progression to larger total filament count and strand number in the course of this work was necessitated by the requirement to spin more dope through the spinneret to stabilize the spinning process. All samples were crimped and packaged in the normal way.

Two of the samples were oxidized on Toho's pilot line and then carbonized and sized on their production line. The precursor visually appeared to be more segmented than standard precursor; however, once the material was tensioned in oxidation, the strands were not easily distinguishable. While the final carbon-fiber product does have a separated appearance, cross filaments are plentiful and some of the strands appear to have consolidated to form larger strands.

The last of three precursor samples produced was also converted into carbon fiber at Toho. This particular sample contained 28 individual strands of 2,000 filaments each. The tow was carbonized and sized with the same polyurethane size used in the ongoing carbon slitting effort (see Phase 2). Because the tow stiffness was enhanced by the size, separating the strands in the tow was even more difficult than for the two similar tows converted and sized with epoxy.

The precursor-splitting trials generally demonstrated that the use of divider pins or grooved bars is feasible to keep strands separate in the precursor state during the spinning process attributable to the toughness of the polymer and the larger filament diameter. However, the use of the same techniques in the carbon conversion process will likely cause excessive filament damage once the polyacrylonitrile (PAN) fiber is converted to a brittle material of much smaller diameter. The implication of the results to date was that the strands must either be maintained as separate entities until sizing application and drying or created at the point of size application and maintained separate through drying, as is done in the carbon slitting process.

The results of these trials were conveyed to precursor manufacturing personnel for final consideration. The decision to terminate this development approach was made after discussing the technical problems with personnel at the precursor manufacturing facility. In the final analysis, the precursor manufacturing team was unable to introduce entanglement or twists in the individual strands of a tow, and carbon-fiber manufacturing personnel were negative on the feasibility of maintaining separation of the strands in the carbon conversion process without causing excessive filament damage. Development activities to produce a stranded roving by modifying the form of the precursor were subsequently discontinued.

Toho Tenax CF Phase 2: The second phase of the project involves direct mechanical slitting of carbon fiber, focusing, in particular, on what happens at the point of subdivision of the tow into strands.

Various types and configurations of slitter rolls were evaluated. The most effective slitting configuration achieved to date uses a single roll, eccentric in shape, with flat bottom grooves, and rotated counter to the direction of the moving tow faster than the absolute speed of the fiber (Figure 1). The eccentric design of the roll allows cross filaments to move between grooves in a gradual way to avoid a build-up of filaments that would otherwise cause stoppage of the operation. The use of multiple rolls and various groove geometries was also evaluated. Additional rolls do not enhance the slitting effectiveness, however.

Critical to the consolidation of the strands after their creation at the surface of the slitter roll is the

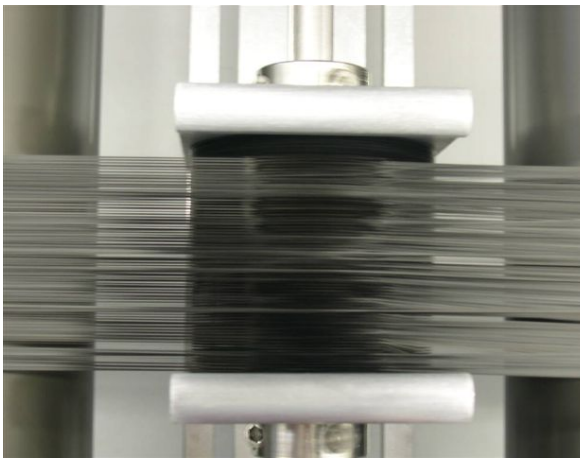


Figure 1. Prototype tow-splitting device.

application of a water-based size. Initial slitting trials used a hand sprayer to apply water directly onto the fiber and slitting roll, but techniques have since been developed to apply the size prior to the slitting roll by drip or kiss-roll application.

Upon completion of the above tasks, lab-scale production of three roving samples was conducted for material evaluations in the P4 process. Carbon-fiber rovings with nominal strand counts of 25, 35, and 50, were produced on the lab-scale slitting line (Figure 2). All of the rovings were produced from 80k carbon tows having a TEX value of approximately 4380. The rovings were sized with the same commercially-available, water-based polyurethane used for all of the carbon slitting trials to date. Some minor fuzzing was encountered in the production of the strands resulting in the formation of small fuzz balls, most of which were manually removed. It is envisioned that in a commercial



Figure 2. Prototype tow-splitting line.

production operation, such fuzz agglomerations would be removed by patented production technology already owned by Toho Carbon Fibers.

Following receipt of the materials, a processing evaluation of the three rovings (25, 35 and 50 split) was conducted on the ACC's P4 preforming machine. These panels were then molded via SRIM and characterized to determine the mechanical properties of the composite. Five kilograms of fiber with each of three split configurations (25, 35, and 50 splits, yielding about 1.5 k, 2.5k, and 3k strands) were evaluated by the ACC. Preforming of the fibers was acceptable for an initial evaluation, although further sizing work is needed to deal with fiber handling issues. The results of mechanical testing from this preforming and molding trial are shown in Table 1.

Table 1. Mechanical Properties of Toho Tenax split-tow carbon-fiber composite.

	Tensile		Compression
	Strength MPa	**Modulus GPa**	**Strength MPa**
Control 12x3k	207	33.4	247
Toho 50x1.5k	194	29.7	250
Toho 35x2.5k	190	32.2	298
Toho 25x3k	190	32.5	297

Mechanical properties are similar to the control, but do not show an improvement with fiber bundle size. Since other work in the ACC has shown the advantage of smaller fiber bundles, this indicates a need for further sizing development to enhance the properties of the random chopped composite.

Toho Tenax CF Phase 3: This phase calls for the development of appropriate fiber sizings for improved handling and fiber/matrix interface with a polyurethane resin system. This has been initiated in conjunction with the processing studies on the fiber-slitting line, and will be continued by Toho research labs in Japan.

Toho Tenax CF Phases 4& 5: The fourth phase is acquisition of a pilot-line for fiber production. The actual extent of the pilot-line is still under discussion with Toho management, and the fifth phase, the optimization of the pilot-line, production of fibers for ACC evaluation, and assessment of

manufacturing costs, will be determined after the results of that discussion are clear.

The program has an anticipated completion date of September 30, 2006. The date has been delayed from the initial schedule by a combination of factors, including the lack of success of the precursor-slitting trials and the acquisition by Toho Tenax. Continuation of this project is currently under review by Toho Tenax management.

Thermoplastic P4 (TP-P4)

Preliminary Processing Studies: To prove out the process concept, an initial series of experimental studies was conducted to demonstrate deposition of polymer matrix materials and reinforcement fibers. In total, 80 blanks were manufactured under a variety of conditions to test deposition reliability and throughput capability. The key technical hurdles, related to fiber and matrix deposition, are considered to be:

- Verification of throughput capability for 45s production cycle times.
- Demonstration of control over fiber distribution.
- Demonstration of process robustness for continuous, uninterrupted operation.

During the concept feasibility trials, attention was focused on material deposition throughput. At present, the TP-P4 processing equipment has shown capability for fiber and polymer deposition, but only at reduced output. This limitation is a function of the equipment design, which was originally commissioned for a previous project. Hence, increased material output will require a re-design of equipment. An example of the material blank that is produced using the current development cell is shown in Figure 3.

As the photograph shows, random deposition of the fibers and matrix is achieved creating a blank similar to conventional glass mat thermoplastic (GMT). Overall, the process concept feasibility studies were considered a success, although the remaining technical hurdles in the list above need to be addressed, and are the subject of further trials scheduled in 2006. The key issue, however, remains throughput capability. Figure 4 shows material throughput requirements if the process were applied



Figure 3. TP-P4 chopped-fiber blank.

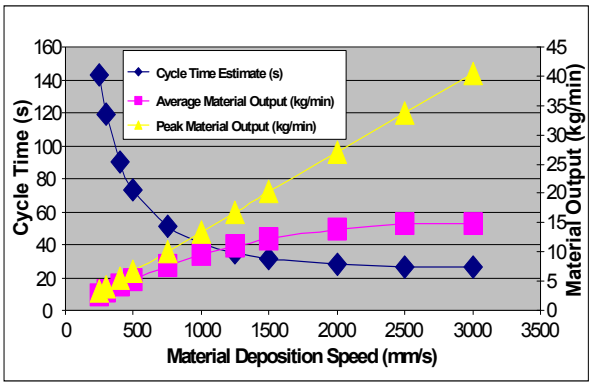


Figure 4. Material deposition vs. production cycle time.

to the production of a vehicle liftgate inner panel. In this example, the deposition speed in the TP-P4 cell is chosen in order to meet the specified annual production volume. For instance, at a high production volume of 100k units per year or more, a cycle time of 40s is desirable to prevent the need for a second manufacturing cell. Based upon these constraints, an average deposition rate of 10kg/min would be required, with a peak deposition capability of 15kg/min. The current TP-P4 is operating at about 10% of this capability. Hence, a parallel effort is focused on the design of new deposition equipment, capable of meeting the target throughput requirements. Fabrication and testing of the new equipment will commence if justified by the results of an economic evaluation of the TP-P4 process technology.

Assessment of Pre-Consolidation Methods: Following material deposition and stabilization, the requirement for a further processing step is anticipated in order to promote wetting of the fiber reinforcement by the polymer matrix. Hence, a variety of techniques are under investigation to determine the most cost-effective processing route. These include double-belt lamination, hot-air or infrared heating, and batch thermal cycling of matched tooling.

The function of the pre-consolidation method within the TP-P4 process is placed into context using Figure 5. In this chart, the material porosity is shown at different stages of processing. Since porosity has a direct impact on final part properties, it is important to track this parameter and determine the effect of processing on the final outcome. When determining the right choice of pre-consolidation method, two factors need to be considered. Firstly, a high level of porosity may be tolerated if a near-zero value can be achieved during the compression molding process. Secondly, the type of porosity, whether within or between fiber bundles (Figure 6), will have an effect on what is manageable during processing. Hence, it may not be required to drive down the bulk porosity to 2% or 3% during consolidation. Instead, the overall process needs to be considered, and the consolidation route selected, based upon process economics. Regarding the latter, results from consolidation studies, which are

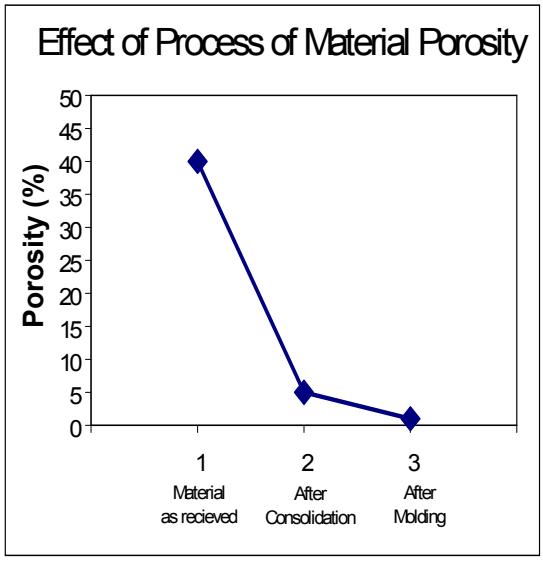


Figure 5. The effect of processing on material porosity.

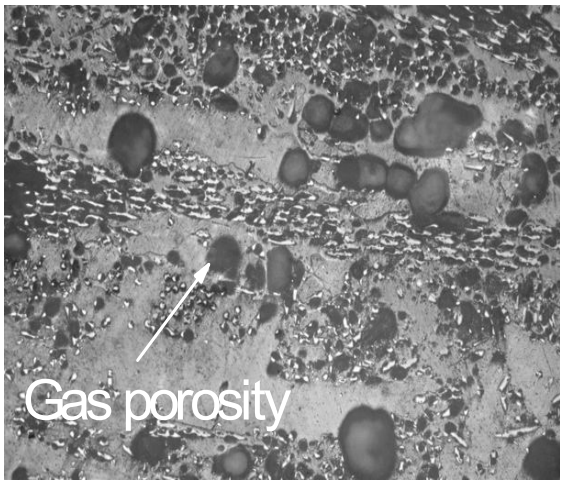


Figure 6. Porosity distribution within TP-P4 materials following pre-consolidation.

ongoing, will be used to specify equipment requirements for full-scale manufacture. Equipment pricing will subsequently be used as input into future cost analysis. The results of this analysis will be presented in a future report.

Economic Analysis: In parallel to process development studies, an analysis of the TP-P4 process has commenced to understand the process economics. The work is divided into three distinct phases.

Phase 1: Preliminary cost analysis based upon assumptions of TP-P4 capability
Phase 2: Experimental studies to corroborate process/equipment assumptions from Phase 1.
Phase 3: Refine cost model and update results based upon studies conducted in Phase 2.

During the first phase of the project, a baseline cost model was created for process technologies that are direct competitors to the TP-P4 concept. These models are now established and will provide a realistic assessment of the cost savings forecast using the new technology. In order to execute a comparative analysis, two target components have been selected as the focus of case studies (a SUV liftgate inner panel and a rear seat-back structure). To date, materials and process data have been gathered for input into the cost model. Outstanding data required to enable the first analysis are being sought with a first series of cost analysis results due by Nov 30th 2005.

TP-P4 Summary: A new, high-volume process technology for the manufacture of thermoplastic composite components is currently under development. The project, which received ACC Board of Directors approval in Q2 2005, commenced by using existing and modified process equipment to prove out initial concept feasibility. Preliminary process studies have demonstrated manufacturing capability and further process investigations are ongoing to improve production robustness and throughput capability. Further scale up of R&D activities will ultimately be contingent upon a positive economic assessment. Preliminary results of the process cost analysis are due by Nov 30th 2005.



Figure 7. Molded Baffling Installed on Underside of Preforming Tool

Focal Project 3 B-Pillar Preforming

In support of Focal Project 3 (FP3), preforming process development has been conducted to facilitate manufacture of B-Pillar Inner and Outer preforms. Preforming development efforts were performed using the revised B-pillar preforming tooling. In the revised tooling, the 'B' surface is the preform deposition surface and the 'A' surface is the consolidation surface. Although the preform and molding tool compatibility issue has been addressed with the revised preform tooling, the inverse orientation of the deposition surface has created additional issues during the material deposition process.

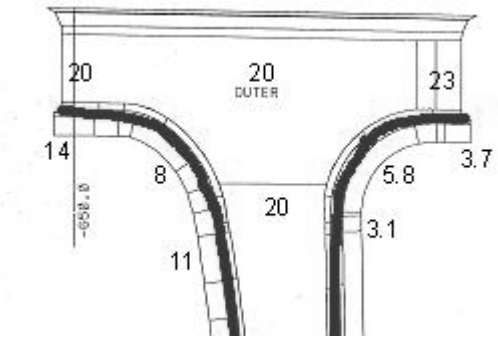


Figure 8. Air flow rates on outer B-pillar with baffles installed (the 2 dark areas).

In an attempt to resolve these issues, it was determined that baffles would be constructed and utilized on the underside of the preform screen. Baffling was constructed by trimming previously-molded B-pillars so that only the flanges and a section of the walls adjacent to the flanges remained. The baffling was installed on the underside of the tooling by fastening it to the existing screen every 250 mm (Figure 7). The baffling was initially installed flush against the screen so that airflow was essentially blocked in the 1.5 mm flanges and lower section of the vertical regions. However, some air flow did occur in these regions, but at much lower values.

Air flow rates were significantly reduced with the baffles installed, primarily in the 1.5 mm flange regions by as much as ten times based upon average anemometer readings (Figure 8). Air flow measurements were recorded as averages taken over ten seconds, with the anemometer held at approximately the same angle and spacing each time.

High air flow rates on the unbaffled tooling (Figure 9) combined with the orientation of flanges relative to thicker regions, encouraged fibers to congregate in the flanges while being chopped. This resulted in excess thickness in the flanges and made it difficult to fill the outside radii with proper fiber amounts. Areal density sampling data indicated regions exceeding 100% by volume for the target fiber volume fraction of 40% at a 1.5 mm thickness. Large areal density variability within the preform has led to subsequent molding issues including fiber-wash and dry regions in the parts. Excessive material density creates "dry spots" in the molded components. Also, fiber crush existed primarily in

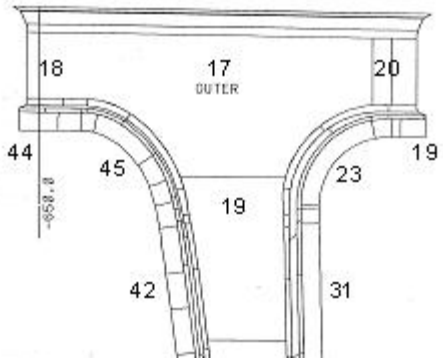


Figure 9. Air-flow rates on outer B-pillar without baffles.

flanges adjacent to thicker regions on the bottom 6 and 8 mm regions of outer and inner B-pillars, respectively.

After inspecting molded B-pillars, it was evident that the air baffles had positively affected preforming optimization efforts with respect to fiber density and dispersion. However, issues still remained such as high fiber density in the 1.5 mm flanges. Adjustments were made to the spacing of the baffles by placing flat washers (~1.5 mm thickness) between the baffles and preform screen. Several spacing ranges were evaluated during preforming. Optimal spacing, and, hence, optimum air flow values were achieved via a 3.0 mm spacing.

Several preforming process variables were also altered in an attempt to optimize the B-pillar preforming along with the air flow being optimized via baffling. Different fiber lengths (12.5, 15, 25, 30, 50, and 100 mm) were utilized throughout different locations. Tool Center Points (TCP) were modified to place the chopper gun closer to the screen in certain regions. Additionally, fiber output, robot speed, air ejector pressure, screen air flow, and robotic positions were modified to varying degrees in an attempt to optimize B-pillar preforms.

Minimal, positive results were realized through modifications to the above listed preforming process variables. Problems still exist with the quantity of fibers that can be placed in the flanges sections (1.5 mm) and radii relative to the amount that can be placed in the thicker regions. When fibers are placed in the flanges at or near the target fiber volume fraction (40%), very low fiber volume fractions will exist in the adjacent radii and thicker regions. However, if fibers are placed in the thicker regions and radii at the target fiber volume fraction, excess fibers will exist in the flanges that are adjacent to these regions.

The combination of near-target fiber volume fraction (40%) in the flanges and slightly reduced fiber volume fraction (30-35%) in the adjacent thicker regions seems to be the best compromise. However, this presents problems in the molding stage of manufacturing, such as fiber-wash, race-tracking, areas of very low fiber density, and areas of excess fiber density leading to fiber crush. Overall, there appears to be more compromise with the revised tooling than with the original tooling, despite baffling being installed on the revised tooling. This is due to the location of the flanges relative to the thicker regions combined with the tooling surface proximity to the flanges, which increases the air flow rates in the region and causes fibers to congregate into the flanges. Also, the flanges are located below the thicker regions, allowing gravity to have a greater effect on the congregation of fibers in the flanges. Optimization efforts are ongoing in an attempt to resolve these issues.

B. Development of Next-Generation Programmable Preforming Process

Co-Principal Investigator; Robert E. Norris, Jr
Oak Ridge National Laboratory
P.O. Box 2008, Oak Ridge, TN 37831-6053
(865) 576-1179; fax (865)-574-8257; e-mail: norrisrejr@ornl.gov

Co-Principal Investigator: Raymond G. Boeman
Oak Ridge National Laboratory
P.O. Box 2008, Oak Ridge, TN 37831-6053
(202) 586-0785; fax (202) 586-7409; e-mail: boemanrg@ornl.gov

Field Project Manager, Composites: C. David Warren
Oak Ridge National Laboratory
P.O. Box 2008, Oak Ridge, TN 37831-6065
(865) 574-9693; fax: (865) 576-4963; e-mail: warrencd@ornl.gov

Technology Area Development Manager: Joseph A. Carpenter
(202) 586-1022; fax: (202) 586-1600; e-mail: joseph.carpenter@ee.doe.gov
Field Technical Manager: Philip S. Sklad
(865) 574-5069; fax: (865) 576-4963; e-mail: skladps@ornl.gov

---

Contractor: Oak Ridge National Laboratory
Contract No.: DE-AC05-00OR22725

Objectives

- Develop the next-generation of low-cost fiber-preforming technologies based on programmable, robotic-controlled, directed chopped-fiber processes for the application of
  - low-cost carbon fiber
  - reinforced thermoplastics
  - hybrid glass-carbon
- Develop supporting technologies required to successfully implement the process technology including
  - preform characterization (e.g., permeability, areal density uniformity)
  - preform process modeling for process effects analysis
- Conduct parametric process studies to investigate fundamental process effects and establish process-property relationships.
- Conduct requisite molding investigations—experimental and through modeling—to elucidate relationship between preform characteristics and moldability.

Approach

- Establish a base research programmable, robotic preforming system for which advanced capabilities (e.g., new chopper designs) can be developed and evaluated.
- Establish a highly instrumented and controlled research molding capability to isolate and investigate the effects of process variables on moldability and mechanical properties.

- Develop new severing technology to facilitate the implementation of low-cost carbon, reinforced thermoplastics, and hybrid glass-carbon products.

Accomplishments

- Completed preliminary acceptance testing on the P4 machine at Aplicator with several recommended improvements to both hardware and software to be implemented prior to shipment.
- Upgraded laboratory utilities to provide dedicated 600A and plant air services to the P4 machine.
- Coordinated with shippers, customs, and plant facilities and equipment crews to get P4 system containers delivered to ORNL and placed in convenient staging locations, and assisted Aplicator crew on initial 3-week effort to complete system basic mechanical installation.
- ORNL personnel completed robotic-specific training at the ABB US Training facility.
- Hosted Aplicator personnel on return 3-week visit to complete installation, checkout, and training of ORNL personnel in operations, maintenance, and system programming. This completed activities necessary for contractual acceptance of the P4 system.
- Obtained various combinations of fibers and binders to establish materials baselines for comparison with previous and ongoing P4 work being conducted by the ACC. Also obtained materials to be used in establishing baseline for related permeability test development.
- Built a sensor test rig and evaluated numerous concepts and techniques for fluid detection sensors and associated data acquisition system in the in-plane permeability test machine. Chose best sensor candidate and set up lab-scale production to complete ~250 sensors for system operation.
- Completed radial flow permeability measurement system and associated controls and data acquisition systems specifically configured for the ORNL-developed sensor system. System checkout and initial permeability measurements to compare with literature values were being taken at the end of this reporting period.
- Initiated planning and identification of equipment requirements necessary to evaluate feasibility of laser severing technology.
- Developed requirements for research press, experimental mold, and injection-molding machine with assistance from the Automotive Composites Consortium Processing Group members. Requirements were utilized to prepare and issue RFQ's for this equipment. Evaluation of submitted bids to get this equipment under contract was being completed at the end of this reporting period.
- Previously developed general modeling approach was expanded to include a new algorithm that made possible quick simulation of tens of thousands of fibers, new algorithms for fast void discovery, an initial model for shaped substrate, and an initial model for mat compression
- Completed ORNL/DOE "Critical Outcome" milestone by demonstrating system functionality of the performing machine in a variety of trials including generation of various spray patterns, preform thicknesses and cut fiber lengths during testing.

Future Direction

- Complete procurement, installation, and integration of injection/compression press, general purpose mold with associated heating system, and resin injection machine.
- Upgrade laboratory structure and utilities as required to accommodate the equipment as described above.
- Demonstrate functionality and utility of the in-plane permeability measurement system by verifying data quality in comparison with data in the literature and conducting measurements on preforms made by simulated split-tow products of varying tow-size.
- Evaluate preform process models relative to physical preform characteristics and expand model capability as resources permit.

- Conduct initial preforming studies with low-cost carbon fiber and various forms incorporating reinforcement and thermoplastic matrix materials "co-processed" through the performing machine.
- Construct and test through-thickness permeability rig as funding and other resources permit.
- Initiate bench-top studies of advanced severing technology.

Introduction

Polymer-matrix composite materials offer a number of benefits in "lightweighting" of automotive and heavy vehicles, including greater stiffness and strength per unit weight than conventional materials, easier formability, less corrosion susceptibility, the ability to tailor properties to specific load requirements, and enhanced noise and vibration damping. However, widespread implementation of carbon-fiber composites, which offer among the greatest mass savings potential, requires lower cost materials and processes than are currently available. Advanced preforming processes offer opportunities to facilitate the widespread use of carbon composites.

Robotic-controlled, programmable, directed-fiber preforming processes have demonstrated exceptional value for rapidly preforming large, glass-reinforced, automotive composite structures. Due to their unique features and flexibility, and to their inherently low scrap rate, they are the most viable candidate processes for making affordable carbon-fiber preforms for a variety of structural automotive components. The Automotive Composites Consortium (ACC) has implemented the Programmable Powdered Preform Process (P4), with glass fibers, very successfully in its truck box program—Focal Project 2 (FP2). Original equipment manufacturers (OEMs) have transferred the technology to commercial applications such as the General Motors (GM) Silverado pickup box and the Aston Martin Vanquish body-side.

Analyses have indicated a potential for greater than 60% mass savings for a carbon-fiber-intensive body-in-white under the assumption of a thickness design constraint of 1.5 mm. The analyses also indicate the potential of saving an additional 15% if the thickness constraint is reduced to 1 mm. Unfortunately, evidence suggests that 1.5 mm may be a practical limit for liquid molding. However, thermoplastics preforms, in which the matrix and fiber are both deposited in the preforming step, offer a potential path to obtaining thinner sections, and consequently additional mass savings as well as greater potential for recyclability. Hybrid-fiber performs offer another potential benefit in terms of economics and property enhancement.

Approach

The objective of this project is to advance directed-fiber preforming processes to effect a further reduction in vehicle mass—relative to glass-fiber composites—while maintaining the economical advantages of net-shape preforming. The project will be executed in three focus areas corresponding to three materials systems: carbon fiber, reinforced thermoplastics, and hybrid glass-carbon fiber. Each focus area will consists of four main tasks concentrating on (1) materials developments, including new fiber product forms and binders; (2) machine developments, particularly new severing technology; (3) process developments, for example, to control areal density uniformity and preform anisotropy; and (4) development of supporting technologies such as modeling and preform characterization techniques. Furthermore, this project will undertake to develop sufficient understanding of fundamental aspects of the process and their effect on preform quality and mechanical properties in the molded part. As such, this project will support, augment, and facilitate the current and future research activities undertaken in the "Development of Manufacturing Methods for Fiber Preforms" project (see report 4.A).

Procurement and Installation of Preforming System

Central to this effort is the implementation of a research-oriented, robotic-controlled, programmable preforming system for installation in the polymer composites laboratories of the Metals and Ceramics Division at the Oak Ridge National Laboratory. This system establishes the base for future hardware developments as well as serving as a research instrument on which parametric process studies will

be conducted. A competitive solicitation was issued in April 2004, vendor selection made in May 2004, and a purchase order let in June 2004. Applicator System AB of Mölnlycke, Sweden, was selected to design and build the system.

The ORNL system was ready for initial acceptance testing and approval for shipment late in the first quarter of FY 2005. This review took place in at Aplicator's manufacturing facility in Sweden in December of 2004. ORNL had a technical and a contractual representative present at this review who were assisted by a technical representative from the Processing Group of the Automotive Composites Consortium. Although the technical review identified several software and hardware items requiring further adjustment and minor modification, the system was deemed ready for shipment upon completion of those items.

The system (see Figures 1 and 2) has a footprint of 9 by 15 m, contains a robot with 7° of freedom and can produce preforms up to approximate dimensions 1 m × 1.2 m × 1.8 m. On the head of the robot is mounted a chopper unit that incorporates the main chopper for spraying the reinforcement fibers and a surface veil chopper. Fiber length is adjustable on-the-fly in two ranges, 20–85 mm and 90–200 mm, as well as continuous. Fiber output is variable and can be as high as 3500 g/min.

Facility modifications and upgrades were required in order to install this machine in the Composites Processing Laboratory at ORNL.

Testing at Aplicator revealed that the machine actually required a single power line supply of at least 500A, versus projections as the machine was being constructed that the unit could be operated from reallocation and combining the capacities from two existing 400A supply lines already present in this laboratory. To provide the necessary capacity, a completely new 600A supply line had to be established in this laboratory and a new building transformer activated. Also beyond the original planning was the need for extensive logistical and rigging support in handling of the large sea-land containers in which the unit was shipped from Sweden. As planned, other support was provided for provision of plant air and overall coordination of activities.

In addition to installation of the P4 system itself and provision of utilities, the use of chopped fibers and powdered binders necessitates that the large air stream utilized to assist in direction, placement, and setting of the prefrom must be filtered prior to release of the air back into the environment. ORNL staff worked with Aplicator, ACC staff, and representatives of firms providing filtration units and installation services to choose an appropriate filtration unit and design this system to fit within facility constraints. Procurement, installation of the filtration unit (shown in Figure 3), and interface with the P4 machine was contracted to a construction firm approved by the building owner as a turn-key job. Also a part of the job was provision of a makeup air system since the filtered air is being exhausted exterior to the building and the building itself is already operating at a higher than desired negative air pressure environment.

During the initial multi-week visit by personnel from Aplicator to install the P4 machine at ORNL, initial system checkout and rudimentary training were conducted. The system met operational targets and items identified for improvement during the pre-shipment evaluation had been completed as desired. Having a basic understanding of the nuances of the ORNL machine and its ABB robotic system, operational personnel from ORNL were sent to robot-specific training conducted at the ABB US Training facility. With this training and some additional checkout activities completed at ORNL, Aplicator returned for more in-depth training and system checkout. During the interim, some minor hardware and software difficulties had been identified. This training has now been completed and the technical difficulties rectified.

As a second, but no less important focus of this follow-on visit, Aplicator worked with ORNL to develop general purpose programs for making the flat plaques that will serve as baseline for much of the initial ORNL work in establishing the machine operational envelope. These programs provide an easily modifiable platform for beginning the development work projected for working with new

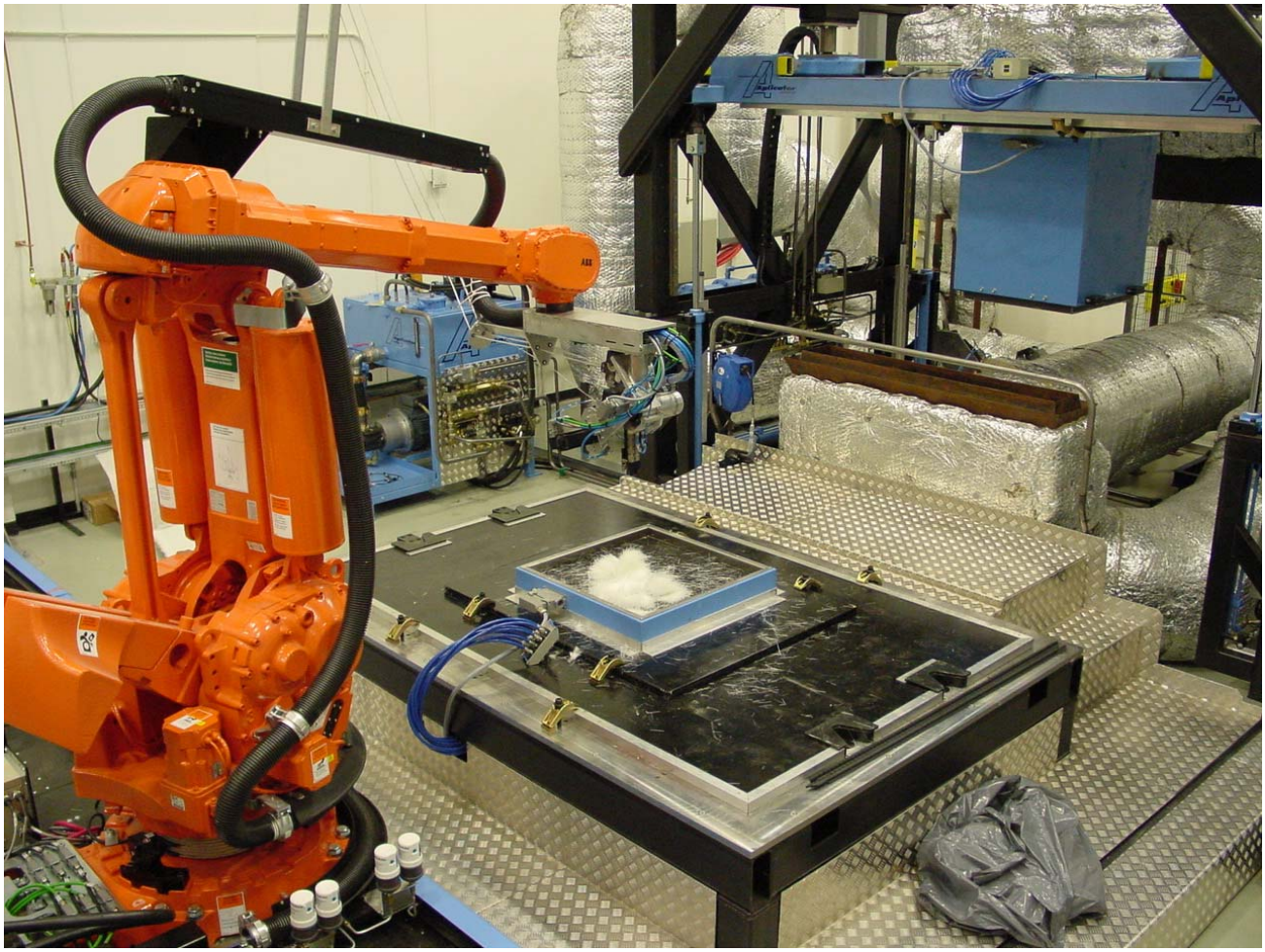


Figure 1. ORNL's new robot-controlled and actuated, programmable preforming system.



Figure 2. Fiber delivery system and operating controls for ORNL's preforming system.



Figure 3. External filter system for ORNL's preforming system.

materials and processes in advancing the state-of-the-art for performing technology using this type of equipment. In fact, these programs were indeed utilized with minor modification in order to meet an ORNL/DOE "Critical Outcome" milestone by demonstrating system functionality in a variety of trials including generation of various spray patterns, preform thicknesses and cut fiber lengths during testing. Future work will also include modifications to the base system in facilitating advanced fiber product forms, including low-cost carbon fiber, reinforced thermoplastics, and glass-carbon hybrids.

Procurement of a Press, Mold, and Injection Machine

Key to being able to demonstrate the advances achieved in performing technology is the ability to demonstrate that these advances translate into improvements in actual completed composites. The best way to effect this demonstration is through injection of resin into the preform and compression of the preform and resin into a composite in the manner in which this would be accomplished in actual composite manufacturing.

During this period, efforts were initiated to identify the most appropriate equipment necessary to do this on a research basis. ORNL staff worked with members of the Automotive Composites Consortium's Processing Group to quantify process equipment requirements and initiate activities necessary to procure a research press, general purpose mold, and injection machine. These requirements were turned into formal RFQ's for designing and building these systems, which were issued to companies that had been identified through ORNL and ACC interactions as having potential to meet or exceed all performance targets. The intelligent-leveling press (see Figure 4) is being designed to accommodate various molds and molding processes and will be instrumented above routine standards in order to provide more process details in experimental research. Nominal pressing capacity is 750 tons. The general purpose plaque mold (see Figure 5) will be designed for instrumented experiments using Structural Reaction Injection Molding (SRIM), Compression Molding of Reinforced Thermoplastics, and Sheet Molding Compound (SMC) processes. This equipment will

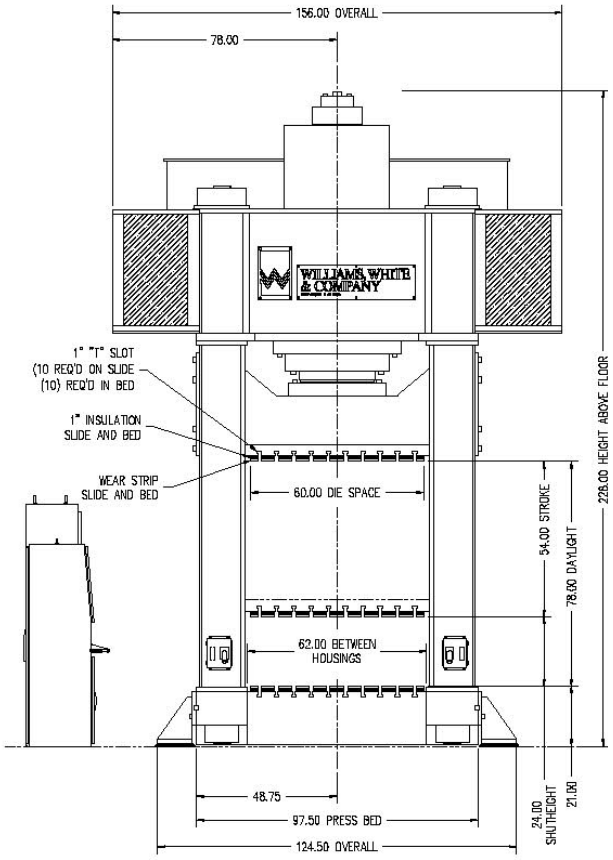


Figure 4. Intelligent-Leveling, 750-net-ton, Injection/Compression Press being procured by ORNL.

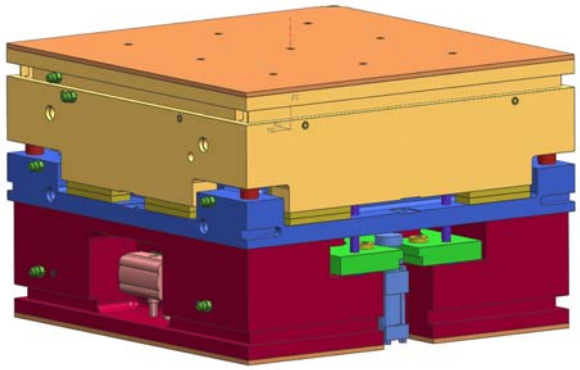


Figure 5. General Purpose Flat Plaque Mold for SRIM, SMC, and Thermoplastics.

allow ORNL to demonstrate preform advances while further investigating advances in the various molding processes themselves.

At the conclusion of this reporting period, the bid packages have been received and the orders will be placed in early FY 2006. It is anticipated that the

mold will be completed in the early portion of the second quarter of FY 2006 while the press will be completed late in the third quarter or early in the fourth quarter of FY 2006. Both will be shipped to ORNL and installed as soon as possible after initial acceptance testing at the vendors. A completion date for the injection machine is dependent on vendor selection, which has not been completed at this time. Also to be determined is need for any structural upgrades needed for the facility to support this equipment. An engineering study is planned for early FY 2006 to quantify these needs and provide any necessary design details along with a cost estimate.

Permeability Measurement

It has been found that injection-compression offers distinct advantages over injection-only liquid molding for the infiltration of high-volume fraction preforms. Consequently, both the in-plane permeability and the through-thickness permeability affect the moldability of the part. Accordingly, two novel research instruments are under development that will provide experimental data to characterize the three-dimensional permeability of the fiber mat preform.

Work continues on the development and implementation of an in-plane rig (see Figure 6) with a flow capacity of 0.33 gpm and a fluid capacity of 2 gal. It can be operated in either constant-flow or constant-pressure mode under feedback control. Maximum pressure and fluid viscosity are 100 psi and 5 poises, respectively. Both platens are instrumented with sensors—a total of 218 sensors—to monitor the flow-front with resolution of 0.25 in. The initial development focused on a sensor concept developed through subcontract to Prof. Richard Parnas at the University of Connecticut. It consisted of a recessed insulated conductor that generates a voltage when the conductive fluid bridges the sensor and the metallic plate. Although the conductive sensor appeared to work adequately in the University of Connecticut laboratory, it has been problematic when implemented in the system at ORNL. Although some effort was continued to improve the accuracy and reliability of the conductive sensors, it was decided to reopen the sensor selection to a variety of concepts identified by the staff at ORNL.

A smaller-scale "sensor test rig" (Figure 7) was fabricated in order to facilitate evaluation of several sensor concepts in a simpler environment than the full-scale test rig. Based on tests of a number of sensor concepts in this rig, it was decided to focus further development and implementation on a novel concept for a temperature sensor that would demonstrate fluid contact by a significant change in temperature caused by the cooling of the test fluid passing over its surface. This potentially patentable concept was successfully evaluated in the sensor test rig and a full complement of sensors for the in-plane test rig were manufactured and installed in the full-scale test rig.

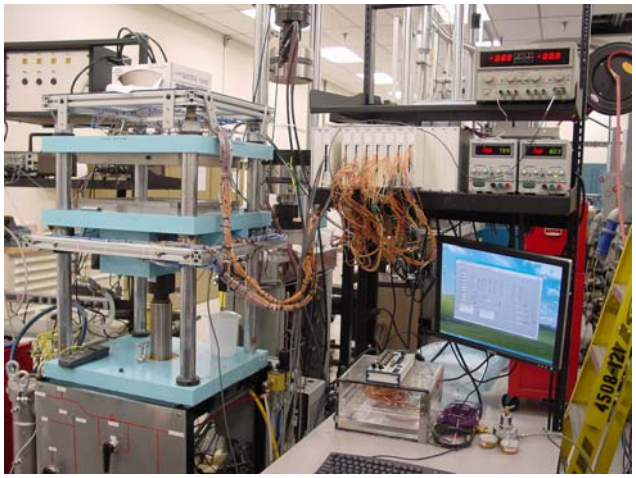


Figure 6. Radial Permeability Test Rig showing associated data acquisition and monitoring station.

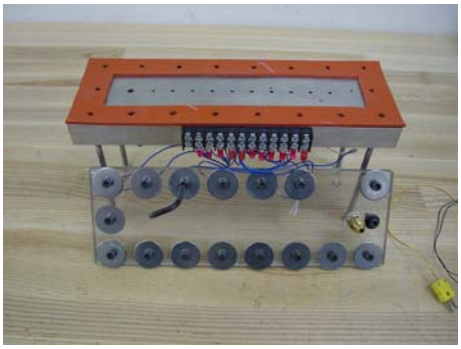


Figure 7. Test rig developed to evaluate sensors that will identify moving fluid front.

A data acquisition and control system has been developed based on National Instruments' PXI hardware and LabVIEW software. Stand-alone program modules have been written to evaluate sensor performance, to conduct the permeability experiments, to analyze the collected data and calculate permeability value, and to review the experiment at reduced speed. The modules that monitor the sensors have been developed for both conductor and thermocouple-based sensors. An example of the real-time display is shown in Figure 8.

An analysis module that takes the elliptical flow front and calculates the in-plane components of the permeability sensor has been developed from expressions provided by Prof. Parnas. Full characterization of the analysis module is now underway following resolution of sensor reliability and accuracy issues.

A through-thickness rig has also been designed and fabrication of most hardware is underway as a lower priority task. Maximum pressure and viscosity are the same as the in-plane rig. The through-thickness rig has a flow capacity of 8 gpm. Through incorporation of a dynamic seal, preform thickness can be changed quickly for successive measurements to evaluate the influence of fiber volume fraction on permeability. This system will be completed and demonstrated as personnel and budgetary resources allow.

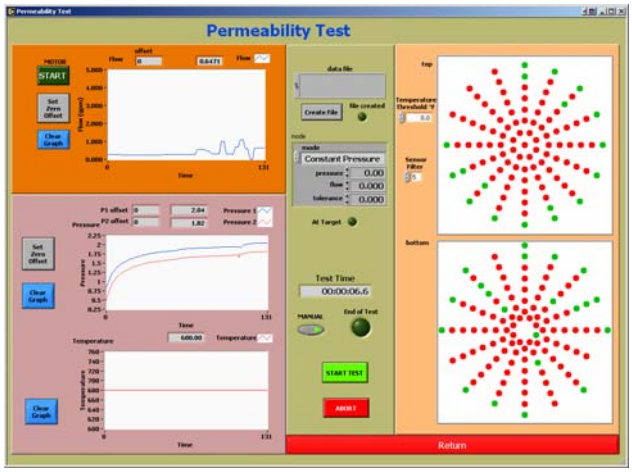


Figure 8. Permeability Test Rig Display showing radial progression of flow front indicated by a change in dot color.

Modeling of Fiber Deposition

A C-based program is under development to analyze the effect of process variables on preform characteristics. The program, FNSim, will be used to evaluate preforms in terms of measures such as fiber run length, fiber connectivity, distribution of voids, etc. FNSim, when correlated with permeability data and areal density measurements, will provide an understanding of the effect of process variables on resulting preforms and their "moldability." Recent advancements to FNSim have included efficiency improvements such that it now can be used on desktop computers as well as enhancement of the previously developed general modeling approach by addition or improvement of many of the capabilities. Examples of these enhancements include a new algorithm that makes quick simulation of tens of thousands of fibers possible, new algorithms for fast void discovery, an initial model for shaped substrate, and an initial model for mat compression. Further development of the model will be continued as program data is available to support model expansion and verification.

Fiber-Severing Technology

Due to significant differences in the physical properties of various reinforcement fibers as well as their available product forms, chopping technology that has been successful for glass fibers systems has demonstrated less-satisfactory results for the carbon-fiber products that are currently available. It is expected that similar results will occur for reinforced thermoplastics and hybrid glass-carbon products. Accordingly, consideration is given in this project to identifying alternative severing technology. A literature and patent search was undertaken to assess promising technologies for bench-top investigation. Possibilities identified include mechanical-based, laser-based, CO_2 pellet, liquid nitrogen, water-jet, and ultrasonic. Based on the information available in the literature and consideration of project team experience in related activities, laser-based choppers appear to offer the most promise.

During this period, effort was initiated to identify equipment and supporting tasks necessary to evaluate and demonstrate the potential for laser severing. Plans are under development to set up a laser system in the laboratory and experiment with a

carbon-fiber tow at the bench scale to define the more detailed laser parameter and control requirements in order to be able to cleanly sever a moving carbon-fiber tow at the speeds required for utilization in the P4 system. Initial work will be done in static tests to determine beam width, power levels versus time, and other necessary information before moving to low speed tests, and then tests at speeds more representative of actual fiber deposition rates. With this background, plans are then to scale up the hardware for on-machine experimentation and demonstration. In addition to severing carbon fiber, future work will address other reinforcing fibers, as well as fibers used as binders, and blends of reinforcing and binder fibers.

Summary

A new project to develop the next-generation programmable preforming process and provide supporting technology to existing performing developmental work was initiated in FY 2004. The research will continue to build on past development and application of directed-fiber preforming processes, namely those of the Programmable Powdered Preform Process (P4), to extend the process to new material systems. Developments are expected to facilitate the use of low-cost carbon fiber, reinforced thermoplastics, and glass-carbon hybrid materials as effectively as is the current state-of-the-art with glass. Utilizing these materials is expected to lead to further reductions in vehicle mass in a more cost-competitive scenario than is currently possible. A preforming system, which will serve as the base for hardware and associated technology developments, was completed and installed in the polymer composites laboratories at Oak Ridge National Laboratory in the second quarter of FY 2005.

The base system is designed around glass-fiber product forms. A literature review has identified alternate severing technologies that may prove more effective for "chopping" the carbon, reinforced thermoplastics, and glass-carbon hybrids under investigation in this effort. During this period, effort was initiated to identify equipment and supporting tasks necessary to evaluate and demonstrate the potential for laser severing.

Efforts are underway to procure the most appropriate press, mold, and injection equipment necessary to demonstrate the advances achieved in performing technology through actual experimental composite manufacturing. ORNL staff has worked with members of the Automotive Composites Consortium's Processing Group to quantify process equipment requirements and write specifications necessary to procure this equipment that will allow ORNL to demonstrate preform advances while further investigating advances in the various molding processes themselves. At the time of this report, evaluation of the bid packages is being completed in order to get the equipment on contract in early FY 2006. Delivery of the experimental mold is anticipated in the second quarter of FY 2006 while delivery and final acceptance of the press is anticipated for the fourth quarter of FY 2006.

Development continued on two novel permeability rigs designed to characterize the preforms' resistance to resin flow during the molding process. The in-plane rig has been constructed and experiments initiated. Issues with initially-provided conductive-sensor reliability and accuracy have been identified, and appear to have been resolved with development and implementation of an entirely new temperature-based sensor concept. The through-thickness rig has been designed and hardware components purchased. A data acquisition, control, and analysis system is continuing to be implemented and fine-tuned for the radial rig and will be used in completion and troubleshooting experiments with the through-thickness rig. Together, the two rigs will provide the three-dimensional permeability data for the comparison of preformed materials as well as development of mold-flow models.

Modeling of the fiber deposition process continues at a low level through the development of an in-house code. The program, FNSim, will be used to evaluate preforms in terms of measures such as fiber run length, fiber connectivity, distribution of voids, etc. Results will be correlated with permeability data and areal density data to assess the affect of process parameters on preform quality as well as the mechanical properties of molded parts. Collectively, the technology under development in this project will advance low-cost processing on two fronts. First, it will provide the opportunity to

employ additional materials in the net-shape preforming process, which is expected to lead to additional mass reduction and/or better performance. Second, it will provide the requisite tools to evaluate the affect of process parameters on the utility and performance of preforms and molded parts.

C. High Volume Processing of Composites

Principal Investigator: Becky Joitke
DaimlerChrysler NA, Advance Vehicle Engineering
CIMS 489-00-00, 1030 Doris Road, Auburn Hills, MI 48326
(248) 754-9761; fax (248) 754-9720; e-mail: rlj@daimlerchrysler.com

Technology Area Development Manager: Joseph A. Carpenter
(202) 586-1022; fax: (202) 586-1600; e-mail: joseph.carpenter@ee.doe.gov
Field Technical Manager: Philip S. Sklad
(865) 574-5069; fax: (865) 576-4963; e-mail: skladps@ornl.gov

---

Contractor: U.S. Automotive Materials Partnership
Contract No.: FC26-02OR22910

Objective

- Develop and demonstrate high-volume manufacturing (molding) processes to produce lightweight composite automotive components.
- Provide process development support to Focal Project 3, B-Pillar molding (ACC080).

Approach

- Benchmark current thermoplastic processes.
- Develop new research programs to study high-volume composite manufacturing processes.
  - Determine the technical feasibility of thermoplastic P4 (TP-P4) for chopped-fiber lay-up.
  - Initiate carbon-fiber sheet molding compound (SMC) program with suppliers.
  - Investigate the use of natural fiber as a lightweight and low-cost alternative to glass fiber.
  - Develop a cost model to determine feasibility of new technologies and the viability of existing technologies.
  - Establish gateways to determine program duration.
  - Propose programs to the Automotive Composites Consortium (ACC) Board of Directors for approval.

Accomplishments

- Completed the design of experiments (DoE) to assess the effects of glass type, glass length, thickness, de-mold time and surface veil of plaques created via the long-fiber injection (LFI) method in partnership with Bayer.
  - A LFI plaque tool was constructed based on an existing reinforced reaction injection molding (RRIM) tool at Bayer but incorporating shear edges and a show surface finished to SPI A2.
  - Based on extensive benchmarking of typical class "A" exterior substrates, the ACC Processing (ACCP) Team identified a "Surface Acceptance Standard" linked to specific quantitative techniques for use in future studies.
- New programs initiated:
  - Develop P-4 chopper gun technology to produce tailored hybrid blanks from a combination of glass, carbon and natural-fiber reinforcements for subsequent hot-flow compression molding.
  - Partner with Fiberforge® to validate materials and processes for application to high-volume automotive production.
  - Investigate DRIFT technology with various fiber reinforcements in polymer systems for structural and semi-structural applications.

- Develop manufacturing processes for carbon-fiber SMC body panels amenable to cost-effective high-volume applications.
- Investigate compatibility of natural-fiber reinforcements with polymer systems for structural and semi-structural applications.
- Develop understanding of soy-based polymers in conjunction with glass and carbon-fiber reinforcements.

Future Direction

- High-volume processing of lightweight structural thermoplastic composites.
  - Characterize panels fabricated with Fiberforge® technology and proceed with optimizing the polymer systems to enhance performance and appearance.
  - Investigate DRIFT technology with various fiber reinforcements in polymer systems for structural and semi-structural applications, including partnership with the ORNL carbon-fiber line.
- Carbon-fiber SMC body panels for exterior and interior applications:
  - Resolve material and processing issues, including physical property variation, mold flow, low-strength knit lines, and surface appearance
- Natural-fiber reinforcements and soy-based polymers:
  - Characterization results will be used to refine testing methods for determining durability properties of natural-fiber composite systems.
  - Optimize fiber surface treatments and polymer systems to minimize the moisture absorption of natural-fiber composite systems.
- TP-P4 project to be encompassed under ACC040.

Introduction

The purpose of this project is to develop the high-volume composite molding technologies germane to automotive production. Previously, this project mainly supported ACC Focal Project 3 (ACC080); liquid molding processes (see report 4.D). Structural reaction-injected molded (SRIM) technology was utilized to mold carbon-fiber preforms of reduced section thickness. Currently, all molding support of Focal Project 3 is being undertaken through its own efforts. Therefore, a new direction has been defined in this project (ACC115), to collaborate with suppliers to develop low-cost, high-volume molding processes compatible with the material property and processing requirements of the automotive industry.

The first of these new programs was initiated in 2004 with Bayer to investigate the feasibility of their long-fiber injection (LFI) molding process. Personnel from the ACC and Bayer collaborated in a study of LFI of polyurethane to assess its potential for achieving a Class "A" automotive finish, and to characterize its structural capability.

Efforts to reach the Class "A" surface requirements, detailed in prior progress reports, were not fully successful due to air entrapment. Solutions for venting the tool and adding vacuum to the system were explored. Considerable reductions in air entrapment were achieved with the vacuum, and the team also found that sections near the lifter area, where the LFI was particularly compressed, were exceptionally free of defects. This program is now completed and published in the ACC Technical Report TR-P05-04.

Five new programs have been proposed, approved, and initiated: 1.) The P4 process, developed within the ACC, is being studied for producing tailored hybrid blanks with a combination of glass, carbon and natural fiber reinforcements. These blanks are to be used for subsequent hot-flow thermoplastic compression molding. 2.) Collaboration with Fiberforge® has been initiated to determine the feasibility of robotic placement of uni-directional fiber tapes in desired orientations, to produce locally-reinforced blanks at high speed. 3) DRIFT®, a patented pultrusion process, will be studied for its ability to support the project objectives and its compatibility. 4.) A program has been initiated to resolve issues with producing carbon-fiber SMC body panels for exterior and interior applications. Finally, 5) natural fibers and soy-based polymers are

being studied for their compatibility with current systems, and their physical characteristics, with the intent of adding the desired feature of sustainability to the other objectives.

To support these initiatives, purchase of two plaque tools, one for compression molding and one for injection molding, was proposed and approved. These molds can be used at various suppliers and national laboratories to create plaques for mechanical testing using various thermoplastics and reinforcements. The compression-molding tool will be delivered 4Q 2005. The injection tool will be completed 1Q 2006.

Thermoplastic P4

Introduction

Examples of thermoplastic composites are widespread within the automotive industry. This is driven in most part by the design flexibility and weight savings realized through the use of low-density polymers. However, material price is a constant consideration and has often prevented the application of thermoplastics to structural components due to the necessity to attach supplementary reinforcements, which in turn drives up cost. The processing concept which is described in the following sections claims to offer two major benefits. First, components are fabricated using commodity raw materials in an attempt to reduce piece cost. Secondly, the process is designed to take maximum advantage of material properties to allow further design optimization. The latter translates into the elimination of secondary reinforcements which provides opportunities for further weight reduction. As a thermoplastic derivative of the P4 Process (Programmable Powdered Preforming Process), the new process is referred to as the TP-P4 process.

Process Concept

Figure 1 shows the basic process concept. In Station 1, reinforcement fiber and polymer are dispensed, using a pre-programmed deposition cycle, onto a perforated screen. Fibers are held in position using air flow through the screen. A stabilization cycle follows to create a rigid blank which can be easily removed and transferred to the next station. The blank is subjected to a pre-consolidation process (Station 2) to promote fiber-bundle wetting. Depending on the consolidation method, the blank may require a further pre-heating step before being placed as a charge into a shear-edge compression-molding tool. The press closure in Station 3 results in hot-flow compression molding of the charge, and formation of the final part shape.

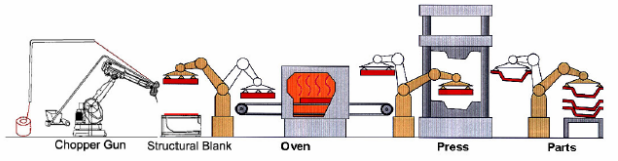


Figure 1. TP-P4 Process Concept.

Notable differences between the original P4 process and the new thermoplastic-based derivative include restricting the fiber deposition to a 2D blank as opposed to a 3D net-shape preform. Furthermore, both the fiber and matrix materials are deposited in the new process, compared to the original P4 process which required a subsequent liquid molding operation. Potential benefits of the process are listed below. The engineering and cost analysis, which form part of the research plan, will address each of these items to validate each of the associated claims.

TP-P4 Process Benefits

- Lower raw material costs and no blank cutting costs.
- Tailored blanks retain fiber length equivalent to glass mat thermoplastic.
- Blank size and shape can be customized for specific applications.
- Local uni-directional fibers can be integrated into the blank for enhanced stiffness and strength. Plus, fibers can be orientated to meet local stiffness requirements.
- Areal density can be adjusted to meet flow condition and press tonnage capabilities.
- Thinner sections are possible where appropriate.
- Option for use of hybrid reinforcement (glass/carbon/natural fiber) within a single blank.
- Applicable to a broad range of thermoplastics applications.

Economic Analysis

An analysis of the TP-P4 process and associated costs has been undertaken in conjunction with Swiss

Federal Institute of Technology (EPFL) Lausanne, Switzerland. This study will also compare the TP-P4 technology to other more conventional thermoplastic technologies. The work is divided into three distinct phases.

Phase 1: Preliminary cost analysis based upon assumptions of TP-P4 capability.

Phase 2: Experimental studies to corroborate process and equipment assumption used in Phase 1.

Phase 3: Refinement of cost model and update of results based upon studies conducted in Phase 2.

During the first phase of the project, baselines cost models have been created for process technologies that are direct competitors to the TP-P4 concept. These models are now established and will provide a realistic assessment of the cost savings forecast using the new technology. In order to execute a comparative analysis, two target components have been selected as the focus of case studies (a SUV liftgate inner panel and a rear seat back structure). To date, materials and process data have been gathered for input into the cost model. Outstanding data, required to enable the first analysis, are being sought with a first series of cost analysis results due by Nov 30th 2005.

The TP-P4 program initiated under the umbrella of ACC115; however, due to the interrelation of this program and the P4 technology, all processing studies have been undertaken under ACC 040. The results of the initial processing studies are therefore presented in the ACC040 Annual Report (see report 4.A).

Fiberforge®

The Fiberforge® process is comparable to the TP-P4, in that it eliminates additional material and process sequences. In the case of the Fiberforge® process, unidirectional tapes are robotically placed to enhance structural performance of specific areas of the components produced. Figure 2 represents an overview of the process. Initial meetings have been held with Fiberforge® to develop a work plan, roles and responsibilities, and a cost analysis. Plaques made via Fiberforge® process, utilizing nylon 6 (PA6) with carbon-fiber reinforcement, are being submitted to the ACC Materials Working Group for analysis and characterization.

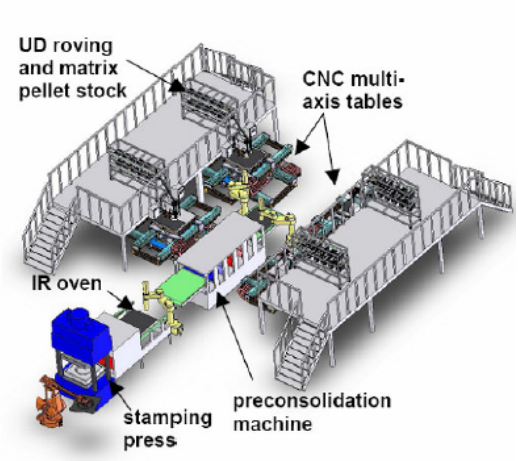


Figure 2. Fiberforge® process diagram.

DRIFT®

In FY 2005, ACC115 began work in conjunction with Oak Ridge National Laboratories (ORNL) to address the compatibility of Directly Reinforced Fiber Technology (DRIFT®) with low-cost carbon-fiber program objectives. DRIFT® is a patented pultrusion process by which tapes, chips, pellets, sheets, or woven fabrics are produced, which then are capable of feeding a variety of molding processes.

Objectives for the studies include optimizing the fiber types, percentages, and types of polymer systems to achieve needed levels of mechanical performance and appearance. Important process characteristics such as low warpage and reduced material system cost will be explored. Test specimens and components will both be tested for characterization and durability for use in structural and semi-structural applications.

Carbon-Fiber SMC

The objectives of this program are to develop high-performance, cost-effective, carbon-fiber SMC materials and associated processing techniques for high-volume automotive components. Initial collaborative meetings with Meridian Automotive Systems have been undertaken to determine future program direction. Experience drawn from Meridian's involvement the DOE *21st Century Truck*

Program was reviewed as well as possibilities of utilizing the ACC-funded Toho/Tenax carbon-fiber splitting technology (see report 4.A).

Natural Fibers and Biocomposites

In FY 2005, work began in conjunction with Pacific Northwest National Laboratory (PNNL) to explore opportunities with natural fibers as reinforcements, and soy-based polymers. The objectives were fourfold:

- Investigate the compatibility of natural-fiber reinforcements with polymer systems, for usage in exterior and interior applications of both structural and semi-structural purpose.
- Optimize fiber surface treatments and polymer systems to enhance compatibility and performance, as well as minimize moisture absorption.
- Develop and conduct characterization and durability evaluations on both test specimens and components.
- Develop the understanding of soy-based polymers with glass and carbon-fiber reinforcements.

Test plaques utilizing a commercially available soy-based vinyl ester resin, reinforced with glass and carbon fiber, were compression-molded at Ashland Chemical. The plaques will be characterized for a direct comparison with petroleum-based resin systems that have been identically reinforced.

In addition, soy-based polyurethane plaques have been provided by Pittsburg State University for characterization; those tests are in progress.

Tool Acquisitions

One of the obstacles identified with studying the consistencies of processing various materials has been the inability to make test plaques. To address this concern, the Board of Directors approved the proposals to build an injection-mold plaque tool and a compression-molding plaque tool.

Each tool was designed to produce a 610 mm x 610 mm (24” x 24”) plaque using a wide variety of materials and be capable of multiple thicknesses. The individual tools can be shipped to various molders to compare samples made from the same tool but with optimum process conditions. In addition, pressure sensors and thermocouples were specified for several positions in each tool so that process data can be collected and compared between trials in a consistent fashion.

In support of numerous ACC projects, a new shear-edge compression tool has been designed and commissioned to enable production of 610 mm x 610 mm flat panels. Test panels, produced using the new tooling, will support process studies and provide a useful source of materials for mechanical testing. A description of the new tooling follows, with key features and capabilities listed below. A 3 D view of the exploded assembly is shown in Figure 3. Tool commissioning trials are complete and the final sign-off is scheduled for November 15th 2005.

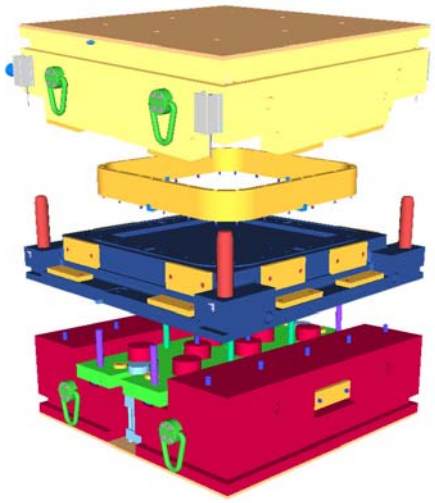


Figure 3. New shear-edge flat panel compression mold.

Basic Tool Description

- Designed for SMC and thermoplastic compression molding.
- Single cavity mold for molding experimental flat plaques, 610 mm x 610 mm (24" x 24") between 1.00 mm and 5.00 mm thick.
- Mold to have external vacuum shroud which should engage with mold open 75 mm and hold 710 mm Hg pressure.
- 6 pressure and 6 temperature transducers each on top and bottom part surfaces.
- LVDTs (displacement transducers) at tool corners to provide position detail for vacuum

system activation and experimental parameter correlation.
- Capability to heat and cool cavity and core to 180°C +/-2°C across part/tool surface using hot oil as the heat transfer median.
- 400 grit finish on core side. 320 draw polish finish on shear edges and other surfaces contacting part.

The injection-molding tool was designed by a team of ACC members and incorporated many "lessons learned" on prior projects. The stringent requirements included options of producing test panels from 2.0 mm to 5.0 mm in thickness, in increments of 0.5 mm, easy access to multiple sensors at prescribed positions, and capability of withstanding high clamp forces without flashing.

The quotation process concluded in the 3rd quarter of 2005 with the selection of Service Mold Inc. Detailed designs are being finalized. Future work includes issuing the purchase orders, proving out the tool once it is completed, and molding plaques from material made with the DRIFT® process for testing. The full requirements list of available on USCAR's VROOM website (www.uscar.org.).

Conclusions

ACC115 explores different approaches to the high-volume processing of composites. Redirection took place early in 2005 as the LFI project with Bayer completed, providing valuable knowledge for future investigations into surface optimization. Since the redirection, five new projects were commissioned, each with the objective of researching ways to save weight in automobiles, at the volumes unique to the industry. Natural fibers and biocomposites also hold future possibilities of less reliance on petrochemicals and greater recyclability.

D. Automotive Composites Consortium Focal Project 3 Composite-Intensive Body Structure

Principal Investigator: Stanley A. Iobst
GM Research & Development
MC 480-106-710
30500 Mound Road
Warren, MI 48090-9055
(586) 986-1223; fax: (586) 986-1207; e-mail: stanley.a.iobst@gm.com

Field Project Manager, Composites: C. David Warren
Oak Ridge National Laboratory
P.O. Box 2009, Oak Ridge, TN 37831-8050
(865) 574-9693; fax: (865) 574-0740; e-mail: warrencd@ornl.gov

Technology Area Development Manager: Joseph A. Carpenter
(202) 586-1022; fax: (202) 586-1600; e-mail: joseph.carpenter@ee.doe.gov
Field Technical Manager: Philip S. Sklad
(865) 574-5069; fax: (865) 576-4963; e-mail: skladps@ornl.gov

---

Contractor: U.S. Automotive Materials Partnership
Contract No.: FC26-02OR22910

Objectives

- Design, analyze, and develop the technology to build a composite-intensive body-in-white (BIW), offering a minimum of 60% weight savings over steel at a cost close to that of steel, while meeting manufacturing, assembly, and performance targets.
- Provide a focus for bringing together technology developed by each of the Automotive Composites Consortium (ACC) working groups through emphasis on carbon-fiber-reinforced composites and the use of hybrid materials, faster manufacturing processes, design optimization including crashworthiness, and rapid joining methods.

Approach

- Optimize the design and complete the finite element analysis for the carbon-fiber composite BIW (Phase 1 - completed).
- Build one part of the BIW (the B-pillar portion of the body side) to demonstrate high-volume processing methods (Phase 2).
- Develop and model a structural test for the B-pillar.

Accomplishments

- Initial preforming, molding, and bonding development of glass-fiber-reinforced B-pillar is completed.
- The final optimization of B-pillar preforming and molding is being completed with glass prior to the carbon-fiber work.
- Fixtures for the B-pillar 3-point bend and torsion tests were designed and built.
- Verified the B-pillar structural testing protocol with glass reinforced inners, outers, and bonded assemblies.

- A predictive model for B-Pillar test modes was completed
- Flow modeling studies for the carbon-fiber B-pillar and the full body side were completed

Introduction

Focal Project 3 (FP3) is intended to be a design and processing study to develop a cost-effective manufacturing scenario for carbon-fiber-intensive composite vehicle structures. All of the materials, manufacturing processes, and fabrication and assembly methods to be considered in this project are to be consistent with the following overall objectives:

- High-volume production techniques (>100,000 units per year)
- Cost parity with equivalent steel structures
- Overall 60% mass reduction relative to steel BIW structure
- Structural performance equivalent to or better than that of a steel structure
- Dimensional tolerance equal to or better than that of steel

We continue to develop the manufacturing processes necessary to demonstrate the body side. Preforming and molding trials continue with the B-pillar tools. Other major activities during this period were the structural testing and modeling of the B-pillar. An injection/ compression mold-filling model was also developed. In addition, a series of carbon-fiber plaques were molded as part of the carbon-fiber development program.

Program Redirection

It became apparent at the beginning of the year that insufficient resources were available within the FP3 program to generate the necessary matching funds to support the full body-side tooling and molding program. It was decided that the B-pillar portion of the body side, illustrated in Figure 1, would be the preforming and molding demonstration project for the Focal Project 3 program. Concurrent with the change in the program scope, the program leadership passed from Nancy Johnson to Stanley Iobst.

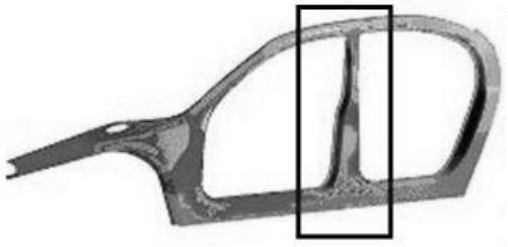


Figure 1. B-pillar section of body side structure.

The ACC is formulating other material and process programs, and it is likely that some of these processes will be demonstrated with the FP3 B-pillar mold. The resources released from the FP3 program are being redirected into the other programs within the ACC Processing Group, and there is actually an increase in the ACC membership to support these new programs.

B-Pillar Preforming Development

In support of FP3, preforming process development has been conducted to facilitate manufacture of B-pillar inner and outer preforms.

Experimental Preforming

Preforming development efforts were performed on the ACC/DOE preforming machine using the revised B-pillar preforming tooling. In the revised Gen-2 tooling, the 'B' surface is the preform deposition surface and the 'A' surface is the consolidation surface. Although the preform and molding tool compatibility issue has been addressed with the revised preform tooling, the inverse orientation of the deposition surface (relative to the original tooling) has created additional issues during the material deposition process.

High fiber density exists in 1.5 mm regions, mainly the flange regions, immediately adjacent to thicker (3, 4, 6, 8 mm) and subsequently higher fiber content sections of the component. A particular region exhibiting this issue on the B-pillar outer preform is shown is Figure 2.

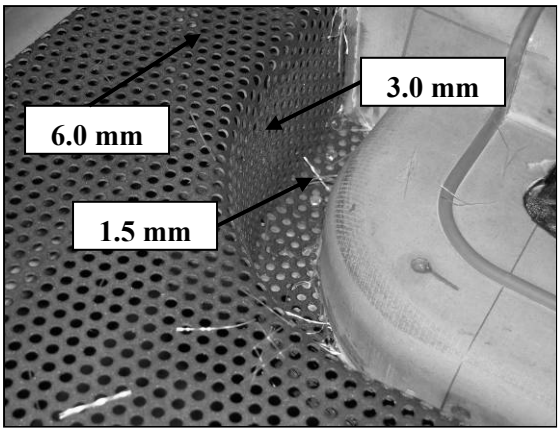


Figure 2. B-pillar outer preform region exhibiting material distribution issues in the 1.5 mm area.

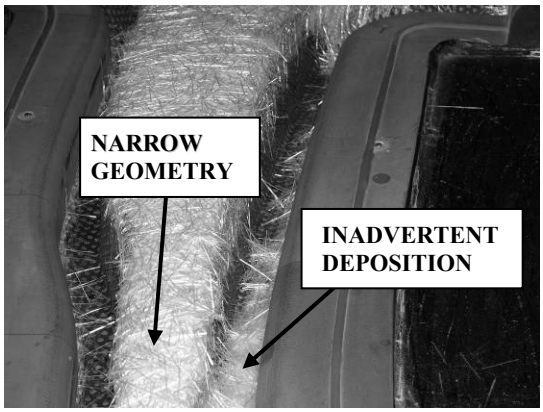


Figure 3. Inadvertent material deposition in 1.5 mm region (B-pillar outer).

This issue is more evident on the B-pillar outer preform; however similar issues also exist on the B-pillar inner in the inverted tooling condition. Despite extensive robotic programming efforts on both the B-pillar outer and inner preforms to alter the robotic positions and path, this issue could not be remedied. Areal density sampling data indicated fiber volume fractions far exceeding the specified fiber volume fraction of 40% even though fiber deposition routines for these regions were deleted from the overall robotic preforming program. A majority of the excess material is deposited in these regions during deposition routines associated with other sections of the component, unrelated to the 1.5 mm flange section (Figure 3).

This is exacerbated depending upon the thickness requirement and part geometry for a region in close proximity to the 1.5 mm regions. For example, narrow part geometries relative to the material deposition pattern will yield higher material concentrations in the associated flange section as the material is inadvertently projected to these regions due to the part geometry (Figure 2). When incorporating the deleted fiber deposition routines for the aforementioned sections of the B-pillar, areal density sampling data suggest greater than 100% by volume for the target fiber volume fraction of 40% at a 1.5 mm thickness.

In an attempt to improve material distribution, additional experiments were conducted via modifications to preforming process variables other than the robotic positions and path. Fiber length, tool center point (TCP) distance, and air velocity through the screen were identified as important preforming process variables. Although material distribution improvements were made through modifications to the above process variables, the magnitude was insufficient to improve conditions in the molded component. This was evident in subsequent molding trials where both fiber wash (insufficient material) and dry spots (excessive material) were still present despite extensive experimental preforming efforts.

Preforming Conclusions

Despite experimental preforming efforts using the revised B-pillar preform tooling, a fully optimized preform has not yet been realized. This may be attributed to a myriad of previously mentioned issues, all leading to inadequate material distribution within the preform. After making insufficient preforming progress with the revised screens, preform development reverted to the original screens.

Based upon the experimental preforming conducted to date on both the original and revised preform tooling, a 1.5 mm part thickness at a fiber volume fraction of 40% may not be feasible and possibly beyond the current process capability. Focal Project 3 B-pillar preforming development efforts are ongoing using the ACC/DOE preforming machine at the National Composites Center in Dayton, Ohio to obtain an optimized preform.

Molding Development

Carbon-Fiber Plaque Molding

A series of preforms using Fortafil (now TohoTenax) fibers were molded. These contained different numbers of splits per roving and were molded over a range of fiber volumes. At a given fiber volume, there was only a small difference in the in-mold pressure between preforms of differing fiber splits. This was unlike the findings from the earlier Hexcel fiber study where the in-mold pressure increased with preforms of smaller fibers.

B-Pillar Molding

There were no full-scale molding trials for molding optimization during this period. The B-pillar molding during first part of the year was to support the evaluation of preforms produced on the Gen-2 screens. It was determined that while some of the preforming problems were solved with the new screens, there were other issues with the new design. Therefore, it was decided to complete the B-pillar development work using the original screens.

After an interruption for the carbon-fiber plaque work and maintenance on the press and preformer, B-pillar molding development has resumed. At this point the preform for the inner panel is nearly optimized and improvements to the outer preform are underway. A critical area of the outer preform has been identified where too much fiber will prevent the mold from fully closing (Figure 4). Heavy fiber loading in other areas of the preform did not have this same detrimental effect.

During the maintenance period, the control system for the French Oil press at NCC was reprogrammed to give a more linear press closing profile. The press closing rate was essentially uncontrolled and varied depending on the resistance to closing. This is demonstrated in Figure 5, which shows the separation between the upper and lower mold halves during the compression stage. The old closing profile was a variable rate event, while the modified closing has a nearly linear position vs. time profile. The improved closing profile will make the press a better tool for the continuing molding trials.

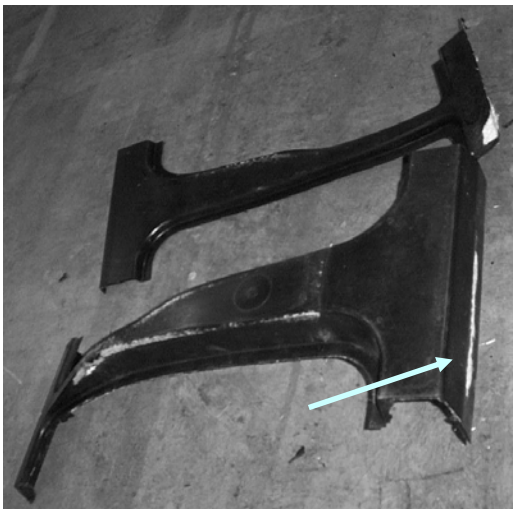


Figure 4. Arrow shows dry glass area in B-pillar where heavy fiber loading holds mold open.

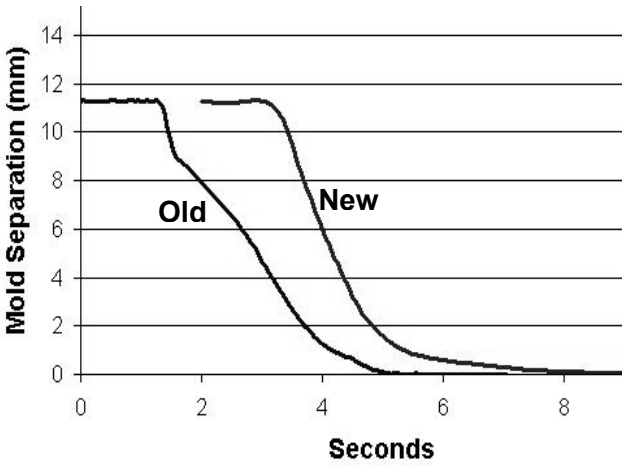


Figure 5. Comparison of old and new, more linear, closing profiles for the NCC press.

Flow Modeling

Prof. Suresh Advani of U. Delaware was contracted to develop a flow model for the molding of carbon-fiber preforms by the injection-compression process used in FP3. The intention was to develop and confirm a flow model with the B-pillar and then extend it to the full body side. This would be used as a design tool to assist in optimizing the location of the injection locations for body side molding.

The flow model has been completed for the B-pillar for both glass and carbon preforms. The predicted filling profile is very close to the observations made with short shots. The body side flow model has been completed for a single injection point, with the full, multiple-injection model to follow.

The mold filling of the full body side was modeled in a similar fashion to the B-pillar. The mold was assumed to be partially open with a gap between the preform and the upper mold half, with the resin injected into this gap (the injection step). This resin is initially pooled on top of the preform as shown in Figure 6 for an actual B-pillar molding. In the compression step, advancing resin front was modeled as the closing mold forced the resin through the preform. In this simulation the resin is considered to first be pooled in the gap between the preform and the mold, next the resin is forced into the preform, and finally the resin is forced throughout the preform, filling the mold. Figure 7 shows the model prediction at a point partway through the compression stroke, where the mold has contacted the preform, but not yet compressed it. At this point, the preform under the original resin pool is fully saturated, but the adjoining areas are only partially filled, and the flow has not yet reached the extreme ends of the mold. This model will be used to determine where additional mix heads need to be located to completely fill a complex part such as the body side.

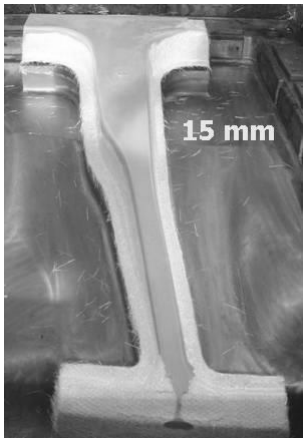


Figure 6. Resin pooled on top of B-pillar preform.

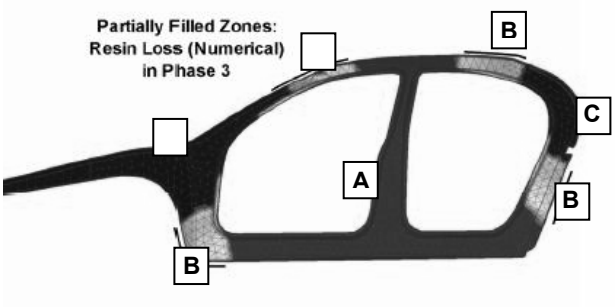


Figure 7. Flow model simulation of partially filled preform. (A) Completely filled preform, (B) partially filled cells, (C) empty preform.

B-Pillar Testing

A combined structural testing and structural modeling effort was established to evaluate the quality of the B-pillar. The B-pillar had not initially been modeled as an independent structure separate from the entire body structure. The structural testing program was therefore set up to define test cases to be modeled, and then provide experimental data to verify the structural model. This model would also predict the response of the structure to local fiber content variations, and also predict the difference between glass and carbon reinforcement.

The approach was to categorize potential defect type, location and magnitude, and then to determine which of the potential tests (loading conditions) would highlight the effects of these defects, and determine which tests are most sensitive to defects. A limited set of physical tests would then be down-selected, and the tests conducted. The tested bonded parts would be available for further analysis to evaluate any damage occurring during the test loading.

The 3-point bending and torsion loading cases were selected for the testing and cases to be modeled. The testing was performed at Defiance Testing & Engineering located in Troy, Michigan. Test fixtures were designed and built for these cases, and testing completed for the glass B-Pillar inners, outers and bonded assemblies. Figure 8 shows a B-pillar outer clamped into the 3-point bend fixture and ready for test.

A total of four B-Pillar inners, four bonded assemblies and four outers were tested in 3-point bend and torsion. It should be noted that the maximum load/torque was determined by loading the first sample of each test near its limits. Audible cracking of the inner panel was detected at 3.6 kN and for the bonded assembly at 2.4 kN. Therefore,

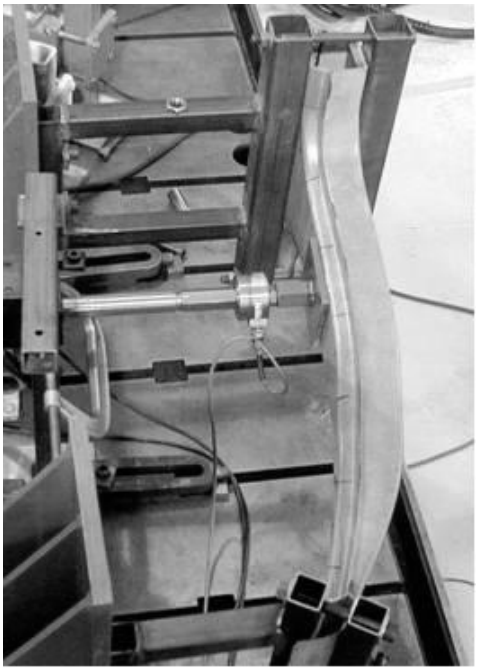


Figure 8. Bonded B-pillar in 3-point bend test fixture.

test loads for the additional parts were limited to 1.8 kN. An example of 3-point bend force-deflection curves for the inner, outer, and bonded assembly is shown in Figure 9. Results from the B-Pillar evaluation testing were used in the ACC FP3 modeling effort to evaluate the models used to predict component stiffness, with those results discussed below. The testing of the glass-reinforced B-pillars was judged to be very satisfactory, and the same procedure will be applied to the carbon B-pillars.

B-Pillar Structural Analysis

For the B-Pillar torsion and bending test cases, finite element analysis (FEA) was carried out using commercial FE code LS-DYNA. The objective was to identify the potential problems in structural analysis and to study the effect of fiber volume fraction on torsion and bending responses.

Variation in thickness and fiber volume fraction of the B-Pillar presents a challenge for FE modeling. The variation in thickness can be modeled via the use of solid elements. However, shell elements are preferred for full vehicle analysis. To develop a FE modeling strategy pertinent to full vehicle analysis, FE model was constructed with shell elements.

Thickness variation was digitized at 0.5 mm interval. Each shell element was assigned a thickness. As an example, Figure 10 presents assigned thickness variation for B-Pillar inner panel.

Two methods were examined to represent the material variation: (1) assume a nominal constant fiber volume fraction (volume %) and (2) divide the B-pillar into different zones based on its approximate fiber volume % and use a stress-strain curve according to its volume %. The material was assumed to be isotropic and modeled with a piecewise linear plasticity model (MAT24).

Torsion and bending simulations were carried out for inner, outer and bonded B-pillar. Torsion simulations were in good agreement with the experimental results in deformed shapes (Figure 11) as well as in responses (Figure 12). For bending cases, simulations predicted a much stiffer response. The FE model was modified with different boundary

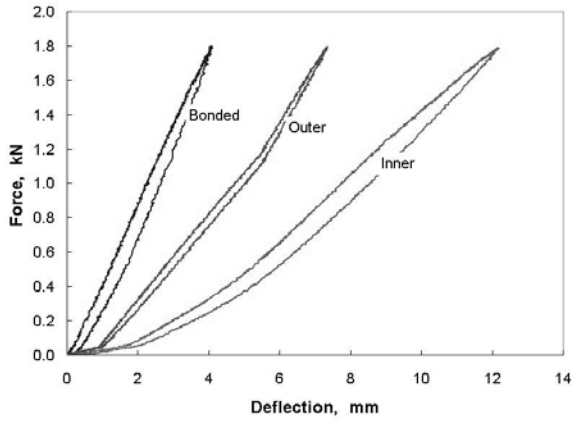
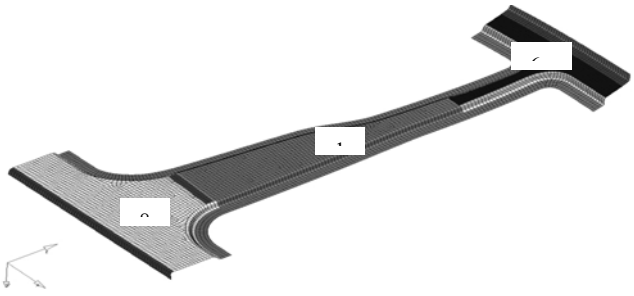


Figure 9. Example of force vs. deflection curves for the bonded B-pillar and the separate inner and outer panels.



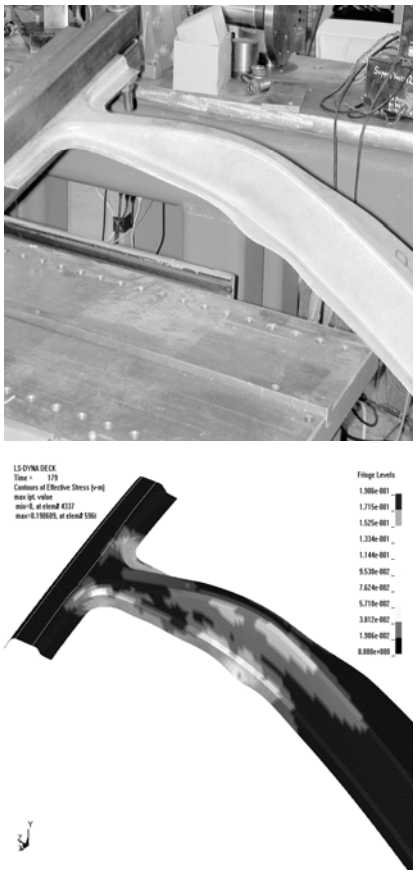


Figure 11. Deformed B-pillar outer in torsion test and simulation.

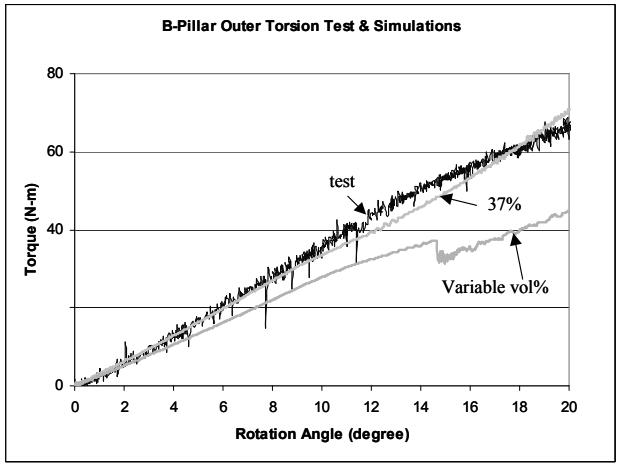


Figure 12. Comparison of simulations with experimental results for B-pillar outer torsion.

conditions and the results indicated that the resin nuggets left on the B-pillar surface prevented the piece being properly clamped in bending test. It is recommended that resin nuggets need to be removed in future tests.

Simulations results indicated that while the FE models with variable fiber volume % gave better correlations, the results of the models with a nominal constant fiber volume % were also acceptable. For the load cases analyzed, when compared to those with variable fiber volume %, the stiffness ratios were in the range of 1.1-1.2 and 0.866-0.95 for simulations with a constant fiber volume % of 37% and 30%, respectively.

The adhesive bond was modeled via tied nodes between the shell elements and the method appeared to be efficient. The width of the bondline was found to have a significant effect on the response (Figure 13). Examination of the hand applied bond line showed it to average less than the bond flange width of 25 mm. Using a bond width of 16 mm in the model gave good agreement with the experimental results.

Summary

Complete optimization of the B-pillar preform has turned out to be more difficult than originally envisioned. With the limited amount of suitable

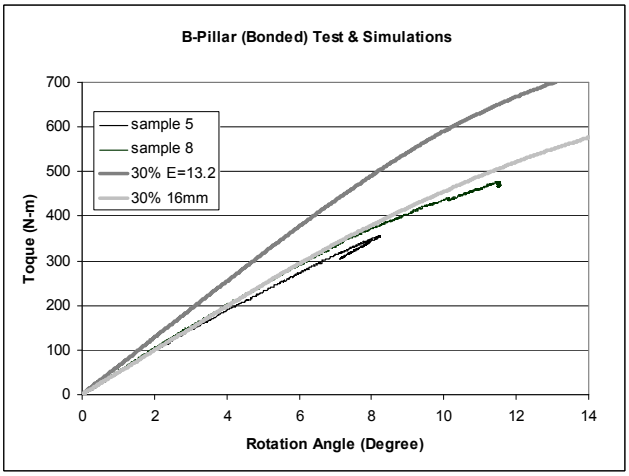


Figure 13. Comparison of experimental results with simulations with 25 mm and 16 mm bond width.

carbon fiber for preforming, it is necessary to optimize the preform with glass prior to the carbon-fiber molding.

The preform optimization is nearing completion and carbon-fiber molding will start in the near future. Most of the remaining items needed for completing the project are in place: the bonder has been tested, the structural testing demonstrated, and the structural model developed.

External Publications

Stanley Iobst, Jeff Dahl, Libby Berger, Jessica Schroeder, Dan Houston, and Mike Mao, "Automotive Composites Consortium B-Pillar Molding Program," Presented at Society of Plastics Engineers Automotive Division, September 12-14, 2005, Troy, MI, and published in the Conference Proceedings.

ACC Technical Reports

Stanley Iobst, "Automotive Composites Consortium Carbon Fiber-SRIM Plaque Molding," May 2005.

E. Low-Cost Test Methods for Advanced Automotive Composite Materials: Creep Compression Fixture

John M. Henshaw
The University of Tulsa
600 South College Ave.
Tulsa, OK 74104
(918) 631-3002, fax:(918) 631-2397, e-mail: john-henshaw@utulsa.edu

Greg Baxter
The University of Tulsa
Mechanical Engineering, KEP L185
600 South College Ave.
Tulsa, OK 74104
(918) 631-2521; e-mail: greg-baxter@utulsa.edu

Ron Cooper
Ford Motor Company
Ford Research Laboratory
MD 3135/RIC Bldg.
P.O. Box 2053
Dearborn, MI 48121
(313) 322-3424; e-mail: rcooper3@ford.com

ACC Project Contact: Dan Houston
Ford Motor Company.
20000 Rotunda Dr., MD 3182 SRL, P.O Box 2053
Dearborn, MI 48121-2053
(313) 323-2879, fax: (313) 323-0514, e-mail: dhousto2@ford.com

Technology Area Development Manager: Joseph A. Carpenter
(202) 586-1022; fax: (202) 586-1600; e-mail: joseph.carpenter@ee.doe.gov
Field Technical Manager: Philip S. Sklad
(865) 574-5069; fax: (865) 576-4963; e-mail: skladps@ornl.gov

---

Contractor: U.S. Automotive Materials Partnership
Contract No.: FC26-02OR22910

Objective

- Design and develop low-cost, reliable fixtures and methods for the characterization of compression creep behavior of automotive composites with and without environmental exposure. Confirm results generated by the new fixture with those from conventional testing systems.
- Incorporate the fixtures and methods in the above objective into industry-standard test methods for automotive composites.
- Using results of short-term tests, develop predictive models for lifetime property degradation.
- Investigate the fundamental damage mechanisms in polymer-matrix, carbon-fiber and E-glass composites as a function of specific, varied mechanical loading with concurrent environmental exposure.

Approach

- Design and develop a compact compression creep test fixture system and confirm its performance.
- Use the new fixture system to develop a compression creep database.
- Develop a standard procedure for compression creep testing using the new system.

Accomplishments – FY 2005

- Final fixture prototype developed and extensively tested.
- Test fixture meets all design and project requirements.

Future Directions

- Continue to evaluate and document fixture performance – final tests in advance of project end date.
- Document standard test procedures.
- Project end date: 12-31-2005

Introduction

Because of insufficient information on the long-term durability of lightweight composite materials, reliable methods and models requiring relatively short-term tests are essential to composites achieving their full potential in the automotive industry. The purpose of this project is to develop simple, low-cost fixtures and methods for the creep and creep-rupture characterization of automotive composites, and confirm the in-situ creep test fixture results with those obtained using conventional testing methods.

Initial Design Concept for the Compression Creep Fixture

Several design specifications were targeted when developing the initial prototype fixture during the first year of this project. The creep compression fixture must simulate in-service loading conditions by allowing the specimen to be exposed to various automotive environments. The fixture must also be lightweight, compact, relatively inexpensive, and portable compared to industry standard dead-weight creep testing fixtures. Lastly, the data generated by the fixture should be of design quality while comparing favorably to ORNL (Oak Ridge National Laboratory) and literature data. A successful fixture will also be corrosion resistant, capable of testing ASTM standard compression coupons, and exhibit no signs of specimen buckling (less than 5% bending).

Prototype 3A Creep Test Results

Test results with the third-generation prototype (Prototype 3) were extremely encouraging, as reported in detail in the 2004 annual report. Previous Prototype 3 test results involving glass-fiber composites in creep compression generally exhibited less than 5% bending. All previous results from prototypes 1 to 3 can be viewed in the 2003 and 2004 annual reports. Modifications made to Prototype 3, resulting in Prototype 3A, have mainly been done to allow the Prototype 3A to be adapted to a variety of external-loading machines (as noted above).

Summary of Prototype 3A Design Detail

The third-generation prototype currently under development utilizes a four-pin design where the specimen fits inside two compression blocks that are pressed toward each other by load-reversing pins (Figure 1). The ends of the pins are threaded into a connecting bracket that, in turn, mounts to either a clevis joint on a spring-loaded moment arm, Figure 5 (a fixture developed in a previous project), a standard load frame (not shown), or a custom load-multiplying creep-rupture fixture developed in a previous project (Figure 2). Prototype 3A is capable of testing compression specimens that are 5 inches long, which is the ASTM standard length. Earlier prototypes utilized an undersized specimen. The prove-out testing continued with evaluating performance of unreinforced poly-vinyl chloride

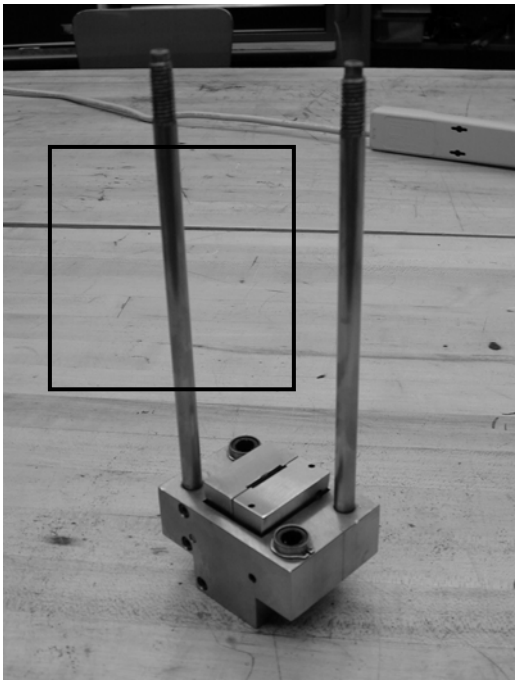


Figure 1. Disassembled creep compression fixture showing one of two load blocks, two of four load-reversing pins, and slot for inserting specimen (inset shows assembled fixture)

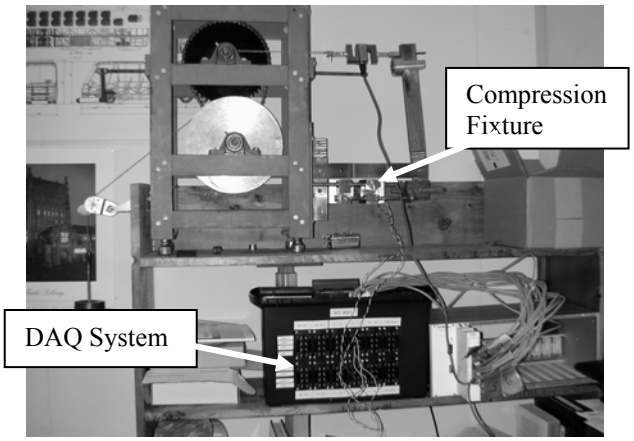


Figure 2. Custom load-multiplying frame with Prototype 3 compression fixture

(PVC) specimens. Results from these tests, while generally good, produced some unexpected results.

At the beginning of some tests, the initial percent difference in strain was inconsistent from one test to another on the same material. It was determined through repeated testing that, in the assembling of the fixture and installation of the specimen, critical variances sometimes occurred.

Since the Prototype 3A compression fixture is made up of many components, differences in assembly sequence were investigated. When disassembled, the fixture is comprised of 6 critical components. When assembled, there are 16 ways in which these pieces can fit together to make the same fixture. It was found that of these 16 configurations, only 4 produced favorable bending results. This was determined by manually compressing a PVC specimen and, as the wedges slid into the compression blocks, visually inspecting bending of the specimen.

Using the 4 best setup configurations, creep compression tests were conducted on PVC and polycarbonate compression specimens. Since these plastics lacked fiber reinforcement, bending loads were immediately evident. Figures 3 and 4

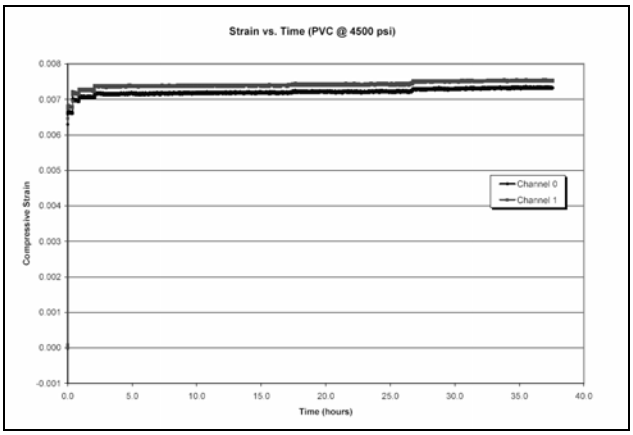


Figure 3. Plot of compressive strain for PVC at 4,500 psi for 38 hours

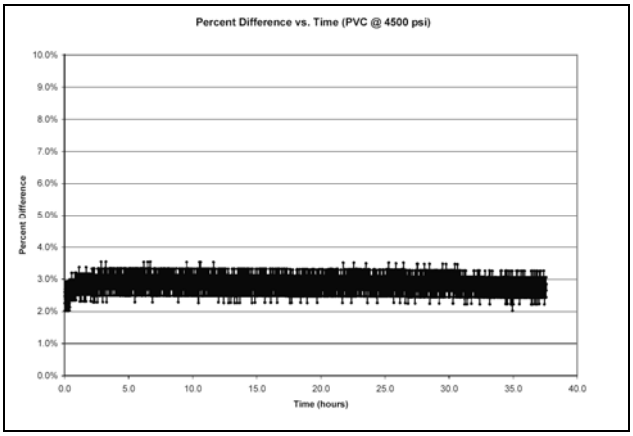


Figure 4. Plot of percent difference for PVC at 4,500 psi for 38 hours

demonstrate the creep compression performance of PVC under 4,500 psi for 38 hours. Figure 3 shows the total strain on a PVC specimen as a function of time, while Figure 4 shows the percent difference in strain between the two sides of the specimen throughout the duration of the test. Note that the percent difference in strain varies between about 2.5% and 3.5%, well under the maximum of 5%. The creep compression test from Figures 3 & 4 was conducted using the compression fixture in the creep-rupture fixture as shown in Figure 2. This creep-rupture fixture is capable of outputting a load 180 times its input. A hanging weight is applied as the input and the load-multiplier arm pulls on the reverse-loading pins in tension causing the compression blocks to come together, putting the specimen wedged within under compression. Because the weight is allowed to hang, the loading is constant.

Constant-Load Testing

As noted above, Prototype 3A is identical to Prototype 3 except for a few modifications to allow it to fit in a variety of external loading frames, such as the tensile creep constant-tress frame (Figure 5). Two modifications were incorporated into the new fixture to simplify loading the sample in the frame and fitting the fixture into the limited working envelope of the constant-stress frame. Pins to secure the cross-head to the loading rods instead of bolts were used to ease loading the fixture into the frame and eliminate uneven loading that can occur if the bolts are not threaded to identical positions on each loading rod. A bolt was added external to the original workspace of the constant-stress fixture to secure one of the two cross-heads. The addition of this bolt allowed the fixture to be more easily loaded into the frame.

A test of the fixture's ability to maintain a constant load was conducted because both modifications created changes to the original fixture loaded in the creep-rupture frame. This was accomplished by replacing the test specimen with a compression load cell (Figure 6). The load cell was compressed to a 506 lbf clamping load and held for 500 hours. The load remained within 10 lbf of 506 lbf (within ±2%) after 500 hours (Figure 7).

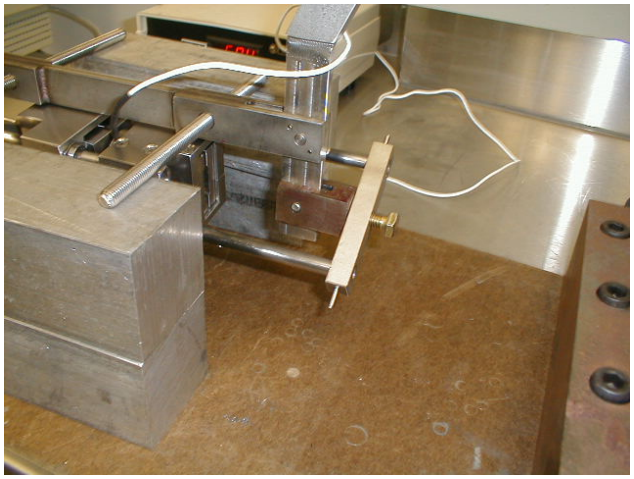


Figure 5. Prototype 3A creep compression fixture modifications to fit in the constant-stress frame

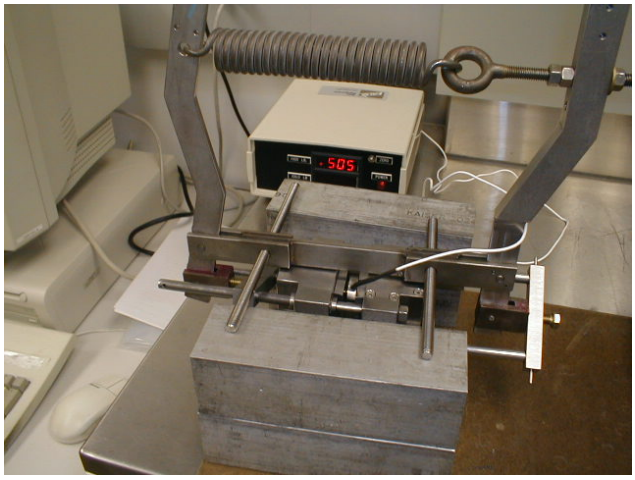


Figure 6. Prototype 3A creep compression fixture static load test

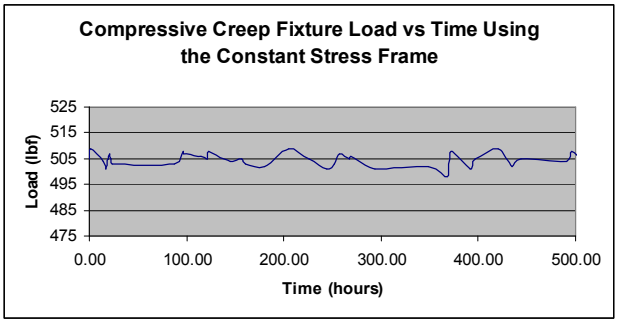


Figure 7. Prototype 3A creep compression fixture load vs. time for a static load of 506 lbf

On-Going/Future Work

- Conduct further creep compression tests in an MTS floor load-frame, comparing results from the two existing fixtures.
- Evaluate creep compression fixture under elevated temperature testing.
- Construct a testing procedure with assembling instructions.

Conclusions

- Controlling assembly of the compression creep fixture is important in terms of ensuring the quality and repeatability of compression test results.
- The current fixture prototype meets design requirements including maximum allowable bending during test (percent difference in strain less than 5%).
- The current fixture maintains applied loads within 2% over long-term testing.

F. Interphase Analysis and Control in Fiber-Reinforced Thermoplastic Composites

Principal Investigator: Jon J. Kellar
Department of Materials and Metallurgical Engineering
South Dakota School of Mines and Technology
501 E. St. Joseph Street
Rapid City, SD 57701-3901
605-394-2343, 605-394-3369, jon.kellar@sdsmt.edu

Technology Area Development Manager: Joseph A. Carpenter
(202) 586-1022; fax: (202) 586-1600; e-mail: joseph.carpenter@ee.doe.gov

---

Contractor: South Dakota School of Mines and Technology
Contract No.: DE-FG02-04ER46117

Objectives

- Develop the science underlying the formation and effects of transcrystalline regions in carbon-fiber-reinforced thermoplastic-matrix composite systems.
- Exploit the understanding developed from the research described above to allow controlled tailoring of the interphase transcrystallinity for specific applications.
- Analyze processing parameters in new thermoplastic-matrix composite technologies, specifically the DRIFT (**D**irect **R**einforcement **F**abrication **T**echnology, Southern Research Institute) and the P4 (**P**rogrammable **P**owered **P**reform **P**rocess, Department of Energy (DOE)/Oak Ridge National Laboratory (ORNL) processes.
- Generate composites with tailored interphases for specific applications of laminates produced by the DRIFT and P4 processes in the FreedomCAR and other DOE initiatives in lighter weight vehicles.

Approach

- Choose matrix materials relevant to the FreedomCAR and DOE automotive lightweight materials initiatives.
- Characterize the chosen matrix materials with respect to mechanical properties and crystallinity.
- Determine the thermodynamic and practical adhesion between the chosen matrix materials and carbon fibers. The carbon fibers will be both sized and unsized.
- Identify and control the presence and size of transcrystalline regions in the matrix material adjacent to the carbon fibers.
- Manufacture laminates using the DRIFT and P4 processes having controlled transcrystalline regions.
- Perform mechanical testing, including tensile testing, impact testing and indentation testing of the laminates having controlled interphases.

Accomplishments

- Demonstrated transcrystalline layer formation for Kevlar and pitch-based carbon fibers and polypropylene matrix.
- Measured matrix crystallinity by differential scanning calorimetry
- Designed an apparatus to allow for controlled, resistive, carbon-fiber heating for thermodynamic adhesion and transcrystallinity experiments.

  - 2 students traveled to University of Alabama-Birmingham to meet with Dr. George Husman and view the DRIFT system in place at that university and to obtain DRIFT samples.
  - Presented a poster at the National DOE/NSF EPSCoR Conference.
- Presented a poster at the Joint North Dakota/South Dakota EPSCoR Conference.

Future Direction

- Thermodynamic and practical adhesion measurements of polypropylene and polyphenylene sulfide with carbon fibers having various (including no) sizings.
- Indentation testing of initial DRIFT laminates with a new nanoindentation machine recently purchased by the South Dakota School of Mines and Technology (SDSM&T).
- Mechanical property determination of matrices and fibers will continue. Much of this work will be performed at SDSM&T, but some single-fiber testing work may be performed at ORNL.
- Measurement of the extent of transcrystalline regions in test pieces will be begun using a new atomic force microscope accessory, to be purchased with funds from this grant to complement the optical microscopy performed thus far.
- Static and dynamic mechanical testing of DRIFT and P4 laminates will be continued.
- Manufacture of a mini-DRIFT system to allow better control of material temperatures and heating and cooling rates and therefore allow controlled sample manufacture has begun.
- Travel by two of the Principal Investigators to ORNL to procure samples, perform testing and better understand the processing techniques used to fabricate samples will occur.

Introduction

Over the past decade considerable effort has been expended to develop a new generation of vehicles that are lighter and more fuel-efficient than today's vehicles. In addition, these vehicles should retain crashworthiness and be of relatively low cost. Targets include reduction in overall weight of approximately 40%, primarily achieved through lighter body and chassis materials. Polymer matrix composites (PMCs) have reached this target with a potential weight savings of 70%. At the current time, PMC technology has, in general, been deemed too costly, as carbon-fiber-based PMCs can cost ten times as much as steel parts. Some of this increased cost is due to the high price of carbon fibers and some due to limitations in the manufacturing process. Many of the problems in the manufacturing process are caused or exacerbated by lack of fundamental scientific knowledge of the interactions between the fibers and matrix materials.

This research is of significance to the DOE Automotive Lightweighting Materials in that it will help develop the necessary science base to allow more complete exploitation of PMCs having thermoplastic matrices. Traditionally, these materials have trailed the use of PMCs having thermosetting matrices, because of processability issues stemming from the low viscosity and wetting of the thermoplastic-matrix material. In addition, thermoplastic matrices are generally less strong and less stiff than thermoset matrices. This liability is further compounded by the fact that most fiber reinforcements associated with thermoplastic-matrix PMCs are of fairly short length, mainly because of the processing limitations mentioned earlier. This latter aspect is relevant because short-fiber reinforcements do not carry load as well as long- or continuous-fiber reinforcements. From the automotive perspective, short-fiber-reinforced PMCs are therefore most utilized in non-structural components. Further comparisons between thermoplastic- and thermoset-matrix PMCs are warranted here to highlight the focus of this research project, namely the role of the interface/interphase region between the fiber and the matrix.

The development of the interphase in thermoplastic PMCs is quite different from that of thermosetting matrices, which tend to be amorphous in nature. Rather, in thermoplastic PMCs, the interphase development is generally due to nucleation and growth of crystallites from the fiber surface rather

than actual chemical reactions within the interphase. The interphases formed in these systems are termed transcrystalline regions, reflecting their dependence upon the thermoplastic crystallinity. There has been much speculation in the literature as to the cause for the formation of the transcrystalline region and its role in bulk composite properties. Several conclusions can be reached. First, the transcrystalline region can grow in size to tens of microns, depending upon such parameters as fiber type, morphology and fiber surface treatments such as sizings. Second, the transcrystalline region can significantly affect properties such as the strength and impact resistance. Also, in some cases different types of transcrystalline interphases may be formed. For instance, both α and β transcrystalline regions were produced around natural fibers in polypropylene-matrix composites. These regions could be altered by inclusion of maleic anhydride in the polypropylene or on the fiber.

With respect to these novel processing routes, two examples are of particular interest to this research. The first is a low-cost process to produce continuous reinforcing fibers with thermoplastic matrices, called the **D**irect **Rei**nforcement **F**abrication **T**echnology (DRIFT) developed by the Southern Research Institute (SRI) and now located at the University of Alabama-Birmingham (UAB). PMCs produced by this continuous-fiber technology could serve as metal replacements in structural applications, specifically for the automotive industry. Keys to optimal utilization of the DRIFT process are fiber wetting, and ultimately adhesion, of the thermoplastic-matrix. Traditionally, sizings are applied to the fibers to help prevent abrasive damage, and assist with lubrication. A major component of the sizing is a coupling agent that aids in wetting, adhesion and hygrothermal stability of the composite. Research conducted in this program will utilize thermoplastic-matrix PMCs produced by UAB using the DRIFT process. The second novel processing route of interest is the Programmable Powered Preform Process (P4). While the P4 technology does allow control over fiber length, its main potential benefit is its ability to circumvent previous PMC process limitations through robotic control. To our knowledge, no fundamental analysis of PMC interphases formed by the P4 technology has been undertaken.

This research program builds upon a multi-disciplinary effort with a strong background in interphase analysis and control in thermosetting PMC systems, and applies this experience to new thermoplastic-matrix PMC systems critical to the future success of Automotive Lightweighting Materials. The research investigates model systems deemed of interest by members of the Automotive Composites Consortium (ACC) as well as samples at the forefront of PMC process development (DRIFT and P4 technologies). Finally, the research investigates, based upon the fundamental understanding of the interphases created during the fabrication of thermoplastic PMCs, the role the interphase play in key bulk properties of interest to the automotive industry.

Project Deliverables

This research will provide a better understanding of the science, particularly with respect to adhesion, of thermoplastic matrices with fiber reinforcements. The adhesion data will be used to identify processing parameters for thermoplastic-matrix composites to tailor transcrystalline interphase formation. Transcrystalline interphases are generally quite large (>10 microns) and can be stronger and stiffer than the matrix material or tougher and with greater work of fracture than the matrix. In addition, this work will produce composite samples using new processing technologies and the scientific knowledge gained with respect to adhesion and interphase formation. These test protocols are important to possible end uses for the tailored PMCs in automotive applications.

Accomplishments

Research accomplishments during the past year occurred in three primary areas: adhesion, mechanical property determination, and extent of crystallinity as a function of formation conditions. Progress in each of the three areas is described below.

Adhesion

In the past year, thermodynamic and practical adhesion research has been mainly focused on designing, manufacturing and calibrating several new testing systems and instrumentation. A new microbond test system has been calibrated for both

thermodynamic and practical adhesion. The new microbond test system utilizes the high-precision force measurements afforded by our dynamic mechanical analyzer (DMA) and precise determination of all the geometric factors associated with microbond testing to achieve the maximum consistency in the microbond test results. This consistency is shown in Table 1 (ci represents confidence interval) in which the new test system decreased the coefficient of variation (COV) by 54% over the best results our research group had previously achieved (ci represents confidence interval). With respect to microbond testing by other groups a similar decrease is observed as typical COV are in the 10-20% range.

In addition, a Nano-XP nanoindenter was purchased during the past year and our group has been working to develop procedures after discussions with Dr. Edgar Lara-Curzio of the Oak Ridge National Laboratory (ORNL) for performing microindentation practical adhesion tests. Initial work of this type has focused on using glass-fiber polypropylene and carbon-fiber polypropylene composites manufactured by the DRIFT process and obtained from Dr. George Husman of the UAB. This initial work has concentrated on identifying the primary issues associated with testing. Of particular importance are obtaining flat surfaces without debonding the fibers from the matrix prior to testing and splitting of the fibers during indentation.

To simulate DRIFT manufacturing of samples for microbond practical adhesion testing and thermodynamic adhesion measurements, a furnace capable of resistively heating carbon fibers was manufactured. Figure 1 shows both an overview and a close-up of the fiber heating assembly of this apparatus. Figure 2 shows the resistance versus temperature of three of the six carbon fibers. The important issue from Figure 2 is that the slope of the resistance-temperature curve is essentially the same for all three fibers. The difference in the data is due to slight differences in the diameter of the carbon fibers. Also, the linearity of the resistance-temperature curve is very high (>0.995) in all cases.

Finally, contact angles of polypropylene on carbon fibers have been measured for slow cooling conditions. In the cases studied thus far, polypropylene has exhibited a close to zero contact angle, indicating that molten polypropylene wets carbon fibers if given sufficient time.

Mechanical Property Determination

To manufacture samples for mechanical testing, a Wabash heatable-coolable press was used to manufacture blanks from which tensile and DMA samples could be cut. As control of the heating and cooling rates is critical for the success of this work, the first area studied was the profile of the heating and cooling rate at different points on the surface of the press. The heating rate was

Table 1. Comparison of microbond test data

Test Data	Average COV/ Average ci (%)	Improvement in Data Scatter COV/ci ratios
2001 data	45.7/18.6	5.0/4.8
2002 data	41.4/19.8	4.5/5.1
2003 data	19.7/8.5	2.2/2.2
Current setup data	9.1/3.9	NA

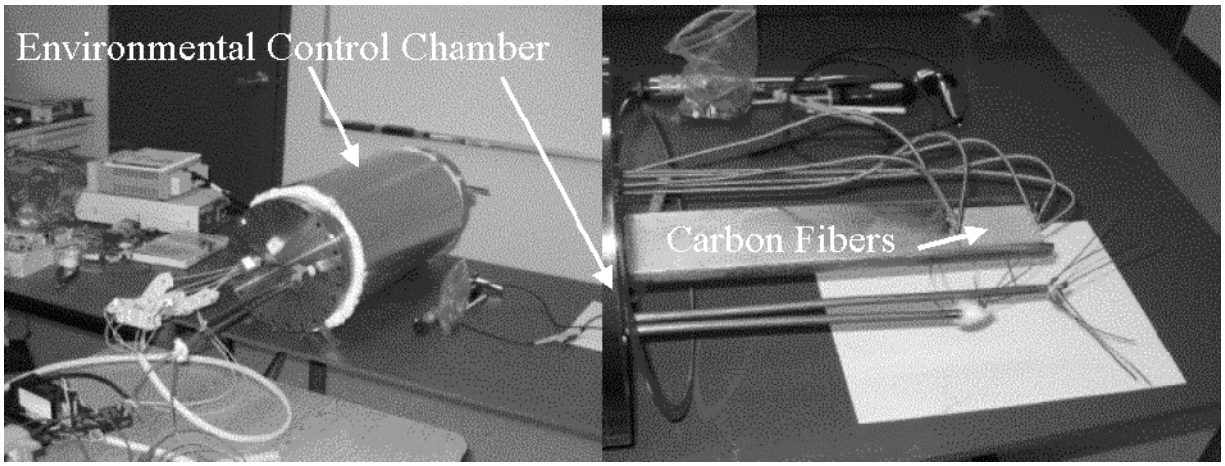


Figure 1. Apparatus for resistively heating carbon fibers. The left photo shows the full apparatus, while the right photo shows a close-up of the fiber-heating portion of the apparatus.

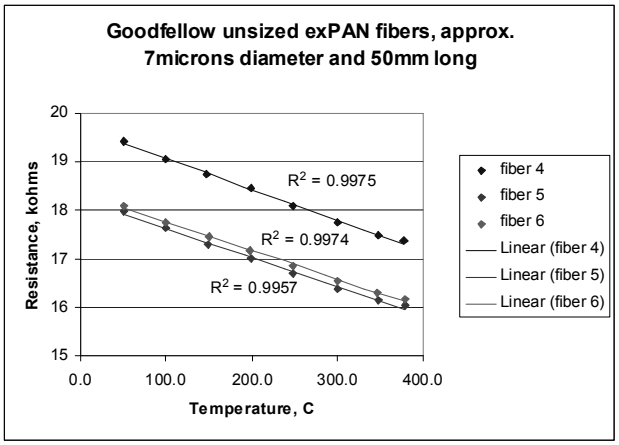


Figure 2. Measured carbon-fiber resistance as a function of applied temperature.

expected to be reasonably consistent across the platens; but, due to the way platen cooling is conducted, the cooling rate (which is more important in this work than the heating rate) was expected to be quite variable. As Figure 3 (right) shows, the heating rate was constant across the platen to about 0.2 ºC for a 6 ºC/minute heating rate. For the cooling rate, the left graph in Figure 3 indicates that the cooling rate varies by about ±2 ºC for an 18 ºC/minute cooling rate. Therefore, the cooling rate varies by about a factor of 3 compared to the heating rate. Examination of Figure 3 indicates that the central region of about 6" by 6" has a relatively stable cooling rate. Hence, mechanical testing samples were cut from this region.

Both tensile testing and DMA samples have been manufactured. The tensile testing has measured the Young's modulus and yield strength of samples made from carbon-fiber polypropylene prepreg (Baycomp) laminates. Thus far, little difference has been observed for different cooling rates. The reasons for this are being studied, but are likely due to the development of the transcrystalline layer in this system.

For DMA testing of bulk polypropylene samples, Figures 4 and 5 show the storage and loss moduli (Figure 4) and creep compliance (Figure 5). The storage and loss moduli are relatively constant as a function of cooling rate between about 5 and 20 ºC/minute. As the crystallinity of the matrix is greater at slower cooling rates compared to faster cooling rates, this indicates that the matrix crystallinity has little effect when a sinusoidal load is applied at 1 Hz with an amplitude of 15 micrometers. Conversely, the creep compliance is a function of the cooling rate, and hence, the matrix crystallinity. The creep compliance was approximately twice as great when the cooling rate was ~7.5 ºC/minute as compared to when the cooling rate was ~21 ºC/minute.

Extent of Crystallinity as a Function of Formation Conditions

Crystallinity formation was studied by two types of experimentation. In one type of experiment, bulk polypropylene samples were placed in a

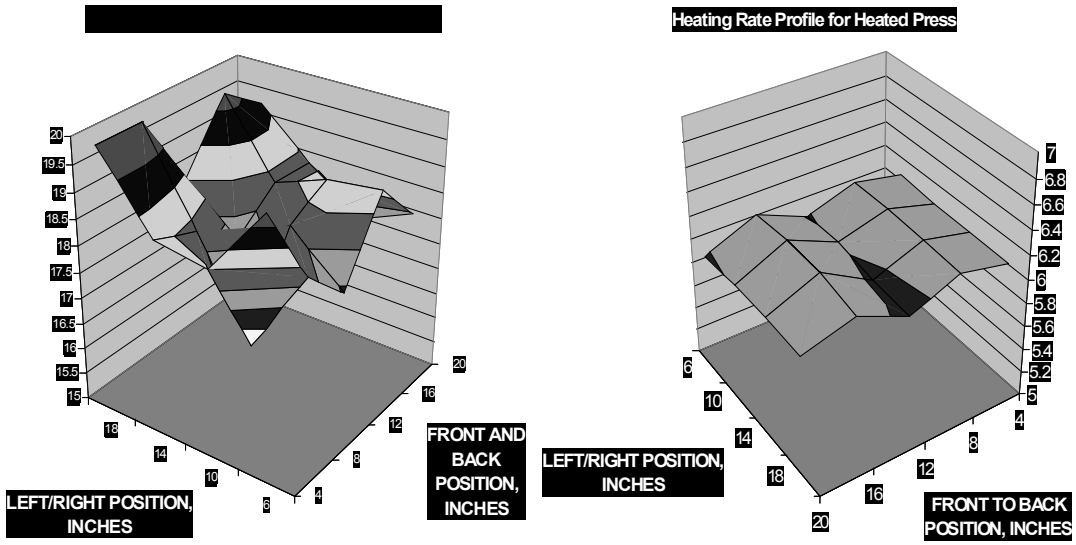


Figure 3. Cooling (left) and heating (right) rate profiles for the Wabash press (the numbers on either side represent the distance from the center of the press).

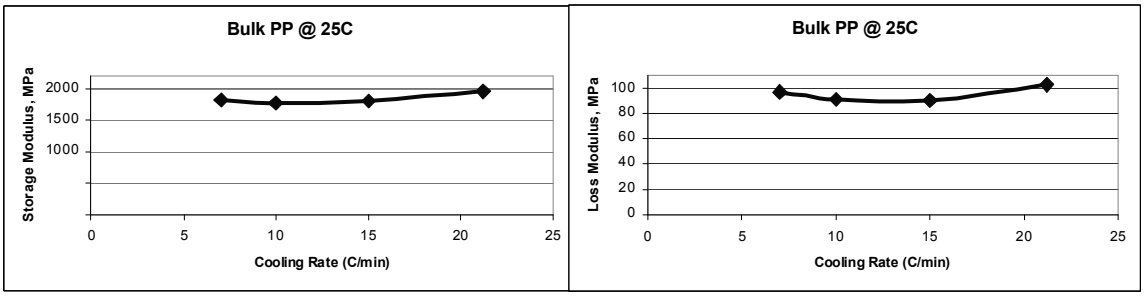


Figure 4. Storage modulus (left) and loss modulus (right) of bulk polypropylene as a function of cooling rate.

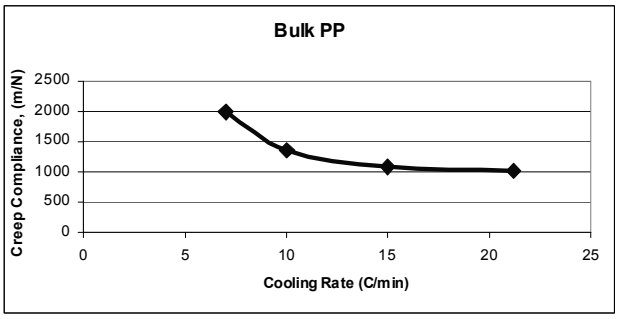


Figure 5. Creep compliance of bulk polypropylene as a function of cooling rate.

differential scanning calorimeter (DSC) and the crystallization endotherm was used to determine the amount of crystallization. Figure 6 shows the results from these two types of experimentation. Isothermal crystallization, Figure 6 (left), shows little difference in the crystallization as a function of hold time at the isothermal crystallization temperature (115 ºC). This is because essentially all the crystallization occurs in the first two minutes. For nonisothermal crystallization, Figure 6 (right), the cooling rate is varied then the amount of crystallization is determined from the endothermic crystallite melting during the next heating cycle. The amount of bulk crystallization is quite dependent upon the cooling rate, for cooling rates less than 10 ºC/minute. Nonisothermal crystallization typically is a better representation of the cooling during DRIFT and P4 processing.

In addition to bulk testing, experiments were conducted to examine transcrystalline layer formation during cooling. These experiments used a hot stage mounted on a polarized microscope

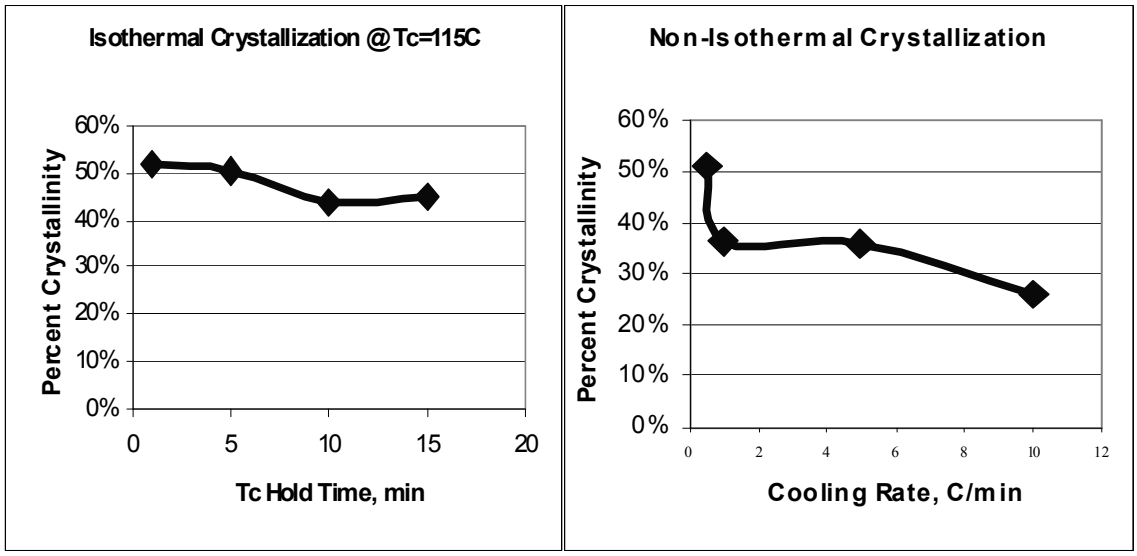


Figure 6. Isothermal (left) and non-isothermal (right) determination of bulk polypropylene crystallization.

stage. Two thin layers of polypropylene with a small number of fibers sandwiched between the layers were placed in the hot stage and heated to approximately 200 ºC for 10 minutes. After this hold, the stage was slowly cooled (~4 ºC/minute) and the crystallization recorded with a video camera mounted to the polarized microscope. Figures 7 and 8 show transcrystalline layer formation for pitch-based, carbon fibers (Figure 7) and Kevlar® fibers (Figure 8). Glass fibers and ex-PAN (polyacrylonitrile) carbon fibers were also tested. The glass fibers used did not show any transcrystallinity, while the ex-PAN fibers intermittently showed transcrystallinity. The ex-PAN transcrystallinity generally took the form of hemispherical regions growing from the fiber surface rather than the more lamellar regions seen in Figures 7 and 8. This is most likely due to the number of nucleation sites on the ex-PAN fibers

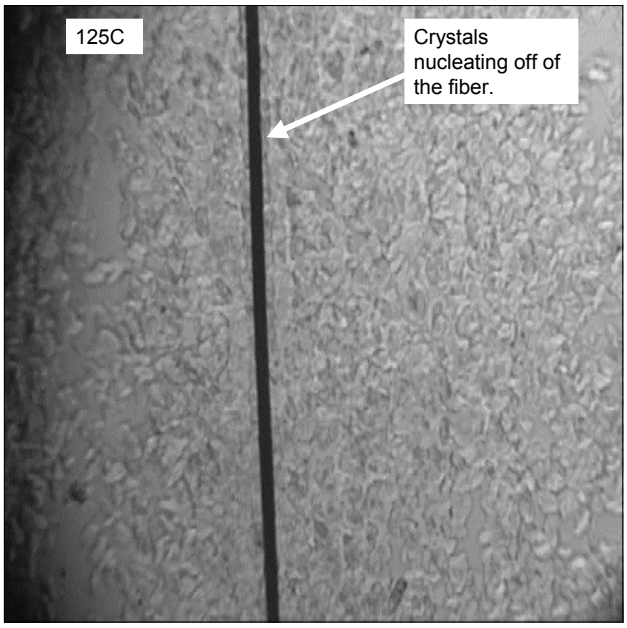


Figure 7. Transcrystalline layer on pitch-based carbon fibers.

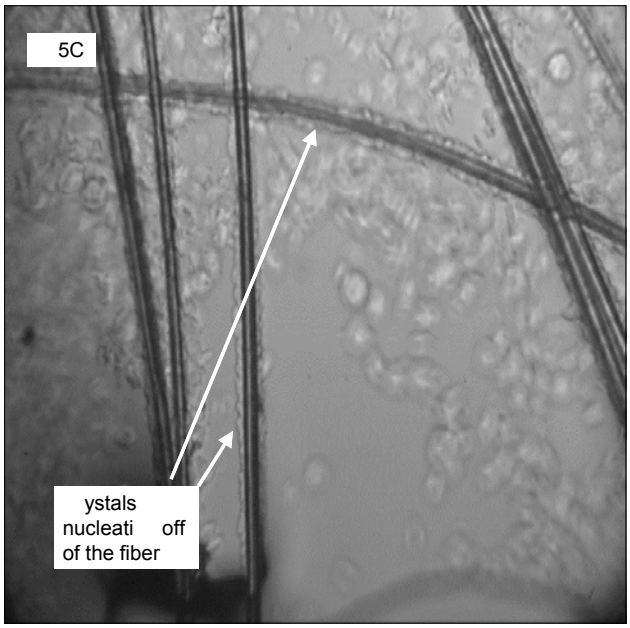


Figure 8. Transcrystalline layer on Kevlar fibers.

being much les than the number of nucleation sites on pitch or Kevlar® fibers. Links to videos of these results can be found at: http://hpcnet.org/thermoplastic.

Summary

Highlights of our FY2005 research include:

1. Demonstrated transcrystalline layer formation for Kevlar and pitch-based carbon fibers and polypropylene matrix.
2. Measured matrix crystallinity by differential scanning calorimetry
3. Designed an apparatus to allow for controlled, resistive, carbon-fiber heating for thermodynamic adhesion and transcrystallinity experiments.
4. 2 students traveled to University of Alabama-Birmingham to meet with Dr. George Husman, to allow better design of a tabletop mini-DRIFT system.

G. Performance Evaluation and Durability Prediction of Dissimilar Material Hybrid Joints

D. L. Erdman
Oak Ridge National Laboratory
P.O. Box 2009, Oak Ridge, TN 37831-8048
(865) 574-0743; fax: (865) 574-8257; e-mail: erdmandl@ornl.gov

Field Project Manager: C. David Warren
Oak Ridge National Laboratory
P.O. Box 2009, Oak Ridge, TN 37831-8050
(865) 574-9693; fax: (865) 574-0740; e-mail: warrencd@ornl.gov

Technology Area Development Manager: Joseph A. Carpenter
(202) 586-1022; fax: (202) 586-1600; e-mail: joseph.carpenter@ee.doe.gov
Field Technical Manager: Philip S. Sklad
(865) 574-5069; fax: (865) 576-4963; e-mail: skladps@ornl.gov

Contractor: Oak Ridge National Laboratory
Contract No.: DE-AC05-00OR22725

Objective

Develop new experimental methods and analysis techniques to enable hybrid joining as a viable attachment technology in automotive structures. This will be accomplished by evaluating the mechanical behavior of composite/metal joints assembled using a variety of hybrid joining methods and quantifying the resultant damage mechanisms under environmental exposures, including temperature extremes and automotive fluids, for the ultimate development of practical modeling techniques that offer global predictions for joint durability.

Approach

- Characterize the structural hybrid joint to quasi-static load conditions.
- Characterize response to fatigue, creep, and environmental exposures.
- Conduct predictive analysis.

Accomplishments

- Conducted replicate fatigue tests at 85%, 70% and 40% of ultimate load for Quantum rails.
- Performed progressive failure analysis with contact and non-linear material behavior using coupled GENOA and ABAQUS codes.

Future Direction

- This project was completed Month 6 FY 2005.

Introduction

Weight can be reduced and fuel efficiency increased in automobiles, without compromising structural integrity or utility, by incorporating innovative designs that strategically utilize modern lightweight materials—such as polymeric composites—in conjunction with traditional structural materials such as aluminum, magnesium and steel. Despite the advantages associated with such dissimilar or hybrid material systems, there is reluctance to adopt them for primary structural applications. In part, this reluctance can be attributed to the limited knowledge of joining techniques with such disparate materials where traditional fastening methods such as welding, riveting, screw-type fasteners, and bolted joints may not be appropriate.

One solution to this problem is the use of hybrid joining techniques by which a combination of two or more fastening methods is employed to attach similar or dissimilar materials. One example is a mechanically fastened joint (i.e., bolted or riveted) that is also bonded with adhesive. These types of joints could provide a compromise between a familiar mechanical attachment that has proven reliability, and the reduction of problematic issues such as stress concentrations and crack nucleation sites introduced by using mechanical fasteners with polymeric composites.

The use of hybrid joining could also lead to other potential benefits such as increased joint rigidity, contributing to overall stiffness gains and a reduction of vehicle mass. Additionally, the use of adhesives in conjunction with mechanical fasteners could significantly reduce stress concentrations, which serve as locations for crack starters. Hybrid joining methods can also provide additional joint continuity to allow increased spacing between fasteners or welds.

Although numerous benefits are derived from using hybrid joining techniques, and the joining of dissimilar materials is becoming a reality, little or no practical information is available concerning the performance and durability of hybrid joints. Therefore this project has taken on the task of developing new technologies to quantify joint toughness and predict long-term durability. This will necessitate identifying and developing an understanding of key issues associated with hybrid joint performance, such as creep, fatigue, and effects of environmental exposure.

To initiate this study, it was necessary to choose a candidate hybrid joint representative of those typically encountered in automobiles. Because of their wide applicability in automotive structures, several combinations of hat-section geometries were considered. Hat-sections can be incorporated into a variety of generic automotive structural components, such as crush-tubes or frame rails, when they are bonded and mechanically fastened to other geometries. For the current study, the Joining Task Force selected a composite hat-section bonded and riveted to a steel base. This selection was made on the basis of general applicability to a variety of automobile structural components. Members of the Joining Task Force identified industry partners for sources for the steel, rivets, composite hat-section, and adhesive.

To determine the influences of the adhesive and the rivets on the structural performance of the rail, it was also decided to investigate bonded specimens without rivets and riveted specimens without adhesive.

Replicate Fatigue Tests of Quantum Rails

Replicate fatigue tests have been performed at 40% of average ultimate static load at room temperature for both loading configurations—hat-in- tension and hat-in-compression. These tests, carried out at frequency of 3 Hz, require significant test machine time, since most specimens incur damage after more than 10^6 cycles. Most specimens reach run-out limit of 10^7 cycles without catastrophic failure. Three replicate fatigue tests at 40% of ultimate load will be completed when two remaining tests in progress conclude.

To date, replicate tests have confirmed our previously reported observations. Specimens reaching high cycle counts during fatigue tests exhibit failure mechanism different from mechanisms observed in quasi-static tests. Specimens containing adhesive bonds have been consistently outperforming specimens with rivets only as illustrated by Figure 1 and Figure 2. Specimens that encountered catastrophic failure,

before reaching run-out limit of 10^7 cycles, have sustained significant damage. Adhesively-bonded specimens developed cracks in the steel substrate, while riveted specimens sustained partial or complete loss of rivets prior to final failure. None of the specimens tested at 40% of ultimate load showed failure modes identical to that of quasi-static test.

Finite Element Modeling

An in-house developed Python code was used to calibrate material properties for input to GENOA. This calibration enables simulation of non-linear behavior of the matrix of the composite, which is important in specimens with ± 45 fiber orientation. Experimental stress-strain curves from coupon tests

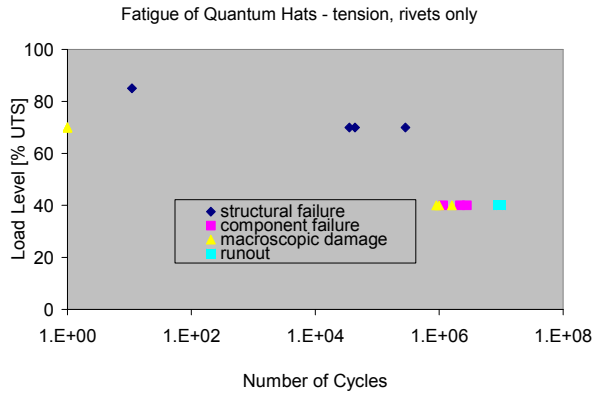


Figure 1. Specimens with rivets only exhibited rivet failure before reaching run-out limit at 40% of ultimate load.

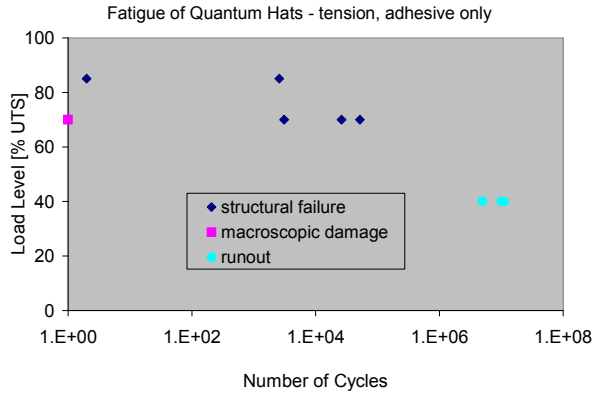


Figure 2. Specimens with adhesive did not exhibit damage before reaching run-out limit.

were matched in equivalent GENOA models. The modified distortion-energy failure criterion was disabled, since it inaccurately predicted premature failure.

Previous GENOA analyses disregarded complex contact conditions that exist in real tests due to unavailability of a contact algorithm in GENOA finite element solver (MHOST). ORNL and Alpha Star collaborated in coupling GENOA and ABAQUS finite element solvers. This development allows analysts to take advantage of multi-scale progressive failure capabilities as well as non-linear and contact capabilities of ABAQUS.

A full model of hat-in-tension presented in Figure 3 was developed. Previously calibrated material properties for $\pm$ 45 cross-ply composite were used along with material properties of adhesive and steel. Figures 4-5 show damage. The sequence of push-through damage due to contact and subsequent failure in the hat was observed in experiments. The model with the disabled modified distortion-energy failure criterion over-predicts ultimate load of the structure and does not reflect the unloading part of the load-displacement curve. The model with all damage criteria active under-predicts ultimate load, as expected based on coupon test calibration; however, the unloading part of the load-displacement curve is reflected in the results. This indicates strong sensitivity of the model on parameters affecting modified distortion-energy criterion. Material calibration is presently being re-visited in order to include all failure criteria in the coupon models.

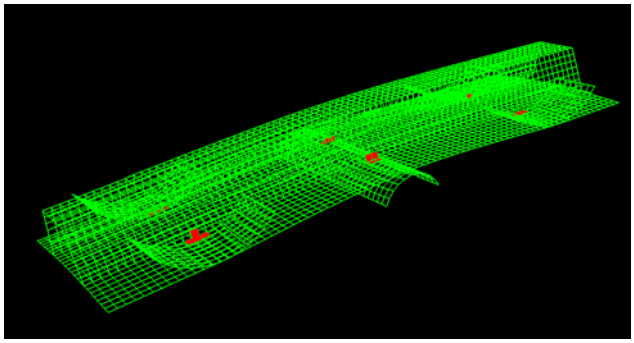


Figure 3. Initial damage due to contact in GENOA model.

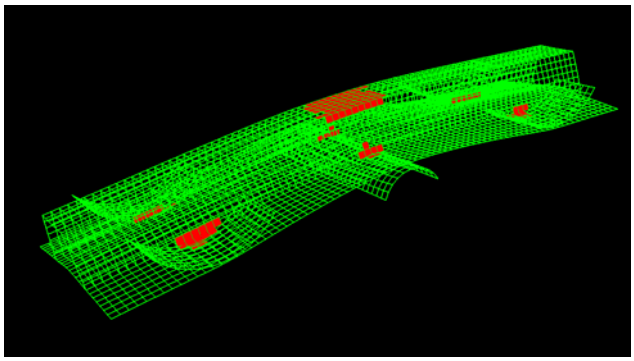


Figure 4. Failure at the top of the hat in GENOA model.

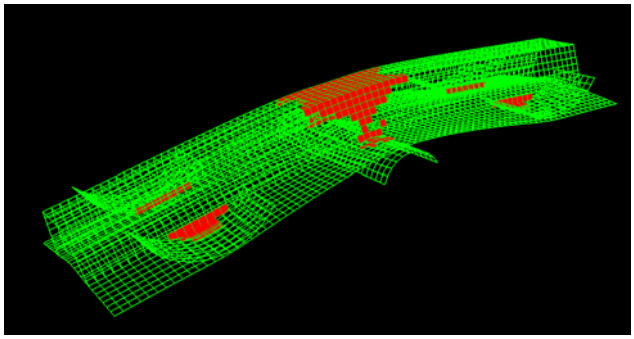


Figure 5. Advanced stage of damage in GENOA model.

Conclusions

Replicate fatigue tests have been conducted and statistical certainty was increased for previous observations. Multi-scale progressive failure analyses with contact and non-linear material behavior have been performed.

Presentations/Publications/Patents

V. Kunc, D. Erdman and L.B. Klett, "Hybrid Joining in Automotive Applications", Presented at the SAMPE 2005 Symposium and Exhibition, Renaissance Long Beach Hotel/Long Beach Convention Center, Long Beach, CA, 1-5 May 2005

H. Durability of Carbon-Fiber Composites

Dan J. Naus (Principal Investigator), J. M. Corum, R. L. Battiste, L. Klett, M. Davenport
Oak Ridge National Laboratory, P.O. Box 2009
Oak Ridge, TN 37831-8056
(865) 574-0657; FAX: (865) 574-6098; e-mail: nausdj@ornl.gov

Technology Area Development Manager: Joseph A. Carpenter
(202) 586-1022; fax: (202) 586-1600; e-mail: joseph.carpenter@ee.doe.gov
Field Technical Manager: Philip S. Sklad
(865) 574-5069; fax: (865) 576-4963; e-mail: skladps@ornl.gov

---

Contractor: Oak Ridge National Laboratory
Contract No.: DE-AC05-00OR22725

Objective

- To develop experimentally-based, durability-driven design guidelines to ensure the long-term (15-year) integrity of representative carbon-fiber-based composite systems that can be used to produce large structural automotive components. Durability issues being considered include the potentially degrading effects of cyclic and sustained loadings, exposure to automotive fluids, temperature extremes, and low-energy impacts from such events as tool drops and kick-ups of roadway debris on structural strength, stiffness, and dimensional stability.

Approach

- Characterize and model the durability behavior of a progression of three representative carbon-fiber composites, each with the same thermoset urethane matrix but having a different reinforcement preform: (1) continuous fiber, ±45° crossply; (2) continuous fiber, quasi-isotropic; and (3) random chopped fiber.
- Replicate on-road conditions in laboratory tests of each composite to generate durability data and models.
- Subsequently shift focus to suitable thermoplastic composites, for which durability issues are generally more significant.
- Develop and publish durability-based design criteria for each composite.

Accomplishments

- Published and distributed a report that reviews measurement and development of crystallinity and its relationship to properties of neat Poly (Phenylene Sulfide) (PPS) and its fiber-reinforced composites (ORNL/TM-2004/304).1
- Published journal article on effect of thermal cycling on carbon-fiber-reinforced PPS composites. 2
- Completed baseline testing (tension, compression, shear, and flexural properties) for all plaques.
- Completed testing to determine effect of strain rate on tensile properties.
- Completed testing to determine effect of sequential loading on stiffness.
- Completed testing to determine effect of prolonged thermal exposure (i.e., up to 1000 hours) on tensile properties.
- Completed testing to evaluate effect of preconditioning temperature on flexural and shear strength.

- Completed environmental screening tests (e.g., short-beam shear strength and weight gain) to establish which, if any, common automotive fluids may have a degrading effect on the properties of the PPS composite material.
- Completed testing to determine effect of prolonged exposure (i.e., 1000 hours) to distilled water or windshield washer fluid on tensile, compressive, and shear properties.
- Completed in-air, room-temperature and in-air elevated-temperature (i.e., 70˚, 90˚ or 120˚C), sustained-load tension tests (94 tests).
- Completed room-temperature, sustained-load tension tests on specimens preconditioned and maintained in either windshield washer fluid or distilled water during testing (43 tests).
- Completed room-temperature and elevated-temperature (120˚C), sustained-compression load testing (19 tests).
- Completed cyclic fatigue tests (88 tests) involving stress ranges from 10 to 90% ultimate tensile strength and test temperatures of room temperature, -40˚, 70˚, or 120˚C.
- Completed mean stress effects cyclic fatigue testing (52 tests).
- Completed uniaxial and biaxial flexural strength testing.
- Carbon-fiber composite data feeding directly into the planning and analysis for the Focal Project 3 carbon-fiber body-in-white.

Future Direction

- Complete durability assessment of carbon-fiber-reinforced PPS material.
- Publish durability-driven design criteria documents for representative thermoplastic composites suitable for automotive structural applications.
- Complete report outlining minimum test matrix for development of design criteria for carbon-fiber-reinforced thermoset and thermoplastic materials.

Introduction

Before composite structures will be widely used in automotive applications, their long-term durability must be assured. The Durability of Carbon-Fiber Composites Project at the Oak Ridge National Laboratory (ORNL) was established to develop the means for providing that assurance. Specifically, the project is developing and documenting experimentally-based, durability-driven design criteria and damage-tolerance assessment procedures for representative carbon-fiber composite systems to assure the long-term (15-year) integrity of composite automotive structures. Durability issues being considered include the potentially degrading effects of cyclic and sustained loads, exposures to automotive fluids, temperature extremes, and incidental impacts from such things as tool drops and kick-ups of roadway debris. Research to determine the effects that these environmental stressors and loadings have on structural strength, stiffness, and dimensional stability is being conducted. The project is carried out in close coordination with the Automotive Composites Consortium (ACC).

It is envisioned that about 15% of the Focal Project 3 (See report 4.D) carbon-fiber-composite body-in-white will utilize directed continuous-fiber reinforcement architectures, while the remainder will employ random chopped-fiber reinforcement. The approach to investigating durability has thus been to address a progression of thermoset composites, each of which has the same urethane matrix:

- reference $[\pm 45]_{3S}$ crossply composite,
- $[0/90/\pm 45]_{S}$ quasi-isotropic composite, and
- randomly-oriented, chopped-carbon-fiber composite.

Characterization of the first two continuous-fiber composites has been completed, and design criteria documents published. In mid-FY 2002, the focus turned to chopped-carbon-fiber composites. Characterization of the randomly-oriented, chopped-carbon-fiber composite was completed in FY 2003

and the durability-based design criteria report published. In FY 2003, investigation of carbon-fiber-reinforced thermoplastic materials for structural automotive applications was initiated. Recent activities associated with evaluation of the thermoplastic material have addressed thermoplastic material characterization, baseline property determination, strain-rate and prior-load tests, environmental effects tests, uniaxial and biaxial flexural strength evaluations, sustained-load tests (tension and compression), and cyclic fatigue tests.

Thermoplastic Material Characterization

The ACC has supplied 46 plaques, 510 mm by 610 mm by about 3-mm thick, for use in durability studies. Plaque reinforcement is symmetrical and consists of 16 plies of carbon-fiber unidirectional tape, $[0/90/\pm45]_{2S}$. PPS is the matrix material.

Processing conditions are very important because they affect the crystallinity of a semicrystalline polymer such as PPS. Crystallinity changes of thermoplastic materials can result in significant changes in the mechanical behavior of composites containing them, particularly with respect to matrix-dominated properties such as compressive strength and creep. For this reason, the ability to precisely characterize the polymer crystallinity in a thermoplastic material becomes an important requirement. Unfortunately, due to the proprietary nature of the material processing, only limited information has been provided by the material supplier on processing of the as-received material.

In addition to information presented previously (Automotive Lightweighting Materials FY 2004 Annual Progress Report) on differential scanning calorimetry (DSC) and x-ray diffraction (XRD) results, a review of literature and contacts with industry has been conducted. Results of this review have been provided in a report that was published and distributed.[1] The objective of this report was to broaden the understanding of low-cost, semi-crystalline thermoplastic resins and composites for use in potential future automotive applications. PPS has an excellent combination of attributes including good mechanical properties and thermal stability, high chemical resistance, low moisture absorption, good weathering resistance, high dimensional stability, low flammability, and excellent processability. Specific areas addressed in the report include: structure of PPS; techniques for measuring crystallinity; crystallinity as a function of prior treatment; crystallization kinetics and morphology; effect of variation of crystallinity on properties of PPS and its composites; environmental stability; unusual effects of cooling rates and degree of crystallinity on mechanical properties of AS4/PPS composites; recent PPS laminate data (Ten Cate Advanced Composites); and recommendations for future research.

Baseline Property Determination

In an attempt to enhance the as-received material crystallinity, tests to establish room-temperature tensile, compressive, and shear properties of as-received material as well as material that had been annealed at 230°C for 2 hours have been completed. Investigation of specimen orientation effects also has been completed.

Table 1 summarizes tensile, compressive, and shear properties obtained for the as-received and annealed materials. Tensile, compression, and shear results represent tests of specimens that were obtained from 36, 10, and 6 plaques, respectively.

Strain-Rate and Prior-Load Tests

Testing to determine the effect of strain rate on tensile properties of the PPS composite has been completed. Four specimens each were tested at testing machine nominal stroke rates of 0.0005, 0.005, 0.05, 0.5, 5.0, and 50.0 in/sec. At rates up to 5.0 in/sec, an averaging extensometer was utilized to obtain strain data; however, at the 50 in/sec rate, strain gages had to be utilized due to difficulties in keeping the extensometer attached to the specimen. Strain rate for each of the specimens was determined using the test text files and determining the slope of the strain versus time curves. Strain rates ranged from 4.21×10^{-05} to 5.11 s^{-1}. Figure 1 presents the ultimate tensile strength as a function of strain rate. These results indicate that the ultimate tensile strength of the material increased slightly (<10%) when the strain rate increased from lowest to maximum. The tensile modulus of elasticity was relatively unaffected by strain rate while the tensile failure strain tended to decrease with increasing strain rate.

Table 1. Baseline properties: as-received material.

Property	As-Received Material	Annealed Material
	Tension	
Strength, MPa	551	539
Modulus, GPa	36.45	37.38
Failure Strain, %	1.53	1.42
Number Tests	207	31
	Compression	
Strength, MPa	295	292
Modulus, GPa	34.26	35.09
Failure Strain, %	0.95	0.92
Number Tests	57	13
	Shear	
Strength, MPa	193	196
Modulus, GPa	13.4	13.60
Failure Strain, %	1.63	1.59
Number Tests	34	12

Specimens oriented in long direction of plaque.

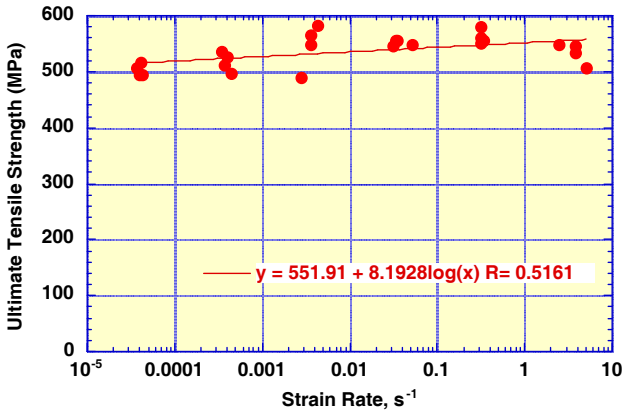


Figure 1. Effect of strain rate on ultimate tensile strength.

Testing to determine the effect of sequential loading on stiffness has been completed. After initial stiffness checks to establish baseline values, four tensile specimens each were subjected to initial loadings of either 20%, 40%, 60%, or 80% of the plaque average ultimate tensile strength (UTS). The specimens were then unloaded and reloaded with the load increased by 20% of the plaque average ultimate tensile strength. This procedure was repeated until the last load cycle in which the specimen was loaded to failure. Specimen modulus of elasticity was determined for each of the load applications. Figure 2 presents average change in

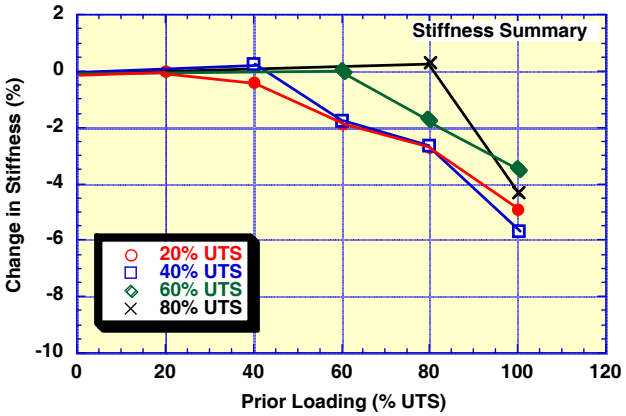


Figure 2. Effect of sequential loading on stiffness.

stiffness for each of the load applications. Results indicate that the first load increment did not produce a change in stiffness, but succeeding load increments produced increased reductions in the modulus of elasticity relative to the baseline values.

Environmental Effects Tests

Four series of tests were conducted that address environmental effects: prolonged thermal exposure on tensile properties, automotive fluids screening, and effect of exposure to distilled water and windshield washer fluid on tensile, compressive, and shear strengths.

Testing to evaluate the effect of prolonged thermal exposure on the ultimate tensile strength, tensile modulus of elasticity, and tensile failure strain has been completed. Either eleven or twelve specimens had been placed into ovens maintained at either 50°C, 70°C, 90° or 120°C. Two or three specimens were removed from each oven after thermal exposure periods of 100 h, 200 h, 500 h and 1000 h; placed into an insulated container and permitted to slowly return to room temperature; and tested to failure. Table 2 summarizes tensile strength results and indicates that although there was a 3 to 13% increase in ultimate tensile strength for specimens preconditioned at 120°C, there was no definite trend indicating significant effects of temperature level or periods of exposure on ultimate tensile strength. Tensile modulus of elasticity and tensile failure strain were unaffected by either the temperature level or the exposure period for the range of values investigated.

Table 2. Effect of elevated temperature exposure on ultimate tensile strength (MPa).

Preconditioning Time, hours	Preconditioning Temperature, °C				
	RT	50	70	90	120
0	594	-	-	-	-
100	-	581	637	632	610
200	-	588	569	573	620
500	-	599	552	572	670
1000	-	595	584	565	625

Environmental fluid screening tests to establish which, if any, common automotive fluids may have degrading effects on the carbon-fiber-reinforced PPS material have been completed. Nine automotive fluids were used in the screening (viz, antifreeze, battery acid, 5% NaCl solution, windshield washer fluid, brake fluid, distilled water, transmission fluid, gasoline, and motor oil). Twenty flexure specimens 12.7-mm-wide by 76.2-mm-long were submerged in each of the automotive fluids. Periodically, the specimens were removed from each of the fluids, measured, weighed, and returned to the appropriate fluid. After exposure periods of 100 h, 200 h, 500 h, 1000 h, and 2000 h, four specimens were tested to determine the effect of fluid exposure on the short-beam shear strength. Figures 3 and 4 present weight change and short-beam shear results obtained for

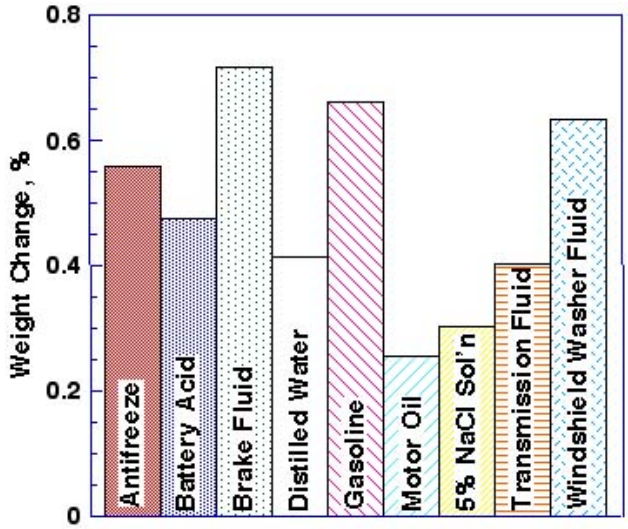


Figure 3. Weight change after 2000 hours exposure to typical automotive fluids.

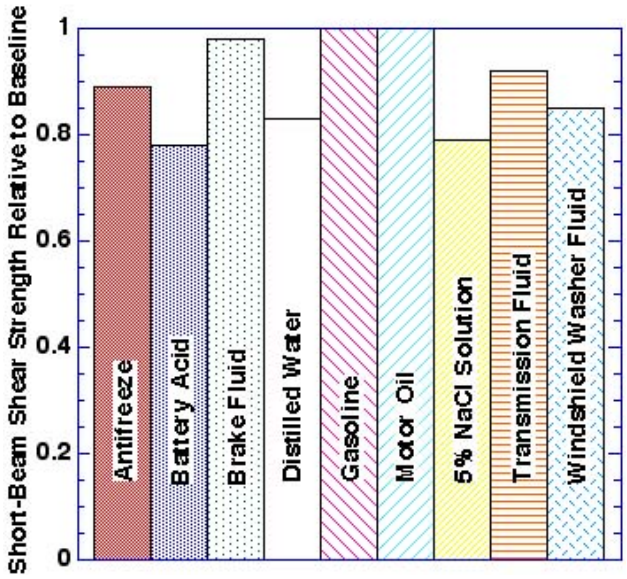


Figure 4. Short-beam shear strength after 2000 hours exposure to typical automotive fluids.

each of the automotive fluids after 2000 hours exposure. Brake fluid, gasoline, and windshield washer fluid produced the largest percentage change in specimen weight; however, these changes are less than 0.7%. No significant change in specimen geometry occurred as a result of the fluid exposure. Battery acid, distilled water, and a 5% NaCl solution had the most effect on short-beam shear strength after 2000 hours exposure.

Tests to determine distilled-water and windshield-washer-fluid effects on tensile, compressive, and shear strength of specimens exposed to these fluids for periods up to 1000 h, have been completed. After 1000 hours exposure to distilled water and windshield washer fluid, the tensile strength decreased 6.8% and 6.3%, respectively; the compressive strength decreased 10.5% and 22.4%, respectively; and the shear strength decreased 34.9% and 31.3%, respectively, relative to the baseline strength. Compressive and shear properties, that tend to be more influenced by the matrix, were affected more significantly by 1000-hour exposure to distilled water and windshield washer fluid than was the tensile strength.

Uniaxial and Biaxial Flexural Strength Evaluations

Testing to determine the effect of thermal exposure on the uniaxial flexural strength and environmental effects on the biaxial flexural strength have been completed. Six specimens each, 76.2-mm long by 12.7-mm wide, were thermally preconditioned at either –40°C, 70°C, 90°C, or 120˚C for one hour prior to testing. Three specimens at each of these preconditioning temperatures were tested in three-point bending (50.8-mm major span) at temperature with the remaining three specimens permitted to return to room temperature prior to testing. Figure 5 summarizes flexural strength results for specimens tested at-temperature and specimens permitted to return to room temperature prior to testing. These results indicate that for specimens tested at-temperature, the flexural strength decreased as the preconditioning temperature increased. For specimens permitted to return to room temperature prior to testing, there was a slight trend for the flexural strength to increase as the preconditioning temperature increased. Results obtained from biaxial flexural tests in which a disk-shaped specimen supported at its edge is loaded by means of a load ring are summarized in Table 3. Results indicate that relative to the baseline value, the biaxial flexural strength was reduced by exposure to distilled water, windshield washer fluid, and elevated temperature.

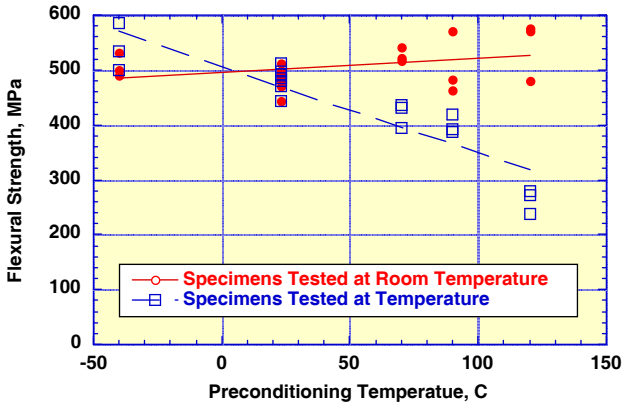


Figure 5. Effect of preconditioning temperature and test temperature on flexural strength.

Table 3. Biaxial flexural test result summary.

Preconditioning Environment	Maximum Load, kN	Displacement at Pmax, mm
Baseline	12.878	5.253
Distilled Water (1000 h Presoak)	9.697	5.011
Windshield Washer Fluid (100 h Presoak)	10.467	4.648
-40°C (1 hour)	14.497	5.672
70°C (1 hour)	10.849	5.296
90°C (1 hour)	10.422	4.920
120°C (1 hour)	6.770	4.590

Sustained-Load Tests

Sustained-load tests have been conducted as part of the overall assessment of the PPS composite material's ability to sustain constant loads for long-time periods. Sixty-one in-air room-temperature tests have been completed with sustained-load levels investigated ranging from 40 to 95% UTS. Thirty-three elevated temperature (70°, 90°, or 120°C) sustained-load tests have been completed with sustained-load levels investigated ranging from 40 to 91% UTS. Forty-three sustained-load tests in which the specimen was subjected to either room-temperature windshield washer fluid (1000 hour presoak) or distilled water (100 hour presoak) while under load have been completed investigating sustained-load levels ranging from 30 to 95% UTS. In addition, 19 compressive sustained-load tests have been completed in air at either room-temperature or 120°C. Figure 6 presents an example of total strain versus time plots for room temperature in-air tests of specimens subjected to sustained loads from 40.0 to 79.9% UTS.

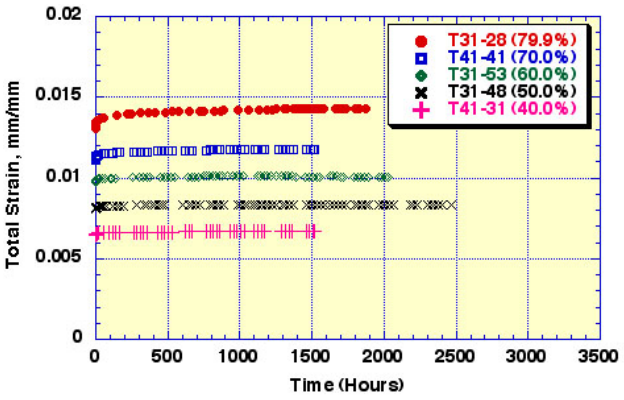


Figure 6. Examples of total strain results for room-temperature tensile creep tests.

Cyclic Fatigue Tests

Eighty-eight cyclic fatigue tests have been completed. Test parameters included the stress range (40 to 90% UTS, R = 0.1), test temperature (room temperature, –40°, 70° or 120°C), and effect of fluids (100-hour presoak in windshield washer fluid or 1000-hour presoak in distilled water). In addition, 52 tests were completed to examine the mean-stress effects (R = 0, R = -1, R = $-\infty$, or 45% mean UTS). Figure 7 presents examples of stress versus cycles-to-failure results for tests involving different environmental exposures. Results such as these will be used to help establish design limits for cyclic loads for the PPS composite.

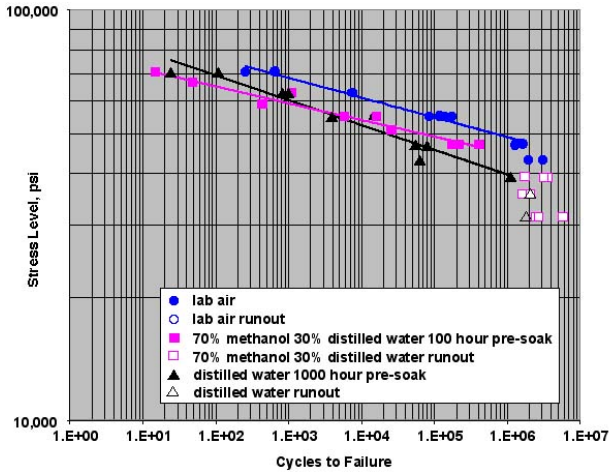


Figure 7. Stress versus number of cycles-to-failure results for various environmental exposures.

Summary and Conclusions

A quasi-isotropic carbon-fiber-reinforced PPS material is being investigated. This is the first thermoplastic material to be studied under the durability program. The ACC has supplied 46 plaques, 510 mm by 610 mm by about 3-mm thick, for use in durability studies. Plaque reinforcement is symmetrical and consists of 16 plies of carbon-fiber unidirectional tape, $[0/90/\pm45]_{2S}$.

Processing conditions for these plaques are very important because they affect the crystallinity of a semicrystalline polymer such as PPS, which can result in significant changes in the mechanical behavior of composites containing them. Because precise processing information on the plaques was not available due to the proprietary nature of the processing, the crystallinity of the material was investigated and a report prepared that presents data and information on the relationship between processing of PPS materials and crystallinity as well as the relationship between crystallinity and material properties.[1] Material characterization studies indicate that processing of the composite was fairly complete producing a crystallinity of about 85% of maximum achievable.

Tests to establish baseline room-temperature tensile, compressive, and shear properties of the PPS composite material have been completed. Additional tests (reported previously) established properties for material that had been annealed at 230°C for two hours in an attempt to increase crystallinity. Tensile, compressive, and shear strength properties of the as-received and annealed material were within 3% of each other tending to indicate that the material supplied possessed good crystallinity.

Strain-rate tests indicated that the material tensile strength increased somewhat (<10%) when the strain rate was increased from 4.21 x 10^{-05} to 5.11 s^{-1}.

Testing to determine the effect of sequential loading on stiffness indicates that the first load increment did not produce a change in stiffness, but succeeding load increments to higher load levels produced increased reductions in the modulus of elasticity relative to the baseline values. Sequential loading from 20 to 80% UTS did not have a significant effect on the ultimate tensile properties of the PPS material (last load cycle) as the tensile strength and tensile failure strain were relatively unaffected and the modulus of elasticity was reduced less than 10%.

Prolonged thermal exposures up to 120°C for periods up to 1000 hours produced a slight increase in tensile strength (3 to 13%); however, other exposure temperatures did not affect results. Tensile modulus of elasticity and strain at failure were not affected by either the exposure temperature or exposure period for the range of values investigated.

Environmental screening tests utilizing typical automotive fluids indicated that windshield washer fluid, gasoline, and brake fluid produced the largest weight gains due to exposure; however, the gains were less than 0.7%. Battery acid, distilled water,

and a 5% NaCl solution had the most effect on short-beam shear strength. Exposure of 1000 hours to either distilled water or windshield washer fluid resulted in decreases in the tensile, compressive, and shear strengths, with the decreases greatest for properties that are more matrix dominated (i.e., compressive and shear).

Flexural results indicated a trend for the flexural strength to decrease as the preconditioning temperature increased when the specimens were tested at temperature; however, when permitted to return to room temperature prior to testing, the preconditioning temperature did not have much effect on the flexural strength.

Sixty-one in-air room-temperature creep tests have been completed with sustained-load levels investigated ranging from 40 to 95% UTS. Thirty-three elevated temperature (70°, 90°, or 120°C) sustained-load tests have been completed with sustained-load levels investigated ranging from 40 to 91% UTS. Forty-three sustained-load tests in which the specimen was subjected to either room-temperature windshield washer fluid (1000 hour presoak) or distilled water (100 hour presoak) while under load have been completed investigating sustained-load levels ranging from 30 to 95% UTS. In addition, 19 compressive sustained-load tests have been completed in air at either room temperature or 120°C.

Eighty-eight cyclic fatigue tests have been completed. Test parameters included the stress range (40 to 90% UTS, R = 0.1), test temperature (room temperature, –40°, 70° or 120°C), and effect of fluids (100-hour presoak in windshield washer fluid or 1000-hour presoak in distilled water). In addition, 52 tests were completed to examine the mean-stress effects (R = 0, R = -1, R = $-\infty$, or 45% mean UTS). Fatigue test results indicate that as the maximum applied stress level increased, the number of load cycles-to-failure decreased (R = 0.1). Also, exposure to either windshield washer fluid or distilled water resulted in a decrease in the number of load cycles-to-failure relative to in-air test results at the same maximum stress level (R = 0.1).

Results contained in this report will be utilized to develop durability-driven design criteria for the quasi-isotropic carbon-fiber-reinforced PPS composite.

References

1. J. E. Spruiell and C. J. Janke, “A Review of the Measurement and Development of Crystallinity and Its Relation to Properties in Neat Poly (Phenylene Sulfide) and Its Fiber Reinforced Composites,” ORNL/TM-2004/304, Oak Ridge National Laboratory, Oak Ridge, Tennessee (August 2004).
2. J. Cao and L. Chen, “Effect of Thermal Cycling on Carbon Fiber-Reinforced PPS Composite,” Proc. of SEM Annual Conference and Exposition on Experimental & Applied Mechanics, pp. 713-716, Portland, Oregon, 2005.

I. Composite Crash Energy Management

Principal Investigator: Richard Jeryan
Ford Research and Innovation Center
2101 Village Road
MD3137 SRL
Dearborn, MI 48124-2053
(313) 594-4903; fax: (313) 337-5581; e-mail: rjeryan@ford.com

Field Project Manager: C. David Warren
Oak Ridge National Laboratory
P.O. Box 2009, Oak Ridge, TN 37831-8050
(865) 574-9693; fax: (865) 574-4963; e-mail: warrencd@ornl.gov

Technology Area Development Manager: Joseph Carpenter
(202) 586-1022; fax: (202) 586-6109; e-mail: joseph.carpenter@ee.doe.gov
Field Technical Manager: Philip S. Sklad
(865) 574-5069; fax: (865) 576-4963; e-mail: skladps@ornl.gov

---

Contractor: U.S. Automotive Materials Partnership (cooperative agreement) Automotive Composites Consortium Energy Management Working Group
Contract No.: DE-FC05-02OR22910

Objective

- Experimentally determine the effects of material, design, environment, and loading on macroscopic crash performance to guide the design and the development of predictive tools.
- Determine the key mechanisms responsible for crash energy absorption and examine microstructural behavior during crash to direct the development of material models.
- Develop analytical methods for predicting energy absorption and crash behavior of components and structures.
- Conduct experiments to validate analytical tools and design practices.
- Develop and demonstrate crash design guidelines and practices.
- Develop and support design concepts for application in demonstration projects.

FCVT R&D Plan: Task 7; Barrier C

Approach

- Conduct experimental projects to increase understanding of the global and macro influences of major variables on crash performance.
- Use the data from these experiments to create crash intuition, guidelines, and rules-of-thumb and data for the validation of analysis developments.
- Conduct microscopic experimental characterization to define the mechanisms that occur during and as a result of the crash process.
- Develop and validate analytical design tools to predict structural crash performance based on both phenomenological and micro-mechanical approaches to material and crash mechanism modeling.

Accomplishments

- A computational model employing a discrete cohesive zone representation of the fracture plane was used to evaluate the performance of composites with two different polymer matrices. The analyses showed that fracture toughness is more critical than material strength when energy absorption is to be maximized.
- The effects of friction on the energy absorption of composites, including the differences between quasi-static and dynamic behavior, have been characterized and reported.
- A novel driven-wedge test technique was developed to effectively determine the stick-slip behavior of bond fractures including the adhesive bond crack initiation and arrest fracture energies.
- The damage evolution testing of sandwich structures has been completed. The testing included Mode-I (DCB), Mode-II (ENF) and Mixed Mode tests.
- A rate-dependent plasticity model, incorporated into the ABAQUS® code, was used to predict the dynamic crush behavior of square and circular tubes with good correlation to experimental results.
- A Schapery-like, thermodynamically-based theory was developed to characterize post-peak progressive (inelastic) damage. The methodology encompasses a mechanism-based damage/fracture model in order to represent degradation at both the micro and macro (structural) levels.
- The modeling and analysis of a [0° 80k / ±45° 12k] tri-axial carbon-fiber braided composite strip subjected to off-axis compressive loading has been completed.
- A rate-independent damage material model was developed under a multi-scale framework based on the mathematical homogenization theory and a novel model reduction technique that represented the damage-induced fields by influence functions. The multiscale model was implemented for two and three-dimensional problems and incorporated into ABAQUS® Explicit using the user material utility.

Future Direction

- Continue the development and validation of both micro-mechanical and phenomenological analytical design tools to predict structural crash performance.
- Expand micro-mechanical approaches to model material and crash mechanisms and explore novel multi-scale approaches.
- Expand focus on design tools suitable for use with random chopped carbon-fiber-reinforced composites.
- Continue the characterization of the energy absorption mechanisms of carbon fiber-reinforced-composites.
- Characterize the critical physical parameters required for analytical model development. Develop test methods to obtain the stress-strain response beyond the peak stress of the materials and expand the current experimental methods to more fully characterize the dynamic material and physical properties needed to advance the modeling capability.
- Determine the effects of manufacturing features and environmental and loading factors, e.g. minor field damage, abrasion, fatigue, and cumulative effects, on the macroscopic crash performance of carbon and carbon/glass hybrid reinforced composites. These results will establish design guidelines and guide the development of predictive tools.
- Develop relationships to implement analytical tools for commercial use.

Introduction

The purpose of the Crash Energy Management Program is to develop and demonstrate the technologies required to apply production-feasible structural composites in automotive crash and energy management applications. Projects within the program are intended to understand the mechanisms of polymer composite crash, develop analytical tools for use in vehicle design and build a knowledge base for the vehicular application of lightweight polymer composites. The projects relate to materials, molding and assembly process and design configurations that are useful in realistic applications. Design analysis methods will be developed that can be used at several different steps in the design process. These

steps require different levels of precision and speed of use and the appropriate tools are expected to include both micro-mechanical and phenomenological approaches.

Static vs. Dynamic Performance

This project's objectives are to experimentally determine the microstructural factors and behaviors that lead to decreased energy absorption when crushing tubes dynamically. In this study, the strain-rate effects of a braided carbon-fiber composite are investigated at the material specimen level. The goal is to determine the source of rate effects using specimen-level tests and develop experimental methods by which candidate materials for energy absorption can be evaluated for their rate sensitivity. The results of this study will be used to develop and enhance analytical models that will need to take into account rate-sensitive material behavior.

In this period, parametric studies using the Discrete Cohesive Zone Model (DCZM) were conducted with regard to fracture toughness. In addition, the DCZM code was used to predict the fracture behavior of Epon and Hetron resin matrix composites. Parametric studies showed that under Mode I conditions when the fracture toughness of the matrix increases, the overall energy absorption capacity of the composite increases. By keeping the fracture toughness as a constant and varying the cohesive strength (i.e., ultimate strength of the material), it is shown that the peak load of initial fracture increases as the strength increases, however, post-peak energy absorption remains the same. These results are important for the design of energy-absorbing structures since it shows that fracture toughness is more important than the strength of the composite when energy absorption is to be maximized. Experimental results using Epon and Hetron composites showed that in the case of Epon specimens, there is less energy dissipation. This was found to be linked directly to the lower fracture toughness of Epon composite compared to the Hetron composite. The conclusion of the study is that the matrix material toughness is a very important factor when designing for energy absorption. A simple DCZM model that takes into account the material strain energy release rate and strength can be used as a tool to design appropriate composite materials for energy-absorbing structures.

Friction Effects on Crash Performance

The objectives of this work are to (1) experimentally determine the relative energy absorption due to each mode of a progressively crushed composite tube and isolate that portion of energy absorption due to friction and (2) evaluate differences in friction energy absorption between quasi-static and dynamic crush.

All dynamic and static testing has been completed and the documentation of the results and conclusions is complete. The results are published by Michigan State University in a Ph.D. dissertation titled "Friction Energy Absorption in Fiber Reinforced Composites" by Thomas J. Brimhall, August 2005. The results are summarized as follow:

Experiments seem to suggest that sliding friction played an important role in the energy absorption of composite crush tubes. In order to separate the sliding friction Specific Energy Absorption (SEA) from the SEA attributable to matrix damage due to bending, an innovative strip testing fixture was designed, fabricated, and tested. When loaded quasi-statically, the SEA of round-cornered square carbon-fiber-reinforced composite tubes was measured to be 30.4 J/g. The SEA of identical crush tubes when tested dynamically (2 m/sec), was measured to be 23.8 J/g, a decrease in SEA of 6.6 J/g. These results are presented in Table 1 along with the individual energy absorption modes and are described below.

Simple mechanical tests were used to isolate and measure four modes of energy absorption: axial corner splitting, delamination, matrix damage due to bending, and sliding friction. The first two of these modes accounted for a low percentage of energy absorption. Fracture energy values were obtained

Table 1. Quasi-static vs. dynamic loaded carbon composite tube crush dynamic load rate (2.0 m/sec).

Energy Mode	Quasi-Static		Dynamic		Difference	
	J/gm	%	J/gm	%	J/gm	%
Delamination	0.84	2.8	0.84	3.5	0	0
Bending	18.9	62.2	18.6	78.1	-0.3	5
Friction	10.6	34.8	4.3	18.1	-6.34	96
Tube Corner splitting	0.063	0.2	0.06	0.3	0	
Total	30.4	100	23.8	100	-6.6	100

from simple tensile testing and used to calculate SEA attributable to tube corner splitting. End notch flexure testing data was used to calculate SEA attributable to composite delamination.

The strip testing fixture was used to measure SEA attributable to matrix damage due to bending and sliding friction. The strip testing fixture has two test configurations that permit the isolation of SEA attributable to sliding friction. Under quasi-static loading, SEA attributable to matrix damage due to bending was found to be 18.9 J/g or 62.2% of the total tube SEA. Under dynamic crush, the SEA attributable to matrix damage due to bending was found to be 18.6 J/gm or 78.1% of the total tube SEA. Carbon-fiber-composite SEA attributable to sliding friction under quasi-static compression was found to be 10.6 J/gm or 34.8% of the total tube SEA. Under dynamic crush, the SEA attributable to sliding friction was found to be 4.3 J/gm or 18.1% of the total SEA. The decrease in sliding friction SEA of 6.3 J/gm accounted for nearly all of the decrease in tube SEA of 6.6 J/gm between dynamic crush and quasi-static compression. Sliding friction was concluded to be responsible for the decrease in tube SEA from quasi-static compression to dynamic crush.

Impact Performance of Bonded Structures

The objectives of this effort are to (1) evaluate the performance of bonded structures under crash loads; (2) examine the influence of bond design concepts, impact velocity, and other material issues; and (3) fabricate new molding tools to produce simulated automotive structures. Visteon Corporation, an automotive supplier, is leading this effort jointly with Focal Project 3 and ACC Energy Management and Joining Work Groups.

An integrated computational and experimental study of the dynamic response and behavior of an adhesively-bonded, automotive sub-structural component under impact loading is undertaken here. The approach consists of characterizing the dynamic fracture of the adhesive material under various mode mixities. Numerical constitutive models of the adhesive are developed and validated.

Experimental work:

A driven-wedge technique has been developed and implemented at the Oak Ridge National Laboratory (ORNL). Tests have been conducted on 12-ply composite adherends, bonded with the SIA adhesive. A special frame, developed to hold a small wedge, was attached to a 1000 lb load cell mounted on the upper crosshead. The lower end of the bonded beam specimen rests on the hydraulic actuator, which is able to force the specimen past the wedge. The setup is illustrated in Figure 1 below.

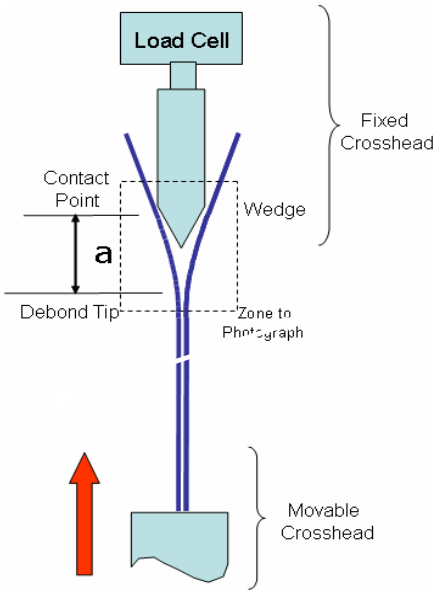


Figure 1. Illustration of driven wedge test configuration.

Tests were conducted over a range of loading rates, up to 1 m/sec, with similar results. This approach has been a major step forward for testing adhesives, showing the substantial stick-slip behavior that is typical of the SIA adhesive material. Rather than obtain only two data points per 12” long double-cantilever beam (DCB) specimen, we are now able to obtain 10 or more data points per specimen. This improves the amount of useful data that can be obtained from a set of specimens, and is believed to offer advantages for future testing needs. Figure 2 illustrates typical results obtained from one specimen that was tested at both 3 and 30 m/min. No significant differences were seen for these rates.

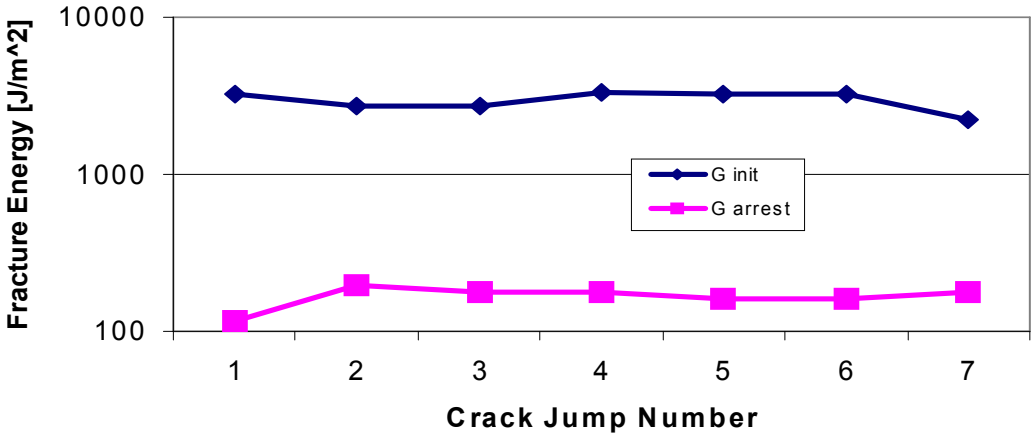


Figure 2. Initiation and arrest fracture energies for bonded 12 ply composite specimens.

Testing of compact tension K_{Ic} specimens at sub-ambient temperatures was continued. When tested cold at 1 m/s, fracture toughness values were on the order of 0.5 MPa $m^{0.5}$, similar to what had been obtained for specimens tested at this rate at ambient conditions. Sub-ambient tests conducted over a range of quasi-static crosshead rates, however, resulted in fracture toughness values that were well above the 1 m/s test results. When tested at slower crosshead speeds at temperatures of -40, -80, -120, and at -160°F, fracture toughness of about 1.5 MPa $m^{0.5}$ was obtained. The results are being analyzed, but application of the time-temperature superposition principle (TTSP) to fracture toughness values does not appear feasible. It is possible that the multiphase components within the formulated adhesive are complicating the time-temperature relationship.

Rate-Dependent Modeling in LS-DYNA:

The preliminary tests on the compact tension test specimens carried out at ORNL showed that the fracture toughness was dependent on the test speeds. A rate-dependent model was formulated to incorporate this behavior in terms of the strain energy release rate and the rate of the opening displacement. The rate-dependent law was implemented in the adhesive elements in the LS-DYNA simulation of the DCB configuration used in the drop-tower tests.

Figure 3 shows the crack length history obtained using the rate-independent and the rate-dependent analysis of a 12-ply composite DCB. The results are obtained using the Tsai and Wu model for the composite damage, which is part of the LS-DYNA material model library (*MAT_054-055). Softening parameters for the progressive damage were not incorporated and are currently being investigated. The results from this preliminary analysis can be considered to be in fair agreement with the experimental result.

Mode II Modeling in LS-DYNA:

Even though the experimental data on Mode II is preliminary, the end-load-split (ELS) falling-wedge test was modeled with the data obtained thus far including some of the Mode I fracture parameters for the SIA adhesive. Also, since the test is dynamic, the force histories from the experiment were not monitored. The simulation matches the experimental results qualitatively. Investigations to obtain a quantitative comparison between the experiments and the simulations are continuing.

Tube Modeling in LS-DYNA

Simulation of the composite tube axial-crush test is being conducted at ORNL using the element deletion scheme in LS-DYNA. These tests are unique in that the crush is performed at a constant velocity, intermediate between quasi-static test speeds and typical impact-sled speeds. Experiments done for the axial crushing of the square composite tube at ORNL were simulated using LS-DYNA. The experiments showed that the composite tubes exhibited extensive material fracture upon impact.

To simulate this kind of fracture in LS-DYNA, shell elements were used to model the composites along

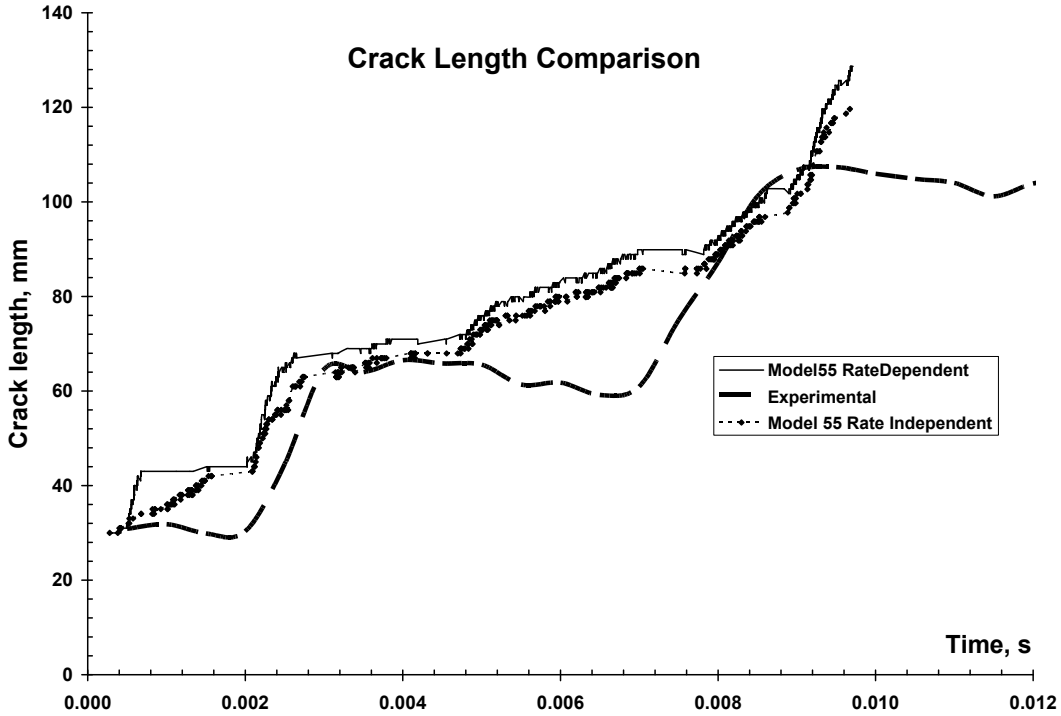


Figure 3. Crack length histories for the SIA-bonded, twelve-ply composite DCB from the falling wedge test, and from rate-independent and rate-dependent LS-DYNA simulations.

with the material model for enhanced composite damage (*MAT_054-055). The built-in criterion for the material model, TFAIL, was used. TFAIL is defined as the time-step criteria for element deletion. The cross-section of the square tube is 100 mm x 100 mm x 2.5 mm. The fracture pattern as well as the peak loads and the load history were compared. The unbonded tube was tested at ORNL at an impact velocity of about 4 m/s. Figure 4 compares the reaction force from the experimental and numerical simulations. The peak loads for each of the time histories are given in parentheses in the legend. Comparison of the two load histories shows that LS-DYNA simulation is not only capable of capturing the right crush mode, but also predicts the peak load reasonably well.

Performance of Novel Sandwich Composites

The objective of this project is to investigate the viability and crashworthiness of novel sandwich composite concepts for automotive applications.

Topics such as wrinkling, face-sheet de-bonding, Poisson's effects and core-skin property mismatch, load-rate effects, impact damage modes, and energy absorption were identified as part of the research effort. The research work being performed at the University of Utah is split into three, phase-specific objectives, of which the first phase has been completed. The current phase involves developing an understanding of the structural response of four selected sandwich composite concepts identified in Phase I. These configurations are:

- Carbon-Epoxy/Balsa
- Carbon-Epoxy/Polyurethane Foam
- P4 Carbon-Epoxy/Polyurethane Foam
- P4 Carbon-Epoxy/Balsa

Numerous structural enhancements have been investigated in the current phase, Figure 5. They include end beveling, vertical edge stitching, perpendicular stitching and vertical webbing. In addition, the current work is also focusing on the details needed in the test fixture to obtain not only high energy absorption in the structural specimens but also consistent test results. The progress thus far has resulted in significant increases in the energy absorption of the above-mentioned configurations, Figure 6. Work is also currently underway to obtain fracture toughness measurements of the face-sheet/core interface. These measurements are input

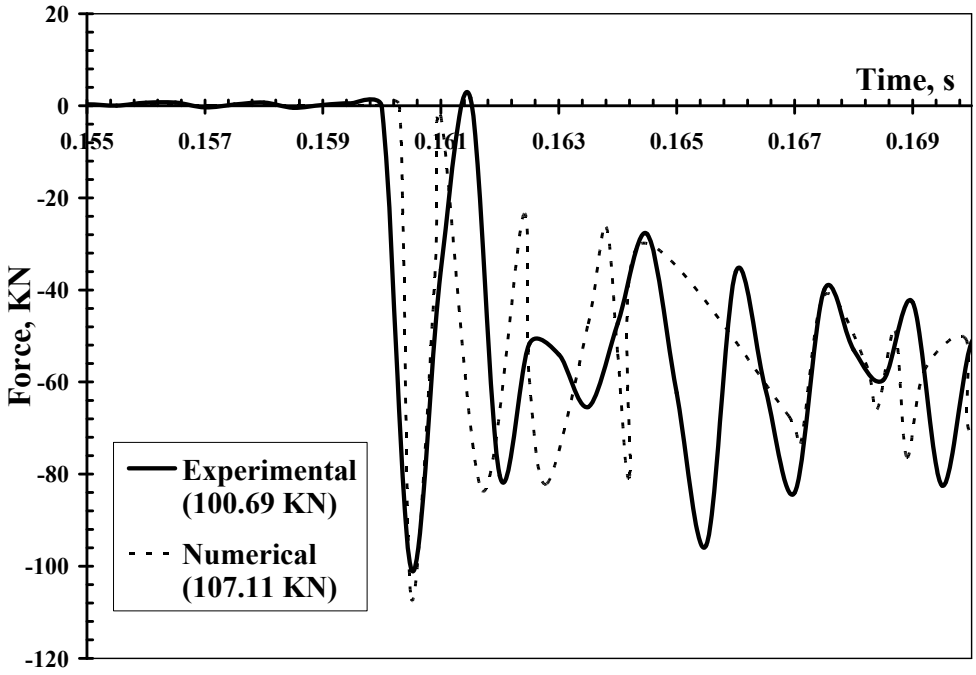


Figure 4. Comparison of force histories for the unbonded tube under an impact velocity of 4m/s.

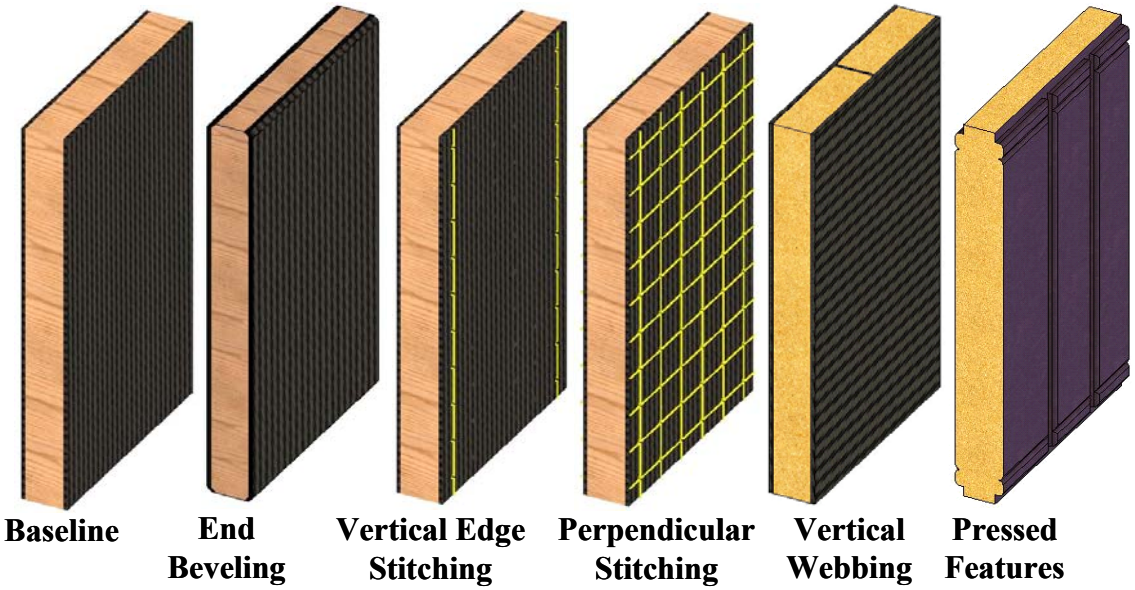


Figure 5. Structural Enhancement Features Being Explored in Phase II.

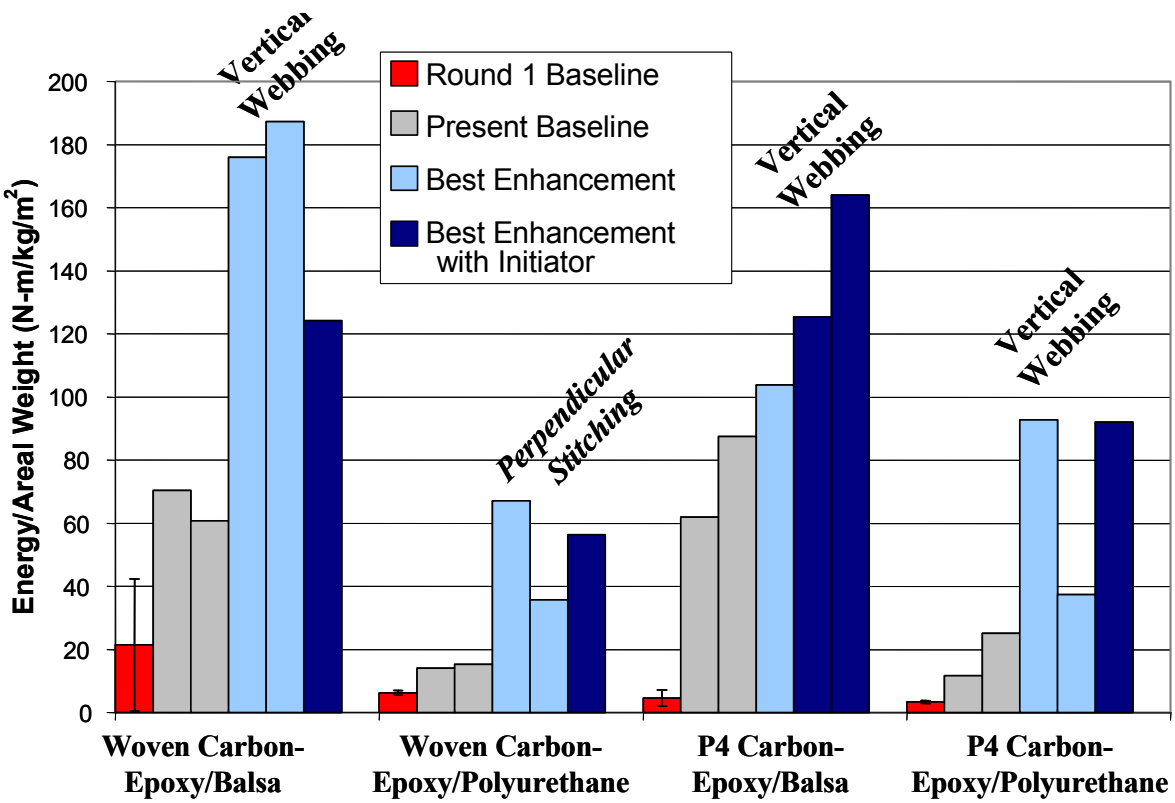


Figure 6. Improvements in Energy Absorption as a Function of the Structural Enhancement and Fixture Position.

to a numerical analysis using the virtual crack closure technique (VCCT) in the commercial software code ABAQUS®.

Energy Absorption of Triaxially Braided Composite Tubes

The objective of the project is to develop a predictive tool for the crush analysis of triaxial braided composite structures under dynamic loads based on a smeared micro-mechanics model. The constitutive law developed for the analysis is based on an anisotropic viscoplastic model proposed earlier by Sun, et al. This viscoplastic law takes into account the effects of strain rate that are necessary to model dynamic behavior.

Fracture of the carbon-composite plies is also modeled in the current simulation. This fracture is not only based on the stresses obtained using the viscoplastic law but also on the critical damage zone that encompasses such fracture stresses. This damage zone takes into account stress concentrations and fiber-tow scissoring. The effect of delay in damage propagation as a result of stress concentration was captured using the fiber bundle theory of Tsai and Hahn specialized for the triaxial braid situation. The effect of stress-concentration was demonstrated by comparing experimental and numerical results in case of a tensile specimen with a hole. The critical damage area approach based on Tsai-Hahn fiber bundle theory was found to be very effective.

The entire modeling approach was demonstrated on dynamic crushing of both square and circular tubes with ±30, 45 and 60 degrees lay-up with very good correlation between experimental and numerical data over a wide range of crush speeds, Figure 7. The constitutive model with scissoring, stress-concentration and rate dependency has been implemented as a Vectorized User Material (VUMAT) subroutine in the explicit version of the commercial software ABAQUS®.

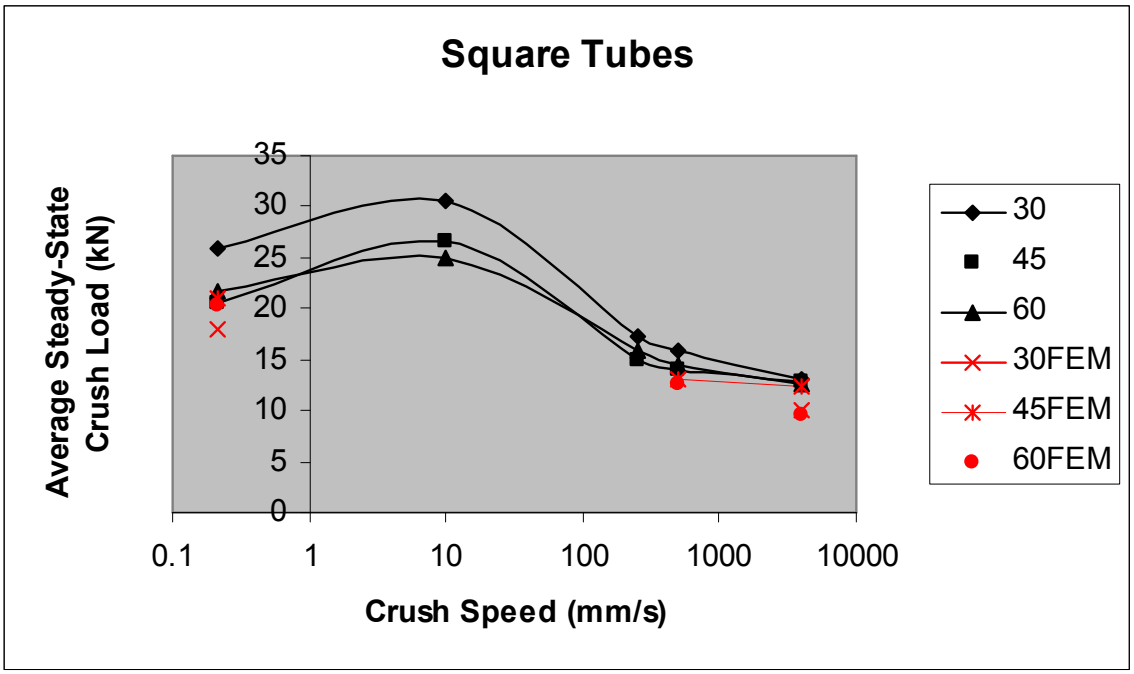


Figure 7. Correlation between Experimental Crush Data and Finite Element Predictions for Carbon-Fiber-Reinforced Square Tubes.

Post-Peak Response Characterization of 2D Triaxially Braided Composites

The objectives of this project are:
1) computationally demonstrate post-peak softening (PPS) observed with single unit-cell structural models on multi-cell structural models;
2) computationally investigate how the hierarchy of damage/fracture modes and the number/arrangement of unit cells affect PPS predictions;
3) computationally investigate how the variation in degree of imperfection in the micro-architecture affects the derived structural properties of the 2D Triaxially Braided Composite (2DTBC); and 4) experimentally test multi-unit-cell structural specimens in order to reflect, refute, or support the finding of the above objectives.

In this project, scalability of macroscopic structural stress-strain relations in 2DTBC will be investigated and studied. Computational models will be employed to demonstrate PPS observed with single-unit-cell structural models on multi-cell unit structural models. The results of such analyses are directly applicable to the development of structural properties of 2DTBC for large-scale finite element (FE) simulations that are needed to assess energy absorption in 2DTBC structural components. Using laser extensometers and speckle photography (for full-field strain measurements), experimental tests to measure PPS on single- and multi-cell 2DTBC will be performed. Further, computational models that incorporate cohesive zones (CZ) within the cell in order to capture experimentally-observed tow/matrix separation will be developed and analyzed including the effect of CZ on PPS. Finally, the computational analyses will be carried further in order to study and characterize the effects of measured architecture imperfections on the single-unit-cell and multi-cell structural stress-strain properties of 2DTBC, including the effects of different types and distribution of imperfection on PPS.

The primary resin matrix materials (Hetron and Epon) were experimentally characterized by measuring their pure (virgin) properties, performing coupon tension tests (with 0 ^{o}, +45^{o}/-45 ^{o} tow orientations), and then using data reduction techniques back-calculated *in-situ* material properties. Compression tests on coupons were also performed in the transverse (matrix-dominated) direction. It was found that *in-situ* matrix properties differ from pure matrix properties, and hence, the *in-situ* properties should be used for subsequent FE

analyses. Since axial fiber tows are the dominant load-carrying component, statistical scanning electron microscopy (SEM) in conjunction with photo-stitching techniques were performed on the Hetron- and Epon-based composites. From the detailed specimen preparation and subsequent SEM images, it was found that unwetted regions inside the tows need to be accounted for in finite element analysis by a reduction in tow cross-sectional area and/or material constants. Such regions that reduce the fiber volume fraction exist in the Hetron-based composite and are usually associated with micro-fracture. Note that Hetron typically exhibits an approximately 10% shrinkage during curing. However, detailed SEM images of Epon-based composite show that the tows are fully wetted and micro-cracks are minimal (typically, Epon exhibits little or no shrinkage while curing). Such a difference might explain (at this stage in the study) the higher energy absorption capacity of the Hetron-based system as compared with the Epon-based system.

Detailed FE models have been developed for a representative unit cell (RUC) for both material systems (Hetron and Epon). A RUC model (which is based on the real geometry) was analyzed using a new method in order to obtain the *in-situ* stress state of the matrix within a braided textile composite. It was found that when performing RUC-based analysis, it is important to recognize volume consolidation processes occurring during manufacturing. For example, when an enlarged cross-sectional image of a multi-layered braided composite is analyzed and the "theoretical" boundaries of adjacent RUCs within this image are marked, one notices that some RUCs are overlapping. To account for this fact in subsequent analyses, a computer program was developed to analyze the image and calculate the "actual" axial fiber-tow area. Based on the latter, the actual fiber volume fraction is recalculated, and the axial fiber-tow modulus within a RUC was adjusted.

An imperfection analysis study on a RUC was performed using FEA. The geometric imperfection was derived from the eigen modes of the RUC with the imperfection amplitude used as a parameter. Nonlinear geometry and nonlinear material properties were included. The analyses demonstrated the imperfection-sensitivity character of this material/ structural system.

It was found that when a plasticity model is used, the Mises stress within the matrix element (in the RUC) has already reached the maximum value specified by the plasticity curve. This results in an artificial stiffening of the matrix. Because inelastic behavior is associated with work-loss, the team has suggested the development and employment of a Schapery-like, thermodynamically-based theory (ST) to characterize the progressive (inelastic) damage. Such an approach requires the definition of internal state variables. Further, the Schapery-like methodology will encompass mechanism-based damage/fracture modeling in order to model degradation at both the micro and macro (structural) levels. The principal investigator (PI) and team have formulated the mathematical basis for this work and have presented it to the sub-group. This formulation shows several relations between internal state variables and the energy of the system, as well the relation between instantaneous moduli in damaged state and virgin state. The PI and team have received 1-ply plaques of the same material systems (Epon- and Hetron-based) and performed coupon-level experiments. Extensive testing was performed on the 1-ply specimens, followed by experimental data processing including the extraction of the ST internal state variables (ISV) for RUC damage modeling.

A computer program was developed to calculate the ISV from the stress/strain test data. This program is incorporated directly into a FEA code so that ISV (implicit to the constitutive law) are automatically calculated during a FEA.

Lateral Impact Study

The objective of the project is to achieve a fundamental understanding of the energy absorbing mechanisms in triaxially braided composites subjected to lateral bending and impact. A combined experimental and analytical approach has been planned and implemented for this purpose. The analytical study has applied the smeared micro-mechanics material model previously developed in the Energy Management Program, available as a user sub-routine with ABAQUS®. Following a correlation study based on a simple test coupon, a

specimen representative of an automotive component subjected to bending impact loads will be evaluated.

The overall study involves three distinct phases: 1) smeared micro-mechanics material model of composite strips under lateral bending, 2) validation of the model using experimental data, 3) extension of the model for designing automotive components. Phase I of the project has been completed with the modeling and analysis of a [0° 80k / ±45° 12k] triaxial carbon-fiber braided composite strip subjected to off-axis compressive loading.

Phase II experimental testing of composite strips to validate the model effectiveness was completed by a university contractor in January 2005. Ninety specimens were tested to characterize the properties of triaxially braided composites in tensile, compression, pure bending and lateral bending.

Continuing software development during the course of this project has produced improvements in the basic ABAQUS® routines. Correlation studies with the updated version of the UMAT subroutine and Phase II test data were reported in May 2005. Problems noted with the test data were identified for further study.

Multi-scale Modeling for Crash Prediction of Composite Structures

The objective of this research project is to develop a material model that considers microstructural aspects of damage and an efficient multi-scale modeling tool that is able to predict dynamic crush response of automotive composite structures at an affordable computational cost.

Four tasks of the research were proposed to accomplish the goal: (1) development of damage models for polymeric composites under the multi-scale computational framework; (2) calibration of the models to the experimental data provided by the ACC; (3) implementation of the developed capabilities into ABAQUS® Explicit, and finally (4) validation of the developed simulation capabilities against the experimental data on tubes in a drop test.

Research efforts so far have focused on Task 1 and Task 3. For Task 1, rate-independent damage material model for polymeric composites has been developed under the multi-scale framework based on the mathematical homogenization theory. At each representative volume element, the fracture of the composite materials was modeled as a progressive debonding and delamination at the material interfaces, as well as the degradation of the phase material properties. Two damage variables were introduced correspondingly to reflect the phase damage and the interface damage between phases using continuous damage mechanics. The constitutive relationship resulting from this microscale damage model is to be used in the numerical simulation of its corresponding macroscale model.

To significantly reduce the computational cost devoted to obtaining the constitutive relationship at each representative volume element for the simulation of the macroscale model, a novel model reduction technique was formulated by representing the damage-induced fields by influence functions. The influence function can be numerically evaluated at preprocessing stage ahead of the macroscale simulation. The model reduction approach was incorporated into the classical nonlinear homogenization theory. The accuracy and the computational cost of the homogenized model with model reduction is a function of the number of degrees-of-freedom used to interpolate the interface damage variables and the number degrees-of-freedom used to interpolate the microscale phase damage variables.

The developed multi-scale model has been implemented for two- and three-dimensional problems and incorporated into ABAQUS® Explicit using the user material utility (Task 3). A number of numerical verifications were conducted by comparing the newly developed multiscale model to the most sophisticated mathematical model involving no model reduction. As shown in Figure 8, a three-dimensional unit-cell problem with interface damage was considered. The unit-cell was under tensions along the 1 and 2 directions. Figure 9 illustrates the damaged unit-cell due to the tensions obtained from the classical unit-cell calculation without the model reduction. Figure 10 shows history curves of the response force along 1

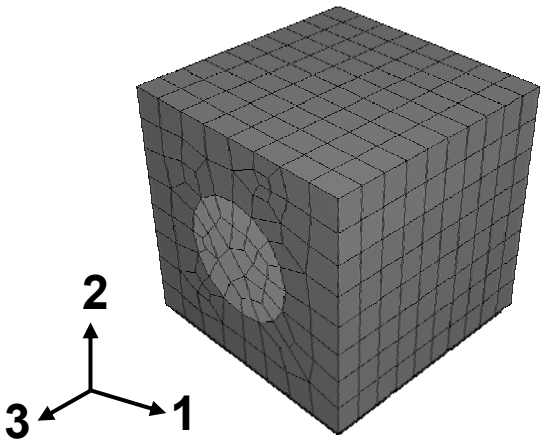


Figure 8. The Unit-Cell Problem.

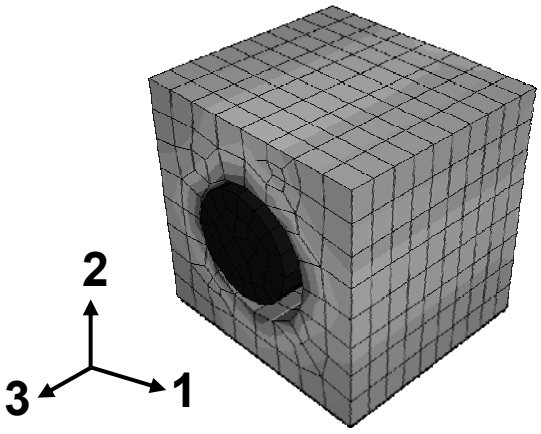


Figure 9. The Deformed Unit-Cell Under Tensions.

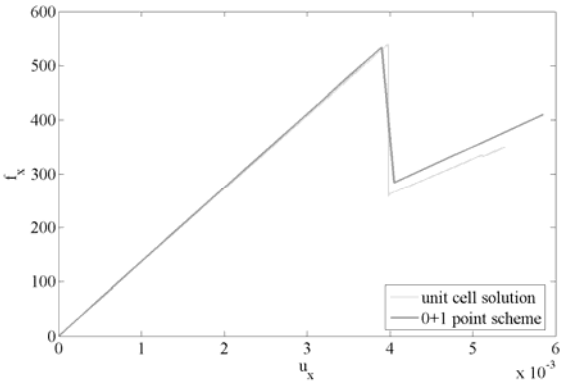


Figure 10. The History Curves of The Response Force Verses The Displacement.

direction with respect to the displacement along 1 direction for the classical unit-cell calculation and the developed unit-cell calculation with the model reduction. In this case, the developed approach only used one degree-of-freedom to approximate the interface damage variable and achieved quite agreeable response to the expensive classical unit-cell calculation, which used more than 1000 degrees-of-freedom.

The next phase of this project will concentrate on the development of the rate-sensitive damage model for interface debonding and phase degradation (completing Task 1), calibration of the developed material models to the experimental data provided by the Automotive Composites Consortium (Task 2) and validation of the simulation capabilities developed against the experimental data on tubes in a drop test (Task 4).

Summary

The Crash Energy Management Program develops and demonstrates technologies that are used to apply production-feasible structural composites in automotive crash and energy management applications. Projects within the program are intended to understand the mechanisms of polymer composite crash, develop analytical tools for use in vehicle design and build a knowledge base for the vehicular application of lightweight polymer composites. During FY2005, in the experimental projects,

The effects of friction on the energy absorption of composites, including the differences between quasi-static and dynamic behavior, have been characterized and reported

A novel driven-wedge test technique was developed to effectively determine the stick-slip behavior of bond fractures including the adhesive bond crack initiation and arrest fracture energies.

A novel driven-wedge test technique was developed to effectively determine the stick-slip behavior of bond fractures including the adhesive bond crack initiation and arrest fracture energies.

In the analytical studies,

- A computational model employing a discrete cohesive-zone representation of the fracture plane was used to evaluate the performance of composites with two different polymer matrices.

The analyses showed that fracture toughness is more critical than material strength when energy absorption is to be maximized.

- A rate-dependent plasticity model, incorporated into the ABAQUS® code, was used to predict the dynamic crush behavior of square and circular tubes with good correlation to experimental results.
- A Schapery-like, thermodynamically-based theory was developed to characterize post-peak progressive (inelastic) damage. The methodology encompasses a mechanism-based damage/fracture model in order to represent degradation at both the micro and macro (structural) levels.
- The modeling and analysis of a [0° 80k / ±45° 12k] triaxial carbon-fiber braided composite strip subjected to off-axis compressive loading has been completed.
- A rate-independent damage material model was developed under a multi-scale framework based on the mathematical homogenization theory and a novel model reduction technique that represented the damage-induced fields by influence functions. The multi-scale model was implemented for two and three-dimensional problems and incorporated into ABAQUS® Explicit using the user material utility.

Bibliography

1. Brimhall, Thomas J. "Friction Energy Absorption in Fiber Reinforced Composites." PhD diss., Michigan State University, 2005.
2. Salvi, Amit G.; Waas, Anthony M.; Caliskan, Ari, Rate-Dependent Compressive Behavior of Unidirectional Carbon Fiber Composites Polymer Composites, Aug 2004, v 25, n4, pp. 397-406.
3. Salvi, Amit G.; Waas, Anthony M.; Caliskan, Ari, Specimen Size Effects in the Off-axis Compression Test of Unidirectional Carbon Fiber Tow Composites, Composites Science & Technology, v 64 n 1, January 2004, pp. 83-97.
4. Kapania, Rakesh K., Makhecha, Dhaval P., Johnson, Eric R., Simon, Josh, Dillard, David A., Modeling Stable And Unstable Crack Growth Observed In Quasi-Static Adhesively Bonded Beam Tests. IMEC204-59765. Proceedings of IMECE'04, 2004 ASME International Mechanical Engineering Congress and Exposition, Anaheim, California, USA, November 13-16, 2004
5. Joshua C. Simón, David A. Dillard, Eric R. Johnson, Characterizing the Impact Fracture Properties of Structural Adhesives, Presented at the 27th Annual Meeting of Adhesion Society, Wilmington, NC, USA, February 15-18, 2004.
6. A. L. Van Otten, N. S. Ellerbeck, D. O. Adams, C. L. Nailadi, K. W. Shahwan, *Evaluation of Sandwich Composites for Automotive Applications,* Proceedings of the 2004 SAMPE Conference, Long Beach, California.
7. Flesher, N.D.; Chang, F-K. Modeling the Response of Braided Composites with Stress Concentrations. 11th US-Japan Conference on Composite Materials. September 9-11, 2004. Yonezawa, Japan.
8. Flesher, N.D.; Chang, F-K. Effect of Cross-Section Configuration on Energy Absorption of Triaxially Braided Composite Tubes. 18th Annual Technical Conference American Society for Composites. Oct. 19-22, 2003. University of Florida.
9. Flesher, N.D. ; Cheng, W. Evaluation of STCrush for Characterization of Crushing Behavior of Composite Tubes. 10th US-Japan Conference on Composite Materials. September 16-18, 2002. Stanford University.
10. Quek SC, Waas AM, Shahwan KW and Agaram, V. Compressive response and failure of braided textile composites: Part 2 - computations, Int J.Nonlinear Mech. 39 (4): 650-663, June 2003.
11. Quek SC, Waas AM, Shahwan KW and Agaram, V. Compressive response and failure of braided textile composites: Part 1 - experiments, Int J. Nonlinear Mech. 39 (4): 635-648, June 2003.
12. Quek, S C, A M Waas, K W Shahwan, and V Agaram, Analysis of 2D Flat Triaxial Braided Composites, Int.J. Mechanical Sciences, 45 (6-7): 1077-1096, 2003.
13. Quek SC, Waas AM, Micromechanical Analyses Of Instabilities In Braided Glass Textile Composites, AIAA J, 41 (10): 2069-2076 Oct. 2003.

J. Crash Analysis of Adhesively-Bonded Structures (CAABS)

Principal Investigator: J. Michael Starbuck
Oak Ridge National Laboratory
P.O. Box 2009, Oak Ridge, TN 37831-8048
(865) 576-3633; fax: (865) 574-8257; e-mail: starbuckjm@ornl.gov

ACC Collaboration Contact: Naveen Rastogi
Visteon Corporation
6100 Mercury Drive, #SW61-025, Dearborn, MI 48126
(313) 755-6264; fax: (313) 755-4229; e-mail: nrastogi@visteon.com

Project Manager, Composites: C. David Warren
Oak Ridge National Laboratory
P.O. Box 2008, Oak Ridge, TN 37831-6065
(865) 574-9693; fax: (865) 576-4963; e-mail: warrencd@ornl.gov

Technology Area Development Manager: Joseph A. Carpenter
(202) 586-1022; fax: (202) 586-1600; e-mail: joseph.carpenter@ee.doe.gov
Field Technical Manager: Philip S. Sklad
(865) 574-5069; fax: (865) 576-4963; e-mail: skladps@ornl.gov

---

Contractor: Oak Ridge National Laboratory
Contract No.: DE-AC05-00OR22725

Objectives

- Develop a comprehensive experimental and analytical methodology to analyze and design adhesively-bonded automotive composite structures to sustain axial, off-axis, and lateral crash/impact loads.
- Determine the rate sensitivity of bonded tubes to crush through experiments on the Oak Ridge National Laboratory (ORNL) Test Machine for Automotive Crashworthiness (TMAC).
- Determine influence of critical joint design parameters, for example, bond length, bond thickness, and fillet, on specific energy absorption.
- Experimentally determine the full-field deformations at joint discontinuities for validation of analytical/numerical results.

Approach

- Coordinate with the bonded-joint experimental and analytical efforts undertaken in the Automotive Composites Consortium (ACC) thrust "Composite Crash Energy Management" (report 4.I)
- Select a substrate, adhesive, and representative subcomponent joint geometry for evaluation.
- Characterize substrate material, adhesive material, and coupon-level joints under static and dynamic loads.
- Build and test unbonded and bonded rail components under static and dynamic crush loads.
- Correlate experimental results with analytical results by developing finite-element-based tools with appropriate material models and progressive-damage algorithms.
- Enhance the understanding of joint performance by conducting full-field deformation measurements.

Accomplishments

- Characterized tensile and fracture toughness of bulk adhesive at quasi-static and dynamic loading rates.
- Completed scanning electron microscopy (SEM) studies to characterize the fracture surface in bulk adhesive compact-tension specimens.
- Characterized static and dynamic behavior of the braided carbon-fiber composite substrate under uniaxial tension loads.
- Completed static and dynamic tests at three different velocities on both unbonded and bonded tubes using TMAC.
- Designed and fabricated a slack adapter for conducting dynamic coupon-level tests.
- Completed static and dynamic tests on specimens having single-lap and double-notch joint geometries to determine influence of critical joint design parameters on specific energy absorption.
- Completed static and dynamic Mode I fracture toughness tests using the double-cantilever-beam (DCB) driven-wedge test.
- Procured new high-rate equipment for conducting coupon-level dynamic tests at higher rates than current equipment capability.

Future Direction

- Complete dynamic testing of substrate, bulk adhesive, and coupon-level joints at rates greater than 1 meter/second.
- Complete Mode II, Mode III, and mixed-mode fracture toughness tests at static and dynamic rates.
- Complete bonded and unbonded tube tests at two additional velocities.
- Install and set-up test equipment for characterizing full-field deformation patterns in adhesive joints.

Introduction

The objective of this project is to develop a comprehensive experimental and analytical methodology to analyze and design adhesively-bonded automotive composite structures to sustain axial, off-axis, and lateral crash loads. This direct-funded project will be closely aligned with the experimental and analytical efforts undertaken by the Automotive Composites Consortium (ACC) "Composite Crash Energy Management" thrust (see report 4.I). The focus of this work, however, will be restricted to the adhesive-joint related issues. The key to the methodology development is the understanding of how critical joint design parameters, for example, bond length, bond thickness, and fillet, affect the energy absorption. Recent investigations at ORNL have provided valuable insight toward the understanding of composite joint performance and composite crashworthiness. The next logical step is determining the correlation between measurable adhesive joint parameters and their influence on the structure to dissipate energy and ultimately predict crashworthiness for a particular composite design.

Experimental tasks include material testing under quasi-static and dynamic loads for substrates, adhesives, and joints; full-field deformation mapping of joints for correlation with computational results; strain-rate sensitivity studies; fracture toughness testing; and test method development as required. These experimental results will provide the building blocks for model developments—first at the coupon level, then progressing in complexity to component level. Correlation with experimental results will provide the basis for which the analytical developments, including development of constitutive laws, materials models, damage algorithms, and new finite elements will be made. Structural tests will be conducted on the new intermediate-rate Test Machine for Automotive Crashworthiness (TMAC)] at ORNL.

Approach and Results

The technical approach involves both experimental and analytical tasks. There are four main tasks:

Task 1—Materials Selection and Screening,
Task 2—Material Characterization,
Task 3—Component Testing, and
Task 4—Computational Tools Development.

Task 1 was completed and reported on in the FY 2002 annual report. The chopped-carbon-fiber prepreg material system selected was characterized from flat plaques provided by the vendor. Discussions with the vendor led to an overly optimistic view of the suitability of the material for this project. Additionally, delays in receipt of the material from the supplier resulted in consideration of a carbon-fiber sheet-molding-component (SMC). Both materials were unsatisfactory due to processing difficultly and material variability. As a result of the variability in the initial material screening tests and difficulty in fabricating tubes with this material, the substrate material was changed to a carbon-fiber braided system. The woven-fabric prepreg is comprised of T300B carbon fiber with a tow size of 3K and 42% (by weight) epoxy resin.

Task 2 was initiated during FY 2002 and has continued through FY 2005. This task focuses on determining the rate dependencies, if any, for mechanical properties of the bulk adhesive, substrate, and coupon-level joints.

Task 3 started in FY 2004 with preliminary tests to determine if the selected composite-tube geometry would provide for a stable progressive crush behavior instead of global buckling. The geometry for the tube was 100 mm by 100 mm square with a 3 mm wall thickness and a 300 mm length. A 45-degree bevel was used for the triggering mechanism. These tests showed that a progressive crush failure mechanism was achievable using this geometry. Therefore, the required unbonded and bonded tubes needed for the remainder of the project were procured from Pacific Composites.
In Task 4, the development of computational tools was subcontracted to Virginia Tech under ACC Cooperative Agreement funding.

Bulk Adhesive Specimen Fabrication

The adhesive used, PL731SI, is a commercially available, two-part epoxy system produced by Sovereign Specialty Adhesives Inc. (Chicago, IL). The bulk adhesive testing consisted of tension, compression, shear, and fracture toughness. In addition, differential scanning calorimetry and dynamic mechanical analysis tests were conducted to verify the degree of cure. The key to this task was the successful fabrication of high-quality specimens (e.g., low void content) to accurately quantify the bulk adhesive mechanical properties. The resin and hardener were mixed at a 4:1 ratio using a MixPac MC 10-24 static mixer on a Profill pneumatic dispenser. The adhesive was degassed by centrifuging for 15 minutes at room temperature in a container that could serve as a syringe for subsequent dispensing. The compression and shear testing were accomplished using cylindrical-rod specimen geometries. Cylindrical-rod specimens were fabricated using centrifugation and glass test tubes as molds. Initial difficulties in producing flat plaques were alleviated by developing a mold-filling process that uses an adequate supply of excess adhesive under pressure to back-fill the mold cavity. The adhesive was carefully squeezed onto a stainless steel plate that had been coated with Lilly RAM 225 mold release to allow for subsequent separation. A dam of silicone rubber tubing and rigid spacers of the desired thickness were used to support a second plate to produce a plaque with consistent thickness. The plates were clamped together and the assembly was held at 125ºC for 60 minutes in a convection oven. The curing procedure was used based on discussions with the manufacturer. Using this technique, neat adhesive plaques were prepared with thicknesses of 8 and 27 mm. High-quality specimens for all bulk adhesive tests were fabricated with these two approaches.

Bulk Adhesive Fracture Toughness

A key parameter in the development of computational models under Task 4 was the rate-sensitive fracture toughness of the bulk adhesive. Miniature compact tension specimens were machined from hockey-puck-shaped adhesive castings. The castings were fabricated with zero voids using the techniques developed for flat plaques and cylindrical rods. Quasi-static and

dynamic fracture toughness tests were conducted on the bulk adhesive using an 8-mm-thick specimen per the geometry specified in ASTM D5045.

Fracture toughness tests of the bulk adhesive were conducted at room temperature on a conventional, closed-loop, servo-hydraulic machine at rates ranging from 10^{-6} to 1 m/s. The load frame was equipped with a commercial slack adaptor or lost-motion device. Checkout tests were completed and it was determined that the target velocities could be achieved prior to the load application. However, at rates of 0.5 and 1 m/sec, it was difficult to accurately detect the relatively small loads generated by the test specimen because of contributions from the momentum of the 4-kg commercial slack adapter. Hence, a much smaller and lighter slack adapter shown in Figure 1 was fabricated in-house by cutting and threading a #2 Morse taper [Standard Extension Drill Socket:1-5161-015]. Fracture toughness tests were successfully repeated at various rates from 10^{-6} to 1 m/sec with three specimens tested at each rate. The new setup, shown in Figure 2, included a smaller load cell, a shorter and simplified load train between the load cell and specimen, and reduced weight on the specimen because of the lighter adapter.

Figure 3 illustrates the fracture toughness over the range of loading rates from 10^{-6} to 1 m/s. Fracture toughness was found to decrease as a function of loading rate, resulting in a drop in fracture toughness at 1 m/sec to about 20% of the value at lower rates. Error bars, which have been included in the figure, show that the data obtained was quite consistent at each condition. While the plane-strain



Figure 1. Small slack adaptor.

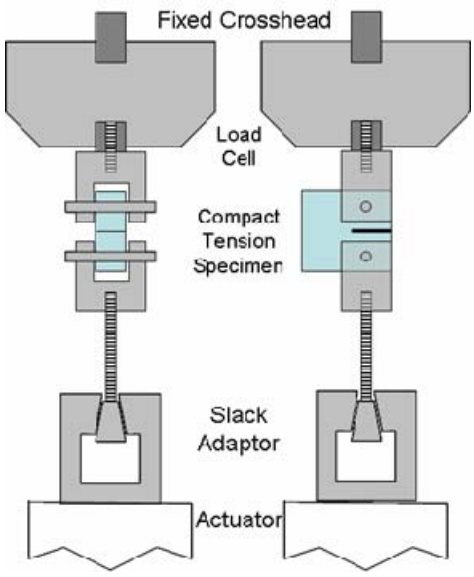


Figure 2. Load train.

fracture toughness, K_{Ic}, was determined from the intercept of a 95% slope with the load trace for the slower rates, the peak load was used to determine the fracture toughness at the higher rates. The dashed line in Figure 3 illustrates fracture-toughness values obtained from using the peak load values at the slower rates.

Figure 4 shows that at the lower rates there was extensive stress whitening and stable crack growth. Stress whitening was significantly reduced at higher testing speeds suggesting that plastic deformation at the crack tip was severely limited at the higher loading rates. Additionally, the failure appeared much more brittle at higher rates.

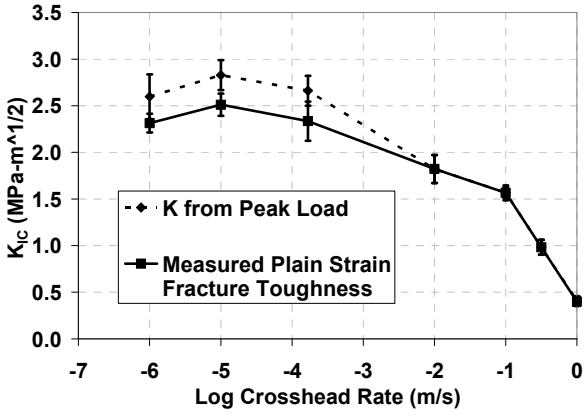


Figure 3. Measured fracture toughness values as a function of crosshead rate.

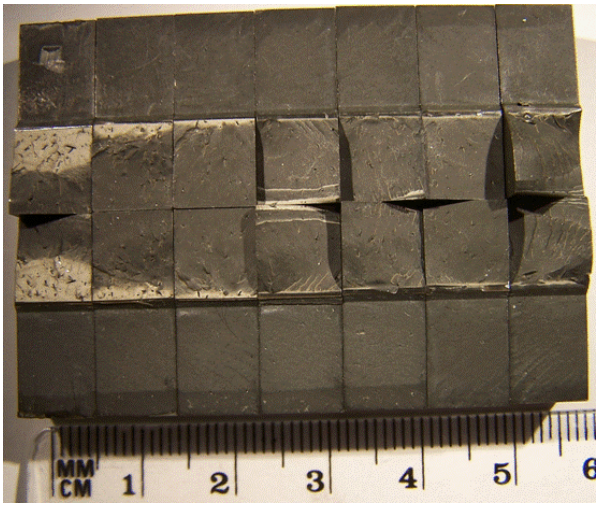


Figure 4. Illustration of typical stress whitening extent for range of crosshead rates in increasing order from left to right.

Bonded and Unbonded Tube Tests

The matrix for the tube testing consisted of crushing tubes having different bond widths and bond thicknesses at different velocities. The test velocities were chosen to be 50 mm/sec, 500 mm/sec, and 5000 mm/sec. The bond line thicknesses were either 0.5 mm or 1.0 mm and the bond width or tube overlap was either 25 mm or 50 mm. Figure 5 shows the test results in terms of the specific energy absorbed (SEA) as a function of test velocity. A snapshot of one of the bonded tubes being crushed at 5000 mm/sec is shown in Figure 6. The results in Figure 5 show a significant decrease in SEA as a function of loading rate with the largest reduction seen to occur above the 500 mm/sec rate.

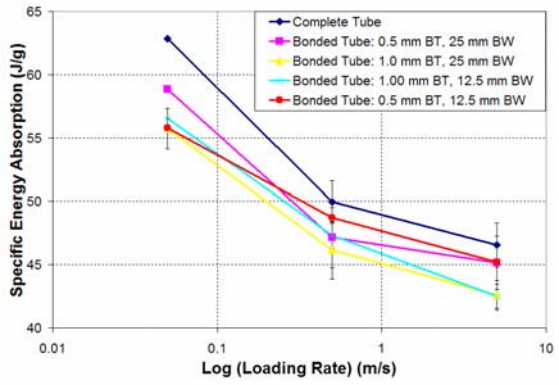


Figure 5. Measured tube SEA as a function of crosshead rate.

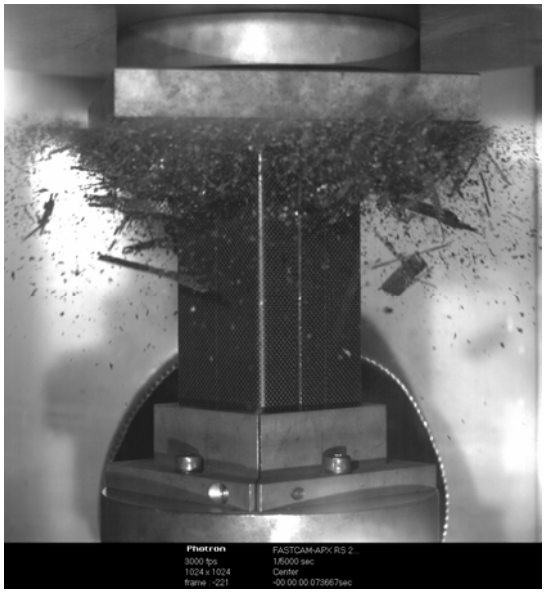


Figure 6. Bonded tube tested at 5000 mm/sec.

Also, the unbonded or complete tubes are seen to have the highest SEA compared to the bonded tubes. The effect of bond width appears to be negligible but there does appear to be a slight effect on bond thickness with the thinner bonds having slightly higher SEAs.

Conclusions

Material characterization tests were completed on bulk adhesive specimens and carbon-fiber woven-fabric substrate specimens. A key parameter for the modeling efforts being conducted at Virginia Tech was the determination of the rate-sensitive fracture toughness for the bulk adhesive. This was accomplished for Mode I by conducting compact-tension tests at different loading rates. The results showed a definite decrease in fracture toughness as the loading rate increased. The Mode I toughness at 1 meter/second was only 20% of the static value. Adhesive-joint specimens are currently being tested to characterize the rate sensitivities for Mode II fracture toughness.

To validate analytical models and to quantify the effect that an adhesive joint has on specific energy absorption, a series of progressive crush tests on composite tubes was conducted using TMAC. Tests on bonded and unbonded tubes were completed at loading rates of 50, 500, and 5000 mm/sec. The SEA's were calculated and the results showed a

decrease in SEA with loading rate for both the unbonded and bonded tubes. This trend is similar to that seen in previous ACC composite tube crush data, where the majority of the decrease in SEA appears to occur below the 500 mm/sec velocity. Additional tube tests are planned to better quantify this effect.

Presentations/Publications/Patents

"Dynamic Testing for Quantifying Rate Sensitivities in Bonded Composite Structures," presented at the 2005 Society for Experimental Mechanics Annual Conference on Experimental and Applied Mechanics, June 7-9, 2005, Portland, Oregon. This paper was given the best paper award in the Advanced Composite Materials and System Track.

"Rate Dependent Cohesive Zone Modeling of Unstable Crack Growth in an Epoxy Adhesive," published in the Proceedings of the 2005 ASME International Mechanical Engineering Congress and Exposition.

K. Engineering Property Prediction Tools for Tailored Polymer Composite Structures

Principal Investigator: Ba Nghiep Nguyen
Pacific Northwest National Laboratory
902 Battelle Boulevard, P.O. Box 999, MS: K5-22, Richland, WA 99354
Phone: 509-375 3634, Fax: 509-375 6736, e-mail: Ba.Nguyen@pnl.gov

James D Holbery
Pacific Northwest National Laboratory
902 Battelle Boulevard, P.O. Box 99, MS: K5-22, Richland, WA 99354
Phone: 509-375 3686, Fax: 509-375 6736, e-*mail: James.Holbery@pnl.gov*

Vlastimil Kunc
Oak Ridge National Laboratory
P.O. Box 2009, Oak Ridge, TN 37831
Phone: 865-574 8010, Fax: 865-574-0740, e-mail: kuncv@ornl.gov

Technology Area Development Manager: Joseph A. Carpenter
(202) 586-1022; fax: (202) 586-1600; e-mail: joseph.carpenter@ee.doe.gov
Field Technical Manager: Philip S. Sklad
(865) 574-5069; fax: (865) 576-4963; e-mail: skladps@ornl.gov

---

Contractor: Pacific Northwest National Laboratory, Oak Ridge National Laboratory
Contract No.: DE-AC06-76RL01830, DE-AC05-00OR22725

Objective

- Enable the optimum design of lightweight automotive structural components using long-fiber-reinforced injection-molded thermoplastic composites (LFTs).

Approach

Phase I: Technical-feasibility assessment

- Perform a technical assessment of current process models and computational methods for short-fiber polymer injection-molded composites in order to determine their accuracy, limitations and potential applications to LFTs.
- Identify the research directions needed to develop process and constitutive models for LFTs.
- Understand and examine the LFT emerging microstructure, characterization techniques and material processing.
- Characterize LFT parts for both fiber orientation and attrition by applying x-ray tomography, automated methods utilizing advanced microscopy combined with polymer matrix etching, and ultrasonic inspection.
- Examine the molding behaviors of glass and carbon fibers.

Phase II: Research and development

- Develop an integrated approach that links process to structural modeling allowing the optimum design of LFT composite structures.

- Establish experimental methodologies for material characterization and testing to develop material property and performance databases and to verify modeling predictions.

Accomplishments

- The technical assessment of current process models has pointed out that the fiber-orientation equation and constitutive relation for short-fiber systems needs to be improved to account for the features of long-fiber systems which are characterized by limited fiber mobility, collective movement of fiber domains, fiber attrition, and bending of fibers.
- An approach to the fiber-suspension flow problem using the smoothed particle hydrodynamics method was formulated.
- Numerical assessment of current process modeling capability was performed for a center-gated disk and an end-gated plaque.
- The project kickoff meeting was organized at the USCAR headquarter on September 1st, 2005. A steering committee composed of Automotive Composite Consortium, American Plastics Council, and National Labs members was formed to follow this project.
- Identified several methods of non-destructively and destructively characterizing LFT composite fiber orientation, and have experimented and conducted proof-of-concept verification of these techniques.
- Identified a specialty material supplier and arranged procurement of materials for molded parts.
- Have identified and secured Tier 1 supplier commitment for molding LFT plaques and test articles for feasibility program. Have begun process of Tier 1 supplier commitment to the full project.
- Have secured commitment with LFT material supplier, both for the feasibility and full program.
- Completed material mold evaluation, identified US manufacturer, obtained mold quotation, and completed investigation of adaptation of PNNL Aarborg 350 injection-molding machine to mold LFT materials.

Future Direction

- The technical feasibility assessment phase will be completed by March 2006 that includes the completion of the assessment of process models and available computational tools to perform the work, the establishment of an experimental methodology, and research directions to develop process models for LFTs,
- Develop a material performance matrix to obtain material parameters for model input.
- Begin developing process and property prediction models for LFTs from April 2006.
- Further develop non-destructive techniques to determine fiber orientation, fiber length, and fiber attrition in molded parts.
- Procure materials and subsequently mold test samples with selected Tier 1 molder.

Introduction

Injection molding of fiber-filled thermoplastics is a multi-step process which consists of i) pre-mixing and pelletizing the fibers and thermoplastic resin, ii) putting the pellets in an injection molding machine that melts them and injects them under high pressure into a mold (*mold filling*) iii) solidifying the as-formed composite in the mold (*packing, holding and cooling*), and iv) ejecting the part. Mold filling is of greater importance in injection molding of fiber-reinforced thermoplastics since the fiber orientations in the part are almost entirely determined by the flow patterns during filling. This phase is characterized by a *time-dependent non-isothermal and non-Newtonian flow* with free surface. As a result, it is very challenging to accurately predict the flow-induced fiber orientation. The difficulty is greater when the fibers are long (> 1 mm) and/or concentrated fiber volume fractions are considered, and the part to be molded presents three-dimensional features. Basically, the mold-filling problem is governed by three general equations from continuum mechanics which express

the balances of mass, momentum and energy of the fiber suspension. To complete the problem formulation, a constitutive relation is needed to describe the suspension behavior, and an equation to describe how the fibers can orient in response to the flow and fiber-fiber interaction must be added. These additional equations are essential but are the main sources of difficulty in process modeling. Therefore, assumptions have often been made to simplify the suspension rheology, flow behavior, coupled phenomena, fiber-fiber interactions, etc.

In the next section, the formulation of the mold filling problem is summarized. Standard assumptions will be mentioned. Also, the limitations of the current models will be clarified. After that, an approach to the mold-filling and fiber-orientation problems using the smoothed particle hydrodynamics method will be presented. The modeling investigation continues with the numerical assessment section in which the particularities of the microstructures of short- and long-fiber systems are discussed. Through the analyses of the end-gated plaque and center-gated disk problems, the limitations of the current process model are pointed out. Finally, the report is completed with the material selection, and non-destructive and destructive techniques evaluations for LFTs.

Status of Current Process Models

Generally, it has been verified that the use of orientation tensors provides an efficient and accurate way to quantify the orientation state. Although injection molding of fiber-reinforced polymers, in general, involves flows of non-Newtonian suspending liquids, the assumption of a generalized Newtonian fluid is useful and allows qualitative predictions of fiber orientations in injection-molded parts. In addition, many of these parts possess thicknesses that are much smaller than other relevant dimensions and, consequently, the generalized Hele-Shaw model, which reduces the fully three-dimensional flow problem to a two-dimensional (2D) formulation for the pressure, is valid to model flows in thin cavities. However, the Hele-Shaw approximation has severe limitations to model flows in three-dimensional (3D) geometries since it does not provide accurate velocity fields in 3D features. Another important assumption consists of solving the flow equations as if the fibers were absent, then using the obtained velocity results to solve the fiber-orientation problem. This uncoupled approach is often acceptable especially in the major (lubrication) part of the flow regions. Fiber-fiber interactions which are important in semi-concentrated and concentrated regimes have been modeled by adding a rotary diffusion term in the Jeffery equation. This term is the key element of the Folgar-Tucker model that is implemented in current commercial process modeling codes. It is noted that capabilities of 3D solutions for the governing equations and/or coupled flow-orientation also exist. 3D analyses using coupled or uncoupled approaches have improved the results for 3D feature problems.

Current process models for injection molding have been applied to short-fiber filled polymers. The fact that these models are able to provide good qualitative fiber orientations is thanks to the acceptable validity of the simplifying assumptions for short-fiber suspensions. However, to date, no models exist to describe the flow of a long-fiber suspension. Here, we arrive at a principal difficulty which is linked to the rheology of the suspension and its microstructure. Long fibers have limited mobility due to their length and multiple fiber-fiber contacts. Hence, they do not freely rotate and convect with the flow. Their behavior needs to be understood and accounted for in the establishment of the fiber-orientation equation. This equation should be able to describe the fiber-fiber interaction when the fibers are long and it should include the effect of fiber breakage during injection molding.

By examining the Folgar-Tucker equation, the limitation of this model can be understood. Advani and Tucker have expressed the Folgar-Tucker model in terms of fiber-orientation tensor components. According to this model, the fibers are convected with the fluid, and they re-orient in response to the deformation and rotation of the fluid according to:

$$\frac{Da_{ij}}{Dt} + \frac{1}{2}(\omega_{ik}a_{kj} - a_{ik}\omega_{kj}) = \frac{1}{2}\kappa(\dot{\gamma}_{ik}a_{kj} + a_{ik}\dot{\gamma}_{kj} - 2\dot{\gamma}_{kl}a_{ijkl}) + 2C_1\dot{\gamma}(\delta_{ij} - 3a_{ij}) \quad (1)$$

where a_{ij} and a_{ijkl} are, respectively, the second-and fourth-order orientation tensors, ω_{ij} is the vorticity tensor, $\dot{\gamma}_{ij}$ is the rate of the deformation tensor whose scalar magnitude is $\dot{\gamma}$. κ and C_{I} are material constants; κ depends on fiber aspect ratio, r_{e}, and C_{I} is called the interaction coefficient. If $C_{\mathrm{I}} = 0$ and $\kappa = (r_{\mathrm{e}}^2 - 1)/(r_{\mathrm{e}}^2 + 1)$, Equation (1) is then Jeffrey's equation for the motion of a rigid, ellipsoidal shape fiber in a Newtonian solvent. This is strictly valid for dilute suspensions in which the fiber-fiber interaction is absent or negligible. Jeffrey's equation imposes no restriction on the fiber aspect ratio. The last term of Equation (1) has been added to model the randomizing effect of fiber-fiber interaction in semi-concentrated suspensions. Here, an important question is raised when applying Equation (1) to long-fiber suspensions, that is, long fibers do not freely rotate and convect with the suspending liquid; they remain organized in domains and have limited mobility. As a consequence, representing the fiber-fiber interaction through a rotary diffusion term dependent on a scalar coefficient (C_{I}) would be only a rough approximation. Furthermore, the assumption that the fibers are rigid cylinders of equal length and diameter is not valid for injection molding of long-fiber-filled polymers since fibers undergo bending and rupture which reduces the fiber length considerably. This is an important issue that has not been addressed until now.

A Smoothed Particle Hydrodynamics Approach to the Fiber Suspension Problem

An alternative approach to model multiphase free surface flows and heat transfer in domains with complex solid boundaries is to use a *Lagrangian particle-based method*. To simulate the mold-filling problem during injection molding, a smoothed particle hydrodynamics (SPH) approach, a meshless Lagrangian method, can be used. In this approach, the fluid is modeled by a discrete set of SPH particles, where each particle represents a finite volume of the fluid. One of the main advantages of SPH for modeling fiber-filled thermoplastics injection molding is that the SPH method does not require explicit interface tracking or contact angle models. In addition, the SPH simulations explicitly conserve mass, momentum and energy. Also, the SPH method is manifestly Galilean-invariant because particle-particle interactions depend on the *relative* particle positions and velocity differences. In particle-based methods, the fluid-fluid interfaces move with the particles, hence there is no need to explicitly track the fluid-fluid interfaces. Processes such as fluid fragmentation and coalescence can be handled without difficulty. In addition, the particle nature of the SPH model allows fluid-solid interactions to be modeled through simple particle-particle interactions. The number of particles needed in SPH simulations is determined only by the required resolution and accuracy of the numerical solutions of the macroscopic governing equations such as the Navier-Stokes equation, continuity equation and energy conservation equation.

In SPH, the fluid is modeled by a discrete set of N SPH particles, where each particle represents a finite volume of the fluid. The size of the SPH particles is defined by the desired resolution of the simulation. The position of the i^{th} SPH particle is denoted by the vector $\mathbf{r}_i$, $i = 1,\ldots,N$, and each particle has a mass, m, and density, ρ_i. The SPH theory is based on the idea that a continuous field $A(\mathbf{r})$ at the position $\mathbf{r}$ can be smoothed by the convolution integral:

$$A_s(\mathbf{r}) = \int A(\mathbf{r}')W(\mathbf{r} - \mathbf{r}', h)d\mathbf{r}' \qquad (2)$$

where $A_s(\mathbf{r})$ is the smoothed field, and the weighting function, W, with a range or support scale h satisfies the normalization condition:

$$\int W(\mathbf{r} - \mathbf{r}', h)d\mathbf{r}' = 1. \qquad (3)$$

The integration in Equation (2) is performed over the entire space of the field, and in the $h \to 0$ limit where W becomes a Dirac delta function, $A_s(\mathbf{r}) \to A(\mathbf{r})$.

Properties associated with any particle i are calculated by approximating the integral in (2) by the sum

$$A_i = \sum_j \Delta V_j A_j W(\mathbf{r}_i - \mathbf{r}_j, h)$$

$$= \sum_j m_j \frac{A_j}{\rho_j} W(\mathbf{r}_i - \mathbf{r}_j, h) \quad (4)$$

where ΔV_j is the volume occupied by particle j, ρ_j is the density at position $\mathbf{r}_j$, and the gradients of these properties are approximated by

$$\nabla A_i = \sum_j \Delta V_j A_j \nabla_i W(\mathbf{r}_i - \mathbf{r}_j, h)$$

$$= \sum_j m_j \frac{A_j}{\rho_j} \nabla_i W(\mathbf{r}_i - \mathbf{r}_j, h) . \quad (5)$$

The motion of each particle is governed by the momentum conservation described by the Navier—Stokes equation which can be written in terms of SPH approximation as

$$\frac{d\mathbf{v}_i}{dt} = -\sum_j m_j \left(\frac{\boldsymbol{\sigma}_j}{\rho_j^2} + \frac{\boldsymbol{\sigma}_i}{\rho_i^2} \right) \nabla_i W\left(\mathbf{r}_i - \mathbf{r}_j, h\right) + \mathbf{g} \quad (6)$$

where $\boldsymbol{\sigma}$ and $\boldsymbol{\tau}$ are total and extra stress tensors given by:

$$\boldsymbol{\sigma} = P\mathbf{I} + \boldsymbol{\tau} . \quad (7)$$

Most of the existing models for fiber orientation in injecting molding operate under a simplifying assumption of fluid incompressibility. SPH allows the fluid flows ranging from essentially incompressible fluids (compressibility less than 0.01%) to highly compressible fluids to be modeled. The density ρi that can be determined from the continuity equation or directly from Equation (4), is given by:

$$\rho_i = \sum_j m_i W\left(\mathbf{r}_i - \mathbf{r}_j, h\right) \quad (8)$$

for $A_i = \rho i$ Mass m_i depends on the volume fraction of the suspending liquid that is related to the volume fraction of fibers. Given the density ρi , the pressure P in Equation (7) is obtained from the equation of state. To simulate the effect of surface tension and fluid-solid interactions, particle-particle interactions were added into Equation (6) leading to the particle equation of motion:

$$\frac{d\mathbf{v}_i}{dt} = \mathbf{F}_i \quad (9)$$

$$\text{Where } \mathbf{F}_i = -\sum_j m_j \left(\frac{\boldsymbol{\sigma}_j}{\rho_j^2} + \frac{\boldsymbol{\sigma}_i}{\rho_i^2} \right) \nabla_i W\left(\mathbf{r}_i - \mathbf{r}_j, h\right)$$

$$+\mathbf{g} + \frac{1}{m_i} \sum_j \mathbf{F}_{ij} \quad (10)$$

where $\sum_j \mathbf{F}_{ij}$ is the force acting on particle i due to the particle-particle interactions with the interaction forces given by

$$\mathbf{F}_{ij} = \begin{cases} s_{ij} \cos\left(\frac{1.5\pi}{3h} \left| \mathbf{r}_j - \mathbf{r}_i \right| \right) \frac{\mathbf{r}_j - \mathbf{r}_i}{\left| \mathbf{r}_j - \mathbf{r}_i \right|}, & \left| \mathbf{r}_j - \mathbf{r}_i \right| \le h \\ 0, & \left| \mathbf{r}_j - \mathbf{r}_i \right| > h, \end{cases} \quad (11)$$

where s_{ij} is the strength of the force acting between particles i and j. Since $\mathbf{F}_{ij} = -\mathbf{F}_{ji}$, the particle-particle interactions conserve momentum.

The fiber orientation at each point of the fluid domain represented by the particle i can be obtained by solving the Advani-Tucker Equation (1) that can be expressed in terms of the SPH discretization.

Current modeling tools for flow-induced fiber orientation relies on finite element (FE) analyses. After the prediction of fiber orientation by a FE processing code, the same mesh is imported into a structural FE code for a structural analysis. By doing so, some numerical problems could arise because the mesh that is good for flow modeling might not be appropriate for a structural analysis (e.g., damage analysis, etc.). The advantage of the SPH approach is that fiber-orientation prediction is not linked to a finite element mesh, but it is linked to the domain which corresponds to the part to be molded. Hence, once fiber orientation has been known at each point of the domain, the domain can be meshed as appropriately as necessary for a structural analysis that makes use of the orientation results.

Finally, it is important to note that the major issue in SPH modeling is related to the high computational cost in comparison with the analyses using the grid-based numerical methods (e.g., finite element methods). To date, the automotive industry is not familiar with the SPH methods. On the other hand, finite element tools are available and will be more effectively explored to handle LFT analyses.

Numerical Assessment [1]

Conventional, short-fiber, thermoplastic composites (SFTs), processed by injection molding, have a layered structure. As shown in Figure 1, the fibers close to the cavity walls are aligned with their neighbors and oriented in the flow direction. This region of the part is called the shell layer. Fiber alignment in the shell is caused by shearing deformation during mold filling; the polymer has high velocity near the midplane of the part and does not slip on the cavity walls. Closer to the midplane of the part, the fiber orientation is nearly random in the flow/crossflow plane, and there may even be a dominant crossflow orientation. This layer is called the core. On a polished cross-section, the human eye will see a sharp transition between the core and the shell. This is apparent in Figure 2(a). However, quantitative measurements show that the transition is actually smooth, as in Figure 2(b).



Figure 1. Cross-section of injection-molded plaque, showing typical core/shell layered pattern of fiber orientation.

A center-gated disk has the same layered structure as a plaque, but the shell layers are thinner, the core is thicker, and the core has a strong crossflow alignment. This is shown in Figure 2(b). The crossflow core in the disk is caused by fluid stretching in the tangential direction as it flows radially outward from the gate. This stretching is strongest at the midplane, where there is no gapwise shearing, whereas the gapwise shearing dominates the fiber orientation near the upper and lower surfaces of the part, as illustrated in Figure 3. At intermediate positions across the thickness, the orientation is a result of the competition between shearing and stretching.

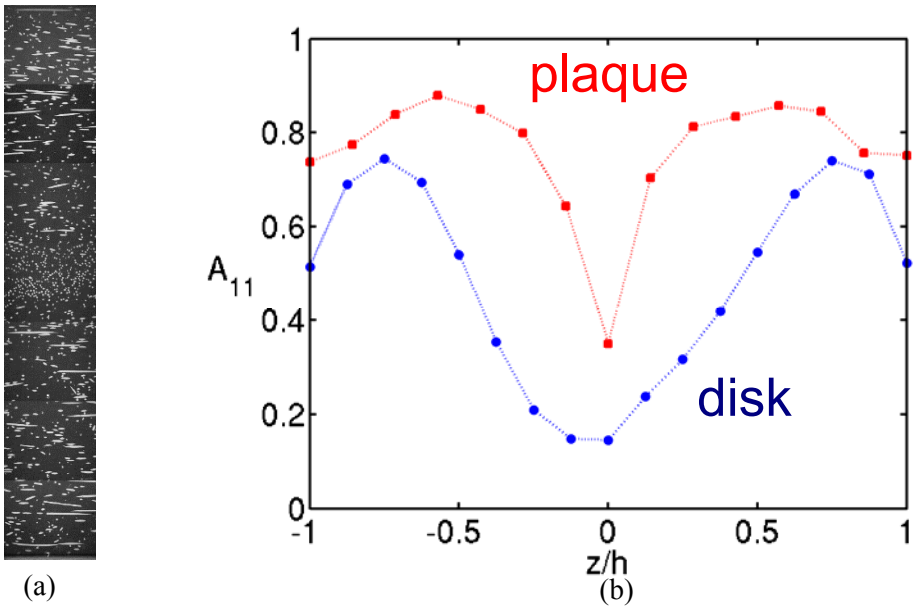


Figure 2. (a) Polished cross-section from an injection-molded SFT. Taken from a region like the white area in Fig. 2. (b) Measured flow-direction orientation in a plaque (upper curve) and center-gated disk (lower curve).

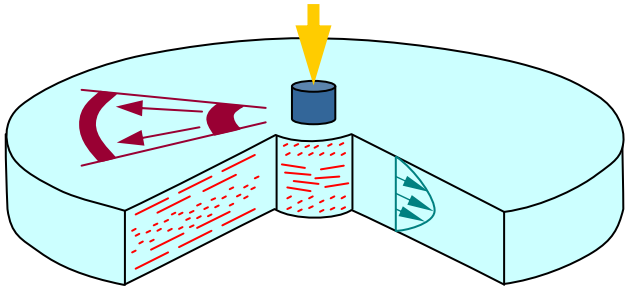


Figure 3. Sketch of fiber orientation structure in a center-gated disk.

Current fiber orientation models for injection-molded SFTs are accurate for parts with long flow lengths, but not as accurate when the flow length is short. Table 1 shows an example. For this table, plaques of two different sizes were molded from a 30% glass-reinforced PBT, General Electric Valox 420. The fiber orientation was measured in each type of plaque, and the elastic modulus was measured in the flow direction (E_{11}) and the crossflow direction (E_{22}). The fiber orientation was also predicted using the standard model. The same micromechanics model was then used to make two predictions for the elastic moduli, one using the measured fiber orientation and the other using the predicted fiber orientation.

Table 1 shows the results. The parts are strongly anisotropic, being almost twice as stiff in the flow direction as in the crossflow direction. However, the part with the shorter 125-mm flow length has less anisotropy than the part with the longer 279-mm flow length. Using the measured orientation to predict the properties results in good agreement for both parts. The predictions based on the predicted orientation are quite good for the long part, but do not capture the increased isotropy for the short flow length. The underlying issue is that the standard theory predicts a core that is too narrow and shell layers that are too thick, compared to experiments (see Figure 4). This deficiency in the standard model is currently being addressed, and there is an improved model developed, by Prof. Charles Tucker and his students at the University of Illinois. Continued work on fiber orientation models is required, even for the familiar SFT materials.

Material Selection and Injection Molding

Materials to be analyzed have been determined to be both glass- and carbon-filled polypropylene and Nylon 6 at a 30% fiber by weight. These materials will be procured by an industrial supplier; currently we are evaluating three material suppliers and will down-select to one supplier for full project participation. The samples will be long fiber between 6-15 □m in length.

Injection-molding-machine adaptation to minimize fiber attrition during long-fiber processing has been investigated during the course of this project. The injection-molding machine will be fixed with low-torque screws that will minimize fiber shearing during the heating and material transfer. Molds will be commercially-available designs produced from matched metal parts; we have identified a company in Greenville, MI that is experienced in producing multi-plate molds capable of producing a variety of sample configurations from a single mold base. In the experimental phase of this program, we will pursue the purchase and installation of one of these systems at PNNL.

Table 1. Comparison of measured and predicted elastic moduli for plaques molded from 30% glass-fiber-reinforced PBT. E11is measured in the flow direction and E22 is measured in the crossflow direction.

Plaque Dimensions (mm)	Property	Experimental (GPa)	Predicted using measured orientation (GPa)	Predicted using predicted orientation (GPa)
76x299x3	E_{11}	8.8	9.1	8.6
76x299x3	E_{22}	4.6	4.4	4.3
75x125x3	E_{11}	7.7	7.5	8.6
75x125x3	E_{22}	5.4	4.8	4.3

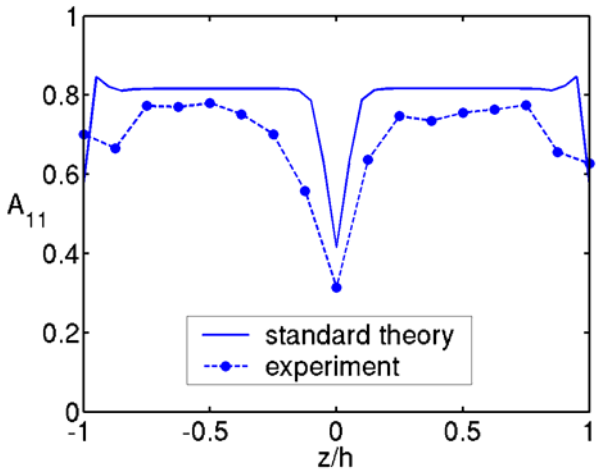


Figure 4. Fiber orientation in a 80x90x2mm plaque of 30% glass/PBT. The predictions using the standard theory give a much narrower core than the part actually has.

Non-Destructive and Destructive LFT Analysis

Short-fiber-reinforced thermoplastics are commonly utilized for applications in the automotive industry due to several factors including commonalities in process equipment with neat resin products, homogeneities within the fiber filler, consistent fiber lengths that are generally 1 mm or less, and a generally well-defined procedure for predicting fiber orientation within the molded part. Long-fiber-filled thermoplastic composites, on the other hand, pose significant challenges in both processing and fiber-orientation prediction. Specifically, factors that are inherent in long-fiber injection-molded parts include fiber breakage, large variations in viscosity due to decreased fiber mobility especially at the mold front, non-homogeneous yield stresses, increased fiber-wall interactions, and poor fiber dispersion that can be manifested in the presence of fiber bundles in the molding. Injection molding of simple geometries will be performed using long glass or carbon fibers. The injection-mold screw must be modified to provide the correct fiber shear to minimize fiber breakage and provide uniform distribution. However, the fiber aspect ratio of long-fibers results in an increased core thickness possibly reflecting the segregated state at which long fibers enter the mold cavity. Steric interactions that inhibit the motion and reorientation of longer fibers can result in the orientation of both the core and shell layers being lower than that of short-fiber composites; all of these factors require that careful experimental characterization and fiber orientation characterization be pursued in conjunction with any fiber orientation prediction modeling.

Nearly any measurement technique could be used provided that it effectively generates images of fibers on 2D sections through the material. Techniques could range from contact x-ray micro-radiography, scanning acoustic microscopy, to nuclear magnetic resonance. For studies of mesostructural artifacts, optical is preferred despite requiring a polished section of the sample.

If samples are to be prepared for 2D optical-reflection microscopy and analysis by image-processing techniques, great care must be taken with both sectioning and final polishing. Physical sectioning of long-fiber reinforcements can easily cause fiber pullout and the sectioning of aligned-fiber composites can leave chipped fibers and fragments at the surface. Clearly, fiber orientation characteristics that result from any 2D image analyzer depend upon the quality of the surface preparation.

Image reconstruction from projections using computed tomography (CT) produces a non-invasive measure of structure from external measurements. In x-ray CT, radiation is passed along straight lines through the object to a detector with the specimen located between the source and detector. With a stationary source and detector, the specimen is rotated and stopped at predetermined locations to acquire projections through the specimen. The projected signal is proportional to the amount of radiation reaching the detector. The logarithm of these measurements can be considered line integrals of the x-ray attenuation coefficients of the specimen; knowledge of all line integrals allows the reconstruction of the interior structure. X-ray tomographic reconstruction produces a two-dimensional map of x-ray attenuation coefficients of the irradiated cross-section of the specimen.

Transmission tomography such as x-ray CT employs scanners capable of discerning between linear attenuation coefficients values by as little as 0.1%. In practice, density measurement from x-ray tomographic data can be performed either by

calibrating the CT machines with objects of known density and obtaining a correlation equation that relates density with attenuation coefficients or by utilizing dual energy scanning to determine directly the density of the material. Typically, volumetric imaging of the sample is obtained by stacking a series of two-dimensional slices of CT image data. The quality and utility of the CT data ultimately depend on the machine resolution.

For many years, the standard method of acquiring a volumetric CT scan has been by scanning a sample one slice at a time. In this method, a linear detector array and an x-ray point source are mounted opposite each other. A fan-shaped x-ray beam traverses the sample and the attenuated fan is stored as a 1D linear image. By rotating the source/detector pair around the sample, a series of linear images are obtained which are subsequently used for the 2D slice reconstruction. A volumetric representation is obtained by advancing the table on which the sample rests after each rotation in order to acquire a stack of such slices. Recently, cone-beam CT has been developed to acquire a 3D data set with only one rotation of the sample. This provides for fast data acquisition and better x-ray utilization. In a cone-beam design, each projection of the object is, in essence, a radiograph. Attenuation measurements are simultaneously made for the entire object rather than for a single slice. The reconstruction algorithm is a generalization in three dimensions of the widely used convolution back-projection method.

Fiber Architecture of Long-Fiber-Reinforced Thermoplastics (LFTs)

The ability to characterize fiber orientation, fiber length and fiber curvature is critical for validation of predictive processing codes and for input to micro-mechanic-based life-prediction software. The ORNL team has been focusing on evaluating various destructive and non-destructive characterization methods. The objective of this study was to evaluate these methods for glass- as well as carbon-fiber-reinforced injection-molded parts. RTP Co. supplied tensile and flex bars molded from VLF 80107 CC natural polypropylene with 40% 11-mm-long glass fibers. Long-carbon-fiber-reinforced thermoplastics were not available on the market, therefore the evaluation was performed on specimens made from AMC 8590 sheet-molding compound by Quantum Composites with 1-inch-long fibers. A flexible surface heater by Thermion was used for evaluation of x-ray techniques with Ni-coated carbon fibers.

X-ray Techniques

X-ray techniques can be used for obtaining two- and three-dimensional information about the fiber architecture of LFT. The utility of x-ray evaluation is dependent on differences in x-ray absorptance of materials used in the composite. Glass-reinforced thermoplastics can be used without modification, while carbon-fiber-reinforced thermoplastics must be modified to obtain sufficient contrast. Two techniques were considered for modification of carbon-fiber-reinforced thermoplastics. Dispersion of metallic particles in the matrix and coating of fibers was considered. Micrographs of particles dispersed in the polymer matrix, obtained from a previous project, were evaluated (Figure 5). It was concluded that this technique was not promising due to the necessity of uniformly dispersing sub-micron-sized particles in the matrix material. Large particles and non-uniformities in particle distribution would cause problems during image analysis. Ni-coated carbon fibers were deemed more suitable for x-ray analyses (Figure 6). It remains to be seen how the coating affects the manufacturing process, fiber length and fiber orientation in long-fiber thermoplastics.

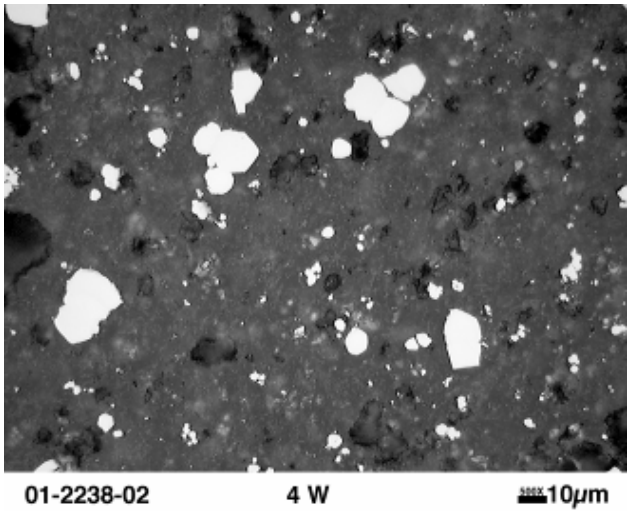


Figure 5. Micrograph of 17% tungsten particles by volume in polymeric matrix (material supplied by Ecomass).

Two x-ray techniques were evaluated: 2D x-ray and 3D x-ray computed tomography. Information from 2D x-ray can provide useful information about fiber distribution spanning several fiber lengths (Figure 7). While it is impossible to resolve the individual fibers due to the number of fibers present in the thickness direction of a typical molded specimen, local fiber density, uniformity of fiber dispersion and general fiber-bundle orientation can be judged from the image. 2D x-ray imaging can be performed rapidly, and commercial equipment is readily available.

3D x-ray computed tomography was used to image individual fibers in LFT (Figure 8). Trade-offs must be made between image resolution, specimen size and time of imaging. Figure 8 shows images of 2x2 mm, 40% glass-reinforced sample with 4.5-micrometer resolution obtained in one hour with equipment available at ORNL. X-ray tomography machines are commercially available; however, the equipment is not as easily accessible as 2D x-ray machines.

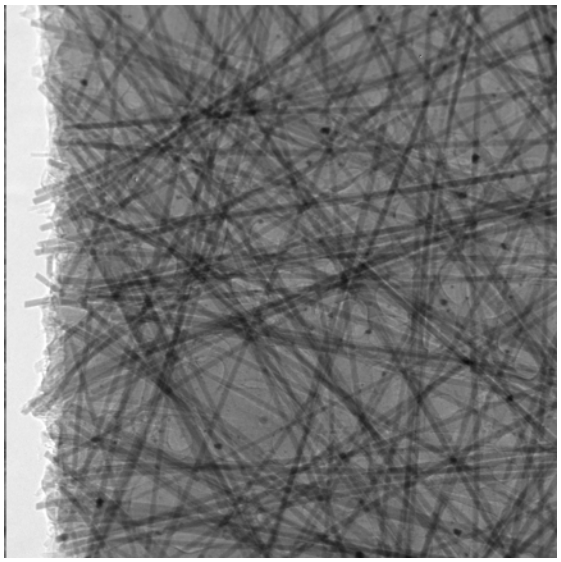


Figure 6. X-ray of Thermion heater containing Ni-coated carbon fibers.

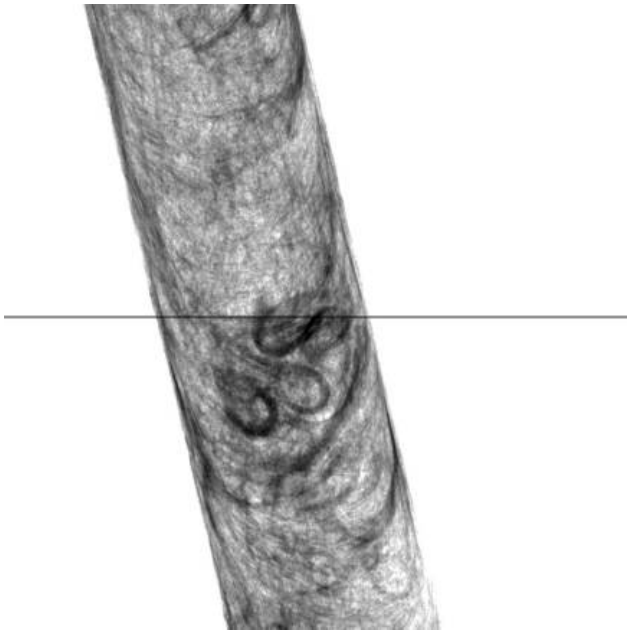


Figure 7. 2D x-ray of 12.5-mm-wide, 40% glass/polypropylene injection-molded tensile bar.

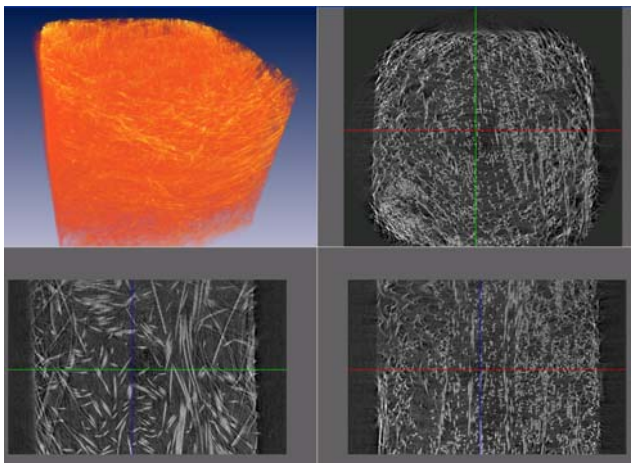


Figure 8. 3D x-ray of 2x2-mm sample of 40% glass/polypropylene - ISO view and three cross-sections.

Obtaining the orientation tensor $\langle a_{ij} \rangle$ requires digital image processing on data obtained from 3D x-ray analysis. Software capable of this analysis in 3D was not available; however, a possible approach for determining $\langle a_{ij} \rangle$ was demonstrated in 2D by analyzing a cross-section. Steerable filters were applied to resolve fibers (Figure 9, Figure 10) before the distribution of fiber orientations was determined (Figure 11).



Figure 9. Threshold filter applied to cross-section obtained from 3D x-ray.

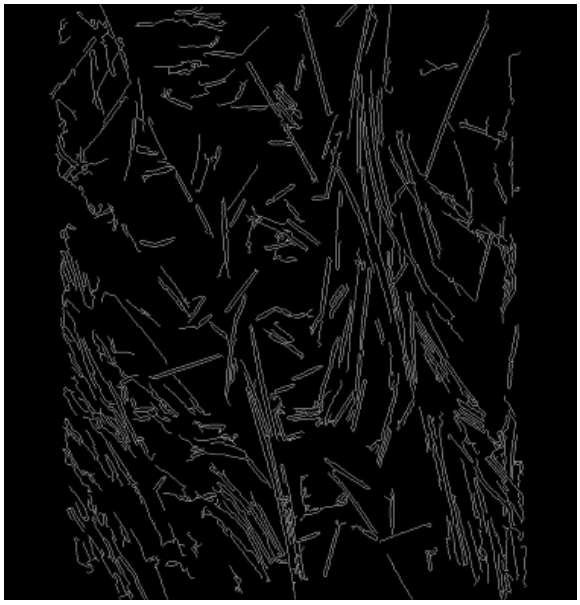


Figure 10. Edge filter applied to cross-section obtained from 3D x-ray.

An ash method was evaluated for fiber length determination. The matrix was burned off from a section of a specimen in a furnace at 600°C. A small amount of fibers was separated from the middle of the section so that the sample would not contain any fibers that were cut before the burn-off. This was accomplished by placing a drop of epoxy adhesive and washing free fibers away after the

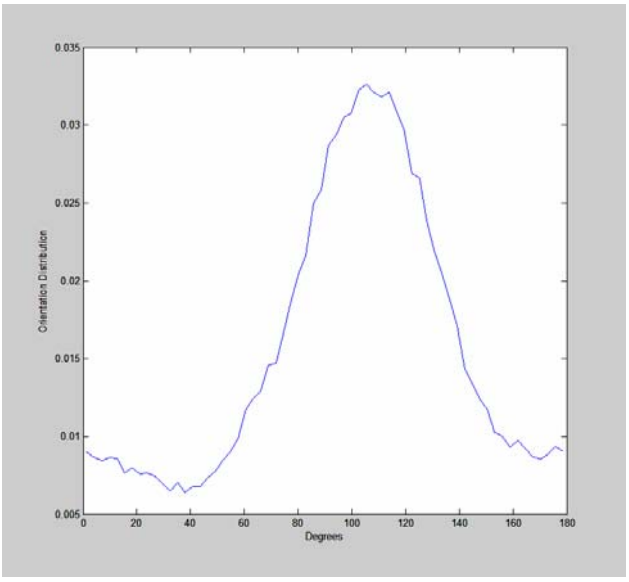


Figure 11. Orientation of fiber cross-sections in a slice from 3D x-ray data.

adhesive set. It is challenging not to break any fibers as the fibers are tightly wrapped and intermingled. The adhesive drop was then burned off and the fibers spread on a Petri dish. Again, separating fibers and fiber bundles is challenging without breaking the fibers. Fibers were then imaged via a scanner. The need for a microscope with an x-y stage and multiple image assembly was eliminated by the use of a scanner. Fiber lengths were then evaluated using ImageJ freeware (Figure 12).

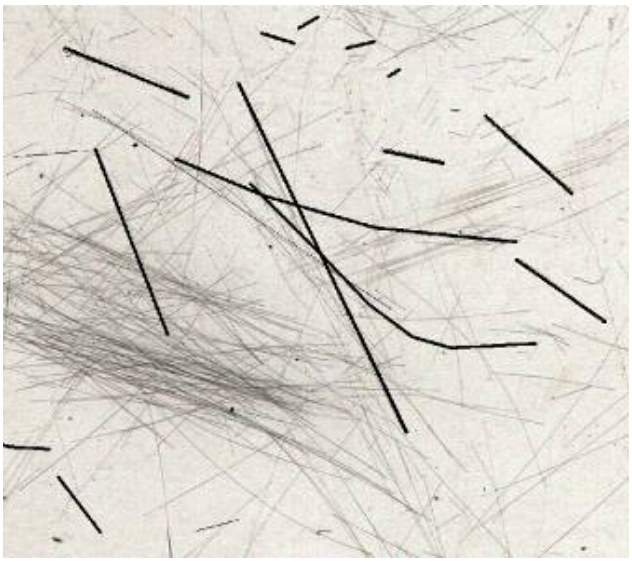


Figure 12. Fibers and their approximation for fiber-length determination.

MRI, c-scan and other acoustic methods were also evaluated; however, initial results did not indicate that these methods would be useful for determination of fiber architecture in LFT.

Conclusions

This report covers five months of work in FY 2005 (the project started in June 2005). Our efforts were focused on evaluating existing process models, computational methods, emerging microstructure, and fiber-orientation characterization tools to determine their accuracy and potential applications to LFTs.

When SFTs are compared to LFTs, many factors suggest that orientation models which work well for SFTs may not work so well for LFTs. Because the fibers in LFTs are nearly an order of magnitude longer than in SFTs, it is expected that fiber-fiber interactions are important over longer length scales. LFTs can have a patchy, domain-like orientational structure, where fibers are aligned similarly to their neighbors. This does not occur in SFTs. Previous experiments on LFTs show a variation in fiber volume fraction across the thickness of molded parts, with higher fiber concentrations near the midplane of the part. Finally, the average fiber length can change significantly during the processing of an LFT, and can vary from location to location within a molded part. None of these factors are accounted for in current models of fiber orientation in SFTs, but all of these factors will affect the mechanical properties of molded parts. Thus, there is a significant need to develop more advanced processing-microstructure models for LFT materials, in order to provide a solid foundation for predictive engineering.

Experimental characterization of the composite microstructure (i.e., fiber-orientation and aspect-ratio distributions, fiber organization structure) is essential since all the modeling work relies on it. Currently, there are promising techniques based on computed tomography that can be used effectively to characterize LFT microstructures.

Reference

[1] Tucker III, CL. “Material on Injection Molding Flow Modeling and Fiber Orientation Modeling.” Internal Report submitted to PNNL.

Presentations/Publications/Patents

Nguyen, BN, Holbery, JD, Johnson, KI, Smith, MT. “Long Fiber Injection Molded Composites: From Process Modeling to Property Prediction” Proceedings of the 5th Annual Automotive Composites Conference and Exhibition, Troy, MI, September 12-14, 2005.

L. Simulation of Injection Molding of Thermoplastics Reinforced with Short and Long Fibers

Principal Investigator: Donald G. Baird
Virginia Polytechnic Institute and State University
Department of Chemical Engineering
Blacksburg, VA 24061
(540) 231-5998, fax: (540) 231-2732, email: dbaird@vt.edu

Co-Principal Investigator: Peter Wapperom
Virginia Polytechnic Institute and State University
Department of Mathematics
Blacksburg, VA 24061
(540) 231-7252, email: pwappero@vt.edu

Technology Area Development Manager: Joseph A. Carpenter
(202) 586-1022; fax: (202) 586-1600; e-mail: joseph.carpenter@ee.doe.gov

Participants
Aaron P. R. Eberle, Ph.D. student, email: eberle@vt.edu
Gregorio Velez, PhD. student, email: gvelez@vt.edu

Contractor: Virginia Polytechnic Institute and State University
Contract No.: DMI-052918

Objective

- Improve predictions of fiber orientation in thermoplastics during injection and compression molding by:
  - Using a theory that couples fiber orientation with flow (Doi Theory).
  - Incorporating the effects of viscoelasticity and the frontal flow region (which is dominated by extensional flow) in the calculations.
- Define and evaluate rheological tests to determine the material parameters for the constitutive relation.
- Evaluate predicted orientation distribution by comparing results to glass-fiber orientation found in an injection-molded part (end and center-gated parts).

Approach

- Conduct transient rheological tests (stress growth/relaxation) on glass-fiber-filled polypropylene systems in which fibers of various length (from 11 mm to 0.5 mm) are used.
- Demonstrate the feasibility of extending Doi's Theory for rigid-rod molecules to the glass-fiber-filled polypropylenes by comparing the transient rheology to that predicted by the theory.
- Fit the model to the transient rheological results to obtain empirical constants for the theory.
- Use the finite element method (FEM) to simulate the flow in three basic mold geometries (tubular element, planar element, center-gated disk).
- Injection mold samples of varying fiber length and matrix viscosity, and quantify fiber orientation.
- Compare model predictions for fiber orientation to that of experimental findings.

Accomplishments

- Rheological characterization and stress growth/relaxation tests were performed on glass-filled polypropylenes containing fibers of various lengths in order to establish a methodology for determining model rheological parameters.
- Model predictions for stress growth/relaxation were performed, and parameter effects on model predictions were investigated.
- The development of a finite element code for simulating Hele-Shaw flow was initiated.
- Two presentations were given, one at the Society of Rheology meeting in Vancouver, BC, Oct. 2005, the other at the annual American Institute of Chemical Engineers (AIChE) meeting in Cincinnati, OH, Nov. 2005.

Future Direction

- Validate transient rheology by comparing data found with parallel-plate rheometer to that of sliding-plate rheometer.
- Fit Doi Model to transient stress growth/relaxation data.
- Develop a unique method for determining model parameters.
- Finish phase one of the FEM model.
- Begin injection molding parts using glass-fiber-filled systems.

Introduction

The purpose of this project is to improve the predictions of fiber orientation during processing of thermoplastics and, hence, the ability to predict stiffness and part dimensional stability. The improvements will be accomplished by using constitutive relations which contain the micro-structural aspects of the reinforced melts and viscoelastic effects.

Glass-Fiber-Filled Polypropylene Rheology

Two fiber-filled polypropylene samples have been used in this work. The first sample is a glass-fiber-filled polypropylene pellet that is formed by pultrusion and then cut into 2.75 mm, 5.5 mm and 11 mm fiber-length samples allowing for the evaluation of fiber length on rheology. The other sample is a glass-fiber-filled polypropylene that has been processed (extruded) and pelletized with an average fiber length of 1 mm. The two samples have a different matrix viscosity.

Rheological testing in the low shear-rate region (0.1-100 s^{-1}) is performed with a Rheometrics Mechanical Spectrometer (RMS-800) fitted with parallel-plate geometry, which allows for gap control. A Göttfert Rheograph 2001 capillary rheometer is used for high shear-rate data (10-2000 s^{-1}). As seen in Figure 1, at low shear rates (.1-10 s^{-1}) there is an obvious increase in the magnitude of stress with increasing fiber length; but at high shear rates the magnitude of the stress for varying fiber length converges to that of the matrix values.

An analysis of the storage modulus (G') of different fiber-filled systems compared to that of the matrix material suggests that the fiber has a dramatic effect on the viscoelasticity of the systems, i.e., relaxation time spectrum. Also, the fiber length is a factor in the relaxation time spectrum as seen in Figure 2.

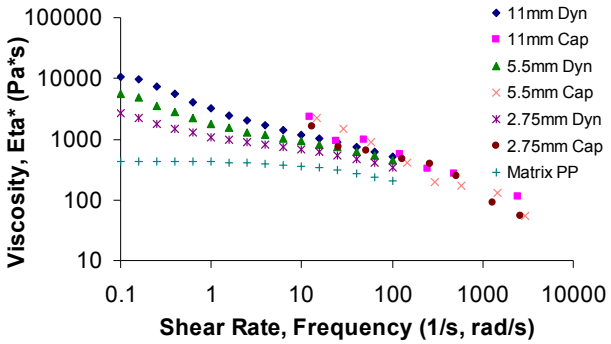


Figure 1. Dynamic and shear viscosity vs. shear rate, frequency for varying fiber length systems, and matrix.

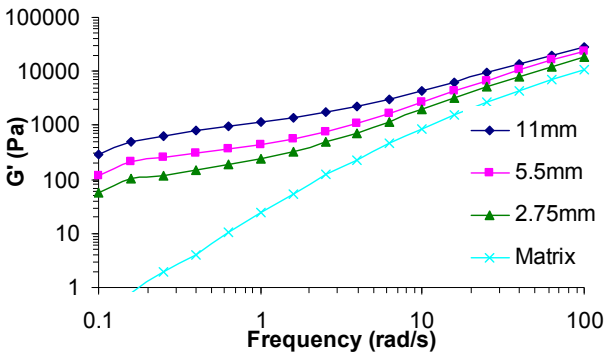


Figure 2. Effect of fiber length on G', compared to matrix viscosity.

Stress growth/relaxation experiments have been performed on all samples. It is found that initial fiber orientation has a large effect on the magnitude of stress overshoot. It is believed that fitting this transient response along with the time for the stresses to relax out of the sample will allow for consistent determination of unique model parameters.

Model: Doi Theory

For this project a constitutive equation is used that couples orientation and flow rather than decouple these events. Doi's Theory was developed for rigid-rod molecules in a solution, and we propose to extend this theory to glass-fiber-filled polypropylene. The model contains two material parameters, ν_1 (constant on the order of unity) and D_r (rotational diffusivity), for which theory gives some methods for calculation. However, when the constants are calculated using this theory, results are unreasonable. This is attributed to the many assumptions made in the development of the theory and the translation from a molecule-solvent system to a fiber-polymer system. For this reason, the material parameters and certain constants have been lumped into three empirical constants for use in fitting the model to transient stress growth/relaxation data. By adjusting these parameters we have found that the Doi theory can predict many of the same transient stress growth/relaxation trends that are found in the fiber-filled systems, i.e., stress growth overshoot, and residual stress in stress relaxation. Though the model can predict stress overshoot, it is still unclear whether the model can predict the magnitude of the overshoot or breadth of time that has been observed for the overshoot to relax to a steady-state stress.

Model: Parameters

A key aspect of this project is determining the material parameters associated with the model. Unique acquisition of these parameters is essential for the accuracy of final results. This is to be accomplished by transient stress growth/relaxation tests on the fiber-filled composites while controlling the initial fiber orientations (initial conditions) in the sample. Evaluation of the model's ability to predict the transient behavior can then be done, and by comparing different initial condition results to model predictions while adjusting the parameters, unique results can be accomplished.

Model: Predicting Fiber Orientation using Finite Element Method (FEM)

Development of a FEM model is a key step to the final goal of increasing the accuracy of predicting fiber orientation in an injection-molded part. The FEM model will be developed and implemented in two phases. In the first phase, the model will be developed for simple pressure-driven flow using the Hele-Shaw approximation, which treats the flow as being dominated by shear flow for the three different die geometries. In the second phase, the code will be adapted to incorporate the kinematics of the flow at the frontal region which has been shown to be dominated by extensional flow (which will play a major role in controlling fiber orientation on the part surface). It is also noted that the quadratic decoupling approximation in Doi's theory will be modified to a Bingham approximation for the frontal flow region.

Conclusions

Although we are in the initial stages of this research project, we have covered a lot of preliminary ground. Rheological classification and transient stress growth/relaxation data for two different glass-fiber-filled systems have been completed. Preliminary model predictions of stress growth/relaxation have shown that Doi's theory simulates many of the interesting phenomena of fiber-filled systems such as stress growth overshoot and stress relaxation which is associated with residual stresses.

Presentations

1. A. P.R. Eberle, D.G. Baird, and P. Wapperom, "Transient Rheology of a Polypropylene Melt Reinforced with Long and Short Glass Fibers," 77th Annual Meeting of The Society of Rheology, October 16-20, 2005, Vancouver, BC, Canada (2005).
2. A. P.R. Eberle, D.G. Baird, and P. Wapperom, "Transient Rheology of a Polypropylene Melt Reinforced with Long and Short Glass Fibers," AIChE Annual Meeting, October 30-November 4, 2005, Cincinnati, OH (2005).

M. A Hierarchical, Structure-Oriented and Stochastic Approach to Model Liquid Molding Processes

Principal Investigator: Thanasis D. Papathanasiou
Department of Chemical Engineering
University of South Carolina
Columbia, SC 29208
Tel: 803-777-7219; fax: 803-777-6245; e-mail: papathan@engr.sc.edu

Technology Area Development Manager: Joseph A. Carpenter
(202) 586-1022; fax: (202) 586-1600; e-mail: joseph.carpenter@ee.doe.gov

National Science Foundation (NSF) Monitor: Mary Lynn Realff
This project was jointly funded by NSF and DOE
(703) 292-7088; fax: (703) 292-9056; email: mlrealff@nsf.gov

Contractor: University of South Carolina Research Foundation
Contract No.: DMI-0522221

Objective

To develop models for the hydraulic permeability of fibrous media, taking explicit account of the underlying microstructure and its variability. A specific task for the preceding period was to explain the scatter in the hydraulic permeability (K) of unidirectional random fiber arrays that is observed computationally as well as experimentally.

Approach

Our approach is computational. A large number of simulations have been carried out, using a parallel implementation of the Boundary Element Method (BEM), in microstructures consisting of ~600 fiber cross-sections placed within a containing unit-cell by a Monte Carlo (MC) procedure. This allows a direct and unambiguous correlation between (K) and the microstructure of the fiber arrays.

Accomplishments

- We find a reduction in (*K)* as the degree of local heterogeneity increases. This reduction follows a power-law, whose exponent is a linear function of fiber content.
- The hydraulic permeability (*K*) is a statistical function of the mean nearest inter-fiber spacing $\langle\delta_1\rangle$
- The mean behavior of (K) can be expressed by the equation $\ln\left(\langle K\rangle/K_{hex}\right)/n = \ln\left(\langle\delta_1\rangle/\delta_{hex}\right)$, where n is a linear function of porosity and K_{hex} and δ_{hex} are also known functions of porosity.

Future Direction (for the next calendar year)

- Further optimize and develop parallel BEM code to run on a Dell cluster.
- Use this code to investigate the changes in (K) brought about by the transition of a microstructure from random to clustered. Develop explicit models that express changes in (K) in terms of microstructural parameters characterizing this transition.
- Directly link the stochastic character of (K) to the microstructural statistics of the fiber array.

- Modify the parallel BEM code to consider problems of linear, compressible elasticity. Use this code to predict the development of stress concentrations that characterizes the transition of uniform fiber arrays to arrays exhibiting various levels of small- and large-scale aggregation.
- Commence the development of a multipole-accelerated BEM code for Stokes flow.

Introduction

Viscous flow through fibrous media is a problem of long-standing interest in engineering due to its importance in the manufacturing and process industries. With specific reference to manufacturing of lightweight materials, flow through fibrous media is of direct relevance to several composites-forming operations such as liquid-molding, pultrusion and autoclave processing. To numerically model flow through fibrous preforms, nodal permeability values must be specified at points dictated by the domain discretization method; the accuracy in the provided permeability data is critical to successful modeling. For this purpose, permeability measurement techniques suitable for fibrous media similar to those used in liquid molding (preforms) have been developed. However, these measurements are known to be subject to large uncertainties, mainly caused by structural variations and/or deformation of the preform during the experiment. Therefore, in parallel with the development of more accurate and faster permeability testing methods, a great deal of effort has been devoted to developing models that would predict the permeability of a fibrous preform based on knowledge of its structure.

The present study is motivated by this need. The particular problem we consider is transverse flow through unidirectional, random fiber arrays. Large discrepancies are routinely observed between theoretical results for such arrays and experimental data obtained in real fiber beds. A notable feature of the permeability as measured in the latter is the substantial scatter in the measured values of (K). It has been widely assumed that these discrepancies are caused by the non-uniformity of real fiber beds. Indeed, fiber packing disorder, fiber bundling and fiber size variations are the norm in fiber preforms. Hence, it is not unreasonable that a function of porosity alone will not be sufficient to explain the observed variability in permeability data. Investigating the possible existence of structure-permeability correlations in disordered fiber arrays is therefore of obvious importance.

Problem Formulation

We consider a fibrous medium composed of long, cylindrical fibers with their axes oriented perpendicular to the direction of bulk flow. The computational unit cell represents a plane cut normal to the fibers' axes. As our focus is on the effect of the spatial distribution of fibers, these are of the same size. A typical unit cell is shown in Figure 1. The porosity of the system is $\phi = 1 - N_f \pi R^2 / A$, where N_f is the number of fibers, R is the fiber radius, and A is the area of the unit cell. The random configuration of fibers is generated by a MC procedure.

The governing equations for slow viscous Newtonian flow across the fibrous medium are the Stokes equations:

$$\nabla \cdot \mathbf{u} = 0 \quad \text{on } \Omega \tag{1}$$

$$\mu \nabla^2 \mathbf{u} = \nabla p \quad \text{on } \Omega \tag{2}$$

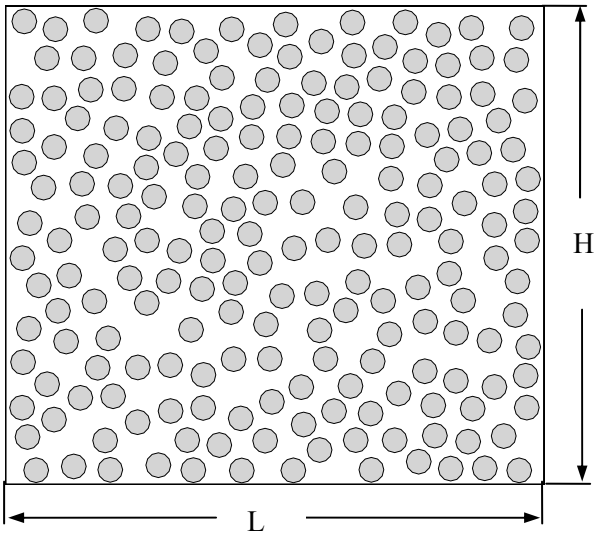


Figure 1. Model geometry used to represent a cross-section of a unidirectional array of randomly-placed fibers.

Here u, p, μ and Ω denote the velocity vector, pressure, viscosity and the 2-D flow domain, respectively. The governing equations can be cast into boundary integral representations involving boundary velocities and tractions only. This technique is well established. Using fundamental solutions, the boundary integral equations are usually written as:

$$c_{ij}(x_p)u_j(x_p) = \int_\Gamma u^*_{ij}(x_q, x_p)t(x_q)d\Gamma - \int_\Gamma t^*(x_q, x_p)u_i(x_q)d\Gamma \quad (3)$$

where u^*_{ij} is the Stokeslet representing the fluid velocity at $\boldsymbol{x_p}$ in the i^{th} direction due to a point force at $\boldsymbol{x_q}$ in the j^{th} direction and t^*_{ij} is the analogous singularity for tractions. Quadratic elements were used to discretize Eq.(3), providing second-order approximations for both geometry and field variables. After discretization, the resulting system of linear equations is usually represented as $[\mathbf{H}]\{\mathbf{u}\} = [\mathbf{G}]\{\mathbf{t}\}$, where {**u**} and {**t**} contain two complete sets of both known and unknown nodal velocity and tractions, respectively; and [**H**] and [**G**] are influence coefficient matrices whose elements are either non-singular or singular integrals. The non-singular integrals were typically evaluated by *10*-point Gauss quadrature. The singular integrals were worked around by the well-known assumption of rigid-body motion, and the weakly-singular integrals were evaluated by Gauss-Laguerre quadrature with the aid of coordinate transformation. To prevent the deterioration of accuracy of numerical quadrature in non-singular integrals, the ratio of the closest distance between two nodes at different elements to the element size should be kept above a certain value. In the worst case, the closest distance between two nodes at different elements is equal to the minimum allowable, nearest inter-fiber spacing, δ_{min}. Therefore, the discretization of fiber surfaces should be finer when δ_{min} gets smaller. In this study, the smallest value of δ_{min} is one tenth of the fiber radius (R). We typically used 24-36 nodes per fiber. This translates to a distance-to-element ratio of 0.25 for less than 10^{-5} error according to an empirical error bound. It was observed that further refinement did not change the results significantly. Also specific to the problem setup, there is one additional unknown of traction at each corner node. This has been treated using the stress balance method.

The main (inherent) shortcoming of the BEM is that its application results in dense and non-symmetric coefficient matrices. In the two-dimensional cases studied here, there are two unknowns for each node, plus four extra unknowns of traction at corner nodes because of the imposed boundary conditions, which result in $2\times(N_f \times M_f + 4 \times M_b + 4)$ degrees of freedom, assuming M_f is the number of nodes per fiber and M_b is the number of nodes per unit-cell edge. The amount of computational work can exceed the capability of a workstation easily as the number of fibers in the unit cell increases. The bottleneck is the main memory (RAM) that can be used; for example, a simulation involving 576 randomly placed fibers results in a system with about 32,000 degrees of freedom and requires about *8* Gb of storage using double-precision arithmetic. For this reason, it is desirable to implement the BEM on a distributed-memory parallel computer. In this study, we implemented a parallel boundary element code which exploits the coarse parallelism in the different phases of the BEM, namely, matrix assembly, solution and post-processing. The solution of the dense linear system is the most time-consuming part in the BEM. In our study, the implementation of the L-U decomposition algorithm in ScaLAPACK is achieved using a two-dimensional block-cyclic data-decomposition scheme. This is scalable in the sense that the memory efficiency is N^2/np, where N is the global matrix size and np is the number of processors used. Our code was written in FORTRAN with function calls to BLACS, ScaLAPACK and MPI libraries.

Microstructure Generation and Quantification

The fiber distributions considered by this study were generated using a MC procedure, which is similar to the method described in Torquato's monograph[1] for generating an equilibrium ensemble of hard disks. The MC process starts with a fixed fiber packing arrangement (square array in our case) and proceeds

[1] Torquato, S. "Random Heterogeneous Materials," 1st edition, Chap. 12:273-277 (Springer-Verlag, 2001).

by randomly and sequentially perturbing the fiber locations. The microstructures generated in this manner are primarily governed by the choice of porosity ϕ and the minimum allowable inter-fiber distance δ_{min}. The latter, defined as the closest distance between fiber surfaces, is the mechanism used to prevent fibers from overlapping during the MC process. Additionally, the unit-cell boundaries act like rigid walls to restrict fibers inside the cell. Such a MC process generates a random field which is short-range correlated. Typical fiber distributions generated in this manner are presented in Figure 2, with differences in ϕ and δ_{min}. It is evident that small values of δ_{min} result in patterns showing local (small-scale) fiber aggregation while large values of δ_{min} lead to more or less uniform distributions that show only small deviations from a hexagonal lattice. The effect of δ_{min} on fiber aggregation is more pronounced when the porosity is large. By varying δ_{min}, a spectrum of fiber distributions can be generated at the same porosity level, ranging from locally aggregated to homogeneous. The possible range of δ_{min} is determined by numerical considerations (at the low end) and by porosity (at the high end). Specifically, the smallest value of δ_{min} was taken to be one tenth of fiber radius (R) to ensure accurate integrations as well as to avoid excessive CPU time, as explained previously. In spite of the artificiality of this choice, we found that when δ_{min} is given small values, the resulting fiber distributions appear similar to the ones we have observed in several liquid molded or pultruded unidirectional composites.

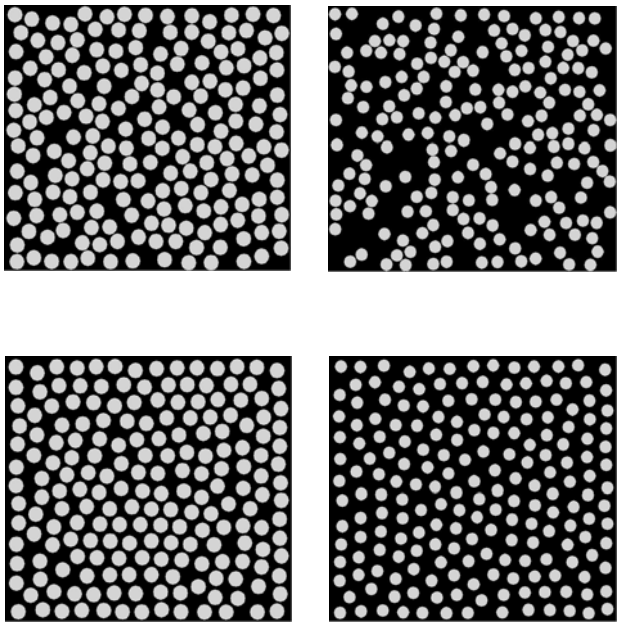


Figure 2. Sample geometries created by the MC process. They exhibit differing degrees of local aggregation. From top left clock-wise (ϕ,δ_1) = (0.5,0.1R); (0.7,0.1R); (0.7,1.0R); (0.5,0.4R)

Prior to any analysis, it is necessary to quantify the microstructure of the fiber distribution first. In this effort, we have investigated the use of the nearest inter-fiber spacing — whose statistics differ between different fiber arrangements. For each fiber one can find a number of 'neighbors', which are assigned with a subscript (i) in such a way that the nearest one corresponds to i=*1* and the others are in ascending order according to relative distances. Thus, the near-neighbor distances are the center-to-center distances from the reference fiber k to its neighbors, which are denoted as $\{d_i^k\}$. The nearest-neighbor distance for a reference fiber k is therefore the minimum in this distance set, i.e., $d_1^{(k)} = \min\{d_i^{(k)}\}$. For a population of fibers, the mean nearest-neighbor distance is denoted as $\langle d_1 \rangle$, which is simply an arithmetic mean. This metric is frequently used to indicate the degree of local heterogeneity in spatial point patterns. Small values of $\langle d_1 \rangle$ are associated with disordered patterns, while large $\langle d_1 \rangle$ indicate a homogeneous arrangement. By subtracting the fiber diameter D, d_1^k is translated to δ_1^k, which is the closest spacing between the reference fiber (k) and its neighbors. Because δ_1^k is more relevant to fluid space, we will use δ_1^k in correlating the microstructure of a fiber array to its permeability in the rest of this paper. We will also refer to the arithmetic mean of $\{\delta_1^k$, k=1…$N_f\}$ as the mean nearest inter-fiber spacing, denoted as $\langle \delta_1 \rangle$.

As is the case in experimental measurement of permeability in fiber preforms, the stochastic nature of the fiber distribution leads to scatter in the computed permeability data. In this study, a number of random realizations (N_r) were generated for each class of fiber distributions characterized by ϕ and $\langle \delta_1 \rangle$ (or δ_{min}), and the permeability values were

computed for the resulting unit cells. The average permeability and its standard deviation are then computed as:

$$\langle K \rangle = \frac{1}{N_r} \sum_{i}^{N_r} K_i \qquad (4)$$

$$\sigma(K) = \frac{1}{N_r - 1} \sqrt{\sum_{i}^{N_r} \left(K_i - \langle K \rangle \right)^2} \qquad (5)$$

Figure 3 shows one representative flow field computed for a unit cell containing *900* fibers using the parallel BEM code.

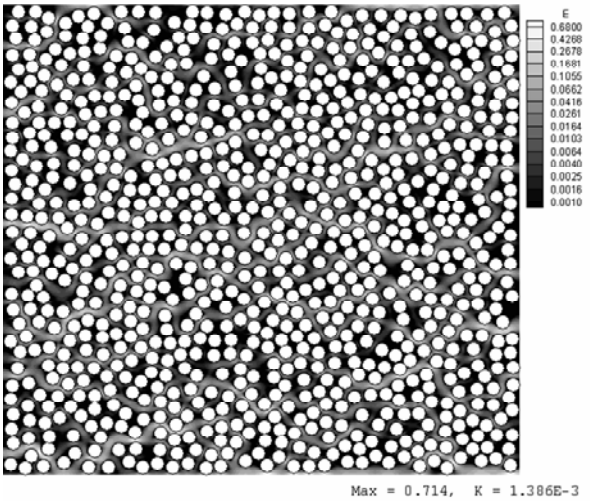


Figure 3. Fluid speed contours for slow viscous flows across a unidirectional fiber array consisting of 900 fibers at ϕ=0.50. Flow is horizontal.

Results

The use of porosity alone is not sufficient to explain the scatter in the permeability of random fiber arrays, whether calculated numerically or determined by experiment. The objective of this study is to link the transverse permeability of random fiber arrays to the geometrical characteristics of these arrays. To do so, the dimensionless permeability data are plotted against $\langle \delta_1 \rangle / R$ in Figure 4. A correlation between K and $\langle \delta_1 \rangle$ is evident. In the porosity range $0.45 < \phi < 0.7$ it

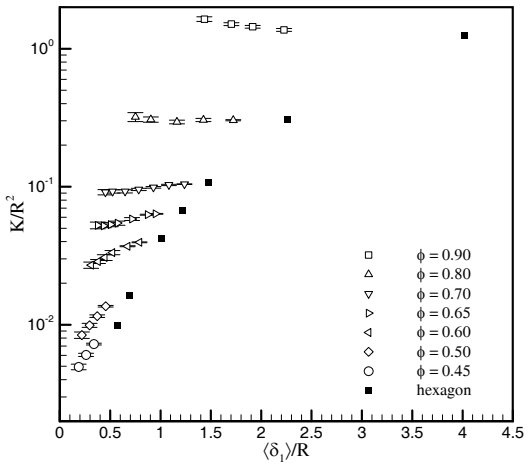


Figure 4. Correlation of the normalized permeability (K/R^2) with the mean nearest inter-fiber spacing, $\langle \delta_1 \rangle / R$. The symbols are mean values and the error bars represent standard deviations ($\pm\sigma$) in each ensemble of data. Each ensemble of data contains *20* runs on geometries of similar spatial statistics. Also shown are permeability values of hexagonal arrays.

appears that decreasing $\langle \delta_1 \rangle$ or, equivalently, moving from a homogeneous system to ones progressively showing higher local aggregation, results in a permeability reduction. This trend is more pronounced at lower porosities ($\phi = 0.45, 0.5$). This permeability reduction, as a result of non-uniformity in fiber distribution (quantified by the Morishita index in that case) was also reported in a recent study[2]. At higher porosities, an opposite trend is shown: at $\phi > 0.7$ as $\langle \delta_1 \rangle / R$ decreases (below ~1.0 for $\phi = 0.8$), the permeability seems to increase. It is necessary to point out that large-scale clustering (in which cluster dimensions are comparable to unit-cell dimensions) does not occur in our systems because of the hard-core distribution statistics implicit in the MC procedure used for microstructure generation. The surprisingly good fit between $<\delta_1>$ and (K) can be qualitatively explained by the fact that, in the absence of large-scale clustering, the flow resistance around each fiber is governed by the narrowest gap separating it from its neighbors. The whole system can then be viewed as a network of flow paths connected in parallel as well as in series. The resistance of each component in the network is

[2] Bechtold, G. and Ye, L. Compos. Sci. Technol. 63:2069-2079 (2003).

determined by the narrowest gap, which is included in the statistics of the inter-fiber spacing (see earlier section). It is therefore not surprising that such a clear correlation exists between $\langle \delta_1 \rangle$ and $<K>$.

In the porosity range of practical interest to composites manufacturing ($0.45<\phi<0.70$), Figure 4 suggests that the functional form which describes the relation between $\langle \delta_1 \rangle$ and K should be:

$$\frac{K}{R^2} = \left(\frac{\langle \delta_1 \rangle}{R} \right)^n f(\phi) \qquad (6)$$

where the exponent n is a function of ϕ as evidenced by the different slopes of the data sets corresponding to different porosities. In seeking a functional form for $f(\phi)$ in Eq.(6), we recall that Eq.(6) should reduce to existing models for the transverse permeability when the fiber array becomes uniform. When the array approaches a uniform hexagonal array, $\langle \delta_1 \rangle$ should equal the inter-fiber spacing of a hexagonal array (δ_{hex}) and the corresponding permeability will be K_{hex}, which is known to be only a function of porosity. For example, at the low porosity limit, K_{hex} and δ_{hex} are given by Eq. (7):

$$K_{hex} = \frac{2}{9\pi\sqrt{3}} \left(\frac{\delta_{hex}}{R} \right)^{5/2} R^2 \qquad (7a)$$

$$\delta_{hex} = 2\left(\sqrt{\frac{1-\phi_{\min}}{1-\phi}} - 1 \right) R \qquad (7b)$$

where $\phi_{min}=1-\pi/\left(2\sqrt{3}\right)$, is the porosity at maximum packing for a hexagonal array. To be asymptotically correct, the form of $f(\phi)$ should therefore be:

$$f(\phi) = \left(\frac{R}{\delta_{hex}} \right)^n \frac{K_{hex}}{R^2} \qquad (8)$$

and thus Eq.(9) yields:

$$\frac{K}{K_{hex}} = \left(\frac{\langle \delta_1 \rangle}{\delta_{hex}} \right)^n \qquad (9)$$

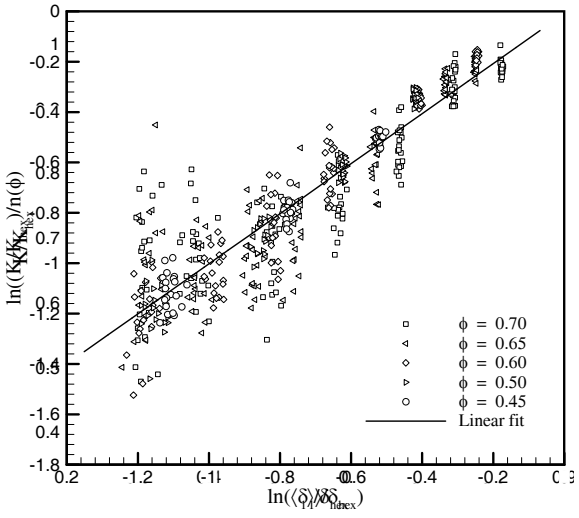
We attempted to scale the computational results of Figure (4) as suggested by Eq. (9). The result is presented in Figure 5(a), in which each data point corresponds to one simulation, characterized by one set of values (ϕ, $\langle \delta_1 \rangle$). As expected by the dependence of the exponent n on ϕ, this scaling does not collapse the data onto one single master curve. Fitting the data as a power function gives the lowest estimate of $n=0.164$ at ϕ=0.7 and the highest estimate $n=0.628$ at ϕ=0.45. It is interesting to note that a plot of n versus ϕ suggests a linear relationship $n=\alpha+\beta\phi$. Therefore an overall correlation between K and $\langle \delta_1 \rangle$ for random fiber arrays can be written as:

$$\frac{K}{K_{hex}} = \left(\frac{\langle \delta_1 \rangle}{\delta_{hex}} \right)^{\alpha+\beta\phi} \qquad (10)$$

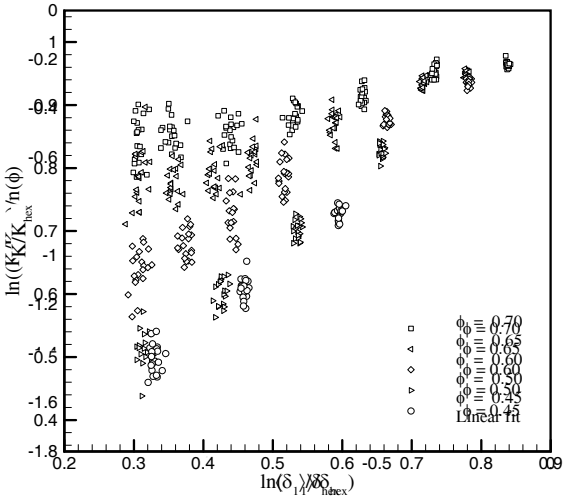
where the constants α and β are determined from a least square fit as $\alpha = 1.51 \pm 0.06$ and $\beta = -1.93 \pm 0.10$. It goes without saying that the linear relationship $n = \alpha+\beta\phi$ can only be considered applicable in the indicated range of ϕ and $\langle \delta_1 \rangle$. Taking logarithms in both sides of Eq. (10) results in:

$$\ln\left(K/K_{hex}\right)/\, n(\phi) = \ln\left(\langle \delta_1 \rangle / \delta_{hex}\right). \qquad (11)$$

The computational data for (K), transformed according to Eq. (11), are plotted in Figure 5 (b). A solid line in Figure 5(b) indicates the least square fit of the data set to a linear model with slope around unity (0.994 ± 0.018) and intercept (-0.008 ± 0.01) very close to zero, exactly as anticipated from Eq.(11). It seems that Eq.(11) predicts the correct average behavior, as the data are indeed shown to be distributed randomly around an average log-linear relationship. In the studied ranges of ϕ and $\langle \delta_1 \rangle$, the permeability follows, on average, Eq. (11), with a scatter that is inversely proportional to $\langle \delta_1 \rangle$. Additionally, the scatter of the permeability values around the mean trend is also related to the variance (σ^2) of δ_1, or, in other words, to the non-uniformity



(a)



(b)

Figure 5. The correlation between permeability and the mean nearest inter-fiber spacing in the porosity range [0.45, 0.70]: (*a*) plot of the reduced permeability (K/K_{hex}) versus $\langle\delta_1\rangle/\delta_{hex}$; *(b-bottom)* plot of $\ln(K/K_{hex})/n$ versus $\langle\delta_1\rangle/\delta_{hex}$. Each data point in the graph is the result of one simulation. The linear fit in *(b)* has a slope of (*0.994± 0.018*) and an intercept of (*-0.008±0.01*).

of the underlying microstructure. Relating the known statistics of (δ_1) to the obtained statistics of (K) is of great practical interest and we are working in this direction.

Conclusion

We carried out an extensive investigation of Stokes flow across a large number of unidirectional, random fiber arrays generated by a MC procedure. This numerically-intensive task was accomplished by developing and running an in-house parallel boundary element code on a distributed-memory parallel computer. The transverse permeability (K) of systems consisting (each) of 576 fibers, calculated in the porosity range $0.45<\phi<0.90$ by averaging over 20 random realizations at each porosity value, was computed. Following this, we point out the need to consider some measure of the underlying fiber spatial statistics as an additional parameter affecting permeability. The microstructural characteristics of the model fiber distributions were analyzed and the mean nearest inter-fiber spacing ($\langle\delta_1\rangle$) was identified as a parameter that correlates with the numerical estimates of (K). Specifically, we found that (K) is a statistical function of $\langle\delta_1\rangle$, with its average behavior ($\langle K\rangle$) expressed by $\ln(\langle K\rangle/K_{hex})/n = \ln(\langle\delta_1\rangle/\delta_{hex})$, where ($n$) is a linear function of porosity and K_{hex} and δ_{hex} are also known functions of porosity. The deviation of (K) from this average behavior is related to the variability of the underlying microstructure, as expressed by the variance of (δ_1).

Presentations/Publications/Patents

X. Chen and T.D. Papathanasiou, 'Understanding the scatter in the permeability of random fiber arrays: A statistical correlation in terms of mean inter-fiber spacing', subm. Physics of Fluids, 10/2005.

N. Modeling and Simulation of Compression Resin Transfer Molding

Principal Investigator: Suresh G. Advani
Department of Mechanical Engineering
University of Delaware
Newark, DE 19716
(302) 831-8975; fax: (302)-831-8525; e-mail: advani@me.udel.edu

Technology Area Development Manager: Joseph A. Carpenter
(202) 586-1022; fax: (202) 586-1600; e-mail: joseph.carpenter@ee.doe.gov

Contractor: University of Delaware
Contract No.: DMI-0521789

Objective

The principal objective in this phase is to build fundamental understanding of flow-compression coupling in the Compression Resin Transfer Molding (CRTM) process and to identify the issues to be addressed in the subsequent analytic, experimental and numerical work.

Approach

We analyzed the existing approach to modeling CRTM, and its shortcomings were examined. New governing equations are being developed. These equations describe all the necessary physical phenomena of the process.

Accomplishments

Analysis of the current modeling approach for CRTM, as well as for some of the physical phenomena involved in the process, such as preform deformation, revealed certain weaknesses in the numerical approach and, more importantly, significant gaps in fundamental understanding of underlying physics.

New governing relations for the general Liquid Composite Molding (LCM) and, in particular, for CRTM have been proposed. These relations describe the process in general and should help not only in process modeling but also in identifying the needs in material characterization.

Future Direction

The current development should be followed by several steps:

1. Build fundamental understanding of flow-compression coupling in the CRTM process with exploratory experiments and closed-form solutions.
2. Develop and experimentally validate the numerical simulation of CRTM to address processing of complex, large-scale structures.
3. Perform parametric studies to identify material and process parameters that significantly impact the process and the yield.

Introduction

All Liquid Composite Molding (LCM) processes require one to place a fibrous preform inside the mold. The mold is sealed and a liquid resin (typically a thermosetting resin due to its low viscosity) is injected to saturate the preform. The fibers in the preform and the preform itself are usually stationary or may undergo slow and small deformation during the injection process. Next, the resin is allowed to cure. During the curing process, the resin cross-links and hardens. Once the resin has sufficiently solidified, the mold is opened and the part is removed.

The resin flow during the preform saturation is of particular interest, as full preform saturation is mandatory to manufacture a successful part. Note that, for textile preforms, this implies *both* the saturation of macro-pores between the fiber tows and the saturation of the micro-pores in the fiber tows.

Flow modeling thus became an important part of the established variations of the LCM process, since, for non-trivial cases, it may defy the intuition of the process designer. For CRTM its importance may be even higher as fast, high-volume production is desired.

The CRTM Process

Unlike the other common variations of LCM, the resin flow during CRTM exhibits three distinct stages. These are shown in detail in Figure 1. All of the phases can be modeled as flow through porous media, but under distinctly different boundary and initial conditions. The three stages are:

(a) Resin injection in the narrow gap between the mold platen and the fiber preform in the mold.
(b) Closing of the gap without direct contact between the mold platen and the preform.
(c) Compaction of the preform by the mold platen along with resin impregnation.

Note that the first stage may overlap with the later ones and, depending on tool geometry and kinematics, a single composite structure may be undergoing different phases in different regions.

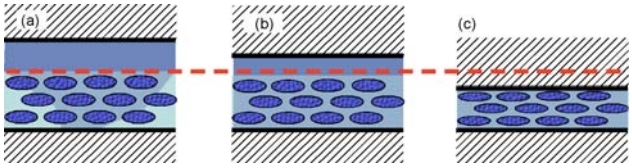


Figure 1. Three stages of CRTM process: (a) Resin injection into the gap. (b) Compression closing the gap, forcing the resin into preform. (c) Final preform compaction.

In the first stage, the resin is injected into the gap between the movable mold part and preform (Figure 1 (a)). It can readily spread through the gap, but it also slowly penetrates into the preform. This situation is similar to the flow in traditional LCM variations with distribution media. In this case, the gap plays the role of highly-permeable distribution media.

In the second stage (Figure 1(b)), the resin injection is discontinued and the mold closure is initiated. The gap between the preform and the mold platen reduces as the mold closes and the resin is displaced and forced into the preform. The gap serves as a flow channel and as a continuous resin source similar to traditional compression-molding squeezing a charge of resin. However, here the resin needs to fill the small gaps in between the fibers of the preform with possible preform compaction as well. As the gap thickness reduces, so does its resistance to the resin flow (permeability) and the resin-flow behavior changes accordingly.

In the final stage (Figure 1 (c)), the gap between the preform and the mold platen is closed, and the mold wall is in contact with the preform and compresses the preform directly. Consequently, the resin is forced out from already-filled regions in the preform to impregnate the remaining unfilled regions.

The averaged preform compaction can be described reliably if the closing speed is known, as the mold platen is in direct contact with the preform. In this case, the average volume fraction, permeability, etc., can be predicted at any time-step during this stage. However, there are currently no means to estimate whether there are local variations in these properties, much less to quantify those variations. Also, if the compaction is driven by applied load, the mold kinetics are unknown and should be predicted by the numerical model.

The advantage of CRTM, as related to more conventional RTM processes, is that it combines the net-shape, high-performance part with the fast cycle time compatible with rapid manufacturing process. In addition, the method inherits the capability to manufacture complex, near-shape part with good surface finish in one step, possibly eliminating a number of assembly steps. These advantages are offset by significant process complexity as demonstrated above.

Current Modeling of CRTM Process

The CRTM process combines elements of conventional RTM and of compression molding. Both these processes were successfully modeled, but the combination of the two is non-trivial. Also, some additional issues are introduced.

The compression creates a resin source in the filled volume and this source is modeled as a constant-flow-rate inlet in every node. It also changes the material properties of the preform.

Our existing model utilizes Liquid Injection Molding Simulation scripting to model the resin flow during CRTM process in 3D or combined 2D/3D. As there is coupling between preform deformation and flow, repetitive modification of both the material parameters and the resin "inlets" is accomplished by script that executes the simulation.

We were able to obtain predictions for simple geometry (Figure 2), but the resulting accuracy was poor. Generally, this method is not acceptable to meet industrial demands and was not accurate enough to install confidence.

Additional Issues to be Considered

There are several additional issues to consider when modeling CRTM which are not modeled by the current approach. The first one lies with possible replacement of kinematically-driven compression by a certain applied load.

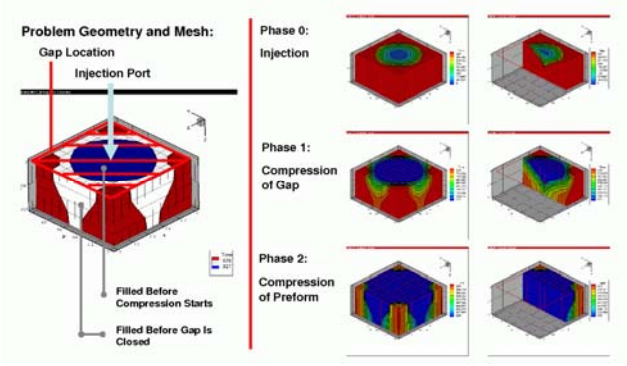


Figure 2. Numerical modeling of resin flow during CRTM injection into rectangular plate.

The prediction of compression forces is difficult even for the kinematically-driven compression as the load is a superposition of resin pressure – which the model predicts – and of forces within the deformed preform. As there are very limited material data and no reliable models for the latter, compression forces can not be predicted with any degree of accuracy. The model cannot, in its current form, predict flow during load-driven compression. While it is theoretically possible to extend it, the extension would compound the performance problems and is, in our opinion, a waste of time.

Another issue is the problem of fiber-tow saturation. The preform of choice consists of fiber-tow strands and the saturation of micro-voids within these strands is imperative. While we have successfully modeled fiber-tow saturation for conventional LCM processes (Figure 3), the approach is not quite suitable for the existing CRTM model because of performance issues.

Process Governing Equations

The preceding analysis indicates that there is a need to fundamentally modify the approach to the modeling. Instead of lumping corrections and "equivalent" properties into the existing model, we need to develop a more general governing equation for flow modeling and to use it in order to (a) create a numerical model and (b) analyze which material data are necessary for reasonably accurate process modeling.

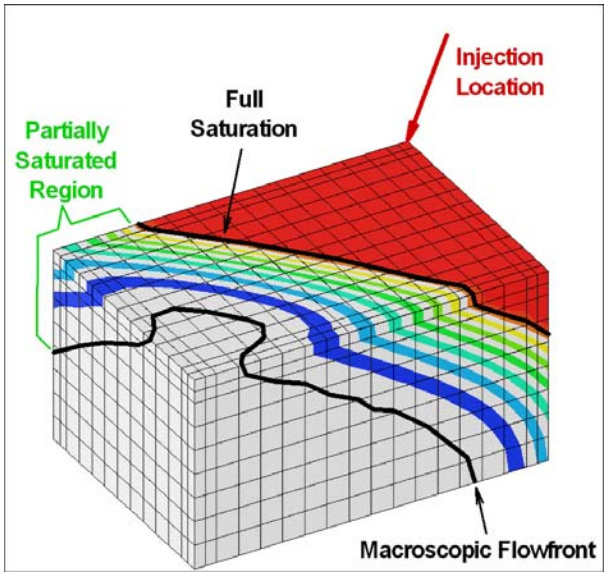


Figure 3. Numerical modeling of dual scale (saturated and unsaturated) flow during RTM resin injection into box-like structure.

The equation must include not only resin pressure and preform saturation that are commonly used to describe the flow in RTM, but also the following:

1. Description of preform deformation in time. This is necessary to obtain acceptable stress prediction for kinematically-driven compression and to model load-driven compression at all.
2. The saturation of micro-pores within fiber tows. This is necessary to predict if the process rate is to be as high as possible. In such a case, the heuristic remedy of conventional RTM of "ramping up pressure and wait" may be suboptimal.

This suggests substituting the usual LCM governing equation

$$\phi \,.\frac{\partial s}{\partial t} = \nabla.\frac{\mathbf{K}}{\eta}.\nabla p$$

where ϕ is the material porosity (constant during the process), **K** its permeability (constant), η the resin viscosity, p the resin pressure and s the saturation by the more involved system.

$$\phi_M.\frac{\partial s_M}{\partial t} + \frac{\partial \phi_M}{\partial t}.s_M + \phi_F.\frac{\partial s_F}{\partial t} + \frac{\partial \phi_F}{\partial t}.s_F = \nabla.\frac{\mathbf{K}}{\eta}.\nabla p$$

$$\phi_M = f(p,...)$$

$$\mathbf{K} = f(\phi_M)$$

$$\phi_f = f(\phi_M)$$

This system contains independent values for porosity and saturation in macro- and micro-pores (ϕ_M, s_M and ϕ_F, s_F) and additional constitutive equations that relate porosity and permeability with material state. One must also add the equation to govern the saturation of micro-pores in the form:

$$\frac{\partial s_M}{\partial t} = f(s_M, p,...)$$

Note that the porosity may be used as the above-mentioned measure of deformation.

The constitutive equations are – apart from permeability-porosity relation $\mathbf{K}=f(\phi_M)$ – insufficiently explored, if explored at all.

Conclusions

The analysis of existing modeling capabilities for the CRTM process revealed weaknesses that cannot be overcome by evolutionary approach; based on the current solutions, a novel approach is needed to provide industry-strength modeling capability for the CRTM process.

A new, more involved, governing-equation system is suggested to include the relevant physical phenomena at a fundamental level, rather than adding them by correctional steps to what is basically an RTM solution.

This analysis also revealed a number of constitutive relations that should be studied to gain better insight into the flow mechanics during the CRTM process.

O. Incorporating Higher-Order Tensors in the Computation of Polymer Composite Mechanical Properties

Principal Investigator: Douglas E. Smith
University of Missouri at Columbia
E2411 Lafferre Hall / MAE Dept., Columbia, MO 65211
(573) 884-6552; fax: (573) 884-5090; e-mail: smithdoug@missouri.edu

Technology Area Development Manager: Joseph A. Carpenter
(202) 586-1022; fax: (202) 586-1600; e-mail: joseph.carpenter@ee.doe.gov

National Science Foundation (NSF) Monitor: Mary Lynn Realff
(703) 292-7088; fax: (703) 292-9056; email: mlrealff@nsf.gov
(This project was jointly funded by NSF and DOE)

Participants: David A. Jack, University of Missouri at Columbia

---

Contractor: University of Missouri at Columbia
Contract No.: NSF Grant DMI-0522694

Objective

- Develop a predictive capability that incorporates higher-order orientation tensors to evaluate mechanical properties of short- and long-fiber-reinforced polymer composites.

Approach

- Development of a model for predicting mechanical properties from higher-order orientation tensors derived from flow simulations or measurements that are not limited by the material symmetry requirements imposed by current models.
- Development of an automated three-dimensional voxel-based finite element modeling technique that may be used to predict the effective mechanical properties of short- and long-fiber suspensions.
- Integration of Micro-CT-derived fiber reconstructions to illustrate the applicability of the proposed approach on production hardware to be obtained from industry or DOE.
- Statistical assessment of mechanical property calculations to address sampling issues associated with using the proposed averaging techniques.
- Demonstration of the proposed methodology on an industrially-relevant polymer composite product where flow simulation software is to be provided by Moldflow Corporation.

Accomplishments

- Developed a statistical sampling approach for predicting the variability of short-fiber composite properties from the mechanical properties of the constituent materials and a fiber-orientation distribution function.
- Derived an analytical relationship between mechanical properties and fiber-orientation tensors for statistically independent short fibers.

Future Direction

- Investigate methods for incorporating fiber interaction into the current statistical sampling methodology.
- Develop a voxel-based, three-dimensional, finite element modeling capability for evaluating effective mechanical properties for short- and long-fiber composites.
- Develop an automated procedure for defining three-dimensional finite element models of a representative cell that may be used with analytically-derived, fiber-orientation distribution functions, or fiber-orientation states obtained from Micro-CT measurements.

Introduction

The purpose of this project is to develop a predictive capability that incorporates higher-order orientation tensors to evaluate mechanical properties of short- and long-fiber-reinforced polymer composites. To realize this goal, the project will develop a computational methodology to predict elastic mechanical properties from orientation tensors of second- and fourth-order which are computed during melt-low simulations. The micromechanics of both short- and long-fiber suspension will be simulated with a voxel-based finite element modeling approach, so that the mechanical properties of randomly-oriented fiber samples can be computed. Simulated fiber- orientation states, as well as those obtained from Micro-CT scans, will serve as input. Finally, fiber-orientation states from industrially-relevant products will be evaluated with the new methodology to assess its applicability for complex geometries.

This report provides a brief description of the three-year project and some preliminary results that have been obtained since its start in September, 2005.

Project Deliverables

The primary deliverable of this research will be a relationship between higher-order (i.e., fourth) orientation tensors and the elastic mechanical properties for short- and long-fiber suspensions. An assessment of the variability of mechanical properties among fiber-orientation states will be provided, along with a computational procedure for evaluating the same properties for a specific orientation state. A final report will be generated to communicate the functional form of the mechanical properties and the relevant model parameters for specific examples studied.

Background

Orientation tensors are used extensively to represent the stochastic nature of polymer-composite fiber suspensions in a form that is suitable for large-scale melt-flow simulations. Orientation tensor research over the past two decades has advanced the state-of-the-art related to polymer composites; however, the use of tensors today is still basically the same as it was when these methods were first developed nearly twenty years ago. In addition, the application of orientation tensors to long-fiber composites is nearly non-existent.

The continued advancement of our basic understanding of short- and long-fiber-reinforced polymer composites is critical in numerous industries including consumer products and automotive which rely heavily on the low cost, design flexibility, and superior performance offered by these materials. A major focus of the National Science Foundation/U.S. Department of Energy/American Plastics Council sponsored workshop[1],co-organized by the PI in June 2004, was the need for the U.S. automotive industry to incorporate more fiber-reinforced polymer composites in the design of future vehicles to reduce the weight, emissions, and fuel consumption.

For example, a specific goal of FreedomCAR is to reduce the weight of an automotive structure by 50% for the same cost and durability as seen in today's products. The key to meeting these objectives is a comprehensive predictive engineering approach that is capable of accurately simulating critical attributes associated with the design of both the product and its manufacturing process. To this end, Figure 1 captures the long-standing vision of an integrated

[1] See http://www.missouri.edu/~desy9b/nsf/index.htm for workshop information.

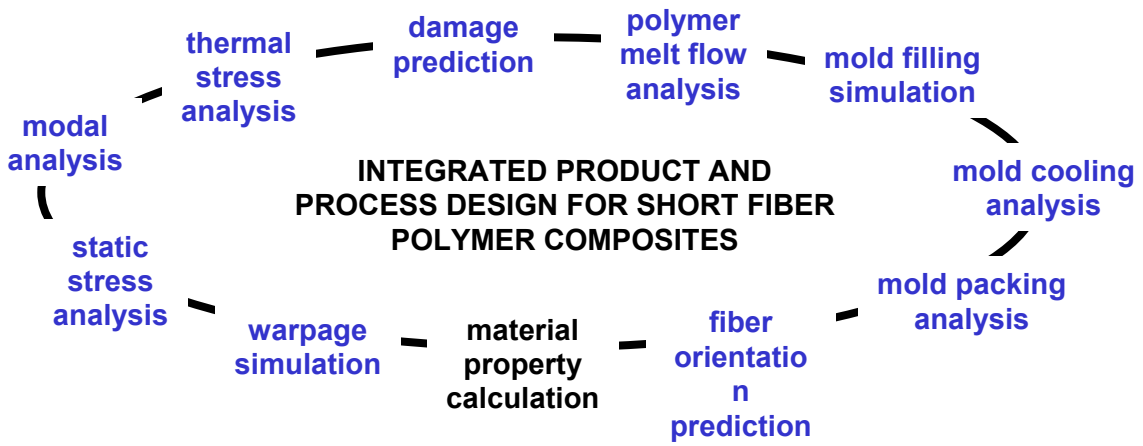


Figure 1. Relationship of product and process attributes in the analysis of short- and long-fiber polymer composites.

product and process design environment for short-fiber reinforced polymer composites. Here, the critical link that connects the computation of materials processing attributes with the prediction of a composite product's performance is the evaluation of structural mechanical properties from melt-flow predictions.

Given the dramatic increases in affordable computing over the past decade, and the anticipated demands on our predictive capabilities for composite materials over the next decade, it is now time to reconsider assumptions that compose today's fiber-orientation models. For example, limiting fiber-orientation predictions to solving for only the second-order orientation tensor components in an effort to reduce computational effort may not be necessary. This project will provide a higher-order approximation to more accurately describe suspension mechanics for complex flow fields such as those where both shear and elongational velocity gradients exist in all three different planes.

Statistical Approach for Computing Mechanical Properties

One task of this research is to develop a statistical approach that may be used to evaluate the variability of mechanical properties of short- and long-fiber composites. Current methods for computing the mechanical properties are limited to short fibers, and provide the deterministic (i.e., averaged) values of properties such as elastic moduli and Poissons ratios. Unfortunately, a finite region within an injection-molded part would be better represented by a statistical sample of the orientation distribution, rather than its mean values. This is particularly important since elastic properties computed by integrating through the thickness of a polymer composite rely on data evaluated over finite sub-regions that may have dimensions on the order of 100 μm.

In our preliminary work, material properties are obtained from the aggregate of unidirectional fibers by computing expected values of the material properties from a known fiber-distribution function. The orientation average, or expectation value, of the material properties of the composite sample is defined for discrete non-correlated fiber distributions as

$$\left\langle C_{ijkl} \right\rangle = \frac{1}{N}\sum_{n=1}^{N}(Q_{pi}(\theta_n,\phi_n)Q_{qj}(\theta_n,\phi_n) Q_{rk}(\theta_n,\phi_n)Q_{sl}(\theta_n,\phi_n)\overline{C}_{pqrs})$$

where N is the number of fibers considered in the sample which is defined by the fiber volume fraction, fiber size, and the volume of a sample of the composite of interest. In this calculation, $\left\langle C_{ijkl} \right\rangle$ is the expectation value of the compliance tensor, $\overline{C}_{pqrs}$ is the underlying unidirectional compliance tensor for a single fiber (computed using the Mori-Tanaka, Halpin-Tsai, or similar inclusion model) and $Q_{ij}(\theta_n,\phi_n)$ is a rotation tensor that transforms

the *n*th fiber into a selected coordinate system. The angles θ and ϕ define the fiber direction as shown in Figure 2. It is important to note that this computation does not account for spatial interactions between individual fibers, and assumes a homogeneous volume fraction, as do other techniques that appear in the literature[2].

The material property expectations are evaluated in this research through Monte Carlo simulations by generating N randomly-oriented fibers for a polymer-composite sample. Then, a similar analysis is used to randomly generate multiple samples which are used to compute the mean and variance of the mechanical properties of interest.

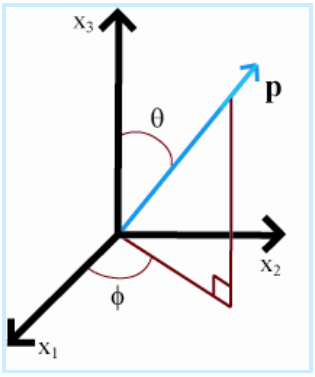


Figure 2. Coordinate system defining fiber direction with the unit vector p(θ,ϕ).

Example Calculations

To illustrate the statistical nature of the mechanical properties of short-fiber composites, we consider the fiber-orientation distribution function

$$\psi(\theta,\phi) = k \sin^n \theta \quad \cos^m \phi$$

where n and m define the amount of fiber alignment, and k is a constant chosen to satisfy the normalization condition. As n and m increase, fibers become more aligned in the x_2-direction in Figure 2. In the first example, we consider a short-fiber sample having a fiber aspect ratio a_r = 100 and a volume fraction V_f = 0.2. A highly-aligned flow is assumed here with $n = m = 60$ which defines the normalization parameter $k = 61/4\pi$. In this example, the fiber and matrix moduli are 10.5 Mpsi and 0.5 Mpsi, respectively, and the fiber and matrix Poissons ratios are 0.2 and 0.35, respectively. The orthotropic material properties computed for this composite appear in Table 1 where mean property values for the Young's moduli (E_1, E_2, and E_3), Poissons ratio (ν_{12}) and shear moduli (G_{12} and G_{23}) are evaluated. Also shown are results computed by the statistical approach presented here for N = 100,000. Table 1 shows that the mean orthotropic material properties obtained from our statistical approach are nearly identical to results published by Advani and Tucker.

Table 1. Elastic properties evaluated from Advani and Tucker, and by the Monte Carlo sampling approach presented here.

material property	Advani and Tucker properties	expected value from 10^5 fiber simulations
E_1 (Mpsi)	2.220	2.224
E_2 (Mpsi)	0.813	0.814
E_3 (Mpsi)	0.813	0.813
ν_{12}	0.333	0.330
G_{12} (Mpsi)	0.293	0.292
G_{23} (Mpsi)	0.254	0.254

In a second example, our statistical approach is used to evaluate the variability in mechanical properties of a short-fiber composite. Figure 3 illustrates a cube of uniformly-random and aligned fibers sampled from the orientation distribution function given above. A Monte Carlo simulation was performed using 100,000 samples from each distribution and histograms of the resulting elastic moduli and Possions ratio appear in Figure 4.

The effect of volume fraction on material property variability is also evaluated using the Monte Carlo simulation method and statistical evaluation described above. Figure 5 illustrates the coefficient

[2] See e.g., Advani, S. and Tucker, C., 'The Use of Tensors to Describe and Predict Fiber Orientation in Short Fiber Composites', *Jn. of Rheology*, Vol. 31, No. 8, pp. 751-784, 1987.

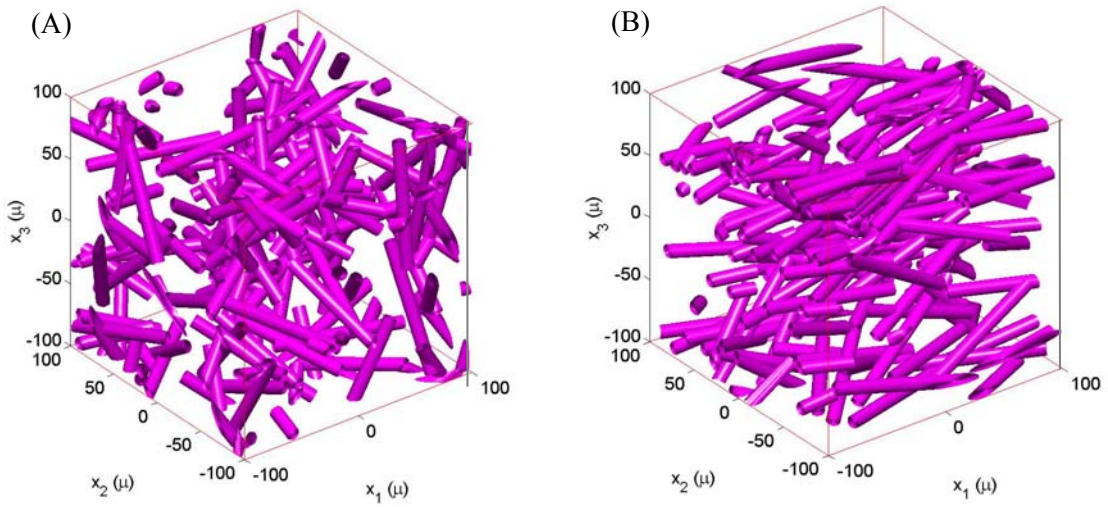


Figure 3. Short-fiber composite samples with $V_f = 0.1$ and $a_r = 10$ for A) a uniformly-random distribution having $k = 1/4\pi$ and $n = m = 0$ and B) a distribution aligned in the x_2 direction with $k = 7/4\pi$ and $n = m = 6$.

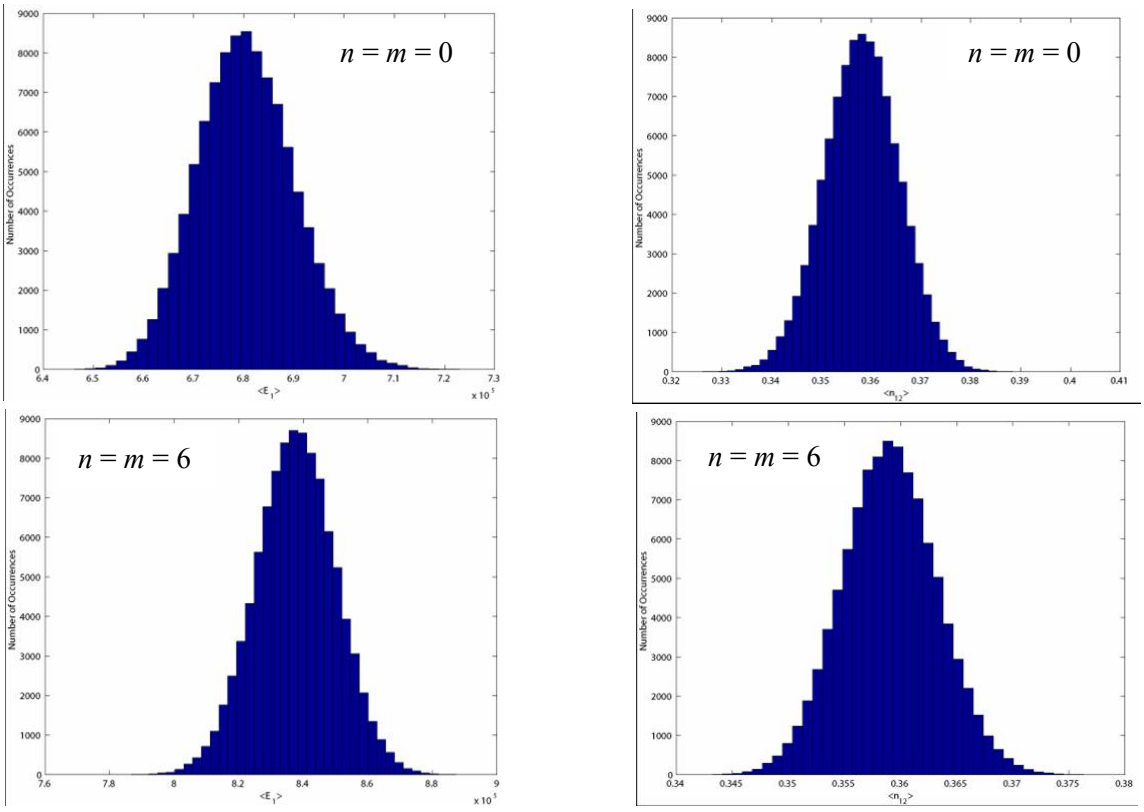


Figure 4. Histograms of selected elastic properties generated from 100,000 samples of fiber-orientation states for uniformly-random and aligned distributions.

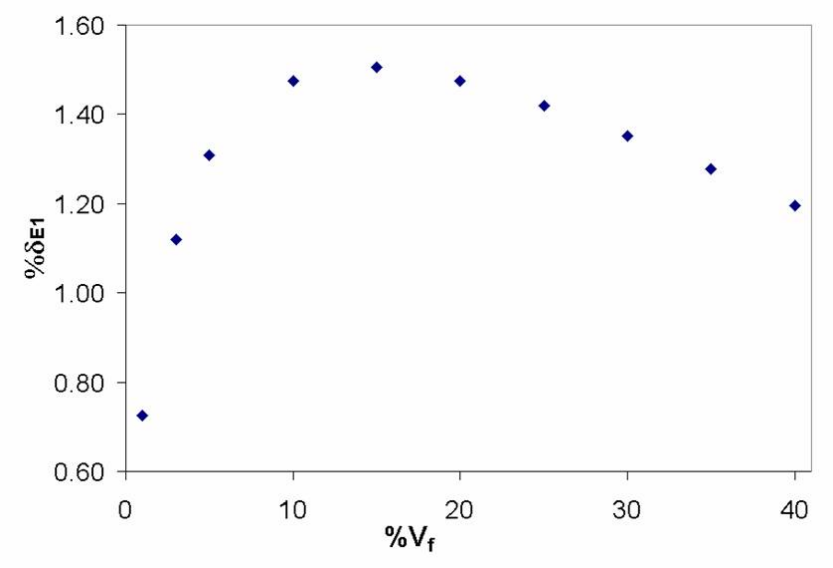


Figure 5. Coefficient of variation as a function of volume fraction for a highly aligned fiber-orientation state ($n = m = 6$).

of variation for the elastic modulus in the x_2 direction defined as

$$\%\delta = \frac{\sigma}{\mu}(100\%)$$

where μ and σ are, respectively, the mean and standard deviation of an elastic property determined through statistical sampling. The results presented here are for the highly-aligned distribution described above. The values illustrated in Figure 5 show that as the volume fraction gets large or small, the decreased influence of orientation reduces δ. It is also seen that δ is a maximum near a volume fraction of approximately 12% for the conditions evaluated here.

Conclusions

This research project focuses on the prediction of elastic mechanical properties from higher-order fiber orientation tensors. As part of this study, computations are being performed to assess the variability in these properties that occurs due to sampling the fiber-orientation distribution function. Preliminary results are presented here for short-fiber composites based on a statistical evaluation of the mechanical property's expected value and Monte Carlo sampling. These results show that both fiber orientation and volume fraction influence property variability

Presentations/Publications/Patents

1. D.A. Jack and D.E. Smith, 'A Statistical Method to Obtain Material Properties from the Orientation Distribution Function for Short-fiber Polymer Composites', IMECE2005-81263, Proceedings of ASME IMECE'05, Orlando, Florida, Nov. 5-11, 2005.

5. JOINING

A. Die-Cast Net-Shaped Hole Process Development for Application of Thread-Forming Fasteners

Principal Investigator: William Charron
Ford Motor Company
17000 Oakwood, Room B154, Allan Park, MI 48101
(313) 805-6628; fax: (313) 594-1898; e-mail: wcharron@ford.com

PNNL Principal Investigator: Dean M. Paxton
Pacific Northwest National Laboratory
P. O. Box 999, Richland, WA 99352
(509) 375-2620; fax (509) 375-2186; e-mail: dean.paxton@pnl.gov

PNNL Contract Manager: Mark T. Smith
Pacific Northwest National Laboratory
P. O. Box 999, Richland, WA 99352
(509) 375-4478; fax: (509) 375-4448; e-mail: mark.smith@pnl.gov

Technology Area Development Manager: Joseph A. Carpenter
(202) 586-1022; fax: (202) 586-1600; e-mail: joseph.carpenter@ee.doe.gov
Field Technical Manager: Philip S. Sklad
(865) 574-5069; fax: (865) 576-4963; e-mail: skladps@ornl.gov

---

Contractor: Pacific Northwest National Laboratory / U.S. Automotive Materials Partnership
Contract No: DE-AC06-76RLO 1830 / FC26-02OR22910

Objectives

- Evaluate the effect of hole size and shape variation on clamp load using thread-forming fasteners (TFFs) in aluminum alloy die castings.
- Evaluate the reusability performance of thread-forming fasteners in aluminum die castings when subjected to repeated assembly/disassembly of a single fastener into the same hole.
- Evaluate the extent to which contamination in the form of debris is produced when inserting TFFs into aluminum die-cast net-shaped holes at 3-diameter thread engagement.
- Identify automotive casting suppliers and collect in-field measurements of variation in size and shape of casting-die hole features and pins.

Accomplishments

- Completed testing and evaluation of the effect of hole size and shape variation on clamp load when using TFFs in aluminum alloy die castings.
- Implemented a test plan recommended by the USCAR Fastener Committee to evaluate the requirements for reusability when assembling TFFs in die-cast net-shaped holes.
- Completed initial reusability testing of selected TFFs in aluminum alloy die-cast net-shaped holes.

- Completed an initial assessment of contamination created during the sequence of assembly/disassembly of TFFs into aluminum die-cast nut specimens at 3-diameter thread engagement.
- Initiated the collection of in-field data from casting suppliers who are taking measurements of hole size, shape, and position variation during production casting operations.

Future Direction

- Execute remaining reusability tests of additional TFFs in aluminum alloy die castings.
- Execute hole size and shape testing of TFFs in magnesium alloy die castings.
- Execute reusability testing of TFFs in magnesium alloy die castings.
- Execute next phase of serviceability, debris, and hole size and shape testing using magnesium specimens.
- Analyze in-field measurement data collected by casting suppliers taking measurements of hole size, shape and position variation during production casting operations.

Introduction

This technical feasibility project is focused on resolving the highest priority technical challenges associated with application of thread-forming fasteners (TFFs) into die-cast, net-shaped holes in aluminum and magnesium alloys which were identified during the initial concept feasibility project completed in 2003. Those priority issues were grouped into 4 technical challenges: (a) casting variation, (b) fastener design, (c) assembly processing and (d) in-service requirements. The major facets of casting variation are cast-hole position, shape and size resulting from the thermal, mechanical and metallurgical effects of the die-casting process. Fastener testing is planned to evaluate the effect of hole size, shape and position on clamp load. In addition, in-field data is being collected from casting suppliers on die-pin wear and degradation. A variety of fastener designs provided by the fastener suppliers and assembly procedures will be evaluated during this testing. Also to be considered in this phase is the closely related in-service issues of contamination and reusability. All of these prioritized issues will be addressed for both aluminum and magnesium alloys during the Phase 1 technical feasibility project.

Background

Progress has been made in applying TFFs into machined or stamped holes featured in automotive applications for general assembly. Use of these fasteners has eliminated the tapping operation and thereby reduced costs, reduced investment, and improved warranty while delivering better joint properties within an assembly.

Opportunities exist to further reduce costs by using TFFs with net-shaped holes in lightweight castings by eliminating the drilling operation and associated equipment investment without sacrificing joint performance. Potential applications for using TFFs in cast components are numerous and include: powertrain (transmissions, engines, and rear axles), chassis (control arms, suspensions) and body structures that utilize large castings (inner doors, liftgates, under-hood attachments and supports). Expanding the use of lightweight materials is the driver behind this project. Little progress has been made in applying this concept to aluminum castings and even less progress has been made with magnesium. Successful development of this idea in cast products will expand the use of lightweight materials due to the proven benefits already achieved in the "as-stamped" applications.

Approach to Hole Size and Shape Variation Testing

Holes in die castings are created by the use of steel pins inserted in specific locations in the die block. The potential exists for the dimensions of the die pin to change in size (diameter) or shape (taper) resulting from repeated contact with the molten metal filling the die cavity. Molten aluminum tends to dissolve some alloy constituents of the steel and this dissolution is a function of temperature. Thus, if dissolution were to occur, it would be most prevalent at the leading end of the pin which is the hottest due to the large die block acting as a heat sink. In addition, exposure to molten aluminum and

magnesium can result in soldering of these alloys onto the pin, which is then cleaned with an emory cloth. Repeated application of this mechanical cleaning process can result in further removal of pin material, thereby changing the diameter of the pin. Both of these changes in time have the potential to cause variation in the desired size and shape of the resulting hole in the die casting. The purpose of this hole size and shape test matrix is to determine the impact of variations from nominal hole size (diameter) and shape (taper) on the resulting clamp load when using a thread-forming fastener. The matrix for this testing includes three different tapers and up to three increments of larger and smaller hole diameters and is presented in Figure 1. The nominal hole for a M6 Taptite 2000 fastener has a 0.5 degree taper with a hole diameter of 5.44 mm at the target thread engagement depth of 15 mm. The variations in size and shape are made relative to this nominal definition. Test plates with a range of hole sizes and shapes were cast from aluminum alloy A380 and machined into individual test specimens as shown in Figure 2.

Clamp load was determined using the LabMaster Fastener Evaluation Test Cell. This unit utilizes a slide-bearing mount for the fastener drive system and mounting for the rotary torque-angle sensor and torque-tension research head. The fastener test system couples with a DC electric nut-runner tool and controller, a rotary torque-angle transducer, a combination thread-torque and clamp-force transducer, and a computer control system for accurate test reproduction and data logging and reporting. The test-stand equipment and Bosch Rexroth nut-runner are shown in Figure 3. The nut-runner was programmed to drive the fasteners to failure at a rundown speed of 240 RPM and the Labmaster software recorded clamp load, input torque and failure torque versus time and angular rotations of the fastener for each test. The failure mode was noted at the end of the test (break the fastener or strip the threads). The fasteners for these tests were coated with Magni 565 and a total of 30 tests were run at each combination of size and shape.

Results for Holes Size and Shape Variation Testing

Clamp load at failure and mode of failure are plotted vs. hole size in Figure 4. As shown in the test matrix, the nominal taper (0.5 degree) was tested at three (0.05 mm) increments above nominal (5.44 mm) and three increments below nominal. At nominal diameter, the average maximum clamp load was 13 Nm and the failure mode in all cases was breaking the fastener. As the hole diameter increased by 0.05 mm, the clamp load decreased to 12 Nm and the failure mode in all cases remained breaking the fastener. As the hole size increased to the next two increments (+0.10 mm and +0.15 mm), the average clamp load continued to decrease to 10 Nm and 9 Nm respectively, and fastener stripping became more prevalent with the larger holes. For hole diameters at nominal +0.10 mm, 1 in 30 fasteners stripped, whereas for hose holes at nominal + 0.15 mm, the failure mode for 15 of the 30 tests was stripping. For the same 0.5- degree taper with hole sizes smaller than nominal, the average clamp load was 14 Nm for all three increments and the failure mode for all cases was breaking the fastener. However, the standard deviation for these three sizes was 2 Nm and the clamp load in all tests fell in the range from 12-16 Nm, whereas the standard deviation at the nominal diameter was 1 Nm and all tests resulted in clamp loads ranging from 12 to 14 Nm. This maybe be indicative of excessive galling of the fastener and would result in poor reusability.

Nominal = 5.44 mm	Nominal - 0.15 mm	Nominal - 0.10 mm	Nominal - 0.05 mm	Nominal	Nominal + 0.05 mm	Nominal + 0.10 mm	Nominal + 0.15 mm
0.5º Taper	X	X	X	X	X	X	X
1.0º Taper	X	X	X				
1.5º Taper	X	X					

Figure 1. Test matrix for hole size and shape variation testing in aluminum alloy A380.

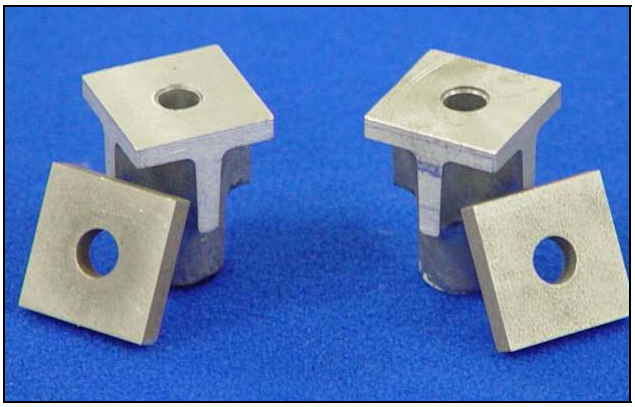


Figure 2. As-cast aluminum nut and washer specimens used for thread-forming fastener torque-tension mechanical testing.

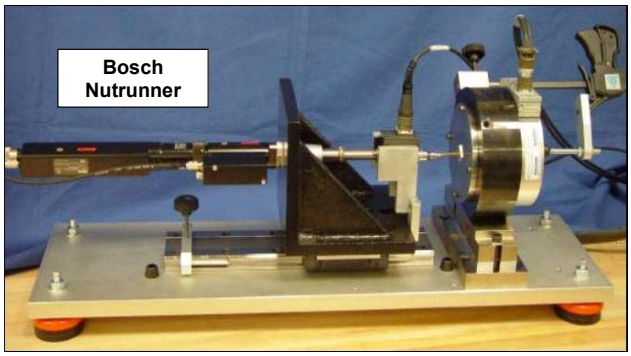


Figure 3. LabMaster Fastener Evaluation Test Cell from RS Technologies with integrated Bosch nutrunner.

In the case of the 1.0-degree taper, three increments below nominal were tested and resulted in average clamp loads increasing from 11.8 Nm at nominal -0.05 mm to 13 Nm at nominal -0.15 mm. For the largest of these holes, 3 out of 30 tests resulted in failure modes of fastener stripping. As the hole diameter decreased, all failure modes were breaking the fastener. Similar to the smaller holes at 0.5 degree taper, the standard deviation in these tests was approximately twice (2 Nm) observed at the 0.5 degree taper hole with nominal diameter (1 Nm). For those holes at the largest taper (1.5 degree), only 2 hole diameters were tested and both resulted in high probability of stripping, i.e. 30/30 at nominal -0.10 mm and 25/30 for the smaller hole at nominal -0.15 mm.

Results from this size and shape test matrix suggest that clamp load performance of nominal hole sizes for 0.5-degree tapered holes is most comparable to hole size of nominal + 0.05 mm. For larger holes, the probability of fastener stripping increases and the clamp load decreases. For 0.5-degree tapered holes smaller than nominal diameter (5.44 mm), the variability in clamp load is almost twice that observed at nominal conditions. The high probability of fastener stripping in both the larger tapered holes indicates this feature is likely limiting in hole geometry.

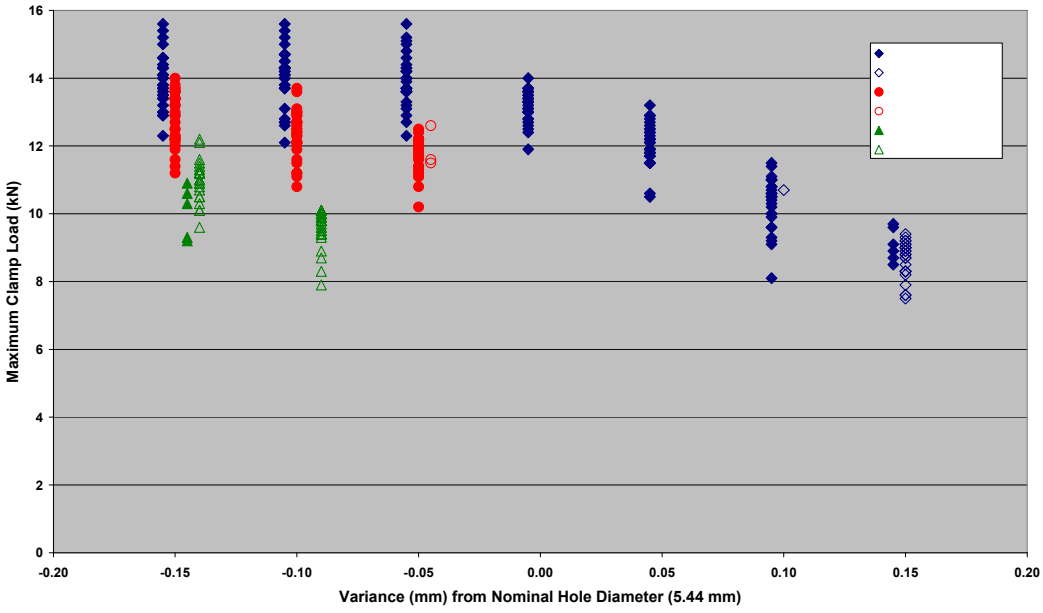


Figure 4. Clamp-load test data for hole size and shape variation test matrix using Taptite with Magni 565 coating at 15 mm thread-engagement depth.

Approach to TFF Reusability Testing

In order to establish a test procedure that would adequately address the issues associated with reusability, the project team requested input from the USCAR Fastener Committee which consists of OEM representatives with expertise in fastener technology and assembly applications. This committee prepared a recommended test procedure to assess reusability performance. This procedure was adopted by the project team and is presented in Figure 5. After initial testing and based on discussions with the Project Fastener Team, the procedure was modified such that the target torque was determined to be the assembly specification torque used to install M6 fasteners on the assembly line, the range of which is 10-12 Nm. With this established, a machine screw was assembled into a tapped hole to a target input torque of 11 Nm and the resulting clamp load recorded. This sequence was repeated 13 more times for a total of 14 consecutive run-downs. On the 15th run-down, the torque limit was removed and the joint was tightened to failure of the fastener. Similar testing was repeated for both the Taptite and ALtracs thread-forming fasteners. The nut-runner was programmed to drive the fasteners to target torque at a rundown speed of 240 RPM and the Labmaster software recorded clamp load, input torque versus time and angular rotations of the fastener for each test. The fasteners for these tests were coated with Magni 565 and a total of 10-15 tests were run at each combination of size and shape.

Results of Reusability Testing

The clamp-load and input torque data for a series of 15 reusability tests using M6 machine screws is presented in Figure 6. The clamp load achieved was ~10 Nm and clamp-load retention was nearly 100% when running the same machine screw into the same hole 14 times. The average data were very repeatable for the 15 fasteners and nut specimens tested as evidenced by the small standard deviation lines bounding the average data. When the same procedure and target torque were applied to Taptite and ALtracs thread-forming fasteners, the resulting clamp load generated was ~ 5 Nm, or 50% of the value generated by machine screws at the same input torque. A series of tests was conducted with each fastener and each showed lower clamp load at the target torque, as shown in Figure 7, for Taptite fasteners. As with machine screws, the average data were very repeatable for the 10 fasteners and nut specimens tested, as evidenced by the small standard deviation lines bounding the average data.

After discussion with the Project Fastener Team, the target torque for all thread-forming fasteners was increased to a value beyond the assembly specification but which matches the clamp load generated by a similar machine screw under the same conditions. In the case of the Taptite fastener at 15-mm thread engagement shown in Figure 7, the new target torque was raised to 17 Nm and it generated ~ 9 Nm of clamp load upon initial testing and showed ~90% clamp-load retention throughout the 14 run-downs. Comparable results were observed for ALtracs fasteners when testing under similar conditions. The lessons learned during this test series will be adopted during future reusability testing for this project, to include 12- and 15-mm thread engagements in aluminum and magnesium nut specimens with a variety of thread-forming fasteners.

Approach to TFF Contamination Testing

Another issue to be investigated during this technical feasibility project is the extent to which contamination in the form of debris is generated while using thread-forming fasteners in die-cast, net-shaped holes. The approach to this test was to run a single fastener into the same hole and measure the metal fines generated as debris in the hole after disassembly of the joint. The debris was collected in a plastic dish and weighed on an electronic balance. In order to collect this debris, assembly of the fastener could not be done using the Labmaster test stand and constant-speed nutrunner assembly tool due to the space constraints of the load cell. Therefore, a hand-held drill was used to run the fastener into a nut specimen held in a bench-top vise. The assembly was performed horizontally with the plastic dish held under the joint during assembly and disassembly to collect any debris. The input torque capability of the hand-held drill was measured on a test piece using the Labmaster and was measured at 12 Nm. This sequence was repeated 9 more times for a single fastener for a total of 10 assembly/disassembly steps. Thread-forming M6 fasteners with the S437 coating supplied by Textron were used for this testing along with the

USCAR Fastener Committee
USAMP Die Cast Net-Shaped Hole Process Development

To: USAMP Die Cast Net-Shaped Hole Process Development Team

cc: USCAR Fastener Committee

Subject: **Die Cast Net-Shaped Hole Process Development - Fastener Service Recommendations**

Objective: Develop a baseline service metric by establishing a target torque with fastener trials, using worst case conditions.

Establish a baseline for screw performance using a machine screw and pre tapped hole:

Tighten 30 fasteners to failure using a torque-tension test method, and record clamp load, torque, & failure mode.

Establish a target torque from this data, based on 80% of the minimum failure.

Record clamp load at the target torque for a minimum of 15 rundowns (unless failure occurs sooner) reusing the same fastener and hole.

On the 15th run, tighten the 30 joints to failure with the previously used torque-tension method.

Establish a target torque using a thread forming screw and non-tapped hole:

Set-up the estimated worst case conditions using a TapeTite 2000 SP thread form, a die cast hole taper with a 0.5^{o} draft angle, a die cast hole at 90% of the screw diameter, and a length of thread engagement equal to 2.0 screw diameters.

Tighten 30 fasteners to failure using a torque-tension test method, and record clamp load, torque (drive and strip), & failure mode.

Determine the drive to strip ratio. It should be a minimum of 4:1.

Establish a target torque that will achieve the same mean clamp load as the machine screw did from the above test at the target torque.

Record clamp load at the target torque for a minimum of 15 rundowns (unless failure occurs sooner) reusing the same fastener and hole.

On the 15th run, tighten the 30 joints to failure with the previously used torque-tension method.

Review the baseline data with the USCAR Fastener Committee.

Figure 5. Recommended test procedure for reusability of thread-forming fasteners into aluminum net-shaped, die-cast holes.

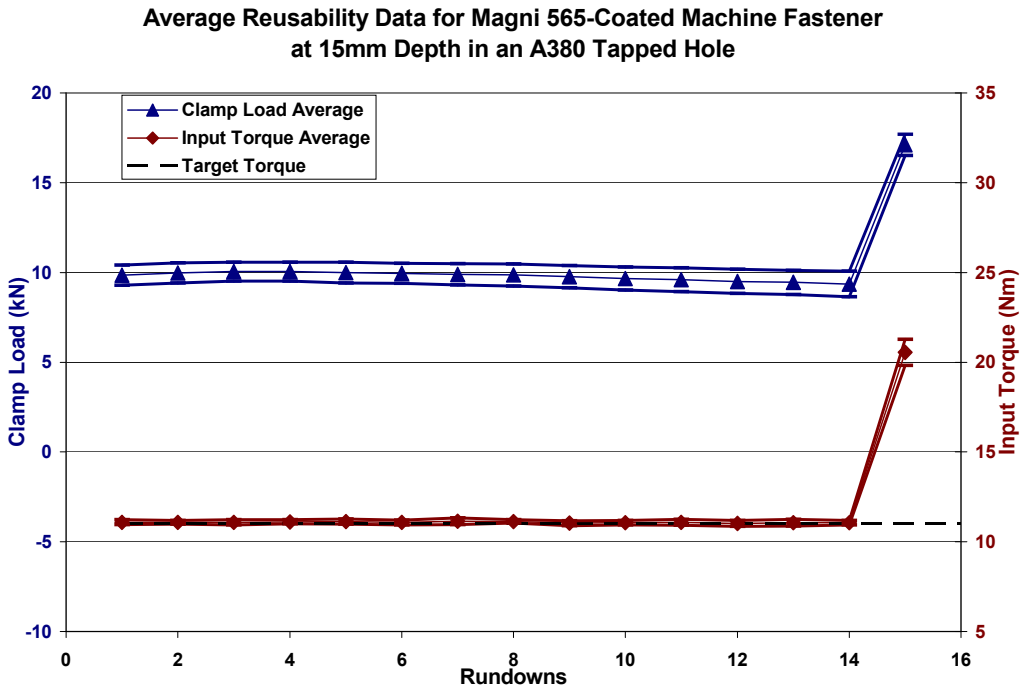


Figure 6. Clamp-load and input-torque data for consecutive rundowns of a single Magni 565-coated M6 machine screw into a drilled and tapped aluminum A380 die-cast nut specimen.

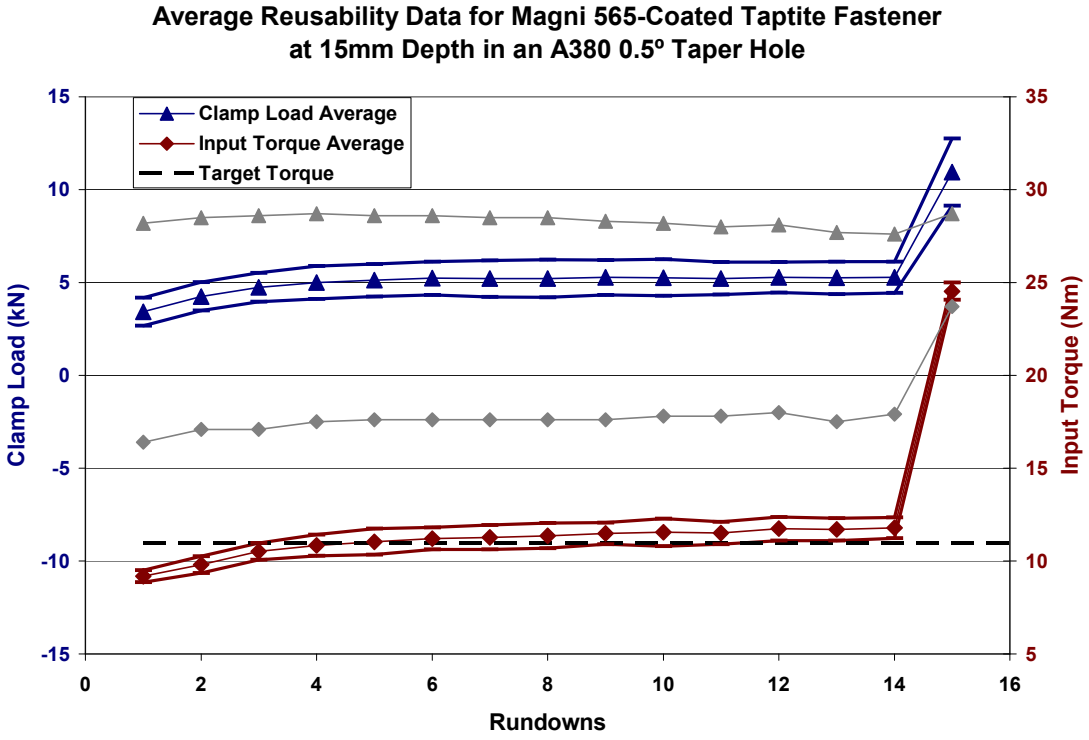


Figure 7. Clamp-load and input-torque data for consecutive rundowns of a single Magni 565-coated M6 Taptite thread-forming into a A380 die-cast nut specimen.

companion machine screws in drilled and tapped holes.

Results for TFF Contamination Testing

The initial contamination test of an S437-coated TFF into a 0.5-degree aluminum nut specimen generated a visible amount of metal fines in the dish which measured 0.035 grams. The next 9 run-downs generated 0.005 grams of additional debris for a total of 0.040 grams. It should be noted that the 0.005 grams is difficult to measure consistently and challenges the resolution of the electronic balance. For the next five tests using similar specimens and fasteners, the total debris collected during each series 10 run-downs of a single fastener into the same hole did not exceed 0.005 grams. The first run-down of the seventh TFF contamination test series performed similar to the first series and generated 0.035 grams of metallic fines, followed by 9 more rundowns that generated an additional 0.005 grams for a total of 0.040 grams. This dramatic variability in debris generation may be impacted by a variation in the horizontal alignment of the fastener/hand-held drill during the assembly process. A similar series of tests was performed using companion machine screws with drilled and tapped die-cast nut specimens. The debris generated during three series of tests with machine screws generated less than 0.005 grams of debris per test series. Again, it should be noted that this level of debris is difficult to measure consistently and challenges the resolution of the electronic balance. The contamination data for all of these tests are summarized in Table 1. For future testing, greater attention to detail will be applied to the alignment of the assembly tool to determine the impact on debris generation.

Approach to TFF In-Field Casting Variation Data

In-field data is being collected from various casting suppliers and analyzed to determine capability and to identify practices for achieving minimal variation in size, shape, and position of as-cast holes. Hole-position data will be measured daily on selected castings and forwarded to PNNL for analysis. Used core pins from the same die-casting dies will be collected and forwarded to PNNL for measurement to determine the rate of variation in size and shape of cast holes.

Laboratory tests have been conducted on the Lab Master Fastener Evaluation Test Cell at PNNL for various combinations of size (diameter) and shape (taper) holes to determine the range of variation that yields acceptable clamp loads. The in-field data and laboratory test-cell data will be compared to identify best practices and to determine gaps for further technical development. Several casting manufacturers are actively involved in the project, with varying stages of participation.

Five are fully engaged in collecting data:

- General Motors
- J R French
- Trace
- Metaldyne
- SPX Contech

Other casters participating in the project activities include:

- DaimlerChrysler
- Meridian
- Intermet
- Lunt

Conclusions

The impact of hole size and shape on clamp load was evaluated for Taptite thread-forming fasteners in aluminum alloy A380. Results from the hole size and shape evaluation indicate that at a taper of 0.5 degree, hole diameters at up to 0.05 mm above nominal (5.44 mm) would generate clamp loads and failure modes comparable to nominal conditions. Above this size, the risk of fastener stripping is high and detrimental to a useful joint. For hole sizes at nominal – 0.05 mm or below, the larger standard deviation is indicative of fastener galling. For holes with tapers at 1.0 and 1.5 degrees, the risk of fastener stripping was high in most cases. For the smaller 1.0-degree tapered holes where stripping did not occur, the standard deviation was large and again indicative of excessive galling.

Initial testing was completed in two areas of fastener serviceability as recommended by the USCAR fastener committee, specifically reusability and contamination. Lessons learned during this series of tests will be applied to future testing of

Table 1. Measurement of contamination in the form of metallic fine debris generated during assembly and disassembly of a single fastener into the same hole 10 consecutive times.

Test #	Fastener Type	Weigh of Debris of 10 rundowns
1	Thread-forming	0.040 grams w/ 0.035 grams on 1st rundown
2	Thread-forming	~0.005 grams
3	Thread-forming	~0.005 grams
4	Thread-forming	~0.005 grams
5	Thread-forming	~0.005 grams
6	Thread-forming	~0.005 grams
7	Thread-forming	0.040 grams w/ 0.035 grams on 1st rundown
8	Machine screw	< 0.005 grams
9	Machine screw	< 0.005 grams
10	Machine screw	< 0.005 grams

both aluminum and magnesium alloys with a variety of fasteners. For tests conducted with the modified procedure, results indicate that when using the same thread-forming fastener into the same hole, clamp load retention was in excess of 90%. Similarly, contamination tests were performed which indicated a minimal amount of debris is generated when thread-forming fasteners are used with as-cast aluminum nut specimens. Lessons learned during both types of testing will be applied to the next phase of work which has prototypical thread-engagement depths of 2 and 2.5 times the fastener diameter.

Future Work

The lessons learned during these initial serviceability tests on reusability and contamination assessment will be employed during future testing of aluminum and magnesium alloys to resolve the key issues identified for investigation during this technical feasibility (see Introduction for definition) project. In addition, in-field data will be collected from participating casting suppliers and analysis of hole size, shape, and position data will be conducted and compared to the clamp-load results generated using Taptite fasteners and aluminum alloy A380. Similar size and shape testing will be conducted on magnesium alloys as well using a variety of thread-forming fasteners.

Presentations/Publications

Abstract accepted by TMS for paper entitled "Application of Thread-Forming Fasteners in Net-Shaped Cast Holes in Lightweight Metal Alloys" to be presented in March 2006.

D. M. Paxton, "Application of Thread-forming Fasteners in Die Cast Net-Shaped Holes", USAMP Casting Off-Site Meeting, Detroit, MI, September 29, 2005.

B. Forming Limits of Weld Metal in Aluminum Alloys and Advanced High-Strength Steels

Project Manager: Richard W. Davies
Pacific Northwest National Laboratory
P.O. Box 999, Richland, WA 99352-0999
(509) 375-6474; fax: (509) 375-5994; e-mail: rich.davies@pnl.gov

Principal Investigator: Frode Stavehaug
Pacific Northwest National Laboratory
P.O. Box 999, Richland, WA 99352-0999
(509) 372-4766; fax: (509) 375-4448; e-mail: frode.stavehaug@pnl.gov

Principal Investigator: Glenn J. Grant
Pacific Northwest National Laboratory
P.O. Box 999, Richland, WA 99352-0999
(509) 375-6890; fax: (509) 375-4448; e-mail: glenn.grant@pnl.gov

Technology Area Development Manager: Joseph A. Carpenter
(202) 586-1022; fax: (202) 586-1600; e-mail: joseph.carpenter@ee.doe.gov
Field Technical Manager: Philip S. Sklad
(865) 574-5069; fax: (865) 576-4963; e-mail: skladps@ornl.gov

Participants
Elizabeth Stephens, Xin Sun, Siva Pilli, Pacific Northwest National Laboratory
USAMP, US Steel, Alcoa, Olympic Controls

Contractor: Pacific Northwest National Laboratory
Contract No.: DE-AC06-76RL01830

Objective

- Develop, validate, and disseminate a combined experimental and numerical method to statistically describe and systematically quantify the forming limits of welded aluminum alloys and high-strength steels.

Approach

- Develop a standard tool for weld process development that will systematically quantify failure probabilities during forming.
- Provide accurate and standardized methods of experimentally characterizing weld-metal formability using unique, but simple test methods available on the shop floor.
- Provide predictive models for more accurate forming simulations of tailor-welded blank (TWB) and hydroforming operations. Predict parts-per-thousand failure rates during production from finite element analysis (FEA).
- Characterize static/fatigue properties and forming behavior of several weld populations and correlate with statistically-based tools.

Accomplishments

- Evaluated competing weld specimen designs by FEA for their suitability in providing statistical information on a given weld methodology or population.
- Experimentally validated specimen designs that produced nearly plane-strain deformation across a welded sample from a simple sample geometry and load-frame test set-up.
- In conjunction with the USAMP steering committee, outlined initial weld populations to be studied to test validity of statistical and predictive methodologies.
- Completed uniaxial tensile testing of laser-welded DP600 to DP600 (1.5 mm to 1 mm thickness) TWBs.
- Constructed theoretical forming-limit diagram for laser-welded DP600 to DP600 TWBs.

Future Direction

- Finish the experimental characterization and validation on select weld populations including friction stir welded and laser-welded specimens.
- Continue development of continuum damage models to create predictive failure tools that can be used to estimate the robustness of a given weld population based on plane-strain performance, microstructural features, and other properties.
- Continue development of Digital Image Correlation for TWBs.
- Commence biaxial testing of TWBs.

Introduction

This work is a collaborative effort between DOE's Pacific Northwest National Laboratory (PNNL), USAMP team of the U.S. Council for Automotive Research (USCAR), US Steel, Olympic Controls and Alcoa. This project will develop, validate, and disseminate combined experimental and numerical methods that systematically quantify the forming limits of weld materials in aluminum alloys and high-strength steels through a combination of experimental and deformation modeling analysis. This work will enable high-volume, robust deployment of tailor-welded blanks (TWB), seam-welded tubes, and tailor-welded tubes in emerging materials.

The deformation of weld materials and their limits of formability are important aspects to both TWB and hydroforming technologies. The conventional low-carbon steels used in automotive applications are easily fusion welded using conventional technologies, and suffer no appreciable strength degradation near the weld. Aluminum alloys are more difficult to weld than low-carbon steels due to high conductivity and reflectivity, and low molten viscosity. Aluminum also has a high propensity for porosity to form during fusion welding, as well as hot cracking and heat-affected- zone (HAZ)-related issues in heat-treatable aluminum alloys. Many of the high-strength steel alloys that are finding increasing application in the automotive industry suffer from degradation of strength in the HAZ. Furthermore, nearly all fusion welds suffer from irregular geometries and elevated levels of surface roughness compared to the parent materials, which also influence formability and component performance.

This project will focus on developing a generalized numerical method to predict material forming limits in weld materials and verifying deformation and forming-limit predictions. The approach will rely on developing standardized test methods for weld material populations to establish a statistical description of material imperfection and mechanical properties in their weld region, and developing statistically-based forming-limit diagrams (FLDs) or continuum damage models that predict material failure in the weld region.

The project includes numerical model development, validation, and supporting experiments. A number of candidate weld methods will be examined in combination with selected aluminum alloys and advanced high-strength steels. The project materials will include 5000 series and 6000 series aluminum alloys, and relevant high-strength steel alloys,

including high-strength low alloy (HSLA), transformation-induced-plasticity (TRIP), and dual-phase (DP) steels. The selection of sheet materials and welding methods will be coordinated with the participating OEMs, and will be representative of high-volume, commercially- viable materials and processing technologies.

The deliverables will include a standard procedure for weld material evaluation coupled with a numerical approach for establishing weld region forming limits. The results will also allow evaluation and development of candidate weld processes and the interaction between materials and weld parameters. The overall objective is to develop test methods and experimental results to enable widespread deployment of weight-optimized TWB and tube hydroforming and to avoid weld failures during production. Figure 1 is a schematic of the typical manufacturing process development.

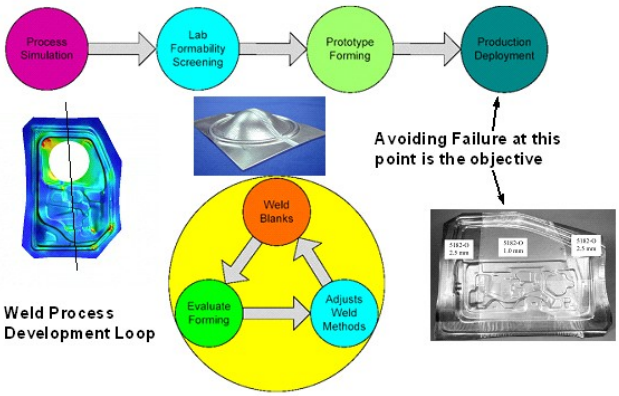


Figure 1. A schematic of the typical manufacturing process development.

Numerical Modeling

During this reporting period, finite element analysis began by first evaluating the forming limits of TWBs. Modeling of TWBs, both aluminum alloys and high-strength steels, is done to aid in the experimental analysis of the deformation of weld materials and their formability limits. A series of tensile tests were modeled and experimentally tested. Initially, a standard ASTM specimen was modeled. The model predicted failure in the thin side of the specimen as expected.

Next, a parametric study was conducted to design a tensile test specimen in which failure would occur in the plane-strain condition. Various length- to-width ratios (not shown here) and several grip dimensions, starting from a regular straight grip to a novel semi-circular grip, were modeled to achieve failure in the plane-strain condition. Figure 2 illustrates the tensile specimen design considered and varying grip design test cases modeled.

Figure 3 illustrates the predicted strain, ε_z, along 'z' in the HAZ prior to failure. It can be seen that an almost plane-strain condition can be achieved with this new tensile test specimen design and with radius grips. Figure 4 shows the stress, σ_y, for grip designs case 'a' and for the regular straight grip design, case 'g'. Note that the stress concentration is lower for case 'a'.

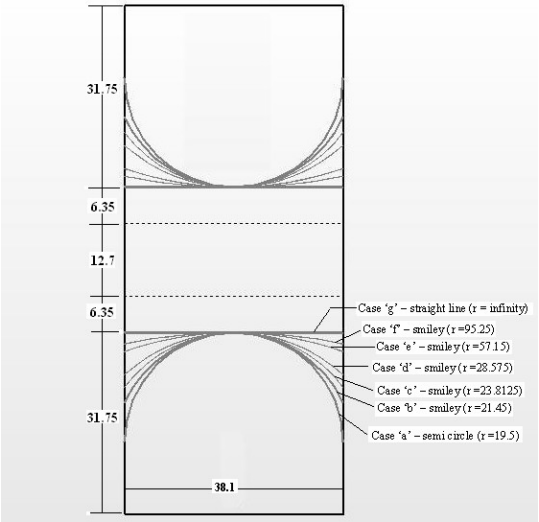


Figure 2. Tensile test specimen design and various grip cases modeled to achieve plane-strain. Dimensions are in millimeters.

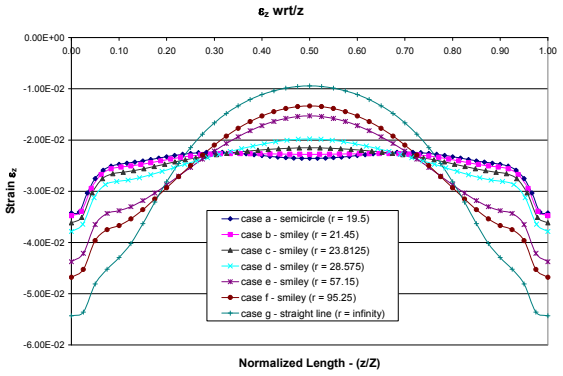
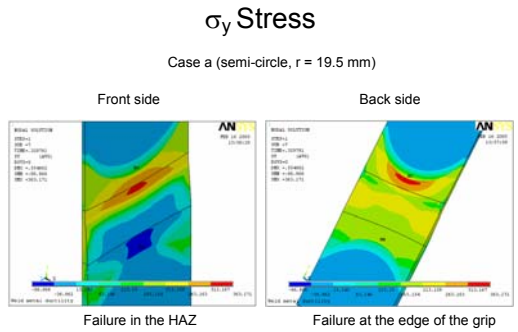
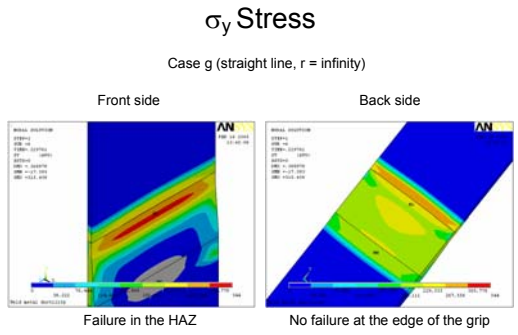


Figure 3. An illustration of the predicted strain, ε_z, with respect to 'z'.



(a)



(b)

Figure 4. Predicted stress results for: (a) Case 'a'. (b) Case 'g'.

Experimental Characterization

The experimental characterization during the first program year has consisted of verifying the grip design, testing of two weld populations and evaluating one alternative method to strain grid analysis, namely, Digital Image Correlation, also known as Speckle Pattern Interferometry.

Tensile Specimen Design

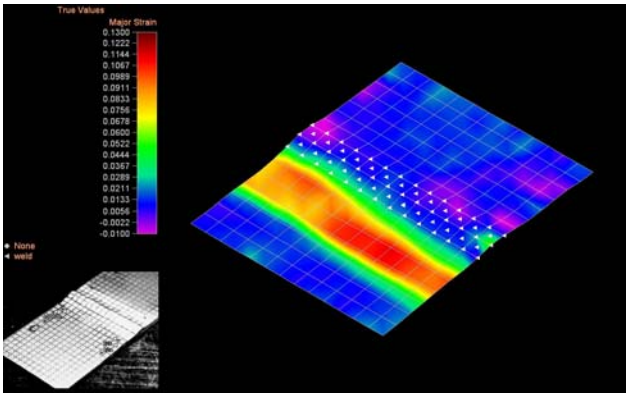
Experimental characterization began with validating the modeling results for the tensile specimen design with case 'g' grips shown in Figure 2. Case 'g' predicted an almost plane-strain condition with no failure at the edge of the grip. Tensile tests were conducted on 5182-O, 2-mm- thick, monolithic sheet specimens. The straight-line grip design had slippage problems due to material flow at the grip edges. A 45^{o} neck was observed in the gage consistent with tensile failure and not plane-strain.

The experimental investigation then continued with the same specimen design, but with the semi-circular grip (case a). Initially, similar necking was observed as in the previous specimens, but with little slippage. The specimen length was then increased to 5 inches (12.7 cm) to ensure a better grip of the specimen. A neck perpendicular to the gage was observed in the center of the longer monolithic sheet specimens, indicative of a plane-strain condition.

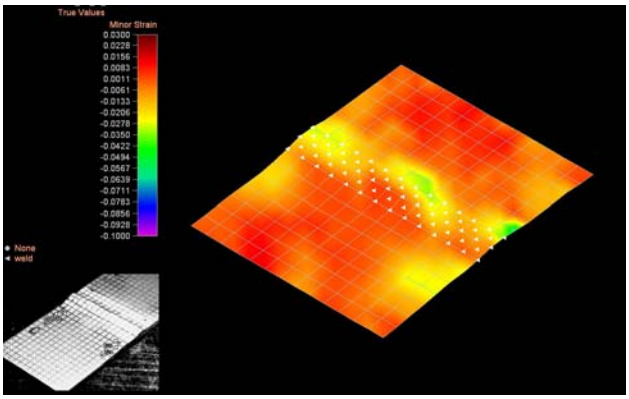
GTAW 5182-O TWB's (2 mm to 1 mm)

A population of gas tungsten arc-welded (GTAW) 5182-O TWB's (2 mm to 1 mm) were prepared to verify the plane-strain condition observed in the monolithic sheet specimens. Thirty specimens were gridded and tested.

In this population, there was only one weld failure. The other 29 specimens failed in plane- strain. The specimens were characterized for surface strains via strain-grid analysis. Figure 5 is representative of the



(a)



(b)

Figure 5. Typical strain-grid analysis results. (a) Major strain. (b) Minor strain.

typical strain results observed. The experimental results to date have shown good correlation with the modeling predictions.

DP600 TWB's (1.5 mm to 1 mm)

Laser-welded DP600 to DP600 TWB's (1.5 mm to 1 mm) were also tested. The total width of the laser-welded zone is small, less than 0.125 inch (3.2 mm).

Sixty samples were tested, 30 samples with a transverse weld orientation and 30 samples with a longitudinal weld orientation. No failures in the weld zone were recorded for the transverse weld samples. All failures were due to localization in the thin sheet (1 mm) far away from the weld and HAZ. Thus, for the transverse weld orientation, failure is determined by the properties of the 1-mm-thick parent sheet material.

In contrast, all longitudinal weld samples failed in the weld and the failure mode is therefore determined by the properties of the longitudinal weld.

Forming-Limit Diagrams

After the completion of the tensile testing, the data were compiled and theoretical FLDs were constructed for both GTAW 5182-O and laser-welded DP600 materials.

The first step in the construction of the FLD is to determine the amount of strain prior to the onset of localization via strain-grid analysis as previously discussed. Figure 6 shows the results of the strain-grid analysis of a representative sample. The data are divided into two groups, safe and localized (necked). From these two data sets, the plane-strain value for the onset of localization can be determined.

The plane-strain values for the onset of localization from all 30 samples in each data set are thereafter used as input into the Marciniak-Kuczynski (M-K) method to predict the theoretical FLD. The theoretical FLD for both GTAW 5182-O and laser-welded DP600 materials based on Weibull distribution of imperfection limits are shown in Figure 7.

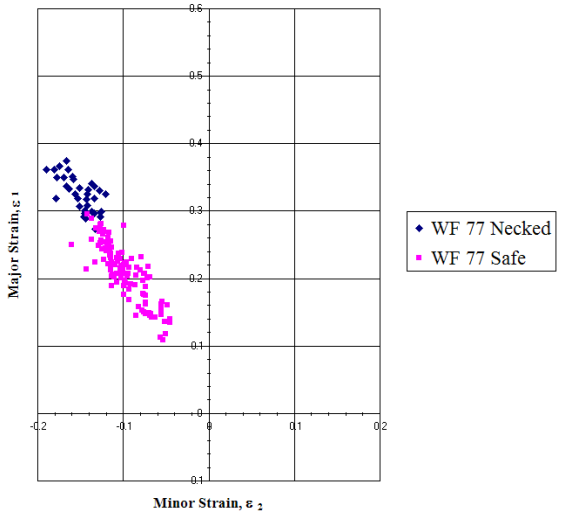


Figure 6. Representative FLD constructed from the strain-grid analysis for one specimen.

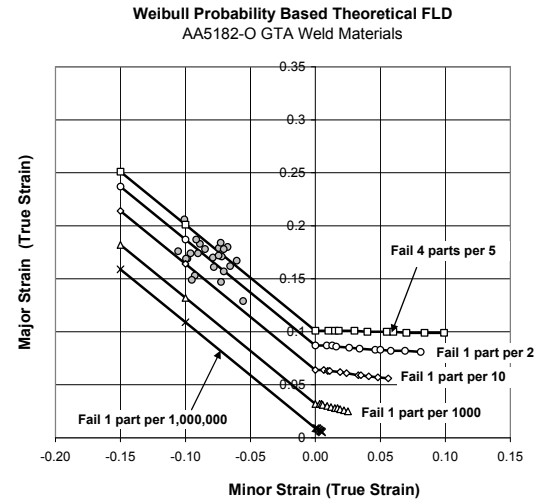
The theoretical calculation of FLD is a powerful tool to predict sheet-metal formability, starting with simple mechanical tensile testing results. This concept will be evaluated during FY 2006.

Digital Image Correlation

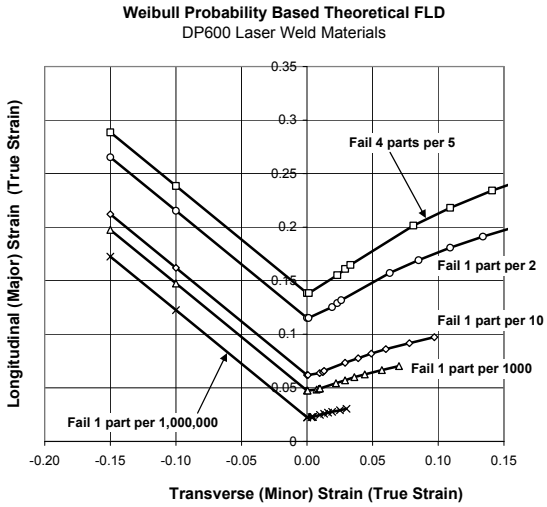
Strain-grid analysis is both time consuming and prone to subjective determination of the onset of localization. In order to address these two issues, we have just begun assessing another strain evaluation method, Digital Image Correlation or Speckle Pattern Interferometry.

Using Digital Image Correlation, a speckle pattern is painted on the sample. Two cameras then record a stereo image of strain accumulation throughout the entire deformation event. The experimental setup is shown in Figure 8.

Digital Image Correlation has very high resolution and non-homogeneous deformation is tracked locally. Since local strains can be tracked, Digital Image Correlation seems ideally suited for non-homogeneous gage areas like welds. Results to date have been very encouraging and Digital Image Correlation will be utilized for the the next material combinations to be tested.



(a)



(b)

Figure 7. Theoretical forming-limit diagrams of (a) GTAW 5182-O. (b) Laser-welded DP600. Both FLD's are based on a Weibull distribution of imperfection levels.

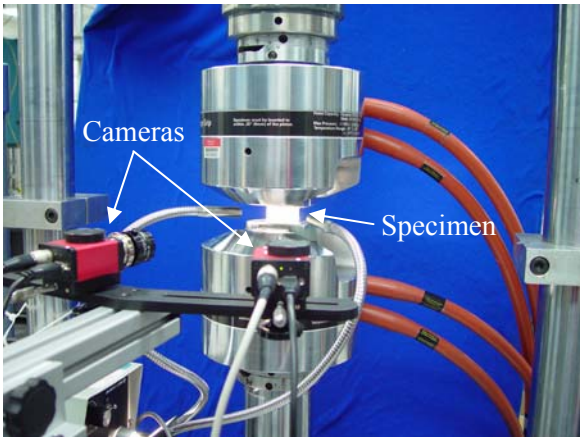


Figure 8. Digital Image Correlation set-up.

Conclusions

From this investigation, the following conclusions were derived:

- FEA can be utilized to evaluate competing weld specimen designs and determine their suitability in providing statistical information on a given population.
- A simple, sample geometry specimen design produced nearly plane-strain deformation across a welded sample.
- In laser-welded DP600 to DP600 TWBs, the properties are determined by the properties of the longitudinal weld.
- Theoretical FLDs can be predicted starting with simple mechanical tensile testing results.
- Digital Image Correlation, or Speckle Pattern Interferometry, has potential to be a more accurate tool to characterize local strain variation than current strain-grid analysis.

C. Friction-Stir Spot-Welding of High-Strength Steel

Principal Investigator: Michael L. Santella
Oak Ridge National Laboratory
1 Bethel Valley Road, Oak Ridge, TN 37831-6096
Phone - 865-574-4805, Fax - 865-574-4928, e-mail: santellaml@ornl.gov

Principal Investigator: Glenn J. Grant
Pacific Northwest National Laboratory
902 Battelle Boulevard, P.O. Box 999, Richland, WA 99352
Phone - (509) 375-6890, Fax - (509) 376-6034, e-mail: Glenn.Grant@pnl.gov

Principal Investigator: Zhili Feng
Oak Ridge National Laboratory
1 Bethel Valley Road, Oak Ridge, TN 37831-6096
Phone - 865-576-3797, Fax - 865-574-4928, e-mail: fengz@ornl.gov

Technology Area Development Manager: Joseph A. Carpenter
(202) 586-1022; fax: (202) 586-1600; e-mail: joseph.carpenter@ee.doe.gov
Field Technical Manager: Philip S. Sklad
(865) 574-5069; fax: (865) 576-4963; e-mail: skladps@ornl.gov

---

Contractor: Oak Ridge National Laboratory & Pacific Northwest National Laboratory
Contract No.: DE-AC05-00OR22725 & DE-AC06-76RLO1830

Objective

- The primary objective of this project is to evaluate the response of high-strength steels to friction-stir spot-welding (FSSW).
- Phase 1 activities will address the critical questions of whether there are tool materials available that have potential for reasonable life, and whether FSSWs made in high-strength steels represent any real advantage over welds made by conventional processes like resistance spot-welding (RSW).

Approach

- The project is a collaboration between ORNL and PNNL, and it includes an advisory committee with representatives of DCX, Ford, GM, two automotive steel suppliers, and a friction stir welding tool supplier.
- Lap joints will be made and used to correlate tensile shear strength with processing parameters and microstructures.
- Tool durability will be evaluated by sequentially making as many welds as possible with each tool material.
- Some relatively simple process modeling will be done with existing capabilities to identify conditions that could improve the business case situation for the process.

Accomplishments

- This is a new project begun during 2005.
- A consensus was achieved on the sheet steels and friction-stir tool materials to include in the Phase 1 study, and all the materials were acquired.
- A consensus was reached on the initial testing and evaluation plans.

- The test plan was initiated.

Future Direction

- Phase 2 activities will develop process models that include weld performance prediction. They will also evaluate joint mechanical properties, assess the potential for in-process NDE, transfer optimized process parameters to a robotic system, and establish the framework of a design database for spot-friction-welded structures.

Introduction

The technology for implementing friction-stir spot-elding (FSSW) of aluminum in automobile manufacturing environments exists. C-gun-type FSSW welding heads have been developed. They have been adapted to robotic systems, and these FSSW systems for aluminum are commercially available. Important questions remain about effective, economical application of FSSW to steels. The critical information that is unknown for auto steel component construction is whether there are tool materials available that have potential for reasonable life, and whether FSSWs made in high-strength steels represent any real advantage over welds made by conventional processes like resistance spot-welding (RSW). If FSSW of high-strength steels can be demonstrated and its advantages over RSW identified, then it will be possible to consider both a more detailed technical study and broader business case analysis for FSSW of high-strength steels (or any steel) in automobile assembly.

Approach

Three uncoated high-strength steels were selected for the Phase 1 study: (1) dual-phased steel, DP780; (2) a steel with transformation-enhanced plasticity, TRIP780; and (3) a hot-stamp boron steel, HSB (sourced from a Swedish supplier). It was agreed to acquire the material in a thickness of 1.5 mm based both on easy availability from the steel suppliers (Mittal Steel Corp. and Gestamp US Hardtech, Inc) and on the level of interest among OEMs.

Two materials were selected for the friction- stir tools: polycrystalline boron nitride (PCBN) and an alloy of tungsten containing 25 wt% rhenium (W25Re). Both materials are available commercially. Two tool designs, shown in Figures 1 and 2, were selected using input from the industry supplier of the PCBN, MegaStir. The tool design shown in Figure 1 is considered relatively conventional, having a pin that protrudes from its main body. The main body is referred to as the shoulder region; its diameter is indicated as 0.4 inches in Figure 1. Figure 2 depicts a 'shoulderless' tool. This geometry was recommended by MegaStir based on their

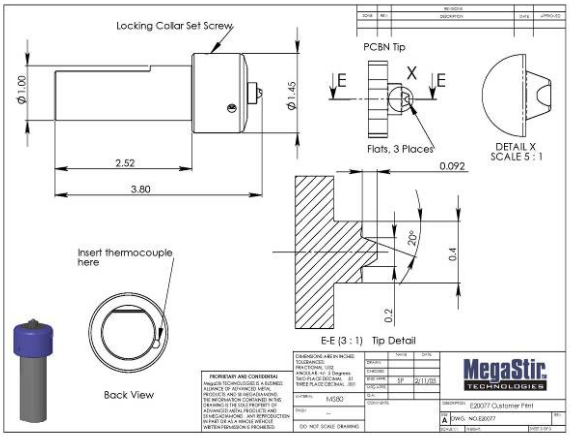


Figure 1. Drawing that illustrates shape of conventional friction-stir pin tool geometry

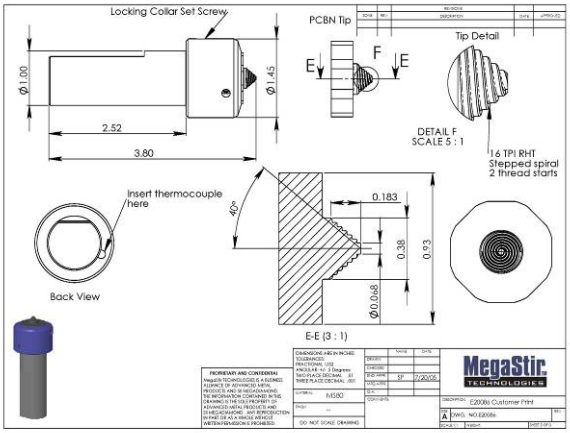


Figure 2. Drawing that illustrates shape of conventional friction-stir shoulderless tool geometry

exploratory work on FSSW. Two tools of each material were made according to both drawings for a total of 4 tools.

Lap joints are being made to measure tension-shear strength, and to correlate strength with processing parameters and microstructures. The spot welds will be made by varying the parameters of tool plunge depth and tool-plunging rate. In addition to these control parameters, a number of other process variables will be recorded for each weld including weld time, spindle torque, normal force, and temperature on the back side of the two-sheet stack-ups.

Joint strength will be correlated with these parameters. Joint strengths will be compared with those of resistance spot-welds using data from published literature and existing databases.

Results and Discussion

Published data indicate the variables of plunge depth and weld cycle time are important for determining spot weld strength in aluminum alloys. Based on this information, the initial testing plan for the high-strength steels was meant to probe this parameter space by plunging to predetermined depths at constant rates, and by including a dwell at the end of each spot-weld program.

The friction-stir machine was used in displacement control during the spot welding. The plunge depths were selected by considering the geometry of the conventional (or pin) tool, Figure 1, and the thickness of the two-sheet stack-ups being used for the welding. The pin extends beyond the plane of the shoulder by about 2.33 mm. The two-sheet stack-up is about 3-mm thick. Consequently, plunging to a depth of 2.3 mm would insert the pin entirely into the stack-up and just start to engage the shoulder of the tool on the surface of the top sheet. Plunging to a depth of 2.9 mm would insert the end of the pin nearly to the bottom surface of the bottom sheet. Based on this reasoning, the plunge depths were varied from 2.3 to 2.9 mm in 0.1 mm steps. Operating the machine in the displacement mode ensured that the desired final plunge depths were achieved.

Because the friction-stir machine was operated in displacement control, the dwell portions of the welding control programs required special consideration. Using a fixed-position dwell in displacement-control mode would permit the normal load on the tool to decrease due to temperature rise at the dwell position. It is believed that maintaining the loading conditions at the dwell position will promote better bonding. Consequently, incorporation of a dwell was accomplished by creating a two-step welding program that involved first plunging to nearly the full desired depth followed by further plunging the final 0.2 mm of depth at a slower rate. Three initial plunging rates were used: 0.4 mm/s, 2 mm/s, and 3 mm/s. The two secondary plunge rates used were 0.07 mm/s and 0.20 mm/s. These secondary plunge segments produced ‘quasi-dwells’ of either 1 s or 3 s at the end of each weld program.

Examples of two weld programs are shown in Figure 3. This procedure resulted in 14 individual welding programs at each plunging rate for a total of 42 individual welding conditions. These 42 sets of conditions encompassed total welding times of 1.70 to 9.75 s.

The initial FSSW trials were conducted at ORNL on September 15-16, 2005, Figure 4. At that time only DP780 and the PCBN tools were available. Spot-welds were made using both the conventional tool and the shoulderless tool. Because the time for experimentation was limited, only selected parameter sets were used for the initial welds. Six parameter sets were chosen to produce plunge depths of either 2.3 or 2.9 mm and weld times of 1.70, 2.05, 3.90, 4.35, 6.25, and 9.75 s. Visual appearance of all welds was good. The PCBN tool did not appear to suffer any significant wear. Lap-joint specimens were scheduled for tension-shear testing and microstructure analysis.

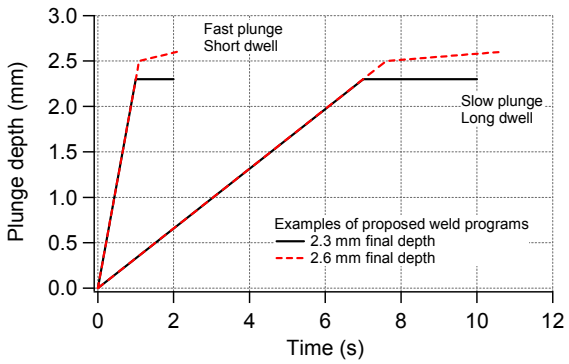


Figure 3. Illustration showing examples of conditions used for friction-stir spot-welding



Figure 4. Participants at initial welding trials held at ORNL. Tsung-Yu Pan (Ford) and Jim Quinn (GM) are seated at the controls for the friction-stir machine. Glenn Grant (PNNL), Russell Steel (MegaStir), and Min Kou (Mittal Steel) observe the proceedings.

Conclusions

Friction-stir spot-welds of acceptable appearance were made on a two-high stack-up of DP780 steel using polycrystalline boron nitride. Two tool geometries were used, that of a conventional pin tool and a shoulderless geometry. Tool wear appeared negligible.

Presentations/Publications/Patents

None

D. Long-Life Electrodes for Resistance Spot-Welding of Aluminum Sheet Alloys and Coated High-Strength Steel Sheet

Principal Investigator: Warren Peterson
Edison Welding Institute
1250 Arthur E. Adams Drive
Columbus, OH 43221-3585
(614) 688-5261; fax: (614) 688-5001; e-mail: warren_peterson@ewi.org

Project Manager: Eric Pakalnins
DaimlerChrysler Corporation
Materials Engineering- Welding
800 Chrysler Drive.
CIMS 482-00-15
Auburn Hills, MI 48326-2757
(248) 576-7454; fax: (248) 576-7490; e-mail: ep18@daimlerchrysler.com

Technology Area Development Manager: Joseph A. Carpenter
(202) 586-1022; fax: (202) 586-1600; e-mail: joseph.carpenter@ee.doe.gov
Field Technical Manager: Philip S. Sklad
(865) 574-5069; fax: (865) 576-4963; e-mail: skladps@ornl.gov

---

Contractor: U.S. Automotive Materials Partnership
Contract No.: FC26-02OR22910

Objective

- Survey the currently available technology for achieving long electrode life.
- Comparatively test a broad selection of existing and developmental electrode technologies that have technical merit.
- Investigate the electrode wear process through a combination of testing, metallography, and computer modeling.
- Evaluate a "best practice" electrode(s) through beta-site automotive production testing. The goal of these tests is to demonstrate the potential to double electrode life in a production environment through changes to electrode materials and/or geometry.

Approach

- Conduct benchmarking (Phase 1). A review of the open-literature, available corporate literature, and interviews of industry experts produced a state-of-the-art report on electrode wear. This phase has been completed.
- Conduct testing (Phase 2). Candidate electrode technologies were screened and in-depth testing of electrodes was performed to help define the mechanism(s) of electrode wear. "Best practice" electrodes for beta-site testing were produced as part of this phase. This phase is complete except for completion of the beta-site tests.
- Computer modeling (Phase 3). Computer models of the electrode metallurgical and mechanical changes that occur as a result of electrode wear were developed. These models helped to investigate the mechanism(s) of electrode wear and define the best-practice electrodes. This phase is complete.
- Beta-site testing of best-practice electrodes in a production environment. This phase of testing is currently in progress.

Accomplishments

Accomplishments that have been completed since the last reporting period:

- Produced "best-practice" electrodes for beta-site testing
- Completed laboratory verification testing of "best-practice" electrodes
- Completed beta-site testing at General Motors on hot-dip-galvanized (HDG) steel
- Initiated beta-site tests at the DaimlerChrysler Windsor assembly plant on galvannealed (GA) steel
- Developed procedures for establishing stepper procedures evaluating comparative stepper-based electrode testing in a production environment
- Established the production stepper schedule for the reduced-face-thickness B-cap M electrode material
- Proposed procedures for comparing "best-practice" electrodes for the DaimlerChrysler beta-site tests

Future Direction

- Complete beta-site tests on the best-practice electrodes at DaimlerChrysler Windsor Assembly Plant on galvannealed steels.
- Complete final report on project.

Introduction

Resistance spot-welding (RSW) has been heavily adopted by the automotive industry due to its relatively low capital and operating costs and the capacity to support high production rates. RSW is commonly used to weld high-strength steel and aluminum in vehicle construction. These materials are commonly selected to reduce vehicle weight and thus improve fuel economy and reduce greenhouse gas emissions. However, electrode wear of coated steels and aluminum continues to be a significant issue. Electrode wear adversely affects the cost and productivity of automotive assembly welding due to reduced weld quality, reliability, and robustness. This mandates increased inspection rates and greater control of welding parameters. Consequently, large potential cost savings and quality improvements are expected from substantial improvements in electrode life.

As technology has developed, few engineering solutions have been successfully introduced into the manufacturing process to manage electrode wear. Weld-current steppers and electrode-cap dressers have been used for many years, but these techniques do not resolve the underlying causes of electrode degradation. More recent efforts to remedy electrode wear have resulted in innovative electrode technologies such as new material compositions, material inserts at the electrode face, surface-coated electrodes, and nontraditional electrode geometries (P-, G- and S-nose). The scope of the present investigation is to objectively evaluate existing and developmental electrode material and geometry technologies to improve electrode life in production.

Review of Previous Work on AMD 302

The overall project organization is schematically illustrated in Figure 1. Prior work covered most of Phases 1 to 3. The current work activities cover the beta-site testing (Phase 2) of electrodes developed from Phases 1-3. The primary scope of work focused on the influence of electrode materials on the electrode life of both aluminum and high-strength galvanized steels. However, after completing several electrode life tests on aluminum using a number of electrode materials, no demonstrable plan based on electrode composition was clearly highlighted. Electrode wear in aluminum occurs through deposition of aluminum onto the face of the electrode. The factors that contributed to reduce sticking of the tip to the aluminum sheet during electrode retraction were opposite to those which improved weld-nugget stability. Additionally, this work showed that the solutions to electrode wear involved much more than just a study of alternate electrode materials. As a result, this part of the program was curtailed and additional efforts were focused on the electrode wear mechanism on steel.

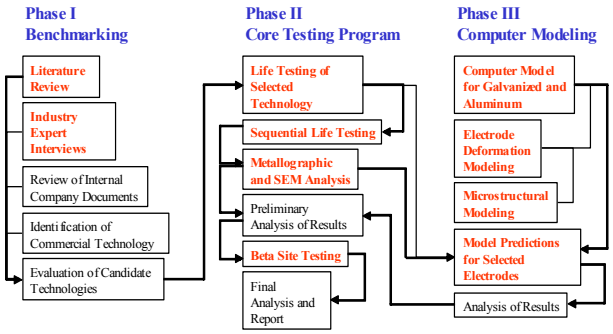


Figure 1. Schematic outline of workscope. Current activities include production of targeted electrodes and beta-site testing in Phase II. Work completed in previous phases include: Benchmarking, core testing, and computer modeling.

Achievement of the program objectives for galvanized steel required a fundamental understanding of how electrode wear occurs. In prior phases of this work, three key processes responsible for electrode wear in resistance-spot-welding (RSW) have been identified, namely, electrode face extrusion, gamma-brass deposition onto the steel sheet, and weld-nugget stability. These three processes have been integrated into a coherent mechanism in this program to describe the weld-nugget failures associated with electrode wear. In summary, the first two wear processes act to enlarge the contact area at the electrode face. This reduces current density and results in an inherent loss of weld-nugget stability in galvanized steels. This mechanism also describes the phenomena of pitting and electrode sticking that is associated with the metallurgical phenomena occurring during electrode wear.

The electrode-wear mechanism developed in this program was based on interpretation of standard electrode life and stepper tests performed on several common electrode geometries that were produced from standard and developmental electrode materials. Computer modeling of the two electrode-enlargement processes described above were developed to better understand significant aspects of the phenomenon such as edge extrusion rate, electrode surface temperature, and brass evolution. This was coupled with information from a detailed metallographic examination of the electrodes at several stages of electrode wear. The metallographic work identified the development, formation rate, and composition of brass alloys and parting layers on the face of the electrodes throughout electrode life. Altogether, this work formed the foundation of the electrode-wear mechanism that described spot-weld behavior during electrode life in galvanized steel.

Electrodes Studied in the Present Phase

The approach used to define the best-practice electrodes for beta-site testing is based on either reducing the electrode surface temperature or maintaining a high current density by promoting a protrusion or narrowed conduction path through the workpieces. These approaches are summarized below:

- **Low Face-Temperature Approach** (reduce rate of electrode face enlargement)
  - Internal fins and reduced face thickness
  - Conductive electrode material
  - Balance conductivity, electrical surface resistance, thermal conductance, and high-temperature strength

- **Sacrificial-Electrode Approach** (maintain current density by protrusion formation)
  - One-dimensional heat flow, face must be hot to maintain protrusion
  - Selective sticking, deformation, and chemical erosion occur sacrificially to maintain protrusion
  - Protrusion formation produces a high current density in the center of the electrode that promotes nugget stability

The latter approach uses either P-cap or G-cap sacrificial-electrode nose geometry with appropriate material to reduce electrode sticking and maintain the protrusion under high heat conditions.

The electrode materials and geometries defined for best practice electrodes are listed in Table 1.

Table 1. Beta-Site Test Electrodes

Material	Electrode Design	Beta Site Test Material	Approach
CuZr	E-cap w/internal fins	HDG	Low Temperature
CuZr	B-cap w/internal fins	GA, HDG	Low Temperature
M material	E-cap	GA, HDG	Low Temperature
M material	B-cap	GA, HDG	Low Temperature
M material	G-cap	GA, HDG	Sacrificial
Al_2O_3 ODS	P-cap	GA, HDG	Sacrificial

The electrode geometries used in the present phase are based on 16 mm-body-diameter with 4.8-mm-flat faces on the B-nose cap designs and 6-mm-flat faces on all other caps. All of the B-cap and E-cap electrodes used a 6- to 7-mm face thickness that increases heat flow to the cooling water channel. The P-cap or G-cap needs high surface temperatures on the electrode face to maintain the protrusion; therefore, no reduced face thickness (10 mm) was incorporated into these designs.

These electrode materials are standard alloys, except the M alloy. This alloy was identified from the previous phases of work. It characteristically produced good welds over a longer numbers of welds compared to the conventional CuZr alloy.

Laboratory Stepper Test Approach

Two sites were selected for beta-site testing, namely the GM Technical Center and DaimlerChrysler's Windsor Assembly plant. The welding parameters, materials, and procedures used in the simulative laboratory tests were replicated as closely as possible to the beta-site application. These tests were used to validate the best-practice electrodes and provide initial welding conditions for the beta-site tests. To better understand the conditions used in the laboratory tests, a description of the GM Technical Center and DaimlerChrysler beta-site tests is provided in the paragraphs that follow.

The GM beta-site tests used the GM WS 5A stepper test. GM performs this test as a standard procedure prior to introducing a new steel, electrode, etc. into production. They compare the stepper to a standardized stepper schedule to determine suitability for production. The same stepper test procedure was used on the prior and present laboratory tests at EWI. The GM test data will provide a separate investigation of electrode performance on the same materials used in previous phases of work. These tests will evaluate selected best-practice electrodes on a different welding machine, operating conditions, and technical staff. They will also use the GM test-termination criterion. The steel used for the GM beta tests will be taken from the 1.1-mm HDG 350 MPa steel remaining from the previous phases of work

The standard GM welding parameters for 1.1-mm 350 MPa HDG steel welded to itself are:

- Weld Time: 16 cycles
- Electrode Force: 670 lbf
- Hold Time: 2 cycles
- Min Button Size: 4.0 mm
- Weld rate: 30 wpm

The DaimlerChrysler beta-site tests are performed on a non-safety-critical part with easy equipment access and plant support. A stationary, rocking-arm AC welder is used in these trials with robotic part manipulation. The electrodes are normally replaced once per shift. Eleven welds are made per part at a welding rate about 30 wpm. This schedule produces about 3400 welds on the electrode at the time the electrodes are replaced.

The materials used for the laboratory tests were donated by DaimlerChrysler. This part welds 0.66-mm DQ galvannealed steel to 1.2-mm DQ GA steel. A weldable sealant is also used at the welding interface.

The standard welding parameters for the 0.66-mm/1.2-mm DQ GA steel application at DaimlerChrysler are:

- Weld Time: 14 cycles
- Electrode Force: 480 lbf
- Hold Time: 2 cycles
- Min Button Size: 3.0 mm

The welding parameters and steels used on both beta-site tests were incorporated in the laboratory tests on hot-dip-galvanized and galvannealed steels. Female electrodes are used at both beta-site tests locations; therefore, female caps were studied in the laboratory tests. However, all of the work performed in previous phases used male electrode designs. The laboratory work validated the targeted electrodes in a female cap design. The laboratory results were compared to the performance of similar electrode design and materials from previous phases of work on this project.

Additionally, both beta-site locations use weld current steppers. Consequently, only stepper testing was used in the laboratory evaluation of the best-

practice electrodes. The GM WS-5 stepper test procedure used in previous phases was again used. A summary of this test procedure is provided below:

- Ensure proper electrode installation in electrode holders
- Begin testing without electrode break-in
- Starting at a low current, increase current in 100 A increments until a minimum button size is established
- Add 500 A to the current required to establish minimum button size
- Weld 98 welds on large test panels to simulate electrode wear
- Make 1 peel test sample, peel test the 100th weld
- Check weld size
- If weld size is greater than minimum button size:
  - Continue at present current level for next electrode wear increment and perform peel test
  - Otherwise, increase current to get minimum button size, add 500 A, and repeat the electrode-wear and peel tests steps listed above

Continue to maintain minimum button size using this procedure until test termination

Examples of stepper test results from a previous phase of the program are shown in Figure 2.

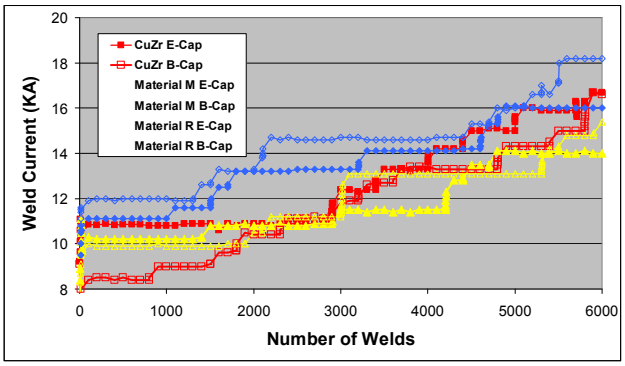


Figure 2. GM WS 5A stepper test results from developmental electrodes studied previously in Phase II. The M electrode is used in the beta-site tests in the current work.

Summary of Laboratory Stepper Test Results

The stepper test results for the electrodes tested in the laboratory in the present phase are summarized in Figure 3. The electrodes and weld schedules tested in the laboratory are summarized in Table 2 below.

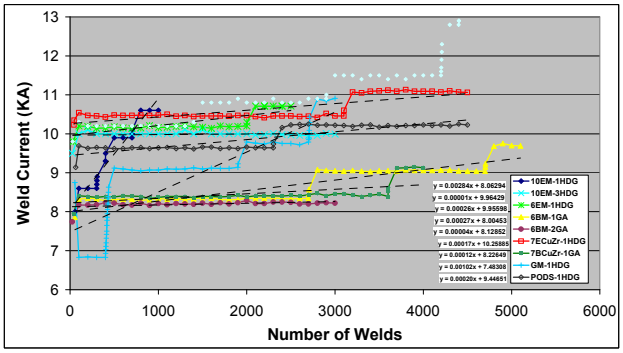


Figure 3. Comparison of limited laboratory tests performed on targeted electrodes in preparation for beta-site testing. The electrodes are listed in Table 2.

Table 2. Electrode designs, electrode materials, sheet materials, and weld schedules for the electrode studies in the laboratory phase of the beta-site testing.

Test	Face Thickness (mm)	Electrode Geometry	Electrode Material	Trial	Steel	Weld Time (cyc)	Electrode Force (lbf)
10EM-1HDG	10	E	M	1	HDG	16	950
10EM-2HDG	10	E	M	2	HDG	16	670
10EM-3HDG	10	E	M	3	HDG	16	670
6EM-1HDG	6	E	M	1	HDG	16	670
6BM-1GA	6	B	M	1	GA	14	480
6BM-2GA	6	B	M	2	GA	14	480
7ECuZr-1HDG	7	E	CuZr	1	HDG	16	670
7ECuZr-1GA	7	B	CuZr	1	GA	14	480
GM-1HDG	9	G	M	1	HDG	16	670
PODS-1HDG	10	P	ODS	1	HDG	12	670

Notes:
Test 1 (10EM-1HDG) was terminated due to use of welding machine with poor cooling. This test had unusually fast electrode wear – very limited analysis. All other trials used original welding machine from previous work.
Test 2 (10EM-2HDG) was terminated quickly due to lack of cooling water. No analysis
Test 6 (6BM-2GA) was performed with sealant.
Test 7 (7ECuZr-1HDG) used internally-finned electrodes
Test 8 (7BCuZr-1GA) used internally-finned electrodes
Test 10 (PODS-1HDG) was performed with a P-cap on top and a CuZr finned B-cap on bottom.

The galvannealed steels in these trials were always tested using the B-nose electrodes while the hot-dip-galvanized steels were always tested using E-nose electrodes. This was done to maximize the work

with the limited budget available for the laboratory testing in this phase.

The laboratory tests on the electrodes were limited to verifying the similar performance of the best-practice electrodes to the characteristics observed previously. This provided the least impact on the budget for this phase. After validating the electrodes in the laboratory, selected electrodes were released for beta-site testing at GM and DaimlerChrysler.

GM Technical Center Beta-Site Test Results

A summary of the beta-site weld trials performed at GM is provided in Figure 4. The maximum electrode face diameter criterion in GM WS 5A was used to terminate each of these tests. The face diameter measurements are made from carbon impressions taken every 500 welds. Testing was stopped when these measurements exceeded 10 mm. The test termination criterion ranked the performance of the standard GM cap (10-mm face thickness CuZr) first at 8000 welds; the 6-mm reduced-face-thickness M electrode second at 7500 welds; and both 7-mm reduced-face-thickness CuZr B-cap and E-cap electrodes, at third with 7000 welds.

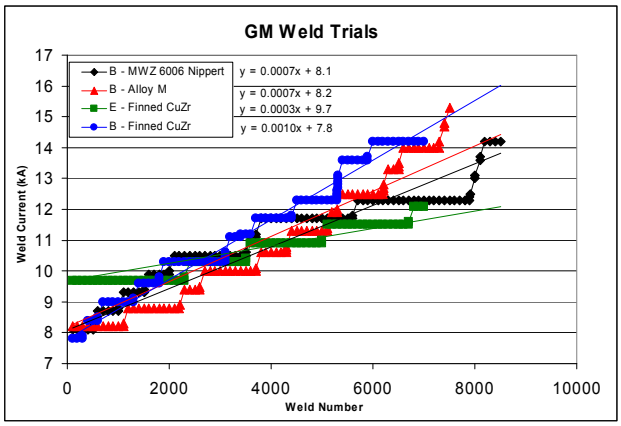


Figure 4. Summary plot showing GM beta-site current stepper test results on 1.1-mm HDG 350 MPa Steel.

Besides the maximum-face-diameter criterion, the maximum current, stepper slope, and other characteristics of the test are also important production considerations. The 7-mm reduced-face, internally-finned CuZr E-cap electrode had the least weld current at 7000 welds compared to the other electrodes and also had the lowest stepper current slope value. Conversely, the 7-mm reduced-face, internally-finned CuZr B-cap electrode had the largest maximum current at 7000 and the highest stepper slope of the beta-site electrodes. The average current and slope values for the GM standard electrode and the 6-mm reduced-face M electrodes were identical. Interestingly, only the standard GM cap did not have indications of boiling behind the cap, as evidenced by a white residue at the water jacket/electrode interface. This suggested that the reduced-face-thickness caps required better water cooling than provided in these trials. Additionally, the weld buttons were more stable for the GM standard CuZr B-cap and the finned CuZr E-cap in this beta-test compared to the other two electrodes. This is contrary to the laboratory testing performed previously, which showed that the M electrode maintained button size until the end of life.

DaimlerChrysler Windsor Assembly Plant Beta-Site Test Results

The stepper-based weld schedule at the DaimlerChrysler Windsor Assembly Plant specifies both a starting current and stepper slope.

Initial observations of the standard production processing of the beta-site test application showed that every weld was made at expulsion for at least the first 2500 welds.

The initial weld schedule was:

- Electrode force: 330 lbf
- Electrode geometry: B-cap with 4.8-mm flat; 16-mm body diameter
- Electrode composition: Composite electrode: Al_2O_3 ODS core with CuZr Body
- Weld time: 14 cycles
- Hold time: 2 cycles
- Initial Current: 9000 A
- Stepper Slope: 2A/weld for 1000 welds, 1.5A/weld for 1500 welds, 1A/weld for 1500 welds

This schedule met the maximum transformer current of approximately 15.5 kA after 1 shift.

Weld quality during the beta-site trials was primarily monitored through periodic component teardowns. Ultrasonic testing was available, but the equipment was out of service during many of the early weld

trials at the facility. Without a non-destructive test method, visual detection of expulsion was the method used to verify the presence of a weld between teardown testing. However, maintaining expulsion accelerates electrode wear and increases the stepper slope rate. Thus, with greater expulsion frequency, higher stepper slopes are expected, limiting the effective electrode stepper life. Alternately, lower current stepper slopes reduce the rate of electrode face enlargement, but endanger weld quality if the stepper slope is insufficient to maintain the minimum weld size. While undersized welds are acceptable in the laboratory to determine the need to increase weld current, they are unacceptable for assembly operations. Additionally, operating current values vary due to differences in materials, prior processing, and setup practice. Therefore, production weld currents must be maintained high enough to produce welds under most normal production conditions. These factors tend to increase the operating weld current level, promoting higher initial currents and stepper slopes.

Selection of the appropriate stepper slope also involves operating below the upper limit of the transformer and acknowledging the opportunities to exchange electrode sets. At the DaimlerChrysler site, the opportunities to change the electrodes for this part occurred during lunch breaks and shift changes. Historically, electrode changes had been made at each lunch break. The goal of the project is to double electrode life in production. However, doubling the electrode life in a 3-shift operation would result in changing the electrodes every other shift. In order to reduce confusion, Windsor personnel suggested changing the electrodes twice daily or every shift and a half. Alternately, the electrodes would have to be changed once per day.

The maximum stepper rates to achieve a 1½- and a 3-shift electrode change is 1.4 amp/weld and 0.7 amp/weld, respectively. This is based on 3400 welds per shift, three shifts (6 break points), and 7000 A maximum difference between initial current and upper limit of the transformer. The actual stepper current slopes would have to be at least less than these average values. Based on the initial trials, it was decided to work toward changing the electrode sets twice daily. This means that the electrodes should be capable of reaching 2 shifts during the weld setup testing. The 2-shift aim indicates that the average maximum stepper rate should be less than 1.0 amp/weld.

The stepper rate for the trials involving the 6-mm reduced-face-thickness B nose M electrodes were based on minimizing the average numbers of expulsions per part. A graphical summary of some of the setup trials performed on this electrode at DaimlerChrysler is shown in Figure 5. This plot shows a moving average of the number of expulsions that occurred out of 11 welds per part made on this application. This expulsion rate is plotted against the number of assemblies made during the trial. While the numbers varied, the traditional average number of assemblies made between electrode changes was approximately 310 assemblies.

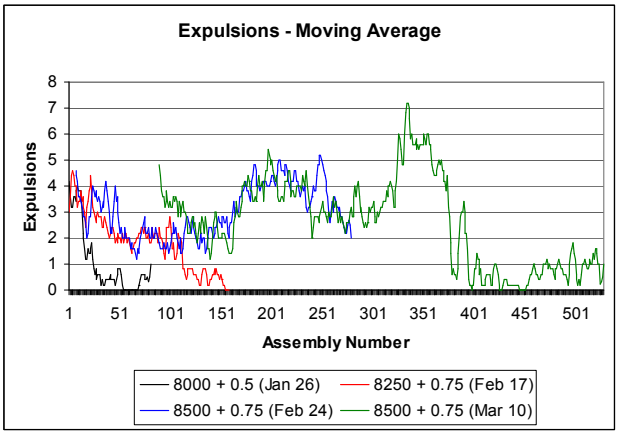


Figure 5. The average number of expulsions per part (11 welds maximum) plotted against the number of assemblies (parts) made for selected trials of the reduced-face-thickness B-cap M electrode during DaimlerChrysler beta-site testing. The individual weld trials show the stages of stepper schedule development. Legend shows the starting current and stepper rate. 11 welds are made per assembly. Approximately 310 assemblies are made each shift.

The first stage of stepper development during these trials was to reduce the initial operating current and stepper slope. A weld schedule suitable for producing welds over 1½ shifts (average 0.75 amp/weld) during the beta-site testing with the M electrode material was:

- Electrode force: 380 lbf

- Electrode geometry: B-cap with 4.8-mm flat face on 16-mm body diameter
- Electrode material: M electrode
- Weld time: 10 cycles
- Hold time: 2 cycles

The expulsion frequency for this stepper is shown in Figure 6. The expulsion frequency for the early part of the stepper was not monitored, but it exactly overlapped the pattern from the previous trials.

Different combinations of stepper slopes were trialed to extend these results through a full second shift. The stepper rate was divided into three portions:

- 0.65 amp/weld for 2500 welds
- 0.76 amp/weld for 2500 welds
- 0.85 amp/weld for 2500 welds

This stepper schedule better maintained the appropriate current density as the electrode face size increased. An example of a weld trial using this stepper schedule is shown in Figure 7. Welding in this trial extended to approximately 2 shifts. Again, the first part of the trial was not monitored, but the average numbers of expulsions in the latter stages of wear was relatively low and weld quality was maintained as verified in teardown tests.

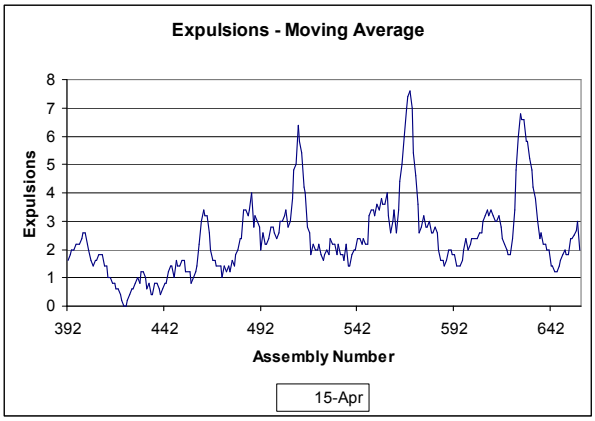


Figure 6. The average number of expulsions per part (11 welds maximum) plotted against the number of assemblies (parts) using reduced-face-thickness B-cap M electrodes during DaimlerChrysler beta-site testing. This trial extended weld quality to 1½ shifts using a three-stage linear stepper schedule. 11 welds per assembly. Approximately 310 assemblies are made each shift.

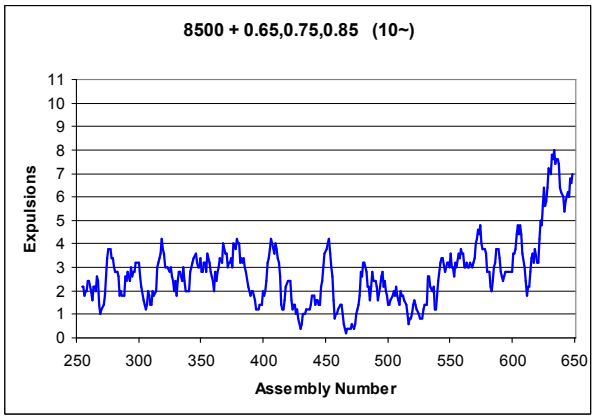


Figure 7. The average number of expulsions per part (11 welds maximum) plotted against the number of assemblies (parts) using reduced-face-thickness B-cap M electrodes during DaimlerChrysler beta-site testing. This trial extended weld quality to 2 shifts using a three-stage linear stepper schedule. 11 welds per assembly. Approximately 310 assemblies are made each shift.

The next stage in the program is to test the reduced-face-thickness B-cap M electrodes in an extended production trial with 2 electrode changes per day over several days of production (at least 12 contiguous shifts).

In an effort to expedite the completion of this work, the work plan to compare the performance of the different best practice electrodes will be based on the minimum stepper rates determined for the M electrode. After adjusting the starting current, weld quality and expulsion frequency will be monitored for a trial up to 2 shifts. If the electrode passes, then a 12-shift weld trial will commence.

Comparison of electrode performance for the alternate electrodes listed in Table 1 (and the current production electrode) will be based on the ability to follow the stepper slope developed for the reduced-face-thickness B-cap M electrode. Experience has shown that if the electrode performance is better than that of the M electrode, then the number of expulsions per part will increase. Conversely, if the performance is worse, then the number of expulsions per part will decrease. A number of other comparisons are also proposed to distinguish between electrodes that can achieve 2 production shifts.

Conclusions

The work performed to date in this phase of the project has shown that the stepper performance of the "best-practice" varieties of electrodes identified in the earlier phases of the program have performed reasonably well in the beta-site tests. Significant results include:

1. Male electrodes appear to provide slightly better stepper-based electrode life compared to female electrode designs.
2. The stepper slope for galvannealed steel is much lower and more repeatable than the slopes produced on hot-dip-galvanized steel.
3. The "best-practice" electrodes developed from the previous phases of this work which incorporate reduced face thickness may be machine- and application- dependent. Specifically, these electrodes may be strongly affected by the lack of cooling water.
4. Stepper slope should increase with increasing numbers of welds to better maintain current density as the cap face increases in size.
5. A plan has been developed to generate stepper schedules in production and efficiently compare different electrodes under production conditions.

Presentations/Publications/Patents

2004. Peterson, W.A., Gould, J.E., Bowers, R., Santella, M., Babu, S. "Evaluation of Electrode Design and Materials for Improving Electrode Life," Sheet Metal Welding Conference XI, Paper 1-6. Sterling Heights, MI (May 11-14). AWS - Detroit Section.

2004. Gallagher, Athwal, K.S.B., Bowers, R., "Evaluation Wear Characterization in Resistance Spot Welding," Sheet Metal Welding Conference XI, Paper 1-5. Sterling Heights, MI (May 11-14). AWS - Detroit Section.

2004. Babu, S., Santella, M., Peterson, W.A., "Modeling of Resistance Spot Welding Electrode Life," Sheet Metal Welding Conference XI, Paper 7-2. Sterling Heights, MI (May 11-14). AWS - Detroit Section.

Acknowledgements

The author would like to acknowledge the members of the AMD 302 project team for their hard work in successfully completing the work to date: Mike Santella and Suresh Babu of the Oak Ridge National Laboratory; Randy Bowers and Jeremy Caron of the University of Windsor; Jerry Gould of the Edison Welding Institute; Eric Pakalnins of DaimlerChrysler; Mike Karagoulis and Peter Sun of General Motors; Arnon Wexler of Ford Motor Company; Brian Swank and Paul Ruess of Outokompu-Nippert; David Fleckenstein of CMW; Bill Brafford and Chuck Pfister of Tuffaloy; Nigel Scotchmer of Huys Industries; and Tom Natale of AK Steel.

The continuing support of our respective companies and the U.S. DOE is gratefully acknowledged.

6. NON-DESTRUCTIVE EVALUATION

A. NDE Tools for the Evaluation of Laser-Welded Metals

Principal Investigator: William Charron
Ford Motor Company
17000 Oakwood
Room B154
Allan Park, MI 48101
(313) 390-3792; fax: (313) 594-1898; e-mail: wcharron@ford.com

Project Administrator: Constance J. S. Philips
National Center for Manufacturing Sciences
3025 Boardwalk
Ann Arbor, MI 48108-3266
(734) 995-7051; fax: (734) 995-1150; e-mail: conniep@ncms.org

Technology Area Development Manager: Joseph A. Carpenter
(202) 586-1022; fax: (202) 586-1600; e-mail: joseph.carpenter@ee.doe.gov
Field Technical Manager: Philip S. Sklad
(865) 574-5069; fax: (865) 576-4963; e-mail: skladps@ornl.gov

---

Contractor: U.S. Automotive Materials Partnership
Contract No.: FC26-02OR22910

This project was completed in FY 2005. A FY 2005 annual report was not submitted, but the final report has been done and is available in USCAR offices (www.uscar.org).

B. NDE Inspection of Resistance Spot-Welds in Automotive Structures Using an Ultrasonic Phased Array

Principal Investigator: Deborah Hopkins, Ph.D.
Lawrence Berkeley National Laboratory
1 Cyclotron Road, MS 46A-1123, Berkeley, CA 94720
(510) 486-4922; fax: (510) 486-4711; e-mail: dlhopkins@lbl.gov

Technology Area Development Manager: Joseph Carpenter
(202) 586-1022; fax: (202) 586-1600; e-mail: joseph.carpenter@ee.doe.gov
Field Technical Manager: Philip S. Sklad
(865) 574-5069; fax: (865) 576-4963; e-mail: skladps@ornl.gov

Participants:
U.S. Automotive Materials Partnership Ultrasonic Phased-Array System for RSW Inspection Project (AMD409) Team
Frédéric Reverdy, Ph.D., Lawrence Berkeley National Laboratory
Daniel Türler, M.S., Lawrence Berkeley National Laboratory
William B. Davis, M.S., Lawrence Berkeley National Laboratory
William Charron, Ford Motor Company
George Harmon, DaimlerChrysler Corporation
Cameron Dasch, General Motors Corporation

Contractor: Lawrence Berkeley National Laboratory
Contract No.: DE-AC03-765F0095

Objective

- Develop a cost-effective ultrasonic phased-array system that is sufficiently fast, accurate, and robust in manufacturing environments to be suitable for inspection of spot welds in automotive structures.

Approach

- Develop a spot-weld inspection system that can be used by operators with minimal training by using state-of-the-art ultrasonic phased-array technology. The multi-element probe allows the ultrasonic energy to be focused at the interface between the welded sheets and electronically scanned through the weld.
- Design and fabricate a miniature mechanical scanner that will allow scanning in the direction perpendicular to the electronic scan to produce two-dimensional images of the weld. The portable system allows more than 3000 signals to be acquired in less than 4 seconds.
- Develop signal-processing and image-analysis software to distinguish satisfactory, undersized, and defective welds and provide dimensional analysis of the weld in a few seconds.
- Minimize the footprint of the probe assembly to ensure access to welds on complex components.
- Design and fabricate a probe housing that meets the size constraints while allowing mechanical scanning over a travel distance of 14+ mm. The housing must also maintain the probe in water and include an outer membrane that confines the water column and provides acoustic coupling to the part under inspection.
- Conduct trials on individual samples made under controlled conditions and on production parts to determine the resolution, repeatability, and accuracy of the prototype system.
- Conduct plant trials to demonstrate the system's ability to characterize welds with sufficient accuracy and repeatability in practice and to demonstrate that the integrated probe housing can be used successfully in a production environment by a skilled and trained operator.

Accomplishments

- Evaluated the performance and limitations of existing ultrasonic phased-array systems.
- Conducted a series of laboratory experiments to evaluate the performance of 5-, 10-, and 17-MHz phased-array probes for characterization of spot-welds in galvanized steel.
- Developed signal-processing algorithms to distinguish between satisfactory, undersized, and defective welds.
- Developed image-processing algorithms that allow three-dimensional analysis of welds.
- Demonstrated the ability to acquire more than 3000 signals per weld and analyze the resulting data in a few seconds to render an estimate of weld quality.
- Developed a difference-equation model that enables simulation as well as signal processing to recover reflectivity estimates, and to detect poor coupling and malfunctioning probe elements. Pre-processing algorithms are used to measure changes in thickness and to detect misalignment of the probe.
- Demonstrated good correlation between ultrasonic measurements, measurements of weld buttons on peeled samples, and metallographic images of cross-sections through welds.
- Designed and fabricated a probe housing that maintains the probe in water, contains a miniature mechanical system that allows linear translation of the probe, and provides an outer membrane that confines the water column while also providing acoustic coupling to the part under inspection. Identified and tested coupling materials that allow satisfactory signals to be obtained outside of a water tank.

Future Direction

- Conduct laboratory experiments on samples prepared under carefully controlled conditions, make measurements on production parts, and conduct plant trials to demonstrate the ability of phased-array systems to inspect spot welds with sufficient accuracy and repeatability for the full range of materials and joint configurations used in production.
- Conduct laboratory experiments to determine the concept feasibility of using ultrasonic phased arrays to inspect welds in aluminum and advanced high-strength steels (AHSS).
- Develop automated classifiers to determine weld dimensions and identify defective welds including cold welds.
- Develop a user interface in conjunction with end users to ensure ease of use and reporting of data in the most useful format for inspectors, welding engineers, and plant managers.
- Develop a fully integrated prototype system suitable for deployment and testing in a manufacturing plant.
- Perform large-scale testing and measurement system analysis.

Introduction

Development of nondestructive evaluation (NDE) techniques is an enabling technology for greater use of lightweight materials in the automotive industry where NDE methods to assure product quality are essential for industry and consumer acceptance of new materials and manufacturing methods. Recent studies have demonstrated cost savings associated with implementing NDE that derive from finding defects early in the production process and reducing waste compared to destructive testing. One of the critical technical challenges in introducing lightweight materials is developing joining technologies and inspection strategies suitable for mass production. At present, the most common methods for inspecting spot-welds in automotive manufacturing are pry checks and physical teardown, during which spot-welded joints are pried apart and the resulting weld buttons are visually inspected or measured with calipers. Although these methods have been used successfully for decades, destructive weld testing has several drawbacks including high costs associated with scrapped material, ergonomic injuries, and the time-lag between the onset and identification of problems. In addition, pry tests and teardowns do not allow plant managers and engineers to easily collect inspection data that would allow them to identify trends and potential problems. Furthermore, these inspection techniques are not viable options for lightweight and

high-strength materials. Composite structures with adhesive-bonded joints cannot be pry checked and aluminum is relatively expensive and more difficult to rework than steel, making pry checks and teardown cost prohibitive. Welds in high-strength steel are often too strong to be pry-checked or torn down and satisfactory welds sometimes fail interfacially rather than by pulling a weld button, making it difficult for inspectors to distinguish between satisfactory and defective welds.

Advances in sensors, computing, communication, and engineering technologies have all played a role in advancing the development of NDE methods with promising automotive applications. For example, ultrasonic phased-array systems have been available since the mid-1970s, but they were prohibitively expensive. In the past decade, prices have dropped dramatically, and increased competition promises additional price reductions in the future. A recent breakthrough is the availability of portable systems that are particularly attractive for use in production environments.

Lawrence Berkely National Laboratory (LBNL) previously evaluated the adequacy of conventional, commercially-available ultrasonic systems for the inspection of spot-welds. These systems are relatively inexpensive and are widely used in European automotive plants, but have not gained widespread acceptance in the United States for reasons that include their dependence on trained operators to set system variables and the need to change probes frequently because of the wide range of materials and sheet thicknesses used in production vehicles. An important goal of the current project is to develop a system that is easier to use. Plant managers also emphasize the need for intuitive user interfaces and summary reports that can be customized for welding engineers and other plant personnel.

To best advance the adoption of lightweight materials while also serving the needs of the auto industry, the current project team has adopted a strategy that strives to develop platforms that add value immediately, minimize barriers to incorporating emerging technologies at a later date, and that are as modular as possible so that they can be easily modified or adapted for new applications. Consistent with that model, the current work is focused on development of a prototype spot-weld inspection platform that integrates the best available ultrasonic phased-array technology with custom-designed signal processing and analysis software, and hardware that will allow the system to be tested and implemented in manufacturing plants as a portable, stand-alone unit.

Ultrasonic Phased-Array Technology

Most commercially-available spot-weld inspection systems use conventional high-frequency, single-crystal ultrasonic probes working in pulse-echo mode. The output from these mono-probes is a single signal that is an integrated response over an area that depends on the diameter of the probe. Different probes must be used for different-sized welds. In contrast, a phased array is composed of many piezoelectric elements that are individually excited by electronic pulses at programmed delay times. As a result, phased arrays have several advantages over conventional ultrasonic probes that derive from the ability to dynamically control the acoustic beam transmitted into the structure under examination. An electronic delay can be applied separately to each electronic channel when emitting and receiving the signal. These delay laws permit constructive and destructive interference of the acoustic wavefront transmitted into the structure, allowing predefined ultrasonic beams to be formed. The acoustic energy can be focused, and delay laws can be used to steer the acoustic beam. Electronic scanning is accomplished by firing successive groups of elements in the array.

Instead of assessing weld quality based on a single signal, as is the case with mono-probes, phased arrays allow thousands of signals to be obtained for individual welds in a few seconds. The ability to perform complex scanning of the acoustic beam through the weld allows greater accuracy in sizing weld nuggets, while also improving the flaw characterization capability. These attributes of phased-array probes allow us to measure the weld-nugget diameter, locate defects, and identify misshapen and burnt welds. In addition, the same probe can be used to inspect different-sized welds and welds in sheets with different thicknesses. It is also possible to electronically compensate for misalignment of the probe with respect to the sample.

To demonstrate concept feasibility, initial experiments were conducted in a water tank or using a confined water column with coupling gel between the probe and the sample. As described below, to allow measurements to be made in a production environment, a self-contained probe housing has been designed and fabricated that maintains the probe in water while also providing acoustic coupling to the part under inspection.

Probe Housing

Although the phased-array probe allows electronic scanning in one direction, mechanical scanning in the perpendicular direction is required to obtain two-dimensional images of the weld. Thus, a plant-deployable unit requires a housing for the ultrasonic probe that maintains the probe in water and contains a miniature mechanical system for linear translation of the probe. The mechanical system designed and encapsulated into the probe housing allows the probe to travel a distance of 14.7 mm. A mechanical drawing of the scanning system is shown in Figure 1a. The small motor used to drive the system has a nominal speed of 4800 RPM and is coupled to a 1:16 gearbox. The drive assembly is separated from the water column containing the probe by two slider plates and O-rings that form a watertight seal. A picture of the integrated probe housing is also displayed in Figure 1b, where the probe assembly is shown on a production part, and in Figure 1c, where the bottom of the housing is visible. The bottom plate was designed with a circular lip to help the outer membrane conform to the surface indentations caused by the welding electrodes.

One of the engineering challenges in designing the housing is minimizing the footprint of the probe assembly, which is essential to ensure access to welds on complex components. The overall footprint of the first prototype, shown in Figures 1b and 1c, is 26 by 44 mm. This design works well on relatively flat components where there is easy access to the welds. In the next several iterations of the probe design, also shown in Figure 1, the bottom section of the housing was tapered to allow improved access to welds on production parts. As shown in Figure 1d, the bottom half of the housing in the latest designs is a cylinder. The probe housing pictured has a circular footprint with a diameter of approximately 2 cm.

Several different designs of the end cap on the probe housing have also been tried, with two objectives: maximizing the ease of changing the membrane that confines the water column, and determining which design provides the best coupling between the membrane and the parts under inspection. Figure 1e shows the end of the probe assembly after being filled with water, and Figure 1d shows one of the membranes used and the bulge in the membrane induced to provide good coupling to welds with deep surface indentations. Experiments are ongoing to determine the best design for inducing and maintaining the bulge in the membrane.

The optimal material for the outer membrane is also under investigation. The material must provide acoustic coupling to the part, which requires that it conform exactly to the surface. Since many welds on production parts are associated with deep surface indentations caused by the welding electrodes, the membrane must be highly pliable, while also being durable enough to withstand thousands of measurements made on rough surfaces with deep indentations. Another important consideration in choosing a material is that it be relatively inexpensive and available off the shelf. Toward that end, experiments have been performed with readily-available materials including finger cots and latex products.

With regard to its acoustic properties, the ideal membrane has an acoustic impedance very close to that of water, and does not attenuate the acoustic signals. Any impedance mismatch between water and the membrane will result in reflection of some of the acoustic energy at the membrane, reducing the energy transmitted into the part, and making it more difficult to analyze the acoustic signals. A recent series of experiments were performed using a newly-available elastomer material specifically designed for ultrasonic inspection. The advantage of Aqualene™ is that it has an acoustic impedance very close to that of water and a very low attenuation coefficient. Initial experiments indicate that the material is also very durable.

Aqualene™ is available in a variety of thicknesses and experiments were conducted to determine the optimal thickness for spot-weld inspection. The

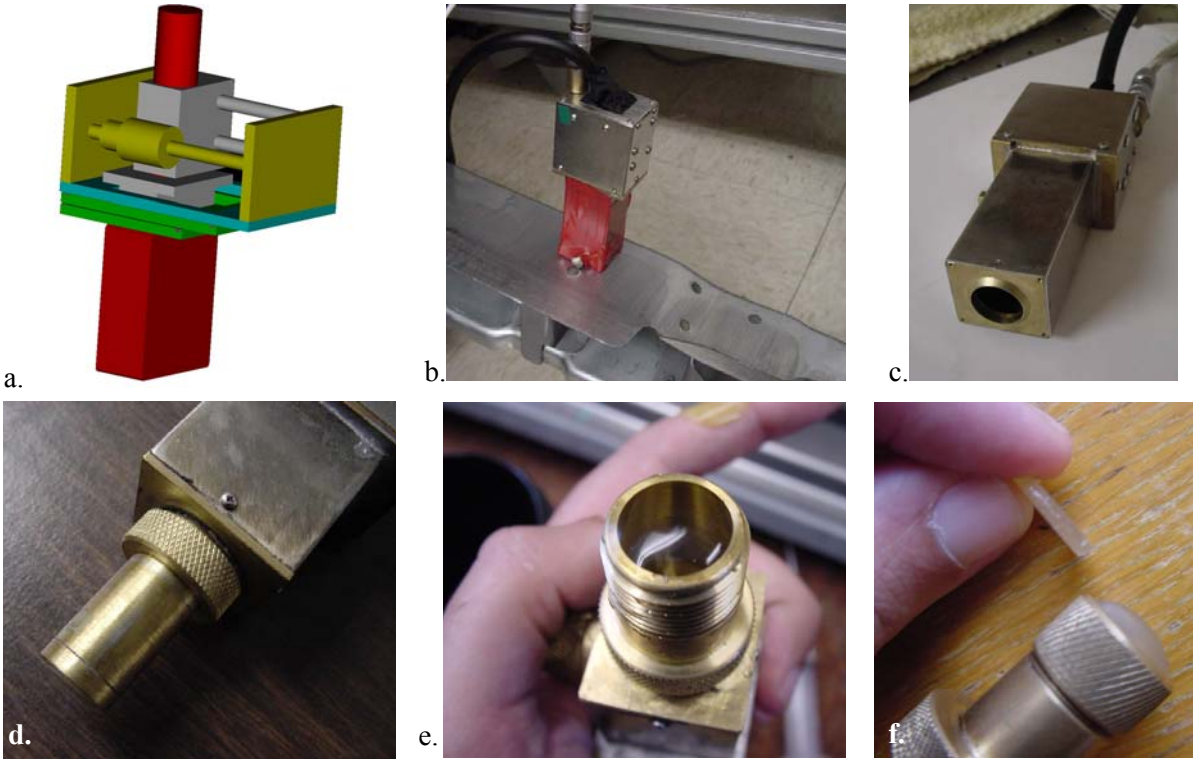


Figure 1. Mechanical drawing of the miniature scanning system (Figure 1a) encapsulated into the prototype probe housing (Figure 1b). The bottom plate of the prototype in Figure 1c has a circular lip to improve coupling between the housing and parts under inspection. In later prototypes, the lower section of the housing was redesigned to be much smaller, for better accessibility to welds on production parts (Figure 1d). After filling the housing with water (Figure 1e), an endcap containing a thin membrane is placed over the tip of the housing assembly (Figure 1f). A bulge is induced in the membrane to improve coupling to parts with deep surface indentations.

tradeoff is between durability and acoustic coupling: the thicker the material, the more durable it is, but the more difficult it is to get good coupling with the part. To evaluate the acoustic coupling, signals obtained using Aqualene™ were compared to signals obtained for the same welds inspected in a water tank. For measurements in the water tank, the outer membrane is removed from the probe assembly, and the sample and probe are submerged. These experiments demonstrated that acceptable results are achieved using an Aqualene™ membrane. Acceptable results are also obtained using finger cots and other off-the-shelf acoustic membranes, which have the advantage of being thinner than the thinnest Aqualene™ currently available (0.5 mm). For welds on production parts with deep surface indentations, membranes thinner than 0.5 mm have been necessary to achieve good coupling with the part. Tradeoffs between price, durability, and coupling will determine the best membrane option for any particular application.

Phased-Array Inspection Strategy

For all experiments performed to date, electronic scanning and focusing laws were combined to inspect the spot welds. The acoustic energy is focused at the interface between the two sheets by applying symmetrical delay laws to the elements of the phased-array probe (see Figure 2). The results presented here were obtained using a new, 17-MHz focused probe. In contrast to the probes used for initial experiments that had flat elements, the 17-MHz probe has curved elements that focus the energy with a natural focal length of 37 mm. When used in conjunction with the delay laws described above that focus the energy from multiple elements, the acoustic beam at the interface between the welded sheets is a circular spot that is scanned across the weld. Using a portable phased-array controller, more than 3000 signals are recorded for each weld in approximately 5 seconds.

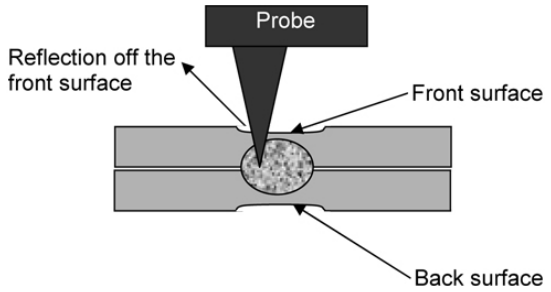


Figure 2. Schematic drawing illustrating focusing of the ultrasonic energy from several phased-array elements at the interface between two spot-welded sheets.

As part of the work underway, experiments are being performed to determine the optimal number of elements to use in the probe. The advantage of using more elements is that more energy is transmitted into the part, and a larger area can be imaged. Disadvantages of using more elements are increased cost; increasing the width of the acoustic beam making it more susceptible to diffraction caused by the indentation at the surface made by the welding electrodes; and requiring the probe housing to be larger to accommodate the larger probe and the wider acoustic beam.

Scanning in one direction is performed by electronically translating the ultrasonic beam across the sample by firing a specified number of elements in sequence. For example, when eight elements are used at a time, the beam is electronically scanned across the weld in steps of one element; that is, elements one through eight are excited to generate the first signal, elements two through nine are excited to generate the second signal, and so forth. To obtain two-dimensional (2-D) images of the weld, the probe is mechanically translated across the weld in the direction perpendicular to the electronic scan.

As described above and illustrated in Figure 2, the acoustic energy generated by several adjacent elements in the probe is focused and transmitted into the test specimen. Some of the energy is reflected off the front surface as indicated in the diagram. In the welded region, the signals pass through both sheets and are reflected off the back surface of the lower sheet. It is interesting to note that the metallurgical changes in the welded area do not cause a change in acoustic impedance large enough to create a noticeable reflection at the boundary of the weld nugget. Outside the welded region, the signals are confined to the top sheet, that is, the acoustic waves are reflected back and forth in the upper sheet and no energy is transferred into the lower sheet.

Signal Processing

The signals recorded while scanning through the weld are currently analyzed in the frequency and time domains with the goal of developing fast and accurate algorithms that work for the wide range of welds found on production parts. For a satisfactory weld, ultrasonic waves are transmitted through the weld nugget and reflected off the back surface of the lower sheet (see Figure 2). In contrast, for a defective weld, incomplete fusion at the interface between the two sheets results in partial reflection of the ultrasonic energy at the interface. This affects the periodicity of the train of echoes, that is, signals that are reflected at the interface have a shorter travel path than signals that propagate through the weld, resulting in echoes in the time domain that are closer together than echoes off the back surface.

Fourier peak ratio and image processing

In the frequency domain, the power spectrum captures the periodicity of the ultrasonic echoes. The relative magnitude of the peaks in the spectra is indicative of the amount of energy reflected at the interface between the welded sheets. For a satisfactory weld, the ultrasonic wave propagates through the weld and reflects back and forth between the front and back surfaces resulting in a peak that corresponds to the travel path through both sheets. For defective welds, where most of the energy is reflected at the interface between the two sheets, there is a peak in the spectrum that corresponds to a travel path equal to twice the thickness of the upper sheet. For each of the 3000 signals that comprise each weld image, the ratio of the peaks in the power spectrum is calculated and then compared to a threshold that is used to create binary images.

The peak-ratio images allow satisfactory and undersized welds to be distinguished according to the size of the area where there is significant transmission of energy into the lower sheet. Although defective welds such as cold welds can

result in a large area of ultrasonic transmission into the second sheet, the Fourier peak ratio indicates that the areas of high transmission are relatively sparse and dispersed compared to the well-defined and concentrated areas for the satisfactory and undersized welds. At present, the quality of the weld is assumed to be associated with the largest contiguous area of transmission. As described below, image-processing techniques are used to identify this area and separate it from the smaller transmission zones. These techniques were developed last year [2], and are only briefly described here.

The first step in processing the peak-ratio images is to extract the largest group of contiguous pixels with high ultrasonic transmission across the interface between sheets, which we assume corresponds to the welded zone. The algorithm used to determine whether individual pixels should be considered connected to or separate from the zone of interest is based on the operation of connected-component extraction. We then apply morphological filters that are commonly used for image processing. The operations applied to the binary peak-ratio images are erosion and dilation, which are used to smooth the boundary of the image and to remove small, isolated holes in the image that result from small defects or a poor signal-to-noise ratio. A processed image is shown in Figure 6c.

As discussed previously, during physical teardown of automotive components, spot-welded joints are pried apart and the resulting weld buttons are visually inspected or measured with calipers. To allow the results of the acoustic measurements to be compared to the size of the weld buttons, it is necessary to estimate weld dimensions from the peak-ratio images. Once the largest contiguous area of high acoustic transmission is identified and extracted, either an ellipse is fit to the area or the total area is calculated as a means of estimating the size of the weld button.

Surface Indentation Measurements

A recent addition to the signal processing software is an algorithm to measure and display the surface indentation caused by the welding electrode for the inspection surface. For our purposes, knowing the depth and location of the top-surface indentation is advantageous for signal processing, and is also important in analyzing the quality of the weld. The criteria used in the automotive industry for assessing weld quality includes specifications for allowable indentation and loss of material. For signal processing, the location of the indentation is being used to locate the weld within the scan region. The estimated location of the weld is used to reduce the number of signals that are processed and analyzed, thus minimizing the total inspection time. As described above, the indentation data are also being analyzed to provide information on weld quality. Excessive indentation and loss of material are indicative of a burnt weld. Although the relationship does not always hold, the depth of the indentation and the size of the weld nugget are often related; thus, the indentation depth may be of some value as a secondary criterion in evaluating quality for those welds that prove difficult to analyze. In addition to indentation depth and size, it is also possible to determine the shape and gradient of the indentation, which provides useful information on the state of the electrodes and may indicate problems in the fit between parts.

Weld Reflectivity

In addition to the signal processing based on Fourier peak ratios, a difference-equation model has been developed that describes the amplitude of the ultrasonic echoes in the time domain as a function of the *reflectivity* of the weld. At each measurement point, the reflectivity measures the share of acoustic energy incident on the interface between the sheets that is reflected. To create images of the welds, the signal obtained at each location during scanning is reduced to a single bounded value (reflectivity), and these values are plotted to create a reflectivity map of the weld. Figure 3 shows reflectivity maps for an undersized, a satisfactory, and a burnt weld.

The peak-ratio method and difference-equation models have different advantages and disadvantages, making it valuable to have two approaches to signal processing. For example, the peak-ratio method is very fast, whereas the difference-equation model enables simulations. Features of the reflectivity model also include the ability to detect and correct for weak signals. Even in a laboratory setting, some weak signals are almost always unavoidably present because the edge of the surface indentation tends to

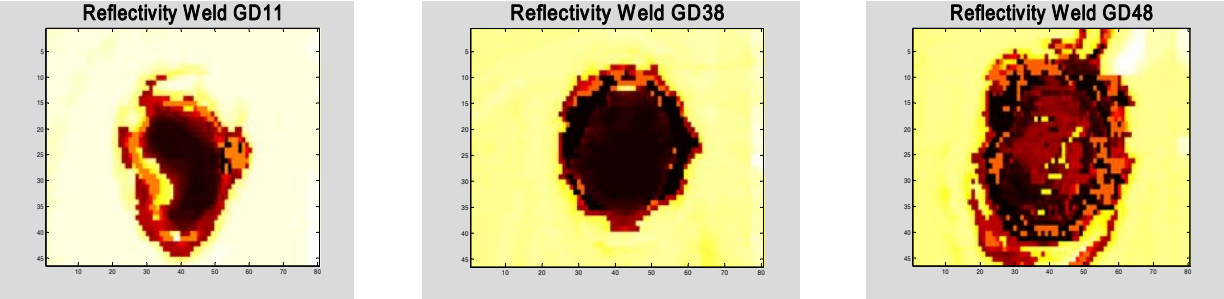


Figure 3. Reflectivity maps obtained for an undersized, a satisfactory and a burnt weld, respectively (left to right). The darkest regions correspond to high transmission of acoustic energy across the interface between sheets, indicative of fusion.

"scatter" the ultrasonic signals. Weak signals may also be present because of poor coupling or because of malfunction of one or more elements in the probe. The software identifies and, as far as possible, corrects for these cases as well.

Metallography

In previous work, metallographic methods were employed to help understand the relationships between ultrasonic signals, the size of the weld nugget, and the dimension of the weld button obtained by peeling the joint. While there is generally a relationship between the size of the weld button obtained from peel tests and the size of the actual weld nugget determined from metallograhy, their dimensions are not exactly the same.

To better understand changes in structure in the welded zone and how these changes are manifested in the ultrasonic signals, as well as to validate LBNL's signal-processing algorithms, a new study was undertaken in collaboration with the Ford Motor Company [3]. For the initial study, Ford created spot-welded test specimens using two sheets of 1.4-mm-thick hot-dipped-galvanized steel. Welds of varying quality were created by varying the number of cycles during welding, while keeping the force and current constant. After LBNL made ultrasonic images of the welds, Ford analyzed a series of vertical cross-sections through each weld. This painstaking process consisted of carefully cutting the weld and the surrounding area out of the test coupons and mounting it in epoxy, and then grinding down the specimen to expose cross sections every few hundred microns through the weld perpendicular to the plane of the interface. Care was taken to ensure that the cross-sections were parallel to one another and to accurately measure the location of each section.

As described above, the samples were created from hot-dipped-galvanized steel, meaning that the surfaces of the sheet metal are coated with a thin layer of zinc. During welding, much of the zinc coating melts and is expelled out of the welded zone. The expelled zinc can form a brazed corona around the weld, and one of the objectives of the study was to determine whether the ultrasonic signals could distinguish between this weak brazed zone and the fused area. To answer this question, the cross sections were polished with a 1-µm grit polish, and optical micrographs of the polished surface were digitally recorded. A metallurgical technique was used to identify and map the location of zinc. The polished surfaces were then treated with a metallographic etch that removed the zinc and revealed the steel grain structure. Optical micrographs of the etched surfaces were carefully studied to identify the fused area at the interface between the two sheets.

Figure 4a shows a cross-section from an undersized weld after etching (Figure 4a). The individual cross-sections were combined to create two-dimensional maps of the welds, as illustrated in Figure 4b, where three zones are identified. The central region marked with heavy dark lines indicates the zone of fully-fused steel. Outside of this area, thin and thick gray lines indicate the regions where zinc is present. Figure 4c shows the estimated weld nugget from the ultrasonic Fourier peak-ratio map superposed on the metallurgical map, showing good agreement between the estimated weld nugget and the fused zone identified in the micrograph.

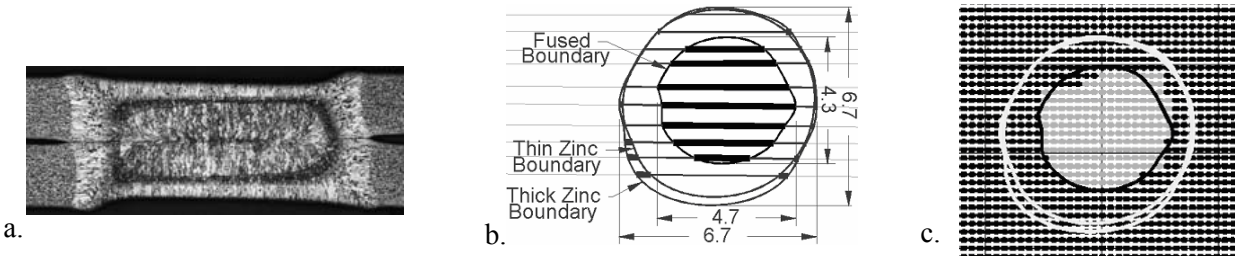


Figure 4. A micrograph of a polished and etched cross section through an undersized weld is shown in Figure 4a. The metallurgical map determined from the micrograph is shown in Figure 4b. The estimated weld nugget from the Fourier peak-ratio map is superposed on the metallurgical map in Figure 4c, showing good correspondence between the estimated weld area and the size determined from the metallurgical analysis. Figures 4b and 4c are reprinted with permission from T. Potter, B. Ghaffari, G. Mozurkewich, F. Reverdy and D. Hopkins, "Comparison of Metallurgical and Ultrasonic Inspections of Galvanized Steel Resistance Spot Welds," *32nd Annual Review of Progress in Quantitative Nondestructive Evaluation*, Copyright 2005, American Institute of Physics.

Although this initial study was promising in that LBNL's signal post processing resulted in images that correlated well with the weld nuggets, the sample size was very small and a larger and more fundamental study was required to establish a physical basis for choosing signal-processing parameters. Toward this end, more than 120 weld coupons were created by Ford, with a range of weld qualities from satisfactory to undersized, cold, and burnt. After LBNL made ultrasonic measurements of the welds using the prototype integrated probe shown in Figure 1b, Ford subjected the welds from each of 15 groups to strength testing, peel testing, or metallurgical analysis. Using a novel technique applied to two welds from each group, Ford created planar sections through the weld parallel to the interface between the sheets. What is particularly appealing about this technique is that it creates a metallographic map in the same plane as the image created from the ultrasonic measurements. In general, good agreement was found between the fused areas identified in the metallographic micrographs and the estimated areas determined from the processed ultrasonic peak-ratio images. Figure 5 is a plot of the weld-nugget areas determined from the metallographic image against the areas estimated from the ultrasonic peak-ratio images, along with the best-fit line from a linear regression. The regression yielded an R-square coefficient of 0.79 (a perfect linear fit would result in a coefficient of 1.0). The line is very close to the 45-degree line, as it should be if the peak-ratio area is a good proxy for the planar-section area.

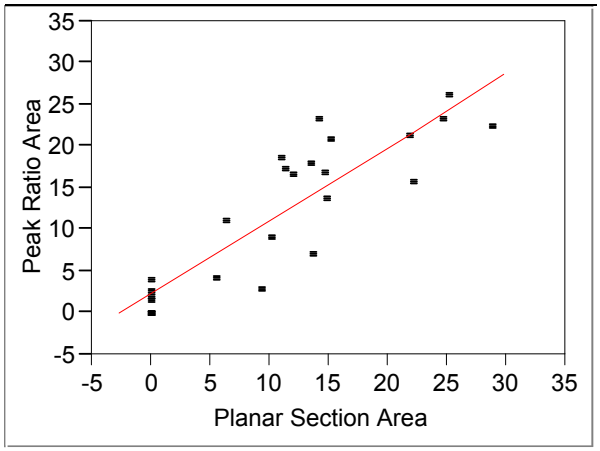


Figure 5. The plot shows the relationship between the weld areas determined from planar-sections and the ultrasonic peak-ratio maps, and the least-squares line fit to the data.

Measurements on Production Parts

To demonstrate technical feasibility of phased arrays for spot-weld inspection, the recently completed prototype probe housing is being used to make measurements on production parts. This was not possible earlier, because it was necessary to design and build the miniature scanning system and the housing that allows the ultrasonic probe to be used outside of a water tank.

To date, preliminary measurements have been made on package trays, apron assemblies, and a truck door. The weld pictured in Figure 6a is on a truck door, and is relatively easy to inspect with the prototype system. The relatively shallow and uniform indentation (Figure 6b) allows good coupling between the probe assembly and the

surface, and the two sheets are reasonably parallel. The measured indentation of the inspection surface is shown in Figure 6b, and the processed peak-ratio image of the weld is shown in Figure 6c.

In general, the quality of the measurements depends in large part on the surface conditions of the parts including the shape and roughness of the surface indentations. For example, very deep spherical indentations make it difficult to get enough energy into the parts to provide a dimensional analysis of the welds, and deep indentations make it difficult to achieve good coupling with the probe. Another challenge arises when the welding electrodes are not aligned, creating non-parallel surfaces. In this case, some of the acoustic energy transmitted into the part is reflected away from the weld, and the reflected signals are not captured by the probe. Non-parallel surfaces and distortion of the parts during welding occurs most often in thin sheets. Surface roughness inside the weld indentation also creates a challenge, because it causes scattering of the acoustic waves. Many of these conditions are associated with burnt welds, in which case it is easy to identify the welds as defective based on excessive material loss and indentation, which is relatively easy to measure. Thus, the weld quality can be determined even though it is difficult to provide a dimensional analysis.

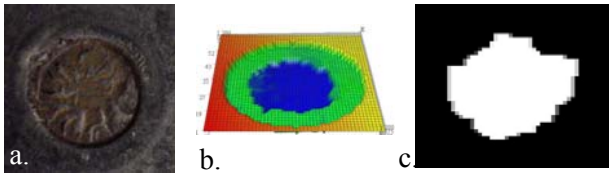


Figure 6. Picture of a spot weld on a truck door (Figure 6a), along with the measured indentation of the inspection surface (Figure 6b) and the processed peak-ratio image of the weld (Figure 6c).

Conclusions

There are substantial challenges in nondestructive testing of welds on automotive parts such as surface roughness, indentations on the surface caused by the welding electrodes, expulsion, and complex geometries that make it difficult to access welds. There is also variability between parts that arises from variations in materials and differences that are inherent in products produced in any large-scale manufacturing operation. Previous work demonstrated the concept feasibility of inspecting spot-welds in steel using ultrasonic phased-array technology. To demonstrate the technical feasibility of phased arrays for spot-weld inspection, a recently completed prototype probe assembly is being used to make measurements on coupons and production parts. This was not possible earlier, because it was necessary to design and build the miniature scanning system and the housing that allows the ultrasonic probe to be used outside of a water tank. Initial experiments were used to guide modifications made to the first prototype to improve accessibility to welds and coupling on production parts. Experiments are underway to validate the results obtained using the prototype probe assembly and LBNL's signal-processing algorithms. Work under way will also yield integrated, real-time diagnostic tools that operate at sufficient speed for assembly-line use. The remaining challenges include determination of resolution limits and the best diagnostic parameters for specific applications, as well as demonstration of robustness, accuracy, and cost-effectiveness under realistic operating conditions.

Presentations

1. F. Reverdy, Lawrence Berkeley National Laboratory, "Inspection of Spot Welds Using a Portable Ultrasonic Phased-Array System," 31st Annual Review of Progress in Quantitative Nondestructive Evaluation, July 25–30, 2004, Colorado School of Mines, Golden, Colorado.
2. D. Hopkins, Lawrence Berkeley National Laboratory, "Development of an Ultrasonic Phased-Array System for Nondestructive Evaluation of Resistance Spot Welds," United States Automotive Materials Partnership (USAMP) — Automotive Materials Division (AMD) Offsite, December 2, 2004, Southfield, Michigan.
3. F. Reverdy, "Spot-Weld Inspection Using an Ultrasonic Phased Array," ASNT Spring Conference, Albuquerque, New Mexico, March 2005.
4. D. Hopkins, "Use of Ultrasonic Phased Arrays for Weld Inspection and Material Characterization," Third US-Japan Symposium on Advancing Applications and Capabilities in NDE, June 20-24, 2005.

Publications

1. F. Reverdy and D. Hopkins, Lawrence Berkeley National Laboratory, "Inspection of Spot Welds Using a Portable Ultrasonic Phased-Array System," *31st Annual Review of Progress in Quantitative Nondestructive Evaluation*, July 25–30, 2004, Colorado School of Mines, Golden, Colorado.
2. F. Reverdy, D. Hopkins, D. Turler, and K. Nihei, "Use of Ultrasonic Phased Arrays for Weld Inspection and Material Characterization," *Proc. Third US-Japan Symposium on Advancing Applications and Capabilities in NDE*, June 20-24, 2005.
3. T. Potter, B. Ghaffari, G. Mozurkewich, F. Reverdy and D. Hopkins, "Comparison of Metallurgical and Ultrasonic Inspections of Galvanized Steel Resistance Spot Welds," *32nd Annual Review of Progress in Quantitative Nondestructive Evaluation*, July 31-August 5, 2005, Bowdoin College, Brunswick, Maine.

7. RECYCLING

A. Recycling Assessments and Planning

Principal Investigator and Field Project Manager: Edward J. Daniels
Argonne National Laboratory
9700 S. Cass Ave., Argonne, IL 60439
(630) 252-5279; fax: (630) 252-1342; e-mail: edaniels@anl.gov

Technology Area Development Manager: Joseph A. Carpenter
(202) 586-1022; fax: (202) 586-1600; e-mail: joseph.carpenter@ee.doe.gov
Field Technical Manager: Philip S. Sklad
(865) 574-5069; fax: (865) 576-4963; e-mail: skladps@ornl.gov

Participants:
This project is conducted as part of a Collaborative Research and Development Agreement (CRADA) between DOE's Argonne National Laboratory, USCAR's Vehicle Recycling Partnership, and the American Plastics Council.
CRADA Partner Principal Investigators:
Michael Fisher, American Plastics Council, (703) 741-5599; e-mail: mike_fisher@plastics.org
Gerald Winslow, VRP, DaimlerChrysler Corp., (248) 512-4802; e-mail: grwx@DCX.com
Claudia Duranceau, VRP, Ford Motor Co., (313) 390-0504; e-mail: cdurance@ford.com
Candace Wheeler, VRP, General Motors Corp., (586) 986-1674; e-mail: candace.s.wheeler@gm.com

---

Contractor: Argonne National Laboratory
Contract No.: W-31-109-Eng-38

Objectives

- Eliminate any real or perceived recycling barriers that might preclude the use of advanced automotive materials.
- Enable the optimum recycling of all automotive materials, current and future, thereby obviating the need for legislative recycle mandates.
- Assess the critical needs for cost-effective recycling of automotive materials and components.
- Establish research priorities to enable cost-effective recycling of advanced automotive materials and components.
- Communicate a collaborative industry/government approach to issues related to the recycling of automotive materials.
- Coordinate research with other agencies and stakeholders in the United States, Europe, and Asia.

Approach

- Consult with automotive manufacturers and recycling industries, the U.S. Council on Automotive Research (USCAR) and its affiliates, national laboratories, universities, and other relevant organizations to assess critical recycling needs/barriers.
- Develop a recycling research plan that will serve as a "working document" to guide the U.S. Department of Energy (DOE) in establishing priority goals, with an initial emphasis on lightweighting body and chassis materials.

- Establish an outreach/communication function to enable cooperation amongst, and leveraging of resources with, all stakeholders and the international community.
- Assist DOE in establishing advanced recycling research and development (R&D) initiatives and provide technical oversight to ensure that priority objectives/goals are accomplished.

Accomplishments

- On September 14, 2005, held a workshop to update the Roadmap for Recycling End-of-Life Vehicles of the Future, which was issued in May of 2001. The updated Roadmap will be issued in the third quarter of FY 2006.
- On September 13, 2005, held a two-year program review that was attended by experts in the field, in addition to the CRADA partners.
- Developed a joint "U.S. ELV (end-of-life vehicle) CRADA" Team presentation kit and brochure.
- Established liaison with the Institute of Scrap Recycling Industries (ISRI) and held several meetings with the CRADA partners and representatives of ISRI in FY 2004 and FY 2005.
- Held a CRADA announcement event at Argonne on December 2, 2004 — the event was attended by representatives of the press, industry, and government.
- Negotiated a CRADA with the Vehicle Recycling Partnership (VRP) and the American Plastics Council (APC) and Argonne National Laboratory (ANL), as partners; effort under the CRADA was initiated in August 2003.
- Prepared a five-year research plan based on (1) the recommendations and priorities identified in the Roadmap and (2) an initial planning meeting with the management council of the VRP of USCAR.

Future Direction

- Continue development and management of the research plan with the CRADA partners.
- Continue ongoing efforts toward the milestones and objectives of the CRADA statement-of-work.
- Continue outreach efforts to broaden the basis for cooperation among stakeholders.
- Continue ongoing project efforts to assist DOE in preparation of planning documents, priority recycling R&D needs, proposal reviews, and related tasks.
- Update the ELV Roadmap as necessary.

Summary

The objective of this project is to establish priorities and develop cost-effective recycling technologies and strategies in support of the U.S. Department of Energy (DOE's) FreedomCAR and Vehicle Technologies (FCVT) Program's long-term objectives and goals. The major goals of this research are to (1) enable the optimum recycling of all automotive materials, (2) ensure that advanced automotive materials that improve the life-cycle energy use of vehicles are not precluded from use as a result of a perception that those materials are not recyclable, and (3) continue to enable market-driven vehicle recycling.

Today, cars that reach the end of their useful service life in the United States are profitably processed for materials and parts recovery by an existing recycling infrastructure (e.g., see Figure 1 in report 7.B). That infrastructure includes automotive dismantlers, which recover useable parts for repair and reuse; automotive remanufactures, which remanufacture a full range of components, including starters, alternators, and engines to replace defective parts; and, ultimately, the scrap processor, which recovers raw materials such as iron, steel, aluminum, and copper from the remaining auto "hulk" after components have been recovered for recycling.

Today, more than 75% of the materials from obsolete cars are profitably recoverable for recycling.
The recyclability of the remaining 25% of the end-of-life vehicles (ELVs) is limited at present by the lack of (1) commercially-proven technologies to identify and cost-effectively separate materials and

components and (2) profitable post-use markets. During the next 20 years, both the number and complexity of ELVs are expected to increase, posing significant challenges to the existing recycling infrastructure. The automobile of the future will use significantly greater amounts of lightweight materials (e.g., ultra-light steels, aluminum, plastics, and composites) and more sophisticated/complex components.

Roadmap Recommendations

A workshop to update the original roadmap, which was published in 2001, was held on September 14, 2005, at Argonne. Representatives from DOE, key stakeholders, and other experts attended the meeting (Exhibit 1). The updated roadmap will be published during the third quarter of FY 2006. The workshop evaluated the original Roadmap and its recommendations. The following were identified as some of the factors that can affect the recyclability of future shredder residue:

- Vehicles containing new materials of construction for lightweighting (composites, light weight steel, aluminum alloys, and magnesium);
- Catalysts for better environmental control; and
- Vehicles powered by fuel cells, electric batteries, hydrogen, and hybrids.

The key recommendations from the original roadmap, which was developed with input from key stakeholders to guide DOE's recycle research, were:

- Come together as a unified recycling community to cost-share in the development of required new technology.
- Incorporate reuse, remanufacturing, and recycling into the design phase for cars whenever possible.
- Recycle as early in the recycling stream as possible, while relying on the market to optimize the value and amount recycled at each step.

Exhibit 1. List of Roadmap Workshop Attendees

Organization	Represented By
American Plastics Council	Trip Allen
Consultant	Richard Paul
American Plastics Council	Mike Fisher
Argonne	Ed Daniels
Argonne	Bassam Jody
Argonne	Pomykala Joe
Argonne	Jeff Spangenberger
Bayer Material Sciences	Don Schomer
DaimlerChrysler	James Frusti
DaimlerChrysler	James Ryan
DaimlerChrysler	Nakia Simon
DaimlerChrysler	Gerry Winslow
Energetics	Melissa Eichner
Energetics	Catherine Jereza
Ford	Claudia Duranceau
Georgia Tech	Bert Bras
Gesing Consultants	Adam Gesing
GM	Steve Cadle
GM	Candace Wheeler
ISRI	Dave Wagger
PURRC	Stephen Niemiec
Rochester Institute of Technology	Nabil Nasr
Steel Recycling Institute	Bill Heenan
Troy Polymers	Ibraham Sendijarevic
Troy Polymers	Vahid Sendijarevic
Univ. of Windsor	Edwin Tam
USCAR	Susan Bairsley
USCAR	Stacey Keast
USCAR	Mike Martin
USCAR	Virginia Smith
USDOE	Joseph Carpenter

- Maintain a flexible recycling process that can adapt to diverse model lines fabricated with different techniques and materials from various suppliers.
- Develop automated ways to recover bulk materials.
- Emphasize R&D on post-shred material identification, sorting, and product recovery.
- Focus R&D efforts on materials not recycled today by sorters (e.g., post-shred glass, rubber, fluids, textiles, plastics).
- Develop uses for recovered materials (whether in the same or different applications) and testing specifications.

- Encourage investment in the infrastructure needed to achieve the recyclability goal. Build on the existing infrastructure.
- Develop a means to prevent the entry of polychlorinated biphenyls and other hazardous materials into the recycling stream and promote acceptable limits in shredder residues.
- Consider the recycling requirements of new technologies entering fleets as early as possible.

The Five-Year R&D Plan

On the basis of the roadmap and continuing discussions with key stakeholders, a five-year research plan was prepared. The plan includes three focus areas, as discussed below.

Area 1. Baseline Technology Assessment and Infrastructure Analysis

The focus of the work under this activity is to develop the tools and document the information necessary to make effective decisions relative to technology needs to facilitate sustainable future vehicle recycling and to make effective decisions regarding the allocation of R&D resources. See report 7.B

Area 2. Materials Recovery Technology Development and Demonstration

Research to be conducted in this area will initially focus on addressing technology needs for post-shred materials recovery, including mechanical recycling and conversion to fuels and chemicals. Projects that enhance pre-shred recovery — including disassembly for materials recovery and direct reuse and remanufacturing of components — will also be considered. In the long term, such components as fuel cells, advanced batteries, and onboard hydrogen reformers are more likely to enter the recycle stream through pre-shred recovery for remanufacturing, repair, and materials recovery. Research will be undertaken to determine the technology needs to ensure the recyclability of these very advanced automotive components. See report 7.E.

Area 3. Recovered Materials Performance and Market Evaluation

Understanding and enhancing recovered materials performance is an essential ingredient to a successful recycling program. This is especially true in automotive systems when the materials and components that are recovered have been in use for an average of from 10–15 years. Area 3 includes projects to quantify the relative performance of recovered materials vis-à-vis new or virgin materials; research on compatibilization of recovered polymers to improve performance properties; development of technologies to upgrade the recovered materials, such as separation of fibers from polymeric substrates; and development of applications for other recovered materials, such as rubber and glass. See report 7.D.

CRADA Projects

A collaborative research and development agreement (CRADA) among Argonne, the Vehicle Recycling Partnership (VRP) of U.S. Council for Automotive Research (USCAR), and the American Plastics Council (APC) has been structured to provide a core team of expertise and the resources to enable the optimum recycling of all automotive materials.

The CRADA team's R&D agenda focuses on the following key objectives:

- Develop and demonstrate sustainable technologies and processes for ELV recycling.
- Demonstrate the feasibility of resource recovery from shredder residue, including materials recovery for reuse in automotive and other applications, chemical conversion of residue to fuels and chemicals, and energy recovery.
- Develop viable strategies for the control and minimization or the elimination of substances of concern.
- Benchmark recycling technology and provide data to stakeholders.
- Stimulate markets for reprocessed materials to support economic collection, processing, and transportation.
- Transfer technology to commercial practice.

This project provides for the overall management of the CRADA team activities and for communication and advocacy with other organizations. The other

major projects that have been initiated under the CRADA include the following:

- Baseline Assessment of Recycling Systems and Technology. (7.A)
- Post-Shred Materials Recovery Technology Development and Demonstration. (7.E)
- Development of Technology for Removal of PCBs and Other Substances of Concern from Shredder Residue. (7.C)
- Compatibilization/Compounding Evaluation of Recovered Polymers. (7.D)

The objectives and progress on these projects are discussed in their respective sections of this report. Effort under the CRADA was initiated in the fourth quarter of FY 2003.

Outreach Efforts

While the CRADA team provides a core of expertise, cooperation with other organizations is key to achieving the overall program objectives. In the United States, a market-driven recycling infrastructure is in place. The CRADA team is actively pursuing cooperation with the organizations and companies that are a part of that infrastructure. Cooperation with other stakeholders is also essential.

Papers outlining the industry/government collaboration have been presented at international conferences. A joint DOE, USCAR, and APC paper on "Market Driven Recycling in North America" was presented as the keynote paper at the 2004 International Car Recycle Congress in Washington, D.C.

Several meetings with representatives of the Institute of Scrap Recycling Industries (ISRI) were held to brief ISRI on the CRADA objectives and projects and to elicit ISRI participation.

To further communicate the U.S. approach to ELV recycling, a one-page CRADA summary and a CRADA brochure have been prepared.

As previously mentioned, a review of the projects and ongoing efforts of the CRADA team was held September 13, 2005 and a workshop was also held on September 14, 2005, to review and update the ELV Roadmap. The updated roadmap will be issued during the third quarter of FY 2006.

Publications

Market Driven Automotive Recycling in North America, Duranceau, C. M., presented at the Institute of Scrap Recycling Industries Shredder Meeting, Dallas, TX (Oct. 30, 2004).

Sustainable End-of-Life Vehicle Recycling: R&D Collaboration between Industry and the U.S. DOE, Daniels, E.J.; Carpenter, J.A., Jr.; Duranceau, C.M.; Fisher, M.M.; Wheeler, C.S.; and Winslow, G.R., JOM, The Mineral, Metals & Materials Society, vol. 56, no. 8, pp. 28–32 (Aug. 2004).

Market Driven Automotive Recycling in North America, Duranceau, C. M., USCAR; Carpenter, J.A., Jr., U.S. DOE; and Fisher, M.M., American Plastics Council, keynote at the 2004 International Car Recycling Workshop, Washington, D.C. (May 19, 2004).

Automotive Materials Recycling: A Status Report of U.S. DOE and Industry Collaboration, Daniels, E.J., in Ecomaterials and Ecoprocesses, Proc. of the International Symposium on Ecomaterials and Ecoprocesses, Vancouver, BC, Canada, pp. 389–402 (August 24–27, 2003).

Effects of Transportation on the Ecosystem, Carpenter, J.A., Jr., in Ecomaterials and Ecoprocesses, Proc. of the International Symposium on Ecomaterials and Ecoprocesses, Vancouver, BC, Canada, pp. 13–22 (August 24–27, 2003).

Automotive Technology: Looking Forward, Sullivan, R.A.; Hamilton, R.D.; and Carpenter, J.A., Jr., in Ecomaterials and Ecoprocesses, Proc. of the International Symposium on Ecomaterials and Ecoprocesses, Vancouver, BC, Canada, pp. 49–67 (August 24–27, 2003).

A Roadmap for Recycling End-of-Life Vehicles of the Future, prepared by Energetics for the U.S. Department of Energy, Office of Advanced Automotive Technologies (May 2001).

B. Baseline Assessment of Recycling Systems and Technology

Principal Investigator and Field Project Manager: Edward J. Daniels
Argonne National Laboratory
9700 S. Cass Ave., Argonne, IL 60439
(630) 252-5279; fax: (630) 252-1342; e-mail: edaniels@anl.gov

Technology Area Development Manager: Joseph A. Carpenter
(202) 586-1022; fax: (202) 586-1600; e-mail: joseph.carpenter@ee.doe.gov
Field Technical Manager: Philip S. Sklad
(865) 574-5069; fax: (865) 576-4963; e-mail: skladps@ornl.gov

Participants:
This project is conducted as part of the Cooperative Research and Development Agreement (CRADA) between DOE's Argonne National Laboratory, USCAR's Vehicle Recycling Partnership, and the American Plastics Council.
CRADA Partner Principal Investigators:
Michael Fisher, American Plastics Council, (703) 741-5599, e-mail: mike_fisher@plastics.org
Gerald Winslow, VRP, DaimlerChrysler Corp., (248) 512-4802, e-mail: grwx@DCX.com
Claudia Duranceau, VRP, Ford Motor Co., (313) 390-0504, e-mail: cdurance@ford.com
Candace Wheeler, VRP, General Motors Corp., (586) 986-1674, e-mail: candace.s.wheeler@gm.com

---

Contractor: Argonne National Laboratory
Contract No.: W-31-109-Eng-38

Objective

- Establish the baseline or state-of-the-art for automotive materials recovery/recycling technology.

Approach

- Review the state-of-the-art of worldwide automotive materials recovery/recycling technologies.
- Develop technology profiles of emerging automotive materials recycling technologies.
- Review international, federal, and state regulatory information regarding vehicle recyclability, substances of concern, and recycle laws and mandates.
- Conduct life-cycle studies to quantify the environmental burdens associated with various end-of-life recycling technologies.
- Conduct reference-case end-of-life recyclability studies.

Accomplishments

- Prepared a draft article that reviewed the state-of-the-art in recycling of vehicles and automotive materials.
- Conducted a literature search that identified mechanical, thermochemical conversion, and energy recovery technologies.
- Conducted life-cycle studies of selected alternative recycle technologies, including mechanical recycling and thermo-chemical conversion of shredder residue to fuels.
- Characterized the existing U.S. recycling infrastructure and derived estimates of automotive recycling rates from the literature.

- Conducted recyclability calculations for reference cases and three lightweight alternatives: lightweight steel, composite materials, and aluminum.

Future Direction

- Update the database of recycling technologies as new technologies emerge, a process that will include visits, as appropriate, to evaluate state-of-the-art material and energy recovery technologies in Japan and Europe.
- Continue life-cycle analysis and comparisons.
- Plan additional recyclability evaluations by using the current study as a starting point for assessing the recyclability of cars of the future.

Summary

The objectives of this project are to bench-mark the automotive materials recycling industry and to compile information in an accessible format regarding the status of existing and emerging recycling technology and research.

The focus of the work under this activity is (1) to develop the tools and document the information necessary to make effective decisions relative to technology needs to facilitate sustainable future vehicle recycling and (2) to make effective decisions regarding allocation of R&D resources.

The state-of-the-art of worldwide automotive materials recovery/recycling technologies and associated resource recovery infrastructures has been reviewed to identify technology gaps and needs and to identify differences in automotive recycling strategies in North America, Europe, and Asia. Technologies that are included in this review include, but are not limited to, post-shred materials recovery technologies, pre-shred materials recovery technologies, materials identification technologies, automated dismantling technologies, technologies for the recycling of specific components of vehicles (such as bumpers and fuel tanks), and thermochemical conversion technologies.

Life-cycle analyses of alternative recycle technologies have also been conducted to identify differences between technologies, such as mechanical recycling vis-à-vis thermochemical recycling, relative to energy and environmental benefits.

Regulations at the international, federal, and state levels are examined to identify the impact that proposed and existing regulations may have regarding recycling of automotive materials.

Reference-case recyclability calculations are made to quantify the expected recyclability of alternative vehicle designs.

Infrastructure

The North American recycling infrastructure has been characterized (Figure 1).

Technology Profiles

The recent literature has been reviewed, and summaries and profiles of available and emerging recycle technologies have been compiled into a draft working document and will be updated annually as new information becomes available.

A bibliography of abstracts of papers that discuss automotive recycling issues has been compiled. The bibliography is organized in the following sections:

- Recycling infrastructure,
- Design for recycling,
- Legal and regulatory issues,
- Life-cycle analysis,
- Research programs,
- Substances of concern,
- Disassembly technologies and case studies,
- Reuse of automotive parts and subassemblies,
- Remanufacturing,
- Mechanical separation technology,
- Thermochemical conversion technology,
- Energy recovery technology,
- Other technology,
- Advanced materials recycle technology, and
- Case studies of materials recycled for auto applications.

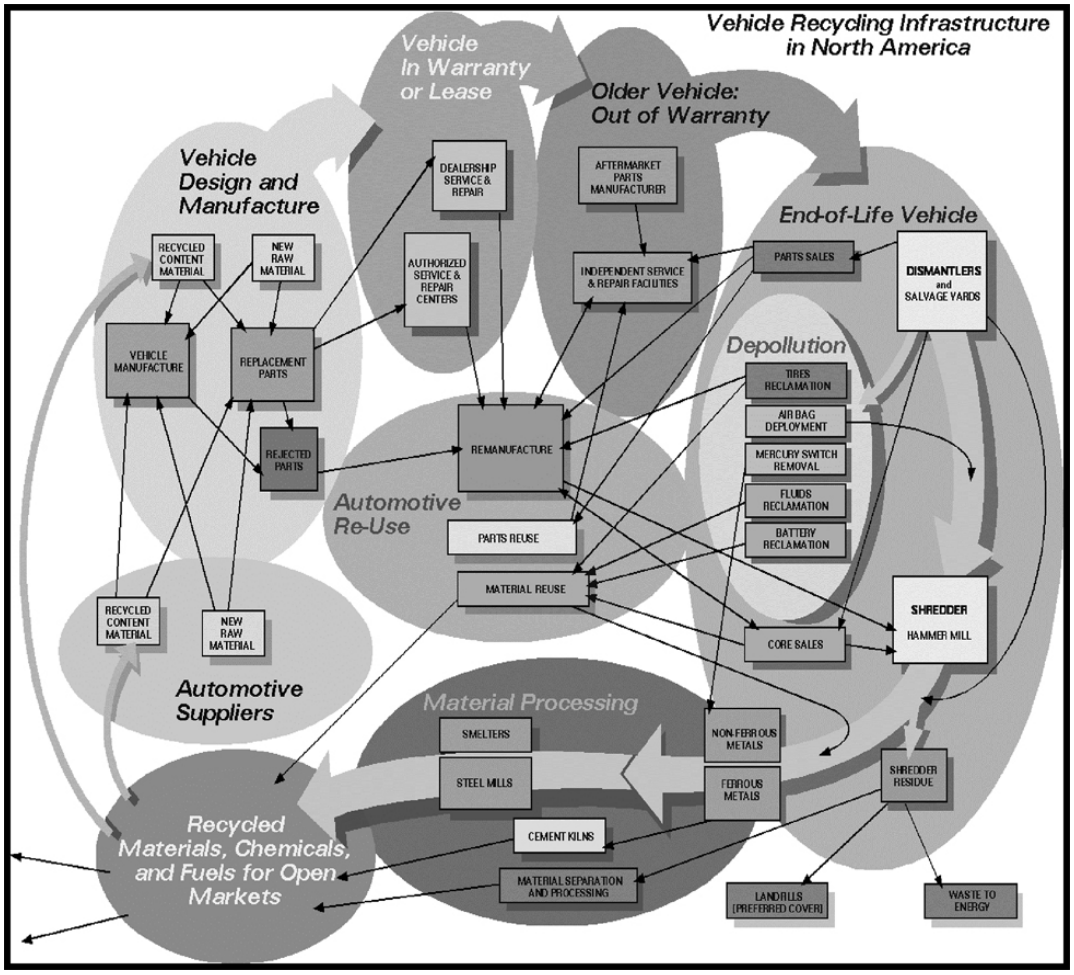


Figure 1. Representation of the North American automotive recycle infrastructure.

The bibliography was compiled from an extensive literature search, which included the following sources:

1. Society of Automotive Engineers (International) World Congresses from 1997 to 2004
2. Environmental Sustainability Conference and Exhibition, 2001
3. Society of Plastics Engineers:
   - ARC '98 Conference
   - ARC '99 Conference
   - ARC '00 Conference
   - GPEC 2002 Conference
   - GPEC 2003 Conference
4. Other conference proceedings:
   - International Automobile Recycling Congress 2001, 2002, 2003, 2004
   - TMS Fourth International Symposium of Recycling of Metals and Engineered Materials, 2000
   - Ecomaterials and Ecoprocesses, The Conference of Metallurgists, COM 2003

At present, the bibliography includes 196 citations (Table 1). References will be added to the bibliography as available.

Recycling Technologies: State-of-the-Art

A draft document describing the state of the art in recycling technologies for end-of-life vehicles, post-shred residue, and automotive materials has been prepared. Because post-shred residue contains residue from shredded white goods and other obsolete items (in addition to vehicles), these were also discussed in the document. The table of contents of this document is shown in Table 2.

Table 1. Citations included in the recycling bibliography (as of September 2005).

Bibliography Section	Number of Citations
Recycling infrastructure	18
Design for recycling	4
Legal and regulatory issues	24
Life-cycle analysis	9
Research programs	10
Substances of concern	5
Disassembly technologies and case studies	9
Reuse of automotive parts and subassemblies	1
Remanufacturing	0
Mechanical separation technology	21
Thermochemical conversion technology	12
Energy recovery technology	16
Other technology	36
Advanced materials recycle technology	7
Case studies of materials recycled for auto applications	24
Total citations	196

Regulatory Situation

The European Union has issued End-of-Life Vehicle Recycle Directives. The enforcement of these directives is, however, the responsibility of each member state. Although the United States has not developed a federal policy or mandate, regulations at the federal and state level can impact the technology needs for recycling automotive materials. For example, U.S. Environmental Protection Agency (EPA) regulations regarding polychlorinated biphenyl (PCB) limits the concentration of PCB on recycled materials to below the detectable limit (i.e., 2 ppm). State regulations regarding mercury and polybrominated diphenyl ethers (PBDEs) can also impede materials recycling.

Life-Cycle Studies

The objective is to use life-cycle analysis to assess the environmental impacts of various mechanical separation technologies and alternative end-of-life recycling technologies. This information will then be used to create a flexible, computerized, life-cycle inventory model, which is process-specific and yet can be modified to include additional recycling technologies and various material inputs. Life-cycle

Table 2. Draft state-of-the-art assessment table of contents.

1.0. Introduction and Background
2.0. The Process of Recycling Automobiles
- Dismantling for Direct Resale
- Shredding

3.0 The Process for Recycling White Goods
- Refurbishing of Units for Resale
- De-Pollution of the Units
- Shredding

4.0. Shredder Residue
- Composition
- Recycling of Materials from Shredder Residue

5.0. Technologies for Concentrating Recyclables from Shredder Residue
- Mechanical Separation Systems
- Gravity Separators
- Electrostatic Separators

6.0. Technologies for Separating and Recovering Products from Shredder Residue
- Argonne's Separation and Recovery of Flexible Polyurethane Foam
- Separation and Recovery of Plastics from Shredder Residue
  - Argonne's Froth Flotation Process
  - The RPI Process
  - The Salyp Process
  - The VW/SiCon Process
  - The Galloo Process
  - The MBA Process
  - The Toyota Process

7.0. Thermochemical Processes for Recycling Shredder Residue
  - CWT Hydrolysis Process
  - TPI Glycolysis Process
  - Other

8.0. Energy Recovery from Shredder Residue
9.0. Substances of Concern
- Polychlorinated Biphenyls (PCBs)
- Heavy Metals
- Flame Retardants

10.0 Recycling of Advanced Vehicles
- Recycling of Fuel-Cell vehicles
- Recycling of Electric and Hybrid Vehicles
- Recycling of Aluminum and Magnesium from New-Generation Vehicles
- Recycling of Composites

11.0 Recycling of Other Vehicle Materials
- Catalytic Converters
- Tires
- Carpet
- Fluids
- Fuel Tanks

involves assessing all of the upstream burdens associated with the production of the materials and energies used in the process, including the transport of all materials to the facility.

PE Europe GmbH, a company that is experienced in conducting life-cycle assessments and in model development using its own GaBi (Ganzheitliche Bilanzerung) software, was contracted to perform these analyses. Two analyses have been done: one for Salyp NV's mechanical separation process and another for Changing World Technologies' (CWT's) thermal conversion process. PE Europe has also developed a flexible end-of-life model, and the model was used to compare the two different approaches to recycling shredder residue. The model allows the user to run simulations on shredder residue separation within different boundary conditions. The following boundary conditions can be modified: (1) shredder residue composition, (2) location of the facility, (3) type and distance of transportation, (4) market values for the separated fractions, (5) new potential applications for separated fractions, and (6) utilization ratio of the facility.

Salyp's separation process combined equipment developed by Argonne National Laboratory (ANL) and several others to create a facility that separates shredder residue into discrete fractions of metals, foam, mixed plastics, and fiber-rich and fines streams. On the other hand, the CWT process converts organic materials into hydrocarbon fuels and other potential products.

Primary data were collected for the Salyp and the CWT processes, including all energy, water, and material inputs, plus data on emissions to air and water, wastes, and products produced. both sets of data were entered into the GaBi software to create a flexible model of the process. Figure 2 illustrates the flow streams for the Salyp case.

In the case of the Salyp separation process, three different scenarios for handling the various materials recovered from shredder residue were determined. These scenarios included using specific material fractions as fuel for cement kilns (energy recovery), as well as using mixed plastics to replace such products as wood pallets and polypropylene (PP) pellets (material substitution). The various scenarios were assessed by using a variety of impact categories, including primary energy demand and CO_2 emissions. In the case of primary energy demand, all scenarios showed a net credit in total energy use. For the three scenarios studied, substituting recovered PP/polyethylene (PE) in a new PP application had the greatest benefit. However, if the mixed plastic stream was used to replace wood (e.g., decking material, park benches, wood pallets, etc.), the benefits to primary energy demand were less than if the recovered materials were simply used for energy recovery. In terms of CO_2 emissions, the PP application again showed the greatest benefit. Substituting PP for wood applications was next with a lower benefit, while the energy recovery scenario showed a negative impact on CO_2.

In the case of the CWT process, two basic scenarios were assessed. They involved using the light hydrocarbon oil generated by the process for fuel oil used in power plants to generate electricity and substituting light hydrocarbon oil for diesel oil (both with and without an added hot-oil processing step). While the oil product generated is more refined than an actual crude oil, it would require additional steps before it could be considered a true diesel oil. Therefore, reality is probably located somewhere between scenarios 1 and 2. In this study, the impact on primary energy demand resulted in a benefit in all cases. The benefits in the diesel substitution case were slightly greater than in the fuel-oil case. In the case of CO_2 emissions, all scenarios again showed an overall benefit. However, the diesel substitution case had a greater benefit than the fuel-oil substitution case.

A comparison of these two technologies is under way. Although early results show that the thermal conversion process has an overall advantage over the mechanical separation process, these results are heavily dependent on the assumed use of the end products in the life-cycle assessment, as well as on key assumptions on contamination and metals recovery. These factors are being addressed.

Recyclability Studies

Recyclability studies are being conducted to examine the effect of using automotive lightweighting material on recyclability. A

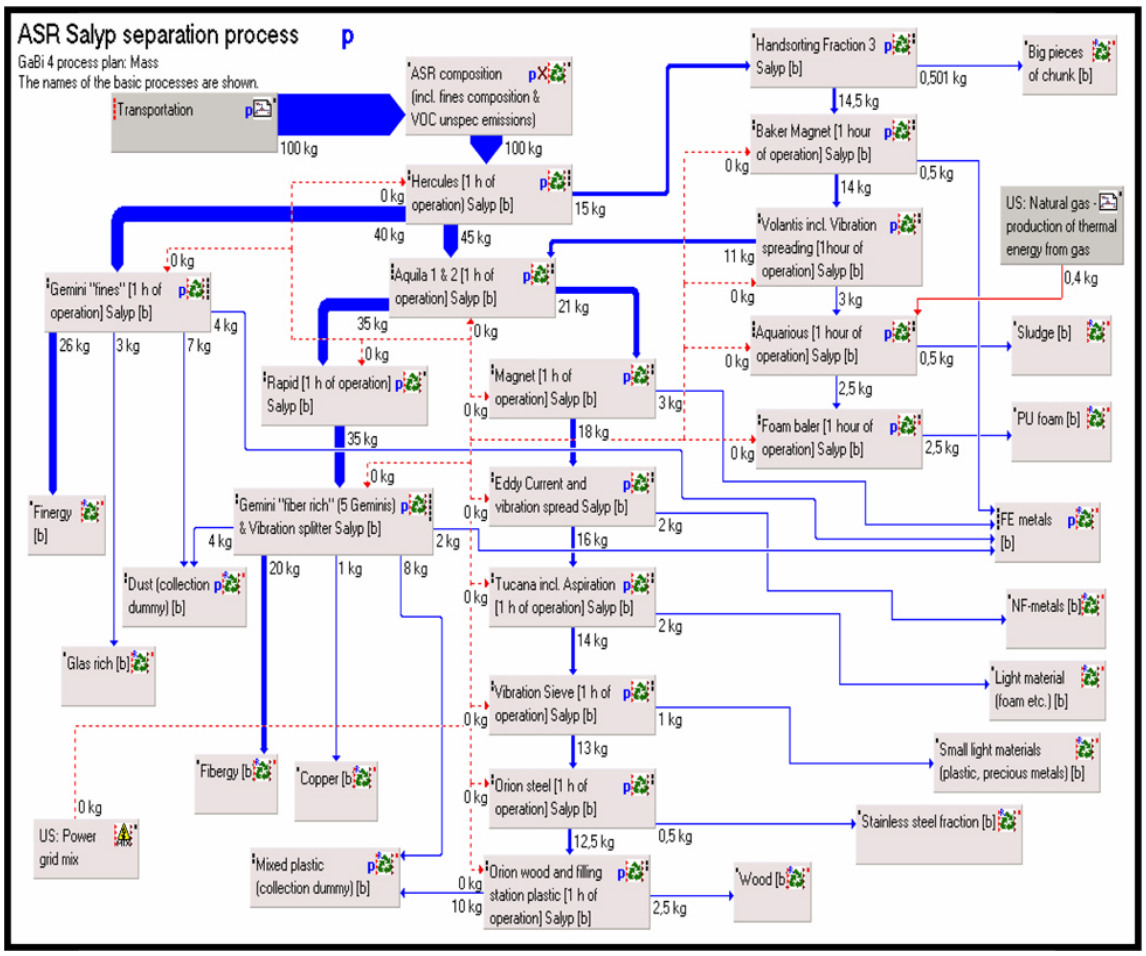


Figure 2. Life-cycle analysis mass-flow representation of Salyp separation process

Toyota Prius hybrid was selected as a reference case. This vehicle is a second-generation hybrid with a gas/electric powertrain. Evaluating the recyclability of this vehicle and its new technology will be a step in identifying changes that will impact end-of-life recycling of vehicles of the future.

In collaboration with Johnson Controls, Inc. (JCI), the VRP dismantled the vehicle according to VRP procedures to single material components and entered data for each part into a database. A material list that identified the breakdown of materials into separate classifications (such as ferrous and non-ferrous metals, as well as composite materials and plastics) was prepared. The materials breakdown is summarized in Table 3. In comparison, the materials composition of a production Ford Taurus is summarized in Table 4.

Table 3. 2004 Toyota Prius materials breakdown.

Materials	Mass (kg)	Percent
Ferrous metals	776.94	60.55
Nonferrous metals	229.99	17.92
Plastics	154.85	12.07
Elastomers	39.66	3.09
Inorganic material	34.71	2.71
Other	28.21	2.20
Organic materials	18.84	1.47
Vehicle mass (less fluids)	1,283.1	100.00

Three different recyclability calculations were made (Table 5). The Federal Trade Commission (FTC) recyclability number is the percentage by weight of the material that is currently being recycled, and it includes metals, fluids less fuel, and batteries. The

Table 4. 2004 Ford Taurus materials breakdown.

Materials	Mass (kg)	Percent
Ferrous metals	1,008.28	70.37
Plastics	154.41	10.78
Nonferrous metals	141.43	9.87
Elastomers	68.71	4.80
Inorganic material	40.91	2.86
Other	17.45	1.22
Organic materials	1.66	0.12
Vehicle mass (less fluids)	1,432.86	100.00

Table 5. Reference case recyclability: 2004 Toyota Prius.

Calculation Method	Recyclability (%)
Federal Trade Commission	80.86
European	97.61
Feasibility of recycling	85.58
Ref. 2000 Ford Taurus	80.50

European guidelines include FTC materials plus fuel at 90% of a full tank, plastics that could be recycled, and up to 10% by weight energy recovery. Note that Europe requires 95% recyclability for new vehicles. The feasibility-to-recycle number includes the FTC materials plus plastics that can be recycled. Changes to the current infrastructure would be required to increase recycling beyond the current FTC percentage.

To establish an indication of the impact of lightweight materials on the reference case recyclability calculations, the 2004 Toyota Prius is compared with a proposed aluminum-intensive lightweight vehicle and a proposed composite lightweight vehicle, both of which are also based on the 2004 Prius. The production 2004 Toyota Prius hybrid vehicle body was steel with an aluminum hood and decklid. The suspension was of steel, except for an aluminum steering knuckle on the front suspension. This vehicle was used as the base for this study.

The aluminum alternative is for a 2004 Toyota Prius with an aluminum body and a magnesium engine cradle and a rear axle substituted for the production parts. In addition, seat frames, body brackets, and the instrument panel cross car beam have been changed from steel to aluminum. As a result, the weight has been reduced by approximately 630 lb or 21%. Because the weight reduction is entirely in the currently recycled portion of the vehicle, the recyclability is adversely affected and is reduced from 80.86% to 76.10%. No changes were made to the currently- nonrecycled portion of the vehicle. Aluminum replaced steel at 50% by weight of the original steel.

The composite alternative is for a 2004 Toyota Prius that consists of (1) a carbon-fiber body with 40% carbon fiber and 60% thermoset polyurethane/urea resin by volume, 49.72% carbon, and 50.28% thermoset polyurethane/urea resin by weight and (2) a magnesium engine cradle and rear axle substituted for the production parts. In addition, seat frames, body brackets, and the instrument panel cross car beam have been changed from steel to composite. As a result, the weight has been reduced by approximately 711 lb, or 24%. Because the weight reduction is entirely in the currently recycled portion of the vehicle, the recyclability is adversely affected and is reduced from 80.86% to 57.20% if none of the composite is recycled or 74% if all of the composite material is recycled. No changes were made to the currently nonrecycled portion of the vehicle. The composite material replaced steel at 40 wt% of the original steel.

There are reductions in all three recyclability calculations for lightweighted vehicles, even though the rest of the vehicle is not changed (Table 6). Where the aluminum and composite material is being recycled, the same amount of material would be disposed of in landfills in each of the three scenarios. The only difference is that the recycled portion of the lightweighted vehicles would be lighter. Although the recyclability would be less, there would be no difference in the amount of material disposed of in landfills, and the lighter vehicles would use less fuel during their life. As can be seen, lightweighting presents challenges in the European market. Note that these calculations do not take into account the downsizing of related components that would accompany any lightweight vehicle, such as powertrains, brakes, and tires. Because the downsized components are high in metallic content, downsizing will further reduce recyclability and make it difficult to meet the European 95% requirement.

Table 6. 2004 Toyota Prius recyclability, reference case vs. aluminum and composite body materials.

Calculation Method	As Produced (%)	Aluminum Body (%)	Composite Body (%)
FTC	80.9	76.1	74.0[a]
European	97.6	96.0	94.5[a]
Feasibility of recycling	88.3	85.6	83.9[a]

[a] If the composite material were not recycled, then the numbers would be FTC, 57.2%; European, 78.2%; and feasibility of recycling, 67.1%. Recycling of the composite material would require significant changes in the current recycling infrastructure. In addition, a market for the recycled carbon fibers would need to be developed. Current technology for recycling carbon fibers results in a 20% loss in fiber properties and would limit their reuse to short-fiber applications.

In conjunction with this study, additional evaluations are planned by using these data as a starting point for assessing the recyclability of cars of the future. The impact of vehicle lightweighting and material selection on recyclability will be evaluated. In addition, the impact of powertrain changes in future vehicles (including hybrid and fuel-cell alternatives) on recyclability will be determined in comparison to powertrains in current vehicles. An assessment of various alternatives on recycling and the effect on the current recycling infrastructure will be produced. No downsizing of other components was included in this study. Future studies will reflect the downsizing of powertrains, brakes, tires, and other components in recyclability calculations. Items requiring further study resulting from these assessments will support future projects to determine the feasibility of various alternative vehicle configurations and choices of materials.

These results demonstrate the need for technology to recycle new automotive material if recycling mandates are to be met and to ensure that lightweighting materials are not excluded because of the inability to recycle them.

Publications

Modular Life Cycle Model — Basis for Analyzing the Environmental Performance of Different Vehicle End-of-Life Options, Binder, M.; Simon, N.L.; Duranceau, C.M.; Wheeler, C.S.; Winslow, G.R., Proc. of the 5th International Automobile Recycling Congress, Amsterdam (Mar. 9-11, 2005).

Modular Life Cycle Model of Vehicle End-of-Life Phase — Basis for Analysis of Environmental Performance, Wheeler, C.S.; Simon, N.L.; Duranceau, C.M.; Winslow, G.R.; Binder, M., SAE Paper 2005-01-0847.

United States National Life Cycle Inventory Database Project, A Status Report, Sullivan, J.L.; Wheeler, C.S.; and Simon, N.L., SAE Paper 2005-01-0852.

C. Development of Technology for Removal of PCBs and Other Substances of Concern (SOCs) from Shredder Residue

Principal Investigator: Bassam Jody
Argonne National Laboratory
9700 S. Cass Ave., Argonne, IL 60439
(630) 252-5279; fax: (630) 252-1342; e-mail: bjody@anl.gov

Field Project Manager: Edward J. Daniels
Argonne National Laboratory
9700 S. Cass Ave., Argonne, IL 60439
(630) 252-4206; fax: (630) 252-1342; e-mail: edaniels@anl.gov

Technology Area Development Manager: Joseph A. Carpenter
(202) 586-1022; fax: (202) 586-1600; e-mail: joseph.carpenter@ee.doe.gov
Field Technical Manager: Philip S. Sklad
(865) 574-5069; fax: (865) 576-4963; e-mail: skladps@ornl.gov

Participants:
This project is conducted as part of the Collaborative Research and Development Agreement (CRADA) between DOE's Argonne National Laboratory, USCAR's Vehicle Recycling Partnership, and the American Plastics Council.
CRADA Partner Principal Investigators:
Michael Fisher, American Plastics Council, (703) 741-5599; e-mail: mike_fisher@plastics.org
Gerald Winslow, VRP, DaimlerChrysler Corp., (248) 512-4802; e-mail: grwx@DCX.com
Claudia Duranceau, VRP, Ford Motor Co., (313) 390-0504; e-mail: cdurance@ford.com
Candace Wheeler, VRP, General Motors Corp., (586) 986-1674; e-mail: candace.s.wheeeler@gm.com

The Polyurethane Recycle and Recovery Council (PURCC) is also participating and cost-sharing in this project.
PURCC Project Lead: Steve Niemic

Contractor: Argonne National Laboratory
Contract No.: W-31-109-Eng-38

Objective

- Develop viable strategies and technology for the control and minimization or elimination of polychlorinated biphenyls (PCBs) and other substances of concern (SOCs) from recycled automotive materials.

Approach

- Identify efficient and environmentally acceptable process solutions for removal of contaminants, including PCBs, from materials recovered from shredder residue.
- Define variances in analytical procedures/test results for PCB analysis.

Accomplishments

- Conducted washing/cleaning tests of plastics recovered from shredder residue in:
  - Proprietary solvent-based solutions and in CO_2 and
  - Equipment using aqueous solutions with surfactants.

- Conducted laboratory tests to develop an understanding of the variability inherent in the analytical procedures for PCB analysis.
- Completed bench-scale screening of 11 surfactants and three organic solvents for removal of PCBs and other contaminants from polymers derived from shredder residues and specified preferred surfactant/cleaning solutions.
- Conducted a seminar with experts to further identify issues with regard to variability in analytical results for PCBs.
- Investigated impact on the analytical results of sample size, extraction solvent, and number of extractions used.

Future Direction

- Conduct additional testing on PCBs removal methods, including steam stripping.
- Integrate washing/cleaning system with the process for polymers recovery from shredder residue and identify necessary modification to facilitate the integration.
- Conduct a cost analysis of modified systems.

Summary

The objective of this project is to develop techniques and/or technology to identify and/or cost-effectively remove polychlorinated biphenyls (PCBs) and other substances of concern (SOCs) from recycled automotive materials.

SOCs can impact the recyclability of automotive materials in a number of ways. Certainly, their presence in either recycled materials and/or materials source stream impact the overall costs of recovering recyclable materials. In some cases, their presence at parts-per-million levels, such as in the case of PCBs, can prevent the reuse of the recovered materials, such as polymers and polyurethane foams.

The strategy that is required for control of the SOCs may vary regionally. For example, requirements are different in Europe, North America, and Asia for various SOCs. Strategies for controlling SOCs can also depend on the technology that is being proposed for recycling the automotive material.

The presence of SOCs in current vehicles and/or in other durable goods that are presently recycled with end-of-life vehicles is likely to impact the materials recycle stream for the foreseeable future. Consequently, the control of certain SOCs will require technology that will effectively remove the SOCs from recovered materials consistent with current regulatory requirements and consistent with the market requirement for the recovered material.

The initial focus of the work in this project is on the development of options and technology for the removal of PCBs from potentially recyclable materials recovered from shredder residue. PCBs, at parts-per-million levels, are routinely found in shredder residue. The source of the PCBs is not completely understood, but historically it has been associated with liquid PCB-containing capacitors and transformers that inadvertently escape the scrap inspections and control process at the shredders.

Evaluation and Testing of Solvent-Based Washing Systems

Three companies with equipment and/or proprietary washing solvents and solutions that could potentially be used for non-aqueous removal of PCBs from plastics recovered from shredder residue were identified by Troy Polymers, Inc. (TPI):

- Environmental Technology Unlimited (Wilmington, North Carolina);
- Cool Clean Technologies, Inc. (Burnsville, Minnesota); and
- ITec Environmental Group, Inc. (Oakdale, California).

Each company was supplied with a sample of plastics with the assigned (determined) concentration of PCBs of 11 ppm. Samples were washed at the three companies, and the washed samples were evaluated for PCB levels.

Environmental Technology Unlimited uses a proprietary METHEX solvent-based system and aqueous-based systems. Environmental Technology Unlimited performed six treatments of shredder residue plastics, and five out of the six washed samples reduced the PCBs concentration to below 2 ppm. The METHEX solvent-based system was superior to the aqueous system.

Cool Clean Technologies technology used CO_2 only. The washing failed to remove the PCBs.
ITec Environment Group reduced PCB levels in the plastics from 11 ppm to 2.8 ppm via solvent washing; no CO_2 treatment, which normally follows the basic process, was used.

On the basis of these results, it appears that Environmental Technology Unlimited and ITec Environmental Group have the technology that could remove PCBs to below 2 ppm. However, at this time, only ITec has the full-scale equipment ready to be integrated with a plastics recycling process.

Evaluation and Testing of Commercially-Available Aqueous-Based Washing Systems

Before testing the solvent-based systems, large-scale cleaning/washing tests were conducted using plastics from shredder residue by means of aqueous solutions and a surfactant previously identified earlier as the most promising from among many tested. The objective was to identify the limitations of the various types of existing washing equipment. Testing was done by using an ALMCO rotary-drum washer equipped with a dryer and SeKoN centrifuge equipment. The tests were carried out on approximately 100 lb of plastic chips each. The particles were between 0.2 and 0.5 in. in size. Under a CRADA contract, GraPar Corporation built, for Troy Polymers, Inc. (TPI), and tested a specially designed machine that has a design capacity of about 300 lb/hour of plastics. TPI conducted further testing on this machine in its facilities.

In each of these large tests, the washed material was "visually" clean in terms of dirt and oils. However, PCBs analyses were highly variable and indicated that in some cases, the PCBs concentration had increased after washing. As a result, it was determined that the PCBs analysis procedures should be reexamined, as is discussed in the next section.

The results suggest that existing aqueous-based equipment, as is, is not likely to reduce the concentration of PCBs to acceptable levels. Modifications are necessary to wash small chips (1/8 to 1/2 in.) of plastics — such as what will be recovered from shredder residue — efficiently and economically.

Evaluation of the Variability of PCB Sampling and Analytical Procedures

The large variability in the analytical results raised questions about the analytical sampling and analyses procedures. Therefore, laboratory experiments were performed to develop an understanding of the variability in PCB analytical procedures and explain the variability in the results.

The variability may be due to a number of factors, including sample size, plastics particle size, PCBs extraction procedure, analytical procedures, and/or interference from other compounds. A one-day seminar was held and attended by analytical experts from the United States and overseas to develop recommendations for improved sampling and analysis techniques specific to plastics chips recovered from shredder residue.

To investigate the possible interference of phthalates in the PCBs analysis, a sample of plastics chips derived from shredder residue was thoroughly mixed and then divided into four parts. The first part was analyzed by using Gas Chromatography and an Electron Capture Detector (GC-ECD) and by using Gas Chromatography/Mass Spectroscopy (GC/MS). The other three parts were spiked with different quantities of phthalates, as shown in Table 1, and the spiked samples were analyzed by using the same

Table 1. Effect of phthalates on PCBs analysis

Weight-Percent of Phthalates added	PCBs Concentration (ppm) by GC/ECD	PCBs Concentrations (ppm) by GC/MS
0	4.6+/-0.3	7.9+/-1.0
0.5	4.7+/-0.3	7.4+/-0.2
1.0	5.1+/-0.6	7.0+/-0.4
2.5	4.8+/-0.3	7.4+/-0.3

two methods. The results show no apparent interference of the phthalates in the PCBs analysis.

To investigate the effects of plastics particle size on extraction efficiency of PCBs, a series of laboratory experiments were conducted at TPI on 300-g samples of plastics with two different particle sizes (one made of chips about 0.2 inch in size and the other was granulated to about 0.04 to 0.08 inch in size). Typically in PCBs analyses, extractions are done on a few grams of material, even though the dirt, oil, and the PCBs are not evenly distributed on the shredder residue plastics.

Samples of the plastics before and after washing were analyzed directly by three different laboratories by using standard PCBs analytical procedures. Extracts from nine sonications of 300-g samples were also analyzed for PCBs by three laboratories. The results (Tables 2–5) show that:

The three labs are fairly consistent for each set of samples.

1. Direct analysis of the samples from the three labs showed that the concentration of PCBs in the granulated plastics was about 5 ppm, and for the un-granulated, it was 10 ppm. Obviously, the granulated samples have larger surface area per unit mass than the other samples. Therefore, more efficient extraction of PCBs from the plastics would be expected in the case of the granulated chips. Because this was not the case, the results indicate that the particle size does not affect the PCB results. Further, the results indicate that the PCBs are on the surface of the plastics and not absorbed in the plastics. After extraction, the samples all had less than 2 ppm of PCBs, except for one sample that showed 2.8 ppm.
2. Calculation of the concentration of PCBs in the original samples based on the determined PCBs in the hexane extracts (prepared via 9 sonications of 300-g samples) showed that the concentrations of PCBs in the granulated samples were comparable with those of the ungranulated samples. These results further indicate that the PCBs are predominantly on the surface of the plastics and not absorbed in the plastics, otherwise the granulated samples would have shown higher concentrations.

In addition, two of the laboratories identified Aroclor 1242 as the only PCB present, while the third laboratory identified Aroclors 1232 and 1254 as the only two present. Each of these Aroclors consists of multiple congeners.

TPI also conducted an analysis of various plastics samples by using GC-ECD and GC-MS methods. The results are compared in Table 6. Results from the two methods are in reasonable agreement, even though the GC-MS method seems to consistently predict higher values.

Evaluation of Soxhlet Method for PCBs Extraction

Successful commercialization of technology for recovering polymers and other materials from shredder residue depends on a reliable and inexpensive technique to analyze samples for PCBs in the recovered polymers in the field. The U.S. EPA and European protocols for PCBs analysis were reviewed and experiments were conducted to gain a good understanding of the requirements for reliable on-site analysis. A Soxhlet-based method appears to be appropriate for testing because of its simplicity and because it is among the methods specified in both the U.S. EPA protocols and in the European protocols (Table 7). Experiments to define the operating conditions for the Soxhlet method were conducted. The results are discussed below.

Selection of a Solvent

Two solvents were tested: hexane and toluene. Three 120-g samples were extracted with hexane for 8 h, and another three 120-g samples were extracted with hexane for 24 hours. Similarly, three 120-g samples were extracted with toluene for 8 h, and another three 120-g samples were extracted with toluene for 24 hours. All extractions were carried out while maintaining the siphoning time at 8- to 10-minute intervals. This procedure resulted in 24 samples of extracts and 12 samples of extracted plastics that were analyzed. The results are summarized in Table 8. The results indicate that hexane is a better solvent because it resulted in less PCBs remaining in the extracted plastics.

Table 2. Concentration of PCBs (ppm) in plastics before and after extraction with hexane (granulated and ungranulated) — analysis by standard PCBs analysis procedures

	Aroclor 1232	Aroclor 1242	Aroclor 1254	Total
Designation	ppm	ppm	ppm	ppm
	Laboratory #1			
Ungranulated before extraction	10.34 +/-1.53	N/D	1.27 +/- 0.29	11.6 +/- 1.51
Ungranulated after extraction	1.06 +/- 0.32	N/D	0.07 +/- 0.01	1.13 +/- 0.32
Granulated before extraction	4.54 +/- 0.84	N/D	0.06 +/- 0.16	5.14 +/- 0.98
Granulated after extraction	0.54 +/- 0.33	N/D	0.07 +/- 0.01	0.60 +/- 0.34
	Laboratory #2			
Ungranulated before extraction	N/D	8.69 +/- 1.02	N/D	8.69 +/- 1.02
Ungranulated after extraction	N/D	2.8 +/- 0.98	N/D	2.8 +/- 0.98
Granulated before extraction	N/D	5.31 +/- 2.04	N/D	5.31 +/- 2.04
Granulated after extraction	N/D	0.75 +/- 0.18	N/D	0.75 +/- 0.18
	Laboratory #3			
Ungranulated before extraction	N/D	9.93 +/- 4.67	N/D	9.93 +/- 4.67
Ungranulated after extraction	N/D	1.57 +/- 0.17	N/D	1.57 +/- 0.17
Granulated before extraction	N/D	3.07 +/- 0.26	N/D	3.07 +/- 0.26
Granulated after extraction	N/D	0.68 +/- 0.27	N/D	0.68 +/- 0.27

Table 3. Concentration of PCBs in the ungranulated samples, as calculated from the analysis of the hexane solution extracts

	Aroclor 1232	Aroclor 1242	Aroclor 1254	Total
Designation	ppm	ppm	ppm	ppm
	Laboratory #1			
Extract 1	8.67 +/- 0.87	N/D	1.02 +/- 0.29	9.69 +/- 0.99
Extract 2	4.59 +/- 1.52	N/D	0.28 +/- 0.05	4.86 +/- 1.49
Extract 3	0.51 +/- 0.09	N/D	0.14 +/- 0.01	0.65 +/- 0.10
Total	**13.76 +/- 2.47**	**N/D**	**1.43 +/- 0.34**	**15.19 +/- 2.57**
	Laboratory #2			
Extract 1	N/D	7.62 +/- 0.58	N/D	7.62 +/- 0.58
Extract 2	N/D	1.44 +/- 0.04	N/D	1.44 +/- 0.04
Extract 3	N/D	0.62 +/- 0.04	N/D	0.62 +/- 0.04
Total	**N/D**	**9.67 +/- 0.65**	**N/D**	**9.67 +/- 0.65**
	Laboratory #3			
Extract 1	N/D	6.56 +/- 0.67	N/D	6.56 +/- 0.67
Extract 2	N/D	1.52 +/- 0.23	N/D	1.52 +/- 0.23
Extract 3	N/D	0.64 +/- 0.03	N/D	0.64 +/- 0.03
Total	**N/D**	**8.71 +/- 0.92**	**N/D**	**8.71 +/- 0.92**

Table 4. Concentration of PCBs in the granulated samples, as calculated from the analysis of the hexane solution extracts

	Aroclor 1232	Aroclor 1242	Aroclor 1254	Total
Designation	ppm	ppm	ppm	ppm
	Laboratory #1			
Extract 1	18.62 +/- 8.99	N/D	2.20 +/- 0.61	20.81 +/- 9.59
Extract 2	2.30 +/- 2.56	N/D	0.25 +/- 0.06	4.86 +/- 1.49
Extract 3	0.62 +/- 0.14	N/D	0.11 +/- 0.01	0.65 +/- 0.10
Total	**21.52 +/- 11.69**	**N/D**	**2.55 +/- 0.67**	**24.07 +/- 12.25**
	Laboratory #2			
Extract 1	N/D	7.24 +/- 0.34	N/D	7.24 +/- 0.34
Extract 2	N/D	1.01 +/- 0.03	N/D	1.01 +/- 0.03
Extract 3	N/D	0.42 +/- 0.03	N/D	0.42 +/- 0.03
Total	**N/D**	**8.67 +/- 0.40**	**N/D**	**8.67 +/- 0.40**
	Laboratory #3			
Extract 1	N/D	6.29 +/- 1.98	N/D	6.29 +/- 1.98
Extract 2	N/D	1.10 +/- 0.06	N/D	1.10 +/- 0.06
Extract 3	N/D	0.48 +/- 0.03	N/D	0.48 +/- 0.03
Total	**N/D**	**7.87 +/- 2.06**	**N/D**	**7.87 +/- 2.06**

Table 5. Comparison of PCBs concentration (ppm) in the starting plastics samples by direct analysis and by calculation based on the amounts in the hexane extracts

Plastics Sample	PCB Concentration by Direct Analysis	PCB Concentration Calculated from PCBs in the Hexane Extracts
Ungranulated, Lab-1	11.6 +/- 1.51	15.19 +/- 2.57
Ungranulated, Lab-2	8.69 +/- 1.02	9.67 +/- 0.65
Ungranulated, Lab-3	9.93 +/- 4.67	8.71 +/- 0.92
Granulated, Lab-1	5.14 +/- 0.98	24.07 +/- 12.25
Granulated, Lab-2	5.31 +/- 2.04	8.67 +/- 0.4
Granulated, Lab-3	3.07 +/- 0.26	7.87 +/- 2.06

Table 6. Comparison of PCBs analysis using GC-ECD and GC-MS methods (extraction was carried out using hexane at 2,000 PSIA and 100°C)

Sample Type	PCB Concentration, Using GC-ECD (ppm)	PCB Concentration, Using GC-MS (ppm)
Ungranulated Chips	7.55	9.67
Ungranulated Chips	3.70	5.07
Ungranulated Chips	1.50	3.3
Ungranulated Chips	1.35	2.66
Granulated Chips	7.56	9.37
Granulated Chips	0.93	1.82
Granulated Chips	0.82	2.11
Hexane Solution	9.93	9.50
Hexane Solution	8.3	11.13
Hexane Solution	1.41	1.72
Hexane Solution	0.78	0.92
Hexane Solution	0.53	0.65

Table 7. Protocols for PCBs analysis

Parameter	European Protocols	U.S. EPA's Protocols	Recommended Protocols
Particle size (mm)	0.5	Not specified	1
Sample size for extraction (g)	3	30	30
Extraction equipment	Soxhlet	Sonication Soxhlet Pressurized fluid	Soxhlet
Extraction time	Not specified	Not specified	>/= 4 h Siphoning cycles at 8–10-min intervals
Solvent	Toluene	Hexane 50/50 Hexane/acetone 50/50 Methylene chloride/acetone	Hexane
Analytical method	MS	GC/ECD MS	MS
Quantification method	6 congeners multiplied by 5	Aroclors	Aroclors

Table 8. Results of the extractions of the 120-g samples with hexane and toluene

Solvent	Extraction Time (h)	Average PCBs in Extract (ppm)	Standard Deviation (ppm)	Average PCBs in Extracted plastics (ppm)	Standard Deviation (ppm)
Hexane	24	9.4	1.5	N.D	0
Hexane	8	9.3	0.8	N.D.	0
Toluene	24	9.8	2.4	1.4	0.2
Toluene	8	9.7	0.9	3.0	0.6
Hexane	4	14.5	2.9	N.D. in samples no. 1 and 2; 1.0 in no. 3	1.0

Determination of Extraction Time

In addition to the experiments discussed above, three additional 120-g samples were extracted with hexane for 4 hours each. This procedure resulted in six samples of extracts and three samples of extracted plastics that were analyzed. The results are also given in Table 8 and indicate that a Soxhlet extraction time of 4 hours is adequate because it reduced the PCBs concentration in the extracted plastics to below the detectable limits in two of the three samples and reduced it in the third to 1 ppm, even though these samples apparently had more PCBs initially as evidenced by the higher level of PCBs in the solvent.

Determination of Adequate Sample Size

In addition to the six 120-gram samples extracted for 24 hours discussed above, six additional 60-gram samples and six additional 30-g samples were processed and sampled in the same manner as before (24-hour extraction time and same siphoning intervals) by using hexane. The results are summarized in Table 9. The results indicate that a sample size of 30 g appears to be adequate.

Sample preparation was also investigated. The results indicated that a well-mixed plastics sample of at least one pound should be granulated to a size of 1 mm and mixed before sampling and analysis is done.

Comparison of the U.S. EPA and the European Quantification Methods

Four of the extracts from the 120-g samples that were extracted with hexane for 24 hours and two of the 120-g samples that were extracted with hexane for 8 hours were also quantified by using the European method. The results were essentially identical within analytical errors (Table 10).

These results lead to the following conclusions:

1. A conventional Soxhlet extractor using hexane is effective for PCBs extraction from plastics.
2. A total extraction time of 4 hours with siphoning intervals of 8–10 min is adequate for complete extraction of the PCBs.
3. The EPA and the European quantification methodologies yield very close results.
4. This method is simple enough to be adopted for field applications.

Publications

Overview of Washing Systems for Commercial Cleaning of Plastics Separated from Automotive Shredder Residue, Sendijarevic, I.; Sendijarevic, V.; Winslow, G.R.; Duranceau, C.M.; Simon, N.L.; Niemiec, S. F.; and Wheeler, C.S., SAE Paper No. 2005-01-0851.

Screening Study to Evaluate Shredder Residue Materials, Sendijarevec, V.; Simon, N.; Duranceau, C.; Winslow, G.; Williams, R.; Wheeler, C.; Niemiec, S.; and Schomer, D., SAE Paper No. 2004-01-0468.

Table 9. Results of the 24-h extractions with hexane of different size samples

Sample size (g)	Average PCBs in Extract (ppm)	Standard Deviation (ppm)	Average PCBs in Extracted Plastics (ppm)	Standard Deviation (ppm)
30	10.8	1.9	N.D	0
60	25.5	12.6	N.D.	0
120	9.4	1.5	N.D.	0

Table 10. Comparison of the U.S. EPA and the European quantification methods

Extraction Time (h)	PCBs According to the EPA Method (ppm)	PCBs According to the European Method (ppm)
24	10.8	9.8
24	9.8	10.9
24	8.0	10.7
24	11.2	11.5
8	11.7	12.3
8	10.8	10.8

D. Compatibilization/Compounding Evaluation of Recovered Polymers

Principal Investigator: Bassam Jody
Argonne National Laboratory
9700 S. Cass Ave., Argonne, IL 60439
(630) 252-5279; fax: (630) 252-1342; e-mail: bjody@anl.gov

Field Project Manager: Edward J. Daniels
Argonne National Laboratory
9700 S. Cass Ave., Argonne, IL 60439
(630) 252-4206; fax: (630) 252-1342; e-mail: edaniels@anl.gov

Technology Area Development Manager: Joseph A. Carpenter
(202) 586-1022; fax: (202) 586-1600; e-mail: joseph.carpenter@ee.doe.gov
Field Technical Manager: Philip S. Sklad
(865) 574-5069; fax: (865) 576-4963; e-mail: skladps@ornl.gov

Participants:
This project is conducted as part of a Collaborative Research and Development Agreement (CRADA) between DOE's Argonne National Laboratory, USCAR's Vehicle Recycling Partnership, and the American Plastics Council.
CRADA Partner Principal Investigators:
Michael Fisher, American Plastics Council, (703) 741-5599; e-mail: mike_fisher@plastics.org
Gerald Winslow, VRP, DaimlerChrysler Corp., (248) 512-4802; e-mail: grwx@DCX.com
Claudia Duranceau, VRP, Ford Motor Co., (313) 390-0504; e-mail: cdurance@ford.com
Candace Wheeler, VRP, General Motors Corp., (586) 986-1674; e-mail: candace.s.wheeler@gm.com

---

Contractor: Argonne National Laboratory
Contract No.: W-31-109-Eng-38

Objectives

- Evaluate the market opportunity for polymers recovered from shredder residue.
- Identify limitations associated with the reuse of the materials as recovered and determine the need for post-processing technology to upgrade the recovered materials to meet the requirements of the market.

Approach

- Specify standard protocols for material testing, content characterization, and performance properties.
- Determine properties of recovered polymers.
- Conduct blending and pelletizing trials of the recovered polymers.
- Conduct mold trials using recovered polymers.

Accomplishments

- Molded auto parts using recovered polypropylene/polyethylene (PP/PE).
- Conducted blending and pelletizing trial.
- Determined physical properties of PP/PE recovered from shredder residue.

- Found that PP/PE recovered by the Argonne process and the Salyp (sink/float) process and recovered in U.S. field trials exhibit equivalent physical properties that are reasonably consistent with those of many virgin PP formulations and co-polymers.
- Compiled a database of physical properties of virgin polymers for comparison with the physical properties of recovered plastics.
- Established a test protocol for material testing, content characterization, and physical properties testing of polymeric materials.

Future Direction

- Continue physical properties testing of recovered polymers.
- Evaluate the market potential for clean mixed plastics streams recovered from shredder residue.
- Update the database of properties of recovered polymers vis-à-vis general purpose virgin polymers.
- Identify candidate automotive applications for recovered polymers.
- Conduct more blending, pelletizing, compounding, and mold trials by using recovered polymers.

Summary

The objectives of this project are (1) to characterize the properties of potentially recyclable automotive materials and (2) to confirm the technical and economic feasibility of using those materials in value-added applications.

The project will initially focus on establishing the properties of polymeric materials that are recovered as part of the Post-Shred Materials Recovery Technology Development and Demonstration project (see report 7.E).

Regardless of the effectiveness of any automotive materials recovery technology, the materials that will be recovered will be, on average, at least 10 to 15 years old. In this project, the performance properties of recovered polymers will be compared vis-à-vis new or virgin materials to establish a database of the properties of recovered automotive polymers. At present, there are few data about the physical properties of polymers recovered from postconsumer durable goods. Absent such data, it is unlikely that sustainable applications for recycled materials will be either identified or developed.

Physical properties testing has been conducted by Midland Compounding, Inc. Midland also conducts composition testing, the results of which are compared with the results of compositional analysis done on recovered materials by Argonne.

Blending and pelletizing of the PP/PE recovered from shredder residue by Argonne has been tested by Palmer Plastics, Inc. More blending and compounding tests will be done, as required, to achieve the desired performance properties of the recovered materials for target applications.

Mold trials using the recovered PP/PE were also done by MGV Enterprises. More molding tests are planned to confirm the technical and economic feasibility of using recycled polymers in specific applications.

Three additional companies — Collins and Aikman Corporation, Enviro-Plas Corporation, and Mayco Plastics, Inc. — have agreed to evaluate, compound, and run mold trials by using recovered materials, subject to the physical properties of the recovered materials.

Polymer Physical Properties and Materials Composition Analysis

Typically, 10-lb samples of recovered materials are used to define physical properties and to characterize the composition of the material.

To quantify the physical properties of the recovered material, a sample is extruded on a single-screw extruder, melt screened through a 40-mesh screen, molded into American Society for Testing and Materials (ASTM) test bars and plaques, and tested. The molded parts and a random selection of regrind

chips from each sample are evaluated for material identification by using infrared spectroscopy.

Physical properties that are measured for each sample include the following:

- Melt flow rate (MFR),
- Izod impact,
- Flexural modulus,
- Tensile strength at yield,
- Tensile strength at rupture,
- Elongation at yield,
- Elongation at rupture,
- Deflection temperature under load (DTUL),
- Gardner impact, and
- Specific gravity (SG).

The physical properties of PP/PE recovered from different shredder residues by Argonne and by Salyp were determined for several samples. The results for the Argonne materials are given in Table 1. Properties of commercially-available PP and PE virgin resins and for PP from dismantled automobiles are presented in Table 2 for comparison. The Izod impact of the recovered material is about three times that of the virgin resins, while the tensile strength of the recovered material is lower than the tensile strength of the virgin resins by about 30%. This phenomenon may be attributed, at least in part, to the presence of thermoplastic olefins (TPO) and rubber in the recovered material, which act as impact modifiers. Recovered samples 8, 9, and 10 listed in Table 1 contained about 2% rubber, while samples 1 through 7 contained about 4% rubber.

The results for the more than 20 PP/PE samples recovered by Salyp from different European and U.S. shredder residues are given in Table 3. The properties of the Salyp-recovered PP/PE are equivalent to the properties of the Argonne-recovered PP/PE.

Polymer Physical Properties Database

A physical properties database has been compiled so that the physical properties of the recovered polymers can be compared with general purpose virgin polymers.

General purpose physical properties have been compiled for the following plastics:

- ABS,
- Nylon (6 cast, 6/6 extruded, 30% glass filled),
- PPO [polyphenylene oxide] (unfilled, 30% glass filled),
- Polycarbonate,
- Polyethylene, low-density polyethylene [LDPE], high-density polyethylene [HDPE], ultra-high-molecular-weight [UHMW] polyethylene,
- Polypropylene,
- Polystyrene (general purpose, high impact), and
- Polyvinyl chloride (PVC).

The Vehicle Recycling Partnership had previously compiled physical properties data on selected polymers that were recovered during the U.S. field trials (see ** in Table 2). These materials were recovered by disassembly. The data from these polymers will also be included in the database so that the physical properties of materials recovered by disassembly can be compared with those of materials that are recovered from post-shred operations.

Blending and Pelletizing of Recovered PP/PE

250 pounds of PP/PE recovered by Argonne were blended with 750 lbs. of supplemental PP copolymer regrind for 15 minutes. The blended material was then run through an extruder and pelletized. The general appearance of the final pellet was excellent (Figure 1). Properties of the recovered material used in blending and the properties of the regrind and of the resulting pellets are shown in Table 4. Standard pelletizing conditions were used. Barrel heats were set from 365°F at the rear barrel zone and increased progressively to 390°F at the front, with six heat zones in between. Screen-changer and breaker- plate heats were set at 405°F, and die heats were set at 395°F. Melt temperature was recorded as 460°F, and drive load and screw speed were set at 60% and 67.5% of the maximum values, respectively. Material output was recorded as 1,400 lb/h. Extra-fine screen packs were used (20/20/20/60/100/20 mesh screens) to remove impurities because this was the first time this material has been tried.

Table 1. Properties of PP/PE recovered by Argonne from different shredder residues.

Property	Sample 1	Sample 2	Sample 3	Sample 4	Sample 5	Sample 6	Sample 7	Sample 8	Sample 9	Sample 10	Average
MFR, g/10min, 230°C, 2.16 kg	10.5	14.9	7.7	10.1	11.4	7.2	8.7	7.2	8.7	7.2	9.4
Izod impact, ft-lb/in., 73°F	12.3	10.5	11.9	10.8	9	10.7	13.2	1.7	2.8	3.3	8.6
Flex mod., 1% secant, 1,000 psi	83	73	89	84	82	101	112	126	127	113	99.0
Tensile strength at yield, 1,000 psi	2.6	2.2	2.7	2.6	2.4	2.8	3.1	3.4	3.3	3.1	2.8
Tensile strength at rupture, 1,000 psi	0.8	1.2	2.1	1.9	1.4	2.5	2.0	3.1	3.1	2.9	2.1
Elongation at yield, %	23.0	20.8	21.1	22.8	20. 6	20. 6	17.1	**	**	**	24.3
Elongation at rupture, %	132	78	233	154	82	251	229	12	14	13	119.8
DTUL (F), at 66 psi	131	131	134	134	138	147	155	**	171	160	145
Gardner impact, 73°F, in.- lb	104	88	136	96	56	144	184	20	32	40	90.0
SG, g/cc	0.94	0.95	0.94	0.95	0.94	0.93	0.93	0.94	0.94	0.94	0.94

** Not tested

Table 2. Comparison of recovered PP/PE with commercial grades of PP & PE (Boedeker) (http://www.boedeker.com/mtable.htm), unless specified otherwise.

Property	PP-Homo Polymer	PP-Co Polymer	PP-FR	Dismantled PP**	Standard PP-Co	LDPE	HDPE
MFR, (g/10 min), 230°C	0.5-136*			17			
Izod impact, ft-lb/in.	1.9	7.5	0.65	1.8	0.7	No Break	3
Flex Mod, 1,000 psi	180	160	145	131.9	120	200	125
Tensile Strength, 1,000 psi	4.8	4.8	4.3	3.1	5.2	2.0	4.6
Elongation, %	12	23	28	18	600	600	900
DTUL (F), at 66 psi	210	173	106	136.5	210	110	--
SG, g/cc	0.905	0.897	0.988		0.90	0.92	0.95
Gardner impact, 73°F, in.- lb	0.9-22*						

* Data from http://www.ed-cam.com/materials/propylene_molded.asp. Ranges are for with and without additives.

** Gallmeyer, W.W.; Duranceau, C.M.; Williams, R.L.; and Winslow, G.R., USCAR U.S. Field Trial for Automotive Polymers Recycling, SAE paper # 2003-01-0645, 2003.

Table 3. Properties of PP/PE recovered by Salyp from different shredder residues.

Property	Salyp Data
MFR (g/10 min), 230°C	2.3–4.6
Izod impact (ft-lb/in.) 73°F	4.7–13.3
Flex mod., 1%, secant, 1,000 psi	81.7–116.5
Tensile strength at yield, 10,00 psi	2.4–2.9
Tensile strength at rupture, 1000 psi	2.2–2.8
Elongation at rupture, %	19–57
DTUL (F), at 66 psi	150–169
Gardner impact, 73°F, in.-lb	190–240
SG, g/cc	0.93

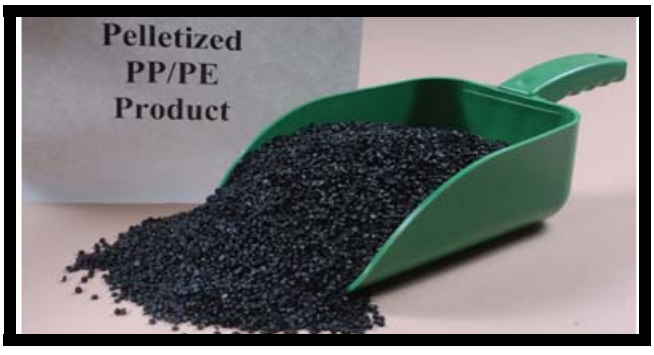


Figure 1. Pelletized PP/PE product recovered from shredder residue.

Table 4. Properties of recovered PP/PE when mixed with regrind.

Property	Argonne, As Recovered Sample 9 (see Table 1)	Regrind, As Is	Pelletized Blend
MFR (g/10 min), 230°C	8.7	3.1	9.2
Izod impact (ft-lb/in.) 73°F	2.8	13.6	10.4
Flex mod., 1%, secant, 1,000 psi	127	157	136
Tensile strength at yield, 1,000 psi	3.3	3.7	3.4
Tensile strength at rupture, 1,000 psi	3.1	2.9	2.3
Elongation at rupture, %	14	125	57
DTUL (F), at 66 psi	171	197	176
Gardner impact, 73°F, in.-lb	32	>320	132
SG, g/cc	0.94	0.91	0.92

In addition, while screen changes are typically performed at pressure differences between 500 psi and 1,000 psi, in this test, changes were performed when the pressure exceeded 500 psi to safeguard against puncturing a screen pack and losing material. Because extra-fine screen packs were used in the test, screen changes were required approximately every five minutes. The results indicated that the recovered PP/PE can be blended with other olefinic regrind and pelletized by using standard processes and equipment.

Mold Trials

Three types of auto parts were molded by MGV Enterprises by using Argonne-recovered PP/PE from shredder residue: knee bolsters, battery trays, and steering column covers (Figure 2). A standard molding machine was used in these trails (Figure 3). No changes to the standard conditions were required to run the recovered material. The limited testing done on the recovered PP/PE fraction shows that quality products, including auto parts, may be produced from the recovered materials. Additives and/or modifiers may be added to meet the specifications of some products.

Recovered Rubber/Plastics Material

A mixed-rubber fraction with about 20% by weight mixed plastics was recovered. A sample of the recovered material was sent for testing by the "TireCycle" process used for recycling rubber. Preliminary tests done on the recovered material indicated that it may be suitable for making construction products, such as roofing shingles. The presence of the plastics in the mixed-rubber material appeared to improve its overall properties, especially its stiffness.

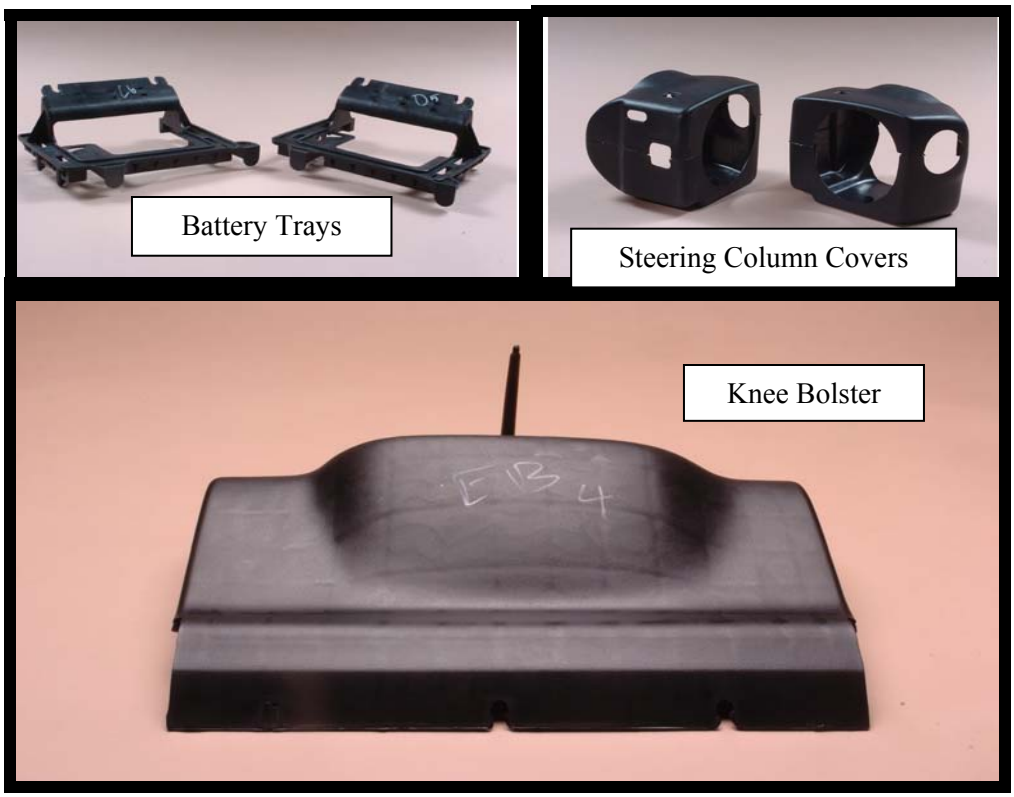


Figure 2. Auto parts molded from PP/PE recovered from shredder residue.



Figure 3. Standard molding machine used in molding auto parts using recovered PP/PE.

E. Post-Shred Materials Recovery Technology Development

Principal Investigator and Field Project Manager: Edward J. Daniels
Argonne National Laboratory
9700 S. Cass Ave., Argonne, IL 60439
(630) 252-5279; fax: (630) 252-1342; e-mail: edaniels@anl.gov

Technology Area Development Manager: Joseph A. Carpenter
(202) 586-1022; fax: (202) 586-1600; e-mail: joseph.carpenter@ee.doe.gov
Field Technical Manager: Philip S. Sklad
(865) 574-5069; fax: (865) 576-4963; e-mail: skladps@ornl.gov

Participants:
This project is conducted as part of a Collaborative between DOE's Argonne National Laboratory, USCAR's Vehicle Recycling Partnership, and the American Plastics Council.
CRADA Partner Principal Investigators:
Michael Fisher, American Plastics Council, (703) 741-5599; e-mail: mike_fisher@plastics.org
Gerald Winslow, VRP, DaimlerChrysler Corp., (248) 512-4802; e-mail: grwx@DCX.com
Claudia Duranceau, VRP, Ford Motor Co., (313) 390-0504; e-mail: cdurance@ford.com
Candace Wheeler, VRP, General Motors Corp., (586) 986-1674; e-mail: candace.s.wheeler@gm.com

Changing World Technologies is cost-sharing on the evaluation of its thermal depolymerization process.
The Polyurethanes Recycle and Recovery Council (PURCC) is also participating and cost-sharing on the evaluation of the Troy Polymers, Inc., polyurethane glycolysis process.

Contractor: Argonne National Laboratory
Contract No.: W-31-109-Eng-38

Objective

- Develop technology for the cost-effective recovery of materials from post-shred residues.

Approach

- Characterize shredder residue from a number of sources to determine composition variability.
- Conduct bench-scale and large-scale process/technology tests to benchmark technology.
- Build and operate a pilot-plant for the separation of shredder residue to produce recovered materials for market evaluation and to provide "control" samples of materials for testing of alternative technologies, as appropriate.
- Conduct cost and performance analysis of alternative technologies to establish the business case for the technologies and to identify technology gaps.

Accomplishments

Mechanical Separation of Shredder Residue

- Processed over 160,000 lbs of shredder residue in Argonne's mechanical separation pilot-plant. Over 50,000 lbs of plastics concentrate were produced. Construction of the plant was completed in the first quarter of FY 2004, and shakedown of the facility occurred during the second and third quarters.
- Increased, through process improvements, yield of polymer concentrate from as low as 40% to 95%.
- Performed mass balance on the process and characterized the shredder residue and the polymer concentrate. Ten shredder residues, including two European and eight United States, were characterized.

Froth Flotation Process for Recovering Plastics

- Completed construction and shakedown of a six-stage froth-flotation plastics separation plant in the first quarter of FY 2005 and started froth-flotation separation trials.
- Recovered over 3,500 lbs of polyolefins (polypropylene [PP] and polyethylene [PE]) product.
- Completed a series of tests to define density distributions and settling velocities of polymers and other materials present in the polymer concentrate.
- Upgraded process to isolate unexpected high content of wood and rubber in the plastics concentrate.

Thermal/Chemical Conversion Processes

- Completed bench-scale and pilot-scale batch testing of Changing World Technologies' (CWT's) thermal depolymerization process for converting shredder residue to fuels.
- Conducted testing in a five-gallon reactor of Troy Polymer, Inc.'s (TPI's) glycolysis process for conversion of urethane foam to polyol initiators. Over 1,200 lbs of foam were used, and over 100 gallons of polyol initiators were produced.

Other Accomplishments

- Completed large-scale tests of Salyp's "thermoplastics sorting" technology by using residue from two European locations and one U.S. location as feed materials.
- Developed an Excel-based process cost model that incorporates two primary modules for the recovery of automotive plastics: the first module includes the unit operations required for recovering a plastics concentrate from shredder residues, and the second module includes the unit operations required to recover selected plastics from the mixed plastics concentrates.

Future Direction

- Continue Argonne froth-flotation campaigns and evaluate process performance and economics; define path forward.
- Complete CWT thermal depolymerization process evaluation; define path forward.
- Complete Polyventure/TPI glycolysis process evaluation; define path forward.
- Test and evaluate the Volkswagon/Sicon (VW/Sicon) technology for separating plastics from shredder residue.
- Update process cost analysis model.
- Review/critique technology developments with representatives of the automotive shredding industry..

Summary

The objective of this project is to develop technology for the cost-effective recovery of materials from post-shred residues. Research will provide data essential to establishing a business case for sustainable recycling of automotive materials from post-shred residue. A wide range of materials recovery technologies is at various stages of development worldwide. Technologies specific to the recovery of materials from post-shred material streams are being evaluated and demonstrated to determine their commercial viability. The performance (e.g., yield, purity, efficiency, and cost) of these emerging technologies will be determined to enable the development of an integrated process for recovering materials from shredder residue.

Research has been completed on the Salyp physical separation/thermosorting process and on Argonne's physical separation process. Research is ongoing on the Argonne froth-flotation process, the Changing World Technologies (CWT) thermal depoly-merization process, and the Polyventure/Troy Polymers process for glycolysis of urethane foam.

Characterization of Shredder Residue

To facilitate the development of technology for the recovery of materials and resources from shredder residue, MBA Polymers characterized five shredder

residues (two European and three American) by using 2-kg samples. The analysis showed significant variations in these samples. For example, the fines in these fractions ranged between 5% and 38%, and foam in the samples ranged between 21% and 37%, which is about four to seven times what is expected for polyurethane foam. These differences are due to a large extent to the small size of the samples used and demonstrate the difficulty in sampling the heterogeneous shredder residue. After processing over 80 tons of shredder residues from five different U.S. shredders in Argonne's mechanical separation plant, which is described in the next section, we observed (Figure 1):

- Large variations in non-plastic materials (e.g., fines, residual metals, rubber and wood) and
- Less-significant variation in the composition of the polymer fraction.

In addition, the polymer concentrate separated from different shredder residues showed, for the most part, little variation (Figure 2), and the weight percent (wt%) of the polymer concentrate recovered from a given source over a six-month period was reasonably consistent (Table 1).

Argonne Pilot-Plant

Argonne's pilot plant consists of two major facilities. The first is a mechanical (physical) separation facility; the second is a wet-density/froth-flotation separation facility. The pilot-plant was used to:

1. Recover materials from shredder residue,
2. Conduct process improvement/integration studies,
3. Provide a capability to produce large samples of recovered materials for market evaluation,
4. Define the effectiveness of alternative separation technologies and systems, and
5. Serve as a user/demonstration facility to conduct separation tests for residue from specific sources.

The mechanical separation facility is shown in Figure 3. The mechanical separation facility processes the raw shredder residue to yield a polymer concentrate and other fractions, as shown in Figure 1.

The wet density/froth-flotation facility is shown in Figure 4. It includes six continuous stages for the separation and recovery of targeted materials from the polymer concentrate derived from shredder residue. Its design capacity is 1,000 lb of mixed plastics per hour.

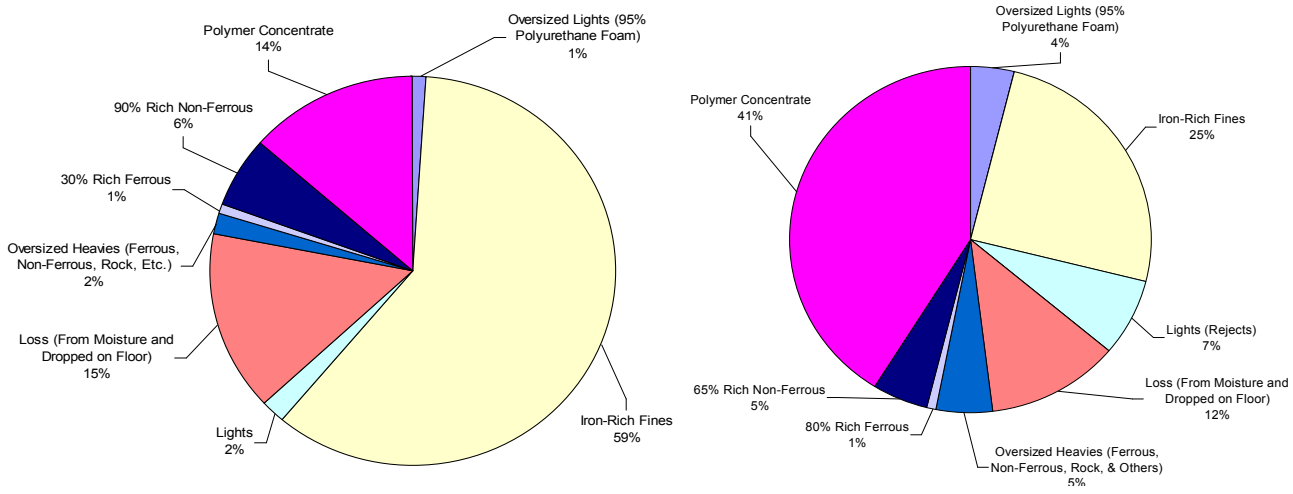


Figure 1. Comparison of shredder residue composition from two shredders.

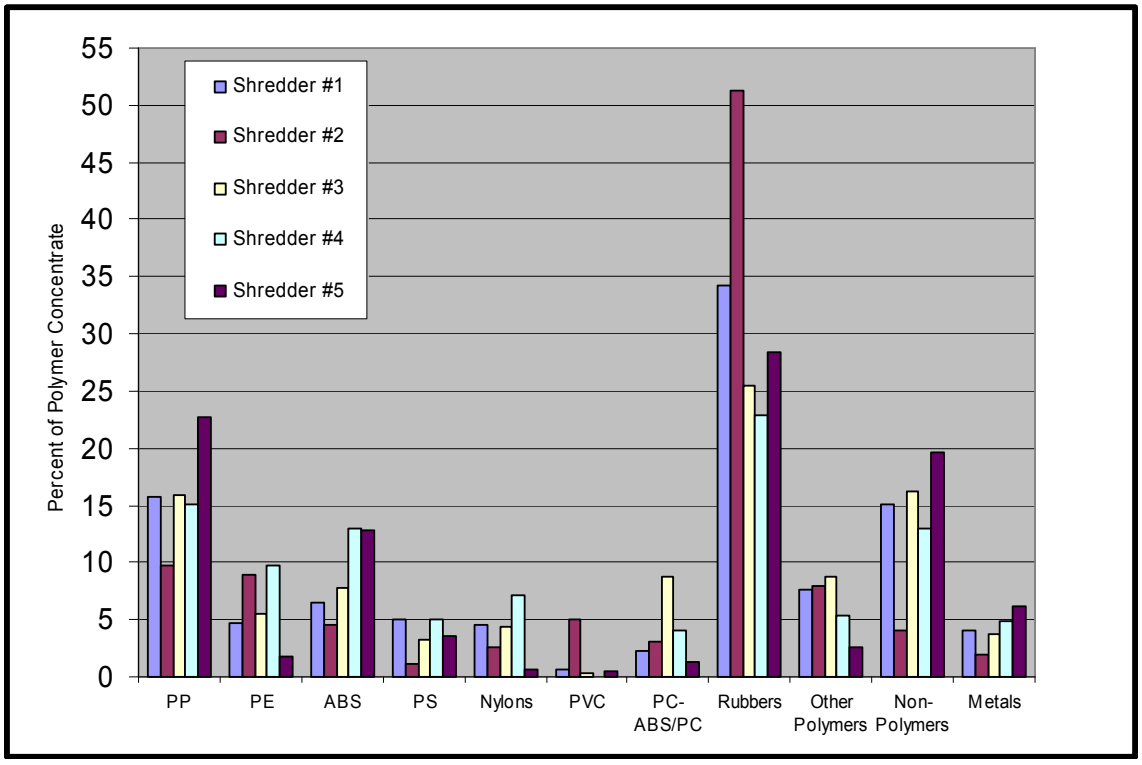


Figure 2. Similarity in composition of polymer concentrate from different shredders.

Table 1. Variability of yield of polymer concentrate from a given source over a six-month period

Run #	Polymer Concentrate (wt%)	Run #	Polymer Concentrate (wt%)
2	41	6	45
3	26	7	37
4	36	8	43
5	39	9	45
		Average	40

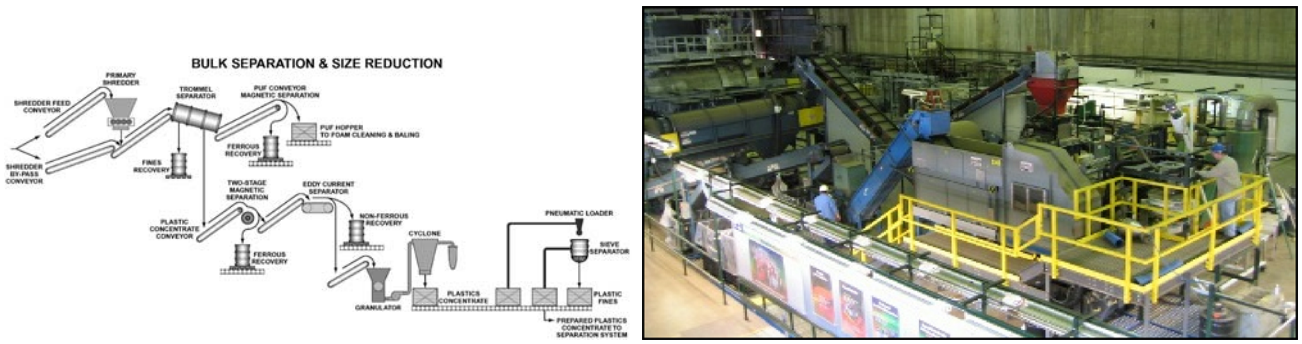


Figure 3. Argonne pilot mechanical separation system for processing raw shredder residue.

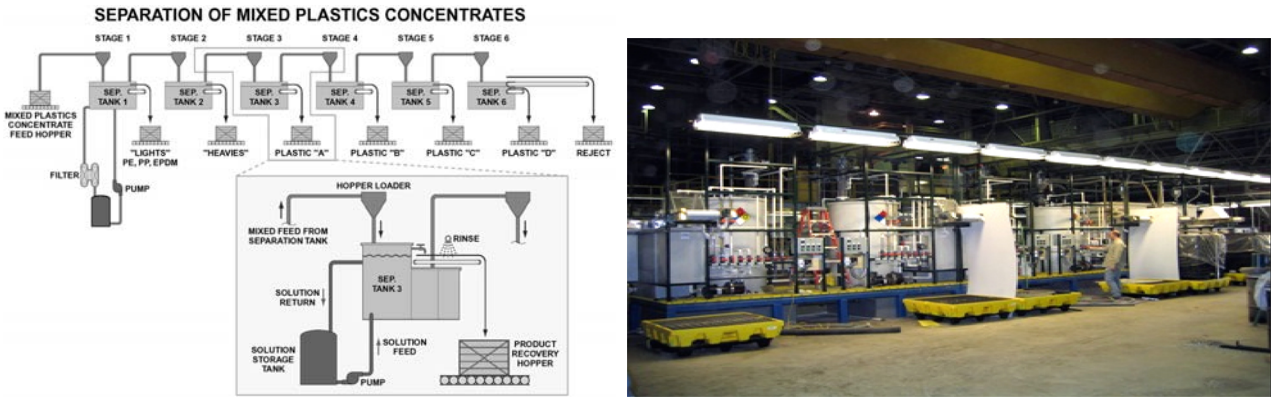


Figure 4. Argonne pilot wet separation system for recovery of plastics from shredder residue.

Mechanical Separation Pilot-Plant

Initially, six campaigns totaling 60,000 lbs of shredder residue were undertaken to debug and shake down the mechanical separation pilot-plant. The average yield of polymer concentrate recovered from these campaigns was only about 17% of the total weight of the shredder residue. This yield was significantly lower than anticipated. Analysis of the various separated streams showed that the recovery of the polymers from shredder residue in the polymer concentrate fraction was also low (40–70%) for the different source materials. As a result, a loss analysis was undertaken. The analysis included sampling and quantification of residual polymers in each of the fractions that are generated in the bulk processing of shredder residue to recover the polymer concentrate. On the basis of this loss analysis, minor process modifications were made, and some of the fractions were reprocessed. As a result, the yield of plastics concentrate more than doubled.

Loss analyses were also conducted on the various non-polymer concentrate fractions after the modifications were made. These analyses indicated that the recovery of polymers targeted for recovery in the polymer concentrate was about 95% of those polymers available in the shredder residue. Although the yield of the polymers targeted for recovery in the polymer concentrate was about 95%, the polymer concentrate also included an unexpectedly high and varying concentration of wood and rubber (Figure 2). The wood content was about 1–4% by weight. In Figure 2, the wood is included in the "non-polymers."

Trials were conducted by using commercially-available air aspirators, classifiers, air-gravity tables, and mineral jigs to remove wood and rubber from the polymer concentrate. Using this equipment did not yield satisfactory results.

Froth-Flotation Pilot-Plant

A shakedown of the wet density/froth-flotation facility was conducted during the second quarter of FY 2005 by using about 4,000 lbs of post-consumer electronics and appliance mixed plastics. These materials were used because their composition is much less variable than the composition of plastics concentrate from shredder residue. The shakedown tests were conducted to target the recovery of acrylo-nitrile-butadiene-styrene (ABS) and polystyrene (PS). Trials were also conducted by using colored plastics supplied through the American Plastics Council. These trials confirmed the effectiveness of the basic system.

The initial trials of the froth-flotation system on shredder residue plastics were complicated by the unexpected high rubber and wood content of the polymer concentrate. Bench-scale tests were conducted to define the specific gravity and settling velocities of the wood and rubber relative to other species in the polymer concentrate. Several plastics, wood, and rubber species were found in every specific gravity range. Several plastics, wood, and rubber species were also found to have overlapping settling velocities. The data indicated that neither specific gravity nor settling velocity differences were large enough to effect the separation of wood and rubber from the plastics.

Trials using various process solution conditions were also conducted. These trials ultimately yielded a set of conditions to remove almost 100% of the wood and to concentrate the rubber into two separate fractions with a nominal loss (less than 5%) of the polymers (such as the polypropylene [PP] and polyethylene [PE]) that are being targeted for recovery. The resultant process conditions have been incorporated into the Argonne froth-flotation process. More than 3,500 lb of a PP/PE fraction that is over 95% PP/PE have been consistently produced. Its wood content is less than 0.2%. The recovered PP/PE has properties similar to those of some commercially-available PP materials. The recovered PP/PE product constituted about 5%–6% of the starting shredder residue weight.

An 80% rubber concentrate was also recovered. A 50-lb sample of the rubber concentrate was submitted for testing by using the "TireCycle" process used for recycling rubber materials. It was determined that the presence of the plastics in the rubber concentrate is likely to improve the properties of the recycled rubber when used to make construction products (such as roofing shingles).

A 75% ABS concentrate has been recovered. The ABS concentrate contained incompatible materials, including filled PP. Trials are ongoing to improve the composition of the ABS concentrate and to recover other polymers from the polymer concentrate.

Changing World Technologies

Changing World Technologies, Inc. (CWT), has developed a thermal conversion process that converts organic material into high hydrocarbon oil. The process was tested for processing shredder residue. The process was able to convert the shredder residue samples into three product fractions: an oil, a gas, and a carbon char. A pilot-scale test apparatus was designed and built by CWT to simulate commercial-scale handling and depolymerization/dissolving of a mixed automotive waste stream (90% shredder residue/10% post-consumer tires). Tests were conducted to confirm the technical and economic feasibility of this process.

In the process, a 1/16-in. mesh vibrating screen was used to separate the fines (mostly inorganic matter), which constituted about 36% of the total shredder-residue sample weight. The shredder residue was supplied by Argonne. About 700 lb of the remaining fines-free material was processed along with 80 lb of shredded tires and 1,700 lb of used motor oil. Samples of the various products were sent out for analysis to determine the fate of the inert solids and contaminants (i.e., heavy metals, polychlorinated biphenyls [PCBs], and chlorine).

Thermal cracking tests of this CWT hydrocarbon fuel were performed in bench-scale Parr reactors to simulate the production of transportation fuels. The products generated were hydrocarbon oil, a fuel-gas, and a solid carbon product. The distribution of oils/gas/carbon fractions was determined to be 84%, 10%, and 6%, respectively. A fractional distillation of the oil was also performed. This process generated gasoline, diesel, and heavy hydrocarbon oils (Figure 5). The distribution was gasoline (12%), middle-distillate (38%), diesel (32%), heavy-oil (15%), and gas (3%).



Figure 5. Left to right: gasoline, middle distillate, diesel, and heavy fuel oil reduced by the CWT process.

Troy Polymers Process for Glycolysis of PUFs

Troy Polymers, Inc. (TPI), has developed a patented process for the conversion of mixed polyurethane foams (PUF), such as that present in shredder residue, into polyol initiators (Figure 6), which can then be utilized to produce urethane products. PUFs first undergo glycolosis, followed by filtration and removal of PCBs and other substances of concern from the liquid glycolyzed product. In a second stage, the glycolyzed products are propoxylated by using propylene oxide to produce polyols.

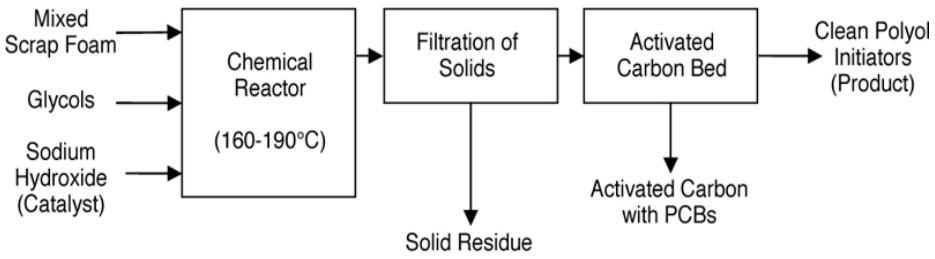


Figure 6. TPI's glycolysis process conceptual process flow sheet.

In FY 2004, bench-scale testing was undertaken to establish proof-of-concept. The results demonstrated the technical feasibility of the process for converting mixed, clean PUF from shredder residue to polyol initiators at a yield of about 88%. The yield for dirty foam was about 72%. The product from dirty foam required extensive filtration to remove the solid residue. The results also indicated that commercially available activated carbons were able to reduce the concentration of PCBs to below 1 ppm.

In FY2005, the process was scaled up in a 5-gal reactor. Scale-up included testing of the filtration of solid impurities and removal of PCBs and other substances of concern from the polyol initiator. Over 1,200 lb of foam separated from shredder residue have been processed, and over 100 gal of polyol initiator have been produced. The effects of temperature, glyocol-to-foam ratio, and catalyst types on the reaction yields have been evaluated. Results indicate that diethylene glycol (DEG) gives a higher yield and allows reaction at lower temperature than dipropylene glycol (DPG). Potassium hydroxide (KOH) was preferred over sodium hydroxide (NaOH) as a catalyst. By using optimized reaction conditions with DEG and KOH catalyst, >90% reaction yields were consistently achieved.

Various filtration methods were also evaluated for the removal of unreacted solids from the polyol initiator. A nylon bag filter was installed in a recirculation loop with the 5-gal reactor to remove solids larger than 200 μm. Although bag filtration worked well on a 5-gal scale, for a production-scale process, continuous filtration systems will most likely be required.

Treatment with activated carbon was also capable of removing PCBs from the polyol initiator to nondetectable levels (<2 ppm). The PCBs are removed more readily from the polyol initiators produced from DEG than DPG. The removal of PCBs via activated carbons from polyol initiator was demonstrated by using Aquasorb 1500 activated carbon. Twenty gallons of the polyol initiator, which had an equivalent weight of 163, was also submitted for propoxylation to Pelron Corporation in Illinois, where two lots were produced. In one lot, the equivalent weight of polyol was 354, and in the other lot, it was 173. That two different equivalent weights were produced proves that polyols with different equivalent weights can be produced from the recycled polyol initiators.

The recycled polyols produced from shredder-residue foam were also tested in preparing rigid PUFs. The recycled polyols exhibited several advantages over the virgin commercial polyols. They were more reactive than the virgin polyols in that they required fewer or no catalysts. Furthermore, the foams based on the recycled polyols had much better flame resistance than the foams based on the virgin polyol.

Initial economic analysis of the process to produce polyol initiator and polyols via propoxylation indicated that the glycolysis process is economical.

Publications

Recycling Shredder Residue Containing Plastics and Foam Using a Thermal Conversion Process, Winslow, G.R.; Appel, B.S.; Adams, T.; Simon, N.I.; Duranceau, C.M.; Wheeler, C.S.; and Sendijarevic, V., SAE Paper #2005-01-0848.

Chemical Recycling of Mixed Polyurethane Foam Recovered from Shredder Residue into Polyurethane Polyols, Sendijarevic, V.; Sendijarevic, I.; Winslow, G.R.; Duranceau, C.M.; Simon, N.I.; and Wheeler, C.S., SAE paper # 2005-01-0850.

Sustainable End-of-Life Vehicle Recycling: R&D Collaboration between Industry and the U.S. DOE, Journal of Metals, Daniels, E.J.; Carpenter, J.A., Jr.; Duranceau, C.; Fischer, M.; Wheeler, C.; and Winslow, G., Vol. 56, No. 8, August 2004.

Advanced Separation of Plastics from Shredder Residue — Mechanical Separation, Salyp Process Technology, Winslow, G.R.; Simon, N.L.; Duranceau, C.M.; Williams, R.; Fisher, M.M.; Kistenmacher, A.; and VanHerpe, I., SAE paper # 2004-01-0469.

Screening Study to Evaluate Shredder Residue Materials, Winslow, G.R.; Wheeler, C.S.; Williams, R.L.; Duranceau, C.M.; Simon, N.L.; and Schomer, D.R., SAE paper # 2004-01-0468.

8. MATERIALS CROSSCUTTING R&D

A. Technical Cost Modeling

Principal Investigator: Sujit Das
National Transportation Research Center
2360 Cherahala Boulevard
Knoxville, TN 37932-6472
(865) 946-1222; fax: (865) 946-1314; e-mail: dass@ornl.gov

Technology Area Development Manager: Joseph A. Carpenter
(202) 586-1022; fax: (202) 586-1600; e-mail: joseph.carpenter@ee.doe.gov
Field Technical Manager: Philip S. Sklad
(865) 574-5069; fax: (865) 576-4963; e-mail: skladps@ornl.gov

---

Contractor: Oak Ridge National Laboratory
Contract No.: DE-AC05-00OR22725

Objectives

- Address the economic viability of new and existing lightweighting materials technologies.
- Develop technical cost models to estimate the cost of lightweighting materials technologies.

Approach

- Address the economic viability of lightweighting materials technologies supported by the ALM.
- Use cost modeling to estimate specific technology improvements and major cost drivers that are detrimental to the economic viability of these new technologies.
- Derive cost estimates based on a fair representation of the technical and economic parameters of each process step.
- Provide technical cost models and/or evaluations of the "realism" of cost projections of lightweighting materials projects under consideration for ALM funding.
- Examine technical cost models of lightweighting materials technologies that include (but are not limited to) aluminum sheet; carbon-fiber precursor and precursor processing methods; fiber-reinforced polymer composites; and methods of producing primary aluminum, magnesium, and titanium and magnesium alloys with adequate high-temperature properties for powertrain applications.

Accomplishments

- Completed a cost-benefit evaluation of the ALM's polymer composites efforts.

Future Direction

- Estimate the impacts of the remaining lightweighting materials areas (i.e., magnesium, steel, metal-matrix composites, aluminum sheet forming, and recycling) supported during the fiscal year 2000–2004 periods.
- Continue individual project-level cost modeling to identify specific technology improvements and major cost drivers that are detrimental to the economic viability of these technologies.

Benefit Evaluation of Polymer Composites

The focus during this fiscal year for this task has been on the benefit evaluation of ALM efforts supported during the fiscal year 2000-2004 periods. The polymer composites efforts, which accounted for a major share of the total ALM funding during the last five-year funding cycle, are only being considered this fiscal year for the benefits evaluation. The benefit evaluation of a specific lightweighting material area is based on a detailed evaluation of a few illustrative projects from that area. The following *five* illustrative projects (along with the major partners listed within parenthesis for each case) were selected from the list of 24 polymer-composites projects supported with a total funding level of around $68 million.

- Automotive Composites Consortium focal project 3 (ACC) (report 4.D);
- Durability of lightweight composite structures (ORNL) (report 4.H);
- Low-cost carbon fibers from renewable resources (ORNL) (report 3.A);
- Low-cost carbon fiber development project (Hexcel/ORNL); and
- Modeling of composite materials for energy absorption (LLNL/ORNL).

These projects mainly cover the carbon-fiber-reinforced polymer-composites focus area examining such issues as durability and safety, important for any lightweighting materials. The R&D projects reflect multiple partners involved in the R&D effort, e.g., national-laboratories-only versus national-laboratories and private-sector collaboration. In choosing the five projects, we also took into consideration the level of funding (one of the larger amounts funded in the polymer-composites area) and project status (e.g., projects completed and those on-going).

Due to the significant focus on the costs of carbon-fiber composites as a means to increase their viability as an option to the automakers, two projects dealing with costs were selected (low-cost carbon fibers from renewable resources and low-cost carbon-fiber development). Similarly, two projects, durability of carbon-fiber composites and modeling of composite materials for energy absorption, fall under the category of enabling technologies, focusing on durability and safety areas, respectively.

The remaining project—composite-intensive body structure for focal project 3—covers the area of polymer-composites manufacturing R&D, has one of the largest budgets, and is 100 percent cost-shared by the auto industry. In addition, it covers technology commercialization. The projects are also reflective of the differences in project partners, i.e., national-laboratories-only in the modeling of composite materials for energy absorption versus private-sector and national- laboratory collaboration in the low-cost carbon fiber development program. Only two projects, i.e., durability of carbon-fiber composites and low-cost carbon-fiber development program, have been completed.

An evaluation framework developed earlier with the goal of evaluating both short-run outputs and long-run outcomes of the R&D projects was selected. The framework consists of four methods using both qualitative and quantitative measures and they are: qualitative assessment, National Research Council indicators, quantitative benefits, and benefit-cost analysis. The first three types of benefits information were collected from the project participants through surveys, which assessed their views about the benefits of projects, including the number of publications produced and graduate students supported by the end of a project and long-term benefits (knowledge-level gained through the publications, human capital investment in graduate students' dissertations and theses produced, and increased international competitiveness of the Big 3 automakers). The benefit-cost analysis is used to monetize values for the benefits and costs of each project. The benefits are estimated based on the projected market penetration of carbon-fiber-composite materials in light-duty vehicles using a Delphi technique.

Overall, the results of the qualitative assessment are positive for the five projects. There was 100 percent agreement that technical objectives were met with the exception of two projects such as the composite-intensive body structure project for focal project 3 which remains to be completed. New knowledge was yielded from all five projects and, in general. collaboration was enhanced through research activities. If future collaboration were uncertain,

issues related to proprietary concerns and finding the correct mix of technical skills were seen as impediments. As one would expect, there was less agreement on whether the results of the project were sufficient for carbon fibers to be a viable option for the automobile sector.

Results of the National Academy of Sciences' indicators show numerous publications (in the range of (9-40) in each R&D effort, where the number of publications appears to be related to the level of involvement of national laboratories and participants. There were mixed perceptions on whether the United States is leading internationally in research on the use of low-cost carbon fibers in the manufacturing of parts for the light-duty vehicles. Most participants indicated the United States was about even or following countries in the European Union or Japan. Nor is the United States perceived as leading in commercialization of carbon fibers in light-duty vehicles. However, there was agreement in all the projects (at least a majority of responses were greater than 50 percent) that the R&D efforts *will* improve the United States' international competitiveness.

The quantitative benefits revealed from this evaluation are quite impressive. Graduate students were involved in each project (maximum 5 per year in one project), even though the project may not have had an active university participant. In addition, patents and copyrights were applied for and received (and future applications are envisioned). Software packages were commercialized in some projects. The reaction of the Big 3 automakers has been favorable on the usefulness of the software.

The results of the economic analyses, primarily the benefit-cost ratios for each of the five projects, are shown in Table 1. The benefit-cost analysis takes into account energy, environmental, and security benefits. The project costs include both federal funding and private-sector matching funds. The base, moderate, and high cases represent low, medium, and high monetary values for energy, environmental, and security savings in Table 1. Note that estimated benefits are based on the projected market penetration of carbon fiber composite materials in light-duty vehicles using a Delphi technique. In every case, the benefit-cost ratios indicate significant benefits for these projects. The fiber development project tops the list, whereas, a significantly higher project cost causes the durability project to be at the bottom of the list. It must be noted, however, that several uncertainties are associated with these numbers, as is typical for benefit-cost analyses. First, the commercialization date and market penetration rates for each technology are uncertain besides the portion of total market penetration that can be accurately attributed to government funding. The analysis assumes dates for initial commercialization and market penetration rates that may or may not come true. Second, the projects reflect uncertainty in the level of benefits associated with each new vehicle that contains new lightweight materials. Third, uncertainties exist concerning the monetary values to be assigned to each benefit, e.g., values of reducing CO_2, oil imports, etc.). Fourth, investment costs to be borne by the automobile manufacturers and their suppliers to implement the new technologies are not fully captured in this analysis.

Table 1. Estimated Benefit-Cost Ratios of Five ALM Polymer-Composite Projects.

Project	Project Cost ($ millions)	B-C Ratio* Base Case	B-C Ratio* Moderate Case	B-C Ratio* High Case
DOE	68.3	29(25)*	62(45)*	124(75)*
Focal Project 3	5.1	90(79)*	193(140)*	388(233)*
Durability	7.2	41(36)*	94(68)*	195(117)*
Renewable Fiber	3.1	89(77)*	200(145)*	417(250)*
Fiber Development Program	3.6	134(117)*	279(202)*	548(329)*
Modeling	4.4	52(45)*	123(89)*	261(157)*

* Numbers inside parenthesis indicate benefit-cost ratios *without* taking into account environmental and security benefits.

Publications

1. "Life Cycle Impacts of Automotive Liftgate Inner," *Resources, Conservation and Recycling,* Vol. 43/4 pp 375-390, Mar. '05.
2. "Cost-Effectiveness of Carbon Reinforced Composite Automotive Part Manufacturing Technologies," presented and published in SAMPE 2005/Long Beach Conference Proceedings, May 1-5, 2005 in Long Beach, CA.

B. Intermediate-Rate Crush Response of Crash Energy Management Structures

Principal Investigator: J. Michael Starbuck
Oak Ridge National Laboratory
P.O. Box 2009, Oak Ridge, TN 37831-8048
(865) 576-3633; fax: (865)-574-8257; e-mail: starbuckjm@ornl.gov

Project Manager, Composites: C. David Warren
Oak Ridge National Laboratory
P.O. Box 2008, Oak Ridge, TN 37831-6065
(865) 574-9693; fax: (865) 576-4963; e-mail: warrencd@ornl.gov

Technology Area Development Manager: Joseph A. Carpenter
(202) 586-1022; fax: (202) 586-1600; e-mail: joseph.carpenter@ee.doe.gov
Field Technical Manager: Philip S. Sklad
(865) 574-5069; fax: (865) 576-4963; e-mail: skladps@ornl.gov

---

Contractor: Oak Ridge National Laboratory
Contract No.: DE-AC05-00OR22725

Objective

- Develop unique characterization facility for controlled, progressive-crush experiments, at intermediate rates, of automotive materials (polymer composites, high-strength steels, and aluminum) and structures.
- Study the deformation and failure mechanisms of automotive materials subjected to crush forces as a function of impact velocity.
- Obtain specific energy absorption and strain data, and correlate with deformation and failure mechanisms to describe the unknown transitional effects from quasi-static to high loading rates for polymer composites.
- Characterize the strain-rate effects for metallic materials and components.
- Provide access to this unique test capability to university, industry, and government users for collaborative research.

Approach

- Develop a unique, high-force (270-kN), high-velocity (8-m/s) servo-hydraulic machine to conduct progressive crush experiments on structural components at intermediate rates.
- Use high-speed imaging to observe and document deformation and damage mechanism during the crush event.
- Conduct strain measurements at discrete locations and explore full-field measurements of strains and curvatures.
- Coordinate polymer composites investigations with the Automotive Composites Consortium (ACC) Energy Management Group.
- Coordinate steel investigations with the Auto/Steel Partnership.

Accomplishments

- Procured high-speed video system.
- Completed glass-fiber-reinforced composite-tube testing that clarified the transition region from static to dynamic.
- Completed tube testing under Stanford University User Proposal,
- Completed preliminary testing on sandwich panels for University of Utah. (See report 4.I.)
- Completed preliminary testing on magnesium tubes for Swinburne University of Technology, Australia.
- Completed tube testing in support of Crash Analysis of Adhesively Bonded Structures (CAABS) Project. (See report 4.J.)
- Completed tube testing in support of the Auto/Steel Partnership Strain-Rate Characterization project. (See report 2.S.)
- Developed improved data acquisition software for strain-gage measurements.
- Developed streamlined software for interfacing force-displacement data with high-speed video.

Future Direction

- Explore techniques for full-field measurements of strains and curvatures.
- Develop User Interaction Plan.
- Support user collaboration as required.

Introduction

Progressive crush is an important mechanism by which the kinetic energy of a traveling automobile is dissipated in a collision to protect the safety of occupants. Unfortunately, the mechanisms governing the progressive-crush response of some emerging automotive materials are not well understood. Additionally, many of these materials are known to exhibit responses that are sensitive to rate of loading.

Understanding the influence of impact velocity on the crush response of materials and structures is critically important for crashworthiness modeling inasmuch as collisions occur at a range of velocities. Additionally, from a structural standpoint, the deformation (or strain) rate is generally not unique from either a spatial or temporal standpoint. Consequently, it is important to quantify the behavior of materials at various strain rates.

Test Machine for Automotive Crashworthiness (TMAC)

Typically, standard test machines are employed for experiments at quasi-static rates, whereas drop towers or impact sleds are the convention for dynamic rates. These two approaches bound a regime within which data, for experiments at constant impact velocity, are not available by conventional experimental practice. This regime is termed herein the intermediate-rate regime and is defined by impact velocities ranging from 1 m/s to 5 m/s. Investigation of rate effects within this regime requires experimental equipment that can supply a large force with constant velocity within these rates. Using a drop tower or sled at intermediate rates, although technically possible, is problematic due to the prohibitively large mass required to maintain constant velocity during the crush. Consequently, the Oak Ridge National Laboratory (ORNL) and the Automotive Composites Consortium (ACC) collaborated to define specifications for a unique experimental apparatus that mitigates the shortcomings of existing equipment. MTS Systems Corporation designed and built the servo-hydraulic test machine, referred to as the TMAC. TMAC is uniquely capable of conducting controlled, progressive-crush tests at constant velocity in the intermediate-velocity range (i.e., less than 5 m/s) because of the large energy available at those rates and to the sophisticated simulation and control software that permits velocity uniformity to within 10%.

The new experimental facility is being used to understand the crush behavior between the static and dynamic (8-m/s) conditions. The installation of the TMAC at its National Transportation Research Center (NTRC) Knoxville, Tennessee, location is shown in Figure 1.



Figure 1. Installation of TMAC in the NTRC Composite's Lab.

Status

Since the last reporting period, activities have focused on supporting users, developing and promoting user interactions, and improving data acquisition.

In FY 2004, a test matrix on glass-fiber-reinforced composite tubes was completed and the experimental data were supplied to the ACC. The tubes were approximately 50 mm x 50 mm square and used an internal plug with a radius as an initiator. A total of 60 tests were initially conducted: six specimens/velocity/material; five velocities (5 mm/sec, 1000 mm/sec, 2000 mm/sec, 3000 mm/sec, and 4000 mm/sec); and two materials (one braided and one fabric). The results showed that the transition between static and dynamic was below the 1000-mm/sec test velocity. In FY 2005, additional tests were run at 250 mm/sec and 500 mm/sec. The results are shown in Figure 2 and clearly indicate that a transition exists. The test specimens have been sectioned and photographed to determine if a physical phenomenon exists that correlates with the transition from static to dynamic test velocity. Complete documentation of this work is in preparation and is being coauthored by Ford Motor Company.

In addition to the glass-fiber-composite tubes tested there were carbon-fiber tubes tested for Ford Motor Company under a user proposal. The objective of this project was to collect experimental data that

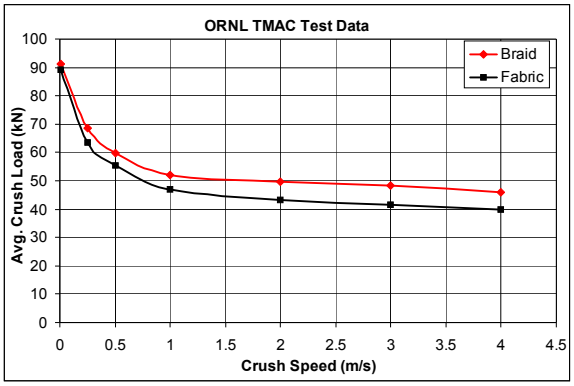


Figure 2. Average crush load versus speed for glass-fiber-reinforced composite tubes.

would help in quantifying the contribution that different failure mechanisms have on the total energy absorbed. This work was completed and the results are to be presented at the 2006 SAMPE Conference.

Stanford University, under ACC Cooperative Agreement funds, has a research project to create a finite element material model that describes the response and failure behavior of braided composite materials. These materials can be used to absorb energy in automotive, aerospace, or other crashes. In order to model the material and to verify numerical predictions, crush tests must be conducted on representative samples, in this case, triaxially-braided composite tubes crushed at several rates using a plug initiator. It is expected that the energy absorption of dynamically-crushed tubes will be lower than statically-crushed tubes that have been crushed previously and that the energy absorption will be sensitive to braid angle.

The scope of work for Stanford University's User Facility proposal included testing of composite tubes to provide essential data for verification of their finite element models. The following tube configurations and velocities were tested.

Square tube

- 30° Braid angle
  - 3 tubes at 1 m/s
  - 3 tubes at 4 m/s
- 45° Braid angle
  - 3 tubes at 1 m/s
  - 3 tubes at 4 m/s
- 60° Braid angle
  - 3 tubes at 1 m/s
  - 3 tubes at 4 m/s

Circular tube

- 30° Braid angle
  - 3 tubes at 1 m/s
  - 3 tubes at 4 m/s
- 45° Braid angle
  - 3 tubes at 1 m/s
  - 3 tubes at 4 m/s
- 60° Braid angle
  - 3 tubes at 1 m/s
  - 3 tubes at 4 m/s

The force and displacement versus time traces, and high-speed video for each test were provided to Stanford University for analysis. This work was part of a graduate student's Ph.D. dissertation. The student has successfully defended his work and publication of these results is in progress. Preliminary tests were completed on sandwich panels for the University of Utah (see report 4.I) and on magnesium tubes for the Swinburne University of Technology, Australia. These tests were conducted to determine appropriate specimen geometries and fixture requirements for future potential user proposals. Examples of these tests are shown Figures 3 and 4 where snap-shot images from the high-speed video were taken. Figure 3 shows a carbon-fiber facesheet with balsa wood core sandwich panel being compressed along one edge. This image captures the sandwich panel failing by buckling and core shear failure. A progressive-crush mode could not be achieved using this specimen geometry and fixture. The University of Utah has redesigned their test fixture and is currently drafting

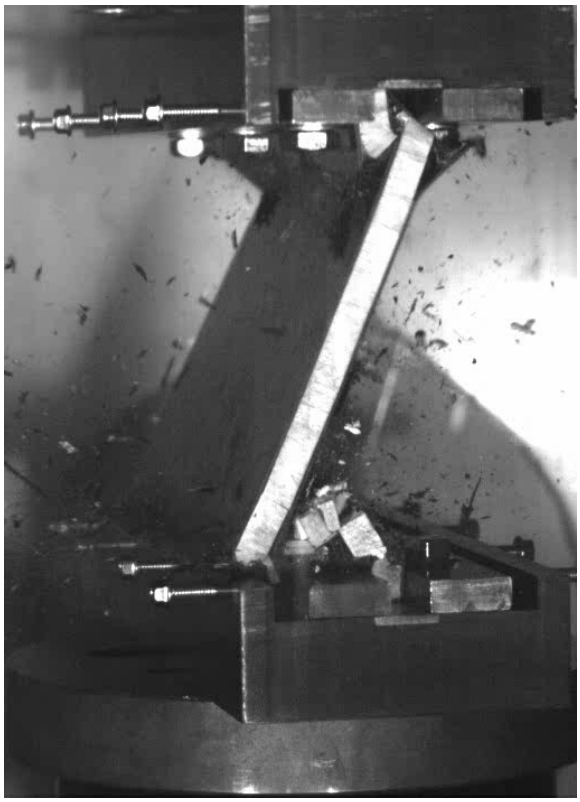


Figure 3. End-loaded compression test on composite sandwich panel having a balsa wood core.

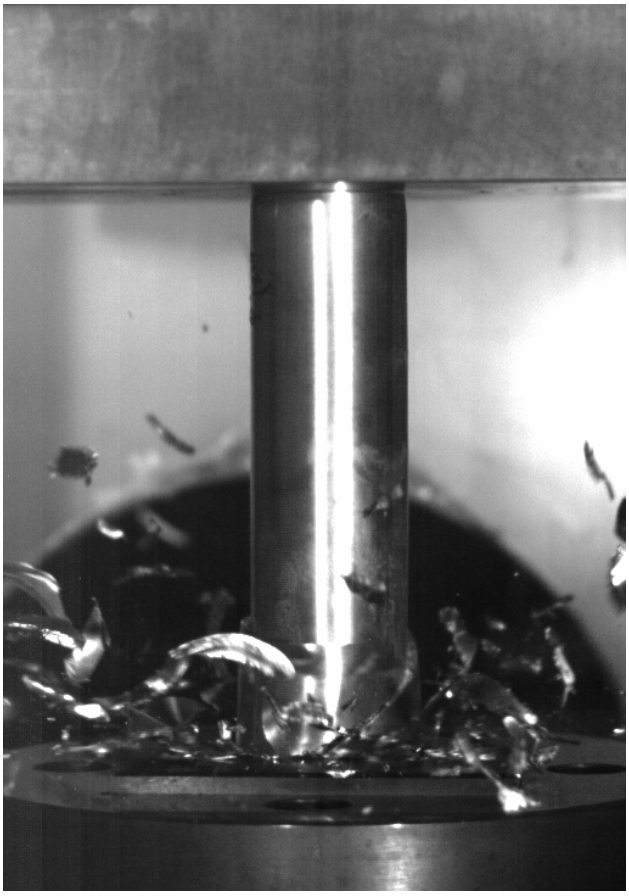


Figure 4. Progressive crush of a magnesium tube.

a new User Facility proposal. A magnesium tube being crushed is shown in Figure 4. This tube underwent a tremendous amount of elastic deformation before failing via multiple fractures. The data from the magnesium tubes tests were provided to the research professor at Swinburne University for his review.

Other interactions with potential users have taken place with Rutgers, Massachusetts Institute of Technology, SAE High Strain Rate Plastics Consortium, General Motors, and Imperial College (London, England).

Project Support Activities

Extensive testing was completed on TMAC in support of both the ACC Crash Analysis of Adhesively Bonded Structures (CAABS) project (see report 4.J) and the Auto/Steel Partnership (A/S-P) Strain-Rate Characterization project (see report 2.S). For the CAABS project, 30 tubes were tested that quantified the effect that adhesive bonds have on energy absorption. In support of the A/S-P project, 30 tubes were tested for determining strain-rate sensitivities in high-strength low-alloy steels and dual-phase steels. Strain gages were used in these tests to locally measure the strains associated with plastic hinge formation in metal tubes undergoing progressive crushing.

Conclusions

TMAC provides a unique capability to measure the specific energy absorption on crush tubes and other specimen geometries as a function of (constant) impact velocity within a range from quasi-static to 8 m/s.

During the past reporting period, tests were conducted to further characterize glass-fiber-composite tubes at 2 velocities below 1000 mm/sec. These tests provided critical data that definitely showed the transition from static to dynamic response that was previously unavailable using other test methods. Also, braided-carbon-fiber tubes were completed for Stanford University under a User's Facility proposal. Additional scoping tests were conducted for the University of Utah and for Swinburne University of Technology, Australia, in support of developing future user proposals. TMAC was also instrumental in meeting project objectives for the CAABS and A/S-P projects. In all of these tests, high-speed video was recorded to document the failure mechanisms using a state-of-the-art CMOS camera that was procured for the TMAC installation.

Presentations/Publications/Patents

None

C. Structural Reliability of Lightweight Glazing Alternatives

Principal Investigator: Moe Khaleel
Pacific Northwest National Laboratory
P.O. Box 999/K7-36
Richland, WA 99352
(509) 375-2438; fax: (509) 375-6605; e-mail: moe.khaleel@pnl.gov

PPG Project Manager: Jim Valimont
(412) 820-8731; fax: (412) 820-8630; e-mail: jvalimont@ppg.com

Technology Development Manager: Joseph Carpenter
(202) 586-1022; fax: (202) 586-1600; e-mail: joseph.carpenter@ee.doe.gov
Field Technical Manager: Philip S. Sklad
(865) 574-5069; fax: (865) 576-4963; e-mail: skladps@ornl.gov

---

Contractor: Pacific Northwest National Laboratory
Contract No.: DE-AC06-76RL01830

Objective

- Optimize glazing systems for cars of the future by decreasing sound transmission while maintaining structural rigidity.
  - Reduce sound transmitted through sidelights by 6 decibel (db) by determining the effect of sidelight shape on sound transmittance, investigating sound-dampening materials for operating sidelight glazing, and quantifying the influence of alternate materials (e.g., laminated glass, bi-layer glass) on sound attenuation.
  - Maintain the level of structural integrity while reducing glass thickness by validating the structural rigidity model for various types of resins used in fixed glazing systems and by expanding/combining existing models to test various alternative constructions and glazing systems for side, rear, and roof windows.
- Reduce vehicle weight through alternate or thinner vision panels and/or by reducing the heat load transmitted through the glass. The goal is to improve the fuel economy of a car by requiring 30% less glass weight.
- Reduce side, rear, and (potentially) roof window glass weight while maintaining acoustics and minimizing price increases.
  - Consider several material options, including laminated glass, cast-in-place, pseudo-laminated glass and bi-layer materials.
  - Enhance fuel economy from reduced solar-energy transmission.
  - Reduce solar-energy transmission through glass by using absorbing substrates and reflective coatings.
  - Quantify gas-mileage improvement opportunities from improvement in solar-energy transmission.

Accomplishments

- Completed fabrication of newly-designed tooling for complex automotive side window shapes and laminates with new interlayer materials.
- Demonstrated feasibility for scaled-up production using resin injection method for large automotive side window laminations.
- Demonstrated strength requirements for 252 g ball impact from 9.14 m.
- Fabricated 30 test windows with new injection method for humidity and ball-drop testing of interlayer material.
- Reduced humidity delamination.

- Conducted initial investigation into surface treatments and edge sealing.
- Demonstrated feasibility of nanocomposites.
- Completed the investigation of edges sealants for further reduction of humidity affects.
- Lamination of large, curved, glass side windows.
- Lamination of soft and hard inclusions in interlayer mix for measuring sound transmission loss differences.
- Correlated modeling efforts to the experimental results from the soft- and hard-inclusion test results.

Future Direction

- Investigate the use of nanoparticles for mechanical property enhancements.
- Investigate non-symmetric laminates for weight reduction.
- Investigate multilayer interlayers for improved acoustical properties and weight reduction.
- Investigate ultra-thin glass layers for weight reduction.

Introduction

This project is a cooperative research and development agreement (CRADA) between the U.S. Department of Energy, Pacific Northwest National Laboratory (PNNL), Visteon Automotive Systems (Glass Division), and PPG, Inc. It started in June 2002, and is expected to be completed in 2006.

The project will evaluate designs for optimized glazing systems to be used in cars of the future and will work to help achieve the goals of FreedomCAR. The primary objective of the project is to reduce vehicle weight, improve fuel economy, and reduce vehicle emissions. However, to achieve these goals, it is necessary to consider the needs for high levels of structural reliability, competitive manufacturing costs, and passenger comfort from the standpoints of minimal acoustical noise levels and controlled interior temperatures. Energy savings will come from reducing weight by using thinner glazing; prior studies at PNNL have shown a potential for 30% reductions in weight from thinner glazing. Energy savings will also come from reducing interior heat loads that, in turn, will reduce the demand for air conditioning. The evaluation of alternative glazing concepts will also seek means to improve acoustical characteristics that will minimize interior noise levels while maintaining glazing at minimal thickness and weight levels.

Lightweight Window Manufacturing

New lightweight window samples were fabricated using 2.3-mm glass plies (a conventional automotive glass ply has a thickness of between 2.4 and 2.6 mm. The new lightweight samples were formed and laminated at PNNL using the newly developed resin injection technique.

New lightweight laminated side glass was fabricated using 2.3-mm plies. The window glass samples that were constructed are 2.3-mm glass, 0.76-mm polymer interlayer, and 2.3-mm glass.

During FY 2005, researchers completed the tool built for demonstration of large side windows with curved surfaces, as shown in Figure 1. The studies conducted demonstrated flow behavior, time to fill, evaluation of void formations, and visual observation for laminate distortion. The material used for the study is the current material that has

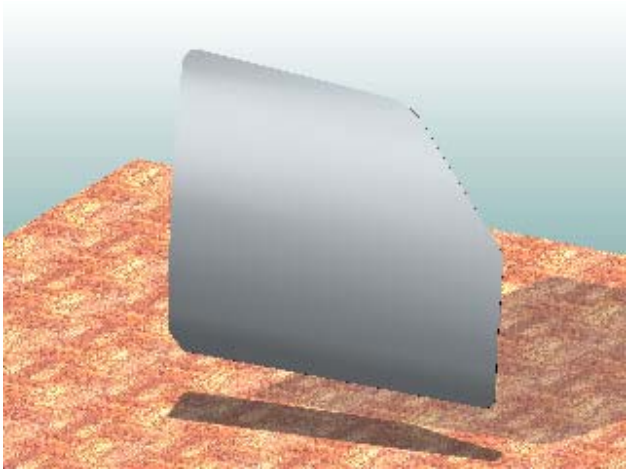


Figure 1. Typical large side window with curved surfaces.

undergone SAE Z26.1 testing with the 12-inch by 12-inch test panels.

Tool Construction

The construction material for the tool build was polymer/fiberglass composite. The matrix was a vinyl ester resin system with a foam core for increased rigidity. The master pattern was created from a current laminated, curved glass window that utilizes the polyvinylbutyral interlayer material. Prior work with this laminated glass provided the availability of thin glass for laminations.

Figure 2 shows the construction of the actual tooling. The outer gray perimeter material is the dam that constrains the resin material to the edge of the glass. The two inner o-rings are seals for vacuum chucking the glass to the mold and resin damming to keep resin out from under the glass.

The two halves are clamped together once the glass layers are chucked up to the mold surface. The resin can then be injected in from one corner and vented out at the other.



Figure 2. Test fixtures for injection process validation.

Flow Behavior and Fill Time

The large-tool-flow experimental setups were first checked for flow behavior and then to determine the time-to-fill. The flow-experiment setup had a diagonal flow length of 1.04 m (41 inches) and an area of approximately 4200 cm. The tool was tilted so there was a 2 cm elevation change from inlet to outlet. This allowed resin to flow evenly through the window and to prevent air from being trapped in the curved shape. The total fill volume was 1.7 liters of resin with 1.8-mm-thick glass laminates and the calculated volume of the window laminate for 5.3-mm-thickness is approximately 720 cm^3. The difference between the total fill volume and calculated volume would be the difference of the fill lines, inlet and outlet reservoirs, and larger separations in the two outer glass surfaces than anticipated.

The resin material had a viscosity of 500 cps and the initial flow test was done with 10 inches of head pressure. The time to fill was 30 minutes. Future testing will be accomplished with resin injection equipment and pressures as high as 1 bar.

Laminate Testing

Laminate testing has been done by both PNNL and PPG. The testing covers a wide variety of tests as shown in Table 1. Tests performed followed the ANSI/SAE Z26.1 criteria for laminated side lights. Although several chemistries have passed most of the required tests, the humidity and impact tests continue to be elusive. Furthermore, material optimization for sound transmission loss is also being investigated. PPG continues to support the project with total light transmission, UV and IR stability, boiling water, humidity, and thermal cycling.

Table 1. Tests performed on laminated glass.

ANSI/SAE Z26.1-1996	PNNL Testing	PPG Testing
1) Light Stability		Pass
2) Luminous Transmittance	Pass	Pass
3) Humidity Test	Pass Rnd 1 Fail Rnd 2	Reduced Signif. Rnd 1 Fail Rnd 2
4) Boil Test	Pass	Pass
5) Impact, Dart (9.14m)		Pass
6) Impact, Ball (9.14m)	Fail Rnd 1 Pass Rnd 2	Fail Rnd 1 No test on Rnd 2 currently
9) Temperature -40°C to 70°C	NT	NT

Humidity Testing

The elusive humidity test has been the most difficult test to pass. One formulation passed, but failed the ball-drop test. Most of the effort put forth has been toward passing this test. The delicate balance of trying to pass one test often upsets several others. However, we have gotten the entire set of tests covered with the exception of the humidity testing. The changes needed to pass the humidity test have had significant changes in the impact testing.

A measurement technique of establishing some type of standard for comparing humidity results is loosely in use. The environmental stability number (ESN) is a number that can be used to compare results from one set of results to another, Table 2. The results must be used with caution. An edge delamination with an ESN of 100 can be different from one sample to the next. For example, 100% of the perimeter could be delaminated in 1/16th of an inch that would give an ESN number of 100, but the same could be true for a small corner delamination that has a depth of ¼ of an inch. It is important to note whether the delamination is equal on all sides or whether it is spotty around the perimeter. See Figure 3 for examples of how the number is determined.

To reduce humidity failure, a couple of approaches have been investigated. Changes to resin chemistry, edge sealing, and surface treatments to the glass are a few of the approaches that have been tested.

The most significant effect was the change in resin chemistry. A 5% change in the resin ratio changed the effect humidity had on delamination by quite some amount. However, this 5% change also reduced the impact properties enough and the lamination failed impact testing. An alternative catalyst is currently being investigated for improved impact properties. The ESN number has been as low as 100. Starting numbers were typically around 2000 prior to resin modification.

Table 1. ESN criteria.

ESN=Pct 1+Pct 2x4+Pct 3x9+Pct 4x16+Pct 5x25	
Percent of perimeter at 1/16th depth	length of delamination less than 1/16th depth/ perimeter
Percent of perimeter at 1/8th depth	length of delamination less than 1/8th depth/ perimeter
Percent of perimeter at 3/16th depth	length of delamination less than 3/16th depth/ perimeter
Percent of perimeter at 1/4th depth	length of delamination less than 1/4th depth/ perimeter
Percent of perimeter greater than 1/4th depth	length of delamination less than 1/4th greater than depth/ perimeter
Highest possible ESN = 2500	

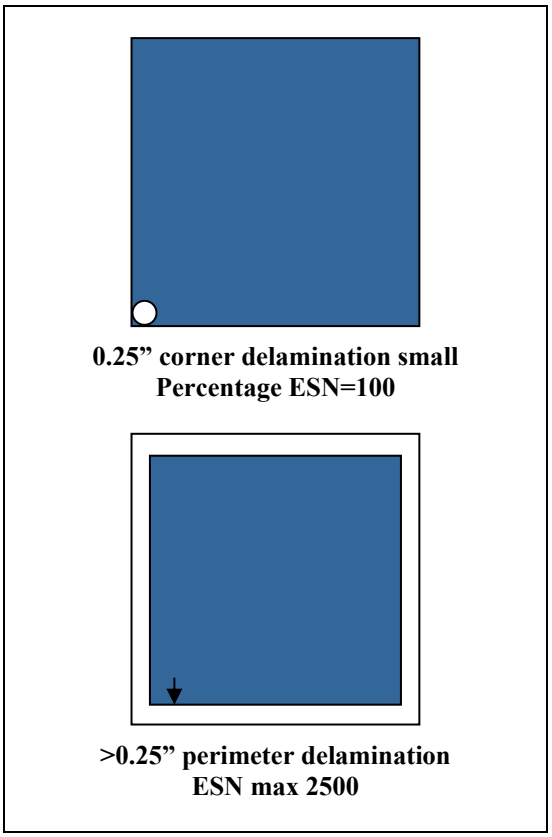


Figure 3. Measurement process for determining ESN number.

An edge-sealing approach was used with UV-curable edge sealants. The sealants were toughened methylacrylates typically used in sealing edges of heads-up display systems. Edge surfaces were prepared by cleaning with the traditional glass-cleaning process used prior to laminating the glass. The other method used was to sand the edges of the glass and then clean. The sealants were then added to the cleaned edges. The initial sealant testing had failed with high ESN numbers over 1500. A second round of testing with better cleaning of the edges and a different set of sealants to try has decreased the ESN number down to the double digits (Table 3).

Table 3. Humidity results with modifications to resin and edge sealing.

Sample	ESN
Standard Mix	2400
5% Resin change	1667
10% Resin change	52
15% Resin change	26
1% Nanoclay	467
Edge Seal #61	16
Edge Seal #68	0
Edge Seal #81	5

A different set of experiments completed the use of self-assembled monolayers. The functionality for the first set of experiments was an isocyanate surface treatment. Past experiments on thinner glass with a different catalyst yielded excellent results. However, the current system did not yield the same results and there are glass panels currently being treated with different functionality for future testing. There was an ESN of zero on past experiments with the previous catalyst and ratio change, the newer catalyst has been less successful.

The last set of experiments used nanoclay materials that serve as a vapor barrier. The ESN number in the I.28E nanoclay resulted in a 467 ESN number while the other less compatible nanoclay I.30E had an ESN of 1152.

Impact Testing

The impact testing for sidelites requires the resistance of a 252 g (0.5 lb) ball passing through or breaking the laminate into large pieces. The laminate must hold together and resist the ball passing through the laminate. There has been great success with this test. However, when optimization for the humidity tests began, the drop test showed the sensitivity of the elongation and toughness.

Figure 4 illustrates how the laminates resist the ball impact. The panel must resist fracturing into several large pieces and restrict the ball from passing through. All of the current panels have passed this test with the standard resin mix. Resin mixes that have been altered to pass the humidity test begin to fail at 5% resin change.



Figure 4. Impact-tested plate with 252 g ball at 9.14 m.

Alternative Laminates for Testing

In Figure 5 there are three different cases of experiments that were performed for process and materials evaluation. The fourth case for comparison is a monolithic glass case.

Case 1 is the baseline comparison of an unfilled resin system. It had several different resin ratios, catalysts, different polymeric materials and cure schedules. Case 1 is what has been reported in past reports and most of this report.

Case 2 is the baseline resin system that is filled with particulates of both hard and soft inclusions of nano-sized materials. There were found to be some definite advantages with these inclusions for the optical transmission and the previously discussed humidity testing.

Case 3 is a multilayer laminate that was processed. These can be made using several different

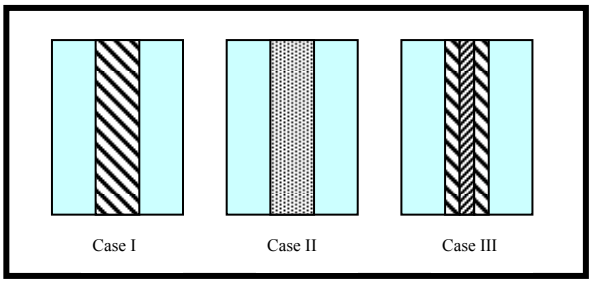


Figure 5. Illustrations of different case studies for alternative laminate possibilities.

combinations of resin blends, filled materials, and bonding agents. These were looked at for the sound transmission as well as impact and humidity tests.

Nanoparticulate Filler Experiments

The technical motivation for case 2 is to leverage the PNNL compounding and resin injection molding of materials for lightweight glazing for automotive side glass and to integrate these advanced composites technologies with surface chemistries for controlling sound, light transmission, and humidity resistance. The approach utilizes the recently-developed polymer system coupled with newly-developed nano-scale particles. This is a further enhancement of the processing and compounding of nano-scale particles for increasing the thermal stability, hardness, elastic modulus, and tensile strength through proper dispersion techniques and unique surface chemistries. An increase in mechanical properties will provide alternative design parameters and unique sound and light filtering. Electrical properties such as conductivity on certain particulates systems could also be utilized that could possibly be used for conducting interlayers for defrosting and other desirable uses.

The inclusion of organic fillers and polymers for commercial applications has been used for many years and are primarily aimed at cost reduction and stiffness improvement of the polymer composite system. A typical loading of greater than 20% by weight of micron-sized particles is generally required to bring realization of the above-stated positive effects. Polymer matrix properties such as processability, appearance, density and aging performance are compromised in systems with particle loadings greater than 20%. Therefore, composites with improved performance and low particle contents are highly desired. Tailored, nano-scale, particle-filled-polymer composites would enable new opportunities within the automotive glazing market for lightweighting of automotive side glass and, furthermore, increase service efficiencies and long-term reliability.

Polymer nanocomposites have drawn considerable attention during the last decade. The most typical fabrication method for polymer nanocomposites is the sol-gel method and it appears to be quite promising. Nanoparticulate are initially dispersed and subsequently mixed with the polymer gel at the molecular or near-molecular level.

The research effort included the following. (1) Evaluation of surface modifications of nanoparticulates for resin compatibility and control of desired properties, Figure 6; (2) Evaluation of soft and hard inclusions as well as plates vs. spheres and their effect on acoustical and optical properties. Figure 7 illustrates the difference between the neat resin and the platelet filled resin; (3) Development of mixing procedures for particulate materials with new resins through a static or ultrasonic mixer and injecting into a usable form for testing; (4) Thermal analysis cross-linking changes and microscopy of mixtures for dispersion; (5) Fabrication of test samples; (6) Testing for mechanical, physical and optical property characterization.

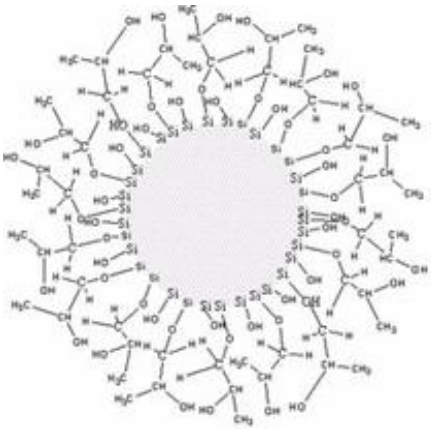
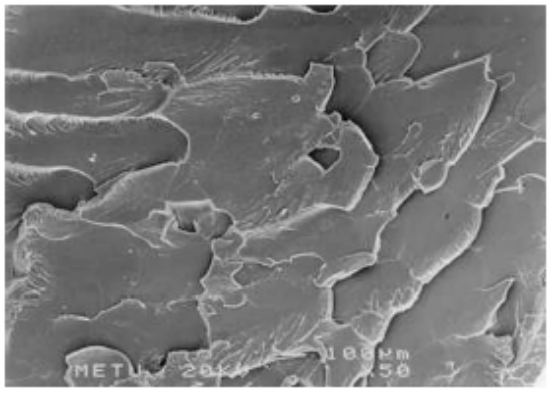


Figure 6. Modified surface of precipitated silica. (http://www.hubermaterials.com)

UV vis data were taken for different concentrations of filler and with different mixing methods. There were also two different surface treatments for testing of compatibility with the filler and resin.

Figure 8 illustrates the effects on transmittance and concentration of particles. With a 1% concentration of particles, one can have a small change on the visible spectrum and modest change to the UV and IR spectrums. The change to the IR spectrum can have a great effect on the heat loading on the interior of a vehicle.

Case three has great potential for using a wide variety of different modulus materials that could be used for sound trapping. This construction also lends



SEM image of neat epoxy

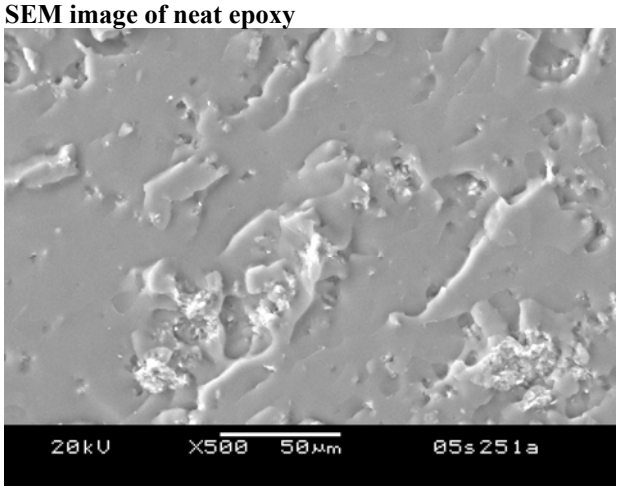


Figure 7. SEM image of cured 1% Nanocor 1.30/proprietary epoxy blend nanocomposite.

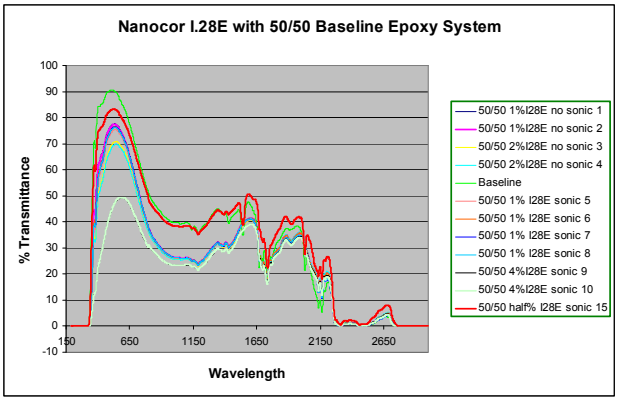


Figure 8. Full Spectrum of different concentrations of nano-particulates and the effect on the spectrum.

itself to alternative design options and adhesion alternatives. Humidity testing did not pass on the initial testing; however, the original goal was to see if it was possible to produce a multilayer laminate.

Sound Measurements and Modeling

Measurements of noise reduction (in decibels) of samples of laminated glass have been made in accordance to SAE J1400, in third-octave bands between 125 Hz and 8 kHz. The samples were mounted between the reverberant chamber and the semi-anechoic chamber. The measured sound transmission losses (STL) were compared with finite-element-determined STL predictions as well as the approximations using elastic-wave-propagation theory through laminated media. Optimized material and geometric parameters for sound insulation were studied using a factorial design method.

Future Work

Future work will focus on laminations of soft and hard inclusions as well as multilayer inter-layers for acoustics and possibly humidity reduction. Specimens will be fabricated for acoustics and material properties testing.

Modeling will be validated from the experimental data on the hard and soft inclusions in the interlayer. Efforts in modeling the sound performance of side lights through optimal multi-layer materials and dispersed particles will continue.

Appendix A. ACRONYMS AND ABBREVIATIONS

A/SP	Auto/Steel Partnership
ALRC	Albany Research Center
ABS	acrylonitrile-butadiene-styrene
ACC	Automotive Composites Consortium
AES	Auger electron spectroscopy
AFS	American Foundry Society
AHSS	advanced high-strength steel
AIChE	American Institute of Chemical Engineers
AISI	American Iron and Steel Institute
AKDQ	aluminum-killed draw-quality
Al	aluminum
ALCOA	Aluminum Company of America
ALM	Automotive Lightweighting Materials
AMD	Automotive Metals Division
ANL	Argonne National Laboratory
ANSI	American National Standards Institute
APC	American Plastics Council
APGE	Association of Petroleum Geochemical Explorationists
ARC	Automotive Research Consortium
ARL	Army Research Laboratory
AS	adaptive simulation
ASME	American Society of Mechanical Engineers
ASNT	American Society for Nondestructive Testing
ASTM	American Society for Testing and Materials
ATC	American Tooling Corporation
AWS	American Welding Society
BCC	body-centered cubic
BEM	boundary element method
BH	blankholder
BHF	blankholder force
BIW	body-in-white
BLR	bolt load retention
BN	boron nitride
BTU	British thermal unit
CAABS	Crash Analysis of Adhesively Bonded Structures
CAD	computer-aided design
CAE	computer-aided engineering
CAFE	Corporate Average Fuel Economy
CAVS	Center for Advanced Vehicular Systems
CD	compact disk
CI	confidence interval
CLiMRI	Canadian Lightweight Materials Research Initiative
COV	coefficient of variation
CP Ti	cold-pressed titanium

CP	cold-pressed
CPMT	Center for Powder Metallurgy Technology
CRADA	Collaborative Research and Development Agreement
CRTM	compression resin transfer molding
CSIRO	Commonwealth Scientific and Industrial Research Organisation
CT	computed tomography
CWT	Changing World Technologies
CY	calendar year
CZ	cohesive zones
DAQ	data acquisition
DB	decibel
DCB	double-cantilever beam
DCX	DaimlerChrsyler
DCZM	discrete cohesive zone mode
DEG	diethylene glycol
DEM	discrete element methods
DFEP	Die Face Engineering Project
DMA	dynamic mechanical analyzer/analysis
DOE	Department of Energy
DoE	design of experiment
DP	dual-phase
DPF	denier/filament
DPG	dipropylene glycol
DQSK	drawing quality special-killed
DRIFT	Direct Reinforcement Fabrication Technology or Directly Reinforced Fiber Technology
DSC	deferential scanning calorimeter/calorimetry
DTUL	deflection temperature under load
EAM	embedded atom method
EBSD	electron back-scattered diffraction
ECD	electron capture detector
E-COAT	electrophoretic primer
EDAG	Engineering Design, Inc.
E-GLASS	electrical glass
ELS	end-load-split
ELV	end-of-life vehicle
EM	electrode materials
EMF	electromagnetic forming
EPA	Environmental Protection Agency
ESN	environmental stability number
ETA	Engineering Technology Associates
EWI	Edison Welding Institute

FCVT	FreedomCAR and Vehicle Technologies
FE	finite element
FEA	finite element analysis
FEM	finite element method
FFC	Fray-Farthing-Chen
FGPC	future generation passenger compartment
FLCA	front-lower control arm
FLD	forming limit diagram
FMVSS	Federal Motor Vehicle Safety Standards
FP2	Focal Project 2
FP3	Focal project 3
FSSW	friction-stir spot-welded
FSW	friction-stir-welded
FTC	Federal Trade Commission
FY	fiscal year
GA	galvannealed
GC/MS	gas chromatography/mass spectroscopy
GENOA	Generalized Optimization and Analysis
GM	General Motors
GMT	glass mat thermoplastic
GPEC	Global Plastics Environmental Conference
GPM	grams per minute
GTAW	gas tungsten arc-welded
HAZ	heat-affected zone
HDG	hot dip galvanized
HDPE	high-density polyethylene
HIP	hot isostatic pressing
HPDC	high-pressure die-casting
HSB	hot-stamped boron
HSLA	high-strength low-alloy
HSS	high-strength steel
IF	interstitial free
IFU	University of Stuttgart
IIHS	Insurance Institute for Highway Safety
IR	infrared
ISO	International Standards Organization
ISRI	Institute of Scrap Recycling Industries
ISV	internal state variable
ITP	International Titanium Powders, Inc.
JCI	Johnson Controls, Inc.
KOH	potassium hydroxide
LabVIEW	Laboratory Virtual Instrumentation Engineering Workbench
LANL	Los Alamos National Laboratory
LBNL	Lawrence Berkeley National Laboratory
LCM	liquid composite molding
LDPE	low-density polyethylene

LFI	long-fiber injection
LFT	long-fiber-reinforced thermoplastic
LIMS	liquid injection molding simulation
LLNL	Lawrence Livermore National Laboratory
LMT	Light Metals Technology
LPPM	low-pressure permanent mold
LSTC	Livermore Software Technology Corporation
LVDT	linear variable displacement transducer
LWB	laser-welded blanks
LWFES	lightweight front end structures
LWFS	lightweight front structure
MAP	microwave-assisted plasma
MC	Monte Carlo procedure
MEL	Magnesium Elektron
MET	Management & Engineering Technologies
MFR	Melt flow rate
MHD	magnetohydrodynamics
MIG	metal inert gas
MIT	Massachusetts Institute of Technology
M-K	Marciniak-Kuczynski method
MPCC	Magnesium Powertrain Cast Components
MS&T	Materials Science and Technology
MSU	Michigan State University
MT	metric tons
MWV	MeadWestvaco
NADCA	North American Die Casting Association
NCAP	New Car Assessment Program
NCC	National Composite Center
NCC	National Composites Consortium
NDE	non-destructive evaluation
NIST	National Institute of Standards and Technology
NM	Newton-meters
NMR	nuclear magnetic resonance spectroscopy
NSF	National Science Foundation
NTRC	National Transportation Research Center
NVH	noise-vibration-harshness
OBD	offset deformable barrier
OD	outer diameter
OEM	original equipment manufacturer
OFCVT	Office of FreedomCAR and Vehicle Technologies
OPT	optimization
ORNL	Oak Ridge National Laboratory
OSU	Ohio State University
P4	programmable powdered preform process
PAN	polyacrylonitrile
PAR	POL Annual Report
PBDE	polybrominated diphenyl ether

PCB	polychlorinated biphenyl
PCBN	polycrystalline boron nitrate
PE	polyethylene
PI	principal investigator
PID	proportional integral derivative
PM	powder metallurgy
PMC	polymer matrix composite
PNNL	Pacific Northwest National Laboratory
PP	polypropylene
PPM	parts per million
PPO	polyphenylene oxide
PPS	polyphenylene sulfide or post-peak softening
PS	polystyrene
PSI	pounds per square inch
PSIA	pounds per square inch absolute
PUF	polyurethane foams
PUR	polyurethane
PURCC	Polyurethane Recycle and Recovery Council
PVB	polyvinylbutyral
PVC	polyvinyl chloride
R&D	research and development
RAM	random access memory
RFQ	request for quotation
RIS	radiographic inspection standards
RMS	rheometrics mechanical spectrometer
RPM	revolutions per minute
RRIM	reinforced reaction injection molding
RSW	resistance spot welding
RTM	resin transfer molding
RUC	representative unit cell
SAE	Society of Automotive Engineers
SAMPE	Society for the Advancement of Material and Process Engineering
SCMD	Structural Cast Magnesium Development
SCP	Springback Compensation Project
SDAS	secondary dendrite arm spacing
SDSM&T	South Dakota School of Mines and Technology
SEA	specific energy absorption
SEM	scanning electron microscopy
SFT	short-fiber thermoplastic composites
SG	specific gravity
SLC	sub-liquidus casting
SMC	sheet-molding compound
SMC	sheet-molding-component
SNL	Sandia National Laboratory
SOC	substance of concern
SOD	Slurry on Demand
SOW	statement of work
SPH	smoothed particle hydrodynamics
SRI	Southern Research Institute

SRIM	structural reaction injection molding
SSM	semi-solid metal
ST	Schapery-like, thermodynamically-based theory
STL	sound transmission losses
SUV	sport utility vehicle
SWSG	structural weld sub-group
TCP	tool center point
TDM	Troy Design and Manufacturing, Co.
TFF	thread-forming fastener
TGA	thermogravimetric
TMAC	Test Machine for Automotive Crashworthiness
TPI	Troy Polymers, Inc
TPO	thermoplastic olefins
TP-P4	thermoplastic P4
TPY	tons per year
TR	technical report
TRC-NCMS	Technologies Research Corp.of the National Center for Manufacturing Sciences
TRIP	transformation-induced plasticity
TTSP	time-temperature superposition principle
TWB	tailor-welded blanks
TYE	tensile, yield, and elongation
UAB	University of Alabama-Birmingham
UDRI	University of Dayton Research Institute
UHMW	ultra-high-molecular-weight
ULC	ultra-large castings
ULSAB	ultra-light steel auto body
UM	University of Michigan
UMAT	user material
USAMP	U.S. Automotive Materials Partnership
USCAR	United States Council for Automotive Research
UT	University of Tennessee
UTK	University of Tennessee at Knoxville
UTS	ultimate tensile strength
UV	ultra-violet
VCCT	virtual crack closure technique
VDA	visualization and data analysis
VPB	viscous pressure bulge
VROOM	Virtual Reality Room
VRP	Vehicle Recycling Partnership
VUMAT	vectorized user material
VW	Volkswagen
WF	warm-forming
WT%	weight percent
XPS	x-ray photoelectron spectroscopy
XRD	x-ray diffraction
YS	yield strength

This document highlights work sponsored by agencies of the U.S. Government. Neither the U.S. Government nor any agency thereof, nor any of their employees, makes any warranty, express or implied, or assumes any legal liability or responsibility for the accuracy, completeness, or usefulness of any information, apparatus, product, or process disclosed, or represents that its use would not infringe privately owned rights. Reference herein to any specific commercial product, process, or service by trade name, trademark, manufacturer, or otherwise does not necessarily constitute or imply its endorsement, recommendation, or favoring by the U.S. Government or any agency thereof. The views and opinions of authors expressed herein do not necessarily state or reflect those of the U.S. Government or any agency thereof.



Printed on
recycled
paper

A Strong Energy Portfolio for a Strong America

Energy efficiency and clean, renewable energy will mean a stronger economy, a cleaner environment, and greater energy independence for America. Working with a wide array of state, community, industry, and university partners, the U.S. Department of Energy's Office of Energy Efficiency and Renewable Energy invests in a diverse portfolio of energy technologies.

For more information contact:
EERE Information Center
1-877-EERE-INF (1-877-337-3463)
www.eere.energy.gov